Trinity College Dublin
Coláiste na Tríonóide, Baile Átha Cliath
The University of Dublin

The Effects of Neuroinflammation and Alzheimer's-like pathology on Gamma Frequency Oscillations in Mice

Hugh Jonathan Delaney

A dissertation submitted to the University of Dublin in candidature for the degree of Doctor in Philosophy

2024

Supervisors:

Prof. Mark Cunningham

Prof. Colm Cunningham

Declaration

I declare that this thesis has not been submitted as an exercise for a degree at this or any other university and it is entirely my own work, except for Figures 5.4, 5.5, and 5.6, in which data were partially collected by Dr Sadia Islam.

I agree to deposit this thesis in the University's open access institutional repository or allow the Library to do so on my behalf, subject to Irish Copyright Legislation and Trinity College Library conditions of use and acknowledgement.

I consent to the examiner retaining a copy of the thesis beyond the examining period, should they so wish (EU GDPR May 2018).

Hugh Delaney

Summary

Gamma frequency (20-80 Hz) oscillations are rhythmic neuronal network activities which are required in many cognitive processes, including working memory and selective attention. Neuroinflammation is increasingly seen as an important factor in neurological and psychiatric disorders, however there is a significant lack of understanding as to how neuroinflammation impacts gamma frequency oscillations in health and disease. Therefore, using *ex vivo* brain slice electrophysiology the effect of neuroinflammation on gamma frequency oscillations was investigated in healthy mice and in APP/PS1 mice (an Alzheimer's disease mouse model).

In young healthy mice exposure to various inflammatory mediators (TNFα, IL-1β, CCL2, CXCL10, and PGE-2) inhibited the normal growth in oscillation amplitude over time and in some instances reduced the oscillation frequency. Therefore, in healthy brain slices, gamma frequency oscillations are sensitive to increased neuroinflammation.

In brain slices from APP/PS1 mice, which carry two mutations that cause early onset Alzheimer's disease, gamma frequency oscillations were found to be disrupted, specifically at 9-11 months the oscillation amplitude and frequency were reduced relative to oscillations in brain slices from age-matched wildtype littermate controls. Additionally, the incidence and length of epileptiform events were increased in APP/PS1 mice. These changes were likely due to the deficits observed in the neuronal networks responsible for generating gamma frequency oscillations in APP/PS1 mice. Specifically, in APP/PS1 mice parvalbumin and somatostatin inhibitory interneurons were shown to be reduced using immunohistochemistry and GABAergic transmission was shown to be altered by pharmacological manipulation.

Given the immune system's active role in Alzheimer's disease and the observed sensitivity of gamma frequency oscillations to neuroinflammation, immune effects on gamma frequency oscillations was investigated in control and APP/PS1 mice. The extent to which the observed

alterations in APP/PS1 mice were due to increased neuroinflammation were investigated by treating mice with a microglial proliferation inhibitor, GW2580, which acts via CSF1R inhibition. This treatment was found to reduce microglial proliferation and reactivity, as intended. Gamma frequency oscillations were partially restored in APP/PS1 mice following GW2580 treatment – the amplitude reduction was reversed, however the incidence of epileptiform activity was increased. This demonstrated that the observed alterations in gamma frequency oscillations in APP/PS1 mice were, to at least some extent, caused by increased neuroinflammation in APP/PS1 mice. Further investigation of neuroinflammatory influences on gamma frequency oscillations in APP/PS1 mice, showed that the inhibitory effect of TNFα and IL-1β on the normal growth of gamma frequency oscillations, previously observed in normal, healthy mice, was not observed in APP/PS1 mice. Although this finding is not intuitive, the data are suggestive of further gamma frequency oscillation disruption in these mice.

Overall, microglia and pro-inflammatory cytokines and chemokines were shown to cause significant alterations to gamma frequency oscillations in brain slices from both healthy control mice and APP/PS1 mice. Delineating the disruptive and beneficial aspects of these alterations will be essential if anti-inflammatory approaches to Alzheimer's disease move towards clinical trials. Therefore, further investigation of neuroinflammatory influences on gamma frequency oscillations is required.

Acknowledgements

I would like to thank my supervisors Prof. Colm Cunningham and Prof. Mark Cunningham. I have learned so much about how to approach scientific research, both experimentally and conceptually. Their shared commitment to research, and to creating a supportive environment in which to do research, has made my experience enjoyable and enriching.

I would also like to thank the members of both Colm and Mark's labs. From Colm's lab, I would like to thank Dr Pierre-Louis Hollier, Dr Paul Denver and Chiara Di Santo for their practical help and advice. They have been a pleasure to work with. Thanks also to former members Dr Arshed Nazmi, Dr Dáire Healy, Louise Riggs-Miller and Dr Sadia Islam for their help when I started in the lab. From Mark's lab, I would like to thank Dr Kate Connor for her advice and encouragement – a conversation with Kate is always very helpful. Thanks too to Dr Vincent Healy, Evgenii Liubishkin and Austin Lacey. I would also like to thank Dr Carol Murray from Physiology for her encouragement and help, especially for introducing me to the behaviour experiments.

I would like to thank the undergraduate and Master's students who worked with me on different elements of this research: Ross Oglesby, Jack Fenton, Rebecca Maher (M.Sc.), Meghan O'Gorman, Rebecca Lynch (M.Sc.), Eoin O'Connor (Laidlaw Scholar), and Seán Hanratty.

I would like to thank those who provided technical expertise for various methods: Dr Barry Moran and Aoife O'Rourke for their assistance in the cell sorting experiments, Dr Daniel Ruiz-Perez for his assistance in developing the method to monitor the oestrous cycle in mice, and Dr Gavin McManus for his is assistance in microscopy. Their expertise in these techniques was invaluable.

Thank you to Prof. Tomás Ryan and Prof. Lydia Lynch for sitting on my thesis committee. Thanks also to Prof. Derek Nolan for his help and guidance throughout my undergraduate

degree. I would also like to thank Dr Clara Ortega de San Luis who has been a constant support since my undergraduate research project.

Thank you to my friends in both TBSI and the Watts building. Especially, Erika Stewart who has been a great friend since day one.

Lastly, I would like to thank my family, especially my parents.

This PhD was funded by the John Scott studentship.

Contents

Index of Figures and Tables

Figures Index

Tables Index

Abbreviations

aCSF	Artificial cerebrospinal fluid
AD	Alzheimer's disease
AMPA(R)	α-amino-3-hydroxy-5-methyl-4-isoxazolepropionic acid (receptor)
ApoE	Apolipoprotein E
APP	Amyloid-beta protein precursor
ATP	Adenosine triphosphate
AUC	Area under the curve
Aβ40/42	40/42-residue form of amyloid-beta
BDNF	Brain-derived neurotrophic factor
CA	Cornus Ammonis
CCL	Chemokine (C-C motif) ligand
cDNA	Copy deoxyribonucleic acid
CNQX	6-cyano-7-nitroquinoxaline-2,3-dione
CNS	Central nervous system
CSF(1R)	Colony stimulating factor (1 receptor)
CXCL	Chemokine (C-X-C motif) ligand
DAB	Diaminobenzene
DAM	Disease-associated microglia
DAMPs	Danger-associated molecular patterns
D-APV	D-2-amino-5-phosphonovalerate
DG	Dentate gyrus
DNA	Deoxyribonucleic acid
EEG	Electroencephalogram
EOAD	Early onset Alzheimer's disease
FACS	Fluorescence-activated cell sorting
FFT	Fast Fourier transform
GABA(R)	Gamma aminobutyric acid (receptor)
GAT3	GABA transporter type 3
GFAP	Glial fibrillary acidic protein

GLAST1	Glutamate aspartate transporter 1
GWAS	Genome-wide association study
HBSS	Hank's buffered saline solution
HCN	Hyperpolarization-activated cyclic nucleotide
Iba1	Ionized calcium binding adaptor molecule 1
IFN-γ	Interferon gamma
IIN	Inhibitory interneuron
IL-1β	Interleukin 1 beta
IL-6	Interleukin 6
IL-34	Interleukin 34
ING	Interneuron network gamma frequency oscillations
iNOS	Inducible nitric oxide synthase
IQR	Interquartile range
LFP	Local field potential
LIF	Leukaemia inhibitory factor
LPS	Lipopolysaccharide
LTP	Long-term potentiation
MACS	Magnetic-activated cell sorting
MEG	Magnetoencephalography
MCI	Mild cognitive impairment
MWM	Morris water maze
NADPH	Nicotinamide adenine dinucleotide phosphate
NBQX	6-nitro-7-sulphamoylbenzo(f)quinoxaline-2,3-dione
NF-κB	Nuclear factor kappa B
NGS	Normal goat serum
NMDA(R)	N-methyl-D-aspartate (receptor)
NO	Nitric oxide
PAMPs	Pathogen-associated molecular patterns
PC	Pyramidal cell
PFA	Paraformaldehyde
PGE2	Prostaglandin E2
PING	Pyramidal-interneuron network gamma frequency oscillations

PNN	Perineuronal nets
PRRs	Pathogen recognition receptors
PS1/2	Presenilin 1/2
PVBC	Parvalbumin basket cell
qPCR	Quantitative polymerase chain reaction
RNA	Ribonucleic acid
RM	Repeated measures
ROS	Reactive oxygen species
SEM	Standard error of the mean
TLR	Toll-like receptor
TNFα	Tumour necrosis factor alpha
TREM2	Triggering receptor expressed on myeloid cells 2
TBS(-T)	Trizma-buffered saline (with Tween)
WT	Wildtype

Chapter 1

Introduction

1.1. Introduction

This thesis aims to answer the specific question: how does the immune system affect neuronal network activity in Alzheimer's disease? There are three topics which must be discussed in order to give context to this question. These three topics are: neuronal network activity, the immune system, and Alzheimer's disease. The research question addressed in this thesis – how does the immune affect neuronal network activity in Alzheimer's disease – is at the intersection of these three topics. In order to fully contextualise the central research question of this thesis the overlap between these three topics must also be discussed. These overlaps are: neuroimmune interactions, neuroinflammation in Alzheimer's disease, and neuronal activity in Alzheimer's disease. Figure 1.1. is a schematic representation of these three topics and the manner in which they intersect one another.

Neuronal activity will be introduced first, with a focus on neuronal oscillations. Following this the immune system will be introduced, with a focus on central nervous system (CNS) immunity. After introducing these two main topics the overlap between these topics will be introduced, namely neuroimmune interactions. This will be followed by an overview of Alzheimer's disease. The interactions between Alzheimer's disease and the other main topics will then be addressed. Specifically, the overlap between the immune system and Alzheimer's disease (neuroinflammation in Alzheimer's disease) and the overlap between neuronal activity and Alzheimer's disease will be introduced.

It is hoped that clear discussion and definition of these topics, and of their interactions, will provide an introduction which gives context to the research question posed above. The research question of this thesis occupies the central section of the Venn diagram in Figure 1.1. This topic – immune effects on neuronal activity in Alzheimer's disease – will be introduced last, and will be the main focus of this thesis.

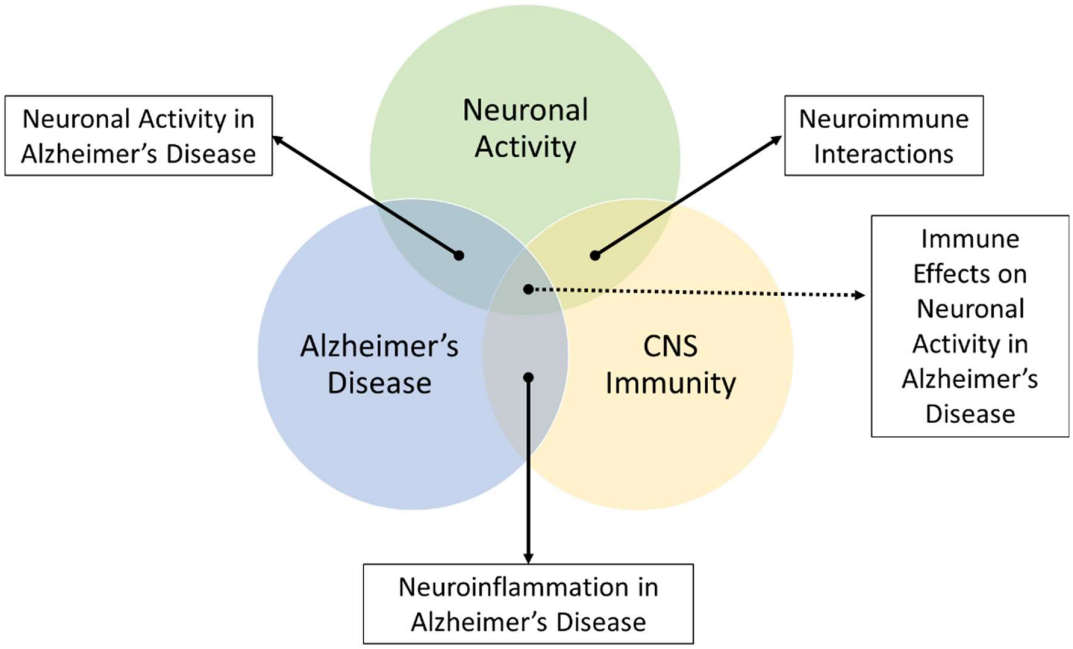

Figure 1.1. Schematic representation of the central research question of this thesis and the topics which it intersects.

1.2. Neuronal activity

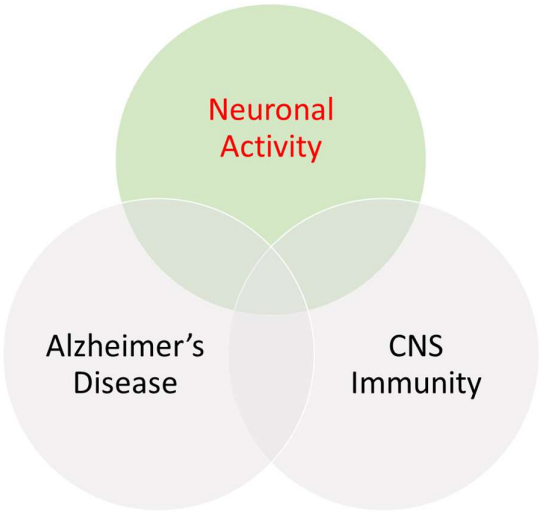

Figure 1.2. Neuronal activity – the focus of this section – and its relation to other topics in this thesis.

The human brain "constructs our perceptions of the external world, fixes our attention, and controls the machinery of our actions" (Kandel et al., 2000). The brain generates all our behaviours; the unconscious control of our breathing, the movement of our fingers, our emotional reaction to our environment – all of these behaviours are orchestrated by the brain. The brain is a complex network of highly interconnected, specialised cells called neurons. Morphologically, neurons consist of a soma (or cell body), which contains the nucleus of the cell. Attached to the soma are long, fibrillar structures which are called dendrites and axons. The ends of these projections are called synapses. Neurons form highly interconnected networks via contacts with one another through their synapses. The number of neurons in the brain and the scale of their interconnectivity are staggering. There are estimated to be 86 billion neurons in the average human brain (Herculano-Houzel, 2009). The number of connections between these neurons (via synapses) is difficult to quantify, but is thought to be in the trillions (Tang et al., 2001).

In addition to being morphologically distinct from other cells of the body, neurons are also functionally distinct. Neurons are capable of generating and transmitting electrical charge. While not unique in their ability to generate electrical charge, the extent to which neurons are electrically active is notable. Electrical charge in neurons arises from the controlled movement of charged particles (ions) across neurons' cellular membrane. The ions responsible for generating electrical charge in neurons are potassium (K^+), sodium (Na^+), calcium (Ca^{2+}), and chloride (Cl^-). Neurons use energy to establish a gradient of these ions across their membranes. Establishing a gradient of ions creates a disequilibrium of both charge and ion concentration. The displacement of ions from an equal distribution across the membrane causes the membrane to have electrical potential. This electrical potential is the basis of neuronal communication via electrical signals.

In a resting state most neuronal membranes have a negative membrane potential that ranges from -80 mV to -65 mV (Abdul Kadir et al., 2018). This means the exterior of the neuronal membrane is more positively charged than the interior of the membrane. This imbalance is caused by the sodium-potassium pump which pumps three Na^+ ions out of the neuron and allows two K^+ ions into the neuron and by potassium leak channels which allow K^+ ions to leave the neuron. This establishes a disequilibrium (or polarisation) in which the outside of the neuron is more positively charged than the inside of the neuron. Changes in membrane potential are the basis of neuronal communication. The membrane potential can become more positive (depolarisation) or more negative (hyperpolarisation)(Figure 1.3). Chemicals called neurotransmitters cause changes in the membrane potential by interacting with ion channels in the neuronal membrane. Generally, neurotransmitters are released by neurons. Depending on the ion channel affected by the neurotransmitter, the membrane potential is increased or reduced.

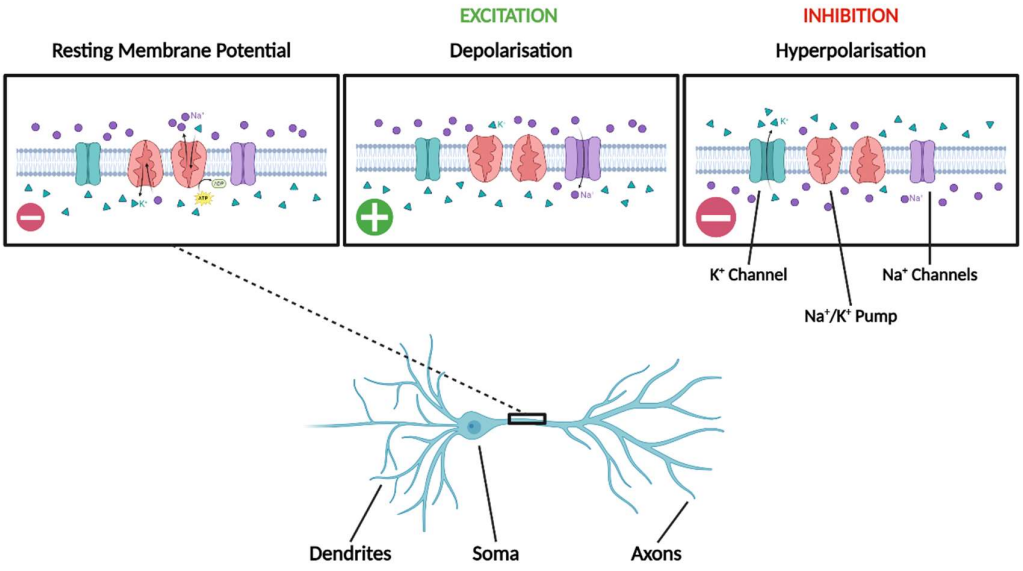

Figure 1.3. Schematic representation of the neuron and molecular basis of electrical charge at the neuronal membrane during resting state, excitation, and inhibition. Purple circles: Na^+ ions, green triangles: K^+ ions. Figure created using BioRender.

The primary neurotransmitters of the brain are glutamate and gamma aminobutyric acid (GABA). Glutamate is an excitatory neurotransmitter which causes certain ion channels, including N-methyl-D-aspartate (NMDA) receptors, α-amino-3-hydroxy-5-methyl-4-isoxazolepropionic acid (AMPA) receptors, and kainate receptors, to open and allow positively charged ions to flow into the neuron. This depolarises, and excites, the neuron. GABA causes ion channels called GABA receptors to open and allow Cl^- ions into the neuron. This hyperpolarises, and inhibits, the neuron. The balance of inhibitory and excitatory inputs a neuron receives determines the neuron's output. When neurons are sufficiently excited, such that the membrane potential increases above -55 mV, an action potential is triggered. Action potentials are rapid, transitory, depolarisations which spread along neurons. Neurotransmitter release is stimulated when action potentials reach the synapse (the connection between neurons). In this manner neurons receive inputs from other neurons via

chemical neurotransmitters which cause changes in the electrical activity of the neuron. This electrochemical communication forms the basis of communication in the brain.

A collection of neurons, connected to one another via synapses, is referred to as a neuronal network. The sum of the activity of the neurons which make up the neuronal network constitutes the network activity. Neuronal networks are responsible for performing a certain computation or generating a certain behaviour. Neuronal networks which share similar functions are organised into larger networks and systems. As a result, certain regions of the brain are associated with certain functions. For example, the hippocampus is critical in memory and learning, while the Broca areas in the frontal lobe are involved in language processing. Therefore, the brain is highly spatially organised from synapses to brain regions. Organisation across physical space is a universal and familiar concept in biology. An idea which is perhaps less familiar however, is organisation across time.

The electrical activity of the brain is generated by billions of neurons. This electrical activity is the sum of ongoing, brief changes in the membrane potential of neurons. How is this activity, which is spread out across time, consolidated? How is the activity of many neurons integrated to give a unified representation of the environment or to support consciousness as "an ongoing, coherent experience" (Kandel et al., 2000)? These questions are central to the so-called "binding problem"; that is: how are the diverse features of an experience unified across a population of neurons into a singular whole (Engel et al., 1992; Gray, 1994; Roskies, 1999)? It has been proposed, in response to this question, that the brain generates synchronous activity which provides a temporal framework upon which dispersed neuronal activity can be organised across time. These synchronous activities are referred to as neuronal oscillations.

1.2.1. Neuronal oscillations

Neuronal oscillations are repetitive electrical activities which occur at a range of frequencies in the brain. The frequencies at which they occur stretch from less than one hertz (i.e. one oscillation per

second) to several thousand hertz (Bullock, 1997; Buzsáki & Draguhn, 2004). This range of frequencies is broken into several frequency bands. Table 1.1 shows these different frequency bands and the frequencies which define each band (Buzsáki & Draguhn, 2004).

Frequency Band Name	Frequency Range
Delta	1.5-4 Hz
Theta	4-10 Hz
Alpha	8-12 Hz
Beta	10-20 Hz
Gamma	20-80 Hz

Table 1.1 Neuronal oscillations frequency bands.

It has been proposed that the synchronous nature of neuronal oscillations provides the brain with a temporal framework in which neuronal activity can occur. That is to say, neuronal oscillations have been proposed as a solution to the "binding problem". For example, in the visual cortex gamma frequency oscillations have been proposed as the means by which various perceived features are combined to give rise to unified perception. The activities of multiple neuronal networks – which are responsible for generating various features of visual perception (colour, shape, opacity etc.) – are coordinated by ongoing, rhythmic gamma frequency oscillations (Eckhorn et al., 1988; Singer & Gray, 1995). Furthermore, in the hippocampus place cells (which encode location-specific information) fire only in specific locations and only at specific phases of ongoing theta frequency oscillations (O'Keefe & Recce, 1993). These examples illustrate the proposed role for neuronal oscillations in which the activity of individual neurons is temporally situated relative to the activity of other individual neurons, via ongoing synchronous network activity. A useful oversimplification

is to compare neuronal oscillations to a metronome or conductor keeping time for the individual members of an orchestra; a pulse onto which activity is superimposed.

Neuronal activities occur across a range of frequencies in the brain. These different frequency oscillations coexist; they compete with and modulate one another. This is referred to as cross-frequency coupling. For example, the amplitude of neuronal oscillations in the gamma frequency band vary as a function of oscillations in the theta frequency band (Bragin et al., 1995). Gamma frequency oscillations are therefore referred to as being nested within the theta frequency oscillation. Oscillations in the gamma band can also be modulated by slow/delta frequency oscillations (Sirota et al., 2003). These interactions between the timekeeping rhythms of the brain have been proposed as means to encode and retrieve information on multiple time scales (Buzsáki & Wang, 2012; Jensen & Colgin, 2007).

The neuronal oscillations which are the central focus of this thesis are those which occur in the gamma frequency range. Oscillations in this frequency range (20-80 Hz), were first observed via electroencephalography (EEG) in the 1930s by Jasper and Andrews. They noted a "rhythm of 40 to 50 per second" during voluntary muscle contraction (Jasper & Andrews, 1938), however the function and mechanism of this activity were not understood. The study of gamma frequency oscillations increased during the 1980s, led by Freeman and his colleagues. They studied the role of gamma frequency oscillations in olfaction (Bressler & Freeman, 1980). Other important work was led by Gray and Singer, who studied gamma frequency oscillations in visual processing (Gray et al., 1989). Further research performed throughout the 1990s showed that gamma frequency oscillations are almost universally present in higher order cognitive processes. Gamma frequency oscillations have been observed during selective attention (Tiitinen et al., 1993), associative learning (Miltner et al., 1999), language processing (Pulvermüller et al., 1995), short term memory (Siegel et al., 2009), dreaming (Llinas & Ribary, 1993), and in response to auditory stimuli (Pantev et al., 1991). These findings resulted in the emergence of a consensus which considers gamma frequency oscillation

generation an essential process in the neuronal computation of cognitive processes. The rhythmic nature of these oscillations is thought to facilitate the communication and coordination of individual neurons. This has been termed communication by coherence (Fries, 2009).

Disruptions in gamma frequency oscillations have been observed in a number of pathological situations – this is not surprising given the involvement of these oscillations in a wide range of neuronal processes. Disrupted gamma frequency oscillations have been observed in neurodevelopmental disorders such as autism spectrum disorder, fragile X syndrome (Ethridge et al., 2016), and schizophrenia (recently reviewed by Sohal (Sohal, 2022)). Aberrant gamma frequency oscillations have also been observed in neurodegenerative diseases such as Parkinson's disease (Guerra et al., 2022; Lofredi et al., 2018) and Alzheimer's disease, as will be discussed in detail later. Additionally, disrupted gamma frequency oscillations have been proposed as biomarker of major depression (Fitzgerald & Watson, 2018). Therefore, it is clear that diseases and disorders which are clinically characterised by cognitive deficits are often associated with disrupted gamma frequency oscillations. This further supports the view that gamma frequency oscillations are essential for normal neuronal processing.

Much of the work described above was carried out by EEG in humans and various animals. This work showed the functional importance and universality of gamma frequency oscillations; however, this work did not lead to a mechanistic understanding of gamma frequency oscillations. Clearer mechanistic understanding came via *ex vivo* brain slice studies. *Ex vivo* brain slices are thin sections of the brain that are maintained in conditions which ensure their viability. The electrical activity of these sections can be studied by inserting an electrode which records the electrical potential in the region close to the electrode. This electrical potential is referred to as the local field potential (LFP). The LFP is the sum of changes in the membrane potentials of neurons proximal to the recording site. Herreras provides a comprehensive overview on the source of this signal (Herreras, 2016). The neuronal networks generating the recorded LFP can be studied by pharmacological or genetic

manipulations of the brain slice. Given the well understood architecture of neuronal circuitry in the hippocampus, many of these studies have been made in brain slices from the rodent hippocampus. This deviates from most of the EEG studies previously mentioned, which were carried out via scalp recordings in humans, meaning the signal recorded is generated by neuronal networks in the cortex. Despite this difference, *ex vivo* studies in rodent brain slices have provided universal mechanistic insights which could not have been gained from EEG studies in humans. For example, work carried out in *ex vivo* brain slices has led to an understanding of the networks and neurotransmission which generate gamma frequency oscillations (Cardin et al., 2009; Sohal et al., 2009; Whittington et al., 1995).

In order to study gamma frequency oscillations in brain slices, it is necessary to be able to induce this activity in a brain slice. Gamma frequency oscillations can occur spontaneously in tissue. However, these oscillations are more commonly induced by the application of certain receptor agonists or by altering the ionic milieu of the slice; this activates the relevant neuronal networks in the brain slice. Additionally, gamma frequency oscillations can be induced by brief tetanic stimulation of the tissue (Traub et al., 2004). Kainate and carbachol are the most commonly used receptor agonists to induce gamma frequency oscillations in hippocampal brain slices (Fisahn et al., 1998). The neuronal network which is activated by these compounds is a highly interconnected network of inhibitory interneurons; this network will now be discussed, followed by a discussion of the proposed mechanisms of action for gamma frequency oscillations.

1.2.2. Parvalbumin inhibitory interneurons

Inhibitory interneurons communicate via GABA. Their output is inhibitory – that is to say, they reduce the probability of action potential generation in post-synaptic neurons. There are many subsets of inhibitory interneurons, often defined by proteins that the interneurons express. The

specific subset of inhibitory interneurons that have been shown to be essential in the generation of gamma frequency oscillations are parvalbumin inhibitory interneurons. Parvalbumin inhibitory interneurons are present in both the cortex and the hippocampus (Celio, 1986; Kosaka tet al., 1987). These neurons form a highly interconnected network which allows them to generate synchronous waves of inhibition that cause the activity of excitatory pyramidal to also become synchronous. The importance of inhibition generated by inhibitory interneurons as means of "phase-locking large numbers of principal [excitatory] cells" was recognised in *ex vivo* brain slice recordings, however the specific subset of interneuron involved was not known (Buhl et al., 1994; Fisahn et al., 1998; Whittington et al., 1995). In parallel to this *ex vivo* brain slice work, *in silico* simulations of neuronal networks confirmed that inhibitory interneurons were capable of entraining synchronous activity in pyramidal cells (Lytton & Sejnowski, 1991).

Parvalbumin inhibitory interneurons were seen as possibly responsible for entraining gamma frequency oscillations due to their ability to generate activity continuously in a fast-spiking pattern (Kawaguchi et al., 1987). Additionally, parvalbumin inhibitory interneurons were known to be highly interconnected via electrical gap junctions (direct contacts between neurons that allow electrical current to spread)(Tamás et al., 2000). Parvalbumin inhibitory interneurons were confirmed as the primary subtype of interneurons involved in the generation of gamma frequency oscillations by genetic manipulations and by optogenetic studies. The genetic ablation of glutamate receptors on parvalbumin interneurons (this essentially knocks-out this network by reducing the excitatory input it receives) causes a reduction in kainate induced gamma frequency oscillations in *ex vivo* brain slices (Fuchs et al., 2007). Two optogenetic studies proved the centrality of parvalbumin inhibitory interneurons in the generation of gamma frequency oscillations. Cardin et al. showed that using optogenetics to depolarise parvalbumin inhibitory interneurons labelled with channelrhodopsin-2 induced gamma frequency oscillations *in vivo* (Cardin et al., 2009). Concurrently, Sohal et al. showed that using optogenetics to hyperpolarise parvalbumin inhibitory

interneurons labelled with a halorhodopsin suppressed gamma frequency oscillations *in vivo* (Sohal et al., 2009). These studies confirmed that parvalbumin inhibitory interneurons are necessary and sufficient for the generation of gamma frequency oscillations.

A second subset of inhibitory interneurons, called somatostatin interneurons, are also viewed as important, but not critically necessary, in the generation of gamma frequency oscillations, in addition to parvalbumin interneurons (Antonoudiou et al., 2020; Veit et al., 2017). Somatostatin interneurons generally project onto the dendritic portion of pyramidal cells, rather than the perisomatic region, which is where parvalbumin interneurons project (Müller & Remy, 2014). Although, the involvement of somatostatin interneurons in gamma frequency oscillations is a relatively recent discovery, the emerging view appears to be that this subset of interneurons is important in modulating gamma frequency oscillations and coordinating the coherence of these oscillations across brain regions (Espinosa et al., 2019; Veit et al., 2017). Parvalbumin interneurons are still viewed as the subset of interneurons primarily involved in the generation of gamma frequency oscillations. Specific features of these interneurons, which enable them to carry out this function, will now be discussed.

A maxim of biology is form follows function; parvalbumin interneurons are not exempt from this rule. The morphological, cellular and molecular characteristics of these interneurons support their physiological function, which is to provide high-frequency inhibitory output to a wide range of targets (Figure 1.4).

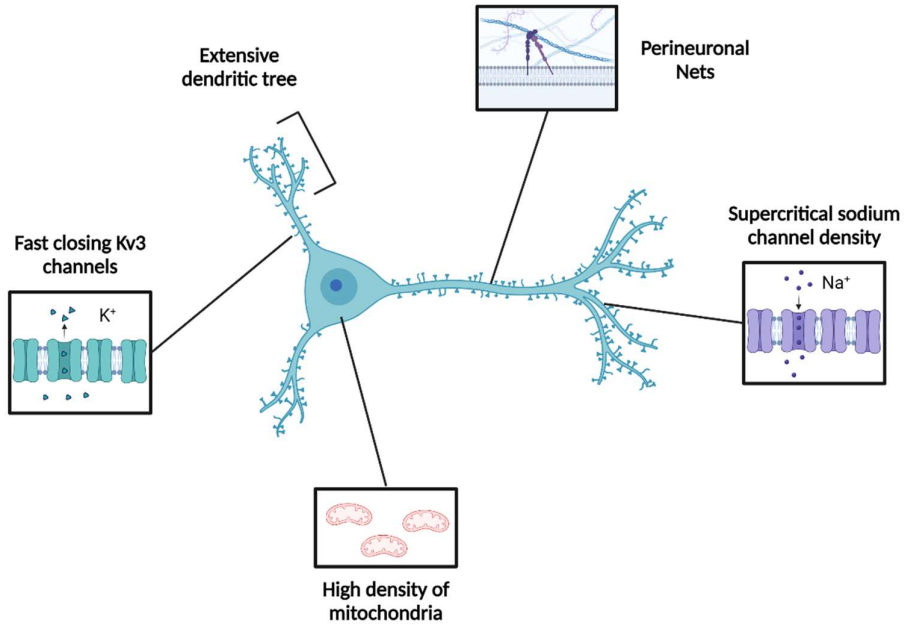

Figure 1.4. Schematic representation of structural and molecular adaptations in parvalbumin interneurons. Figure created using BioRender.

Parvalbumin interneurons have extensive dendritic trees. In the hippocampus, their dendrites run radially from the soma and cross all the layers of this laminar region. The dendrites are aspiny and are tightly packed with mitochondria (Gulyás et al., 1999). This dendritic tree receives an enormous amount of innervation. Estimates of the total number of synapses which converge on a single parvalbumin interneuron range from 16,000 to 35,000. The vast majority of these inputs are excitatory (Gulyás et al., 1999; Tukker et al., 2013). The large dendritic tree of parvalbumin interneurons allows these cells to receive widely convergent input from a large number of neurons, in effect allowing them to sample the network activity. A distinct feature of the parvalbumin interneuron dendritic tree is the extent to which dendrites are highly interconnected by gap junctions. In the cat visual cortex, a single parvalbumin interneuron was found to have on average 60 gap junctions with other cells. This formed a network of serially interconnected cells that could

be “traced laterally in a boundless manner” (Fukuda et al., 2006). The parvalbumin interneuron dendritic tree can therefore be said to be large, interconnected and diversely innervated.

The inhibitory output of parvalbumin interneurons is mediated via their heterogeneous axonal structures. Parvalbumin interneurons are broken into subgroups based on their post-synaptic axonal projections. These subgroups are basket cells, axo-axonic cells, and bistratified cells. Axo-axonic cells project onto the axon initial segment of pyramidal cells, basket cells project onto the perisomatic region of pyramidal cells and bistratified cells project onto distal dendrites. The most common of these groups is parvalbumin basket cells (PVBC), as a result this group is the most widely studied (Bezaire & Soltesz, 2013). PVBC have a roughly circular axonal arborisation which is approximately 45 mm in total length. It is estimated that each PVBC innervates between 1,500 and 2,000 pyramidal cells. The perisomatic inhibition of pyramidal neurons by PVBC is critical in the generation of gamma frequency oscillations. PVBC also project onto other parvalbumin interneurons with equal probability, further connecting the interneuron network (Sik et al., 1995). For a comprehensive review on the differences between these populations see Booker and Vida (Booker & Vida, 2018). This summary shows that the morphological features of parvalbumin interneurons are optimised to receive diverse input and generate inhibitory output to a range of locations.

Parvalbumin interneurons are also known as fast spiking interneurons; this is due to their high firing rate. An early study of these interneurons found that they had a spontaneous firing rate of 20-80 Hz, that is, within the gamma frequency range. Their spikes are narrow, 0.8 msec on average, and display a deep, fast after-hyperpolarisation which lasted several milliseconds (Kawaguchi et al., 1987; Schwartzkroin & Mathers, 1978). This ability to generate “rapid, even trains of spikes” enables parvalbumin interneurons to generate continuous inhibitory output to their diverse targets (Schwartzkroin & Mathers, 1978). The cellular and molecular characteristics of these interneurons support this function.

As can be surmised, the generation of such high levels of activity is energetically demanding. Generating action potentials is energetically expensive. The Na+/K+ ATPase ion pump is the main consumer of adenosine triphosphate (ATP) in neurons (Astrup et al., 1981). Given parvalbumin interneurons fire at the rates described above, it can be deduced that the Na+/K+ ATPase pump is highly active in these cells. This high energetic demand is met by an abundance of mitochondria. Staining for cytochrome C, an electron carrier in the electron transport chain localised to the mitochondria, reveals that parvalbumin interneurons have more mitochondria than both other interneuron populations and pyramidal cells (Gulyás et al., 2006).

Perineuronal nets (PNN) also support parvalbumin inhibitory interneuron's high spiking rate. PNN are a type of extracellular matrix which form around neurons, predominantly around fast-spiking interneurons. PNN are heterogeneous structures made up of proteoglycans. The components of these nets are released by neurons and glia in response to neuronal activity. They can also be modified by proteinases. For a comprehensive review on PNN see Testa et al. (Testa et al., 2019). A variety of features of PNN play a role in supporting the high spiking rates seen in parvalbumin interneurons. One such feature is their polyanionic nature. By creating a highly negatively charged microenvironment immediately adjacent to the parvalbumin interneurons membrane, PNN contribute to ion sorting. Specifically, they create an inwardly directed force for chloride ions and an outwardly directed force for potassium ions. This increases the resting membrane potential in a manner that does not require energy from the parvalbumin interneuron itself (Morawski et al., 2015). In addition to altering excitability and so aiding high spiking rates, PNN also have a protective function. It has been shown that PNN protect parvalbumin interneurons against oxidative stress (Cabungcal et al., 2013). This feature is particularly relevant in this population of interneurons given their reliance on oxidative metabolism, as discussed. This extracellular feature of parvalbumin interneurons both alters their ability to undergo fast spiking rates and protects them from the waste products generated in the maintenance of these fast-spiking rates.

In addition to cellular specialisations, parvalbumin interneurons are also molecularly tailored to support high rates of activity. The expression of certain ion channels in parvalbumin interneurons enable them to sustain their high spiking rates. Firstly, the axons of parvalbumin interneurons express a supercritical density of sodium channels (generally Nav1.1 type channels)(Ogiwara et al., 2007). This excess density of sodium channels increases the speed with which action potentials can propagate. Indeed, action potential propagation has been reported to occur at a velocity of 0.5 ms^{-1} in parvalbumin interneurons (H. Hu & Jonas, 2014). This is quick when compared to other action potential propagation velocities, for example the velocity in granule cells in the dentate gyrus has been reported as 0.24 $msec^{-1}$ (Schmidt-Hieber et al., 2008). The second molecular adaptation in parvalbumin interneurons also relates to sodium channels. Dendritic expression of voltage-gated sodium channels is low in these interneurons. This reduces the propensity for backpropagation of action potentials from the soma into the dendrites (H. Hu et al., 2010). Given the high activity levels of parvalbumin interneurons, backpropagation could result in an endless positive feedforward loop. This adaptation evades a risk associated with almost continuous activity in a neuron. The dendrites of these interneurons mostly express potassium channels; this is the source of the third molecular adaptation discussed here. Specifically, the potassium channel most expressed in parvalbumin interneurons is the voltage gated Kv3 type. Kv3 type potassium channels close with deactivation rates approximately ten times faster than other voltage-gated potassium channels (Kaczmarek & Zhang, 2017). The result of this increased deactivation speed is a reduction in the refractory period that follows an action potential.

It is clear that parvalbumin inhibitory interneurons are exquisitely optimised, both structurally and molecularly, to generate and maintain high frequency oscillations in the gamma frequency range. These adaptations are summarised in Figure 1.4. They are highly-interconnected and capable of generating and maintaining high frequency inhibition. These features are critical to the generation of gamma frequency oscillations, the proposed mechanisms of which will now be discussed.

1.2.3. Mechanisms of gamma frequency oscillation generation

There are two proposed mechanisms for the generation of gamma frequency oscillations. These are the interneuron network gamma frequency oscillations (ING) model and the pyramidal-interneuron network gamma frequency oscillations (PING) model. Figure 1.5 is a schematic representation of these two models. The inhibitory interneuron network discussed above is involved in both mechanisms. It is not clear which model best represents the *in vivo* generation of gamma frequency oscillations (Tiesinga & Sejnowski, 2009). There is some suggestion that these models may in fact compete *in vivo* (Viriyopase et al., 2016). Nevertheless, the ability to generate gamma frequency oscillations by both mechanisms, in *ex vivo* brain slices, is a useful experimental tool.

Per the PING model, the activation of both the inhibitory interneuron network and of pyramidal cells, which mutually project onto one another, is required to generate gamma frequency oscillations. This mechanism of gamma frequency oscillation induction is how gamma frequency oscillations are induced by kainate and carbachol in *ex vivo* brain slices. In this model, pyramidal cells excite the inhibitory interneuron network. Due to the highly interconnected nature of the inhibitory interneuron network, the activity across this network becomes synchronised. As a result the inhibitory output of the network becomes rhythmic and entrains oscillatory activity in the pyramidal cells. In this model of gamma frequency oscillation generation, the oscillation arises from the mutual interaction between pyramidal cells and a network of inhibitory interneurons. As mentioned, carbachol and kainate induce gamma frequency oscillations via this mechanism; however, they do so with slight differences. Kainate depolarises pyramidal cells by binding to kainate receptors, which triggers an influx of sodium and potassium ions; this collapses the membrane potential (Robinson & Deadwyler, 1981). The excitatory output of pyramidal cells, in the form of glutamate, projects onto and activates the inhibitory interneuron network (Kuramoto et al., 2022). In addition to this activation, kainate binds to kainate receptors on interneurons and produces "a massive and sustained

excitation" of the interneurons. This results in a large inhibitory output which projects mostly onto the perisomatic region of excitatory pyramidal cells (Cossart et al., 1998). This rhythmic output, which occurs in the gamma frequency range due to the natural firing rate of parvalbumin interneurons, entrains an oscillation in the activity of the pyramidal cells.

Carbachol acts via a similar mechanism. However, the neurotransmission which underlies kainate-induced gamma frequency oscillations is glutamatergic – that is based on the transmission of glutamate – while the neurotransmission which underlies carbachol-induced gamma frequency oscillations in cholinergic – that is based on the transmission of acetylcholine. Carbachol binds to muscarinic and nicotinic receptors on pyramidal cells, which causes the depolarisation of these neurons (Cole & Nicoll, 1984). Activation of the pyramidal cells by carbachol results in the activation of the inhibitory interneuron network. As with kainate-induced gamma frequency oscillations, the rhythmic inhibitory output of the interneuron network entrains oscillatory activity in the pyramidal cells (Ma & Patel, 2022). Carbachol-induced gamma frequency oscillations in *ex vivo* brain slices are abolished by the pharmacological blockade of $GABA_A$ receptors (with bicuculline methochloride) and by the blockade of non-NMDA-glutamate receptors (with the AMPA receptor antagonist 6-nitro-7-sulphamoylbenzo(f)quinoxaline-2,3-dione (NBQX))(Fisahn et al., 1998). Similarly, kainate-induced gamma frequency oscillations are abolished by the pharmacological blockade of $GABA_A$ receptors (with bicuculline) and by the blockade of glutamate receptors (with the AMPA and kainate receptors antagonist 6-cyano-7-nitroquinoxaline-2,3-dione (CNQX)) (Khazipov & Holmes, 2003). This confirms the involvement of both inhibitory transmission, via $GABA_A$ receptors on pyramidal cells, and of excitatory transmission, via NMDA and AMPA receptors on interneurons, in both kainate- and carbachol-induced gamma frequency oscillations.

Per the ING model, the activation of the inhibitory interneuron network alone is sufficient to induce gamma frequency oscillations. As with the PING model, activation of the highly interconnected

network of inhibitory interneurons leads to synchronous activity which entrains the gamma frequency oscillation. Unlike the PING model, in the ING model pyramidal cells are not activated, nor do they activate the inhibitory interneuron network (Whittington et al., 2000). This mechanism of gamma frequency oscillation generation is at the basis of gamma frequency oscillations induced by tetanic stimulation of the brain slice. Oscillations induced in this manner were impervious to blockade of ionotropic glutamate receptors using D-2-amino-5-phosphonovalerate (D-APV) and CNQX, but they were abolished by the blockade of $GABA_A$ receptors by bicuculline (Whittington et al., 1995). This suggests that the oscillation is based on inhibitory neurotransmission generated by the inhibitory interneuron network – hence it was abolished by blocked GABAergic transmission. It also suggests that glutamatergic transmission from pyramidal cells to inhibitory interneurons via ionotropic glutamate receptors is not required to generate the oscillation – hence it is not affected by blockade of ionotropic glutamate receptors. This differs from the PING mechanism, which does involve ionotropic glutamatergic transmission. Further evidence for this model comes from optogenetic studies which show the light-induced activation of channelrhodopsin-2 labelled inhibitory interneurons was sufficient to induce gamma frequency oscillations (Cardin et al., 2009), and from computer simulations which have also shown that activation of the inhibitory interneuron network alone is sufficient to induce gamma frequency oscillations and it is not also necessary to activate pyramidal cells (Traub, Whittington, Colling, et al., 1996, p. 199; Whittington et al., 1995). As mentioned, the model that represents physiological reality is a matter of debate. However, both models attribute a central role to the inhibitory interneuron network, which subsequent research has shown to be predominated by parvalbumin interneurons. Irrespective of which model explains gamma frequency oscillations as they occur *in vivo*, the use of kainate and carbachol to induce gamma frequency oscillations in *ex vivo* brain slices dictates that the gamma frequency oscillations generated here are based on the PING model.

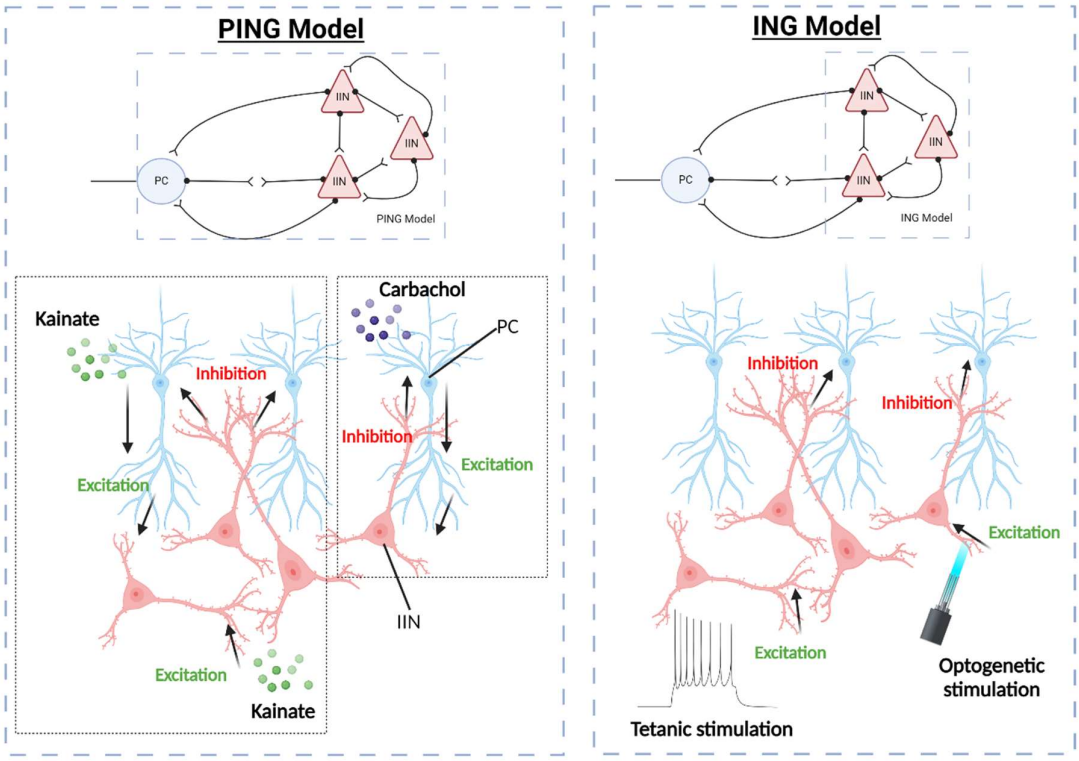

Figure 1.5. Schematic representation of proposed models of gamma frequency oscillation generation. (Left) The PING model, in which both pyramidal cells and inhibitory interneurons generate gamma frequency oscillations. Kainate activates both interneurons and pyramidal cells while carbachol activates just pyramidal cells. (Right) ING model, in which inhibitory interneurons generate gamma frequency oscillations. Optogenetic or tetanic stimulation activation interneurons only. Excitatory pyramidal cells (PC) are represented by a blue circle and inhibitory interneurons (IIN) are represented by red triangles. Figure created using BioRender.

1.3. Central Nervous System Immunity

Until this point, the only cells of the central nervous system which have been discussed are neurons. Clearly, these cells are central to the functioning of the brain. However, these cells are not only the only cells in the brain: among the many cell populations in the brain there are also cells of the immune system. The innate immune system of the CNS is the second main topic of this thesis.

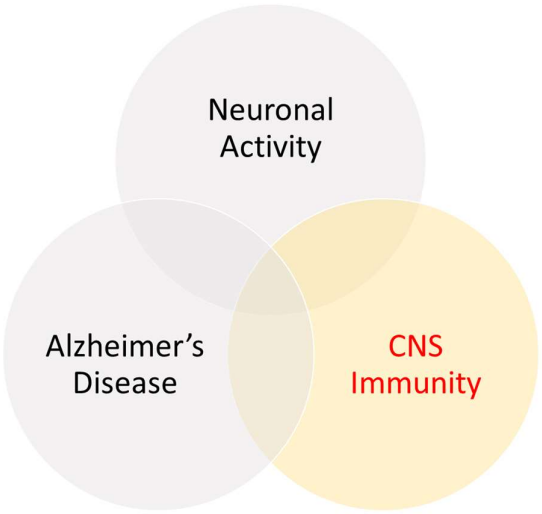

Figure 1.6. CNS immunity – the focus of this section – and its relation to other topics in this thesis.

It is through the immune system that the body responds to disruptions to homeostasis. These disruptions include infection, injury and proliferation of cancerous cells. The immune system has two arms: innate immunity and adaptive immunity. The innate immune system responds to a large array of molecular signals that are indicative of injury or infection in a rapid but relatively nonspecific manner. The adaptive immune system is activated when these molecular signals are particularly severe or chronic. The adaptive immune system mounts a specific immune responses against specific antigens. The adaptive immune system responds to disruptions in a more specific, but slower, manner that requires the activation and proliferation of specific clones of T cells (which kill infected

and cancerous cells, as well as coordinate the inflammatory response) and B cells (which produce antibodies). Through the maintenance of memory T and B cell populations, the adaptive immune system also maintains a memory of the disruptions encountered; this enables it to mount a rapid response should any disruption be reencountered.

The innate immune system identifies disruptions to the tissue via the detection of molecules referred to as pathogen associated molecular patterns (PAMPs) and damage associated molecular patterns (DAMPs). Innate immune cells engulf the source of the PAMPs or DAMPs (for example, a bacterium, a virus-infected cell, or a necrotic cell). This process of engulfment is called phagocytosis. Phagocytosis effectively removes and clears disruptions in the environment. The engulfed body is digested and parts of the digested body may be presented on the surface of the cell to the adaptive immune system. The adaptive immune system mounts a specific response to the source of disruption, as it is presented on the antigen-presenting innate immune cell. Antibodies produced by B cells as part of the adaptive response, increase the rate of phagocytosis by tagging the source of disruption. Antibodies also induce a killing system called complement. The complement system eliminates bodies which have been tagged with antibodies. This response or process described above is termed the inflammatory response or inflammation.

Inflammation is a complicated, controlled process with multiple cell types involved across the entire body. Cells of the immune system communicate throughout the inflammatory response. Immune cells communicate via extracellular molecules called cytokines. Cytokines bind to their receptors and induce a range of changes, for example: cell migration, cell proliferation, and increased phagocytosis. In addition to promoting the inflammatory response, it is also necessary to resolve or terminate the inflammatory response, as without resolution it may become a destructive process. This regulated suppression of inflammation is also mediated by immune cells, again communicating via cytokines and lipid mediators, such as resolvins. Thus, the immune system is a dynamic, complex system

consisting of a range of cell types with specialised functions. The immune system recognises departures from homeostasis and attempts to restore homeostasis via the inflammatory process.

The brain was originally thought to be immune privileged, that is to say it is inaccessible to immune cells (Medawar, 1948). This view has largely been revised. However, the immunity of the brain is correctly still considered to be different to immunity of the periphery. (The term "immune privilege" is still used by some to describe this unique immunity, rather than to describe the absence of immunity (Mapunda et al., 2022)). The parenchyma of the brain is protected from the periphery by several barriers which are collectively known as the blood-brain barrier. This generally prevents immune cells in the periphery from moving into the parenchyma of the brain, however the brain has specialised immune cells which are resident in the parenchyma. For the purposes of this thesis the focus will be on the resident macrophage population of the brain, microglia, and on astrocytes, which can adopt some inflammatory features of immune cells during pathology in the brain.

1.3.1. Microglia

Non-neuronal cells in the brain are referred to as glial cells or glia, this comes from the Latin for glue as they were thought to hold neurons together. The immunity of the brain is predominantly innate, that is to say, it is nonspecific and rapid in its response to disruption. The primary immune cells of the brain are microglia, a brain-resident macrophage population. Microglia account for approximately 5-10% of all cells in the brain (Dos Santos et al., 2020; Korin et al., 2017). Microglia are derived from myeloid progenitors which arise before embryonic day eight and are ontologically distinct from other phagocytes of the immune system (Ginhoux et al., 2010). The morphology of microglia is influenced by their environment. In homeostatic conditions, microglial cells have, as described by Nimmerjahn, "small rod-shaped somata from which numerous thin and highly ramified processes extend symmetrically". The somata of these cells do not migrate through the

tissue. The processes however are highly motile. By cycles of formation and withdrawal of their processes microglial continuously probe their environment (Nimmerjahn et al., 2005). By continually sampling their environment for PAMPs and DAMPs, microglia cells are able to identify disruptions which require a response.

Microglia have genetically predefined receptors which allow them to sense both PAMPs and DAMPs; these are referred to as pathogen recognition receptors (PRRs). Microglia sense various microbial infections via these PRRs. For example, microglia recognise various bacterial products such as lipopolysaccharide (LPS) via Toll-like receptor (TLR) 4 (TLR4) and flagellin via TLR5 (Hayashi et al., 2001; Poltorak et al., 1998). Microglia can also sense viral infections by sensing viral double-stranded ribonucleic acid (RNA) via TLR3 (Town et al., 2006). In addition to sensing infections via PAMPs, microglia sense damaged cells resulting from injury or disease via receptors for DAMPs; examples include, sensing ATP via P2Y12, and damaged nucleic acids via the cGAS-STING signalling pathway (Gulen et al., 2023; Haynes et al., 2006).

Upon binding of their PRRs, microglia undergo phenotypic changes which enable them to respond appropriately to the source of disruption. The nomenclature of these phenotypic changes is a matter of debate. Current consensus appears to favour the term "reactive". In the past pro-inflammatory, M1, and amoeboid have all been used to describe the phenotypic move away from homeostasis. Homeostatic microglia have been described as anti-inflammatory, quiescent, and ramified (Paolicelli et al., 2022). Within the field there is a movement away from viewing microglial phenotypes as discrete dichotomies and instead viewing microglial phenotypes as existing on a multivariate continuum. As put by Waddington, 'cells are residents of a vast 'landscape' of possible states, over which they travel during development and in disease" (Waddington, 1957). The binding of PRRs to their ligands drives rapid changes in gene expression which result in a reactive phenotype that is particular to the stimulus. Reactive phenotypes involve morphological, functional, and molecular changes (Figure 1.7). In response to sensing a source of disruption and becoming reactive, microglia

retract their highly ramified process and generate new protrusions which tend to be more motile. The somata of microglia also become larger in reactive microglia (Stence et al., 2001).

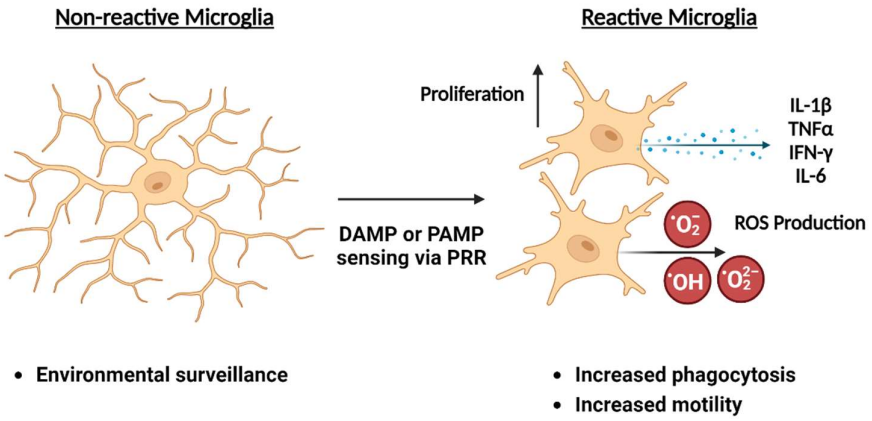

Figure 1.7. Schematic representation of non-reactive and reactive microglia with a selection of the changes observed in reactive microglia. Figure created using BioRender.

In addition to these morphological changes, the function of reactive microglia changes from their homeostatic function, which is one of surveillance. Reactive microglia move their processes towards the source of disruption and attempt to phagocytose these disruptors. For example, this may be a ruptured cell, which have been shown to be phagocytosed by microglia (Davalos et al., 2005; Hughes et al., 2010; Koizumi et al., 2007). These changes are driven by PRRs binding their ligands. For example, the detection of ATP via P2Y12 is required to increase microglial motility, while the detection of uridine diphosphate via P2Y6 is required to increase the phagocytic activity of microglia (Kettenmann, 2007). Reactive microglia also produce cytotoxic factors – these are proteins capable of damaging or killing injured or infected cells. These cytotoxic factors include reactive nitrogen intermediates and superoxide radicals, also known as reactive oxygen species (ROS) (McDonald et al., 1997; Meda et al., 1995).

In various states of reactivity, arising from various types of stimulation, microglia can secrete cytokines, which coordinate and promote the inflammatory response. The principal cytokines produced by reactive microglia are interleukin 1 beta (IL-1β), tumour necrosis factor alpha (TNFα), interferon gamma (IFN-γ), and interleukin 6 (IL-6) (Giulian et al., 1986; Hide et al., 2000; Jekabsone et al., 2006; Kawanokuchi et al., 2006; Suzumura et al., 1996). These cytokines orchestrate the inflammatory response in both microglia themselves (via autocrine signalling) and in other cells (via paracrine signalling). The effects of these cytokines include: increasing microglial proliferation (TNFα, IL-1β, IL-6 (Mander et al., 2006; Streit et al., 2000)), activating astrocytes (TNFα, IL-1β (Liddelow et al., 2017)), induction of apoptosis (TNFα signalling via TNFR1 (Micheau & Tschopp, 2003) and IL-1β via caspase activation (Thornton et al., 2006)), promotion of cell survival (TNFα and IL-1β signalling via nuclear factor kappa B (NF-κB) (Jefferies et al., 2001; Nidai Ozes et al., 1999)), promotion of the antigen presenting ability of microglia (IFN-γ via increased major histocompatibility complex expression (Suzumura et al., 1987)), generation of ROS (IFN- γ, (McDonald et al., 1997)), neuronal support via induction of brain derived neurotrophic factor (BDNF)(IL-6 (Murphy et al., 2000)). This non-exhaustive list shows the diversity of processes which microglia are involved in during the inflammatory response. The battery of cytokines produced by reactive microglia are central drivers of the inflammatory response in the brain.

Microglial homeostasis and survival is maintained via colony stimulating factor 1 receptor (CSF1R) signalling – this is a feature shared with other macrophages in the body (Elmore et al., 2014). CSF1R is a receptor tyrosine kinase which is activated by its ligands: colony stimulating factor 1 (CSF1), and interleukin-34 (IL-34)(H. Lin et al., 2008). CSF1 is produced by microglia, astrocytes, and oligodendrocytes in the CNS, while IL-34 is produced predominantly by neurons (Cahoy et al., 2008). When activated, CSF1R dimerises and sets in a motion a phosphorylation cascade which activates a range of proliferation and survival pathways, including the PI3K/Akt pathway (Kelley et

al., 1999) and the ERK1/2 pathway (Gangoiti et al., 2008; Stanley & Chitu, 2014). Signalling via the CSF1R has been shown to be critical in microglia survival and proliferation. Blocking either or both CSF1 and IL-34 inhibited the development, maintenance, and proliferation of microglia (Easley-Neal et al., 2019). While blocking CSF1R with small molecule inhibitors, such as PLX3397 or GW2580, depleted microglial density and proliferation (Elmore et al., 2014; Olmos-Alonso et al., 2016). Therefore, as well as being physiologically relevant, manipulation of the CSF1R signalling pathway is a useful experimental tool to investigate the role of microglia in a range of pathologies (Askew et al., 2024; Di Nunzio et al., 2021).

To conclude, microglia are the primary immune cell of the brain. During homeostasis they constantly survey the environment. In response to disruptions to homeostasis they undergo functional and morphological changes, as well as centrally orchestrating the inflammatory response, which enables the restoration of homeostasis.

1.3.2. Astrocytes

Astrocytes account for 20-40 % of all glial cells, although there is significant species-related variability in astrocyte numbers (Pelvig et al., 2008; Verkhratsky & Nedergaard, 2018). Astrocytes originate from the neuroepithelium-derived radial glia, meaning they share their developmental origin with that of neurons (Kriegstein & Alvarez-Buylla, 2009). However, unlike neurons, astrocytes retain their proliferative capacity postnatally (Ge et al., 2012).

Astrocytes are divided into two subtypes based on their morphology: protoplasmic and fibrous. Protoplasmic astrocytes are found throughout the grey matter, while fibrous astrocytes are found throughout the white matter. Morphologically, protoplasmic astrocytes have a dense, highly-branched, sphere of processes which emerge from the somata. Fibrous astrocytes have longer processes emerging from the somata which are less spherical than in protoplasmic astrocytes

(Sofroniew & Vinters, 2010). Similar to microglia, astrocytes occupy primarily exclusive zones in the brain; their processes do not significantly overlap (Bushong et al., 2002).

The primary homeostatic function of astrocytes is to support neuronal survival. Astrocytes promote neuronal survival by supporting neuronal metabolism, neurotransmission, and neuronal blood supply (Figure 1.8).

Neurons are extremely energetically demanding. In order to meet this energetic demand, astrocytes provide neurons with metabolic support. Neurons primarily rely on oxidative phosphorylation, while astrocytes primarily rely on glycolysis (Barros et al., 2009). The neuron-astrocyte lactate shuttle hypothesis proposes that neuronal metabolism relies on the lactate generated by glycolysis in astrocytes. This hypothesis additionally proposes that neuronal glutamate release stimulates glycolysis in astrocytes, therefore by this neuron-astrocyte relationship, neurons are able to scale their metabolism via astrocytes in activity-dependent manner (Pellerin & Magistretti, 1994). Neurons generate high levels of ROS, as they are heavily reliant on oxidative phosphorylation. Astrocytes provide the brain with an antioxidative system in the form of ascorbic acid and glutathione, this protects neurons from potentially damaging ROS (Makar et al., 1994). Further metabolic support is provided by astrocytes in the form of glycogen storage. Neurons do not store energy in the form of glycogen, instead this function is performed by astrocytes (Cataldo & Broadwell, 1986). In some senses therefore, neurons have outsourced critical elements of their metabolism to astrocytes.

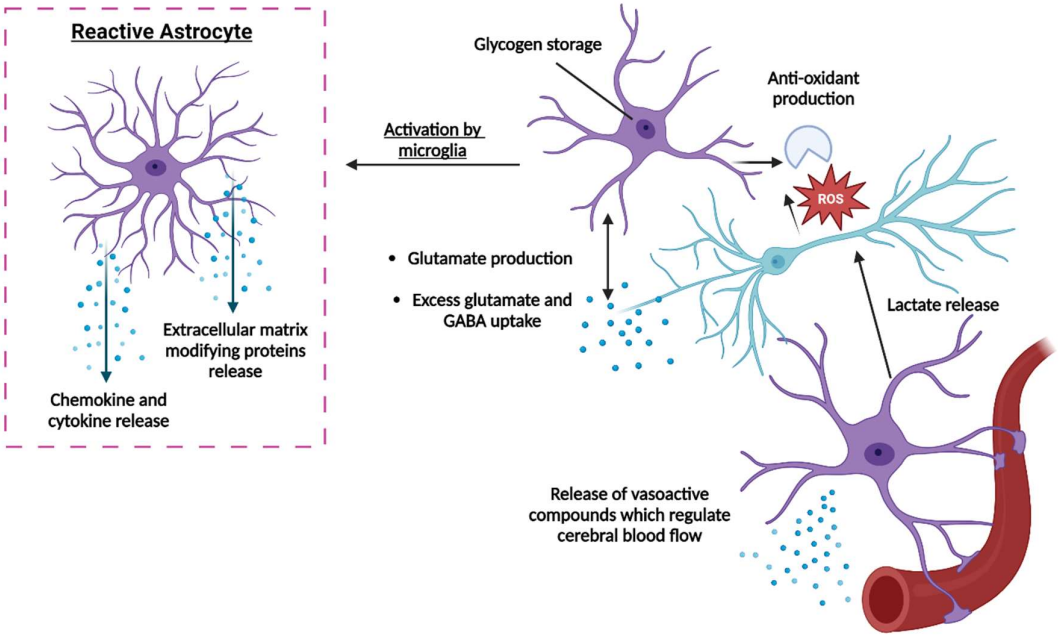

Figure 1.8. Schematic representation of astrocyte function in both homeostasis and inflammation (inset). Figure created using BioRender.

Astrocytes have a key role in neurotransmitter regulation. The awareness of astrocyte involvement in neurotransmission at the neuronal synapse has led to the concept of the tripartite synapse (Araque et al., 1999). The essence of this concept is that in response to neuronal activity, astrocytes are capable of producing their own transmitters which can modulate neuronal activity. Astrocytes influence neuronal activity by regulating neurotransmitter levels at the synapse. Astrocytes generate neurotransmitters and also uptake any excess neurotransmitter. Astrocytes are also responsible for cycling glutamate (the main excitatory neurotransmitter of the central nervous system) via uptake of glutamate from the synaptic cleft, conversion to glutamine by glutamine synthetase, and export to the neuron and conversion back to glutamate by glutaminase (Hertz et al., 1999). Thus, in addition to being the main sink for glutamate, astrocytes are also the main source of glutamate (Danbolt, 2001). The reuptake of glutamate from the synaptic cleft improves the signal-to-noise ratio of glutamate signalling and also reduces the excitotoxic effects of glutamate. Additionally, astrocytes

are capable of regulating GABA levels at the synapse by uptake via GABA transporter type 3 (GAT-3)(Kersanté et al., 2013). Therefore, astrocytes control the levels of both inhibitory and excitatory neurotransmitters at the synapse. This, along with the production of glutamate, gives astrocytes a key role in neurotransmission regulation.

Astrocytes further support neuronal survival by controlling blood supply to the brain. Astrocytic endfeet cover almost all (approximately 99%) of the vasculature of the central nervous system (Mathiisen et al., 2010). The neurovascular unit (formed by astrocytic endfeet, the vasculature of the brain, and neurons) controls the cerebral blood flow in a neuronal-activity-dependent manner. Astrocytes are central to this process, which is known as functional hyperaemia. In response to glutamate release from neurons, astrocytes produce prostaglandins, epoxyeicosatrienoic acids, and release potassium ions which all cause vasodilation in the vasculature of the brain (Metea & Newman, 2006; Paulson & Newman, 1987; Zonta et al., 2003). This increases cerebral blood flow and provides the oxygen and energy needed to support neuronal activity. Astrocytes also produce arachidonic acid derivatives in response to glutamate release from neurons. Arachidonic acid is also vasoactive, it causes vasocontraction which reduces cerebral blood flow (Metea & Newman, 2006). The production of arachidonic acid instead of vasodilatory compounds appears to be regulated by the local oxygen concentration (MacVicar & Newman, 2015). In summary, astrocytes are an essential component of the neurovascular unit and regulate cerebral blood flow in response to neuronal activity.

Astrocytes can also behave, in some respects, like immune cells. As with microglia, they undergo phenotypic changes in response to disturbances in the brain. This phenotypic change has been termed neurotoxic, activated, and astrogliosis. The current consensus is that the terms “reactive astrogliosis” or “reactive astrocytes” are best suited to describe this phenotypic change (Escartin et al., 2021). As with microglia, it is now clear that there is “no prototypical reactive astrocyte”; instead reactive astrocytes exist along a continuum of context-dependent states (Escartin et al., 2021). For

the most part, astrocyte reactivity is induced by cytokines released by reactive microglia (Holm et al., 2012; Liddelow et al., 2017). Astrocytes have limited ability to directly sense disruptions to homeostasis, this detection is predominantly mediated by microglia.

As with microglia, astrocyte reactivity is accompanied by morphological changes. Reactive astrocytes become hypertrophic, however the overlap between individual astrocytes remains low (Wilhelmsson et al., 2006). This morphological change is associated with cytoskeletal reorganisation. Therefore, increased expression of several cytoskeleton proteins (Glial fibrillary acidic protein (GFAP), Vimentin) are used as markers of astrocyte reactivity. In severe cases of astrocyte reactivity, astrocytes form a glial scar. This scar is thought to function as a containment mechanism at sites of severe neurotrauma or infection (Sofroniew, 2009).

The functional changes associated with astrocyte reactivity have been investigated by transcriptomic analysis of gene expression. The specific transcriptomic profile detected was dependent on the manner in which reactivity was induced. This reinforces the point that astrocyte reactivity is context-dependent. Broadly, however, this analysis showed an increase in expression of extracellular matrix modifying proteins, cell proliferation markers, neurotrophic factors (including BDNF and leukaemia inhibitory factor (LIF)), chemokines (including chemokine (C-C motif) ligand (CCL) 2, chemokine (C-X-C motif) ligand (CXCL) 1, CXCL2, CXCL10, IL-6), complement pathway proteins, and antigen processing and presentation proteins (Hasel et al., 2021, 2023; Matusova et al., 2023; Zamanian et al., 2012). The diversity of these changes reflects the diversity of functions carried out by reactive astrocytes. These include: glial scar formation (via extracellular modifying proteins), neuronal support (via neurotrophic factor production), recruitment of peripheral immune cells (via cytokine production), and synapse engulfment (via the complement pathway).

To conclude, astrocytes have an essential role in maintaining neuronal activity during homeostasis. This includes metabolic support, regulation of neurotransmission, and regulation of cerebral blood

flow. During periods of disruption, reactive astrocytes are induced by reactive microglia. Reactive astrocytes are a heterogeneous, dynamic population of cells with a range of neurotoxic and neurotrophic functions.

1.4. Immune effects on neuronal activity

As initially stated, this thesis aims to answer the specific question: how does the immune system affect neuronal network activity in Alzheimer's Disease? Both the immune system and neuronal activity, with a focus on neuronal oscillations, have been introduced. Before introducing and discussing the third element (Alzheimer's disease), interactions between neuronal activity and the immune system will be discussed. As before, there will be a focus on gamma frequency neuronal oscillations as a form of neuronal activity. Neuron-microglia and neuron-astrocyte interactions will be discussed, followed by a discussion of the specific effects of certain inflammatory mediators on neuronal activity.

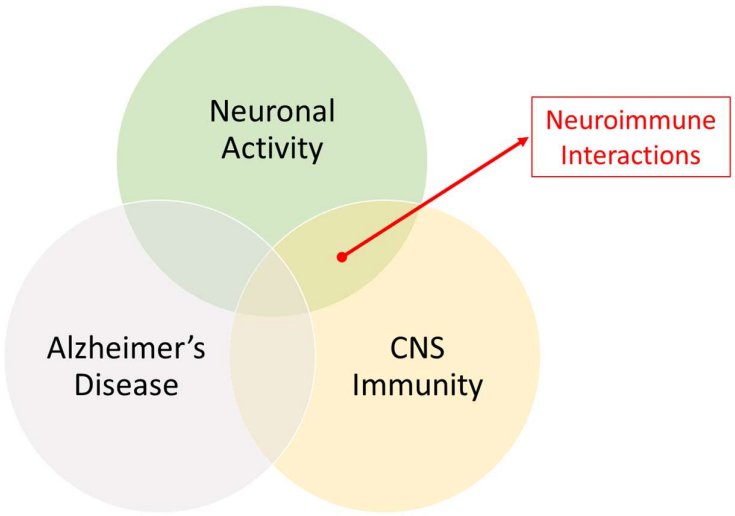

Figure 1.9. Neuroimmune interactions – the focus of this section – and their relation to other topics in this thesis.

1.4.1. Microglia-neuron interactions

There is clear evidence that microglia and neurons reciprocally modulate one another (Pósfai et al., 2019). Microglia express a wide array of receptors that detect neurotransmitters (Marinelli et al., 2019). This allows microglia to modulate their behaviour in response to neuronal activity. For example, microglia express AMPA and kainate receptors, the activation of which enhances the production of TNFα (Noda et al., 2000). Additionally, microglia express $GABA_B$ receptors, the activation of which induces a potassium conductance in microglia and attenuates the release of IL-6 (Kuhn et al., 2004). Therefore, neurotransmission by neurons impacts microglia. Additionally, neurons express proteins which are not neurotransmitters and directly affect the microglial phenotype. Neuronal expression of CD200 maintains the non-reactive, homeostatic phenotype in microglia (Hoek et al., 2000). Similarly, expression of the chemokine CX3CL1 by neurons keeps microglia in the non-reactive phenotype (Maciejewski-Lenoir et al., 1999; Nishiyori et al., 1998).

As well as neurons affecting microglia, microglia affect neurons. This is seen most clearly in microglial surveillance and regulation of synapses. Microglial surveillance is directed towards active synapses. It has been shown that microglia make approximately five minute-long contacts with active synapses at a frequency of approximately once an hour (Wake et al., 2009). Beyond network surveillance, microglia shape neuronal circuits. This is especially prominent during development in a process known as synaptic pruning (Katz & Shatz, 1996). Microglia sense neuronal activity in the developing brain and preferentially remove weaker synaptic inputs via the complement system (Schafer et al., 2012; Stevens et al., 2007).

Although only briefly introduced, there is a clear bi-directional relationship between microglia and neurons in health and disease. This is a large area of current study. Therefore, focus will be limited to microglia interactions with gamma frequency oscillations.

The primary evidence that gamma frequency oscillations affect microglia comes from experiments in which gamma frequency oscillations were induced both by optogenetics and non-invasively by visual and auditory stimulation in 5XFAD mice (an Alzheimer's disease model). The induction of gamma frequency oscillations altered the microglial phenotype. Microglia became more phagocytic and their cell bodies became larger. Additionally, microglia expansion was increased by induction of gamma frequency oscillations. These changes were not associated with random frequency stimulation, suggesting there is a specific effect of gamma frequency oscillations on microglia. The induction of gamma frequency oscillations resulted in reduced plaque burden and disease severity in the Alzheimer's mouse model, these beneficial effects were proposed to be mediated via the induced increase in microglial expansion and phagocytic capacity (Iaccarino et al., 2016; Martorell et al., 2019). The mechanism underlying the effect of gamma frequency oscillation induction on microglia has been investigated. In wildtype mice, non-invasive stimulation (using sensory stimulus) of gamma frequency oscillations activates the NF-κB and MAPK pathways within minutes of gamma frequency oscillation induction. This leads to an increase in the production in the visual cortex of a range of cytokines, most notably IL-6, IL-4, CXCL1, CSF1, and CXCL9 (Garza et al., 2020). These cytokines are likely part of the mechanistic link between microglia changes in response to increased gamma frequency oscillations, as discussed above. The profile induced by 40 Hz light stimulation differs from the immune response to light stimulation at 20 Hz, random light stimulation and the response to acute challenge with LPS (Garza et al., 2020). This suggests that oscillatory activity in the gamma frequency band promotes a distinct immune response. It has also been proposed that the induction of gamma frequency oscillations promotes glymphatic clearance of amyloid-beta plaques by stimulating the influx of cerebrospinal fluid and efflux of interstitial fluid in the cortex of 5XFAD mice (Murdock et al., 2024). Although there are still outstanding mechanistic questions, this preclinical work has led to the development of clinical trials in which gamma frequency oscillations are non-invasively induced in individuals with mild cognitive

impairment (MCI) or prodromal Alzheimer's disease (Adaikkan & Tsai, 2020; Chan et al., 2022). However, there are questions around the reproducibility and interpretation of these findings. It has been suggested that the strategy used in these experiments to non-invasively induce gamma frequency oscillations only induces this activity in the visual cortex, and not in the hippocampus, as was reported. This study also failed to reproduce the effects of non-invasively induced gamma frequency oscillations on amyloid-beta plaque burden and microglia, however this does not necessarily invalidate the finding that optogenetically-induced gamma frequency oscillations are beneficial in 5XFAD mice (Soula et al., 2023). This remains a significant caveat to this body of work.

In addition to neuronal oscillations affecting microglia, microglia have been shown to affect gamma frequency oscillations. The activation state of microglial appears to determine the effect which microglia have on gamma frequency oscillations. In organotypic hippocampal cultures, the power (which is the square of the amplitude) of acetylcholine-induced gamma frequency oscillations was significantly increased when microglia in the culture were activated via TLR4 with LPS (10 μgmL^{-}) or with IFN-γ (100 $ngmL^{-}$). The frequency of the oscillation was slightly reduced when the culture was treated with LPS or IFN-γ alone. Treating the culture with both LPS and IFN-γ led to widespread cell death and an almost total loss of oscillatory activity. Parvalbumin cells were shown to be reduced following treatment with LPS and IFN-γ, however MAP2 labelling shows this is not a population-specific loss. These findings suggest that the power of gamma frequency oscillations is increased when microglia are stimulated by either LPS or IFN-γ alone, but is reduced in the presence of severe inflammation (LPS with IFN-γ), while the frequency of the oscillation is reduced in both scenarios. The effect on power is at least partially mediated by nitric oxide (NO) released from microglia as treating the LPS and IFN-γ activated cultures with 1400W, an inhibitor of inducible nitric oxide synthase (iNOS), partially rescued the power of the gamma frequency oscillations; however, its frequency remained significantly reduced (Papageorgiou et al., 2016). This

suggests that different types of microglial stimulation drive different responses in gamma frequency oscillations. Similar studies in postnatal organotypic hippocampal cultures have shown that chronic activation of microglia by IFN-γ leads to a reduction in oscillation frequency, an increase in oscillation power at moderate levels microglial activation and a reduction in power at high levels of microglial activation. A central role for microglial-produced NO in the disruption of gamma frequency oscillations is also proposed in these studies (Dikmen et al., 2020; Schilling et al., 2021; Ta et al., 2019). Chronic activation of microglia via GM-CSF (also known as CSF2) also affected the frequency of gamma frequency oscillations and caused the emergence of neural burst firing. GM-CSF treatment induced an increase in microglial proliferation but did not increase the production of pro-inflammatory cytokines (Dikmen et al., 2020). Additionally, single activation of either TLR2 or TLR3 reduced the frequency of acetylcholine-induced gamma frequency oscillations but did not affect the power of the oscillations, whereas activation of TLR2 or TLR3 paired with IFN-γ led to a total ablation of gamma frequency oscillations. These disruptions are again suggested to be via NO production (the disruptions were partially reversed by treatment with 1400W (an iNOS inhibitor) and treatment with apocynin (a nicotinamide adenine dinucleotide phosphate (NADPH) oxidase inhibitor), possibly acting on parvalbumin interneurons which are sensitive to oxidative stress (Schilling et al., 2021). Therefore based on this work, led by Kann, there is evidently a means of communication whereby microglia are capable of modulating both the power and frequency of gamma frequency oscillations, this is likely via the production of NO which acts on parvalbumin inhibitory interneurons. Although these findings discussed above indicate that there is a relationship between microglia and gamma frequency oscillations, it has been reported, also by Kann et al., that non-activated microglia are dispensable in the generation and maintenance of gamma frequency oscillations (Lewen et al., 2020). This finding is yet to be corroborated *in vivo*. Regardless of this, it points to the possibility that it is only activated microglia which are capable of affecting gamma frequency oscillations.

In vivo work in rodents also shows that activated microglia can impact gamma frequency oscillations. Peripheral challenge with LPS (1 $mgkg^{-1}$) induces transient microglial activation, along with widespread peripheral immune activation. Microglial activation, following LPS challenge, is correlated with an increase in spontaneous gamma frequency band power in freely moving rats. In mice, the activation of microglia following challenge with peripheral LPS is associated with a reduction in inhibitory synaptic input to cortical projection neurons. This reduced inhibitory activity is possibly responsible for the observed increase in gamma frequency oscillation power (Chen et al., 2014).

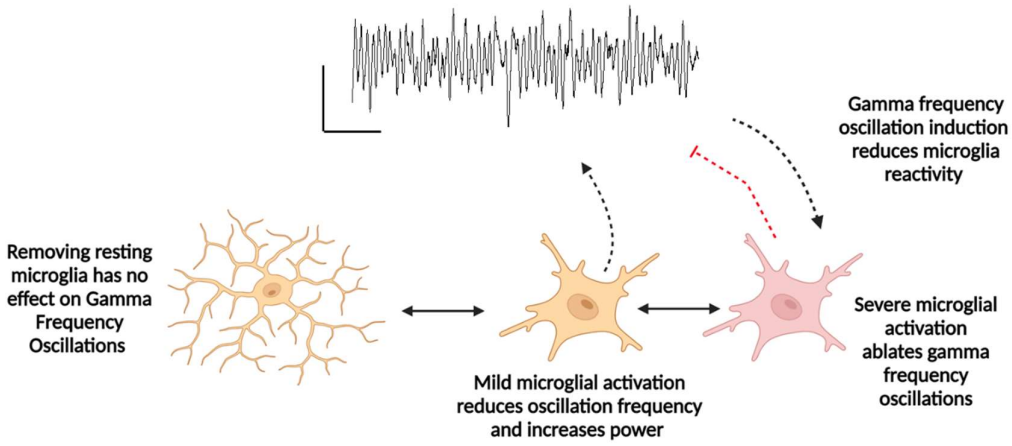

Figure 1.10. Schematic representation of putative bidirectional interactions between gamma frequency oscillations and microglia. Figure created using BioRender.

In summary, activated microglia, or at any rate acute inflammatory activation, clearly impacts gamma frequency oscillations. Broadly, activated microglia appear to reduce gamma frequency oscillation frequency. Mild microglial activation appears to increase gamma frequency oscillation amplitude while severe microglial activation appears to significantly reduce gamma frequency oscillation amplitude (Figure 1.10). Changes in the environment, which result from microglial activation, impact on the ability of inhibitory interneuron networks to generate gamma frequency

oscillations. The mechanisms by which microglia impact gamma frequency oscillations require further investigation.

1.4.2. Inflammatory mediators and gamma frequency oscillations

The effect of specific immune mediators, chemokines and cytokines, on gamma frequency oscillatory activity has also been studied to a limited extent. These are the molecules by which immune cells communicate and execute their functions. There are very few studies which examine the direct effect of exposure to inflammatory mediators on gamma frequency oscillations, this represents a significant gap in our current knowledge. The few studies which have been carried out, as well as the effect of various inflammatory mediators on relevant electrophysiological parameters, will now be summarised. The effects of inflammatory mediators on neuronal activity have been well reviewed elsewhere, therefore this section will focus on the effect on gamma frequency oscillations and related activities only (Zipp et al., 2023).

TNFα is an pro-inflammatory cytokine which has been studied in relation to gamma oscillations. In neonatal rats, administration of intracortical LPS (10 μg in 2 μL, which is a notably high dose) causes spontaneous gamma frequency oscillations to occur less frequently. However, they occur with increased mean duration. The amplitude and frequency of the oscillations are not significantly changed. Treating the LPS-treated rats with anti-TNFα antibodies prevented the changes in oscillatory activity. This suggests that TNFα is mediating these disruptions to gamma frequency oscillations (Nimmervoll et al., 2013). This is consistent with the observation that TNFα can directly influence the activity of neurons. TNFα, derived from glia, is necessary and sufficient for synaptic scaling – a process in which excitatory synapses in a network increase their activity in response to reduced network activity (Stellwagen & Malenka, 2006). TNFα's role in synaptic scaling is likely mediated via its ability to increase the synaptic expression of AMPA receptors and

simultaneously decrease synaptic expression of $GABA_A$ receptors (Beattie et al., 2002; Stellwagen et al., 2005). Furthermore, in brain slices from an Alzheimer's disease mouse model (*Trem2*^{R47H}) synaptic inhibitory transmission was observed to be reduced in TNFα-dependent manner (Ren et al., 2021). These findings show that TNFα is capable of directly affecting the excitatory-inhibitory balance of neural networks. When viewed alongside the observed TNFα-dependent effect of LPS on gamma frequency oscillations it seems probable that this cytokine has an effect on oscillations in the gamma frequency range, however this has not yet been directly examined.

IL-1β is also a pro-inflammatory cytokine. The effect of IL-1β on neuronal activity has been widely studied, for example its effect on long term potentiation (for review see: (M. A. Lynch, 2015)), however the direct effect of this cytokine on gamma frequency oscillations has not been greatly investigated. Intra-striatal injection of IL-1β (50 μg/mL) reduced the power of stimulus-evoked gamma frequency oscillations in freely moving mice (Bray et al., 2016). This is consistent with the observation that IL-1β (30 ng/mL) reduces GABAergic transmission in CA1 pyramidal neurons in hippocampal slices from wildtype mice. This reduction was also seen when hippocampal slices were incubated with microglia, activated by TNFα and IFN-γ, and abrogated when co-incubated with the IL-1β receptor antagonist IL-1ra (Nisticò et al., 2013). This suggests that IL-1β from microglia can alter inhibitory transmission in hippocampal neuronal networks. Although the direct effect of IL-1β on gamma frequency oscillations was not examined in this study, or any other study, it is likely that this altered inhibition leads to perturbations in oscillatory activity.

Chemokines are signalling molecules which induce and direct the movement of immune cells in a process known as chemotaxis. It does not appear that the effect of any chemokines on gamma frequency oscillations has been directly investigated. However, it seems likely, based on previous research, that these molecules have an effect on gamma frequency oscillations. For example, CCL2 (which recruits monocytes and basophils to the site of inflammation) increases the amplitude of GABA-evoked currents in rodent cortical brain slices (Caioli et al., 2013). This effect of CCL2 on

$GABA_A$ receptors strongly suggests that CCL2 may possibly impact gamma frequency oscillations, however this is yet to be investigated. Similarly, CXCL10 (which recruits monocytes, T cells, natural killer cells, and dendritic cells to the site of inflammation) has been shown to reduce the expression of $GABA_A$ and $GABA_B$ receptors, as well as the GABA-producing enzyme GAD65/67, in cultured hippocampal rat neurons (Cho et al., 2009).

Interferons are cytokines involved in the innate immune response. They are especially active in the immune response to viruses. Investigations have been made into the effect of the type II interferon, IFN-γ, on acetylcholine-induced gamma frequency oscillations in postnatal organotypic slice cultures. IFN-γ reduced the frequency, but did not affect the power, of acetylcholine-induced gamma frequency oscillations. The effect of IFN-γ was shown to be mediated via microglia. Specifically, it is mediated by increased nitric oxide release from these cells (Ta et al., 2019). Other work suggests that the effect of IFN-γ on oscillatory neuronal activity may not be entirely mediated by microglia, and additionally IFN-γ can act directly on neurons. IFN-γ, derived from meningeal T cells, acts directly on neurons to increase GABAergic inhibition. This process is required for normal social behaviour (Filiano et al., 2016). Type I interferons can also act directly on neurons. In the rat cortex, oscillatory activity was slowed by application of IFN-β, a Type I interferon. This was not however in the gamma frequency range. Additionally, Type I interferons modulate intrinsic neuronal excitability by reducing the hyperpolarization activated nonselective ion current via inhibition of the hyperpolarization-activated cyclic nucleotide (HCN)-gated channel subunit HCN1 (Stadler et al., 2014). Predicting an effect of type I interferons on gamma frequency oscillations should be tempered by the finding that IFN-α (a type I interferon) had no effect on acetylcholine-induced gamma frequency oscillations in an organotypic culture (Ta et al., 2019).

To conclude, although the research in this area has been relatively limited there is evidence to support the view that cytokines and chemokines are capable of modulating gamma frequency

oscillations. The exact effect of each mediator is yet to be untangled but it is clear that these mediators can affect neuronal activity and neuronal oscillations.

1.4.3. Astrocyte-neuron interactions

The primary function of astrocytes is to support neuronal activity. Therefore they have many interactions with neurons. Several of these interactions were discussed previously. The possible interactions between astrocytes and gamma frequency oscillations will be focussed on here.

Astrocytes have been shown to be required for gamma frequency oscillation generation. In hippocampal brain slices, astrocytes were genetically altered to express tetanus toxin, this blocked glutamate release. Carbachol-induced gamma frequency oscillations in these brain slices had normal amplitude and peak frequency but they had shorter duration. Furthermore, in an *in vivo* model, with inducible tetanus toxin expression in astrocytes, low gamma (20-40 Hz) band power was reduced and the animals had reduced performance on a novel object recognition test (Lee et al., 2014). Additionally, it has been shown that reduction of astrocyte number in the medial prefrontal cortex of rats, using L-alpha aminoadipic acid, diminished gamma band power and impaired cognitive flexibility (Brockett et al., 2018). These findings suggest that the integrity of astrocytic function is required for maintaining normal gamma frequency oscillations. Reductions in astrocyte number or function negatively impacts gamma frequency oscillations and subsequently negatively affects cognitive function. Given the crucial role astrocytes have in supporting neuronal activity, it is perhaps not surprising that disruption of astrocytes negatively impacts gamma frequency oscillations.

Several studies have investigated the mechanistic consequences of astrocyte disruption on gamma frequency oscillations. Generally, these studies find that disruption of astrocyte function leads to an inability to maintain the environment required to generate gamma frequency oscillations. For example, astrocytes buffer the high levels of K^+ ions associated with sustained neuronal activity

(Walz, 2000). Impairing the ability of astrocytes to clear potassium, by blocking potassium channels using barium chloride, increased neuronal excitability and gamma frequency oscillation amplitude, leading to a hyperexcitable phenotype (Bellot-Saez et al., 2018). Similarly, astrocytes buffer the fluctuations of Ca^{2+} ions associated with neuronal activity. Astrocytes produce a calcium binding protein S100β which has been linked to gamma frequency oscillation promotion. The presence of extracellular S100β enhances kainate-induced gamma frequency oscillations via the RAGE receptor (Sakatani et al., 2008). Infusion with S100β increases cross frequency coupling between theta and gamma frequency oscillations, as well as improving cognitive flexibility in rats (Brockett et al., 2018). Interestingly, the release of S100β, from astrocytes, was found to be dependent on neuronal activity, specifically glutamate release (Sakatani et al., 2008). This suggests that in response to sustained neuronal activity astrocytes release S100β in order to buffer extracellular calcium. Blocking the ability of S100β to bind to calcium inhibits rhythmogenesis in neuronal networks in brain slices (Morquette et al., 2015). Therefore, gamma frequency oscillations are promoted by, and require, astrocytic buffering of calcium via S100β. The importance of S100β in gamma frequency oscillations is supported by the observation that conditions associated with increased S100β are also associated with disrupted gamma frequency oscillations: Alzheimer's Disease, epilepsy and schizophrenia (Herrmann & Demiralp, 2005; Lara et al., 2001; Liang et al., 2019; Peskind et al., 2001).

There is some very preliminary evidence that gamma frequency oscillations can modulate astrocytes. In an AD mouse model (5XFAD), increasing gamma frequency activity by auditory stimulation results in increased numbers of astrocytes and increased levels of S100β (Martorell et al., 2019). Therefore, similar to microglia, there is a possibility that gamma frequency oscillations can modulate astrocytes. However, it is well established that astrocytes are required for gamma frequency oscillation generation and maintenance. Alterations in astrocyte number or function have a negative impact on gamma frequency oscillations in a variety of models.

1.4.4. Clinical examples of immune effects on neuronal activity

Useful evidence that the immune system affects neuronal activity can be obtained by briefly considering some clinical phenomena. The output of the brain is behaviour and cognition, there are several instances in which changes in the immune system lead to alterations in behaviour and cognition.

The most notable and widespread example of the immune system impacting behaviour is in sickness behaviour. This refers to the collective changes which take place during infectious disease. These changes include lethargy, depression, anorexia, and reduced social motivation (Devlin et al., 2021; Hart, 1988). These behaviours represent an adaptation which promotes the fight against the infectious pathogen. These behaviours conserve energy and also limit the spread of infection to other individuals (Eisenberger et al., 2010). Sickness behaviour is driven by the immune system's response to infection (C. Cunningham et al., 2007; Erickson & Banks, 2011). Infection is associated with a wave of changes in the immune system, therefore it is difficult to identify the specific effects of various immune cells and mediators, as well as the neuronal correlates of sickness behaviour (Salvador et al., 2021). Nevertheless, sickness behaviour is a clear example of changes in the immune system affecting neuronal activity.

The clinical phenomenon delirium is another example of how changes in the immune system can affect neuronal activity. Delirium is defined as an acute decline in attention and cognition in persons who are 65 and older (Inouye, 2006). Delirium occurs in 15-53% of elderly patients post-operatively and 70-87% of elderly patients in intensive care units (Agostini & Inouye, 2003; Pisani et al., 2003). This distressing, acute cognitive dysfunction therefore represents a widespread condition which affects aged individuals during periods of elevated systemic inflammation (as well as many other acute medical and physiological triggers). Given the role gamma frequency oscillations play in cognitive function, it is very likely that they are disrupted during episodes of delirium. In patients

with delirium, recordings with EEG showed an increase in delta frequency oscillations and a reduction in alpha frequency oscillations (Numan et al., 2017; van Dellen et al., 2014). Despite multiple studies using EEG in individuals with delirium, the effect of delirium on gamma frequency oscillations is not commonly reported (Nishizawa et al., 2023; Shinozaki et al., 2018). In freely moving rats, injection with LPS (1 mg/kg) caused a reduction in theta frequency oscillation power and an increase in delta frequency oscillation power. Hippocampal and medial prefrontal cortex gamma frequency oscillations were reported to be unchanged (Mamad et al., 2018). While in mice which underwent caecal ligation and puncture (a model of sepsis and severe systemic inflammation) gamma frequency oscillation was reported to be increased during illness (Consoli et al., 2023). It is clear therefore that the immune changes which drive delirium result in changes to oscillatory activity, however there is little evidence to suggest that gamma frequency oscillations are specifically affected in delirium. There have been several studies which suggest that there is however some interaction between these oscillations and delirium. In a mouse model of sepsis (caecal ligation and puncture) neuroinflammation caused a reduction in neureglin1-ErbB4 signalling in the hippocampus and a reduction in stimulus evoked gamma frequency oscillation power (Gao et al., 2017). Neureglin1, a trophic and differentiation factor expressed in the hippocampus by pyramidal cells, is a ligand for ErbB4 receptors which are predominantly expressed on parvalbumin interneurons. Unsurprisingly, given the centrality of these cell types in gamma frequency oscillation generation, neureglin1 increases the power of kainate-induced gamma frequency oscillations in an *ex vivo* brain slice model (Fisahn et al., 2009). Other studies have used caecal ligation and puncture to model sepsis and investigate the neuronal consequences of widespread inflammation. In rats caecal ligation and puncture reduced the number of parvalbumin synapses in the perisomatic domain of pyramidal cells. This change was accompanied by a reduction in hippocampal slow gamma power and cognitive impairments (M. Ji et al., 2020). These studies indicate that severe peripheral inflammation is

associated with changes in gamma frequency oscillations as a result of specific changes in the cell populations which underlie these oscillations.

The research above amounts to a compelling argument that there is crosstalk between neuronal activity (with a focus on gamma frequency oscillations) and the immune system. There are clear interactions between the immune cells of the CNS and gamma frequency oscillations. For microglia, these interactions are bidirectional; gamma frequency oscillations are capable of modulating microglial function and *vice versa*. Likewise, astrocytes are required for the generation and maintenance of gamma frequency oscillations. In addition to the evidence of interactions between glia and gamma frequency oscillations, there is a limited amount of research into how immune mediators – cytokines and chemokines – modify gamma frequency oscillations. The mechanistic basis of these effects is likely a combination of mediators acting directly on neurons and mediators acting via glia to affect neurons. Delineating this requires significantly more research and will be a key subject of this thesis.

1.5. Alzheimer's Disease

The key research question of this thesis is to address whether and how neuronal oscillations are affected by the immune system in Alzheimer's disease. Two elements of this question have been discussed, neuronal activity and the immune system of the CNS, as well neuroimmune interactions. The third large element of this question will now be introduced, specifically Alzheimer's disease.

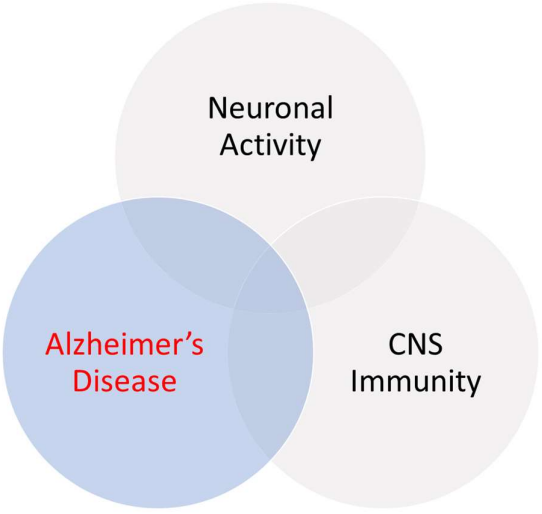

Figure 1.11. Alzheimer's disease – the focus of this section – and its relation to other topics in this thesis.

The Alzheimer's Disease International organisation estimates that there are currently over 50 million people living with dementia worldwide. This figure is expected to increase to 152 million by 2050 (Alzheimer's Disease International, 2019). Alzheimer's disease is the most common cause of dementia and is estimated to account for 60-80% of cases of dementia (Barker et al., 2002; Kapasi et al., 2017). The Alzheimer's Association estimates that currently, approximately one in nine individuals aged 65 and older has Alzheimer's disease in the United States (Alzheimer's Association Report, 2023). To put this in perspective, the number of people predicted to have Alzheimer's disease in 2050 (approximately 122 million) is significantly greater than the current population of Ethiopia (approximately 112 million), a country with the twelfth largest population in the world (United Nations, 2019). There are currently eight drugs available for treating Alzheimer's disease. Two of these drugs (aducanumab (which is being discontinued) and lecanemab) are monoclonal antibody therapies, which slow the rate of cognitive decline to some extent. However, to quote the Alzheimer's Association "lecanemab is not a cure for Alzheimer's disease". Lecanemab has moderate efficacy and possibly serious side effects (Alzheimer's Association Report, 2024).

Therefore, the development of effective methods to diagnose and treat this rapidly growing disease is a significant and urgent challenge.

Alzheimer's disease is neurodegenerative disease clinically characterised by cognitive and behavioural impairment; this includes impairments in learning and recall, impaired reasoning and handling of complex tasks, and changes in personality and comportment (McKhann et al., 2011). At a neuropathological level, Alzheimer's disease is defined by the deposition of extracellular amyloid-beta plaques, the development of neurofibrillary tangles of phosphorylated tau, and widespread loss of synapses by neurodegeneration (Glenner & Murphy, 1989; Goedert et al., 1988; Kidd, 1963; Masters & Beyreuther, 1987; Terry et al., 1964).

The complete aetiology of Alzheimer's disease is unclear; many factors have been found to contribute to the risk of disease. The causes of the disease can however be segregated based on the age of disease onset. Indeed, it could be argued that the disease itself should be segregated into separate diseases based on the age of onset. Early onset Alzheimer's disease (EOAD) or familial Alzheimer's disease, arbitrarily defined as having symptom onset and disease diagnosis before 65 years of age, has been found to be due to mutations in at least one of three genes: presenilin 1 (PS1), (Sherrington et al., 1995) presenilin 2 (PS2) (Levy-Lahad et al., 1995; Scheuner et al., 1996), and amyloid-beta protein precursor (APP) (Goate et al., 1991). Therefore, in these instances, the primary cause of the disease is genetic. The protein products of the genes listed above are involved in the processing of the amyloid-beta protein pathway. APP is a transmembrane protein which exists in several isoforms. APP is the starting point of the amyloid pathway. The exact function of APP remains unknown; it has been proposed as a regulator of both glutamatergic and GABAergic neurotransmission, as well as possibly being an antimicrobial peptide (Dunot et al., 2023; Kesika et al., 2021). The various isoforms of APP are produced by a group of enzymes called secretases. In the healthy brain, cleavage of APP by beta secretase and gamma secretase results in the production of a 40-residue peptide (Aβ40) and a small amount of a 42-residue peptide (Aβ42)(Figure 1.12). PS1 and PS2, which are

among the mutated genes that cause EOAD, are catalytic subunits of the gamma secretase complex (Oikawa & Walter, 2019). Missense mutations in APP, PS1 and PS2 result in an increased production of Aβ42. This product of APP cleavage is less soluble and more hydrophobic than shorter length fragments and has a greater tendency to form aggregates. These aggregates act as seeds or nuclei for the formation of larger plaques of amyloid-beta, which incorporate many shorter residue peptides (Jarrett et al., 1993). These amyloid plaques are a hallmark of Alzheimer's disease. Loss of amyloid-processing pathway control and plaque formation is thought to be the first pathological event which sets in train a series of events which ultimately result in Alzheimer's disease. This is the amyloid cascade hypothesis (Figure 1.12).

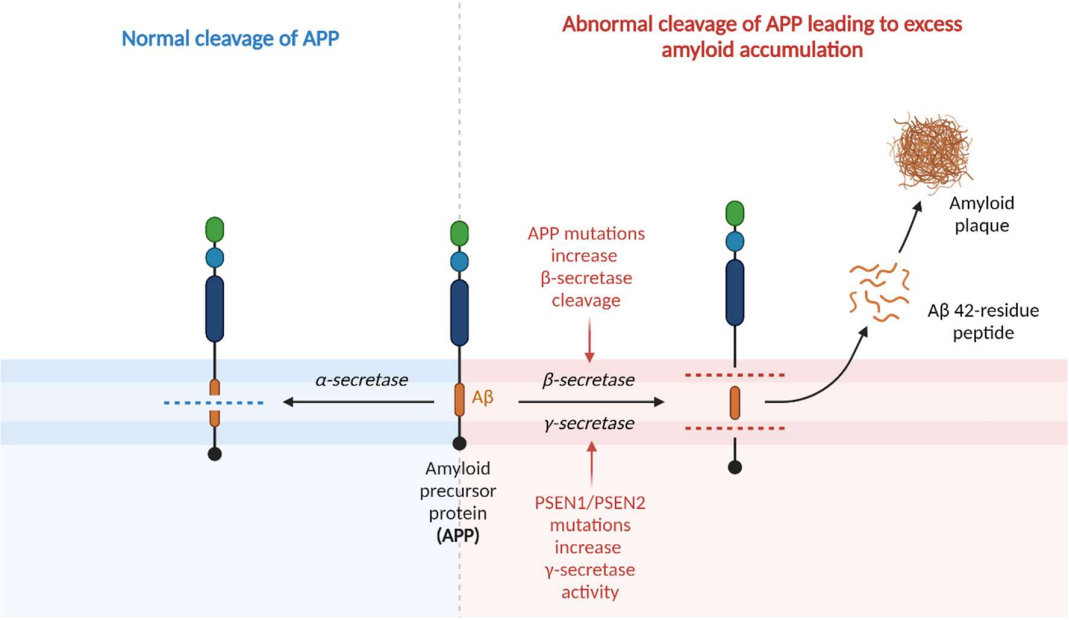

Figure 1.12. Schematic representation of the amyloid hypothesis. Figure created using BioRender.

However, EOAD only accounts for a small minority of Alzheimer's disease cases; a meta-analysis of a range of studies predicts EOAD accounts for 6.1% of all Alzheimer's disease cases (Zhu et al., 2015). Therefore, in only a very small group of patients does the simple proposal that increased

Aβ42 production, as a result of gene mutations, serve as a satisfactory answer for what is causing Alzheimer's disease pathology. This fact has not prevented the widespread study of this pathway and the development of disease models based on amyloid overproduction alone.

The remainder of Alzheimer's disease cases (i.e., the vast majority) have a later age of onset and are referred to as sporadic or late-onset Alzheimer's disease. An enormous number of causes have been proposed to contribute to risk of developing this form of the disease. These include genetic and environmental causes.

The largest risk for all Alzheimer's disease is age. As populations age the incidence of Alzheimer's disease increases exponentially (Hirtz et al., 2007; Rocca et al., 1991). Ageing has been defined as "the time-dependent functional decline that affects most living organisms" (López-Otín et al., 2013). Ageing is a complex process which is unlikely to have a single cause. All biological organisms can be broken down into systems with specific functions from the level of molecules to organs. These systems interconnect and respond to changes in one another. Ageing is the accumulation of change and loss of function in these systems. In Alzheimer's disease the accumulation of certain losses of function, as results of environmental influences and pre-existing vulnerabilities, leads to extensive, degenerative brain pathology.

The close association between ageing and Alzheimer's disease should perhaps inform the way we think about Alzheimer's disease pathogenesis. Similar to ageing, Alzheimer's disease should perhaps be thought of as the emergence of a loss of function in a range of interconnected systems of the brain and the periphery. Instead of searching for a single cause of disease we should consider how a range of possible events or predetermining factors interact over time and cause the same disease state. In Alzheimer's disease a variety of changes in certain systems leads to widespread system collapse in the brain. Just as with ageing which has no set roadmap but a broadly consistent phenotype, the pathway to Alzheimer's disease can be varied but the outcome is relatively consistent. This view

should also inform our hopes for a therapy for Alzheimer's disease. Complex problems and questions rarely have simple answers. In place of single silver bullet therapy, we should perhaps instead place our hopes in combination therapies or lifestyle changes which increase and bolster overall brain health and integrity. Although a comparison has been made here to ageing, it should be noted for clarity that Alzheimer's disease is not inevitably associated with ageing; only 32% of individuals aged 85 years or older are estimated to have Alzheimer's disease (Hebert et al., 2013). It is also important to state that pathological processes occur in individuals who develop Alzheimer's disease that are not occurring, at least to the same extent, in those who do not develop Alzheimer's disease (Ince, 2001).

A wide range of environmental factors have also been linked to increased risk of Alzheimer's disease. Again, none of these factors in isolation lead to Alzheimer's disease pathology. Often the increased risk from these proposed factors is extremely small. These findings are beyond the present scope and are reviewed elsewhere (A Armstrong, 2019; Killin et al., 2016; Livingston et al., 2024).

Late-onset Alzheimer's disease, while not fully monogenic, also has genetic risk factors. Heritability has been estimated to range from 60-80% (Gatz et al., 2006). The greatest genetic risk factor for late-onset Alzheimer's disease is the ε4 allele of the *APOE* gene (Corder et al., 1993; Strittmatter et al., 1993). Apolipoprotein E (ApoE), the protein product of the *APOE* gene, is a lipid transporter. It has been shown that ApoE is essential for intracellular degradation of amyloid-beta and that the ε4 allele protein product results in less efficient amyloid clearance (Jiang et al., 2008; C. C. Liu et al., 2017). Another risk factor rooted in genetic alterations is Down's syndrome (trisomy 21); in which the APP gene, located on chromosome 21, is triplicated (Sleegers et al., 2006). It has been shown that 75-88% of individuals with Down' syndrome who are over 65 years of age develop dementia (Evenhuis, 1990; Lai & Williams, 1989). Mutations in many other genes have been linked to increased risk of the disease (Kunkle et al., 2019). Many of these mutations are in immune-related genes, for example CD33 (Bertram et al., 2008) and triggering receptor expressed on myeloid cells

2 (TREM2) (Jonsson et al., 2013); this had led to an increased focus on neuroinflammation in Alzheimer's disease, and will be discussed in detail in the next section.

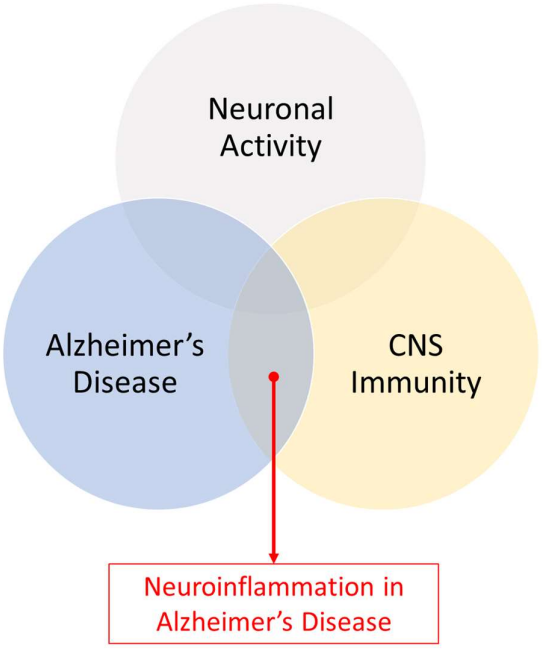

Figure 1.13. Neuroinflammation in Alzheimer's disease – the focus of this section - and its relation to other topics in this thesis.

1.6. The immune system in Alzheimer's disease

The emergence of Alzheimer's disease represents a profound departure from homeostasis. Given the significant disruption to homeostasis caused by the emergence of pathology,Alzheimer's disease is associated with widespread changes in the immune system. Beyond simply reacting to the emergence of pathology, alterations in the immune system can increase the risk of developing Alzheimer's disease and affect disease progression. Therefore, the changes in the immune system should not only be considered a consequence of Alzheimer's disease, but also a key risk factor for disease development and progression.

Microglia sense the emergence of amyloid plaques via a number of different PRR. For example, TLR4 with TLR2, mediated by CD14, can detect amyloid-beta oligomers (Y. Liu et al., 2005; Reed-Geaghan et al., 2009). Similarly, TLR4 with TLR6, mediated by CD36, can detect amyloid-beta oligomers (Momtazmanesh et al., 2020; Stewart et al., 2010). The activation of these PRR by amyloid-beta plaques causes microglia to become reactive. The reactive phenotype acquired by microglia (proximal to plaques) in Alzheimer's disease has been profiled using transcriptomics. Microglia with this phenotype have been termed disease associated microglia (DAM). The DAM profile is characterised by increased expression of genes relating to phagocytosis (*Tyrobp*, *Trem2*, *Ctsd*, *Axl*), pathogen recognition (*Clec7a)*, the complement cascade (*Itgax*), proteases (*Timp2*), and lipid metabolism (*Lpl*, *ApoE*), and a downregulation of homeostatic genes (*P2ry12*, *P2ry13*, *Cxc21*, *Tmem119*)(Keren-Shaul et al., 2017). These changes reflect the functional change in microglia in response to the detection of amyloid-beta oligomers, specifically, microglia recognise amyloid-beta plaques and attempt to clear them by phagocytosis (Keren-Shaul et al., 2017). Therefore, in the early stages of disease, microglia would appear to have a beneficial role in Alzheimer's disease and they counter the emergence of Alzheimer's pathology (Fan et al., 2017; Femminella et al., 2019). However, the role of the immune system in Alzheimer's disease is more complicated than simply resisting Alzheimer's pathology. Alterations in the immune system contribute to both the risk of developing Alzheimer's disease and the progression of Alzheimer's disease.

There is non-mechanistic clinical evidence available which suggests that the immune system can affect the risk of developing Alzheimer's disease. It appears that reducing peripheral and CNS immune activation reduces the risk of developing Alzheimer's disease. This is suggested by the observation that treatment with non-steroidal anti-inflammatory drugs reduces the development of Alzheimer's disease (Hoozemans et al., 2008; Leoutsakos et al., 2012). Similarly, routine vaccinations have been shown to also reduce the risk of developing Alzheimer's disease (Harris et al., 2023). Additionally, individuals who experience an episode of delirium, as a result of large

systemic inflammation, have an increased risk of developing Alzheimer's disease (Davis et al., 2012; Witlox et al., 2010). These findings all suggest that reducing immune activation reduces the risk of developing Alzheimer's disease, and, by extension, excessive immune activation is a risk factor for developing Alzheimer's disease.

Genome-wide association studies (GWAS) and mechanistic studies have demonstrated that the immune system increases the risk of developing Alzheimer's disease when it fails to carry out its normal functions in the brain. This is demonstrated by the observation that many genetic risk factors for Alzheimer' disease encode for proteins with immune-related functions. For example, a certain *Trem2* variant has been identified as a highly significant genetic risk factor for developing Alzheimer's disease (Guerreiro et al., 2013; Jonsson et al., 2013). TREM2 is primarily expressed on microglia in the brain (Sessa et al., 2004). TREM2 binds to anionic lipids – including ApoE-containing phospholipids – and possibly directly to amyloid-beta, these ligands lead to activation of TREM2 signalling (Jendresen et al., 2017; Y. Zhao et al., 2018). TREM2 is essential for microglial activation and amyloid-beta plaque clearance. A deficiency in TREM2 impaired the ability of microglia to cluster around and clear amyloid-beta plaques in Alzheimer's disease mouse models (Ulland & Colonna, 2018). TREM2 facilitates amyloid plaque clearance and promotes microglia survival and reactivity (Y. Wang et al., 2015). Additionally, TREM2-deficient microglia did not acquire the reactive phenotype typically seen proximal to amyloid-beta plaques (disease-associated microglia profile)(Keren-Shaul et al., 2017; Zhou et al., 2020). Microglia lacking TREM2 also had profound metabolic impairments, including deficient glycolysis, ATP levels, and mTOR activation (Ulland et al., 2017). Stimulation of TREM2 with agonistic antibodies has been posited as a potential therapeutic strategy in Alzheimer's disease; the idea being that TREM2 activation promotes the protective function of microglia in Alzheimer's disease (Schlepckow et al., 2023).

Similarly, certain variants of *CD33* have been linked to increased risk for developing Alzheimer's disease (Bertram et al., 2008; Tortora et al., 2022). CD33 is an inhibitory receptor expressed on

microglia (L. Zhao, 2018). In response to binding sialic acid (in glycoproteins and glycolipids) CD33 initiates cellular signalling which inhibits phagocytosis (Crocker et al., 2012). The variants of *CD33* associated with Alzheimer's disease have increased expression relative to non-risk variants. This leads to a reduction in amyloid-beta phagocytosis and clearance by microglia with increased CD33 expression (Griciuc et al., 2013). Knocking out CD33 expression in microglia led to an increased phagocytic capacity, but also increased ROS production (Wißfeld et al., 2021). As with TREM2, CD33 has been proposed as a therapeutic target in Alzheimer's disease. It has been shown that gene therapy – using a microRNA to target CD33 expression – reduced amyloid-beta plaque burden and neuroinflammation in the APP/PS1 Alzheimer's disease model (Griciuc et al., 2020).

These examples (TREM2 and CD33) demonstrate that loss of function in the ability of microglia to clear amyloid-beta plaques increases the risk of developing Alzheimer's disease. Therefore, the immune system is not simply reactive in Alzheimer's disease, it can also contribute causally to disease development.

The immune system can also promote the progression of Alzheimer's disease. In Alzheimer's disease microglia are chronically activated by the presence of amyloid plaques. This results in microglia no longer having beneficial effects on Alzheimer's pathology, instead they promote pathology progression. In response to increased amyloid-beta microglia increase their expression of the complement cascade components (C1q, C3, CR3). This leads to an increase in complement-dependent synapse loss (Hong et al., 2016). Therefore, reactive microglia lead to excess synapse loss and neurodegeneration in response to amyloid-beta. In this manner, microglia promote Alzheimer's pathology.

Furthermore, microglia can also promote the accumulation of amyloid-beta plaques. The NLRP3 inflammasome is a protein complex which promotes inflammation by the protein cleavage and consequent maturation of IL-1β and IL-18 (Martinon et al., 2002). NLRP3 inflammasome

assembly involves a multi-protein complex that includes NLRP3, caspase 1, and ASC. These ASC specks form in the cytoplasm and are essential to the caspase-mediated cleavage of IL-1β, however they can also be released by immune cells to propagate inflammation (Franklin et al., 2014). These ASC specks, released by microglia, can seed the formation of amyloid-beta plaques and it has been shown that disease progression and functional deficits (behavioural and electrophysiological) are mitigated in NLRP3 knockout mice (Heneka et al., 2013; Venegas et al., 2017). Therefore, microglial products actively promote the development of Alzheimer's pathology.

Similarly, ApoE, a lipoprotein transporter, strongly modulates the progression of Alzheimer's disease. The ApoE-epilson-4 allele of *ApoE* is the strongest risk factor, while the APoE-epilson-2 allele is the strongest genetic protective factor, for late-onset Alzheimer's disease (Corder et al., 1993; Reiman et al., 2020). ApoE is primarily released by astrocytes, however its production is downregulated in reactive astrocytes and upregulated in reactive microglia (Grubman et al., 2019; Uchihara et al., 1995). ApoE binds to amyloid-beta and promotes the formation of amyloid-beta plaques (Holtzman et al., 2000; Strittmatter et al., 1993). The ApoE4 allele has the strongest effect on the promotion of amyloid plaque formation, which is consistent with it being the greatest risk factor for late-onset Alzheimer's disease (C. C. Liu et al., 2017). In addition to simply promoting the formation of amyloid-beta plaques, the ApoE also appears to affect microglial reactivity via TREM2 (Jendresen et al., 2017; Krasemann et al., 2017). In mice with the ApoE4 allele transcriptomic analysis of microglia showed a shift towards a pro-inflammatory phenotype, demonstrated by an increase in multiple *Serpina3* genes (which are protease inhibitors)(N. Zhao et al., 2020). Furthermore, microglia derived from induced pluripotent stem cells from ApoE4 allele carriers, had reduced phagocytic capacity for amyloid-beta (Y.-T. Lin et al., 2018). ApoE is therefore a product of immune cells which strongly modulate Alzheimer's disease progression. This has led to many ApoE-directed therapeutic approaches (Serrano-Pozo et al., 2021). These examples

demonstrate that as well as increasing the risk for developing Alzheimer's disease, molecules produced by cells of the immune system can promote disease progression.

Another consequence of long-term microglial activation in Alzheimer's disease is the phenomenon known as microglial priming (Neher & Cunningham, 2019). The primed immune system can become hypersensitive and may generate an exaggerated response to acute inflammatory stimulation. This was first shown in the ME7 model of prion disease (which shows robust chronic neurodegeneration in the hippocampus). Microglia in animals with neurodegeneration had a greater inflammatory response to challenge with LPS than microglia in normal animals. This heightened response included greater expression of pro-inflammatory cytokines (such as IL-1β and TNFα) and increased cell death (C. Cunningham et al., 2005). These initial findings in the ME7 model have since been replicated in many different animal models of neurodegeneration, including the APP/PS1 model of Alzheimer's disease (Godbout et al., 2005; Holtman et al., 2015; Lopez-Rodriguez et al., 2021; Pott Godoy et al., 2008). Astrocytes are also primed to produce exaggerated responses to acute inflammatory stimulation in both the ME7 model and the APP/PS1 model of neurodegenerative disease (Hennessy et al., 2015; Lopez-Rodriguez et al., 2021). Therefore, in Alzheimer's disease, the immune system of the brain is primed to respond in an exaggerated manner to any further inflammatory stimulation. This represents a profound disruption as a result of Alzheimer's pathology. The exaggerated response to acute immune activation in diseased animals is also associated with marked transient cognitive deficits that are not seen in healthy animals (Lopez-Rodriguez et al., 2021; Murray et al., 2012). (These acute and transient cognitive deficits which accompany the exacerbated immune response in aged mice or mouse models of neurodegeneration, have been used to model aspects of delirium). The superimposition of acute systemic inflammation in animal models of chronic neuropathology has negative consequences for the rate of disease progression (C. Cunningham et al., 2009; Field et al., 2010; Torvell et al., 2019). This is also true of acute inflammation and episodes of delirium in the progression of Alzheimer's disease and other

dementias (Davis et al., 2012; Fong et al., 2009; Holmes et al., 2009). These findings show that secondary inflammatory insults can trigger acute cognitive disruption (plausibly via immune priming) and set in motion a process of accelerated neurodegeneration.

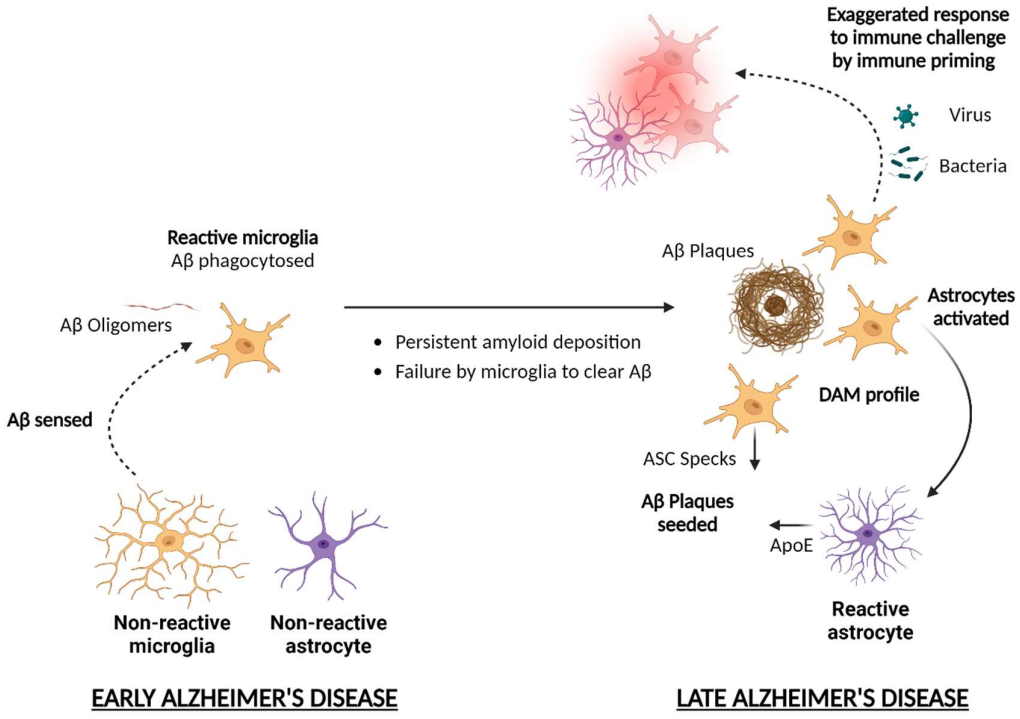

Figure 1.14. Schematic representation of immune changes in Alzheimer's disease. Amyloid-beta (Aβ). Figure created using BioRender.

In summary, the immune system is heavily involved in Alzheimer's disease. Initially, the immune system has a beneficial role in limiting the emergence of Alzheimer's pathology. Impairments in this initial immune response can increase the risk of developing Alzheimer's disease. Persistent Alzheimer's pathology leads to chronic activation of the immune system which promotes neurodegeneration and plaque deposition. The immune system also becomes primed which leads to exaggerated responses to further inflammatory stimulation – this results in cognitive deficits and

accelerated neurodegeneration. Therefore, in Alzheimer's disease the immune system has a varied role – it is initially beneficial but ultimately it contributes to disease progression.

1.7. Neuronal Dysfunction in Alzheimer's Disease

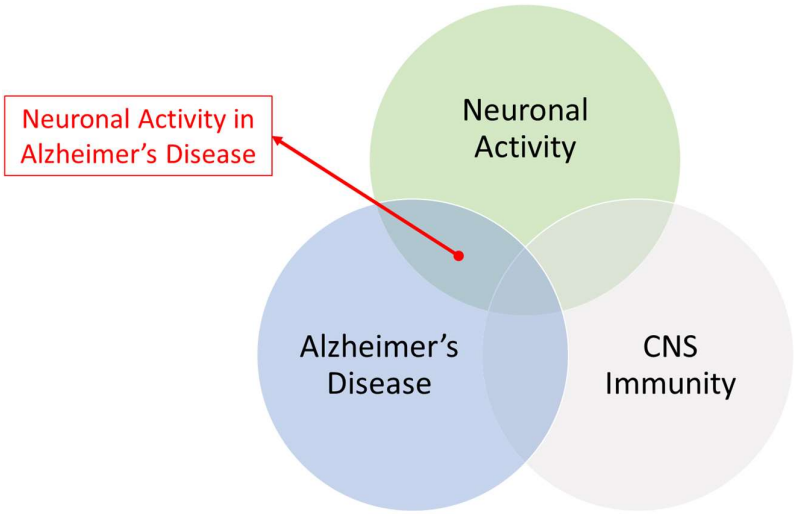

Figure 1.15. Neuronal activity – the focus of this section - in Alzheimer's disease and its relation to other topics in this thesis.

Alzheimer's disease is primarily a neurodegenerative disease. Therefore, in Alzheimer's disease there are widespread changes to neurons and neuronal activity. In Alzheimer's disease neuronal networks become more sparse as neurodegeneration progresses. It has long been known that the greatest correlate to cognitive function in Alzheimer's disease is not extracellular amyloid-beta plaques or neurofibrillary tau tangles, but is synaptic density (DeKosky et al., 1996; Terry et al., 1991). Degeneration in neurons is therefore the primary cause of clinical symptoms of Alzheimer's disease. Neurodegeneration in Alzheimer's disease is concentrated on certain populations of neurons. The loss of one such population, cholinergic neurons (which communicate via the transmission of

acetylcholine), forms the basis of the so-called cholinergic hypothesis. This hypothesis proposes that the loss of cholinergic neurons and acetylcholine neurotransmission is, at least, a partial driver of both Alzheimer's pathology and clinical symptoms (Francis et al., 1999; Hampel et al., 2018). This has led to the therapeutic use of acetylcholinesterase inhibitors as a treatment for the symptoms of Alzheimer's disease (Güntekin et al., 2023). There are many neuronal changes in Alzheimer's disease beyond the brief description provided here, however this section will focus on changes in gamma frequency neuronal oscillations and the incidence of epilepsy in Alzheimer's disease

1.7.1. Neuronal Oscillations in Alzheimer's Disease

Clinical studies carried out with EEG have shown that neuronal oscillations are disrupted in individuals with Alzheimer's disease. The general nature of this disruption is an increase in delta and theta frequency band activity and a decrease in alpha and beta frequency band activity (Huang et al., 2000; Jelic et al., 1996). Oscillations in the gamma frequency band have also been observed to be disrupted in Alzheimer's disease. Early reports suggested that gamma frequency activity was "less intense" and the "waveform was deteriorated" in individuals with Alzheimer's disease (Ribary et al., 1991) More recent work has expanded this initial definition of pathological gamma frequency oscillations in Alzheimer's disease.

Gamma frequency oscillation power, that is the proportion or amplitude of the oscillation in the gamma frequency range, is a frequent measure of gamma frequency oscillation activity. Table 1.2 and Table 1.3 detail the results of a comprehensive review of studies of gamma band power in Alzheimer's disease. These studies were carried out in both humans and a range of animal models. Upon initial inspection, the findings in this area may appear contradictory and inconclusive. However, closer examination shows that several findings are consistent across this area of research. The first commonality is cortical gamma frequency oscillation power appears to be increased in

individuals with Alzheimer's disease. This observation is common in individuals with Alzheimer's disease and in rodent models of Alzheimer's disease (Başar et al., 2016; Güntekin et al., 2023; Gurevicius et al., 2012; Jin et al., 2018; Osipova et al., 2006; Van Deursen et al., 2008; van Deursen et al., 2011; J. Wang et al., 2002, 2017; Wiesman et al., 2021)(Table 1.2).

Reports of changes to gamma frequency oscillation amplitude in the hippocampus are less consistent, however closer examination leads to some shared findings (Table 1.3). All the studies carried out in the hippocampus are from animal models of Alzheimer's disease, which is a limitation of these results. This limitation arises from the invasive nature of hippocampal recording *in vivo*. A consistent finding of these studies is that hippocampal gamma frequency oscillation amplitude is reduced in several animal model studies (at 8 months); namely, the amyloidogenic models: TAS10, J20, and 5XFAD (Driver et al., 2007; Rubio et al., 2012; Stoiljkovic et al., 2016).

The findings relating to hippocampal gamma frequency oscillation amplitude at younger ages are less consistent, specifically in the APP/PS1 model. At 2-4 months hippocampal gamma amplitude is unaffected in the amyloidogenic models: J20, TgCRND8, and APP/PS1 (Goutagny et al., 2013; Hollnagel et al., 2019; Rubio et al., 2012). This is contradicted by a study which found hippocampal gamma frequency oscillation amplitude to be increased at 3.5 months in the APP/PS1 model (Papazoglou et al., 2016). The findings from the APP/PS1 model at 3 months are therefore varied. Hollnagel et al. recorded gamma frequency oscillations induced by carbachol in *ex vivo* brain slices while Papazoglou et al. recorded spontaneous activity using *in vivo* EEG (Hollnagel et al., 2019; Papazoglou et al., 2016). Due to the differing experimental approaches, it is difficult to compare these studies. The *in vivo* finding that gamma frequency oscillations are larger in the APP/PS1 model at 3 months is supported by the observation that parvalbumin interneurons are hyperexcitable at 3 months in APP/PS1 mice (Hijazi et al., 2020). A separate, and experimentally distinct, study in the tauopathy model (TauP301L) showed that gamma frequency oscillation amplitude was reduced in mice at 3 months (Ahnaou et al., 2019). In younger mice with emerging Alzheimer's-

like pathology it is therefore difficult to see a consistent effect on gamma frequency oscillation amplitude.

There are few studies which examine hippocampal gamma frequency oscillation amplitude at late stages of pathology (i.e., beyond 12 months). In the amyloidogenic model TAS10, it has been reported that hippocampal kainate-induced gamma frequency oscillation amplitude does not differ from age-matched controls (Driver et al., 2007). Kainate-induced gamma frequency oscillation amplitude has been shown to be reduced, while carbachol-induced gamma frequency oscillations are unchanged, in the CA3 region of 5XFAD mice at 12-19 months (Mackenzie-Gray Scott et al., 2022).

Changes in gamma frequency oscillation amplitude seem more complicated in the hippocampus than in the cortex. In the cortex, gamma frequency oscillation amplitude is increased (Başar et al., 2016; Güntekin et al., 2023; Gurevicius et al., 2012; Jin et al., 2018; Osipova et al., 2006; Van Deursen et al., 2008; van Deursen et al., 2011; J. Wang et al., 2002, 2017; Wiesman et al., 2021)(Table 1.2). Changes in gamma frequency oscillation amplitude in the hippocampus are not consistent across age. Gamma frequency oscillation amplitude has been observed to have been increased or unchanged at the early stages of pathology and consistently reduced at later time points. It is commonly reported that gamma band power is reduced in Alzheimer's disease (Herrmann & Demiralp, 2005; Palop & Mucke, 2016). Based on the results discussed, it is clear this statement needs refinement. Changes in gamma frequency oscillation power/amplitude vary with brain region and with age.

As well as the amplitude or power, other metrics are used to study neuronal oscillations. Oscillatory activities in the brain coexist and interact with one another. The strength of cross frequency coupling between gamma frequency oscillations and lower frequency oscillations is increased in individuals with Alzheimer's disease (J. Wang et al., 2017). This heightened cross frequency coupling has been

suggested to represent a compensatory mechanism in the degenerating brain. However, this clinical finding is not supported by preclinical models. In many Alzheimer's disease models (5XFAD, APP23, APP-knock in and CRND8) theta-gamma cross frequency coupling is impaired (Goutagny et al., 2013; Ittner et al., 2014; Nakazono et al., 2017; Stoiljkovic et al., 2016). A similar metric used to study oscillations is the extent of synchronization or coherence between oscillations recorded at different locations in the brain. Synchronization is well reported to be reduced in individuals with Alzheimer's disease (Koenig et al., 2005; Stam et al., 2002; Tao & Tian, 2005). An additional metric used to study neuronal oscillations is the latency of oscillation emergence. Oscillation emergence has been shown to be delayed in individuals with Alzheimer's disease (Başar et al., 2016).

Very few of the studies described above comment on the frequency of gamma frequency oscillations, however in individuals with Alzheimer's disease the frequency of cortical gamma frequency oscillations has been observed to be reduced relative to healthy controls (Güntekin et al., 2023)

It is apparent from these findings that the effect of Alzheimer's disease on gamma frequency oscillations is varied and not easily classified, however what can be stated is that gamma frequency oscillations are disrupted in Alzheimer's disease. Given the role of gamma frequency oscillations in many higher order cognitive processes, and the deficit in these processes in individuals with Alzheimer's disease, it is not unreasonable to suggest that deficits in gamma frequency oscillations contribute to the clinical symptoms of Alzheimer's disease. This is supported by the observation that the extent to which gamma frequency oscillations were deficient was predictive of cognitive status in individuals with Alzheimer's disease (Wiesman et al., 2021).

These alterations in gamma frequency oscillations are a potential diagnostic biomarker for Alzheimer's disease. The excellent white paper by Babiloni et al. provides an overview of the clinical potential of EEG and magnetoencephalography (MEG) in the earlier diagnosis of Alzheimer's disease (Babiloni et al., 2020).

Author	Year	Average Age	Region Recorded	Gamma Type	Gamma Power in AD Cohort	Region Affected
Osipova	2006	72.5	Whole head	Auditory steady state response	**Increased**	Both hemispheres
van Deursen	2008	75.2	Cortex	1. Resting state, 2. Music listening, 3. Story listening, 4. Movie watching task	**Increased**	Parietal and occipital lobes
van Deursen	2011	75.2	Cortex	1. Resting state - eyes open, 2. Auditory steady state response	**Increased**	1. AD > Control at T5, T6, O2. 2. AD > MCI at T6 only
Basar	2016	67.53	Cortex	1. Sensory evoked - visual stimulation 2. Event related - oddball paradigm	**No difference/ increased**	Cortex
Wang	2017	76.88	Cortex	Resting eye closed	**Increased**	Midline frontal, central-parietal and occipital
Gaubert	2019	76.41	Cortex	Spontaneous activity while awake and relaxed	**Increased**	Cortex
Wiesman	2021	69.3	Cortex	Visuospatial task	**Increase**	Occipital cortex
Güntekin	2023	73.1	Cortex	Eyes open and eyes closed immobility	**Increased**	Cortex

Table 1.2. Changes in gamma frequency oscillation power in clinical studies of Alzheimer's disease (AD). Table shows the reference, the average subject age in the AD group, the region studied, the task during which gamma frequency oscillations were recorded, the observed changes in gamma frequency oscillation power and the region in which the effect was observed.

Author	Year	Model	Age	Region Recorded	Gamma Type	Gamma Power in AD Model	Region Affected
Wang	2002	APP/PS1	7-13 months	Hippocampus and Cortex	Spontaneous activity during alert immobility	Increased	Cortex
Driver	2007	TAS10	8 and 16 months	CA3	Kainate-induced	8 months - reduced 16 months - no difference	CA3
Rubio	2012	J20	2 and 8-9 months	Hippocampus - CA1	Spontaneous activity in freely moving mice	8 months - reduced 2 months - no difference	CA1
Gurevicius	2012	APP/PS1	16-17 weeks	Hippocampus and thalamus - implanted electrodes Cortex - scalp electrodes	Spontaneous activity in freely moving mice	Increased	Thalamus and frontal cortex
Goutagny	2013	TgCRND8	1 month	Hippocampus	Spontaneous activity	No difference	Hippocampus
Colby-Milley	2015	TgCRND8	3,7, and 11 months	Cortex	Spontaneous activity	Increased	Cortex
Stoiljkovic	2016	5XFAD	8 months	Hippocampus - CA1	Nucleus pontis oralis stimulation induced in anaesthetised mice	Spontaneous - no difference Stimulation-induced -	CA1
Papazoglou	2016	APP/PS1	14-19 weeks	Scalp electrode - Primary motor cortex Implanted electrode - CA1	Spontaneous activity in freely moving mice	Increased	CA1

Author	Year	Model	Age	Region Recorded	Gamma Type	Gamma Power in AD Model	Region Affected
Gillespie	2016	APOE-KI	4-5 and 12-18 months	Hippocampus	Activity during resting immobility	SWR-associated gamma - reduced Spontaneous gamma	Hippocampus
Iaccarino	2016	5XFAD	3 months	CA1	Spontaneous activity	Theta - no difference SWR - reduced	Hippocampus
Klein	2016	APP/PS1	4-5 months	Entorhinal cortex	Kainate-induced	Reduced	Lateral Entorhinal Cortex
Nakazono	2017	hAPP-KI	5 months	Medial entorhinal cortex	Spontaneous activity in anaesthetised mice	No difference	Medial Entorhinal Cortex
Ahnaou	2019	TauP301L	3 months	Frontal Cortex, CA1, CA3	Spontaneous activity while awake and freely moving	Reduced	Hippocampus
Stoiljkovic	2019	APP/PS1	6-12 months	CA1	Nucleus pontis oralis stimulation induced and spontaneous activity	Reduced	Hippocampus
Jin	2018	APP/PS1	14-16 months	Cortex, hippocampus and	Free moving EEG, Auditory evoked potential	Increased	Cortex, dentate gyrus, thalamus
Hollnagel	2019	APP/PS1	3 months	CA1 and CA3	Carbachol-induced gamma	No difference	Hippocampus
Mackenzie-Gray Scott	2022	5XFAD	3-4 and 12-19 months	CA1 and CA3	Kainate- and carbachol-induced gamma oscillations	Carbachol - no difference Kainate - reduced	CA3

Table 1.3. Changes in gamma frequency oscillation amplitude in preclinical studies of Alzheimer's disease (AD). Table shows the reference, the Alzheimer's disease model used, the age of the animal, the region study, the nature of gamma frequency oscillations, the observed effect of gamma frequency oscillation amplitude and the region in which the effect was observed. SWR denotes sharp wave ripple.

1.7.2. Epilepsy in Alzheimer's Disease

Epilepsy is the most common neurological disorder in the world; it is estimated that 50 million people worldwide have an epilepsy diagnosis (WHO, 2001). This disorder has a range of causes and manifestations, however it is most simply defined as a predisposition to recurrent seizures which result from excessively synchronised activity in the brain. This excessively synchronised activity occurs in hyperexcitable groups of neurons.

A link between epilepsy and Alzheimer's disease is long-recognised. The second individual diagnosed with Alzheimer's disease (Johann F.) experienced epileptic seizures (Alzheimer, 1911). However, sufficient interest has not been paid to this link until relatively recently. Neurodegeneration is known to be associated with epilepsy. As early as 1880 Sommer observed gross atrophy in the medial temporal lobe of patients with chronic epilepsy (Sommer, 1880). Therefore, seizures in Alzheimer's disease were thought to be associated with chronic neurodegeneration in the late stages of the disease. Recent work has shown that an re-evaluation of this view is necessary.

Individuals with Alzheimer's disease are at a greater risk of developing late-onset epileptic seizures than non-demented individuals (Hauser et al., 1986; Hesdorffer et al., 1996; Romanelli et al., 1990). The incidence rate of seizures in Alzheimer's disease patients has been reported as ranging from 1.5% to 23% (Scarmeas et al., 2009; Volicer et al., 1995). The risk of seizures is greater in Alzheimer's disease patients at any age than would be expected in a healthy population of the same age. The risk is greatest however for younger individuals with Alzheimer's disease (Amatniek et al., 2006; Cook et al., 2015; Irizarry et al., 2012). This is consistent with findings which strongly

associate seizures with EOAD. In patients with this form of the disease the incidence of seizures ranges from 33% to 57% (Cabrejo et al., 2006; Mann et al., 2001). Seizures have been observed in individuals with a range of EOAD-associated mutations. An inexhaustive summary of these observations are listed in Table 1.4 (for a detailed listing see: (Larner & Doran, 2006)). Seizures are also very common in individuals with Down's Syndrome that develop Alzheimer's disease. Studies have reported that as high as 78% and 84% of patients with both Down's Syndrome and Alzheimer's disease developed epileptic seizures (Evenhuis, 1990; Lai & Williams, 1989). These findings suggest that the emergence of epilepsy in the early stage of Alzheimer's disease is somehow coupled to aberrations in the amyloid pathway.

Mutation	Reference
Presenilin 1 mutation L420R	(Shrimpton et al., 2007)
Presenilin 1 mutation L166P	(Moehlmann et al., 2002)
Presenilin 1 mutation N135S	(Rudzinski et al., 2008)
APP duplication	(Wallon et al., 2012)

Table 1.4. List of EOAD mutations linked to epilepsy in carriers

The nature of seizures experienced by those with Alzheimer's disease makes it difficult to accurately assess the incidence of seizures in Alzheimer's disease. A retrospective study of individuals with AD and epilepsy found that 72% experienced complex partial seizures, which are non-convulsant (Rao et al., 2009). The subtle nature of these types of seizures, along with the individual's cognitively impaired condition, makes diagnosis of seizures difficult. This means it is likely that the incidence of seizures in Alzheimer's disease is under-reported. This view is supported by studies of

epileptiform activity using electroencephalogram in individuals with Alzheimer's disease. In an Alzheimer's disease cohort of 33 individuals (mean age: 62 years) 42.4% of patients had subclinical epileptiform activity. None of these individuals had a history of seizures (Vossel et al., 2016). This is further supported by a study which found that non-convulsive epilepsy preceded MCI diagnosis by 4 to 7 years in individuals which went on to develop sporadic Alzheimer's disease (Cretin et al., 2016). This suggests that aberrant neuronal activity, specifically neuronal hyperexcitability, is common in the early stages of Alzheimer's disease. This has been shown to have consequences for disease progression. The presence of epileptiform activity is associated with a 2.5 increase in the rate of cognitive decline in individuals with Alzheimer's disease or MCI, compared to Alzheimer's disease and MCI individuals without epileptiform activity (Vossel et al., 2013, 2016). This suggests that epileptiform activity promotes neurodegeneration.

The emergence of hyperexcitable, epileptiform activity is also seen in mouse models of Alzheimer's disease. Epileptiform activity has been observed in mouse models which overexpress amyloid-beta (hAPP and APP/PS1 mice) (Cramer et al., 2012; Palop et al., 2007; Verret et al., 2012). This activity has been attributed to: hyperexcitability induced by amyloid-beta, deficits in inhibitory interneurons, and deficits in synaptic plasticity (Busche et al., 2008; Palop & Mucke, 2016).

The increased epileptiform activity observed in Alzheimer's disease is consistent with the increase in gamma frequency oscillation power in the cortex of individuals with Alzheimer's disease and models. There is a suggestion that the increased excitability in the Alzheimer's brain may represent a compensatory mechanism in the early stages of disease (Dickerson et al., 2005; Gaubert et al., 2019; Jones et al., 2017). However, there is some doubt as to whether hyperexcitability in Alzheimer's disease is truly a positive change (Targa Dias Anastacio et al., 2022). In one clinical study individuals with MCI were given levetiracetam, an anti-epileptic drug which reduces neurotransmission by binding the synaptic vesicle protein SC2A (B. A. Lynch et al., 2004). This treatment reduced neuronal hyperactivity and led to improved performance in memory tasks (Bakker

et al., 2012). This has been recapitulated in Alzheimer's disease mouse models. Treating APP/PS1 mice with levetiracetam reduced epileptiform discharges and reversed behavioural impairments (Sanchez et al., 2012). This suggests that considering hyperexcitability as compensatory may be incorrect and instead hyperexcitability negatively contributes to disease symptoms and progression.

While it remains true that the majority of Alzheimer's disease patients that develop seizures do so late in the disease course and this is viewed as a result of severe neurodegeneration, it is evident from the above findings that epileptiform activity can be present in the prodromal and early stages of Alzheimer's disease (Risse et al., 1990). It is also clear that the presence of epilepsy is associated with accelerated disease progression (Vossel et al., 2013, 2016). Therefore, this hallmark of disease should be considered in any theory of Alzheimer's disease pathogenesis and its use as a diagnostic biomarker should be explored.

In conclusion, the activity of neuronal networks is profoundly impaired in Alzheimer's disease. The development of disease is accompanied by hyperexcitability in the form of epileptiform activity and increased amplitude in cortical gamma frequency oscillations. In the hippocampus a more complicated progression occurs, gamma frequency oscillations appear to be initially increased in amplitude and then reduced at later disease stages.

1.8. Immune effects on neuronal activity in Alzheimer's disease

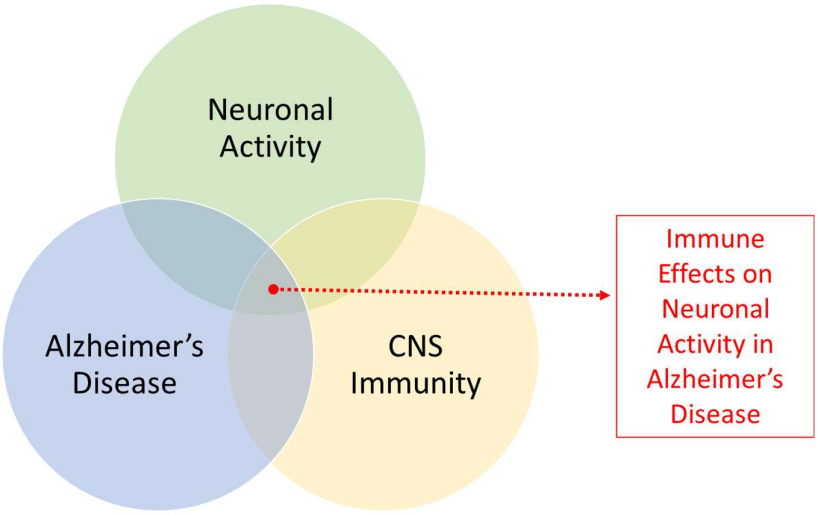

Figure 1.16. Immune effects on neuronal activity in Alzheimer's disease – the focus of this section – and their relation to other topics in this thesis.

The preceding sections give context to the central research question of this thesis, specifically, how does the immune system affect neuronal activity in Alzheimer's disease? Gamma frequency neuronal oscillations have been shown to be a critical network activity involved in higher order cognitive processes. Gamma frequency oscillations are clearly disrupted in Alzheimer's disease, along with other dysfunctions in neuronal network activity. Alzheimer's disease is also known to be associated with, and affected by, widespread changes in the immune system. There is emerging evidence that gamma frequency oscillations are modulated by the immune system. However, there has been very little research into the effect the immune system has on gamma frequency oscillations in Alzheimer's disease.

To what extent are changes in the immune system responsible for deficits in gamma frequency oscillations in Alzheimer's disease? How do gamma frequency oscillations in Alzheimer's disease

respond to increases in inflammation? Does reducing inflammation improve gamma frequency oscillations in Alzheimer's disease? These are all questions which this thesis aims to address.

Given that there are widespread changes in the immune system in Alzheimer's disease, it is difficult to isolate the effect of the immune system on gamma frequency oscillations in the disease state. Therefore, gamma frequency oscillations in brain slices from young wildtype mice will be treated with various inflammatory mediators. This will elucidate the effect of key inflammatory mediators on gamma frequency oscillations. It is hypothesised that key pro-inflammatory mediators, including IL-1β, TNFα, and CCL2, will have negative effects on gamma frequency oscillations.

In order to investigate gamma frequency oscillations in the presence of amyloidosis, gamma frequency oscillations will be induced and recorded in hippocampal brain slices from wildtype littermate controls and from the double transgenic APP/PS1 Alzheimer's disease model, a mouse generated using two well described mutations in APP and PS1 which cause EOAD (Radde et al., 2006). It is hypothesised that gamma frequency oscillations will be disrupted in APP/PS1 mice relative to wildtype littermate controls. The negative impact of inflammatory mediators on gamma frequency oscillations in wildtype mice may be similar to the deficits observed in APP/PS1 mice. This would support a causative role for specific inflammatory mediators in gamma frequency oscillation deficits in Alzheimer's disease.

In addition to examining inflammatory mediators in isolation, the effect of acute inflammatory stimulation on gamma frequency oscillations in brain slices from APP/PS1 mice will be investigated. As microglial priming may cause the immune system of the diseased or aged brain to become hypersensitive to acute immune stimulation, it is of interest therefore to determine if acute inflammatory challenges to gamma frequency oscillations in brain slices from APP/PS1 mice leads to an exaggerated or altered neurophysiological response relative to the response seen in wildtype littermate controls.

Lastly, the extent to which changes in gamma frequency oscillations in APP/PS1 mice are due to changes in the immune system will be investigated by reducing microglial proliferation in APP/PS1 mice. Microglia are the primary immune cell of the CNS. By CSF1R inhibition, microglial proliferation will be reduced in APP/PS1 mice. CSF1R inhibition has been shown to reduce inflammation and disease progression in mouse models of Alzheimer's disease (Olmos-Alonso et al., 2016). Gamma frequency oscillations will be induced in brain slices from these mice. This will investigate the extent to which changes in microgliosis drive changes in gamma frequency oscillations in Alzheimer's disease. It is hypothesised that reducing microglial proliferation will have a protective effect on gamma frequency oscillations in APP/PS1 mice.

In summary, by a variety of approaches, this thesis aims to investigate the effect of the inflammation on gamma frequency oscillations in the hippocampus of normal mice and from a mouse model of Alzheimer's disease. Given the emerging understanding that the immune system has a significant role in Alzheimer's disease, and the observed deficits in neuronal network activity in Alzheimer's disease, it is hypothesised that the immune system will impact gamma frequency oscillations in Alzheimer's disease.

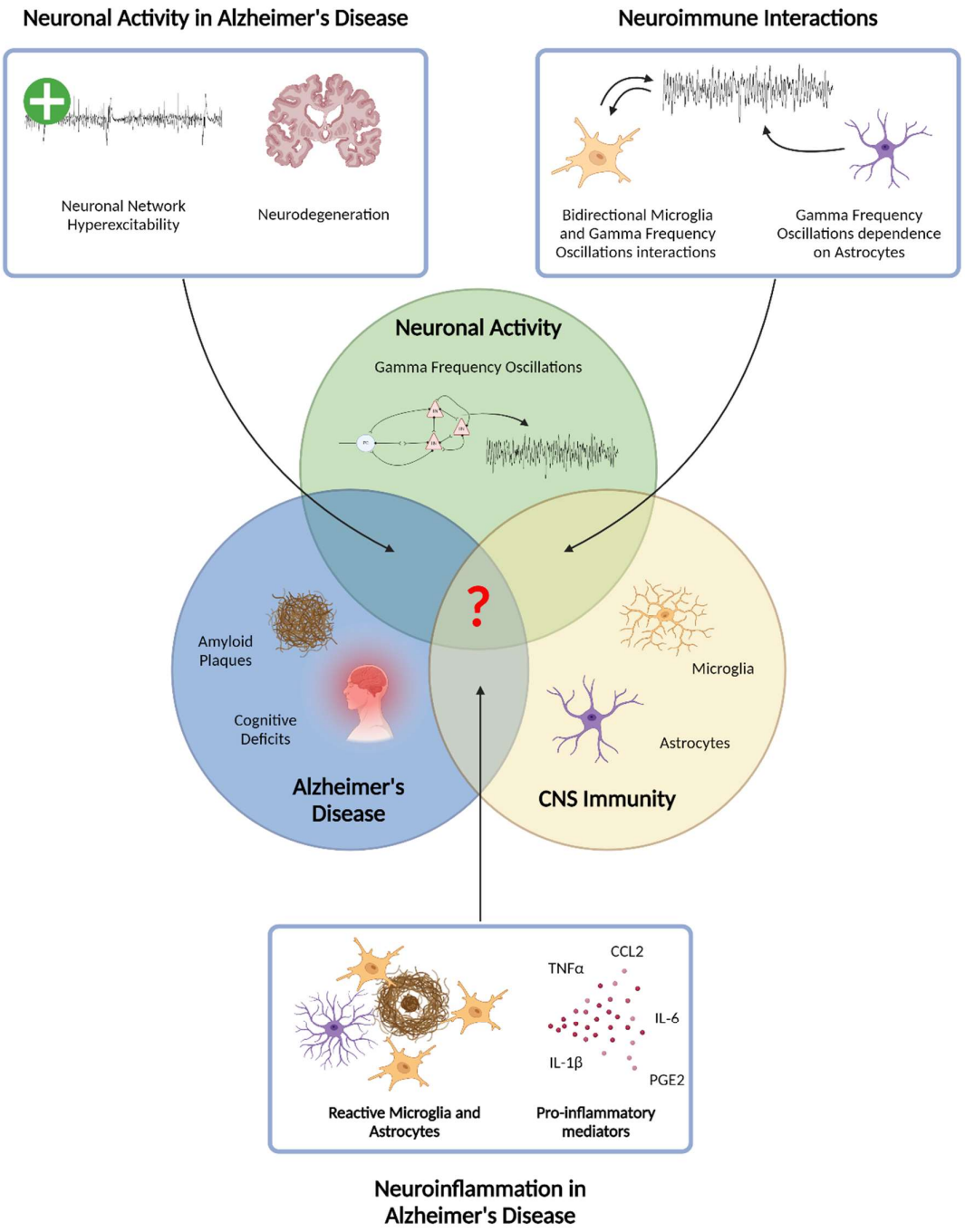

Figure 1.17. Summary of Neuronal Activity, CNS Immunity, and Alzheimer's Disease, and their interactions. Figure created using BioRender.

Chapter 2

Methods

2.1. Animals

Mice were kept in the Trinity College Dublin Comparative Medicine Unit. All procedures were carried out in accordance with EU Directive 2010/63/EU and with the approval of the Trinity Animal Welfare Body. Animals were fed *ad libitum*. C57BL/6J strain mice were used as wildtype animals. The Alzheimer's disease model used was APPSwe/PS1dE9 (APP/PS1) mice (Jax strain #005864, +/0) on a C57BL/6J background. These experiments have been approved by Trinity College Dublin Animal Research Ethics Committee and licensed by the Health Products Regulatory Authority under the individual licence AE19136 I540 granted to Hugh Delaney, and the project licences AE19136 P065 and AE19136 P155 granted to Dr Colm Cunningham.

2.2. Brain slice preparation

The mouse from which brain slices were to be prepared was placed in a bell jar. Several minutes before placing the mouse in the bell jar, the anaesthetic isoflurane (1000 mg/g, 4-5 mL, Vetpharma) was added to tissue in the base of the bell jar. The mouse inhaled the vaporised anaesthetic and was anaesthetised. Unconsciousness was verified by tilting the jar and ensuring the mouse no longer displayed the righting reflex. Once unconsciousness was confirmed, the mouse was removed from the bell jar and administered a lethal overdose of ketamine (100 mg/mL, 0.3 mL, Chanelle) and xylazine (2% w/v, 0.1 mL, Chanelle) intramuscularly to the sartorius muscle. The area where the injection was administered was lightly palpitated to aid the dispersion of the anaesthetic. Unconsciousness was verified by testing the pedal withdrawal reflex. In order to preserve neuronal network integrity, mice underwent transcardial perfusion with an oxygenated, ice-cold sucrose solution (Djurisic, 2020). The components of this solution, which is an artificial cerebrospinal fluid (aCSF), are listed in Table 2.1. Transcardial perfusion was carried out by opening the mouse along the midline and exposing the heart. The perfusing

solution (sucrose supplemented aCSF) was administered via a needle inserted into the left ventricle of the heart. The aorta was incised immediately after the needle was inserted. The perfusing solution (20-25mL) was perfused at a rate of 25 mL/min using a perfusion pump (Pump 11 Elite, Harvard Apparatus). The animal was then decapitated and the brain was removed. The brain was submerged in ice-cold, oxygenated sucrose-supplemented aCSF while brain slices were prepared.

Compound	Supplier	Product Code	Concentration
Sodium carbonate [$NaHCO_3$]	Sigma-Aldrich	223530	24 mM
Potassium chloride [KCl]	Sigma-Aldrich	P3911	3 mM
Sodium phosphate [NaH_2PO_4]	Sigma-Aldrich	S9390	1.25 mM
Magnesium sulphate [$MgSO_4$]	Sigma-Aldrich	M7506	2 mM
Calcium chloride [$CaCl_2.2H_2O$]	Sigma-Aldrich	223506	2 mM
Glucose [$C_6H_{12}O_6$]	Sigma-Aldrich	G8270	10 mM
Sucrose [$C_{12}H_{22}O_{11}$]	Sigma-Aldrich	S0389	252 mM

Table 2.1. Contents of artificial cerebrospinal fluid supplemented with sucrose.

The cerebellum and olfactory bulbs were removed. The brain was mounted horizontally, cortex-side-down on the vibratome stage. Glue (Vetbond, 3M) was used to fix the brain in place. Horizontal sections (400 μm thick) of the brain were cut using a vibratome (5100mz, Campden Instruments). The hippocampus was micro-dissected out of the brain slices. Extreme care was taken not to touch or damage the hippocampus. Hippocampal sections were mounted on tissue paper (lens cleaning paper, Whatman) and were allowed to recover at room temperature for 40

minutes at the interface of an unmodified aCSF solution and carbogen (95% oxygen, 5% carbon dioxide, BOC gases). The contents of this unmodified aCSF solution are listed in Table 2.2.

Compound	Supplier	Product Code	Concentration
Sodium carbonate [$NaHCO_3$]	Sigma-Aldrich	223530	24 mM
Potassium chloride [KCl]	Sigma-Aldrich	P3911	3 mM
Sodium phosphate [NaH_2PO_4]	Sigma-Aldrich	S9390	1.25 mM
Magnesium sulphate [$MgSO_4$]	Sigma-Aldrich	M7506	2 mM
Calcium chloride [$CaCl_2.2H_2O$]	Sigma-Aldrich	223506	2 mM
Glucose [$C_6H_{12}O_6$]	Sigma-Aldrich	G8270	10 mM
Sodium chloride [NaCl]	Sigma-Aldrich	S9888	126 mM

Table 2.2 Contents of artificial cerebrospinal fluid.

2.3. Brain slice recording

Brain slices recording took place in chambers with controlled conditions. The temperature was held at 32-34 °C using a heated water pump system. Gamma frequency oscillations have been shown to be temperature sensitive, this was accounted for by ensuring brain slices were evenly distributed across the temperature range (C. Lu et al., 2012). The chambers were constantly oxygenated with carbogen (95% oxygen, 5% carbon dioxide, BOC gases). The chamber was perfused with oxygenated aCSF (see Table 2.2) at a rate of 1.25 mL/min. After placing the slice in the recording chamber, at the interface of an aCSF solution and carbogen gas, it was allowed to recover for 15 minutes.

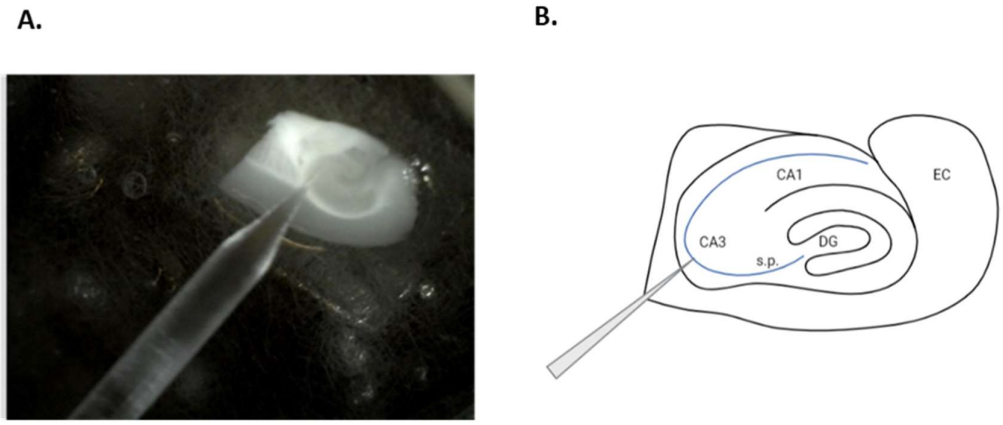

Figure 2.1. A. Image of micropipette inserted in the CA3 region of a hippocampal brain slice. Image acquired with Dino-Lite camera. **B. Schematic representation of hippocampal section with recording electrode inserted in stratum pyramidale in the CA3 region.** Regions of the hippocampus labelled: CA3, dentate gyrus (DG), CA1, entorhinal cortex (EC). The stratum pyramdiale (s.p.) is represented in blue. Figure created using BioRender.

Micropipettes were prepared from capillary tubes (30-0050, Harvard Apparatus) using a micropipette puller (Model P-1000, Sutter Instrument). Micropipettes, filled with aCSF, were attached to electrodes and inserted into head stages (D-71732 Tamm, NPI Electronic). Using micromanipulators attached to the head stage, micropipettes were inserted into the stratum pyramidale in the CA3 region of the hippocampus. A camera (5MP Dino-Lite Premier, Dino-Lite Digital Microscope) was used to visualise and magnify the slice. Figure 2.1 shows the location targeted.

The acquired signal was passed through an extracellular amplifier (EXT-10-2F, NPI Electronic), a noise filtering device (Humbug, Quest Scientific) and an analogue to digital convertor (Micro 1401 Mk II, CED) and finally to a computer where it was visualised and processed. The programme Spike2 (Cambridge Electronic Design) was used to collect and visual the recordings. Figure 2.2 is a schematic of the set-up used to acquire LFP recordings from the hippocampal

brain slices. The acquisition settings used on the amplifier and processing software are shown in Table 2.3.

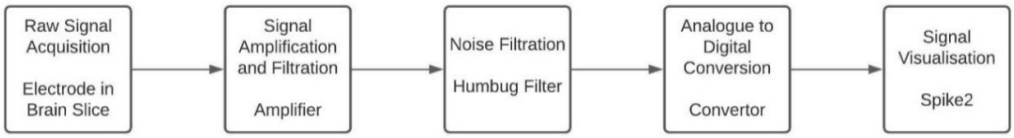

Figure 2.2. Schematic representation of electrophysiology data acquisition. Scheme shows order of data acquisition, processing and visualisation

Parameter	Value
Gain	1000
Analogue to digital conversion rate	5000 kHz
Scale	2500
Offset	0
High pass filter	100 Hz
Low pass filter	1 or 10 Hz

Table 2.3. Data acquisition settings for electrophysiology recordings. Extracellular amplifier, analogue to digital convertor, and Spike2 computer programme settings.

2.4. Gamma frequency oscillation induction

Two models of gamma frequency oscillations in brain slices were used. In the first model kainate (100 nM, Sigma-Aldrich) in aCSF was perfused across the brain slice. In the second model carbachol (20 μM, Sigma-Aldrich) in aCSF was perfused across the brain slice. In both models the emergence and progression of the oscillation was visualised and analysed in Spike2. A script was used which showed the real-time extracellular local field potential and generated a Fast Fourier transform every ten seconds from the real-time oscillation. This script also plotted amplitude and frequency parameters taken from the Fast Fourier transform. This enabled the stability, amplitude, and frequency of the oscillation to be approximated in real-time.

2.5. Established gamma frequency oscillation challenges

Once a stable gamma frequency oscillation was induced, baseline activity was recorded for at least 20 minutes. The oscillation was challenged by adding the compound of interest to the aCSF, with either kainate or carbachol also present, depending on the model in use. Following the challenge period, the compound of interest was removed and the perfusion solution in use prior to the challenge was returned, i.e., kainate or carbachol in aCSF. Table 2.4 lists the compounds used to challenge gamma frequency oscillations.

2.6. Emerging gamma frequency oscillation challenges

In order to capture the longer-term effects of neuroinflammation on gamma frequency oscillations, brain slices were incubated for three hours at the interface of carbogen and oxygenated aCSF supplemented with various inflammatory mediators. These mediators are listed in Table 2.5. Following this incubation brain slices were moved to a recording chamber and gamma frequency oscillations were induced as before.

Compound	Concentration	Product Code	Supplier
Gabazine	100-800 nM	SR95531	Sigma-Aldrich
Tiagabine hydrochloride	120 μM	4256	Tocris
TNFα	1-50 ng/mL	315-01A	Peprotech
IL-1β	10 ng/mL	401-ML	Biotechne
CCL2	1-50 ng/mL	250-10	Peprotech
PGE2	50 ng/mL	14010	Cayman Chemical
CXCL10	50 ng/mL	300-12	Peprotech
CCL11	50 ng/mL	SRP4029	Sigma-Aldrich
Anti-TNFα Antibody	100 ng/mL	MAB4101	Biolegend

Table 2.4. Compounds used to challenge gamma frequency oscillations, with the concentration used and supplier listed.

Compound	Concentration	Product Code	Supplier
TNFα	10-50 ng/mL	315-01A	Peprotech
CCL2	50 ng/mL	250-10	Peprotech
PGE2	50 ng/mL	14010	Cayman Chemical
CXCL10	50 ng/mL	300-12	Peprotech
CCL11	50 ng/mL	SRP4029	Sigma-Aldrich

Table 2.5. Compounds used to challenge gamma frequency oscillation emergence, with the concentration used and supplier listed.

2.7. Gamma Frequency oscillation analysis

Gamma frequency oscillations were first analysed by Fast Fourier transform. This is a mathematical method which decomposes waveforms into their constituent frequencies. Fourier transforms were performed in Spike2. A script was written to automate this process. The Fast Fourier transform block size was set to 8192, this showed the results in 4096 bins with a resolution of 0.61 Hz. The window type applied was a Hanning window. The script returned parameters generated from the Fast Fourier transform in the 20-80 Hz range (which was taken as the gamma frequency range), these were: the area under the curve, the peak amplitude, and the peak frequency. Figure 2.3 shows the representative results of a Fast Fourier transform carried out on ongoing gamma frequency oscillations. The parameters extracted from this analysis are also highlighted.

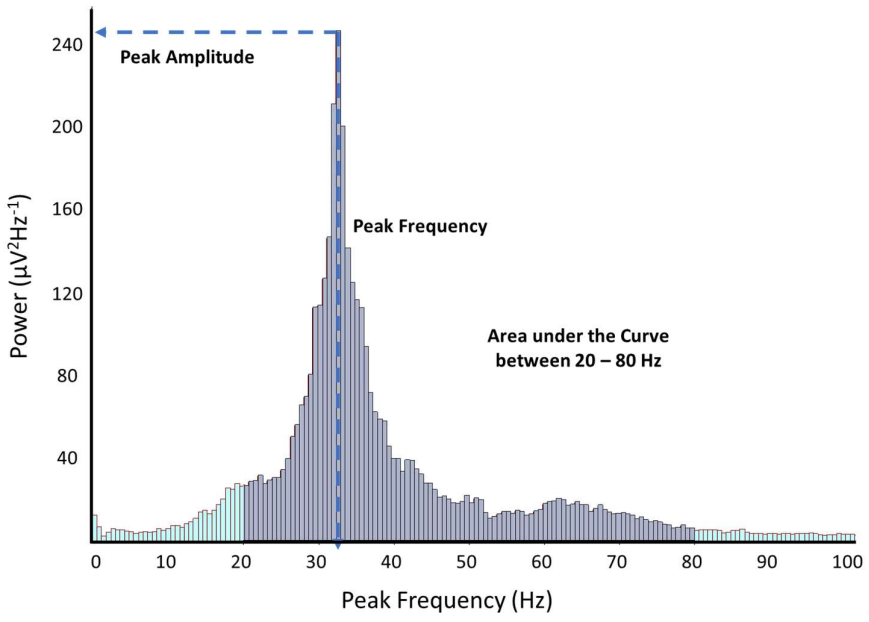

Figure 2.3. Representative results from a Fast Fourier transform carried out on gamma frequency oscillations. Parameters extracted from Fast Fourier transform marked: the area under the curve, peak amplitude, and peak frequency – between 20 and 80 Hz. Figure extracted from Spike2.

In order to reduce the slice-to-slice variability, z-scores were generated for each of the parameters extracted from the Fast Fourier transform. Using the 20 minutes of stable baseline activity (recorded before the oscillation was challenged) the baseline mean and standard deviation of each parameter were determined. A z-score was calculated for each parameter during each minute of the exposure and post-exposure period. The formula for calculating the z-score is below:

$$\boldsymbol{z\ score} = \frac{X - \mu}{\sigma}$$

Where: X is the parameter value during some minute during or after the exposure, μ is the mean parameter value during the baseline, and σ is the standard deviation of the parameter during the baseline.

In addition to analysing the oscillatory activity, epileptiform activity embedded in the oscillation was also analysed. Epileptiform events were defined as events which had an amplitude five standard deviations greater than the mean amplitude of the ongoing gamma frequency oscillation. For each slice, the mean amplitude and standard deviation of the ongoing oscillation were calculated based on a manually selected period of recording that did not have any epileptiform activity. In ten minutes of ongoing activity, instances when the recording crossed the amplitude threshold (defined as five standard deviations larger than the mean ongoing activity) were recorded along with their amplitude and length. Quantification parameters generated for each epileptiform events were: event amplitude, event length, and event frequency. The MATLAB programme script used to quantify epileptiform events is in the appendix to this chapter.

2.8. Oestrous cycle monitoring

It has been observed that gamma frequency oscillations can be affected by the oestrous cycle in female mice (Barth et al., 2014). Therefore, it was of interest to determine the stage of the oestrous cycle for female mice at the time of death.

Immediately post-perfusion, vaginal lavage was performed. Before carrying out the lavage, in order to reduce the number of urea crystals in the sample, traces of urine were removed by rinsing the exterior of the genitalia with deionised water. Physiological saline (0.9 % w/v NaCl in H_2O, 100 μL, Sigma-Aldrich) was flushed in and out of the vagina 7-10 times. The pipette tip was positioned at the opening of the vagina. The collected vaginal sample was placed on a slide and allowed to air dry; this took up to several hours.

Once the sample was entirely dry it was stained using modified Wright's stain (Sigma-Aldrich). Between 0.5 and 1 mL of the stain was placed on the sample. After 30 seconds an equal volume of deionised water was added to the stain on the slide. The stain was gently blown on to ensure mixing. Following 90 seconds, the stain was removed with excess deionised water. Care was taken not to wash the deionised water directly onto the sample in order to avoid removing the sample. The edges of the slide were then dried with tissue paper and allowed to air dry for 30 minutes.

The stained sample was visualised using an objective microscope (Olympus CX21, Olympus). The stage of the oestrous cycle was determined based on the presence of certain cell types and the relative abundance of these cell types. The cell types which fluctuate across the oestrous cycle are leukocytes, cornified epithelia, and non-cornified nucleated epithelia. Figure 2.4 shows how the relative abundance of these cell types changes across the oestrous cycle. Using the tool in Figure 2.4, the stage of the oestrous cycle was determined and recorded. The sample was imaged using a camera attachment (Eyecam Plus, Brunel).

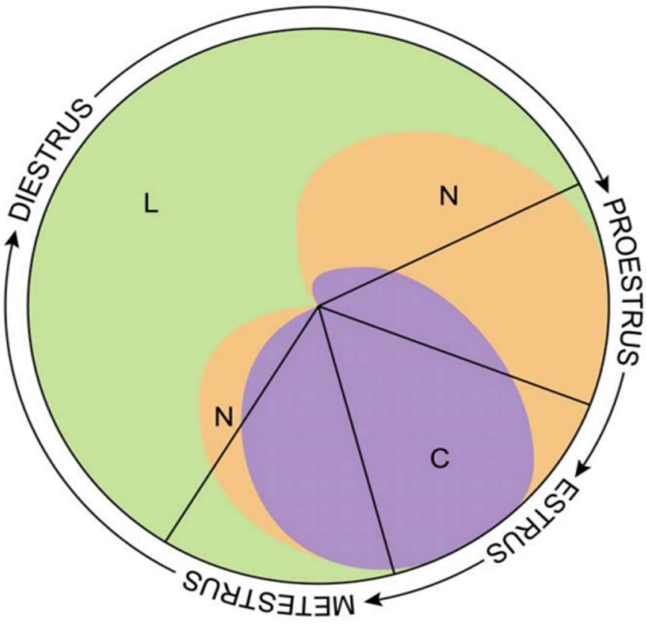

Figure 2.4. Oestrous cycle stage identification tool. The four stages of the oestrous cycle are represented with arrows indicating the order in which the stages occur. The size of the quadrants is approximate to the relative length of each of the phases. The three cell populations, and their relative abundance during each phase, are represented by the coloured areas (green = leukocytes, orange = nucleated epithelia, purple = cornified epithelia). Figure taken from Byers et al. 2012.

2.9. Immunohistochemistry

Slices of brain tissue used for electrophysiology were fixed in paraformaldehyde (PFA) (4% w/v in phosphate buffered saline 1X, Sigma-Aldrich) immediately after electrophysiology. Slices were kept in PFA for a minimum of 48 hours at 4 °C. Brain tissue collected for immunohistochemistry which did not undergo electrophysiology recordings was also fixed in PFA (4% w/v).

Preserved brain slices were sectioned from 400 µm to 40 µm using a freezing sledge microtome (1400, Leitz). In order to cryopreserve the tissue, prior to sectioning slices were transferred from PFA to a sucrose-supplemented Trizma-buffered saline (TBS) solution (30% w/v sucrose in Trizma (0.06% w/v) and NaCl (0.85% w/v) in water, pH 7.4, Sigma-Aldrich). Sectioned slices

were serially distributed across a 24-well plate to representatively capture all depths within the slice. Larger PFA-fixed brain tissue was sectioned in the same manner.

The protocol used for each antibody was optimised. Therefore the protocol differs for each antibody. Table 2.6 lists the specific protocols for each antibody. A general protocol will now be described.

Throughout the protocol, sections were agitated on a rocking plate. In order to perform antigen retrieval in PFA-fixed tissue, sectioned brain slices were incubated several times in hot sodium citrate (50 mM, pH 6, 85 °C, Sigma-Aldrich) for five minutes. Following this antigen retrieval step, the tissue underwent three five-minute washes in TBS or TBS with Tween (TBS-T)(TBS with Tween-20 (0.05% v/v), Sigma-Aldrich). The endogenous peroxidase activity was quenched by incubating the tissue for 30 minutes in a hydrogen peroxide solution (H_2O_2 (0.3% v/v) in methanol (70% v/v) in TBS or H_2O_2 (0.3% v/v) in TBS, Sigma-Aldrich). This was followed by three five-minute washes in TBS/TBS-T as before.

Off-target binding was blocked by incubating the tissue in a blocking solution. The blocking solution was either casein (casein (1% w/v) in TBS, VWR, or normal goat serum (NGS)(5% v/v) in TBS, Vector Laboratories). Again, the tissue underwent three five-minute washes. The tissue was then incubated in the relevant primary antibody diluted in TBS with Tween (0.05% v/v) or Triton (0.03% v/v, Sigma-Aldrich) and NGS (5% v/v). Table 2.7 details the primary antibodies and their concentrations. Tissue was incubated for at least 12 hours in the primary antibody at 4°C.

The primary antibody was then removed, and the tissue underwent three five-minute washes in TBS/TBS-T. The tissue was incubated for two hours in the relevant biotinylated secondary antibody diluted in TBS with Tween (0.05% v/v). Table 2.8 details the secondary antibodies. The secondary antibody used depended on the host species of the primary antibody.

After the secondary antibody incubation was complete the tissue underwent three further five-minute washes in TBS/TBS-T. Tissue was then incubated in horseradish peroxidase conjugated to streptavidin (Vector Laboratories) for one hour. Following this, the tissue underwent three five-minute TBS/TBS-T washes. The chromogenic reaction was then carried out. Tissue was incubated in a diaminobenzene (DAB) solution (diaminobenzene and urea hydrogen peroxide in water, Sigma-Aldrich). In some instances, ammonium nickel sulphate (0.06% w/v, Sigma-Aldrich) was added to the chromogenic reaction to give the precipitate a black colour. The tissue underwent a final three five-minute washes in TBS/TBS-T. The tissue was then mounted on slides coated in a gelatine solution with chromium potassium sulphate dodecahydrate. The slides were left to dry overnight.

The following day, slides were washed briefly (less than ten seconds) in a bath of deionised water. Slides were passed through a concentration gradient of ethanol (70%, 95%, 100% v/v in water). Slides spent five minutes in each concentration of ethanol. Slides were incubated twice in the 100% ethanol solution, in separate baths. Finally, slides were incubated in a xylene-substitute solution (Sigma-Aldrich) for five minutes, twice. Coverslips were placed on the slides. DPX (Sigma-Aldrich) was used as a mounting medium. Slides were allowed to dry.

Antibody	Buffer	Antigen Retrieval	Quenching	Blocking	Primary Antibody
Parvalbumin	TBS	2 x 5 mins Sodium Citrate	0.3% H_2O_2 in 70% Methanol	1% Casein 1 hour	1:5000, >12 hours 0.05% Tween 5% NGS
Somatostatin	TBS	3 x 5 mins Sodium Citrate	0.3% H_2O_2 in TBS	5% NGS 2 hours	1:5000, >12 hours 0.1% Triton 5% NGS
Neu-N	TBS	2 x 5 mins Sodium Citrate	03% H_2O_2 in TBS	5% NGS 1 hour	1:2000, >12 hours 0.05% Tween 5% NGS
GFAP	TBS-T	2 x 5 mins Sodium Citrate	0.3% H_2O_2 in TBS	5% NGS 1 hour	1:6000, >12 hours 0.05% Triton 5% NGS
Iba1	TBS-T	2 x 5 mins Sodium Citrate	0.3% H_2O_2 in TBS	5% NGS 1 hour	1:2000, >12 hours 0.05% Triton 5% NGS
PU.1	TBS-T	2 x 5 mins Sodium Citrate	0.3% H_2O_2 in TBS	5% NGS 1 hour	1:250, >48 hours 0.3% Triton 5% NGS
p16	TBS-T	2 x 5 mins Sodium Citrate	0.3% H_2O_2 in TBS	5% NGS 1 hour	1:300, >48 hours 0.3% Triton 5% NGS
Synaptophysin	TBS-T	2 x 5 mins Sodium Citrate	0.3% H_2O_2 in TBS	5% NGS 1 hour	1:330, >12 hours 0.1% Triton 5% NGS

Table 2.6. Summarised protocols for each antibody.

Target	Manufacturer	Host Species	Product Code	Dilution
Parvalbumin	Sigma-Aldrich	Mouse	P3088	1:5000
Somatostatin	BMA Biomedicals	Rabbit	T-4103	1:5000
Neu-N	Millipore	Guinea Pig	MAB377	1:2000
GFAP	Dako	Rabbit	M0761	1:6000
Iba1	Wako	Rabbit	019-19741	1:2000
PU.1	Cell Signalling	Rabbit	2266	1:250
p16	Abcam	Rabbit	ab211542	1:300
Synaptophysin	Abcam	Rabbit	ab18258	1:330

Table 2.7. Primary antibodies used with supplier and concentration listed.

Target	Manufacturer	Host Species	Product Code	Dilution
Anti-Mouse	Vector Laboratories	Goat	BA-9200-1.5	1:200
Anti-Guinea Pig	Vector Laboratories	Goat	BA-7000-1.5	1:200
Anti-Rabbit	Vector Laboratories	Goat	BA-1000-1.5	1:200

Table 2.8. Secondary antibodies used with supplier and concentration listed.

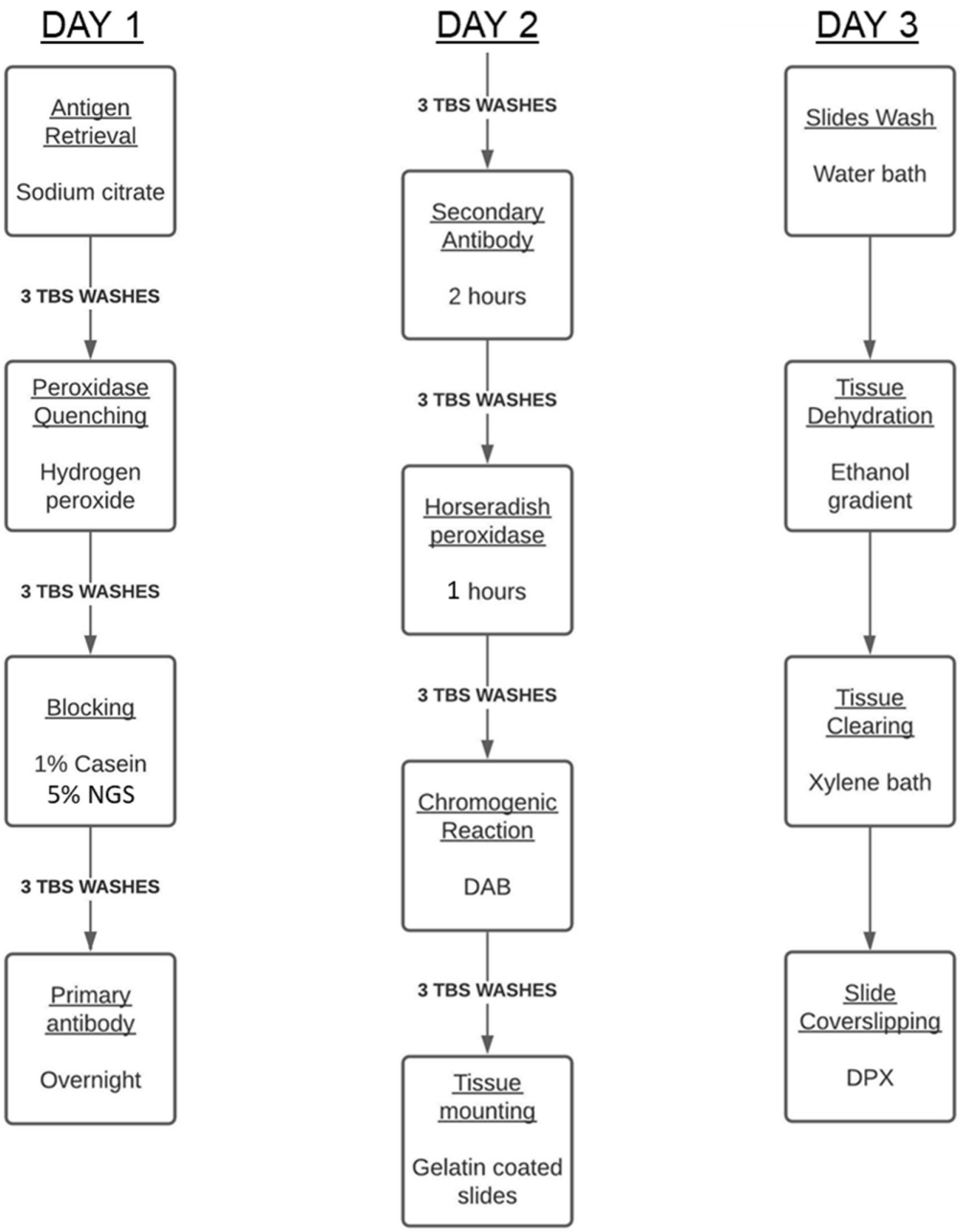

Figure 2.5. Flow-chart representation of the immunohistochemistry protocol. The protocol for day 1, 2, and 3 are in columns 1, 2, and 3 respectively.

2.10. Immunohistochemistry analysis

Tissue was visualised using a light microscope. Images were acquired using a camera insert on the microscope (Olympus CX21 with Eyecam Plus, Brunel and DM3000 Imaging microscope, Leica). In ImageJ (Schindelin et al., 2015), with reference to a brain atlas the various subregions of the hippocampus were identified. Immunohistochemistry for parvalbumin, somatostatin, and PU.1 was manually quantified in ImageJ. Cell counts were expressed as densities by measuring the area of the regions quantified.

Immunohistochemistry for GFAP and Ionized calcium binding adaptor molecule 1 (Iba1) were quantified by measuring the percentage area stained in ImageJ.

Immunohistochemistry for NeuN was automatically quantified in ImageJ using a macro optimised on a manually quantified representative sample of images. Cell counts were expressed as densities by measuring the area of the regions quantified.

2.11. Histology – Harris haematoxylin and Congo red

In order to provide context to certain immunohistochemistry staining, Harris haematoxylin (VWR) was used as a nuclear counterstain. Tissue mounted on slides was placed in Harris haematoxylin for 5 seconds. Slides were then transferred to an acid alcohol solution (1% v/v concentrated hydrochloric acid in 70% v/v ethanol) for 10 seconds to allow the Harris haematoxylin stain to differentiate. Slides were briefly washed in a bath of deionised water. Slides were then moved to Scott's tap water (0.2% w/v potassium bicarbonate, 3% w/v magnesium sulphate) for 10 seconds. Following Harris haematoxylin staining slides were dehydrated and cover-slipped as normal.

Amyloid-beta plaques were visualised by carrying out Congo Red staining. Tissue mounted on slides was placed in Congo Red stain (0.5% w/v Congo Red (Sigma-Aldrich) in 50% v/v ethanol)

for 15 minutes. Slides were then washed in two baths of deionised water; excess stain was removed by dipping the slides in the first, and then the second, water bath for approximately 5 seconds in each. The stain was differentiated by placing the slides in alkaline alcohol (1% v/v of 1% w/v sodium hydroxide in 50% v/v ethanol). The intensity of the staining was monitored by periodically checking the slides under the microscope throughout the differentiation. Generally, the differentiation took 20-25 minutes. After the differentiation was completed, slides were placed in regular tap water for one minute. Slides were then dehydrated and cover-slipped as normal.

2.12. GW2580 study

In order to study the contribution of microglial proliferation to observed changes in the APP/PS1 brain, both APP/PS1 mice and wildtype littermate controls were treated with an inhibitor of colony stimulating factor receptor 1 (CSFR1). The inhibitor used (GW2580) was made up in the mice's diet and administered over a period of three months. GW2580 (LC Laboratories, Boston) was made up in the mice's diet by TestDiet at a concentration of 1000 ppm (20 g of drug in 20 kg of diet). The control group in this study were given an identical diet to mice on the GW2580 diet, less the GW2580.

Throughout the treatment mice were monitored to ensure they were consuming the modified diet and that they were not adversely affected by the diet. Prior to assigning mice to their treatment group, mice in the cohort were ranked based on their performance in Y-maze testing. This ensured that the control and treatment groups were balanced with respect to baseline cognitive ability. Throughout behavioural testing the experimenter was blinded to the mouse's genotype, however it was not possible to blind the treatment group as the GW2580-suplpemented diet is red while the control diet is brown.

2.13. Y-maze

APP/PS1 mice and wildtype littermate controls underwent Y-maze training in order to determine their baseline cognitive status prior to assigning them to treatment groups in the GW2580 study. This paradigm tests mice's ability to learn an exit location with reference to extra-maze visual cues. A clear Perspex Y-maze with three arms (length: 30 cm, width: 8 cm, height: 13 cm) was positioned a fixed position. Visual cues were placed around the maze at heights that made them clearly visible from within the maze. The base of the maze was filled with water (20-22 ˚C) to a height of 2 cm. Mice were assigned an exit arm which was fixed across all training trials. Exit arms were assigned in a balanced manner based on both sex and genotype. Mice were trained across four days with 12 trials on each day. The purpose of training being that each mouse would learn its assigned exit arm. For each trial, mice were first moved to a holding cage for 15 seconds to ensure they were fully aroused. Mice were then placed in one of the two maze arms, which were not their assigned exit arm, in a pseudorandom order. The time taken to locate the exit and the sequence of arms entered were recorded. If mice took more than 60 seconds to locate the exit they were directed to the exit using a guillotine arm. Mice exited the maze via a burrow tunnel, which was used to return them to their home cage.

Following four days of training , the location of the exit arm was changed. This is known as a reversal assay. This tests how well mice can discard what they have previously learned and learn a new exit location. The cohort underwent 12 trials with the new exit location across a single day. The success and speed with which they learned, or did not learn, the new exit location was used to rank the mice. In instances where mice could not be separated based on their performance in the reversal assay, the time it took for mice to learn the original exit location (which was taken as having consecutive 5 correct trials) was used to rank mice.

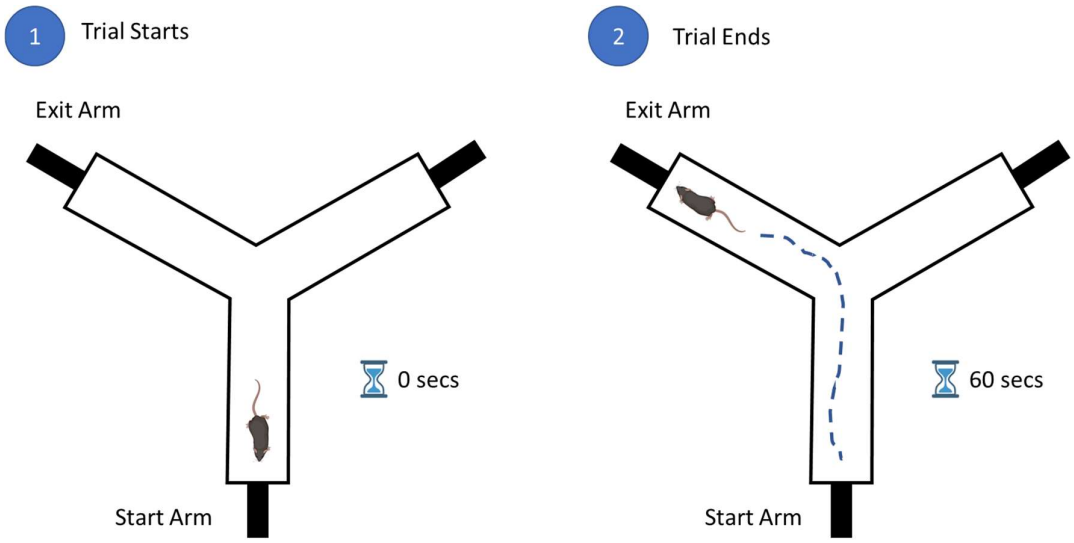

Figure 2.6. Schematic representation of a successful trial in the Y-maze. Mice have 60 seconds to find their designated exit arm.

2.14. Spontaneous alternation in a T-maze

In order to assess hippocampal function and short-term memory, mice underwent spontaneous alternation testing in a T-maze. The protocol described by Deacon et al. was used (Deacon & Rawlins, 2006). The T-maze used had arms which were 30 cm long and 9 cm wide. A partition which was 14 cm long was placed in the centre of the maze. The maze was 20 cm in height. Guillotine doors were suspended at a height of approximately 5 cm at the entrance to two of the arms. In order to motivate the mice to explore the maze, bedding from a cage housing the opposite sex to the mouse being tested was scattered on the maze floor.

For a trial, the mouse was placed in the central start arm facing the wall. The mouse was allowed to choose an arm to enter (left or right). After entering one of the two arms, the mouse was enclosed in the chosen arm by closing the guillotine door. The mouse was left in its chosen arm for 30 seconds. The mouse was then removed from its chosen arm and returned to the start arm. With the central partition removed and both of the guillotine doors open, the mouse was allowed

to choose one of the arms (left or right). If the mouse chose a different arm than its first choice it received a score of one and was considered to have recalled its initial choice and to have spontaneously alternated on its next choice. If the mouse chose the same arm as its first choice it received a score of zero and was considered to have forgotten its initial choice. Mice underwent 10 trials over two days (5 trials per day). Mice which did not move or make a choice in 90 seconds were considered to have failed the trial.

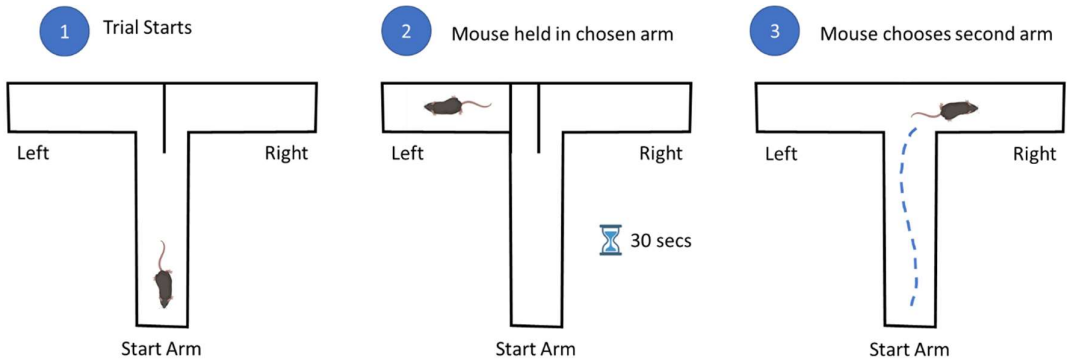

Figure 2.7. Schematic representation of a successful trial in the T-maze. Mice initially choose the left or right arm. Mice are then held in their chosen arm for 30 seconds. Mice are returned to the start arm and allowed to choose the left or right arm. In a successful trial mice will choose the opposite arm to their initial choice.

2.15. Morris water maze

Mice were trained on the Morris water maze (MWM) to assess their ability to use visual-spatial cues to learn the location of a hidden platform. In a tank of diameter 150 cm, filled with water to 31 cm, a platform (with diameter 11.5 cm) was submerged 1 cm below the surface of the water. Visual cues were prominently positioned outside the maze. The water was at a temperature of 20-21 °C and coloured with tempura paint powder. The maze was divided into four quadrants – North, South, East, and West. Each mouse was pseudo-randomly assigned a fixed platform

location within one the four quadrants. Mice were trained to learn this location across 20 trials. Prior to training mice were handled once a day for approximately a week in order to familiarise them with the experimenter. Mice underwent five days of training with four trials on each day. Before each trial mice were moved to a holding cage for one to three minutes. For each trial, mice were moved in a cupped hand to the maze and gently placed facing the wall of the maze in a pseudorandomised starting location – this location was never in the quadrant which contained the platform. Mice were given 60 seconds to locate the platform. Using a camera, mounted on the ceiling, the mice were recorded in the maze. Using ANY-maze software the location and speed of the mice were tracked and recorded. ANY- maze also recorded the time taken to locate the platform. Once the platform was located, mice were removed from the maze, dried by hand, and placed in a heated (35 ˚C) recovery cage. If the platform was not found within 60 seconds, mice were guided to the platform. In instances where the mouse was guided to the platform, they were left on the platform for 15 seconds to facilitate learning and then moved to the recovery cage.

After 20 trials of training were completed the mice underwent a single probe trial to test how well they had retained the location of the platform. The probe trial took place a day after the last day of training. During the probe trial the platform was removed from the maze. For the probe trial, the start position of each mouse was in the quadrant opposite the quadrant in which the platform had been located during training. The probe trial lasted 60 seconds. ANY-maze recorded the amount of time spent in each quadrant and the number of times the location where the platform had been was manually counted. Mice were considered to have learned and retained the platform location if they spent the majority of their time in the quadrant which had contained the platform. The ability of mice to locate a clearly visible platform was assessed in order to confirm that differences observed in learning were not due to visual deficits in any mice. Two trials were carried out in which a flag (width: 25 cm, height: 17cm) was attached to the platform. The flag-platform

was located in the quadrant opposite the quadrant which contained the platform during training. Additionally, three trials were carried out in which the platform was raised 1 cm above the level of the water. Again, the visible platform was not located in the quadrant which contained the platform during training. Trials were carried out as they were during training. Mice which did not readily locate the visible platform were considered to have visual deficits.

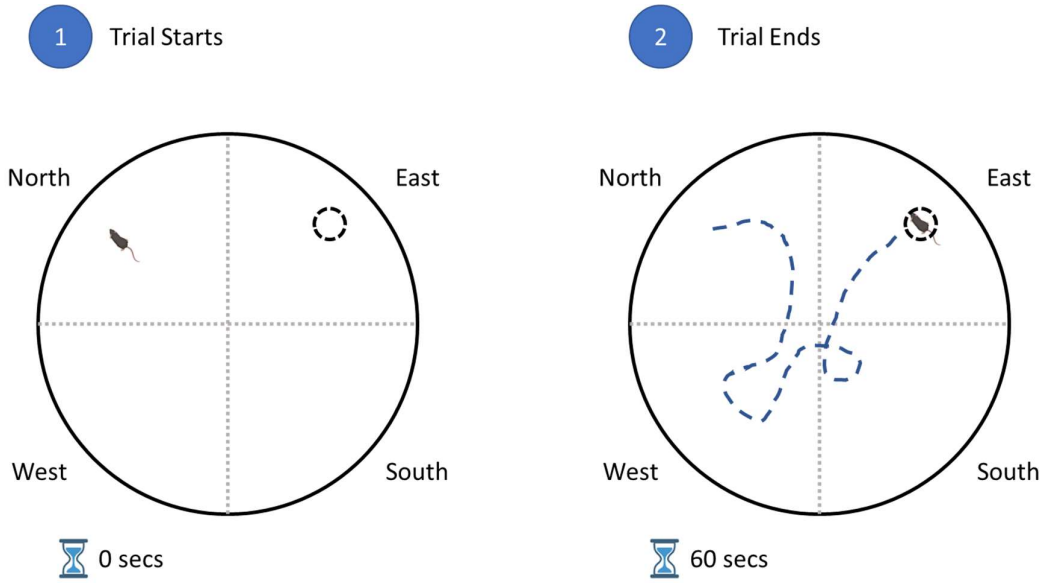

Figure 2.8. Schematic representation of a successful trial in the Morris water maze. Mice are placed in a quadrant which does not contain the hidden platform (small dashed circle). The trial ends when mice locate the hidden platform or when 60 seconds have elapsed.

2.16. Glial cell isolation by fluorescence-activated cell sorting

In order to examine the effects of GW2580 treatment in APP/PS1, glial cells were isolated using fluorescence-activated cells sorting (FACS) and underwent gene expression analysis by quantitative polymerase chain reaction (qPCR). Mice were terminally anaesthetised with sodium pentobarbital administered interperitoneally (2 g/kg, Euthatal). In order to partially clear the brain parenchyma of blood, animals were briefly transcardially perfused with heparinised saline

(0.9% w/v NaCl, 0.1% v/v Heparin, 5mL, Leo Pharma). Following perfusion, the animal was decapitated and the brain was removed. The brain was bisected along the midline. Using two pairs of tweezers, on an ice-cold petri-dish, the hippocampus and overlying cortex was dissected and placed in Hank's buffered saline solution (HBSS)(Sigma-Aldrich) on ice.

In the bowl of a sterile spoon, using a sterile scalpel blade, the extracted brain tissue was chopped to a fine consistency. The homogenised tissue was transferred to 2 mL of an enzymatic digestion (foetal bovine serum (5% v/v, Biosciences), HEPES in HBSS (10 μM, Sigma-Aldrich), Collagenase A (2mg/mL, Roche), DNase (2U/mL, ThermoFisher)) and incubated at 37 °C for 45 minutes. Every five minutes the solution was mixed by inversion. Every 15 minutes, the solution was triturated by slow, repeated passage through a pipette, approximately 20 to 30 times. In order to minimise cell lysis, care was taken not to aggressively or quickly passage the solution through the pipette. The homogeneous post-digestion solution was filtered using a 70 μm cell strainer (Sigma-Aldrich). The solution was washed through the strainer with chilled magnetic-activated cell sorting (MACS) buffer (Miltenyi). The filtered solution was centrifuged (1400 rpm, 4 °C, ten minutes). The supernatant created by centrifugation was discarded as it only contained the digestion solution and MACS buffer.

The pellet generated by centrifugation was resuspended in 50 μL of a blocking solution (CD16/CD32 antibody at 1 in 100 in MACS buffer, Fisher Scientific) which blocks Fc receptors and reduces off-target antibody binding. The resuspended pellet was incubated on ice in the blocking solution for 20 minutes. The primary antibodies were then added directly to the sample and blocking solution. The primary antibodies used were: CD11b FITC (to label microglia)(BioLegend), CD45 APC (also to label microglia)(BioLegend), and GLAST ASCA-1-PE (to label astrocytes)(BioLegend). The cell viability dye, 7-Aminoactinomycin D (7-AAD)(BD Biosciences), was also added to each sample (5 μL per sample). All antibodies were used at a final concentration of 1 in 100 in MACS buffer. The final volume of the solution was

approximately 100 μL, as 50 μL of the primary antibody and 7-AAD solution was added to the sample which was resuspended in 50 μL of the blocking solution. The samples were incubated on ice in the primary antibody solution for 30 minutes. The excess, unbound antibody was removed by adding MACS buffer and centrifuging (1400 rpm, 4 ˚C, ten minutes) the samples. The supernatant was once again discarded. The pellet was gently resuspended in 200 μL of MACS buffer.

The digested, antibody-labelled samples were sorted using a BD FACS Aria Cell sorter in the Flow Cytometry Facility by Dr Barry Moran and Ms. Aoife O'Rourke. Sorted cells were collected directly into 800 μL of LS-Trizol (Biosciences) and stored on ice. Trizol maintains RNA integrity while also lysing cells. The sorted cell populations were selected using the gating strategy in Figure 2.9. For both populations, debris was initially removed based on the forward-scatter area (which is indicative of cell size) versus the side-scatter area (which is indicative of cell granularity or complexity). Doublets were removed by two sequential gating strategies – firstly, using forward-scatter area versus forward-scatter width, and secondly, side-scatter area versus side-scatter width. Having identified single cells, dead cells were excluded using the viability dye 7-AAD (which binds to DNA in lysed cells) versus forward-scatter area. Microglia and astrocytes were identified using fluorescence from the primary antibodies used to label the sample versus the forward-scatter area. Microglia were defined as high-CD11b-FITC and intermediate CD45-APC labelled cells. Astrocytes were defined as high GLAST-1-PE labelled cells.

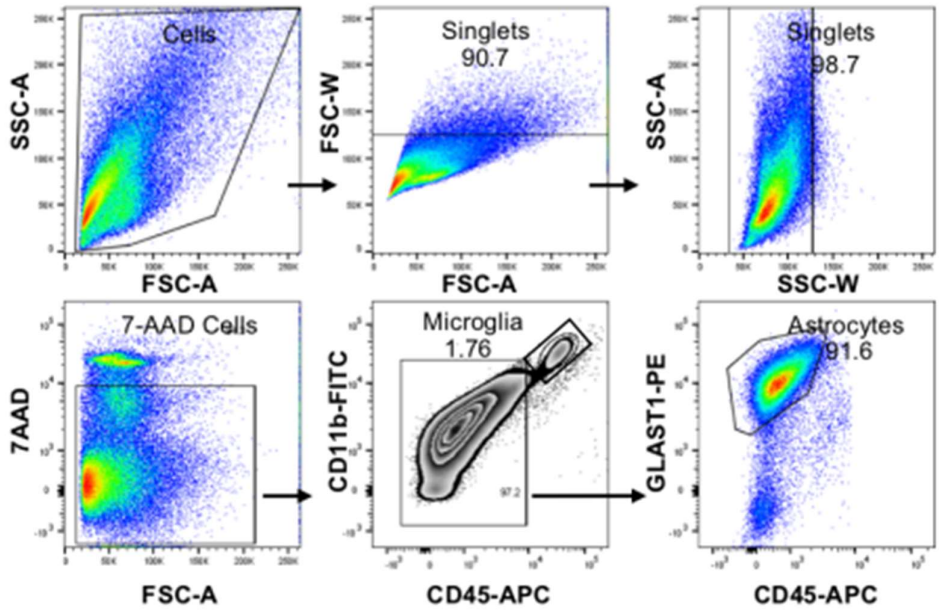

Figure 2.9. Gating strategy used in FACS to isolate microglia and astrocytes. All cells were initially sorted based on forward and side scatter to isolate single cells. Live cells were selected based on the viability marker 7-AAD. Microglia were identified based on high CD11b-FITC and intermediate CD45-APC staining. Astrocytes were identified based on high GLAST1-PE staining.

No more than 80,0000 cells of either cell type were collected. This was in order to avoid diluting the Trizol reagent. This threshold was almost always reached for astrocytes. However, it was never reached for microglia.

2.17. RNA isolation

The sorted cells in Trizol were vortexed for approximately 10 seconds. In order to isolate the RNA from the Trizol, 200 µL of chloroform (Sigma-Aldrich) was added to the sorted cells in Trizol. The samples were shaken vigorously for 15 seconds to thoroughly mix the Trizol and chloroform. The samples were incubated for 3 minutes at room temperature. The samples were

then centrifuged (12,000 g, 4 °C, 15 minutes) to separate the solution into an aqueous and organic phase. The aqueous phase, which contains the RNA, was carefully removed and transferred to a LoBind Eppendorf tube. The RNA was precipitated by adding 500 µL of isopropanol to the isolated aqueous phase. The samples were incubated for 10 minutes at room temperature following this addition. To further aid precipitation, 10 µL of glycogen (ThermoFisher) was added to the samples. At this point, the samples were stored overnight at minus 20 °C.

The following day, the samples were centrifuged (12,000 g, 4 °C, 10 minutes). The supernatant was discarded and the pellet, which contained the RNA, was kept. The pellet was washed by adding ice-cold ethanol (75% v/v) and centrifuging the sample (7,500 g, 4°C, 10 minutes). Following this wash, the supernatant was discarded. The pellet was gently resuspended in a DNase digestion solution (DNase in DNase RDD buffer and RNase free water). After 15 minutes at room temperature, the DNase digestion was stopped by adding ethanol (75% v/v). The samples were then centrifuged (7,500 g, 4 °C, 10 minutes). The supernatant was discarded. The pellet was dried for 10 minutes at room temperature. The pellet was then resuspended in 20 µL of RNase-free water with a RNase inhibitor (Ribolock at a 1 in 100 dilution, Fisher Scientific) added. The RNA concentration of each sample was determined using the Nanodrop ND1000 spectrophotometer (Thermo Fisher Scientific). Samples were stored at minus 80 °C.

2.18. cDNA synthesis

In order to examine gene expression in isolated cells, copy DNA (cDNA) was synthesised from isolated RNA. The iScript cDNA synthesis kit (BioRad) was used to synthesis cDNA. This high sensitivity kit was required given the low RNA concentration in cells isolated by FACS. A separate reaction was prepared for each sample in a PCR tube. As per the kit instructions, RNA was added to the reaction at a concentration of 3 ng/µL. The reaction also contained 5X iScript

Reaction Mix (4 μL), iScript Reverse Transcriptase (1 μL), and RNase-free water (adjusted based on RNA volume to being overall volume to 20 μL). Two controls were also prepared for each cDNA synthesis. The first control did not have any RNA, this was to control for any possible RNA contamination in the cDNA synthesis. The second control did not have any reverse transcriptase, this was to control for any possible DNA contamination in the cDNA synthesis. Once all reaction mixes were complete, the samples were picofuged for approximately 30 seconds. Samples were loaded in the thermocycler (Peltier Thermal Cycler PTC-200). The thermocycler cycle had three stages: firstly, the samples were heated to 25 ˚C for 5 minutes to prime the reaction mix, secondly, the samples were heated to 46 ˚C for 20 minutes to activate the reverse transcriptase, thirdly, the samples were heated to 95 ˚C for one minute to inactivate the reverse transcriptase. The thermocycler then cooled to 4 ˚C and held at this temperature until the samples were removed and stored at 4 ˚C. Prior to use, post-cDNA synthesis, the samples were picofuged for approximately 30 seconds. The samples were also diluted one in two with RNase-free water. This was done to increase the volume of cDNA added to the PCR reaction in order to improve pipetting accuracy.

2.19. Polymerase chain reaction

Gene expression in isolated cells was examined by qPCR on cDNA synthesised from the isolated RNA. The qPCR was carried out in 384 well plates (with a reaction mix volume of 15 μL). Primers were either designed using the National Institute of Health Primer-BLAST tool (Ye et al., 2012) or were taken from publications. When possible, forward and reverse primers were designed to amplify a region which crossed an intron-intron border. In these instances the SYBR-Green reporting system was used. When it was not possible to design primers which crossed an intron-intron border a probe was also designed to recognise a sequence within the amplicon.

When both a probe and forward and reverse primers were in use, the TaqMan reporting system was used. The primers used are available in the appendix to this chapter.

The PCR reaction mix was made up for each well as per Table 2.9. The reaction mix (13 μL) was added to each well. cDNA from each the samples was added to separate wells in duplicate (2 μL). Additionally, a serially diluted standard curve of cDNA, prepared with RNA which was expected to contain the gene of interest, was added to the plate. This allowed the Ct values for each of the samples to be expressed as relative concentrations. The plate was sealed using ABI Prism optical adhesive cover and briefly centrifuged (1400 rpm, < 1 minute).

Component	Volume per sample (μL)	
	SYBR-Green	TaqMan MasterMix
Master Mix	7.5	7.5
RNase free water	4.5	4
Probe (6.25 μM)	0	0.5
Forward Primer (6.25 μM)	0.5	0.5
Reverse Primer (6.25 μM)	0.5	0.5

Table 2.9. PCR reaction mix. Volume per sample required for both reporting systems.

The PCR was run on the Quantstudio 5 machine. The PCR reaction cycle was made up of four stages. Firstly, the reaction was held at 50 ˚C for 2 minutes. Secondly, the reaction was then held at 95 ˚C for 10 minutes. The reaction was then cycled 55 times between the third and fourth stages. In the third stage the reaction is at 95 ˚C for 10 seconds. In the fourth stage the reaction is at 60 ˚C for 30 seconds. The reporter systems detect the amount of amplification of the gene of interest which has occurred at the end of each cycle. SYBR-Green is a dye which binds to double-stranded cDNA. The TaqMan system measures the displacement of the probe during amplification.

PCR data were normalised to expression of a housekeeping gene in order to account for differences in sample quality. 18S, a ribosomal subunit gene, was used as a housekeeping gene.

2.20. Statistical analysis

All statistical analysis was carried out using GraphPad Prism.

Data were tested for normality using the Shapiro-Wilk test. Where data were parametric the mean ± SEM was plotted. Where data were non-parametric the median ± IQR was plotted. Unless otherwise stated, the mean ± SEM is plotted in the figures.

The number of mice in the sample size is denoted by N, while the number of replicates (for example, brain slices or tissue sections) is denoted by n.

Hypothesises based on simple comparisons between two groups with a single experimental variable were tested using paired or unpaired t-tests (parametric data) or Mann-Whitney test (unpaired non-parametric data) or Wilcoxon test (paired parametric data).

Hypothesises which were based on comparisons between two or more groups with multiple experimental variables were tested using ANOVA. In instances where there were two variables (for example, age and genotype) a 2-way ANOVA was used. In instances where there were three variables (for example, age, genotype, and treatment) a 3-way ANOVA was used. Multiple comparisons were made when there was a hypothesis that specific experimental groups would differ from one another. Tukey's range test was used to correct for the effect of making multiple comparisons.

In all testing the level of significance is taken to be $p < 0.05$. For comparisons made by t-tests, Wilcoxon tests, and Mann-Whitney test, significant p values are reported using the asterisk, where: * = $p < 0.05$, ** = $p < 0.01$, *** = $p < 0.005$, and **** = $p < 0.005$. For comparisons made by ANOVA, significant main effects of variables are reported using the hash symbol (#)(where: # =

$p < 0.05$, ## = $p < 0.01$, ### = $p < 0.005$, and #### = $p < 0.005$) while significant effects found by multiple comparisons are reported using the asterisk (where: * = $p < 0.05$, ** = $p < 0.01$, *** = $p < 0.005$, and **** = $p < 0.005$).

Correlations were tested by calculating the Pearson correlation coefficient.

The frequency of categorical outcomes were tested using Fisher's exact test.

Appendix – Chapter 2

MATLAB programme used to automatically quantify epileptiform events

```
%{ The intial section (lines 16-33) of this programme is part of CEDS64ML, an SON MATLAB interface. Developed by: Cambridge Electronic
Design Limited 2014 CEDS64ML is free software: you can redistribute it and/or modify it under the terms of the GNU General Public
License as published by the Free Software Foundation, either version 3 of the License, or (at your option) any later version.The
seizure quantification core kernel (lines 74-98) was written by Dr. Katherine Newling and used with her permission. All other sections
were developed for this thesis.

%}

% This function opens a file and reads the data from a waveform channel as 32-bit floats.
% clear workspace
clear;
% add path to CED code
cedpath = 'C:\Users\hughb\OneDrive\Documents\MATLAB\CEDMATLAB\CEDS64ML';
addpath( cedpath );
CEDS64LoadLib( cedpath );
% load ceds64int.dll
CEDS64LoadLib( cedpath );

% Open a file - path needs to be single inverted commas
fhand1 = CEDS64Open( 'D:\1_Data\1_Electrophysiology_Recordings' );
if (fhand1 <= 0); unloadlibrary ceds64int; return; end
% ends script if unable to open file


% Threshold setting - based on region without events. Time period used - find this region by manually inspecting trace. Also need to
set channel to be analysed.

StartTimeT = CEDS64SecsToTicks(fhand1,XX);
EndTimeT = CEDS64SecsToTicks(fhand1,XX);
Channel = XX;

% Call data for threshold setting

[ fReadT, fValsT, fTimeT ] = CEDS64ReadWaveF( fhand1, Channel, 100000, StartTimeT,EndTimeT);
Freq = CEDS64IdealRate( fhand1, 1 );

% Use findpeaks to find amplitude of data called - threshold is 5 standard deviations from mean amplitude of ongoing oscillation

[pks] = findpeaks(fValsT);
STDEV = std(pks);
AVERAGE_HEIGHT = mean(pks);
threshold = AVERAGE_HEIGHT+(5*STDEV);


% Call data for event Quantification. Set Time Window - this is time period to be analysed

StartTime = CEDS64SecsToTicks(fhand1,XX);
EndTime = CEDS64SecsToTicks(fhand1,XX);


% Call data for event quantification and plot data called

[ fRead, fVals, fTime ] = CEDS64ReadWaveF( fhand1, Channel, 3000000, StartTime,EndTime);
Freq = CEDS64IdealRate( fhand1, 1 );

plot(fVals);

% Event Quantification using function defined below. Gapsize is 5000 as acquisiton rate is 5000 data points per second.

getBurstParameters(fVals,threshold,5000);


% Quantification function definition

function [coastline,numBursts, burstLengths, burstAmps] = getBurstParameters(data,threshold,gapsize)

coastline = sum(abs(diff(data)));

highpoints= find(data>threshold);
begins = highpoints(1);
ends = [];
burstLengths = [];
burstAmps = [];

for i = 1:length(highpoints)-1
    if ((highpoints(i+1)-highpoints(i)>gapsize))
        ends = [ends;highpoints(i)];
        begins = [begins;highpoints(i+1)];
    end
end
ends = [ends;highpoints(length(highpoints))];

for j = 1:length(begins)
    burstLengths = [burstLengths;(ends(j)-begins(j)+1)];
    burstAmps = [burstAmps;max(data(begins(j):ends(j)))];
end
numBursts = length(burstLengths);

% Print results to excel file

filename = "C:\Users\hughb\OneDrive\Documents\MATLAB\";
sheet = "BASELINE";

xlswrite(filename,numBursts,sheet,"A2");
xlswrite(filename,burstAmps,sheet,"C2");
xlswrite(filename,burstLengths,sheet,"D2");

end
```

Primers used for qPCR

Gene	Oligonucleotide	Sequence
18s	Forward	5'-CGCCGCTAGAGGTGAAATTCT-3'
	Reverse	5'-CATTCTTGGCAAATGTCTTTCG-3'
Ccl2	Forward	5'-GTTGGCTCAGCCAGATGCA-3'
	Reverse	5'-AGCCTACTCATTGGGATCATCTTG-3'
	Probe	5'-TTAACGCCCCACTCACCTGCTGCTACT-3'
Ccl3	Forward	5'-CCCAGCCAGGTGTCATTTTCC-3'
	Reverse	5'-GCATTCAGTTCCAGGTCAGTG-3'
Ccl4	Forward	5'-CTCAGCCCTGATGCTTCTCAC-3'
	Reverse	5'-AGAGGGGCAGGAAATCTGAAC-3'
Cxcl1	Forward	5'-CACCCAAACCGAAGTCATAGC-3'
	Reverse	5'-AATTTTCTGAACCAAGGGAGCTT-3'
Cxcl10	Forward	5'-GCCGTCATTTTCTGCCTCAT-3'
	Reverse	5'-GCTTCCCTATGGCCCTCATT-3'
	Probe	5'-TCTCGCAAGGACGGTCCGCTG-3'
Gfap	Forward	5'-CTCCAACCTCCAGATCCGAG-3'
	Reverse	5'-TCCACAGTCTTTACCAGATGT-3'
Glul	Forward	5′-GGGCTACTTTGAAGACCGT-3'
	Reverse	5′-TTCGTCGCCTGTTTCGT-3'
Glut1	Forward	5'-TCTCGTCGGCCTCTTTGTT-3'
	Reverse	5'-GCAGAAGGGCAACAGGATAC-3'
Hes5	Forward	5'-GGTGGAGAAGATGCGTCGG-3'
	Reverse	5'-GCGAAGGCTTTGCTGTGTTT-3'
Il1b	Forward	5'-GCACACCCACCCTGCA-3'
	Reverse	5'-ACCGCTTTTCCATCTTCTTCTT-3'
	Probe	5'-TGGAGAGTCTGGATCCCAAGCAATACCC-3'
Pai-1	Forward	5'-GGGACACCCTCAGCATGTTC-3'
	Reverse	5'-TGTTGGTGAGGGCGGAGA-3'
	Probe	5'-TCGCTGCACCCTTTGAGAAAGATGT-3'
P16	Forward	5'-GTCGCAGGTTCTTGGTCACT-3'
	Reverse	5'-CATGTTCACGAAAGCCAGAGC-3'

Gene	Oligonucleotide	Sequence
P21	Forward	5'-TCCAGACATTCAGAGCCACAG-3'
	Reverse	5'-CAAAGTTCCACCGTTCTCGG-3'
Tgfb	Forward	5'-CGTGGAAATCAACGGGATCA-3'
	Reverse	5'-GGCCATGAGGAGCAGGAA-3'
	Probe	5'-ACCTGGGCACCATCCATGACATGA-3'
Tnfa	Forward	5'-CTCCAGGCGGTGCCTATG-3'
	Reverse	5'-GGGCCATAGAACTGATGAGAGG-3'
	Probe	5'-TCAGCCTCTTCTCATTCCTGCTTGTGG-3'
Vimentin	Forward	5'-GCTGCAGGCCCAGATTCA-3'
	Reverse	5'-TTCATACTGCTGGCGCACAT-3'

Table 2.A.1. Primer sequences.

Chapter 3

Inflammation and Gamma Frequency Oscillations in Healthy Mice

Introduction

Gamma frequency neuronal oscillations are rhythmic neuronal network activities that occur at a frequency of 20 to 80 Hz. Gamma frequency neuronal oscillations are observed during many cognitive activities and are required for normal brain functioning. As well as being functionally relevant, gamma frequency oscillations serve as a useful *in vitro* model of neuronal network activity (Buzsáki & Wang, 2012).

Gamma frequency neuronal oscillations can be induced in rodent hippocampal brain slices using kainate or carbachol (Fisahn et al., 1998; Whittington et al., 1995). These compounds, at relatively low concentrations, initiate the neurotransmission and neuronal activity required for gamma frequency oscillations. Later sections of this thesis will address the effect of age, Alzheimer's-like pathology and neuroinflammation on gamma frequency oscillations; but it was necessary to first ensure that gamma frequency oscillations could be established in hippocampal brain slices from young, healthy, non-transgenic (C57BL/6J) mice. Gamma frequency oscillations were induced using both the kainate and carbachol and a comparison of these models was carried out in young (3-4 months) C57BL/6J mice.

It has been shown that gamma frequency oscillations are affected by the oestrous cycle in female mice (Barth et al., 2014). Specifically, gamma frequency oscillation amplitude is increased during the oestrous stage of the cycle. This factor was identified as a potential confounder and was therefore investigated. In a group of young female C57BL/6J mice vaginal lavage samples were taken at the time of death. A histological stain was used to determine the stage of the oestrous cycle at death. The effect of the oestrous cycle on gamma frequency oscillation amplitude and frequency was examined using the stage of the cycle determined by vaginal lavage.

Having characterised and validated the experimental models of gamma frequency oscillations which were to be used, research questions could be addressed. The question addressed in this

chapter is: how does inflammation affect gamma frequency oscillations? This question was examined by studying the effect of certain inflammatory mediators on gamma frequency oscillations in hippocampal brain slices from young, healthy C57BL/6J mice.

Inflammation is the body's response to departures from homeostasis usually as a result of injury, infection, or disease. Inflammation is mediated by cells of the immune system which communicate via inflammatory mediators called cytokines, chemokines, and prostaglandins. These molecules are the key molecular mediators of inflammation. The effect of a selection of these cytokines, chemokines, and prostaglandins on gamma frequency oscillations was examined. The inflammatory mediators were chosen based on their position at the top of the pro-inflammatory cascade (cytokines IL-1β, TNFα) and based on their dual roles as chemoattractants with neuromodulatory actions (chemokines CCL2, CXCL10, and CCL11) (Rostène et al., 2007; Salvador et al., 2021). The selection of the lipid mediator prostaglandin E2 is based on its widely described impacts on neuronal function through multiple specific receptors expressed on distinct neuronal populations (EP1-EP4) (Lenz et al., 2011; Sang et al., 2005; Saper et al., 2012). During neuroinflammation brain tissue may be exposed to many of these mediators simultaneously. By exposing gamma frequency oscillations to this selection of mediators, at physiologically relevant concentrations, it was hoped to simulate an altered inflammatory milieu in the brain, and to isolate the effects of individual mediators on gamma frequency oscillations.

The effect of inflammation on gamma frequency oscillations was studied using two approaches. Firstly, established gamma frequency oscillations were exposed to the inflammatory mediator of interest and the effect of this exposure was monitored both during the exposure and for 60 minutes after the exposure had ended. Secondly, brain slices were incubated for three hours in the presence of the inflammatory mediator of interest. The effect of this incubation on the emergence of gamma frequency oscillations in the brain slice was monitored over 60 minutes. These two approaches aimed to capture the variety of ways in which inflammatory mediators can

act on both neurons and glia. The first approach (challenging established gamma frequency oscillations) investigates the immediate effect of exposure to inflammation on ongoing, established network activity. Any effect of inflammation in this experimental approach is likely mediated via inflammatory mediators acting directly on neurons or glia. The second approach (studying the emergence of gamma frequency oscillations post-incubation in the presence of an inflammatory mediator) investigates the longer-term effect of inflammation on neuronal networks responsible for generating gamma frequency oscillations. It is possible that any effect of inflammation in this experimental approach is mediated via changes in protein expression (namely receptors or neurotransmitters). These two approaches aimed to capture the effects of various inflammatory mediators on: established neuronal network activity during and following a short exposure to the inflammatory mediator (approach 1), and on the ability of neuronal networks to generate network activity following a long exposure to the inflammatory mediator (approach 2).

Results

3.1. Gamma frequency oscillations in young mice

Prior to investigating the effects of inflammation on the activity of neuronal networks, it was necessary to show that gamma frequency oscillations could be induced in brain slices from young (3-4 months) C57BL/6J mice (male and female). Gamma frequency oscillations were induced with kainate (100 nM) or carbachol (20 μM) in *ex vivo* brain slices. Approximately 15-20 minutes following the application of carbachol or kainate, the hippocampal local field potential (recorded in the CA3 subregion) grew in amplitude and became ordered and rhythmic. This was in contrast to the low amplitude, disordered local field potential observed in untreated slices (Figure 3.1, A). The activity was confirmed to be a neuronal oscillation in the gamma frequency range (20-80 Hz) by fast Fourier transform frequency via. Carrying out Fast Fourier decomposition on ongoing oscillatory activity showed a clear band of increased activity at approximately 30 Hz (Figure 3.1, B).

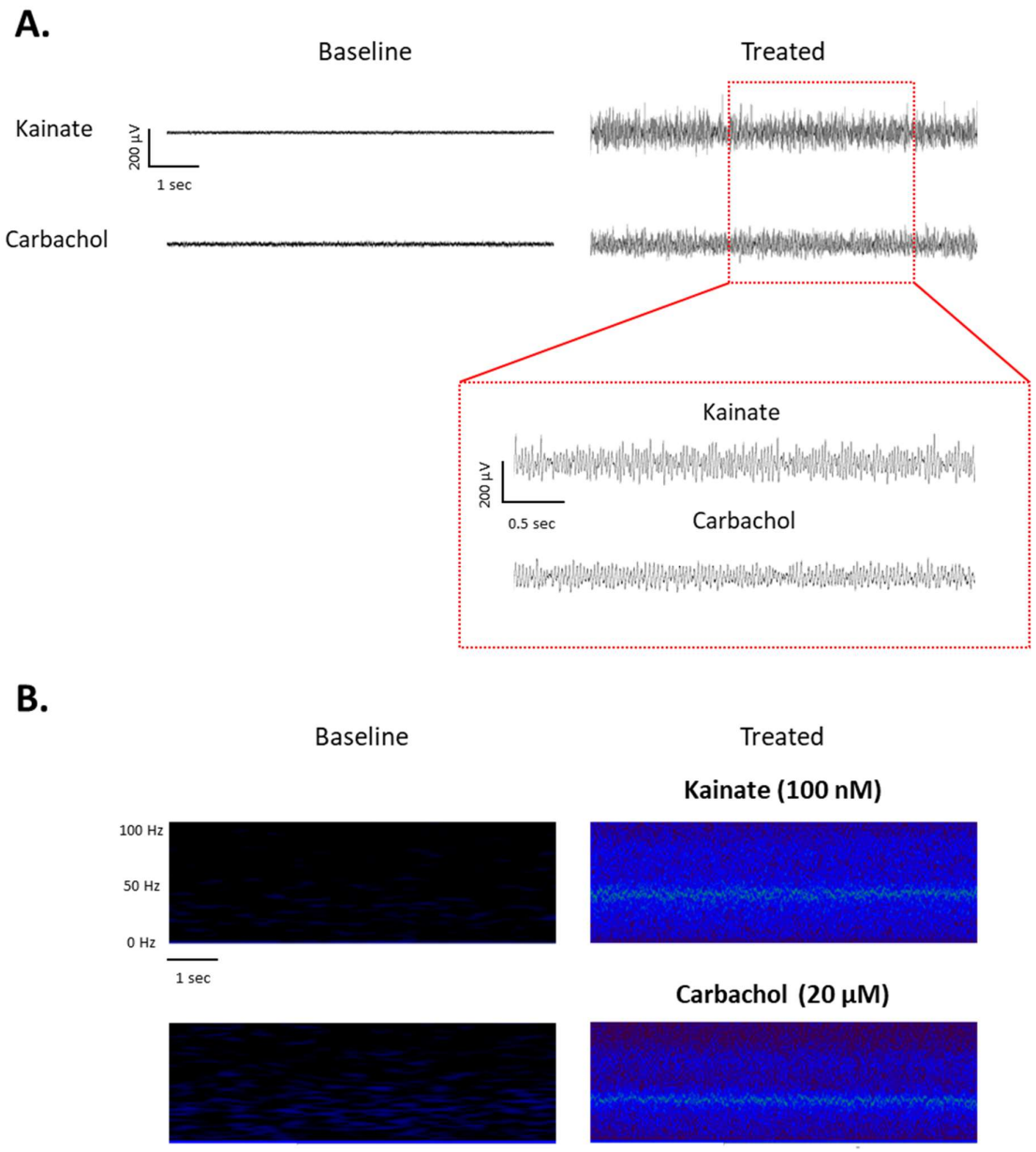

Figure 3.1. Gamma frequency oscillations in brain slices from young C57BL/6J mice. (A) Representative recorded local field potentials in brain slices from C57BL/6J mice in their naïve state (left) and treated with kainate (top-right) and carbachol (bottom-right). (B) Ongoing frequency decomposition by FFT on the representative traces shown in (A).

3.2. Kainate- and carbachol-induced gamma frequency oscillations

The two models of inducing gamma frequency oscillations were compared in brain slices from C57BL/6J mice (3-4 months, male and female). Gamma frequency oscillations were induced by treating brain slices with kainate (100 nM) or carbachol (20 μM). Gamma frequency oscillations were allowed to emerge and stabilise. Fast Fourier transform analysis was performed to determine the amplitude and frequency composition of the activity.

There were no significant differences in kainate- and carbachol-induced gamma frequency oscillations (Figure 3.2). The gamma frequency oscillation amplitude was not significantly different in these two models of gamma frequency oscillation induction. This was demonstrated by the area under the curve (kainate: 5,443 ± 1,458 $\mu V^2 Hz^-$, carbachol: 2,855 ± 695 $\mu V^2 Hz^-$; $p = 0.222$; Figure 3.2, C) and the peak amplitude (kainate: 540.4 ± 168.5 μV, carbachol: 361.1 ± 132.1 μV; $p = 0.522$; Figure 3.2, D). Similarly, the oscillation peak frequency was not significantly different in either model (kainate: 31.48 ± 0.87 Hz, carbachol: 31.48 ± 1.88 Hz; $p = 0.997$; Figure 3.2, E). The pooled Fast Fourier transforms (Figure 3.2, A, B) showed that although the parameters extracted from the Fast Fourier transform analysis were not significantly different in kainate- and carbachol-induced gamma frequency oscillations, there were differences in the frequency distribution of gamma frequency oscillations in these models. Kainate-induced gamma frequency oscillations formed a broader peak than carbachol-induced gamma frequency oscillations. There was also more activity at frequencies below the main oscillation peak in carbachol-induced gamma frequency oscillations than in kainate-induced gamma frequency oscillations. Broadly, however there were no significant differences in kainate- and carbachol-induced gamma frequency oscillations.

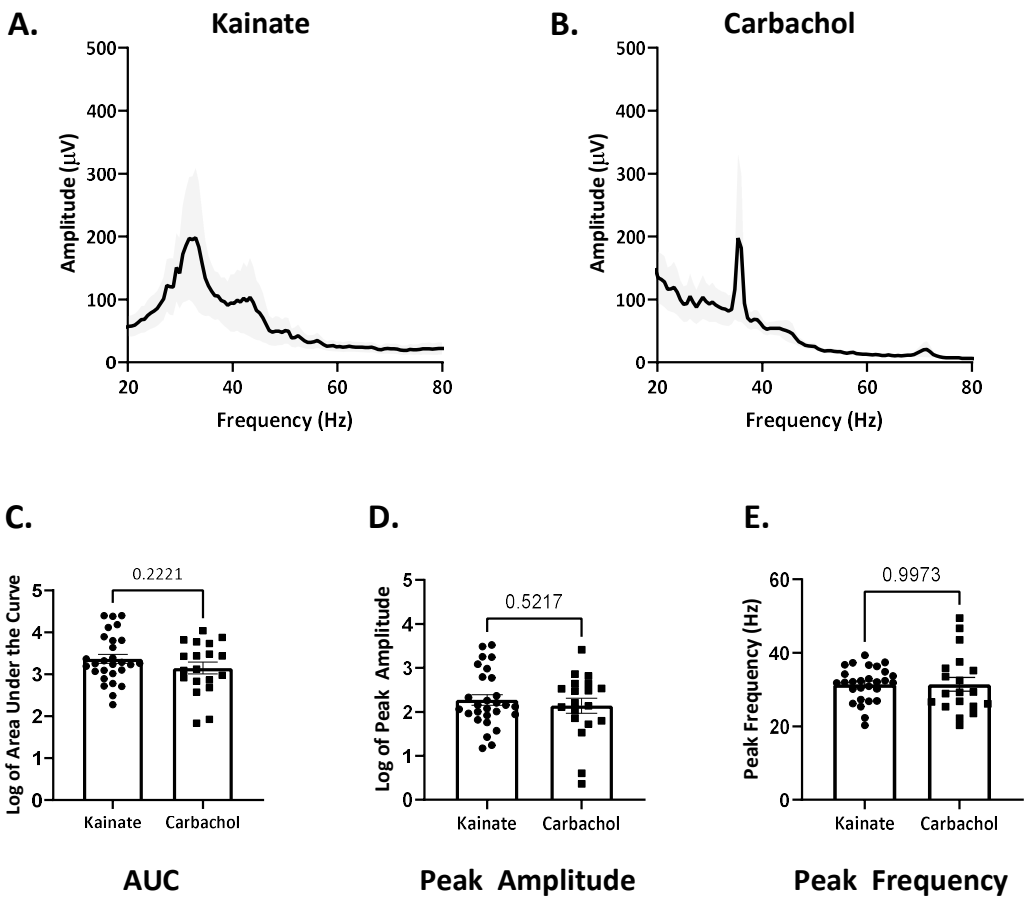

Figure 3.2. Comparison of kainate- and carbachol-induced gamma frequency oscillations. Pooled Fast Fourier transforms for (A) kainate- and (B) carbachol-induced gamma frequency oscillations in brain slices from C57BL/6J mice (3-4 months, both sexes). Parameters from Fast Fourier transforms: (C) Area under the curve (AUC), (D) Peak Amplitude, and (E) Peak Frequency. Data in C and D are log transformed. Unpaired t-test. Kainate: n = 77, N = 28; Carbachol: n = 42, N = 19.

3.3. Gabazine treatment of gamma frequency oscillations

Gamma frequency oscillations are known to be dependent on the transmission of GABA, this is a defining feature of oscillations in this frequency range. In order to confirm that the oscillations induced by kainate and carbachol were gamma frequency oscillations, brain slices with established oscillations were treated with the $GABA_AR$ antagonist, gabazine (500 nM) for 30 minutes (Figure 3.3, A). Treatment with gabazine significantly reduced oscillation peak frequency in both kainate- and carbachol-induced gamma frequency oscillations.

Following treatment with gabazine, in brain slices with kainate-induced neuronal oscillations, there was a significant reduction in the neuronal oscillation frequency (Baseline: 36.1 ± 0.55 Hz, Gabazine: 20.98 ± 0.98 Hz; p = 0.002; Figure 3.3, E), suggesting that the oscillatory activity in the gamma frequency range had been abolished by $GABA_AR$ blockade. There was no significant effect of gabazine treatment on the oscillation amplitude (area under the curve: Baseline: 1,530 ± 428.9 $\mu V^2\ Hz^-$, Gabazine: 1,440 ± 1240 $\mu V^2\ Hz^-$, p = 0.936; peak amplitude: Baseline: 145.8 ± 43.89 μV, Gabazine: 97 ± 63.05 μV, p = 0.381; Figure 3.3, C, D).

Carbachol-induced gamma frequency oscillations were also sensitive to $GABA_AR$ blockade. Following treatment with gabazine, in brain slices with carbachol-induced neuronal oscillations, there was a significant reduction in the neuronal oscillation frequency (Baseline: 28.10 ± 0.80 Hz, Gabazine: 20.43 ± 0.06 Hz; p = 0.0123; Figure 3.3, I). There was a non-significant decrease in carbachol-induced gamma frequency oscillation amplitude following treatment with gabazine (area under the curve: Baseline: 131.8 ± 69.44 $\mu V^2\ Hz^-$, Gabazine: 60.72 ± 23.65 $\mu V^2\ Hz^-$, p = 0.2780; peak amplitude: Baseline: 6.98 ± 2.89 μV, Gabazine: 1.71 ± 0.51 μV, p = 0.2611; Figure 3.3, G, H).

Overall, the neuronal oscillations induced by kainate and carbachol were shown to be sensitive to $GABA_AR$ blockade, demonstrating they were gamma frequency oscillations.

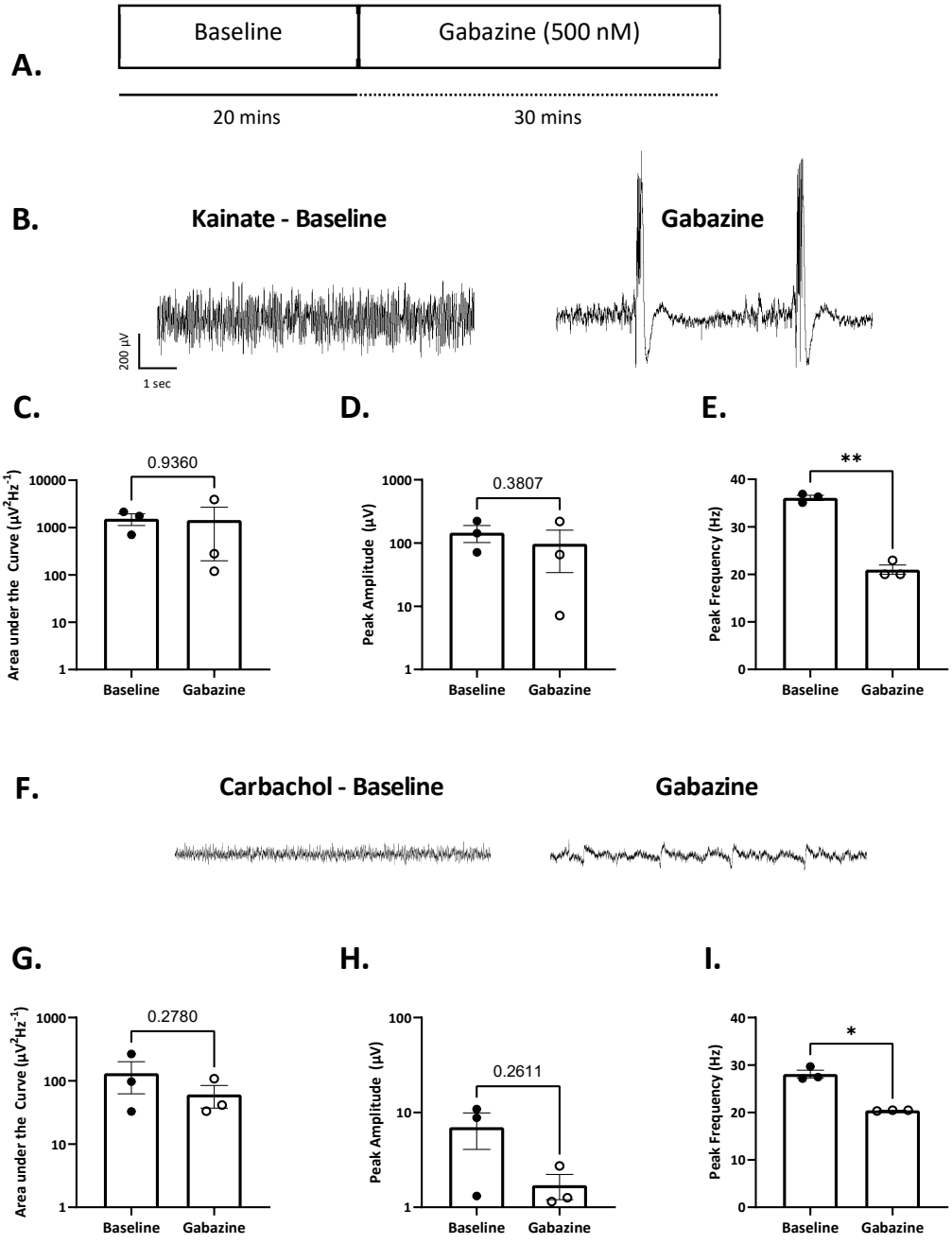

Figure 3.3. Treatment of kainate- and carbachol-induced gamma frequency oscillations with gabazine. (A) Experimental design for treatment with $GABA_AR$ antagonist gabazine. Kainate-induced gamma frequency baseline and gabazine-treated (B) representative traces, (C) area under the curve, (D) peak amplitude, and (E) peak frequency. Carbachol-induced gamma frequency baseline and gabazine-treated (F) representative traces, (G) area under the curve, (H) peak amplitude, and (I) peak frequency. Gamma frequency oscillations in brain slices from C57BL/6J mice (3-4 months, both sexes). Paired t-test, where * = $p < 0.05$. Kainate and carbachol: n = 5, N= 3.

3.4. Preparing brain slices by decapitation versus transcardial perfusion

Initially brain slices were prepared by decapitating mice and extracting the brain. Brain slices were prepared by decapitation from a group of APP/PS1 mice and wildtype littermate controls at 18-25 months. In 32% of brain slices (17 of 53 brain slices) prepared by decapitation it was not possible to generate gamma frequency oscillations by the application of kainate (100 nM)(Figure 3.4, A).

This failure to generate gamma frequency oscillations in brain slices prepared by decapitation did not occur to the same extent in APP/PS1 mice and wildtype littermate controls, or in male and female mice. In brain slices prepared by decapitation gamma frequency oscillations were not generated in: 27% of brain slices from APP/PS1 mice (9 of 33 brain slices), 40% of brain slices from wildtype littermate controls (8 of 20 brain slices), 60% of brain slices from female mice (13 of 22 brain slices), in 13% of brain slices from male mice (4 of 31 brain slices; Figure 3.4, B-E).

These differences presented a limitation to the study of gamma frequency oscillations in APP/PS1 mice and wildtype littermate controls. Therefore, based on these difficulties in brain slices prepared by decapitation, it was decided that brain slices would be prepared by transcardial perfusion as this has been shown to be a superior method of brain slice preparation (M. O. Cunningham, Unpublished; Djurisic, 2020). Preparing brain slices by perfusion resulted in the induction of gamma frequency oscillations in notably more brain slices (96%, 74 of 77 brain slices) than in those prepared by decapitation (Figure 3.4, A).

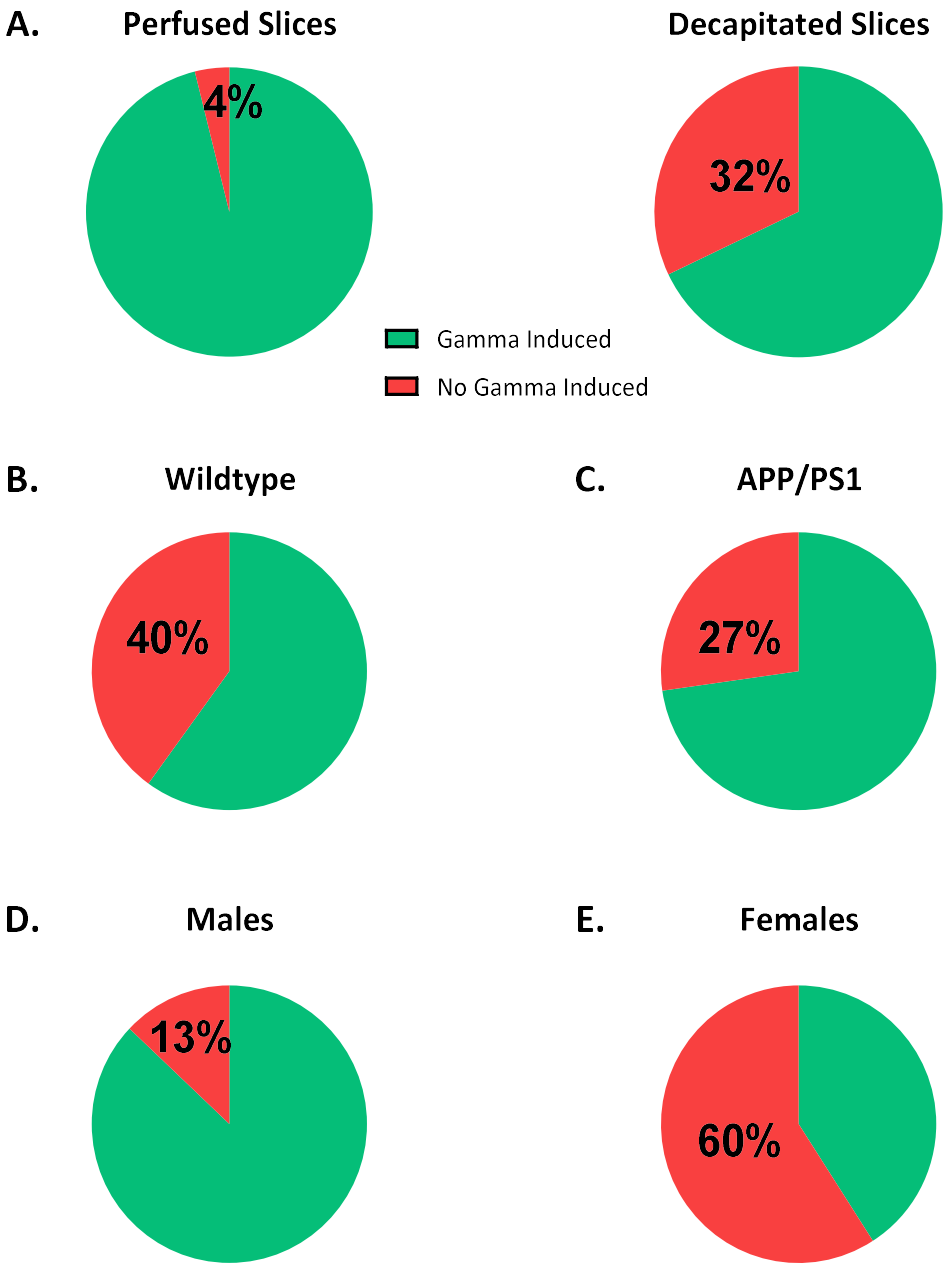

Figure 3.4. Gamma frequency oscillations induction in brain slices prepared by decapitation and by perfusion. (A) Percentage of brain slices prepared by perfusion and by decapitation from APP/PS1 mice and wildtype littermate controls (aged 18-25 months) which successfully generated gamma frequency oscillations treated with kainate (100 nM). (B-E) The percentage of slices prepared by decapitation which generated gamma frequency oscillations separated by sex and genotype. Perfusion: Wildtype: n = 43, N = 15; APP/PS1: n = 34, N = 16. Decapitation: Wildtype: n = 20, N = 8; APP/PS1: n = 33, N = 6.

3.5. Oestrous cycle stage detection

It has been previously observed that the oestrous cycle can have a significant effect on gamma frequency oscillations (Barth et al., 2014). Therefore, the effect of the oestrous cycle on both kainate- and carbachol-induced gamma frequency oscillations was investigated. Vaginal sample were taken by lavage from both APP/PS1 mice and wildtype littermate controls at 3-4, 9-11, and 20-24 months. The samples were stained with Wright's stain and the stage of the oestrous cycle was determined by examining the cell populations present (Figure 3.5, A-D).

At 3-4 months, each stage of the oestrous cycle was detected at a frequency which is approximate to the relative length of that stage (dioestrus: 58% of mice, proestrus: 5% of mice, oestrous: 29% of mice, metestrus: 8% of mice; Figure 3.5, E). Therefore, the oestrous cycle was occurring normally at 3-4 months and the method utilised was capable of detecting each stage of the cycle.

A clear effect of age was observed on oestrous cycles (Figure 3.5, F-H). At 3-4 months the oestrous stage was detected in 29% of mice (7 of 24 mice). At 9-11 months the oestrous stage was detected in 27% of mice (4 of 15 mice). At 20-24 months the oestrous stage was detected in 0% of mice (0 of 11 mice). Therefore, any sex differences observed at 20-24 months were not related to the oestrous cycle as mice were no longer cycling at this age.

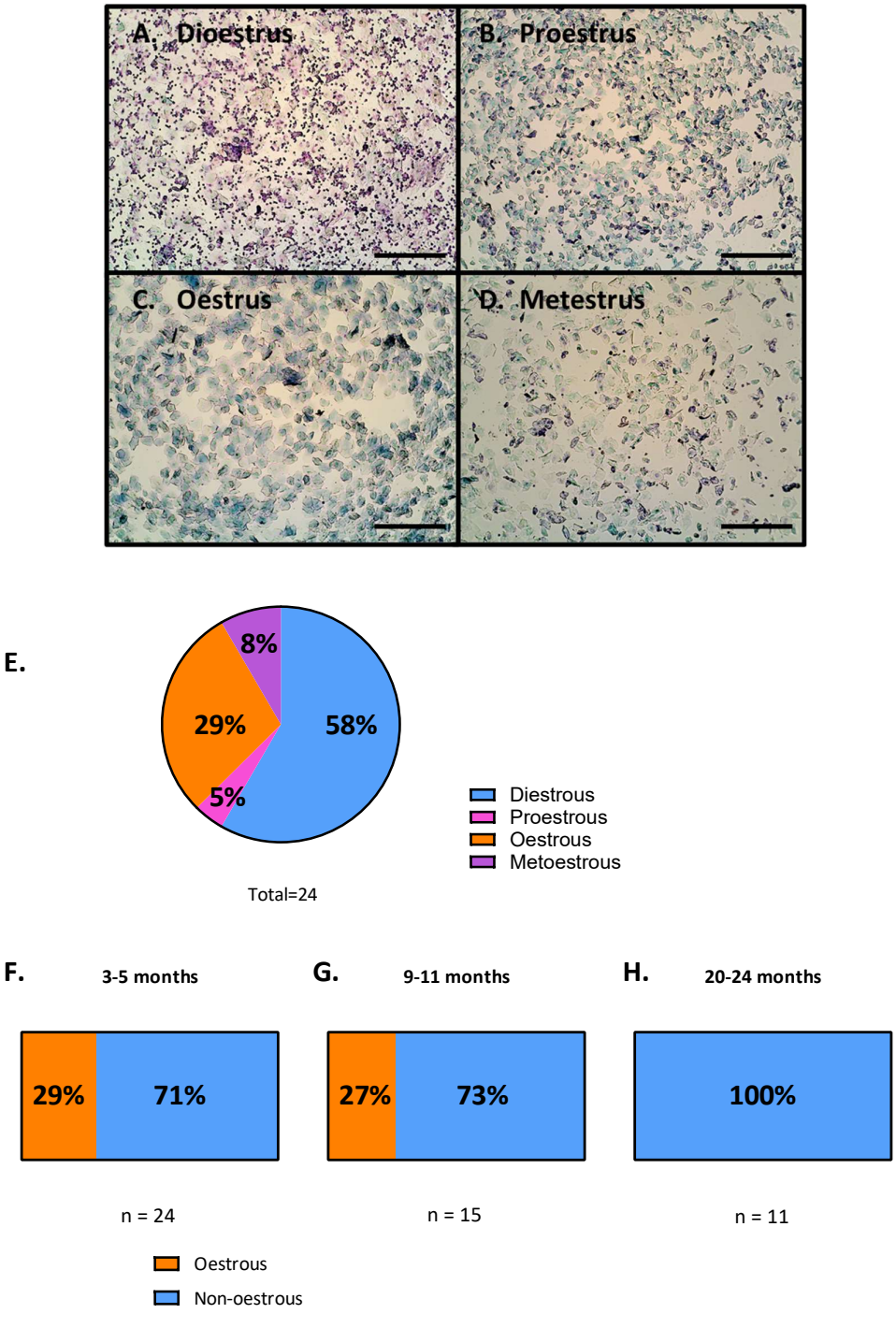

Figure 3.5. Detection of the oestrous cycle stage in mice. (A-D) Representative images of the four cycle stages: (A) Dioestrus, (B) Proestrus, (C) Oestrous, and (D) Metestrus. (E) Frequency at which each stage was detected at 3-4 months. (E-H) Frequency at which oestrous and non-oestrous stages were detected at 3-4, 9-11, and 20-24 months. Samples taken by vaginal lavage and stained with Wright's modified stain. 10X magnification. Scale bars: 250 µm. 3-4 months: N = 24, 9-11 months: N = 15, 20-24 months: N = 11.

3.6. The effects of the oestrous cycle on gamma frequency oscillations

The effect of the oestrous cycle on both kainate- and carbachol-induced gamma frequency oscillations was examined in brain slices from C57BL/6J mice at 3-4 months. No significant differences were found in kainate- or carbachol-induced gamma frequency oscillations across the oestrous cycle (Figure 3.6).

For kainate-induced gamma frequency oscillations, there was a non-significant reduction in oscillation amplitude in the oestrous stage, relative to the non-oestrous stages. This was demonstrated by the area under the curve (oestrous: 17,841 ± 14,180 μV^2 Hz^-, non-oestrous: 30,531 ± 11,480 μV^2 Hz^-; $p = 0.078$; Figure 3.6, A) and the peak amplitude (oestrous: 1,777 ± 1,421 μV, non-oestrous: 3,485 ± 1,432 μV; $p = 0.081$; Figure 3.6, B). The peak frequency parameter was not significantly different in the oestrous stage versus the non-oestrous stages (oestrous: 31.33 ± 1.06 Hz, non-oestrous: 31.25 ± 1.09 Hz; $p = 0.965$).

No notable effect of the oestrous cycle was observed for carbachol-induced gamma frequency oscillations in brain slices from C57BL/6J mice at 3-4 months. This analysis was limited as only two mice were detected in the oestrous stage of the cycle. However, no differences were observed in oscillation amplitude (area under the curve: oestrous: 1,774 ± 953.9 μV^2 Hz^-, non-oestrous: 3,118 ± 1,749 μV^2 Hz^-; peak amplitude, oestrous: 203.9 ± 98.00 μV, non-oestrous: 248.1 ± 114.3 μV) or in oscillation frequency (peak frequency, oestrous: 36.48 ± 7.10 Hz, non-oestrous: 28.12 ± 1.36 Hz).

Therefore, in the absence of any observed effects of the oestrous cycle on either kainate- or carbachol-induced gamma frequency oscillations, it was not necessary to stratify data collected from female animals based on this factor.

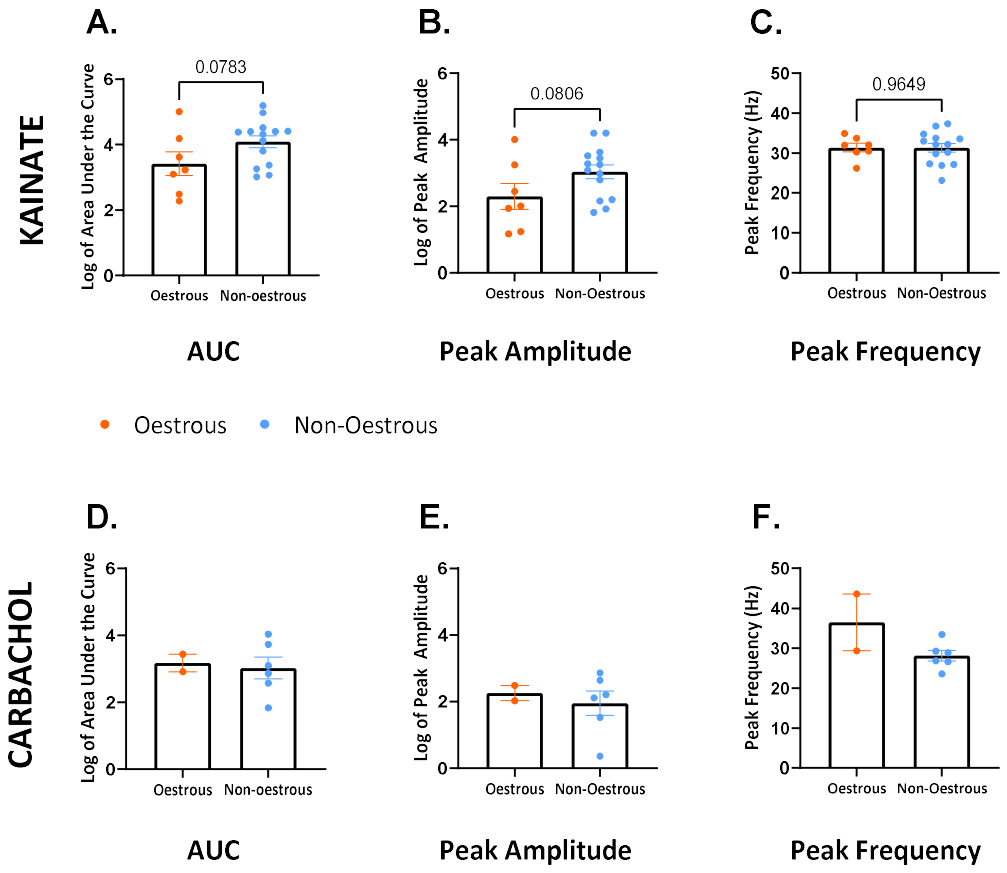

Figure 3.6. The effect of the oestrous cycle on kainate- and carbachol induced gamma frequency oscillations. Kainate-induced gamma frequency oscillation (A) area under the curve, (B) peak amplitude, and (C) peak frequency. Carbachol-induced gamma frequency oscillation (D) area under the curve, (E) peak amplitude, and (F) peak frequency. Gamma frequency oscillations in brain slices from C57BL/6J mice at 3-4 months. Mice in the oestrous stage (orange) and non-oestrous stage (blue). Data in A, B, D, and E are log transformed. Unpaired t-test. Kainate: oestrous: n = 21, N = 7, non-oestrous: n = 32, N = 16; Carbachol: oestrous: n = 4, N = 2, non-oestrous: n = 11, N = 6.

3.7. The behaviour of established gamma frequency oscillations over time

Before studying the effect of inflammation on established gamma frequency oscillations, it was necessary to establish how gamma frequency oscillations behaved in the absence of any intervention. This served as a control for the effect of time on gamma frequency oscillations.

Gamma frequency oscillations were induced with kainate (100 nM) in brain slices from C57BL/6J mice at 3-4 months. The growth of the oscillation was observed in real-time by continuous frequency decomposition by Fast Fourier transform. The representative trace in Figure 3.7, A demonstrates the initial growth in oscillation amplitude which is followed by a period of relative stability and slower growth in amplitude. This period in which the oscillation amplitude was no longer rapidly growing was considered the baseline. The baseline was allowed to continue for 20 minutes. From the established baseline, the oscillation was observed for 90 minutes with no interventions. During this 90 minute period, the oscillation amplitude, as measured by the area under the curve and peak amplitude, significantly increased over time (Figure 3.7, C, D). The area under the curve increased from 42,782 ± 19,572 $\mu V^2 Hz^-$ at the baseline to 89,770 ± 35,304 $\mu V^2 Hz^-$ at 90 minutes after the baseline ($F_{1.794,41.26} = 21.47$, $p < 0.0001$). The oscillation peak amplitude was also significantly increased from 3,649 ± 1,882 μV at the baseline to 6,793 ± 3,336 μV at 90 minutes after the baseline ($F_{1.986,45.67} = 19.26$, $p < 0.0001$). In order to further visualise the changes which occurred, z-scores were calculated for each of the parameters extracted from the Fast Fourier transforms (Figure 3.7, F-H). Z-scores were calculated with reference to 20 minutes of stable activity during the baseline. The mean and standard deviation for each parameter during the 20 minute baseline were used to calculate the distance from the baseline for each parameter during the 90 minute observation period. This accounted for the variability between different brain slices in baseline amplitude. The calculated z-scores for the area under the curve and the peak amplitude clearly showed an increase over time

relative to the baseline. At 90 minutes the area under the curve z-score was 18.41 ± 4.98. Similarly, at 90 minutes the peak amplitude parameter z-score was 12.76 ± 3.767. The increase in kainate-induced gamma frequency oscillation amplitude over time was further displayed by the pooled Fast Fourier transforms, which showed the frequency decomposition of the oscillation at the baseline and 90 minutes after the baseline (Figure 3.7, B).

The peak frequency of the oscillation was stable over time (Baseline: 29.78 ± 0.83 Hz, 90 minutes after the baseline: 28.62 ± 0.97 Hz; Figure 3.7, E). Therefore, there was no significant change in the peak frequency of kainate-induced gamma frequency oscillations over time ($F_{2.582, 59.38} = 1.204$, $p = 0.313$).

To conclude, kainate-induced gamma frequency oscillations in brain slices from C57BL/6J mice at 3-4 months, in the absence of any intervention, significantly increased in amplitude and had a stable peak frequency over time.

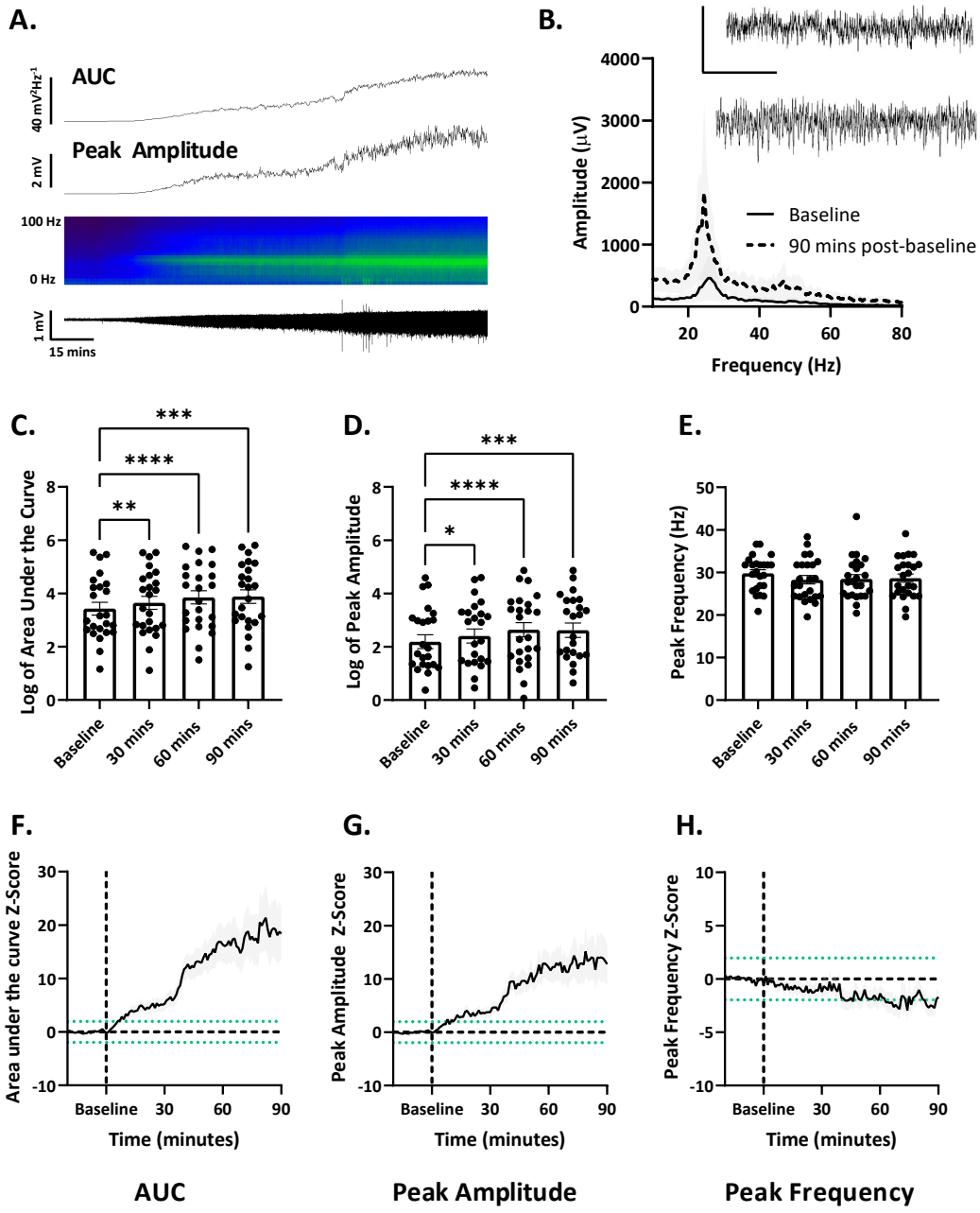

Figure 3.7. The behaviour of established gamma frequency oscillations across time. (A) Representative trace and amplitude parameters showing oscillation growth. (B) Pooled FFTs and representative traces for kainate-induced gamma frequency oscillations at baseline and 90 minutes post-baseline in brain slices from C57BL/6J mice at 3-4 months, both sexes. (C) Area under the curve, (D) peak amplitude, (E) peak frequency of oscillations over 90 minutes. (F, G, H) Z-scores of (C, D, E) respectively. Dotted green line represents $p < 0.05$. Data in C and D are log transformed. RM ANOVA with Tukey post-hoc corrections: * = $p < 0.05$, ** = $p < 0.01$, *** = $p < 0.001$, **** = $p < 0.0001$. Scale bars: 400 μV, 2 seconds. n = 24, N = 24.

3.8. The effect of inflammation on gamma frequency oscillations

The effect of inflammation on gamma frequency oscillations was examined using two methods. Both of these methods were carried out in brain slices from young (3-4 months), C57BL/6J mice (both sexes) in order to isolate the effect of inflammation from the APP/PS1 genotype and from age-related changes. These two methods were carried out in kainate-induced gamma frequency oscillations (Figure 3.8).

For the first method, gamma frequency oscillations were established in brain slices by adding kainate (100 nM). Once the amplitude of gamma frequency oscillations was no longer growing rapidly and a stable baseline had been established, the brain slice was exposed to various inflammatory mediators for 30 minutes. The effect of this exposure on established gamma frequency oscillations was observed during the exposure and for 60 minutes after the exposure ended (post-exposure period).

For the second method, brain slices were incubated in various inflammatory mediators for three hours. Gamma frequency oscillations were then induced in the inflammatory-mediator-treated brain slices by adding kainate (100 nM). The emergence of gamma frequency oscillations in inflammatory-mediator-treated brain slices was observed over 60 minutes.

In summary, these two approaches examined the effect of inflammation on established gamma frequency oscillations and the effect of inflammation on the emergence of gamma frequency oscillations.

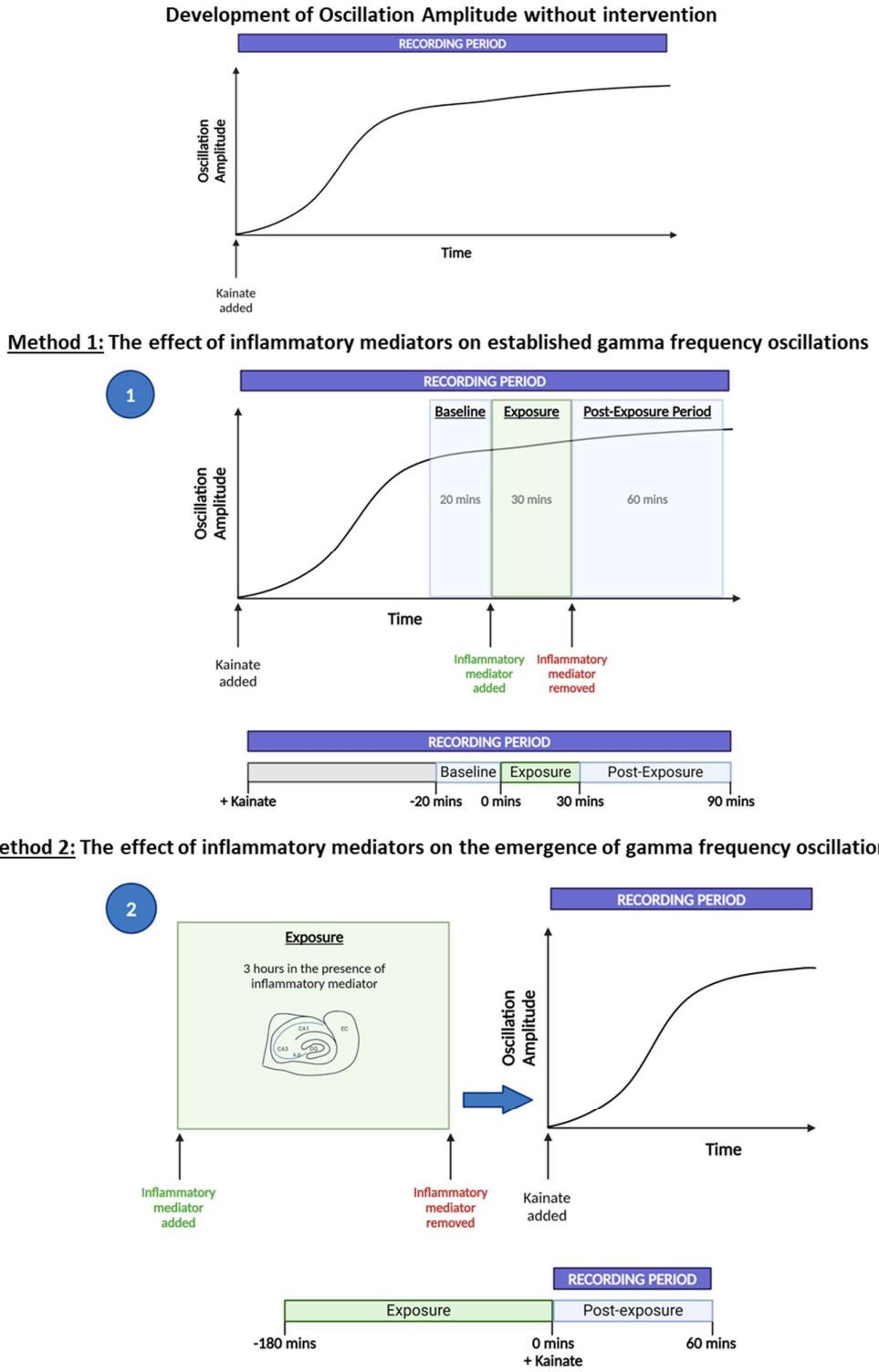

Figure 3.8. Experimental design studies on the effect of inflammation on gamma frequency oscillations. Method 1: the effect of inflammatory mediators on established gamma frequency oscillations. Method 2: the effect of inflammatory mediators on the emergence of gamma frequency oscillations.

3.9. The effect of TNFα on established gamma frequency oscillations

The effect of TNFα on established kainate-induced gamma frequency oscillations in brain slices from C57BL/6J mice at 3-4 months was examined by exposing brain slices with established gamma frequency oscillations to TNFα at a range of concentrations. As before, the growth of the oscillation was observed in real-time by continuous frequency decomposition by Fast Fourier transform. When the oscillation reached a stable baseline, slices were exposed to TNFα (1 ng/mL, 10 ng/mL, 50 ng/mL) for 30 minutes and the effect of this exposure was monitored both during exposure and for the following 60 minutes. In untreated brain slices kainate-induced gamma frequency oscillation amplitude significantly increased over time and the oscillation frequency remained stable. Exposure to TNFα at a range of concentrations inhibited the normal increase in oscillation amplitude and also significantly decreased the oscillation frequency (Figures 3.9 and 3.10).

In untreated slices the area under the curve and peak amplitude slices increased over time (Table 3.1). In slices treated with 1 ng/mL, 10 ng/mL, and 50 ng/mL TNFα both the area under the curve and the peak amplitude did not increase to the same extent as in untreated slices (Table 3.1). Therefore at three concentrations, TNFα inhibited the normal growth in kainate-induced gamma frequency oscillation amplitude. This was also demonstrated by the z-scores calculated at 90 minutes post-exposure for the area under the curve (untreated: 18.41 ± 4.98, TNFα 1 ng/mL: 4.83 ± 4.86, TNFα 10 ng/mL: 3.85 ± 2.24, TNFα 50 ng/mL: 4.17 ± 2.22) and peak amplitude (untreated: 12.76 ± 3.77, TNFα 1 ng/mL: 5.73 ± 4.54, TNFα 10 ng/mL: 2.28 ± 1.65, TNFα 50 ng/mL: 7.16 ± 4.58). There was no significant effect of treatment with TNFα on the area under the curve ($F_{3,53} = 0.33$, $p = 0.8026$) or on the peak amplitude ($F_{3,53} = 0.66$, $p = 0.6571$), however there was a significant effect of time on both parameters (Area under the curve: $F_{2,\ 106.3} = 6.28$, $p = 0.0026$, peak amplitude: $F_{2.1,\ 111.5} = 6.37$, $p = 0.002$) and a significant interaction between time

and treatment with TNFα for the area under the curve ($F_{9,159}$ = 0.13, p = 0.0231) but not the peak amplitude ($F_{9, 159}$ = 1.66, p = 0.1029; Figure 3.10). This demonstrated that gamma frequency oscillation amplitude was increasing over time in both TNFα-treated slices and untreated slices, but treatment with TNFα significantly inhibited this growth in oscillation amplitude.

	Baseline AUC (μV^2 Hz^-)	90 minutes post-exposure AUC (μV^2 Hz^-)	Baseline Peak Amplitude (μV)	90 minutes post-baseline Peak Amplitude (μV)
Untreated	42,782 ± 19,572	89,770 ± 35,304	3,649 ± 1,882	6,793 ± 3,336
TNFα 1 ng/mL	51,114 ± 30,929	65,013 ± 26,157	8,455 ± 5,877	8,788 ± 4093
TNFα 10 ng/mL	36,970 ± 17,135	27,253 ± 7,522	2,134 ± 916.3	3,129 ± 941.4
TNFα 50 ng/mL	18,057 ± 6,000	23,815 ± 7,565	1,360 ± 572.6	2,115 ± 737.1

Table 3.1. Amplitude parameters over time in untreated and TNFα-treated brain slices.

In untreated brain slices the peak frequency was stable over time (baseline: 29.78 ± 0.83 Hz, 90 minutes post-baseline: 28.62 ± 0.97 Hz). In brain slices exposed to TNFα (1 ng/mL, 10 ng/mL, and 50 ng/mL) the oscillation frequency was reduced. The baseline frequencies of the oscillation in slices treated with 1 ng/mL, 10 ng/mL, and 50 ng/mL TNFα were 29.49 ± 1.86 Hz, 33.46 ± 1.97 Hz, and 31.11 ± 1.62 Hz, respectively. TNFα At 90 minutes post-TNFα treatment the peak frequencies were reduced to 25.36 ± 1.94 Hz, 29.25 ± 1.92 Hz, and 26.31 ± 1.62 Hz, respectively. These reduction in oscillation frequency are also demonstrated by the peak frequency z-scores at 90 minutes post-exposure (untreated: - 1.70 ± 0.82, TNFα 1 ng/mL: -3.94 ± 0.62, TNFα 10 ng/mL: -2.78 ± 0.72, TNFα 50 ng/mL: -3.46 ± 1.18). There was no significant effect of treatment with TNFα on peak frequency ($F_{3, 53}$= 1.12, p = 0.3513) but there was significant effect of time ($F_{2.306,122.2}$ = 16.83, p < 0.0001). Post-hoc testing showed that there were no significant

differences between times in untreated brain slices, only in TNFα-treated slices. There was no significant interaction between time and treatment with TNFα ($F_{9, 159}$= 1.61, p = 0.1173).

The inhibitory effect of TNFα treatment on oscillations amplitude growth and oscillation frequency was present at each dose of TNFα used. Post-hoc testing does not show any significant differences in the effect of different concentrations of TNFα.

To conclude, exposure to TNFα inhibited the growth in kainate-induced gamma frequency oscillation amplitude and reduced oscillation frequency.

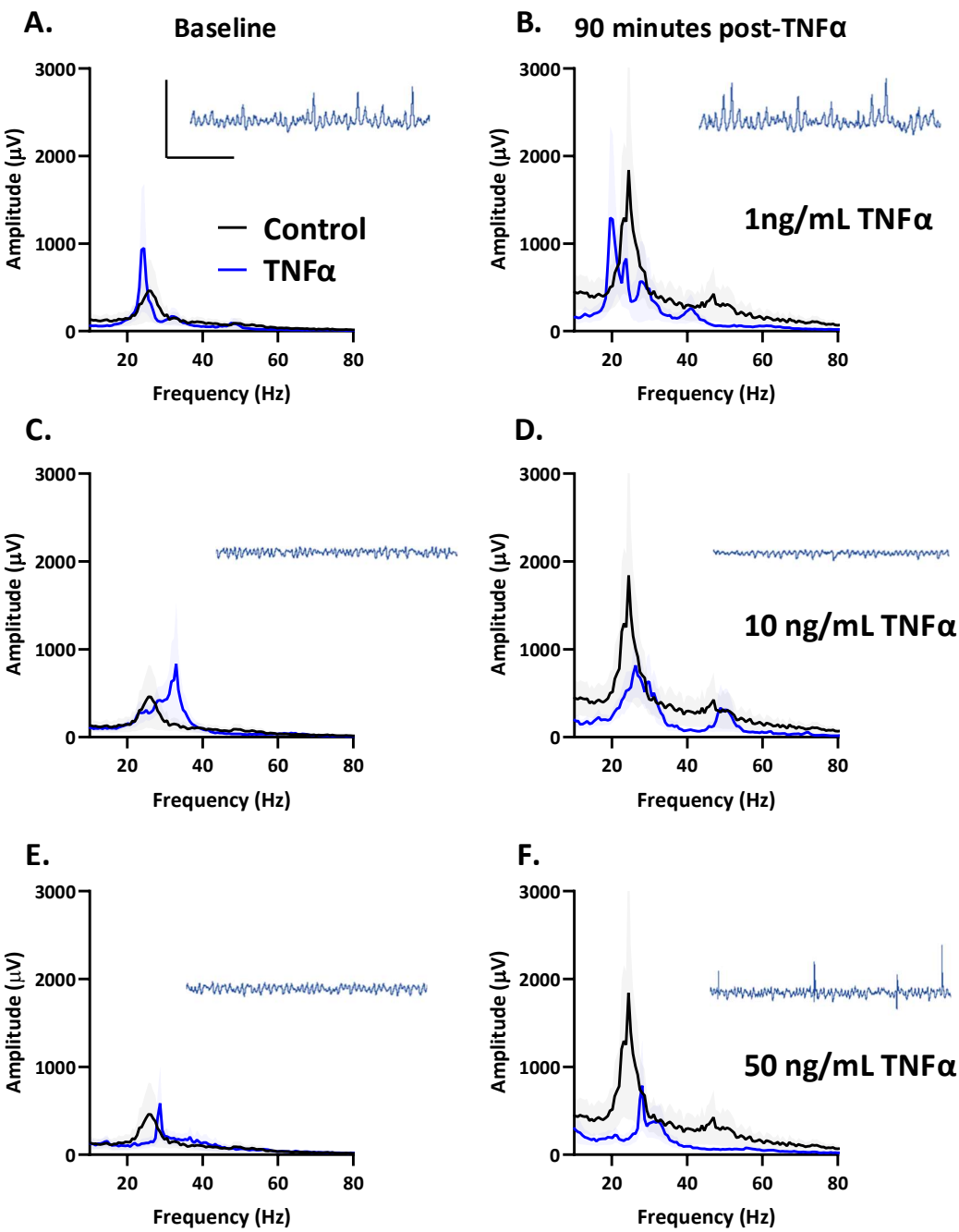

Figure 3.9. The effect of TNFα on established gamma frequency oscillations. Pooled FFTs and representative traces for kainate-induced gamma frequency oscillations at a (A, C, E) Baseline and (B, D, F) 90 minutes post-exposure to TNFα at (A, B) 1 ng/mL, (B, C) 10 ng/mL, and (E, F) 50 ng/mL. Gamma frequency oscillations induced with kainate (100 nM) in brain slices from C57BL/6J mice at 3-4 months. Scale bar: 2000 μV, 0.5 seconds. TNFα 50 ng/mL: n = 14, N = 14; TNFα 10 ng/mL: n = 11, N = 11; TNFα 1ng/mL: n = 8, N = 8.

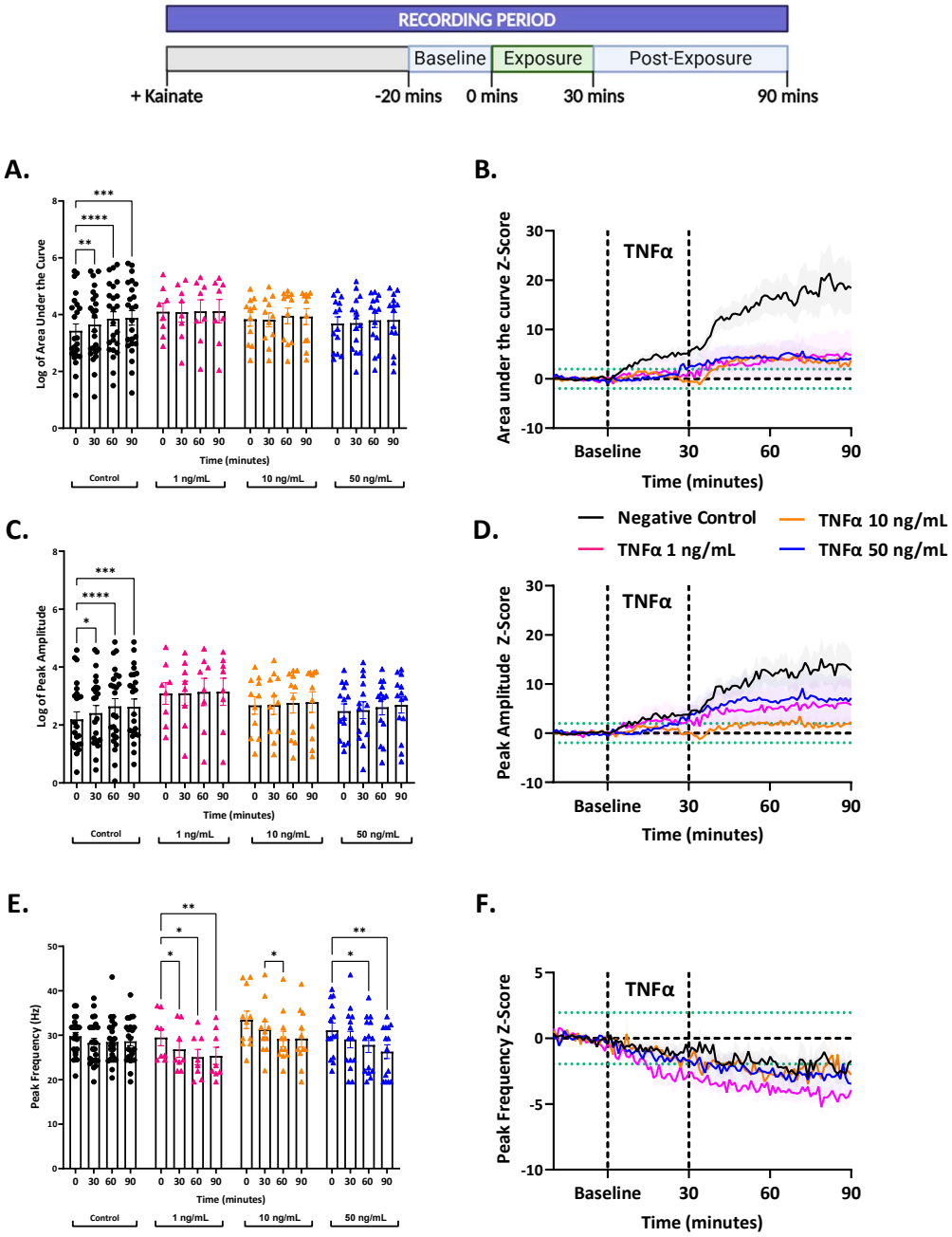

Figure 3.10. The effect of TNFα on established gamma frequency oscillations. (A) Area under the curve, (C) peak amplitude, and (E) peak frequency across 90 minutes of established oscillations in brain slices from C57BL/6J mice (3-4 months) exposed to TNFα (1, 50, 10 ng/mL) for 30 minutes. (B, D, F) Z-scores of (A, C, E) respectively. Dotted green line represent $p < 0.05$. Data in A and C are log transformed. 2-way ANOVA RM with Tukey post-hoc corrections: * = $p < 0.05$, ** = $p < 0.01$, *** = $p < 0.001$, **** = $p < 0.0001$. Control: n = 24, N = 24; TNFα 50 ng/mL: n = 14, N = 14; TNFα 10 ng/mL: n = 11, N = 11; TNFα 1ng/mL: n = 8, N = 8.

3.10. The effect of TNFα on gamma frequency oscillation emergence

Brain slices were treated with TNFα (10 ng/mL and 50 ng/mL) for three hours before gamma frequency oscillations were induced with kainate (100 nM). The effect of this 3 hour treatment with TNFα on the emergence of gamma frequency oscillation was observed over 60 minutes (Figure 3.11).

In untreated slices the oscillation amplitude increased over 60 minutes. The area under the curve stabilised at approximately 7500 μV^2Hz^- and the peak amplitude stabilised at approximately 600 μV. The peak frequency in untreated slices increased from 20 Hz to stabilise at approximately 30 Hz. Treatment with TNFα at 50ng/mL, but not at 10 ng/mL, significantly inhibited the amplitude and frequency of the gamma frequency oscillations which emerge in treated slices (Figure 3.11). The reduced growth in gamma frequency oscillation amplitude following treatment with TNFα (50ng/mL) was demonstrated by the reduction in the area under the curve and the peak amplitude at 60 minutes after application of kainate (area under the curve: 2594.57 ± 1712.18 μV^2Hz^-, peak amplitude: 263.18 ± 152.51 μV). There was a significant effect of time on both the area under the curve ($F_{1.361,42.2} = 8.70$, $p = 0.0024$) and peak amplitude ($F_{1.458,45.2} = 5.69$, $p = 0.0119$). Post-hoc testing showed this effect occurred from 25 to 37 minutes after kainate application in slices treated with TNFα at 50ng/mL relative to both untreated slice and slices treated with TNFα (10ng/mL). There was no significant effect of treatment with TNFα on area under the curve ($F_{2, 31} = 2.11$, $p = 0.1388$) or peak amplitude ($F_{2, 31} = 1.72$, $p = 0.1962$), or significant interaction with treatment and time ($F_{120, 1860} = 0.98$, $p = 0.5464$, and $F_{120, 1860} = 0.91$, $p = 0.7560$).

In untreated brain slices the peak frequency was 29.84 ± 2.06 Hz at 60 minutes after kainate application. The peak frequency of the oscillation which emerged following kainate application was reduced in TNFα-treated slices. In TNFα-treated brain slices, at 60 minutes after kainate

application treatment the peak frequency was 23.23 ± 2.07 Hz for 50 ng/mL TNFα and 25.39 ± 3.19 Hz for 10 ng/mL TNFα. There was a significant effect of treatment with TNFα on the peak frequency of emergent gamma frequency oscillations ($F_{2,31}$ = 4.25, p = 0.0234). As the oscillation frequency increased over time in both treated and untreated slices, there was also significant effect of time ($F_{7.297,226.2}$ = 3.27, p = 0.0021); there was no interaction between time and treatment with TNFα ($F_{120, 1860}$ = 1.18, p = 0.0913). Unlike the effect of TNFα treatment on amplitude, which only occurred at 50 ng/mL, the effect of TNFα on emergent gamma frequency oscillation peak frequency occurred at both concentrations.

To conclude, the gamma frequency oscillations which emerged following kainate application in brain slices treated with TNFα for 3 hours had reduced frequency (for TNFα at 10 ng/mL and 50 ng/mL) and reduced amplitude (for TNFα at 50 ng/mL) compared to the gamma frequency oscillations which emerge following kainate treatment in untreated brain slices.

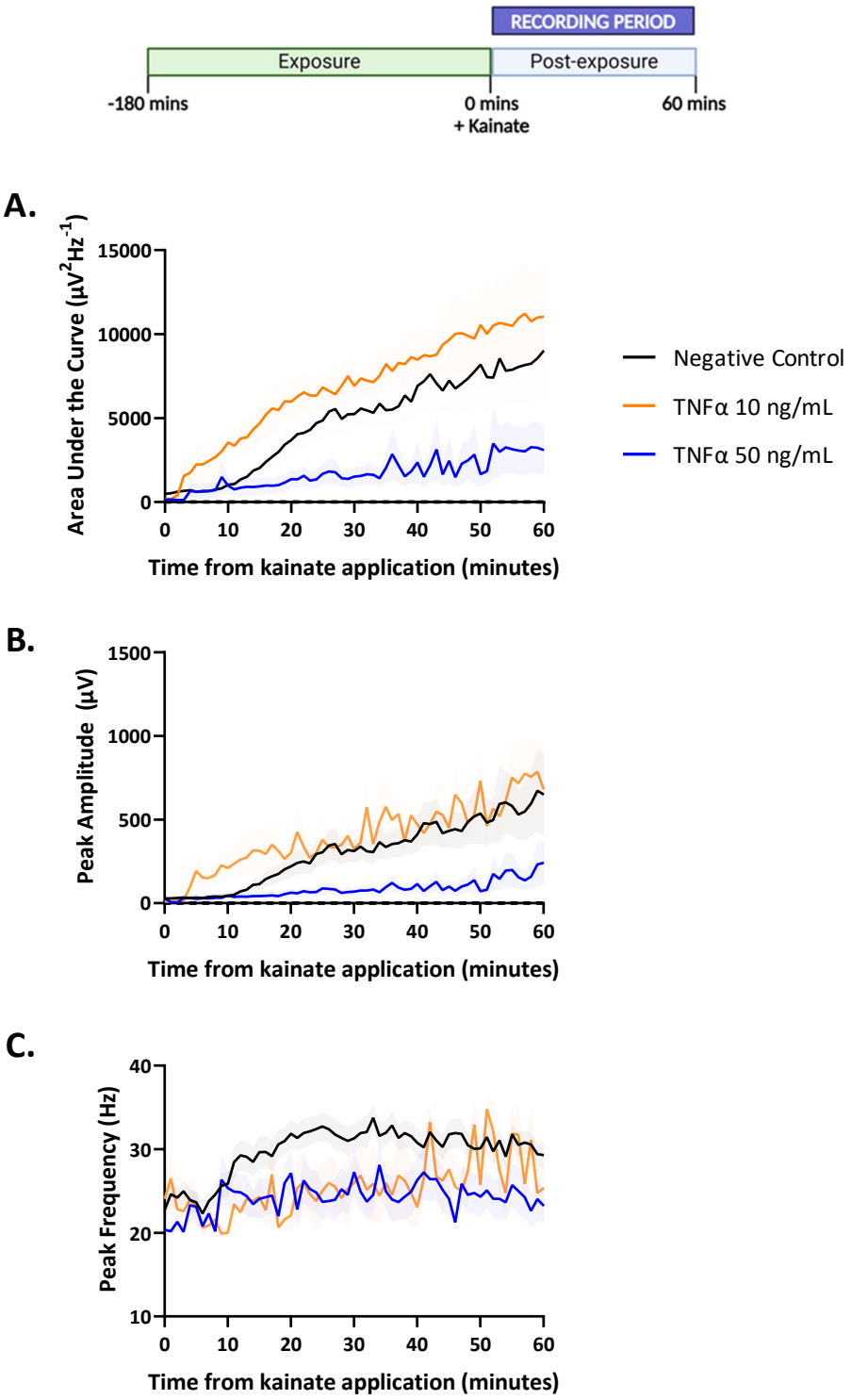

Figure 3.11. The effect of TNFα treatment on gamma frequency oscillation emergence. Kainate-induced gamma frequency oscillation (A) Area under the curve, (B) peak Amplitude, and (C) peak frequency, in brain slices treated for 3 hours with TNFα (50 ng/mL, 10 ng/mL). Control: n= 24, N = 22; TNFα 50 ng/mL: n = 9, N = 7; TNFα 10 ng/mL: n = 6, N = 5.

3.11. The effect of CCL2 on established gamma frequency oscillations

The effect of CCL2 on ongoing kainate-induced gamma frequency oscillations in brain slices from C57BL/6J mice at 3-4 months was examined by exposing brain slices with established gamma frequency oscillations to CCL2 at a range of concentrations (1 ng/mL, 10 ng/mL, and 50 ng/mL) for 30 minutes. The effect of this exposure was monitored both during exposure and for the following 60 minutes. In untreated brain slices kainate-induced gamma frequency oscillation amplitude significantly increased over time and the oscillation frequency remained stable. Exposure to CCL2 at 1 ng/mL and 10 ng/mL inhibited the normal increase in oscillation amplitude. Exposure to CCL2 at all concentrations decreased the peak frequency of the gamma frequency oscillation (Figures 3.12 and 3.13).

	Baseline AUC ($\mu V^2 Hz^-$)	**90 minutes post-exposure AUC ($\mu V^2 Hz^-$)**	**Baseline Peak Amplitude (μV)**	**90 minutes post-baseline Peak Amplitude (μV)**
Untreated	42,782 ± 19,572	89,770 ± 35,304	3,649 ± 1,882	6,793 ± 3,336
CCL2 1 ng/mL	19,651 ± 131,95	18,661 ± 10,079	2,857 ± 2,064	1,931 ± 1,229
CCL2 10 ng/mL	31,112 ± 13,927	35,756 ± 16,506	2,809 ± 1,326	3,032 ± 1,658
CCL2 50 ng/mL	26,474 ± 9,616	46,633 ± 16,620	2,104 ± 915.5	3,374 ± 1,197

Table 3.2. Amplitude parameters over time in untreated and CCL2-treated brain slices.

In untreated slices the area under the curve and peak amplitude slices increased over time. This growth in oscillation amplitude was inhibited in slices treated with CCL2 at 1 ng/mL and 10 ng/mL, but not at 50 ng/mL. This was demonstrated by both the area under the curve and the peak amplitude (Table 3.2). This was also demonstrated by the z-scores calculated at 90 minutes post-exposure for the area under the curve (untreated: 18.41 ± 4.98, CCL2 1 ng/mL: 9.92 ± 5.34, CCL2 10 ng/mL: -0.84 ± 2.56, CCL2 50 ng/mL: 7.58 ± 1.77) and peak amplitude (untreated:

12.76 ± 3.77, CCL2 1 ng/mL: 6.03 ± 3.60, CCL2 10 ng/mL: -0.07 ± 1.65, CCL2 50 ng/mL: 6.95 ± 2.23). There was no significant effect of treatment with CCL2 on the area under the curve parameter ($F_{3,54} = 0.48$, $p = 0.7008$) or on the peak amplitude parameter ($F_{3,54} = 0.67$, $p = 0.5742$), however there was a significant effect of time on both parameters (Area under the curve: $F_{1.889, 102} = 15.77$, $p < 0.0001$, peak amplitude: $F_{1.909, 103.1} = 11.03$, $p < 0.0001$) and a significant interaction between time and treatment with CCL2 for the area under the curve ($F_{9,162} = 3.88$, $p = 0.0002$) and peak amplitude ($F_{9,162} = 3.21$, $p = 0.0013$). This demonstrated that gamma frequency oscillations were increasing over time in both CCL2-treated slices and untreated slices, but treatment with CCL2 significantly inhibited this growth in oscillation amplitude.

In untreated brain slices the peak frequency was stable over time (baseline: 29.78 ± 0.83 Hz, 90 minutes post-baseline: 28.62 ± 0.97 Hz). In brain slices exposed CCL2 (1 ng/mL, 10 ng/mL, and 50 ng/mL) the oscillation frequency was reduced. The baseline peak frequencies of the oscillation in slices treated with 1 ng/mL, 10 ng/mL, and 50 ng/mL CCL2 were 30.84 ± 2.77, 28.74 ± 2.37 Hz, and 33.02 ± 1.22 Hz, respectively. At 90 minutes post-CCL2 treatment the peak frequencies were reduced to 27.55 ± 2.37 Hz, 24.68 ± 1.66 Hz, and 27.99 ± 1.55 Hz, respectively. There was no significant effect of treatment with CCL2 on peak frequency ($F_{3, 54} = 0.8625$, $p = 0.4662$) but there was significant effect of time ($F_{2.612,141} = 9.417$, $p < 0.0001$). Post-hoc testing showed that there were no significant differences between times in untreated brain slices, only in CCL2-treated slices. There was no significant interaction between time and treatment with CCL2 ($F_{9, 1162} = 1.333$, $p = 0.2235$).

To conclude, exposure to CCL2 inhibited the growth in kainate-induced gamma frequency oscillation amplitude and reduced oscillation frequency. This effect was strongest at 10 ng/mL CCL2.

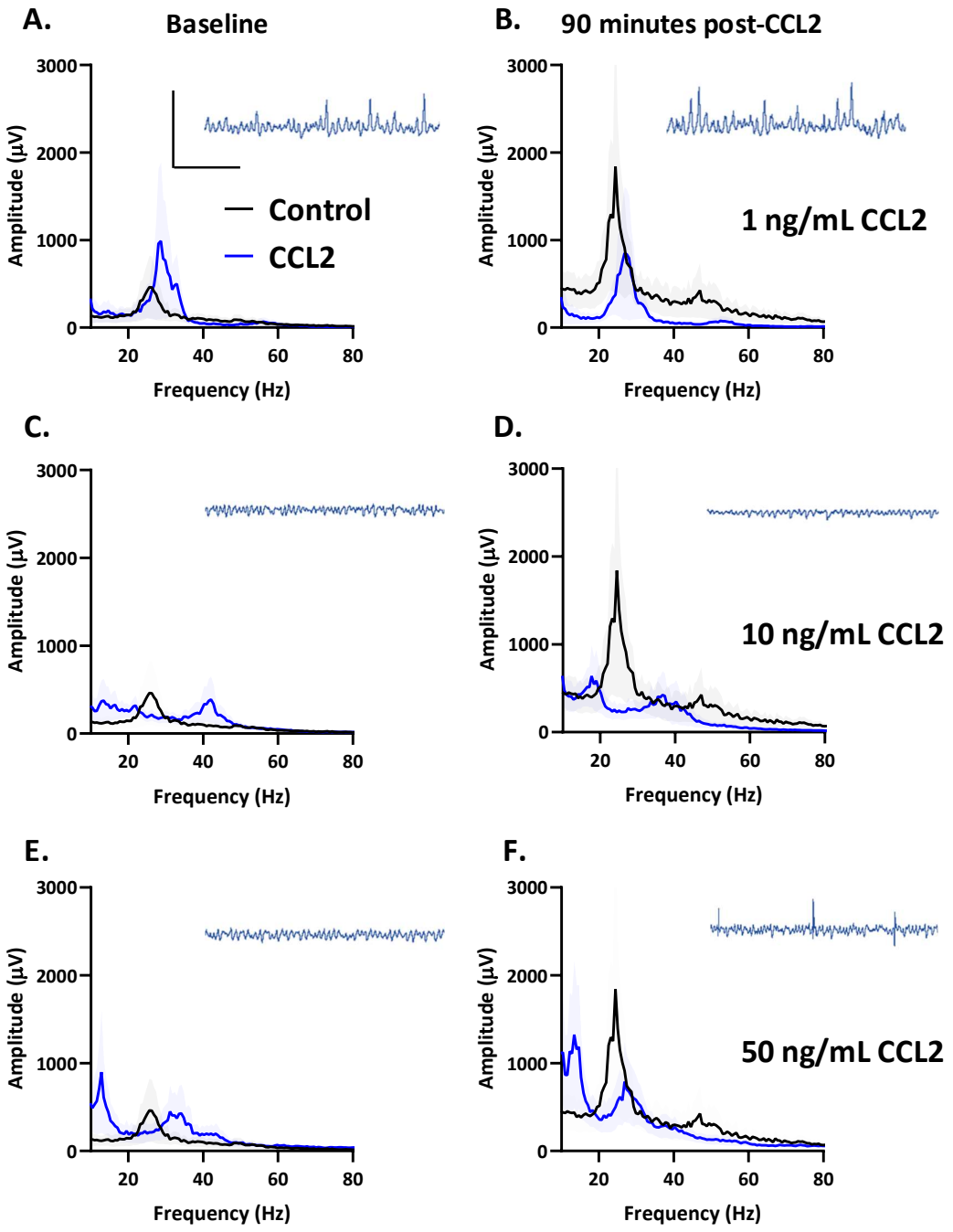

Figure 3.12. The effect of CCL2 on established gamma frequency oscillations. Pooled FFTs and representative traces for kainate-induced gamma frequency oscillations at a (A, C, E) Baseline and (B, D, F) 90 minutes post-exposure to CCL2 at (A, B) 1 ng/mL, (B, C) 10 ng/mL, and (E, F) 50 ng/mL. Gamma frequency oscillations induced with kainate (100 nM) in brain slices from C57BL/6J mice at 3-4 months. Scale bar: 2000 µV, 0.5 seconds. Control: n = 24, N = 24; CCL2 50 ng/mL: n = 17, N = 17; CCL2 10 ng/mL: n = 10, N = 10; CCL2 1 ng/mL: n = 7, N = 7.

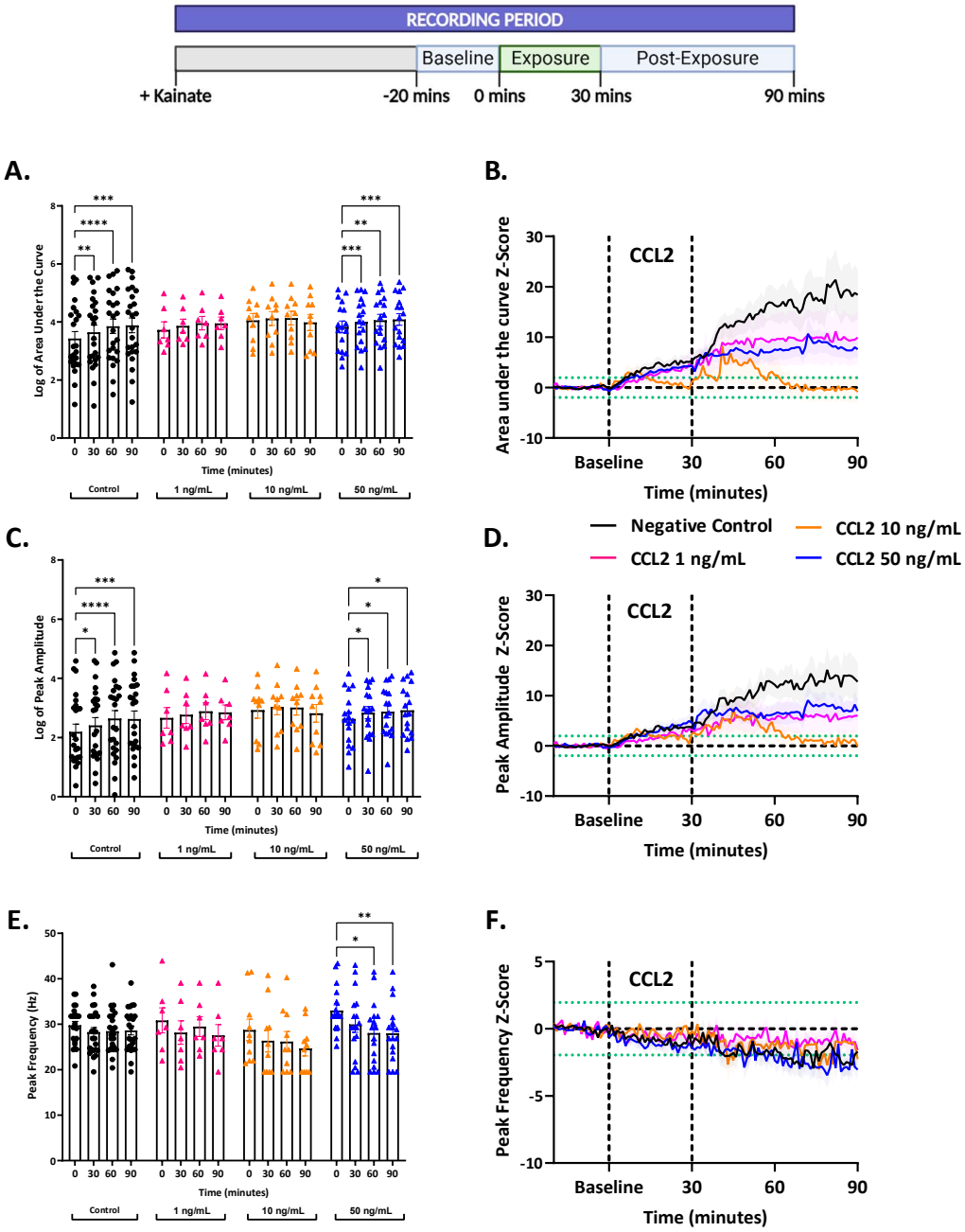

Figure 3.13. The effect of CCL2 on established gamma frequency oscillations. (A) Area under the curve, (C) peak amplitude, and (E) peak frequency across 90 minutes of established oscillations in brain slices from C57BL/6J mice (3-4 months) exposed to CCL2 (1, 50, 10 ng/mL) for 30 minutes. (B, D, F) Z-scores of (A, C, E) respectively. Dotted green line represent $p < 0.05$. Data in A and C are log transformed. 2-way ANOVA RM with Tukey post-hoc corrections: * = $p < 0.05$, ** = $p < 0.01$, *** = $p < 0.001$, **** = $p < 0.0001$. Control: n = 24, N = 24; CCL2 50 ng/mL: n = 17, N = 17; CCL2 10 ng/mL: n = 10, N = 10; CCL2 1 ng/mL: n = 7, N = 7.

3.12. The effect of CCL2 on gamma frequency oscillation emergence

Brain slices were treated with CCL2 (50 ng/mL) for three hours before gamma frequency oscillations were induced with kainate (100 nM). The effect of this 3 hour treatment with CCL2 on the emergence of gamma frequency oscillation was observed over 60 minutes (Figure 3.14).

In untreated slices the oscillation amplitude increased over 60 minutes. The area under the curve parameter stabilised at approximately 7,500 μV^2Hz^- and the peak amplitude parameter stabilised at approximately 600 μV. The peak frequency in untreated slices increased from 20 Hz to stabilise at approximately 30 Hz. Treatment with CCL2 significantly inhibited the amplitude and frequency of the gamma frequency oscillations which emerge in CCL2-treated slices (Figure 3.14). The reduced growth in gamma frequency oscillation amplitude following treatment with CCL2 was demonstrated by the reduction in the area under the curve and the peak amplitude at 60 minutes after kainate application (area under the curve: 4,583.38 ± 2,435.13 μV^2Hz^-, peak amplitude: 314.57 ± 155.52 μV). There was a significant effect of time on both the area under the curve ($F_{1.347,35.03} = 5.87$, $p = 0.0134$) and peak amplitude ($F_{1.416, 36.81} = 4.91$, $p = 0.0221$). Post-hoc testing shows this effect occurred from 17 to 35 minutes after kainate application in slices treated with CCL2. There was no significant effect of treatment with CCL2 on area under the curve ($F_{2, 26} = 1.31$, $p = 0.2631$) or peak amplitude ($F_{1, 26} = 0.98$, $p = 0.3307$), or significant interaction with treatment and time ($F_{60, 1560} = 0.560$, $p = 0.9942$, and $F_{60, 11560} = 0.43$, $p > 0.9999$).

In untreated brain slices the peak frequency was 29.84 ± 2.06 Hz at 60 minutes after kainate application. The peak frequency of the oscillation which emerged following kainate treatment was reduced in CCL2-treated slices. In CCL2-treated brain slices, at 60 minutes after kainate application the peak frequency was 26.99 ± 2.55 Hz. There was no significant effect of treatment with CCL2 on the peak frequency of emergent gamma frequency oscillations ($F_{1, 26} = 0.69$, $p = 0.4139$). As the oscillation frequency increased over time in both CCL2-treated and untreated

slices, there was a significant effect of time ($F_{5.771, 150} = 3.74$, $p = 0.002$) and there was no interaction between time and treatment with CCL2 ($F_{60, 1560} = 0.75$, $p = 0.9233$).

To conclude, the gamma frequency oscillations which emerged following kainate application in brain slices treated with CCL2 for 3 hours had reduced frequency and reduced amplitude compared to the gamma frequency oscillations which emerge following kainate application in untreated brain slices.

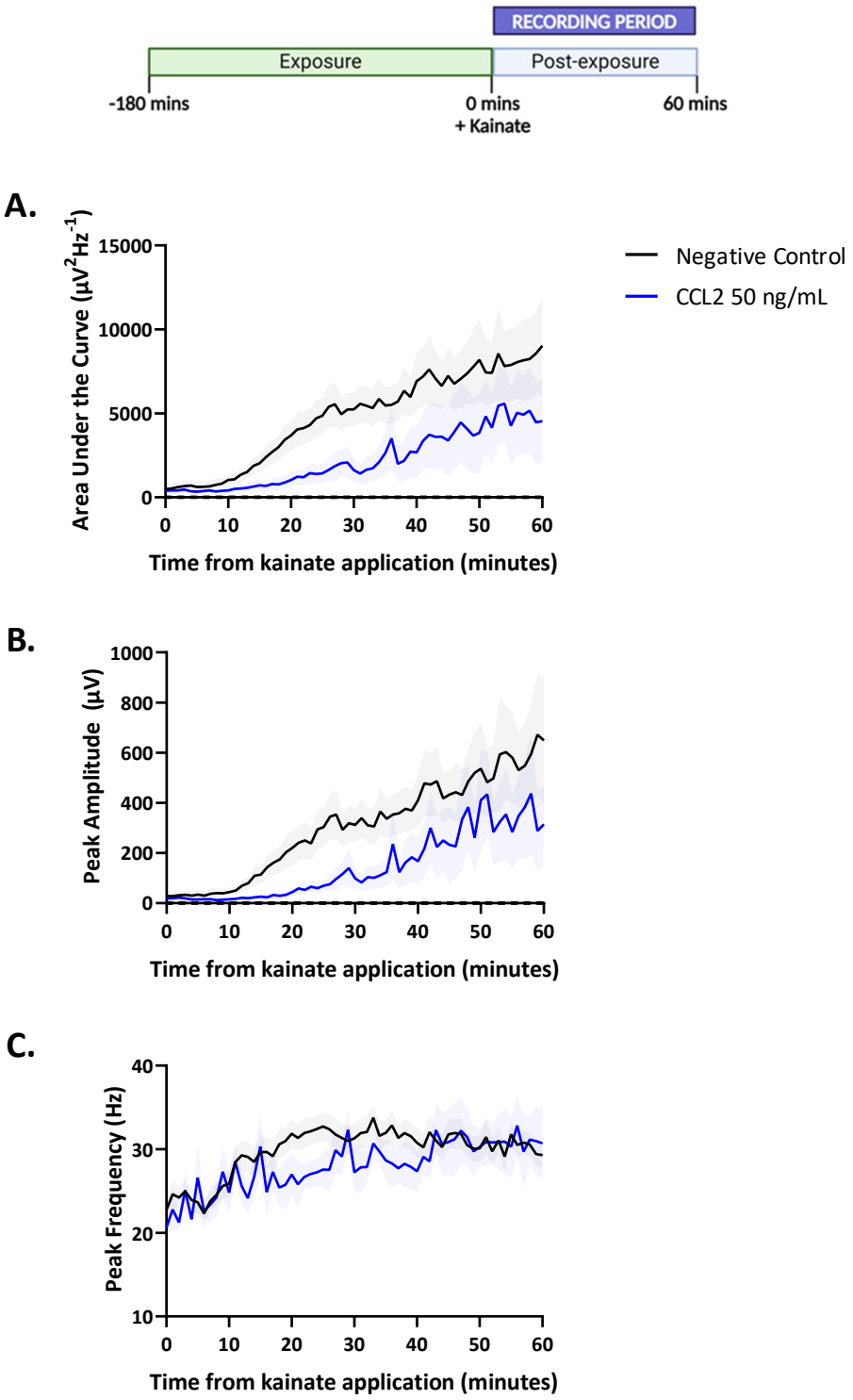

Figure 3.14. The effect of CCL2 treatment on gamma frequency oscillation emergence. Kainate-induced gamma frequency oscillation (A) Area under the curve, (B) peak amplitude, and (C) peak frequency, in brain slices treated for 3 hours with CCL2 (50 ng/mL). Control: n = 24, N = 22; CCL2 50 ng/mL: n = 8, N = 6.

3.13. The effect of IL-1β on established gamma frequency oscillations

The effect of IL-1β on ongoing kainate-induced gamma frequency oscillations in brain slices from C57BL/6J mice at 3-4 months was examined by exposing brain slices with established gamma frequency oscillations to IL-1β at 10 ng/mL for 30 minutes. The effect of this exposure was monitored both during exposure and for the following 60 minutes In untreated brain slices kainate-induced gamma frequency oscillation amplitude significantly increased over time and the oscillation frequency remained stable. Exposure to IL-1β inhibited the increase in oscillation amplitude observed in untreated slices. Exposure to IL-1β did not affect the oscillation frequency (Figure 3.15).

In untreated slices the area under the curve increased from 42,782 ± 19,572 μV^2Hz^- to 89,770 ± 35,304 μV^2Hz^- at 90 minutes after the baseline. Similarly the peak amplitude in untreated slices increased from 3,649 ± 1,882 μV at the baseline to 6,793 ± 3,336 μV at 90 minutes after the baseline. At baseline, in slices treated with IL-1β the area under the curve was 45,203 ± 38,460 μV^2Hz^-. At 90 minutes post-IL-1β treatment the area under the curve was 36,368 ± 29,305 μV^2Hz^-. This represented a decrease in oscillation amplitude, unlike the increase observed in untreated slices. Therefore IL-1β inhibited the growth in kainate-induced gamma frequency oscillation amplitude. This finding was reinforced by the peak amplitude, the normal growth of which was inhibited by exposure IL-1β. The peak amplitude at baseline for brain slices treated with IL-1β was 5,777 ± 5,223 μV. At 90 minutes post-IL-1β treatment the peak amplitude was 5,272 ± 4,664 μV. This is further demonstrated by the z-scores calculated at 90 minutes post-exposure for these parameters (area under the curve: untreated: 18.41 ± 4.98, IL-1β: 1.14 ± 2.19; peak amplitude: 12.76 ± 3.77, IL-1β: 1.84 ± 1.18). There was no significant effect of treatment with IL-1β on the area under the curve parameter ($F_{1,27}$ = 0.39, p = 0.5395) or on the peak amplitude parameter ($F_{2.302, 62.16}$ = 0.61, p = 0.4411), however there was a significant effect of time

on both parameters (area under the curve: $F_{2.019, 54.52} = 4.43$, $p = 0.0162$, peak amplitude: $F_{2.302, 62.16} = 4.93$, $p = 0.0076$) and a significant interaction between time and treatment with IL-1β for the area under the curve ($F_{9, 81} = 3.82$, $p = 0.0129$) but not for the peak amplitude ($F_{3, 81} = 2.38$, $p = 0.0761$; Figure 3.15). This demonstrated that gamma frequency oscillations were increasing over time in both IL-1β-treated slices and untreated slices, but treatment with IL-1β significantly inhibited this growth in oscillation amplitude.

In untreated brain slices the peak frequency was stable over time (baseline: 29.78 ± 0.83 Hz, 90 minutes post-baseline: 28.62 ± 0.97 Hz). In brain slices exposed IL-1β the oscillation frequency is also stable over time (baseline: 30.13 ± 1.85 Hz, 90 minutes post-IL-1β: 29.41 ± 2.62 Hz).

To conclude, exposure to IL-1β inhibited the growth in kainate-induced gamma frequency oscillation amplitude but did not reduce oscillation frequency.

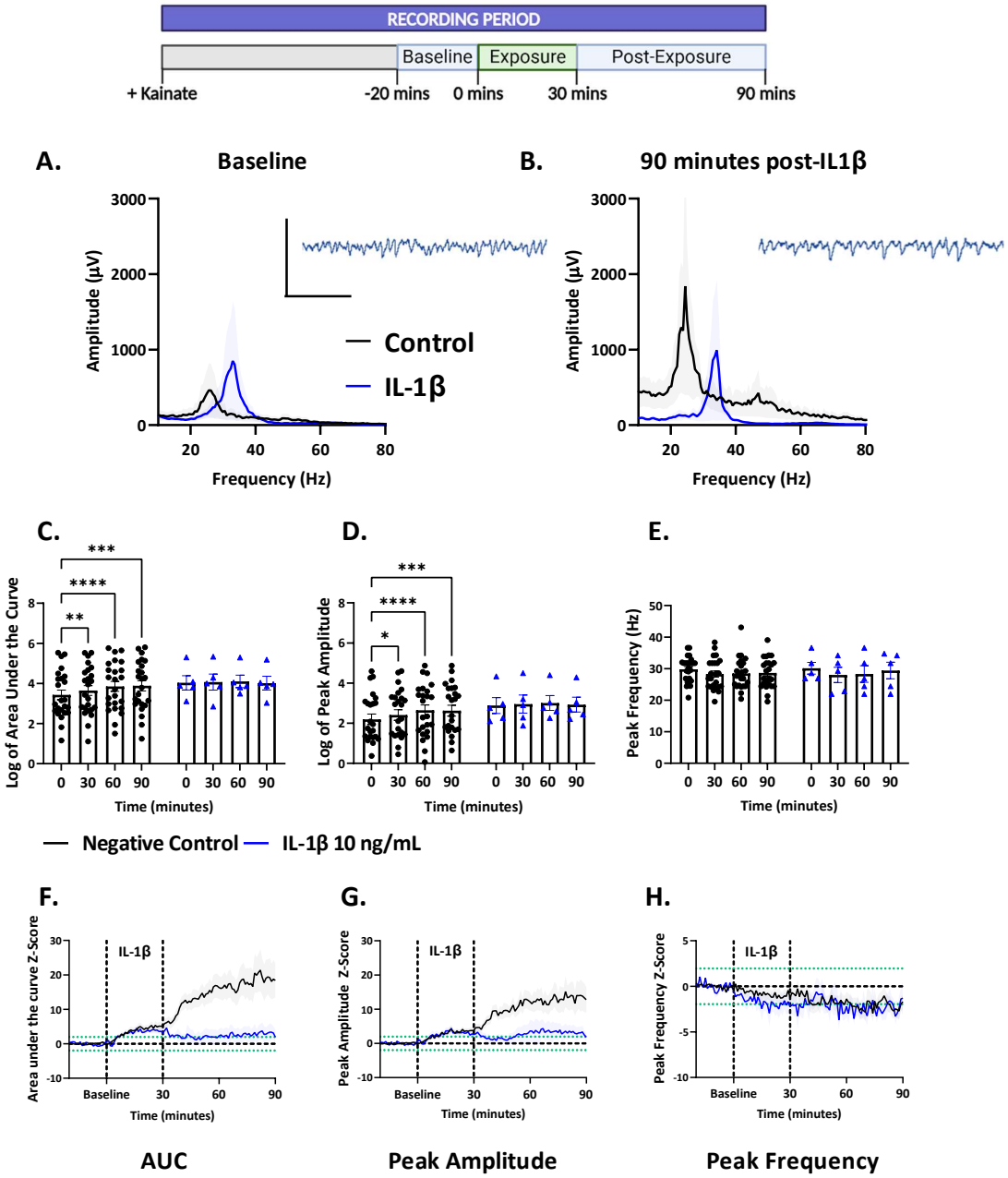

Figure 3.15. The effect of IL-1β on established gamma frequency oscillations. Pooled FFTs and representative traces for kainate-induced gamma frequency oscillations at a (A) Baseline and (B) 90 minutes post-exposure to IL-1β (10 ng/mL). (C) Area under the curve, (D) peak amplitude, and (E) peak frequency across 90 minutes of gamma frequency oscillations in brain slices from C57BL/6J mice at 3-4 months.(F, G, H) Z-scores of (C, D, E) respectively. Dotted green line represent $p < 0.05$. Data in C and D are log transformed. 2-way ANOVA RM with Tukey post-hoc corrections: * = $p < 0.05$, ** = $p < 0.01$, *** = $p < 0.001$, **** = $p < 0.0001$. Scale bar: 2000 μV, 0.5 seconds.Control: n = 24, N = 24; IL-1β 10 ng/mL: n = 5, N = 5.

3.14. The effect of PGE2 on established gamma frequency oscillations

The effect of prostaglandin E2 (PGE2) on ongoing kainate-induced gamma frequency oscillations in brain slices from C57BL/6J mice at 3-4 months was examined by exposing brain slices with established gamma frequency oscillations to PGE2 at 50 ng/mL for 30 minutes. The effect of this exposure was monitored both during exposure and for the following 60 minutes In untreated brain slices kainate-induced gamma frequency oscillation amplitude significantly increased over time and the oscillation frequency remained stable. Exposure to PGE2 inhibited the normal increase in oscillation amplitude. Exposure to PGE2 also decreased the oscillation frequency (Figure 3.16).

In untreated slices the area under the curve increased from 42,782 ± 19,572 μV^2Hz^- to 89,770 ± 35,304 μV^2Hz^- at 90 minutes after the baseline. Similarly the peak amplitude in untreated slices increased from 3,649 ± 1,882 μV at the baseline to 6,793 ± 3,336 μV at 90 minutes after the baseline. At baseline, in slices treated with 50 ng/mL PGE2 the area under the curve was 9,343 ± 5,829 μV^2Hz^-. At 90 minutes post-PGE2 treatment the area under the curve was 12,749 ± 6,625 μV^2Hz^-. This represented a smaller increase than the increase seen in untreated slices. Therefore PGE2 inhibited the growth in kainate-induced gamma frequency oscillation amplitude. This finding was reinforced by the peak amplitude, the normal growth of which was inhibited by exposure PGE2. The average peak amplitude parameter at the baseline for brain slices exposed to PGE2 was 616.7 ± 433.2 μV. At 90 minutes post-PGE2 treatment the peak amplitude was 857.5 ± 473.2 μV. This is further demonstrated by the z-scores calculated at 90 minutes post-exposure for these parameters (area under the curve: untreated: 18.41 ± 4.98, PGE2: 9.54 ± 5.54; peak amplitude: 12.76 ± 3.77, PGE2: 7.51 ± 4.68). There was no significant effect of treatment with PGE2 on the area under the curve parameter ($F_{1, 31} = 0.8266$, $p = 0.3703$) or on the peak amplitude parameter ($F_{1, 31} = 0.81$, $p = 0.3754$), however there was a significant effect of

time on both parameters (Area under the curve: $F_{1.813, 56.19} = 11.16$, $p = 0.0001$, peak amplitude: $F_{1.874, 58.11} = 10.15$, $p = 0.0002$). There was a trend towards a significant interaction between time and treatment with PGE2 for the area under the curve ($F_{3, 93} = 2.32$, $p = 0.0802$) and for the peak amplitude ($F_{3, 93} = 1.61$, $p = 0.1935$; Figure 3.16). This demonstrated that gamma frequency oscillations were increasing over time in both PGE2-treated slices and untreated slices, but treatment with PGE2 inhibited this growth in oscillation amplitude.

In untreated brain slices the peak frequency was stable over time (baseline: 29.78 ± 0.83 Hz, 90 minutes post-baseline: 28.62 ± 0.97 Hz). In brain slices exposed to PGE2 the oscillation frequency was reduced. The baseline frequency of the oscillation in slices treated with PGE2 was 33.44 ± 0.79 Hz. At 90 minutes post-PGE2 treatment the peak frequency was reduced to 30.32 ± 0.72 Hz. There was no significant effect of treatment with PGE2 on peak frequency ($F_{1, 31} = 3.25$, $p = 0.0811$) but there was a significant effect of time ($F_{2.821, 87.46} = 4.61$, $p = 0.0057$). Post-hoc testing showed that there were no significant differences between times in untreated brain slices, only in PGE2-treated slices. There was a trend towards a significant interaction between time and treatment with PGE2, suggesting the effect of time on peak frequency was varied by treatment with PGE2 ($F_{3, 93} = 2.35$, $p = 0.0776$). To conclude, exposure to PGE2 inhibited the growth in kainate-induced gamma frequency oscillation amplitude and reduced oscillation peak frequency.

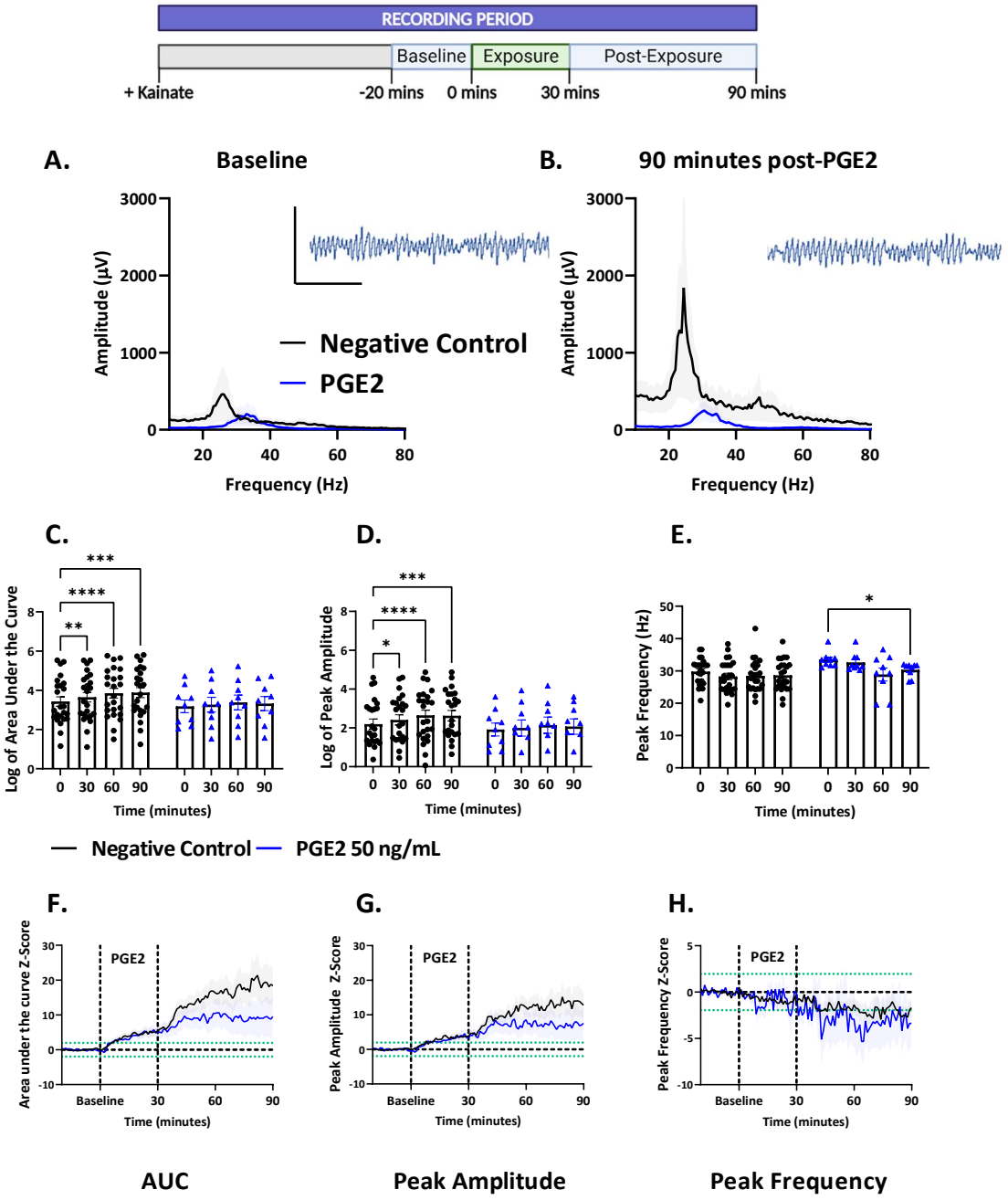

Figure 3.16. The effect of PGE2 on established gamma frequency oscillations. Pooled FFTs and representative traces for kainate-induced gamma frequency oscillations at a (A) Baseline and (B) 90 minutes post-exposure to PGE2 (50 ng/mL). (C) Area under the curve, (D) peak amplitude, and (E) peak frequency across 90 minutes of gamma frequency oscillations in brain slices from C57BL/6J mice at 3-4 months.(F, G, H) Z-scores of (C, D, E) respectively. Dotted green line represent $p < 0.05$. Data in C and D are log transformed. 2-way ANOVA RM with Tukey post-hoc corrections: * = $p < 0.05$, ** = $p < 0.01$, *** = $p < 0.001$, **** = $p < 0.0001$. Scale bar: 2000 µV, 0.5 seconds. Control: n = 24, N = 24; PGE2 50 ng/mL: n = 9, N = 9.

3.15. The effect of PGE2 on gamma frequency oscillation emergence

Brain slices were treated with PGE2 (50 ng/mL) for three hours before gamma frequency oscillations were induced with kainate (100 nM). The effect of this 3 hour treatment with PGE2 on the emergence of gamma frequency oscillation was observed over 60 minutes (Figure 3.17).

In untreated slices the oscillation amplitude increased over 60 minutes. The area under the curve parameter stabilised at approximately 7,500 μV^2Hz^- and the peak amplitude parameter stabilised at approximately 600 μV. The peak frequency in untreated slices increased from 20 Hz to stabilise at approximately 30 Hz. Treatment with PGE2 significantly inhibited the amplitude, but not the frequency, of the gamma frequency oscillations which emerged in PGE2-treated slices (Figure 3.17). The reduced growth in gamma frequency oscillation amplitude following treatment with PGE2 was demonstrated by the reduction in the area under the curve and the peak amplitude at 60 minutes after kainate application (area under the curve: 1,797.11 ± 904.43 μV^2Hz^-, peak amplitude: 98.15 ± 42.89 μV). There was a significant interaction between time and treatment with PGE2 on both the area under the curve ($F_{60, 1620} = 1.73$, $p = 0.0006$) and the peak amplitude ($F_{60, 1620} = 1.54$, $p = 0.0057$). There was a significant effect of time on area under the curve ($F_{1.318, 35.59} = 4.54$, $p = 0.0304$) but not on peak amplitude ($F_{1.366, 36.89} = 3.18$, $p = 0.0705$). This demonstrated the amplitude of the oscillation which emerged was growing in both untreated slices and slices treated with PGE2, but treatment with PGE2 was significantly inhibiting the growth of oscillation amplitude. There was no significant main effect of treatment with PGE2 on area under the curve ($F_{1, 27} = 3.32$, $p = 0.0797$) or peak amplitude ($F_{1, 27} = 2.75$, $p = 0.1086$).

In untreated brain slices the peak frequency was 29.84 ± 2.06 Hz at 60 minutes after kainate application. The peak frequency of the oscillation which emerged following kainate application was similar in PGE2-treated slices. In PGE2-treated brain slices, at 60 minutes after kainate application the peak frequency was 28.97 ± 4.25 Hz. There was no significant effect of treatment

with PGE2 on the peak frequency of emergent gamma frequency oscillations ($F_{1, 27} = 1.66$, $p = 0.2091$). As the oscillation frequency increased over time in both treated and untread slices, there was a significant effect of time ($F_{6.657, 179.7} = 3.95$, $p = 0.0006$) and there was no interaction between time and treatment with PGE2 ($F_{60, 1620} = 1.17$, $p = 0.1813$).

To conclude, the gamma frequency oscillations which emerged following kainate application in brain slices treated with PGE2 for 3 hours had reduced amplitude, but similar frequency, compared to the gamma frequency oscillations which emerged following kainate application treatment in untreated brain slices.

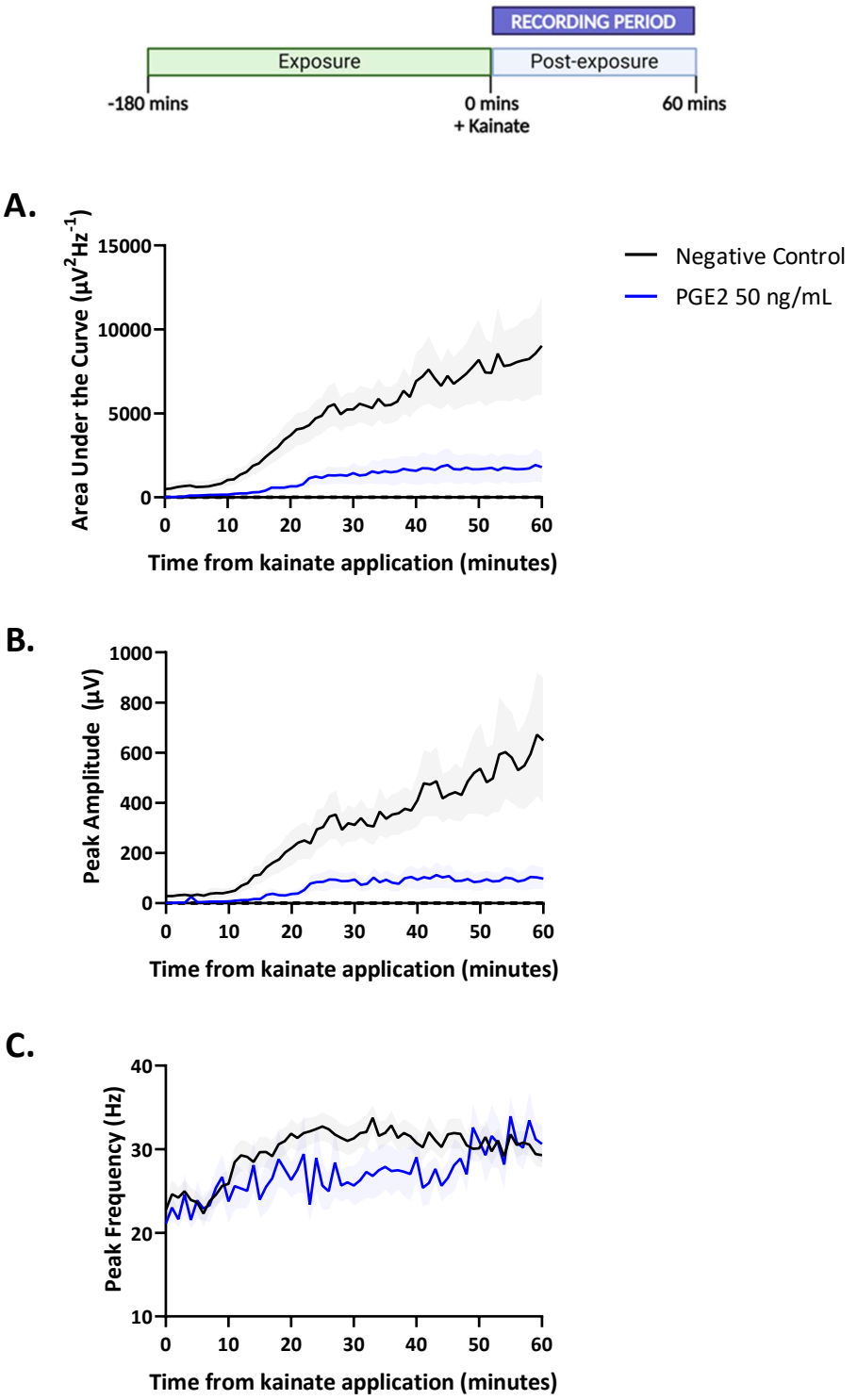

Figure 3.17. The effect of PGE2 treatment on gamma frequency oscillation emergence. Kainate-induced gamma frequency oscillation (A) Area under the curve, (B) peak amplitude, and (C) peak frequency, in brain slices treated for 3 hours with PGE2 (50 ng/mL). Control: n = 24, N = 22; PGE2 50 ng/mL: n = 8, N = 7.

3.16. The effect of CXCL10 on established gamma frequency oscillations

The effect of CXCL10 on ongoing kainate-induced gamma frequency oscillations in brain slices from C57BL/6J mice at 3-4 months was examined by exposing brain slices with established gamma frequency oscillations to CXCL10 at 50 ng/mL for 30 minutes. The effect of this exposure was monitored both during exposure and for the following 60 minutes. In untreated brain slices kainate-induced gamma frequency oscillation amplitude significantly increased over time and the oscillation frequency remained stable. Exposure to CXCL10 inhibited the normal increase in oscillation amplitude. Exposure to CXCL10 did not affect the oscillation frequency (Figure 3.18).

In untreated slices the area under the curve increased from 42,782 ± 19,572 μV^2Hz^- to 89,770 ± 35,304 μV^2Hz^- at 90 minutes after the baseline. Similarly the peak amplitude in untreated slices increased from 3,649 ± 1,882 μV at the baseline to 6,793 ± 3,336 μV at 90 minutes after the baseline. At baseline in slices treated with CXCL10 the area under the curve was 6,117 ± 2,775 μV^2Hz^-. At 90 minutes post-CXCL10 treatment the area under the curve was 7,197 ± 3,673 μV^2Hz^-. This represented a smaller increase than the increase observed in untreated slices. Therefore, CXCL10 inhibited the growth in kainate-induced gamma frequency oscillation amplitude. This was reinforced by the peak amplitude parameter, the normal growth of which was inhibited by exposure CXCL10. The average peak amplitude parameter at the baseline for brain slices exposed CXCL10 was 353.5 ± 33.8 μV. At 90 minutes post-CXCL10 treatment the peak amplitude was 352.4 ± 146.5 μV. This is further demonstrated by the z-scores calculated at 90 minutes post-exposure for these parameters (area under the curve: untreated: 18.41 ± 4.98, CXCL10: 5.17 ± 3.22; peak amplitude: 12.76 ± 3.77, CXCL10: 6.38 ± 4.75). There was no significant effect of treatment with CXCL10 on the area under the curve parameter ($F_{1,28} = 0.23$, $p = 0.6388$) or on the peak amplitude parameter ($F_{1, 28} = 0.26$, $p = 0.6151$), however there was a

significant effect of time on both parameters (Area under the curve: $F_{2.020, 56.56} = 7.48$, $p = 0.0013$, peak amplitude: $F_{2.027, 56.75} = 6.97$, $p = 0.0019$) and a significant interaction between time and treatment with CXCL10 for the area under the curve ($F_{3, 84} = 2.87$, $p = 0.0411$) but not for the peak amplitude ($F_{3, 84} = 2.20$, $p = 0.0942$; Figure 3.18). This demonstrated that gamma frequency oscillations were increasing over time in both CXCL10-treated slices and untreated slices, but treatment with CXCL10 significantly inhibited this growth in oscillation amplitude.

In untreated brain slices the peak frequency was stable over time (baseline: 29.78 ± 0.83 Hz, 90 minutes post-baseline: 28.62 ± 0.97 Hz). In brain slices exposed CXCL10 at 50 ng/mL the oscillation frequency was also stable over time (baseline: 31.28 ± 1.75 Hz, 90 minutes post-CXCL10: 29.08 ± 2.543 Hz).

To conclude, exposure to CXCL10 inhibited the growth in kainate-induced gamma frequency oscillation amplitude but did not reduce oscillation frequency.

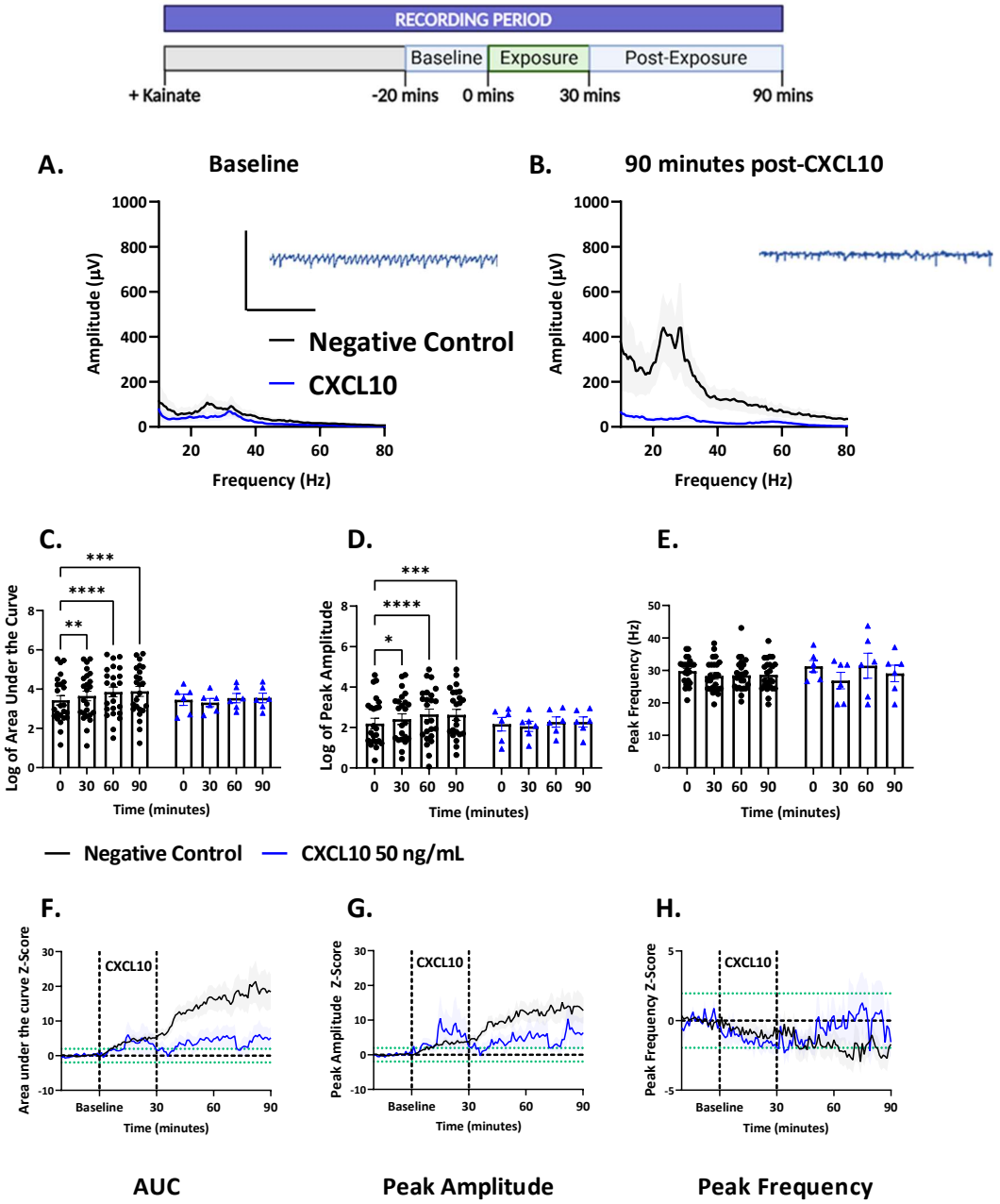

Figure 3.18. The effect of CXCL10 on established gamma frequency oscillations. Pooled FFTs and representative traces for kainate-induced gamma frequency oscillations at a (A) Baseline and (B) 90 minutes post-exposure to CXCL10 (50 ng/mL). (C) Area under the curve, (D) peak amplitude, and (E) peak frequency across 90 minutes of gamma frequency oscillations in brain slices from C57BL/6J mice at 3-4 months.(F, G, H) Z-scores of (C, D, E) respectively. Dotted green line represent $p < 0.05$. Data in C and D are log transformed. 2-way ANOVA RM with Tukey post-hoc corrections: * = $p < 0.05$, ** = $p < 0.01$, *** = $p < 0.001$, **** = $p < 0.0001$. Scale bar: 2000 µV, 0.5 seconds. Control: n = 24, N = 24; CXCL10 50 ng/mL: n = 6, N = 6.

3.17. The effect of CXCL10 on gamma frequency oscillation emergence

Brain slices were treated with CXCL10 (50 ng/mL) for three hours before gamma frequency oscillations were induced with kainate (100 nM). The effect of this 3 hour treatment with CXCL10 on the emergence of gamma frequency oscillation was observed over 60 minutes (Figure 3.19).

In untreated slices the oscillation amplitude increased over 60 minutes. The area under the curve parameter stabilised at approximately 7,500 μV^2Hz^- and the peak amplitude parameter stabilised at approximately 600 μV. The peak frequency in untreated slices increased from 20 Hz to stabilise at approximately 30 Hz. Treatment with CXCL10 significantly inhibited the amplitude, but not the frequency, of the gamma frequency oscillations which emerged in CXCL10-treated slices (Figure 3.19). The reduced growth in gamma frequency oscillation amplitude following treatment with CXCL10 was demonstrated by the reduction in the area under the curve and the peak amplitude at 60 minutes after kainate application (area under the curve: 2,050.11 ± 1,890.23 μV^2Hz^-, peak amplitude: 77.58 ± 72.75 μV). There was no significant effect of time or of treatment with CXCL10 on area under the curve ($F_{1.31, 31.44} = 2.27$, $p = 0.1362$, $F_{1, 24} = 2.46$, $p = 0.1302$) or peak amplitude ($F_{1.358, 32.59} = 1.58$, $p = 0.2230$, $F_{1, 24} = 2.01$, $p = 0.1693$). There was no significant interaction between time and treatment with CXCL10 for either the area under the curve ($F_{60, 1440} = 1.23$, $p = 0.1136$) or the peak amplitude ($F_{60, 1440} = 1.04$, $p = 0.3887$). Post-hoc testing shows that the area under the curve of the oscillation that emerged in CXCL10-treated slices was significantly reduced compared to untreated slices between 30 and 40 minutes after kainate application. Despite no main significant statistical effects of time or treatment with CXCL10 on oscillation amplitude, there was a clear reduction in the amplitude of the gamma frequency oscillation that emerged after treatment with CXCL10 compared to those that emerged in untreated slices.

In untreated brain slices the peak frequency was 29.84 ± 2.06 Hz at 60 minutes after kainate application. The peak frequency of the oscillation which emerged following kainate application was significantly reduced in CXCL10-treated slices. In CXCL10-treated brain slices, at 60 minutes after kainate application the peak frequency was 23.13 ± 2.13 Hz. There was a significant effect of treatment with CXCL10 on the peak frequency of emergent gamma frequency oscillations ($F_{1, 24} = 4.95$, $p = 0.0358$). There was no significant effect of time ($F_{5.912, 141.9} = 1.49$, $p = 0.1861$) and there was no interaction between time and treatment with CXCL10 ($F_{60, 1440} = 0.73$, $p = 0.9366$).

To conclude, the gamma frequency oscillations which emerged following kainate application in brain slices treated with CXCL10 for 3 hours had reduced amplitude and reduced frequency compared to the gamma frequency oscillations which emerged following kainate application in untreated brain slices.

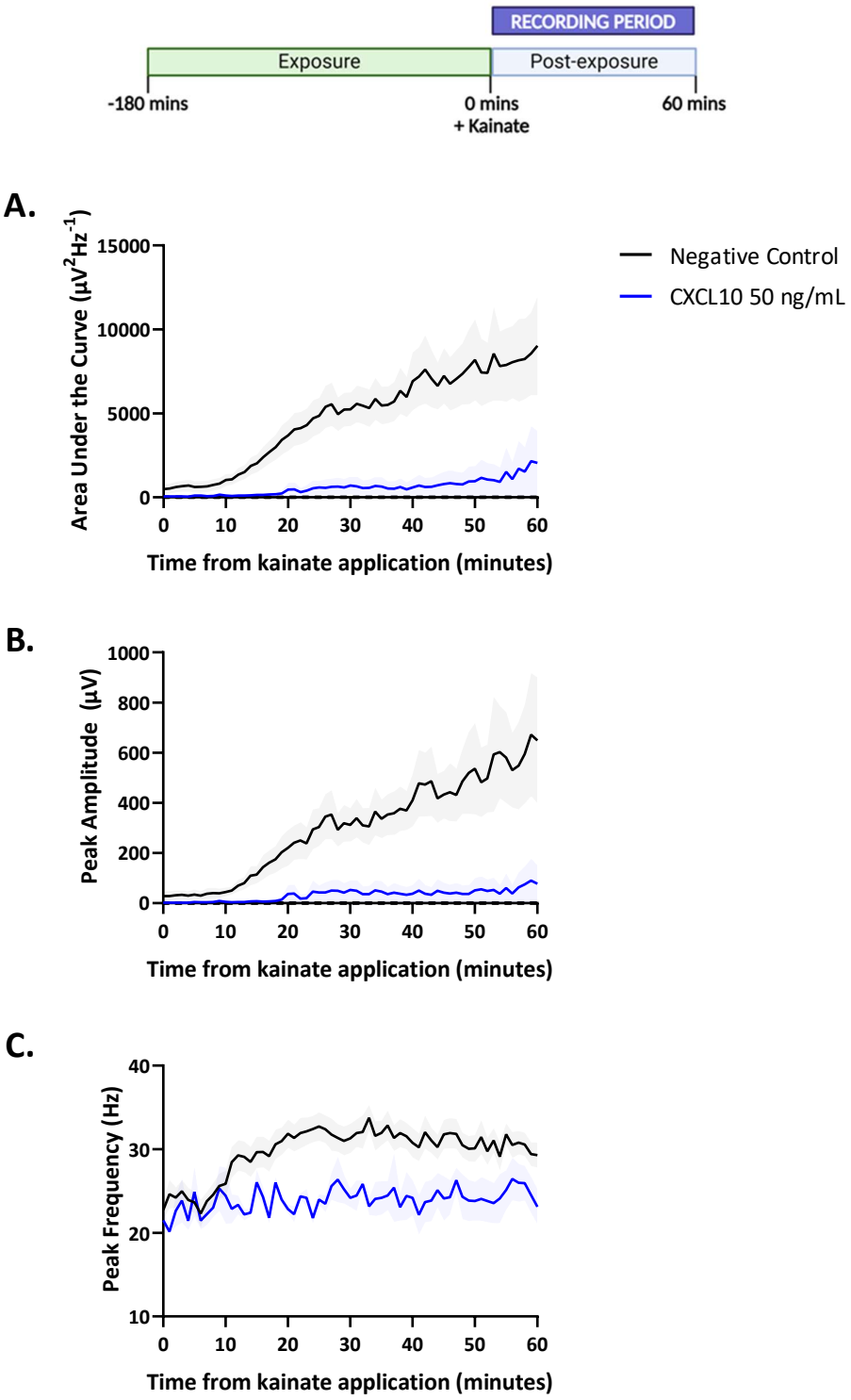

Figure 3.19. The effect of CXCL10 treatment on gamma frequency oscillation emergence. Kainate-induced gamma frequency oscillation (A) Area under the curve, (B) peak amplitude, and (C) peak frequency, in brain slices treated for 3 hours with CXCL10 (50 ng/mL). Control: n = 24, N = 22; CXCL10 50 ng/mL: n = 6, N = 4.

3.18. The effect of CCL11 on established gamma frequency oscillations

The effect of CCL11 on ongoing kainate-induced gamma frequency oscillations in brain slices from C57BL/6J mice at 3-4 months was examined by exposing brain slices with established gamma frequency oscillations to CCL11 at 50 ng/mL for 30 minutes. The effect of this exposure was monitored both during exposure and for the following 60 minutes In untreated brain slices kainate-induced gamma frequency oscillation amplitude significantly increased over time and the oscillation frequency remained stable. In slices exposed to CCL11 the gamma frequency oscillation amplitude also significantly increased over time and the oscillation peak frequency was stable (Figure 3.20).

In untreated slices the area under the curve increased from 42,782 ± 19,572 μV^2Hz^- to 89,770 ± 35,304 μV^2Hz^- at 90 minutes after the baseline. Similarly the peak amplitude in untreated slices increased from 3,649 ± 1,882 μV at the baseline to 6,793 ± 3,336 μV at 90 minutes after the baseline. At baseline, in slices treated with CCL11 the area under the curve was 6,397 ± 3,739 μV^2Hz^-. At 90 minutes post-CCL11 treatment the area under the curve was 49,690 ± 40,905 μV^2Hz^-. This represented a similar increase to the increase observed in untreated slices. This finding was reinforced by increase in the peak amplitude. The peak amplitude at baseline for brain slices exposed CCL11 was 458.1 ± 337.9 μV. At 90 minutes post-CCL11 treatment the peak amplitude was 2,599 ± 1,791 μV. As expected, there was no significant effect of treatment with CCL11 on the area under the curve parameter ($F_{1,27} = 0.31$, $p = 0.5854$) or on the peak amplitude parameter ($F_{1, 27} = 0.28$, $p = 0.6012$), however there was a significant effect of time on both parameters (area under the curve: $F_{1..849, 49.93} = 13.04$, $p < 0.0001$, peak amplitude: $F_{1.929, 52.08} = 14.14$, $p < 0.0001$). There was no significant interaction between time and treatment with CCL11 for the area under the curve ($F_{3, 81} = 0.73$, $p = 0.5396$) or for the peak amplitude ($F_{3, 81} = 0.82$, $p = 0.4854$; Figure 3.20). This demonstrated that gamma frequency oscillations were increasing over

time in both CCL11-treated slices and untreated slices, and treatment with CCL11 had no effect on this growth in oscillation amplitude.

Z-scores were calculated as before for each of the parameters extracted from the Fast Fourier transforms (Figure 3.20). The z-scores demonstrated that the oscillation amplitude grew over time in untreated slices (area under the curve: 18.41 ± 4.98, peak amplitude: 12.76 ± 3.77). Following exposure of the brain slices to CCL11 the amplitude of kainate-induced gamma frequency oscillations increased over time to a similar extent as observed in untreated brain slices. The area under the curve z-score is 24.54 ± 12.07 and the peak amplitude z-score is 20.78 ± 13.07 at 90 minutes after exposure to CCL11.

In untreated brain slices the peak frequency was stable over time (baseline: 29.78 ± 0.83 Hz, 90 minutes post-baseline: 28.62 ± 0.97 Hz). In brain slices exposed CCL11 at 50 ng/mL the oscillation frequency was also stable over time (baseline: 32.34 ± 2.23 Hz, 90 minutes post-CCL11: 28.99 ± 2.52 Hz).

To conclude, exposure to CCL11 had no effect on the growth in kainate-induced gamma frequency oscillation amplitude or the oscillation frequency.

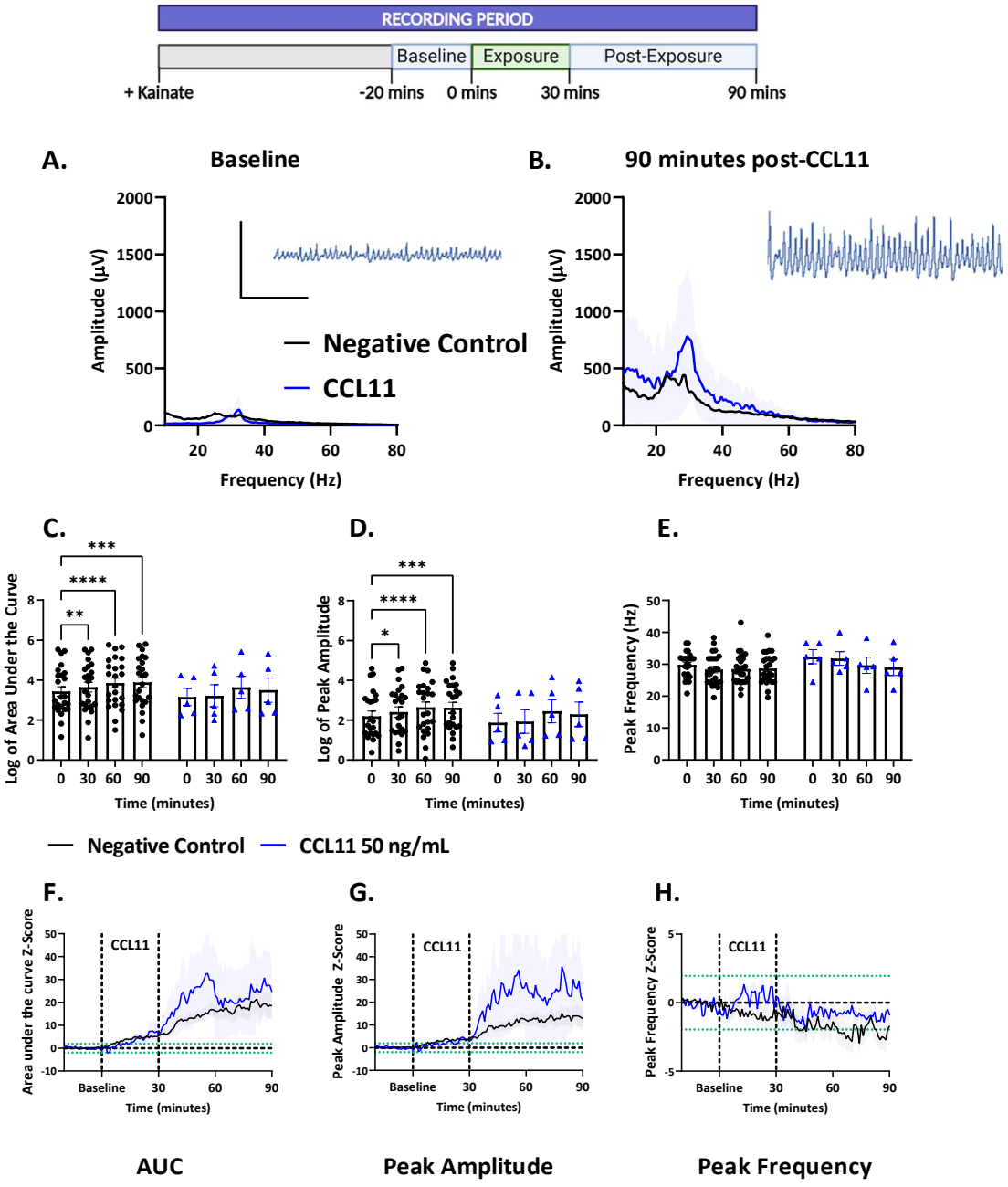

Figure 3.20. The effect of CCL11 on established gamma frequency oscillations. Pooled FFTs and representative traces for kainate-induced gamma frequency oscillations at a (A) Baseline and (B) 90 minutes post-exposure to CCL11 (50 ng/mL). (C) Area under the curve, (D) peak amplitude, and (E) peak frequency across 90 minutes of gamma frequency oscillations in brain slices from C57BL/6J mice at 3-4 months.(F, G, H) Z-scores of (C, D, E) respectively. Dotted green line represent $p < 0.05$. Data in C and D are log transformed. 2-way ANOVA RM with Tukey post-hoc corrections: * = $p < 0.05$, ** = $p < 0.01$, *** = $p < 0.001$, **** = $p < 0.0001$. Scale bar: 2000 µV, 0.5 seconds. Control: n = 24, N = 24; CCL11 50 ng/mL: n = 5, N = 5.

3.19. The effect of CCL11 on gamma frequency oscillation emergence

Brain slices were treated with CCL11 (50 ng/mL) for three hours before gamma frequency oscillations were induced with kainate (100 nM). The effect of this 3 hour treatment with CCL11 on the emergence of gamma frequency oscillation was observed over 60 minutes (Figure 3.21).

In untreated slices the oscillation amplitude increased over 60 minutes. The area under the curve parameter stabilised at approximately 7,500 μV^2Hz^- and the peak amplitude parameter stabilised at approximately 600 μV. The peak frequency in untreated slices increased from 20 Hz to stabilise at approximately 30 Hz. Treatment with CCL11 did not significantly impact the amplitude or the frequency of the gamma frequency oscillations which emerged in CCL11-treated slices (Figure 3.21). The growth in gamma frequency oscillation amplitude following treatment with CCL11 was demonstrated by the area under the curve and the peak amplitude at 60 minutes after kainate application, which were similar to those seen in untreated slices (area under the curve: 4,710.59 ± 2,799.34 μV^2Hz^-, peak amplitude: 265.65 ± 185.83 μV). There was no significant effect treatment with CCL11 on area under the curve ($F_{1, 24} = 0.72$, $p = 0.4032$) or peak amplitude ($F_{1, 24} = 0.80$, $p = 0.3807$). There was also no significant interaction between time and treatment with CCL11 on both the area under the curve ($F_{60, 1440} = 1.23$, $p = 0.1136$) and the peak amplitude ($F_{60, 1440} = 0.34$, $p > 0.999$). However, there was a significant effect of time on both the area under the curve ($F_{1.310, 31.44} = 4.29$, $p = 0.0369$) and a trend towards significance for the effect of time on the peak amplitude ($F_{1.360, 32.65} = 2.89$, $p = 0.0875$), as these parameters were increasing over time in both CCL11-treated slices and untreated slices.

In untreated brain slices the peak frequency was 29.84 ± 2.06 Hz at 60 minutes after kainate application. The peak frequency of the oscillation which emerged following kainate application was unchanged in CCL11-treated slices. In CCL11-treated brain slices, at 60 minutes after kainate application the peak frequency was 35.04 ± 3.07 Hz. There was no effect of treatment

with CCL11 on the peak frequency of emergent gamma frequency oscillations ($F_{1, 24} = 1.45$, $p = 0.2409$) and there was no interaction between time and treatment with CCL11 ($F_{60, 1440} = 0.77$, $p = 0.9072$). However, there was a significant effect of time as the peak frequency increased over time in both CCL11-treated and untreated slices ($F_{6.392, 153.4} = 4.48$, $p = 0.0002$).

To conclude, the gamma frequency oscillations which emerged following kainate application in brain slices treated with CCL11 for 3 hours had similar amplitude and frequency compared to the gamma frequency oscillations which emerged following kainate application in untreated brain slices.

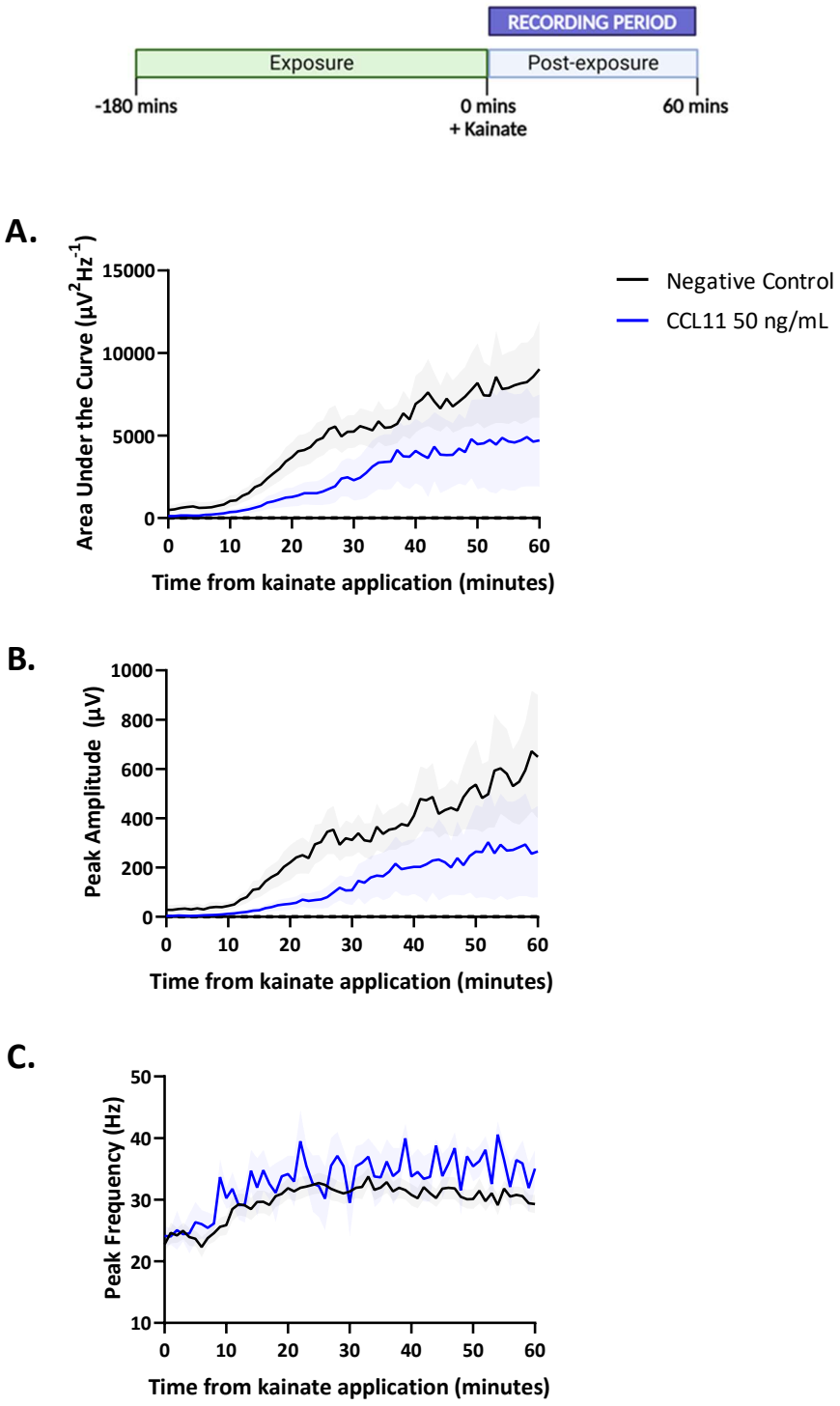

Figure 3.21. The effect of CCL11 treatment on gamma frequency oscillation emergence. (A) Kainate-induced gamma frequency oscillation (A) Area under the curve, (B) peak amplitude, and (C) peak frequency, in brain slices treated for 3 hours with CCL11 (50 ng/mL). Control: n = 24, N = 22, CCL11 50 ng/mL: n = 7, N = 4.

3.20. A comparison of the effects of various inflammatory mediators

The magnitude of the effect of exposure to various inflammatory mediators on established kainate-induced gamma frequency oscillations was taken from the area under the curve and peak amplitude z-scores at 90 minutes following exposure to each mediator.

The magnitude of the effect of each inflammatory mediator was compared in a heatmap (Figure 3.22, A). For most inflammatory mediators tested (TNFα (1ng/mL, 10 ng/mL, 50 ng/mL), CCL2 (1ng/mL, 10 ng/mL), IL-1β (10 ng/mL), and PGE2 (50 ng/mL), CXCL10 (50 ng/mL)), the exposure of the brain slice to the inflammatory mediator inhibited the growth in gamma frequency oscillation amplitude. CCL11 (50 ng/mL) did not however have an inhibitory effect on the growth of oscillation amplitude over time. CCL2 (10 ng/mL) had the largest inhibitory effect on the growth of gamma frequency oscillation amplitude. IL-1β (10 ng/mL) had the second largest inhibitory effect on the growth of gamma frequency oscillation amplitude.

The effect of exposure to various inflammatory mediators on the peak frequency of kainate-induced gamma frequency oscillations was less consistent than the effect on gamma frequency oscillation amplitude (Figure 3.22, B). Exposure to many inflammatory mediators had little effect on oscillation peak frequency (CCL2 (1 ng/mL), IL-1β (10 ng/mL), CCL11 (50 ng/mL). The remaining inflammatory mediators (TNFα (1ng/mL, 10 ng/mL, 50 ng/mL), CCL2 (10 ng/mL, 50 ng/mL), PGE2 (50 ng/mL), CXCL10 (50 ng/mL) tested reduced the peak frequency to a greater extent than it was reduced in the absence of any intervention. Exposure to TNFα (1 ng/mL) had the largest effect on gamma frequency oscillation peak frequency. Exposure to PGE2 (50 ng/mL) had the second largest effect on gamma frequency oscillation peak frequency.

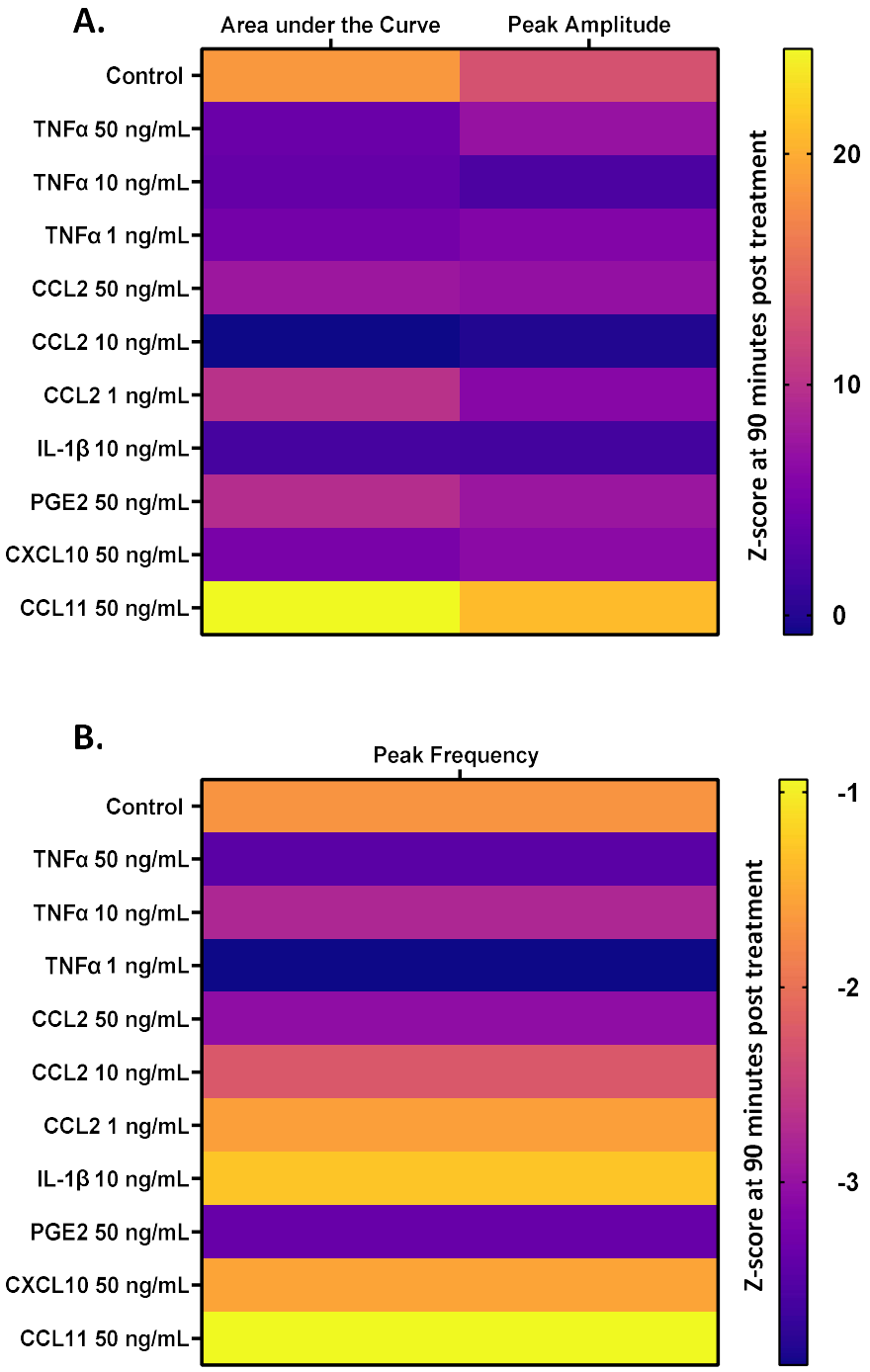

Figure 3.22. A comparison of the effect of various inflammatory mediators on gamma frequency oscillation (A) amplitude and (B) oscillation frequency. Heatmap shows the peak frequency z-score at 90 minutes following no intervention (control) and following exposure to TNFα (1ng/mL, 10 ng/mL, 50 ng/mL), CCL2 (1ng/mL, 10 ng/mL, 50 ng/mL), IL-1β (10 ng/mL), PGE2 (50 ng/mL), CXCL10 (50 ng/mL), and CCL11 (50 ng/mL).

Discussion

Successful establishment of gamma frequency oscillations

The primary experimental method used in this thesis is *ex vivo* electrophysiology using hippocampal brain slices from mice. The neuronal network activity which is the focus of this thesis is gamma frequency neuronal oscillations. Gamma frequency oscillations were successfully induced using kainate and also using carbachol in brain slices from C57BL/6J mice at 3-4 months. These models of gamma frequency oscillation are well established, nevertheless it was important to verify that they could be established successfully (M. O. Cunningham et al., 2003; Hormuzdi et al., 2001; Traub et al., 2000). A defining feature of gamma frequency oscillations is their dependence on GABAergic transmission. This is due to the rhythmic inhibitory (GABAergic) output of highly interconnected inhibitory interneurons which entrains the activity of excitatory pyramidal cells into a synchronised neuronal oscillation in the gamma frequency band (Buzsáki & Wang, 2012). Blockade of GABAergic transmission using gabazine, which is a $GABA_A$ receptor antagonist, resulted in the collapse of both kainate- and carbachol-induced gamma frequency oscillations. This is represented by the reduction in oscillation frequency following application of gabazine. This is consistent with the literature (Fisahn et al., 1998, 2004) and confirms that the neuronal oscillation induced behaves pharmacologically as expected for gamma frequency oscillations.

Having successfully established gamma frequency oscillations in brain slices from C57BL/6J mice at 3-4 months, a comparison was made between kainate- and carbachol-induced gamma frequency oscillations. No significant differences were found between kainate- and carbachol-induced gamma frequency oscillation amplitude or frequency. A systematic comparison of kainate- and carbachol-induced gamma frequency has not yet been carried out by the field, based on the available literature. However, several studies have made use of both models of gamma

frequency oscillations. Based on these studies, it appears that oscillation frequency is similar in kainate- and carbachol-induced gamma frequency oscillations (Mackenzie-Gray Scott et al., 2022; Wójtowicz et al., 2009). Mackenzie-Gray Scott reports an increase in oscillation amplitude in kainate-induced gamma frequency oscillations relative to carbachol-induced gamma frequency oscillations, however this study uses a higher concentration of kainate (400 nM) than used here (100 nM)(Mackenzie-Gray Scott et al., 2022). Wójtowicz reports a similar amplitude in kainate- and carbachol-induced gamma frequency oscillations (Wójtowicz et al., 2009). Therefore, given the reliance of both of these models on fundamentally the same network of cells (inhibitory interneurons and pyramidal cells) and the findings of others', the observation that kainate- and carbachol-induced gamma frequency oscillations have similar frequency and amplitude seems reasonable.

Oestrous cycle effects on gamma frequency oscillations

Gamma frequency oscillations have been shown to be affected by the oestrous cycle in female mice. *In vivo* electrophysiological recordings in cycling female mice shows an increase in gamma frequency oscillation amplitude during the oestrous phase of the oestrous cycle. This increase is posited to be due to a reduction in δ-$GABA_AR$ subunit expression on pyramidal cells and interneurons (Barth et al., 2014). This elegant work, which links molecular changes to known clinical phenomena (for example menstrual-associated changes in memory capacity (Bayer et al., 2014)) was not replicated here; no effect of the oestrous cycle was observed on kainate- or carbachol-induced gamma frequency oscillations. This is possibly due to differences in the experimental system, oestrous cycle differences were observed by *in vivo* electrophysiology rather than by *ex vivo* electrophysiology as used here. A significant possibility is that the mice used here were not undergoing normal oestrous cycling. The mice used were both virgin and housed with females only. In order to replicate the effects of the oestrous cycle on gamma frequency

oscillations it may be necessary to either house the female mice with male mice or to expose the female mice to bedding from male mice. However, the observation that the oestrous cycle has no notable effect on gamma frequency oscillations meant that this factor did not have to be considered and controlled for in other experiments.

The effects of inflammation on gamma frequency oscillations

Having established that gamma frequency oscillations could be established and addressed the possibility of confounding effects of the oestrous cycle, the central question of this thesis was approached. That is, how does the immune system affect gamma frequency oscillations? Specifically, the effect of inflammation on gamma frequency oscillations was investigated. This was investigated in young C57BL/6J mice using two experimental approaches. Firstly, established gamma frequency oscillations were exposed to various pro-inflammatory mediators (cytokines and chemokines). Secondly, brain slices were treated with various pro-inflammatory mediators for 3 hours and the gamma frequency oscillations which emerged following treatment with kainate were studied. Only kainate-induced gamma frequency oscillations were investigated in these studies.

The concentrations of the pro-inflammatory cytokines used were selected based on a literature review which indicated the concentration range at which these mediators are thought to occur in both health and disease, additionally, the concentration at which effects on other neurophysiological parameters have been reported was considered. For example, TNFα has been reported to be at approximately 20 ng/mL and CCL2 at approximately 300 ng/mL in APP/PS1 mice challenged with LPS (Schmöle et al., 2015). While IL-1β has been reported to be at approximately 30 ng/mL in the hippocampus of APP/PS1 mice (Gu et al., 2021). The pro-inflammatory mediators used have been previously used at various concentrations, some of which are notably high. For example, the effect of TNFα on synaptic scaling was carried out with TNFα

at 1 and 10 μg/mL (Stellwagen et al., 2005; Stellwagen & Malenka, 2006). However, the majority of the effects of proinflammatory mediators on neurophysiological parameters have been observed in the nanogram per millilitre range (Blank & Prinz, 2017; A. J. Cunningham et al., 1996; Singh et al., 2019; Zhou et al., 2011). It was observed that gamma frequency oscillations grow rapidly in amplitude to reach a baseline state, these were considered established gamma frequency oscillations. In untreated slices, from this baseline state the oscillation amplitude continues to grow slowly and the frequency remains stable. In slices treated with various pro-inflammatory mediators the amplitude does not continue to grow to the same extent as in untreated slices. Before addressing possible mechanisms by which treatment with pro-inflammatory mediators are inhibiting the normal growth of gamma frequency oscillation amplitude, it is necessary to consider the possible mechanistic basis of the observed growth in gamma frequency oscillation amplitude in untreated slices. Gamma frequency oscillations emerge when highly interconnected networks of inhibitory interneurons are activated and begin to generate rhythmic inhibitory activity which entrains an oscillation in excitatory pyramidal cells. In kainate-induced gamma frequency oscillations inhibitory interneurons are activated by kainate binding to kainate receptors on inhibitory interneurons and by kainate binding to kainate receptors on pyramidal cells which subsequently excite inhibitory interneurons.

One possible basis for the observed growth in oscillation amplitude in untreated slices is an increase in the homogeneity of the excitatory input onto the inhibitory interneuron network. Gamma frequency oscillations have been shown to be sensitive to the heterogeneity of the excitatory input which activates the inhibitory interneuron network (X.-J. Wang & Buzsáki, 1996; White et al., 1998). In an established gamma frequency oscillation, by definition, the excitatory output of pyramidal cells becomes more synchronised and homogenised, this would led to a more homogeneous excitatory input onto inhibitory interneurons. In effect this becomes a positive feedback mechanism in which the rhythmic inhibitory output of inhibitory interneurons

is promoted by causing the excitatory input from pyramidal cells (which activates inhibitory interneurons) to become more synchronised. This self-promoting feature may account for the increase in oscillation amplitude over time in untreated slices.

A second possible explanation for the increase in gamma frequency oscillation amplitude over time is that some form of synaptic plasticity is modulating the strength of the connections in the neuronal network generating the oscillation. There are various synaptic pairings in the gamma frequency oscillation generating network, specifically: pyramidal cell-pyramidal cell, pyramidal cell-interneuron, and interneuron-pyramidal cell. Each of these synapses have been shown to undergo potentiation during gamma frequency oscillations. Ongoing gamma frequency oscillations in the CA1 subregion lead to a potentiation in the recurrent excitatory synapses between pyramidal cells. Both the excitatory postsynaptic potential amplitude and action potential hyperpolarization size are increased in ongoing gamma frequency oscillations at these synapses (Whittington et al., 1997). The potentiation of these synapses between pyramidal cells leads to an increase in the long-range synchrony of gamma frequency oscillations (Traub, Whittington, Stanford, et al., 1996). In addition to the potentiation of synapses between pyramidal cells, synapses between pyramidal cells and interneurons are also potentiation as by ongoing gamma frequency oscillations. The strength of these synapses (as measured by the spike transmission probability) was found to be positively correlated with the power of the local field potential in the gamma frequency band. The long term potentiation (LTP) of these synapses was inhibited by genetically knocking out γCaMKII in parvalbumin-positive inhibitory interneurons. Blocking this process of synaptic strengthening inhibited the strengthening of rhythmicity in gamma frequency oscillations in freely moving mice (He et al., 2021). Therefore, the strengthening of these synapses may also contribute to the amplitude growth of gamma frequency oscillations over time. Finally, the GABAergic synapses between interneurons and pyramidal cells are also potentiated by ongoing gamma frequency oscillations. In the cortex, pyramidal cell firing

leads to LTP of perisomatic GABAergic synapses which project from parvalbumin interneurons onto pyramidal cells, which are known to be critical for gamma frequency oscillation entrainment. This potentiation was dependent on post-synaptic increases in calcium which resulted in increased NO production. NO then acts via presynaptic guanylate cyclase to increase GABA release, so causing potentiation of these synapses (Capogna et al., 2021; Lourenço et al., 2014). These various forms of synaptic potentiation are likely mechanisms which contribute to the observed growth in gamma frequency oscillation amplitude in untreated slices.

Although not experimentally shown, it seems probable that the growth in established gamma frequency oscillation amplitude is due to various forms of synaptic plasticity. Therefore, the reduced growth in established gamma frequency oscillation following exposure to various pro-inflammatory mediators is possibly due to a disruption of these synaptic mechanisms. The relatively short timescale on which these effects are seen suggests that the pro-inflammatory molecules are acting as neuro-modulators, specifically they are acting on pre-existing proteins rather than causing widespread changes in protein expression.

No experimental investigations were made into the possible mechanistic basis of the reduced growth in gamma frequency oscillation amplitude following exposure to various pro-inflammatory mediators. However, in the literature there are many examples of these pro-inflammatory mediators affecting the activity of neurons. TNFα, which inhibits the growth of gamma frequency oscillation amplitude and reduced the frequency of the oscillation, is required for synaptic scaling (Stellwagen & Malenka, 2006). Synaptic scaling is the process by which all synapses on a neuron are uniformly changed in response to sustained activation. Additionally, TNFα has been shown to enhance the synaptic efficacy of pyramidal cells by increasing surface expression of AMPA receptors (Beattie et al., 2002). Therefore, it is very likely that exposure to TNFα interferes with the normal synaptic plasticity which occurs during gamma frequency oscillations. Similarly, CCL2 is known to be neuro-modulatory. Application of CCL2 to

hippocampal brain slices enhanced neuronal excitability and increased synaptic transmission (Zhou et al., 2011). Likewise, in cultured brain slices application of CXCL10 enhanced neuronal excitability and increased synaptic transmission (Nelson & Gruol, 2004). Prostaglandin-E2 has also been shown to be neuro-modulatory. In hippocampal slices PGE2 enhanced the amplitude and frequency of EPSPs (Sang et al., 2005). Early work on the inhibitory effects of IL-1β on LTP suggested that it is a neuro-modulatory cytokine (A. J. Cunningham et al., 1996; Katsuki et al., 1990). Additional studies on IL-1β have shown that it also increases neuronal excitability. It does so by co-localising with NMDAR and enhancing calcium flux through the receptor (Viviani et al., 2003). There is currently an increased in interest in the neuro-modulatory properties of inflammatory mediators and various reviews detail the many neuro-modulatory effects of these molecules (Salvador et al., 2021; Vezzani & Viviani, 2015; Zipp et al., 2023). It is not possible to conclude on the mechanism by which exposure to pro-inflammatory mediators inhibits the growth in established gamma frequency oscillation amplitude. However, based on the literature available it is probable that these mediators are acting in a neuro-modulatory fashion to alter the normal plasticity which occurs in established gamma frequency oscillations. It is possible that each mediator has a separate mechanism of action by which it disrupts synaptic plasticity or that the effects of each mediator converge on a single mechanism – it is not possible to conclude on this.

In some instances, exposure to pro-inflammatory mediators significantly reduced the frequency of the established gamma frequency oscillations; specifically, CCL2 (at 50 ng/mL and 10 ng/mL), TNFα (at all concentrations studied), and PGE2. Again it is difficult to conclude on the mechanism of this decrease in peak frequency. It is possible that these mediators interfere to such an extent with normal synaptic plasticity that they cause the oscillation to slow in frequency.

The second approach used to study the effect of inflammation on gamma frequency oscillations was to study the kainate-induced gamma frequency oscillations which emerge after the treatment

of brain slices with pro-inflammatory mediators for three hours. This longer-term treatment aimed to investigate the effects of inflammation which may arise following inflammation driven changes in gene and protein expression. Treatment with various pro-inflammatory mediators inhibited the amplitude and frequency of emergent kainate-induced gamma frequency oscillations. Therefore, the functionality of the neuronal networks responsible for generating gamma frequency oscillations was impaired by treatment with pro-inflammatory mediators. Increased inflammation drives a wide range of changes, therefore it is difficult to identify specific mechanisms that might cause this inflammation-induced impairment. One possible change associated with inflammation which can be confidently ruled out is any effect from the recruitment of peripheral immune cells. The tissue treated was hippocampal brain slices which is entirely removed from the periphery, therefore the impairment in emergent gamma frequency oscillations is not due to the recruitment of peripheral immune cells.

The first possible contributor to this impairment is metabolic stress induced by inflammation. Gamma frequency oscillations are extremely energetically demanding and are sensitive to alterations in metabolism. In cultured hippocampal brain slices mild metabolic stress (by inhibition of complex one in the electron transport chain) reduced the amplitude of carbachol-induced gamma frequency oscillations and reduced the synchrony with which ensembles of pyramidal cells fire (Elzoheiry et al., 2020). Additional work in the same experimental model shows that gamma frequency oscillations are sensitive to both the source and concentration of metabolic fuel available. In low glucose environments the amplitude of carbachol-induced gamma frequency oscillations is reduced. Gamma frequency oscillations can also use pyruvate and lactate as fuel sources, however this reduces the amplitude of the oscillation (Galow et al., 2014). Inflammation arising from any one of the pro-inflammatory mediators is associated with metabolic disruptions. For example, reactive microglia undergo metabolic reprogramming, with a shift from oxidative phosphorylation towards glycolysis (Baik et al., 2019). Disruptions in

metabolism would negatively impact the ability of parvalbumin inhibitory interneurons to generate their energetically demanding fast spiking activity, and so entrain gamma frequency oscillations. This is a possible contributor towards the reduction in emergent gamma frequency oscillation amplitude and frequency following treatment with pro-inflammatory mediators.

A second possible contributor to the impairment in emergent gamma frequency oscillations is an increase in oxidative stress following treatment with various pro-inflammatory mediators. Reactive microglia produce ROS (McDonald et al., 1997; Meda et al., 1995). As with metabolic stress, oxidative stress likely has a negative impact on the sensitive inhibitory interneuron networks responsible for generating gamma frequency oscillations. In hippocampal cultures, increased oxidative stress (by reducing NMDAR function and by reducing glutathione) reduced gamma frequency oscillation amplitude and frequency via decreased expression of parvalbumin (Hasam-Henderson et al., 2018). Therefore it is probable that increased oxidative stress caused by treatment with pro-inflammatory mediators negatively impacts emergent gamma frequency oscillations. Further effects from increased ROS production are possible given some ROS are known to be neuro-modulatory. NO has been shown to reduce gamma frequency oscillation amplitude and frequency in cultured hippocampal slices (Dikmen et al., 2020; Schilling et al., 2021; Ta et al., 2019). NO can act as a neurotransmitter and can modulate the activity of neurons directly (Lonart et al., 1992). It is therefore possible that increased ROS production leads to alterations in neuronal activity in addition to negatively impacting the inhibitory interneuron network responsible for generating gamma frequency oscillation via oxidative stress.

Briefly, a single exception to the pro-inflammatory mediators studied is CCL11. CCL11 was not found to affect either established or emergent gamma frequency oscillations. CCL11 has been linked to cognitive impairments in mice (Villeda et al., 2011) and in individuals with long-COVID (Fernández-Castañeda et al., 2022). Therefore the failure of CCL11 to impact gamma

frequency oscillations was surprising. This is possibly due to the concentration of CCL11 used (50 ng/mL) or perhaps the requirement for some additional stimulation alongside CCL11.

In conclusion, treatment with pro-inflammatory mediators had a negative impact on both established and emergent gamma frequency oscillations. Pro-inflammatory mediators inhibit the growth of established gamma frequency oscillation amplitude and in some cases reduce the frequency of the oscillation. Given the short timescale on which these changes occur, these changes are likely due to pro-inflammatory mediators disrupting the normal synaptic plasticity mechanisms which occur in established gamma frequency oscillations. Treatment of brain slices with pro-inflammatory mediators for three hours prior to induction of gamma frequency oscillations reduced the amplitude and frequency of emergent gamma frequency oscillations. This is possibly also via disruptions in synaptic plasticity. Alternatively, and or additionally, the impairment in emergent gamma frequency oscillations is due to widespread metabolic and oxidative stress following treatment with the pro-inflammatory mediators.

Limitations

The work presented and discussed above has several limitations which constrain the interpretation of the data. Firstly, the amplitude parameters used to describe the gamma frequency oscillations are highly variable. This variability likely arises the brain slice preparation process; it is highly likely that certain perfusions and brain extractions generate higher quality brain slices than others. Additionally, variability is created by differences in the electrode location between experiments. Although best efforts were made to fix the recording location, there were inevitably differences in the electrode location. The highly variable nature of the baseline gamma frequency oscillations prior to any form of treatment is therefore a limitation in the interpretation of these data. However, the use of z-scores partially addresses this limitation.

Chapter 4

Gamma Frequency Oscillations in APP/PS1 Mice

Introduction

Gamma frequency oscillations are known to be involved in multiple cognitive processes – including working memory (Siegel et al., 2009), dreaming (Llinas & Ribary, 1993), and selective attention (Tiitinen et al., 1993). Gamma frequency oscillations are also a useful model of neuronal network activity. Gamma frequency oscillations have been observed to be altered in both individuals with Alzheimer's disease and Alzheimer's disease animal models. Specifically, cortical gamma frequency oscillations appear to have increased amplitude in individuals with, and preclinical models of, Alzheimer's disease (Başar et al., 2016; Güntekin et al., 2023; Gurevicius et al., 2012; Jin et al., 2018; Osipova et al., 2006; Van Deursen et al., 2008; van Deursen et al., 2011; J. Wang et al., 2002, 2017; Wiesman et al., 2021), while hippocampal gamma frequency oscillations appear to be unaffected or have increased amplitude at 3 months (Goutagny et al., 2013; Hollnagel et al., 2019; Papazoglou et al., 2016; Rubio et al., 2012) and reduced amplitude at approximately 8 months in various amyloidogenic Alzheimer's disease models (Driver et al., 2007; Rubio et al., 2012; Stoiljkovic et al., 2016). The specific nature of the alterations in gamma frequency oscillations in Alzheimer's disease is not yet fully understood. Therefore, gamma frequency oscillations were induced in hippocampal brain slices from APP/PS1 mice and age-matched wildtype littermate controls of both sexes. As with Alzheimer's disease, the pathology in the APP/PS1 mouse becomes progressively worse with age. In order to capture these age-related changes two timepoints were chosen to assess gamma frequency oscillations: 9-11 and 20-24 months. At 9-11 months the Alzheimer's-like pathology is known to be well established in APP/PS1 mice (Radde et al., 2006). While, at 20-24 the pathology has fully developed (Rupp et al., 2011).

Both kainate- and carbachol-induced gamma frequency oscillations were characterised in APP/PS1 mice and wildtype littermate controls. As kainate- and carbachol-induced gamma

frequency oscillations have different underlying mechanisms (primarily kainate relies on glutamatergic transmission (Robinson & Deadwyler, 1981) while carbachol relies on cholinergic transmission (Cole & Nicoll, 1984)), it was of interest to determine if these two models behaved differently in APP/PS1 mice and wildtype littermate controls, or if these models behaved differently at different ages. Generally, kainate-induced gamma frequency oscillations have been the model most studied in Alzheimer's disease models (Driver et al., 2007; Klein et al., 2016; Mackenzie-Gray Scott et al., 2022) however, carbachol-induced gamma frequency oscillations have also been studied (Hollnagel et al., 2019; Mackenzie-Gray Scott et al., 2022).

This investigation also considered spatial heterogeneity of the hippocampus. It has been shown that gamma frequency oscillations can be varied across the hippocampus (Castelhano et al., 2022). This suggests that the region chosen to prepare brain slices is important. In order to account for this potential source of difference, and to investigate if gamma frequency oscillations were affected a in specific region of the hippocampus in APP/PS1 mice, brain slices were chosen from across the dorsal-ventral axis of the hippocampus and gamma frequency oscillations were compared. This has not been carried out in previous studies of gamma frequency oscillations in *ex vivo* brain slices from Alzheimer's disease mouse models.

Gamma frequency oscillations are known to be dependent on highly-interconnected networks of inhibitory interneurons, specifically parvalbumin- and somatostatin-positive interneurons (Antonoudiou et al., 2020; Cardin et al., 2009; Sohal et al., 2009). These interneurons are known to be sensitive to both metabolic and oxidative stress and may be reduced in Alzheimer's disease (Hijazi et al., 2023). Therefore, it is important to characterise the density of these inhibitory interneuron networks in APP/PS1 mice in order to establish whether the networks responsible for generating gamma frequency oscillations are altered. The activity of these networks was also further investigated by blocking GABAergic transmission using the $GABA_A$ receptor antagonist, gabazine. Gamma frequency oscillations are known to be dependent on GABAergic

neurotransmission and the extent to which this varied in brain slices from APP/PS1 mice and wildtype littermate controls was of interest as an indicator of overall inhibitory tone.

Therefore, this systematic investigation, which took account of age, sex, different models of gamma frequency oscillation induction, and location in the hippocampus, provided a thorough characterisation of gamma frequency oscillation and their underlying neuronal correlates in APP/PS1 mice.

Results

4.1. Kainate-induced gamma frequency oscillations in APP/PS1 mice

Gamma frequency oscillations were induced in hippocampal brain slices by the bath application of kainate (100 nM). The growth of the oscillation was observed in real-time by continuous frequency decomposition by Fast Fourier transform. When the oscillation had stopped growing it was considered to have reached a baseline. In this relatively stable state amplitude and frequency parameters were measured for the oscillation. The peak amplitude and the area under the curve of the Fast Fourier transform are amplitude measures while the peak frequency is a measure of the oscillation frequency. In APP/PS1 mice, the oscillation amplitude and frequency were reduced at 9-11 months, while the oscillation amplitude was increased and the frequency was unchanged at 20-24 months (Figure 4.1).

In normal mice (wildtype littermate controls) at 9-11 months kainate-induced gamma frequency oscillations had a peak frequency of 32.99 ± 1.29 Hz. The amplitude of kainate-induced gamma frequency oscillations in wildtype littermate controls at 9-11 months was indicated by the area under the curve (3064 ± 831.6 $\mu V^2 Hz^-$) and peak amplitude (283.8 ± 105.1 μV). The peak frequency was similar at 20-24 months in these mice (31.54 ± 1.02 Hz). However, at 20-24 months the amplitude of kainate-induced gamma frequency oscillation was increased relative to the amplitude at 9-11 months (area under the curve: 6614 ± 2868 $\mu V^2 Hz^-$, peak amplitude: 283.8 ± 105.1 μV). Therefore, kainate-induced oscillations were larger but occurred at the same frequency in wildtype littermate controls at 20-24 months relative to at 9-11 months.

In APP/PS1 mice at 9-11 months kainate-induced gamma frequency oscillations had a peak frequency of 28.71 ± 1.25 Hz, this was a significant reduction relative to wildtype littermate controls at the same age ($p = 0.0280$). The amplitude of kainate-induced gamma frequency oscillations was also significantly reduced at 9-11 months in APP/PS1 mice relative to wildtype

littermate controls (area under the curve: 1170 ± 224.8 $\mu V^2 Hz^-$, p = 0.0248, peak amplitude: 74.48 ± 12.06 μV, p = 0.0077).

In APP/PS1 mice at 20-24 months, the peak frequency of kainate-induced gamma frequency oscillations was 30.53 ± 1.15 Hz, this was increased relative to APP/PS1 mice at 9-11 months and similar to wildtype littermate controls at 9-11 and 20-24 months. The amplitude of kainate-induced gamma frequency oscillation was also increased in APP/PS1 mice at 20-24 months (area under the curve: 12,410 ± 4144 $\mu V^2 Hz^-$, peak amplitude: 675.3 ± 210.6 μV) relative to APP/PS1 mice at 9-11 months and to wildtype littermate controls at 9-11 and 20-24 months. Examination of the pooled Fast Fourier transforms showed this increase in amplitude largely occurred at lower frequencies. Therefore, kainate-induced gamma frequency oscillations in APP/PS1 mice had reduced frequency and amplitude at 9-11 months, and had similar frequency and increased amplitude at 20-24 months, relative to wildtype littermate controls.

There was a significant effect of the APP/PS1 genotype on peak frequency ($F_{1, 56}$ = 4.94, p = 0.0302) however there was no significant effect of age ($F_{1, 56}$ = 0.02, p = 0.5052) or interaction between the APP/PS1 genotype and age ($F_{1, 56}$ = 1.905, p = 0.1730). Therefore, for kainate-induced gamma frequency oscillations, the peak frequency was significantly reduced in APP/PS1 mice. Post-hoc analysis showed that this effect occurred in APP/PS1 mice at 9-11 months.

In summary, kainate-induced gamma frequency oscillation amplitude and frequency were significantly reduced in APP/PS1 mice at 9-11 months. Oscillation amplitude was increased in both APP/PS1 mice and wildtype littermate controls at 20-24 months.

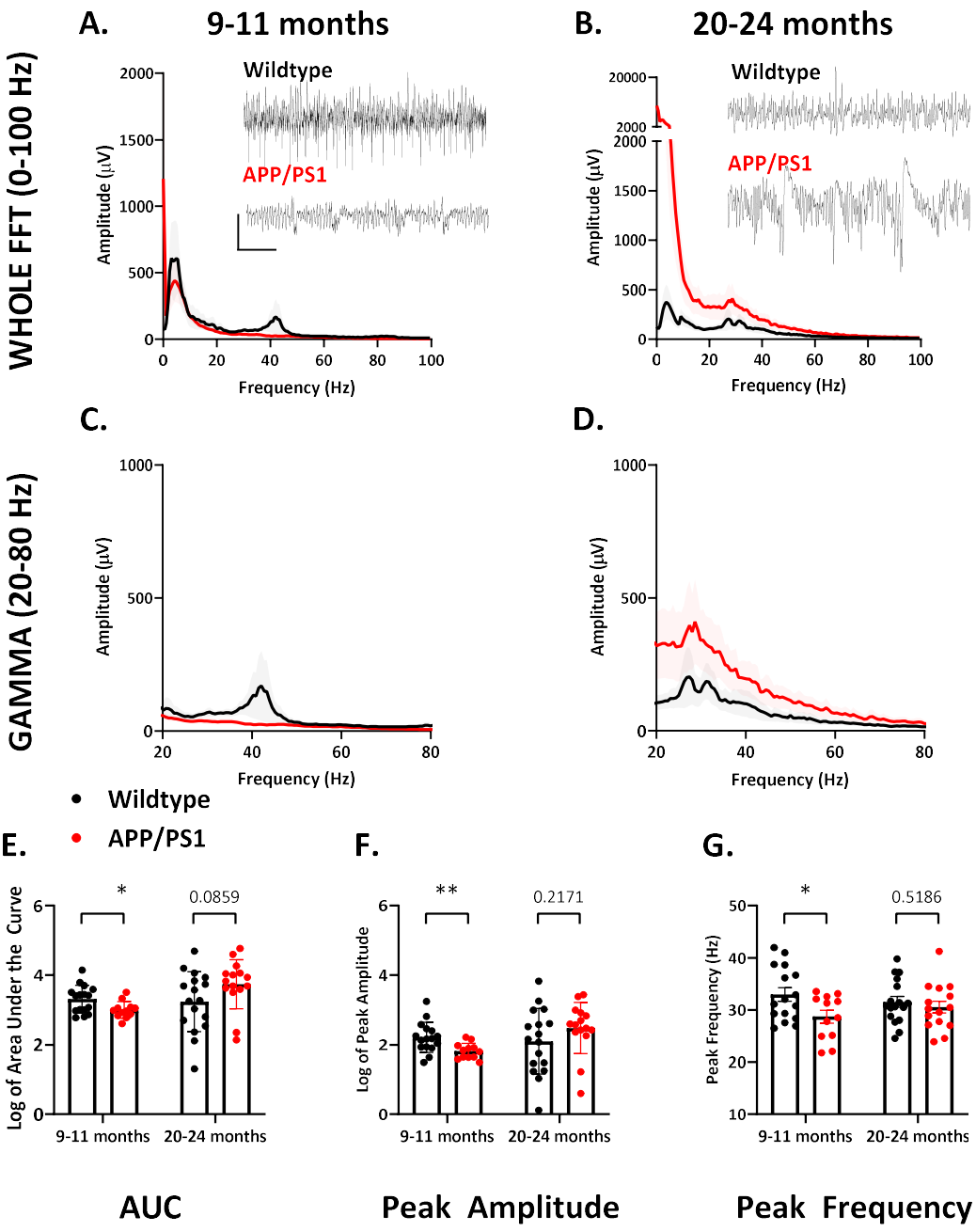

Figure 4.1. Kainate-induced gamma frequency oscillations in APP/PS1 mice. (A-D) FFTs pooled for APP/PS1 (red) and wildtype (black) mice at (A, C) 9-11 and (B, D) 20-24 months across (A, B) 0-100 Hz and (C, D) 20-80 Hz. (E) Area under the curve, (F) peak amplitude, (G) peak frequency parameters from FFTs. Data in E and F are log transformed. Unpaired t-tests: * = $p < 0.05$, ** = $p < 0.01$. 9-11 months: APP/PS1, n = 43, N= 12, wildtype, n = 49, N = 16; 20-24 months: APP/PS1, n = 40, N = 15, wildtype, n = 46, N = 17.

4.2. Kainate-induced gamma frequency oscillations across the hippocampus

Gamma frequency oscillations were recorded across the hippocampus in order to determine if the observed deficits in kainate-induced gamma frequency oscillations in APP/PS1 mice were associated primarily with a specific region of the hippocampus. Gamma frequency oscillations were induced by the application of kainate (100 nM) in brain slices taken from three regions – dorsal, medial, and ventral – across the hippocampus (Figure 4.2). The region recorded did not have a significant effect on either the amplitude or frequency of kainate-induced gamma frequency oscillations in APP/PS1 mice or in wildtype littermate controls

In wildtype littermate controls at 9-11 and at 20-24 months the amplitude of kainate-induced oscillations was similar across the hippocampus and was not affected by the region recorded. This was demonstrated by the area under the curve which was approximately 1,000 $\mu V^2 Hz^-$ in the regions studied. Similarly, the peak amplitude was approximately 100 μV in the regions studied. The peak frequency of kainate-induced gamma frequency oscillations in wildtype littermate controls at 9-11 months was similar in slices taken from the dorsal and medial regions of the hippocampus (approximately: 35 Hz) but was reduced in slices taken from the ventral region of the hippocampus (approximately 30 Hz). At 20-24 months dorsal and ventral slices had reduced peak frequency (approximately 30 Hz) relative to medial slices (approximately 35 Hz). Therefore, in wildtype littermate controls the region recorded did not have a notable impact on kainate-induced gamma frequency oscillations, aside from some minor effects on oscillation frequency.

In APP/PS1 mice at 9-11 and at 20-24 months the amplitude of kainate-induced oscillations was similar across the hippocampus and was not affected by the region recorded. This was demonstrated by the area under the curve which was approximately 700 $\mu V^2 Hz^-$ at 9-11 months, and was approximately 6,000 $\mu V^2 Hz^-$ at 20-24 months. Similarly, the peak amplitude was approximately 75 μV at 9-11 months, and was approximately 275 μV at 20-24 months. The peak

frequency of kainate-induced gamma frequency oscillations in APP/PS1 mice at 9-11 months was similar in slices taken from the dorsal and ventral regions of the hippocampus (approximately: 30 Hz) but was reduced in slices taken from the ventral region of the hippocampus (approximately 22 Hz). At 20-24 months medial slices had reduced peak frequency (approximately 22 Hz) relative to dorsal and ventral slices (approximately 30 Hz). Therefore, the APP/PS1-associated changes in kainate-induced gamma frequency oscillation amplitude and frequency were evenly spread across the hippocampus.

At 9-11 months the area under the curve was significantly reduced in APP/PS1 mice ($F_{1, 53}$ = 4.07, p = 0.0487) but was not significantly affected by the region recorded ($F_{2, 53}$ = 0.52, p = 0.5167), nor was the effect of the APP/PS1 genotype affected by the region recorded ($F_{2, 53}$ = 0.17, p = 0.8468). The same was true for the peak amplitude parameter (APP/PS1: $F_{1, 53}$ = 5.07, p = 0.0285, Region: $F_{2, 53}$ = 0.65, p = 0.5246, APP/PS1 X Region: $F_{2, 53}$ = 0.04, p = 0.9655). Similarly, at 20-24 months the area under the curve was significantly increased in APP/PS1 mice ($F_{1, 61}$ = 5.29, p = 0.0249) but was not significantly affected by the region recorded ($F_{2, 61}$ = 0.27, p = 0.7645), nor was the effect of the APP/PS1 genotype affected by the region recorded ($F_{2, 61}$ = 0.38, p = 0.6842). The same trend was true for the peak amplitude parameter (APP/PS1: $F_{1, 61}$ = 1.83, p = 0.1810, Region: $F_{2, 61}$ = 0.08, p = 0.9229, APP/PS1 X Region: $F_{2, 61}$ = 0.16, p = 0.8556). Similarly, the reduction in oscillation frequency in APP/PS1 mice occurred across the hippocampus. This reduction was significant at 9-11 months ($F_{1, 57}$ = 8.88, p = 0.0042) and trended towards significance at 20-24 months ($F_{1, 62}$ = 3.20, p = 0.0784). There was no effect on peak frequency of the region recorded at 9-11 months ($F_{2, 57}$ = 2.33, p = 0.1065) or at 20-24 months ($F_{2, 62}$ = 0.21, p = 0.8092), nor was the effect of the APP/PS1 genotype affected by the region recorded at 9-11 months ($F_{2, 57}$ = 2.07, p = 0.1356) or 20-24 months ($F_{2, 62}$ = 0.20, p = 0.8230). Therefore the region recorded did not have a significant effect on oscillation amplitude or frequency.

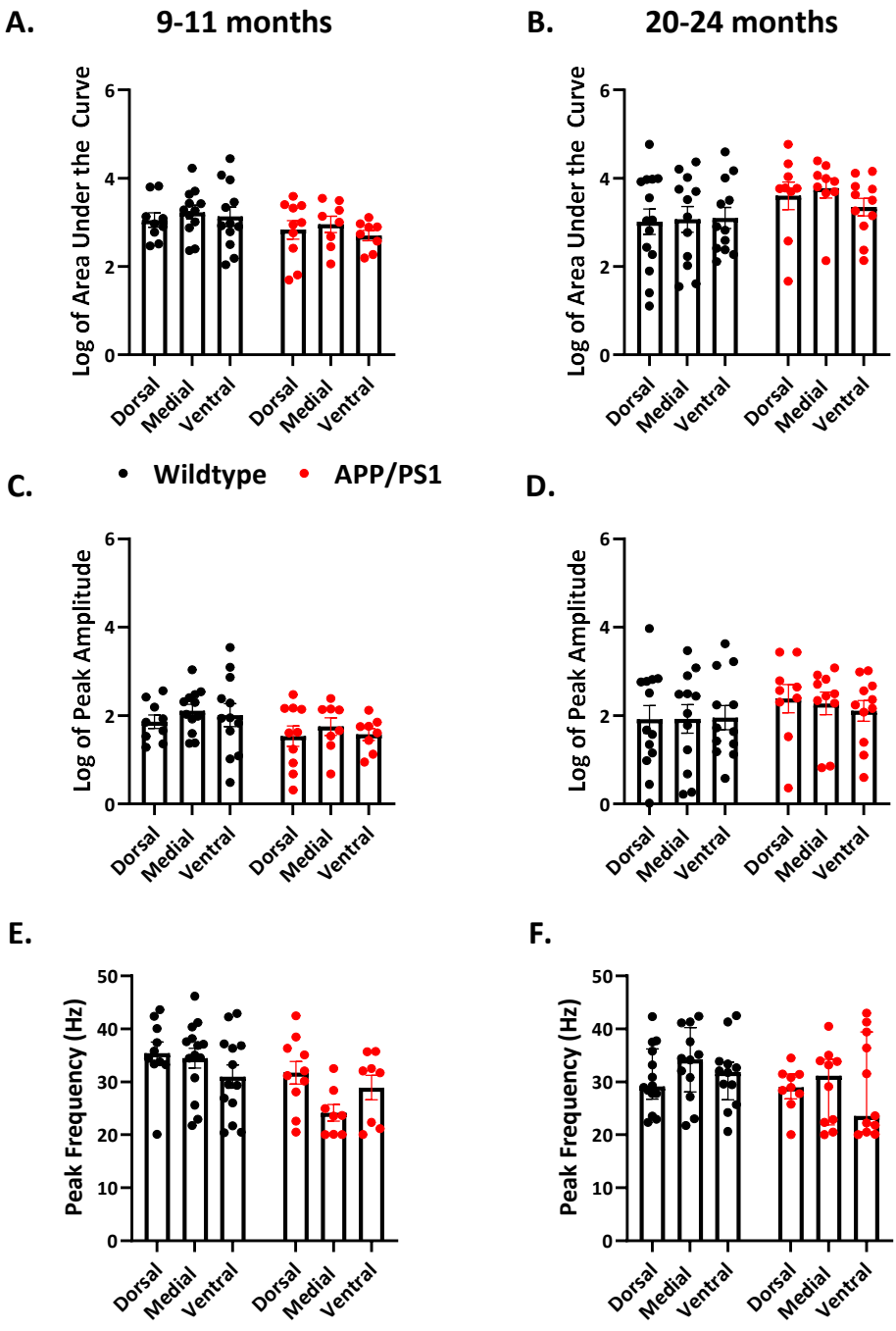

Figure 4.2. Kainate-induced gamma frequency oscillations across the hippocampus. (A, B) Area under the curve, (C, D) peak amplitude, and (E, F) peak frequency of gamma frequency oscillations induced by kainate (100 nM) in APP/PS1 (red) and wildtype mice (black) at (A, C, E) 9-11 and (B, D, F) 20-24 months. Data in A-D are log transformed. Median and IQR plotted in E and F. 2-way ANOVA, main effect of genotype in bold: # = $p < 0.05$, ## = $p < 0.001$. 9-11 months: APP/PS1, n = 43, N = 12, wildtype, n = 49, N = 16; 20-24 months: APP/PS1, n = 40, N = 15, wildtype, n = 46, N = 17.

4.3. Sex differences in kainate-induced gamma frequency oscillations

Biological sex has a known effect on the progression of Alzheimer's-like pathology in APP/PS1 mice (Aggarwal & Mielke, 2023). Therefore, the effect of sex on kainate-induced gamma frequency oscillations was examined (Figure 4.3).

The amplitude and frequency of kainate-induced gamma frequency oscillations were increased in female wildtype mice at 9-11 months relative to males (area under the curve: males: 2,315 ± 691.4 $\mu V^2 Hz^-$, females: 3,813 ± 1525 $\mu V^2 Hz^-$, peak amplitude: males: 172.1 ± 42.71 μV, females: 395.5 ± 204.8 μV, Peak frequency: males: 31.29 ± 1.96 Hz, females: 34.41 ± 1.79 Hz). At 20-24 months the amplitude and frequency of kainate-induced gamma frequency oscillations in females were reduced relative to 9-11 months and also relative to male mice at 20-24 months (Area under the curve: males: 9630 ± 5255 $\mu V^2 Hz^-$, females: 3220 ± 1159 $\mu V^2 Hz^-$, peak amplitude: males: 1138 ± 731.8 μV, females: 262.5 ± 116.7 μV, peak frequency: males: 32.94 ± 1.28 Hz, females: 29.96 ± 1.52 Hz). From an unequal position at 9-11 months, in which females had increased amplitude and frequency of kainate-induced gamma frequency oscillations, female wildtype littermate controls at 20-24 months experienced a greater reduction in oscillation amplitude and frequency relative to males.

In APP/PS1 mice at 9-11 months there were no notable sex differences in the amplitude or frequency of kainate-induced gamma frequency oscillations (area under the curve: males: 1098 ± 270.3 $\mu V^2 Hz^-$, females: 1220 ± 350.7 $\mu V^2 Hz^-$, peak amplitude: males: 80.53 ± 22.82 μV, females: 70.16 ± 14.19 μV, peak frequency: males: 30.64 ± 1.15 Hz, females: 30.65 ± 2.57 Hz) At 9-11 months, the APP/PS1-associated reduction in oscillation amplitude and frequency occurred in both sexes and was not significantly affected by sex (area under the curve: $F_{1,24} = 0.45$, $p = 0.5099$, peak amplitude: $F_{1,24} = 0.21$, $p = 0.6536$, peak frequency: $F_{1,24} = 0.57$, $p = 0.4593$). However, given the increased oscillation amplitude and frequency in female wildtype littermate controls at 9-11

months, the reductions in female APP/PS1 mice represented a greater reduction than those in male APP/PS1 mice. In APP/PS1 mice at 20-24 there were also no notable sex differences in the amplitude and frequency of kainate-induced gamma frequency oscillations (area under the curve: males: 15445 ± 8717 $\mu V^2 Hz^-$, females: 10386 ± 4142 $\mu V^2 Hz^-$, peak amplitude: males: 722.6 ± 401.9 μV, females: 643.8 ± 248.5 μV, peak frequency: males: 29.86 ± 1.41 Hz, females: 30.98 ± 1.73 Hz). At 20-24 months, the APP/PS1-associated increase in kainate-induced gamma frequency oscillation amplitude was not significantly affected by sex (area under the curve: $F_{1,24} = F_{1,28} = 0.44$, $p = 0.2371$, peak amplitude: $F_{1,28} = 1.0$, $p = 0.3233$, peak frequency: $F_{1,28} = 0.36$, $p = 0.5544$).

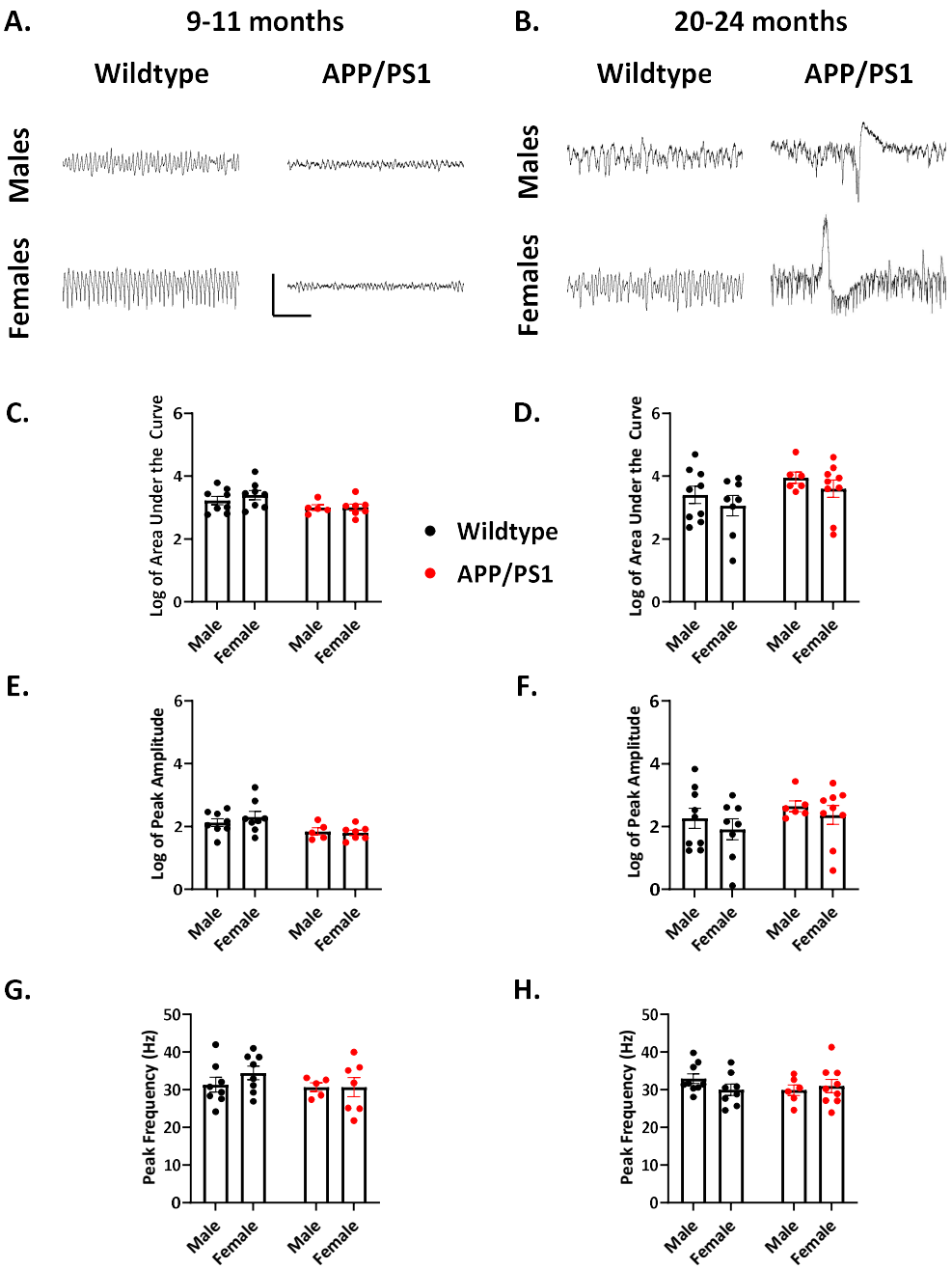

Figure 4.3. Sex effects on kainate-induced gamma frequency oscillations. (A, B) Representative traces of gamma frequency oscillations induced by kainate (100 nM) in APP/PS1 (red) and wildtype mice (black), (C, D) Area under the curve, (E, F) peak amplitude, and (G, H) peak frequency) at (A, C, E, G) 9-11 and (B, D, F, H) 20-24 months in both sexes. Data in A-D are log transformed. 2-way ANOVA. 9-11 months: male APP/PS1, n = 18, N = 5, female APP/PS1, n = 25, N = 7; male WT, n = 26, N = 8, female WT, n = 23, N = 8; 20-24 months: male APP/PS1, n = 14, N = 6, female APP/PS1, n = 26, N = 9; male WT, n = 26, N = 9, female WT, n = 20, N = 8.

4.4. Carbachol-induced gamma frequency oscillations in APP/PS1 mice

Gamma frequency oscillations were induced by treating the brain slice with carbachol (20 μM). The growth of the oscillation was observed in real-time by continuous frequency decomposition by Fast Fourier transform. When the oscillation had stopped growing it was considered to have reached a baseline. In this relatively stable state amplitude and frequency parameters were measured for the oscillation (Figure 4.4).

In wildtype littermate controls at 9-11 months carbachol-induced gamma frequency oscillations had a peak frequency of 27.89 ± 0.85 Hz and an amplitude indicated by the area under the curve (1,637 ± 424.0 $\mu V^2 Hz^-$) and peak amplitude (92.25 ± 20.0 μV). At 20-24 months, the peak frequency of carbachol-induced gamma frequency oscillation was 26.0 ± 1.70 Hz, this was similar to that at 9-11 months. While the oscillation amplitude was increased relative to the amplitude at 9-11 months (area under the curve: 2,950 ± 655.9 $\mu V^2 Hz^-$, peak amplitude: 232.4 ± 52.07 μV). The pooled Fast Fourier transforms showed that carbachol-induced gamma frequency oscillations lacked a well-defined oscillation peak. At 20-24 months the oscillatory activity was more centred around the peak frequency at 20-24 months compared to 9-11 months. Therefore, at 20-24 months in wildtype littermate controls, carbachol-induced oscillations were larger, but occurred at the same frequency, relative to at 9-11 months.

In APP/PS1 mice at 9-11 months carbachol-induced gamma frequency oscillations occurred at a frequency of 26.40 ± 1.23 Hz, this was similar to the peak frequency in wildtype littermate controls at the same age. The oscillation amplitude was also similar in APP/PS1 mice relative to wildtype littermate controls at 9-11 months (area under the curve: 1,249 ± 442.2 $\mu V^2 Hz^-$, peak amplitude: 96.94 ± 27.94 μV). In APP/PS1 mice at 20-24 months, the peak frequency of carbachol-induced gamma frequency oscillations was 24.39 ± 1.17, this was reduced relative to APP/PS1 at 9-11 months and relative to wildtype littermate controls at 9-11 and 20-24 months.

In APP/PS1 mice at 20-24 months, as in wildtype littermate controls, the amplitude of carbachol-induced gamma frequency oscillation was increased (area under the curve: 2,287 ± 492.9 $\mu V^2 Hz^-$, peak amplitude: 240.3 ± 63.14 μV) relative to APP/PS1 mice and wildtype littermate controls at 9-11 months. The pooled Fast Fourier transforms showed this increase in amplitude largely occurred at lower frequencies and there was no clear peak of gamma frequency activity.

There was no significant effect of the APP/PS1 genotype ($F_{1, 60} = 1.17$, $p = 0.2834$) or of age ($F_{1, 60} = 3.35$, $p = 0.0724$) on peak frequency. Therefore, carbachol-induced gamma frequency oscillation peak frequency was not significantly impacted by age or the APP/PS1 genotype.

There was a significant effect of age on the area under the curve ($F_{1, 60} = 7.60$, $p = 0.0077$) and on peak amplitude ($F_{1, 60} = 8.32$, $p = 0.0054$). While there was no significant effect of the APP/PS1 genotype on the area under the curve ($F_{1, 60} = 0.22$, $p = 0.6422$) or peak amplitude ($F_{1, 60} = 0.006$, $p = 0.9342$). This demonstrated that carbachol-induced gamma frequency oscillations were significantly increased at 20-24 months.

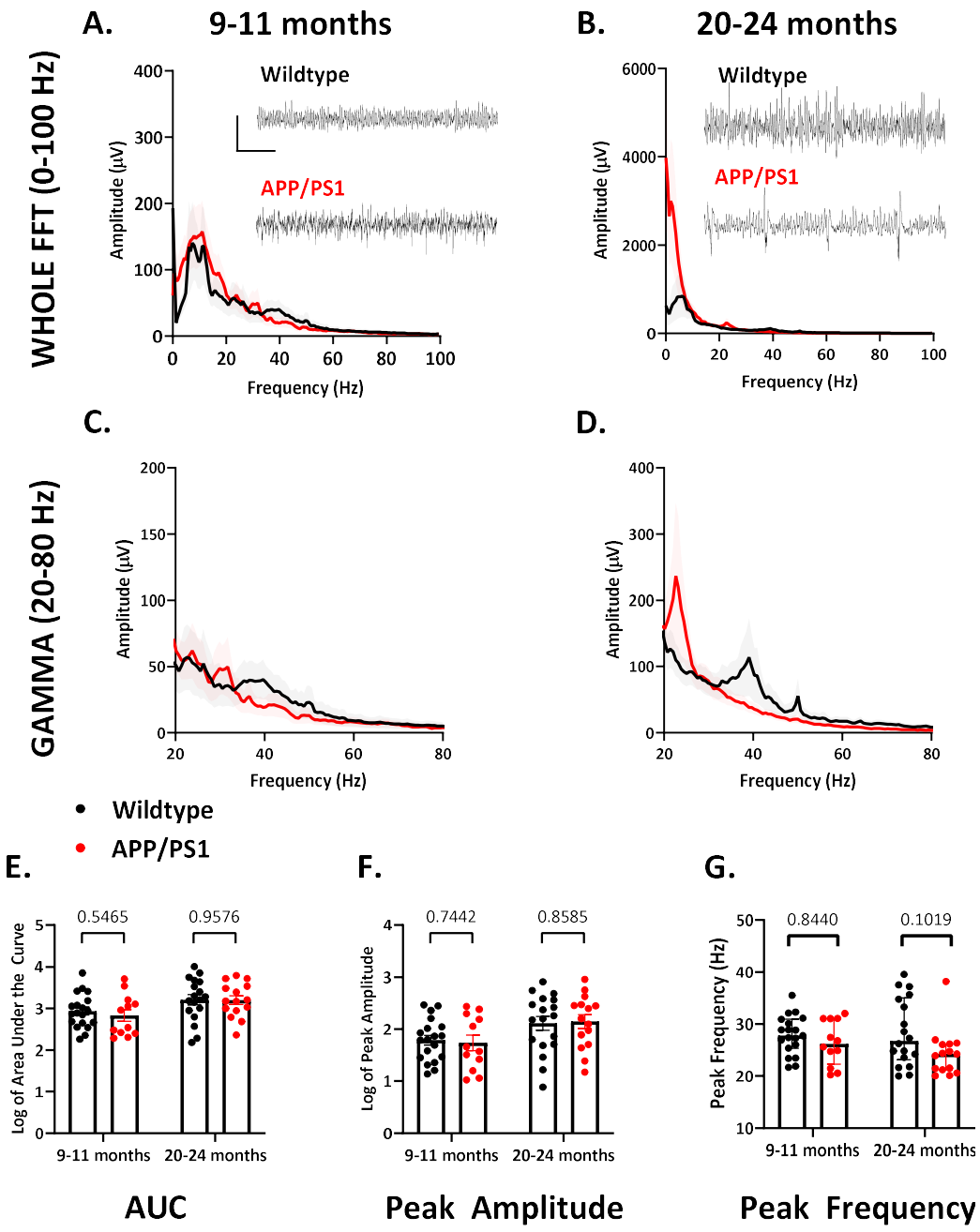

Figure 4.4. Carbachol-induced gamma frequency oscillations in APP/PS1 mice. (A-D) FFTs pooled for APP/PS1 (red) and wildtype (black) mice at (A, C) 9-11 and (B, D) 20-24 months across (A, B) 0-100 Hz and (C, D) 20-80 Hz. (E) Area under the curve, (F) peak amplitude, (G) peak frequency parameters from FFTs. Data in E and F are log transformed. Median and IQR plotted for data in G. Unpaired t-test. 9-11 months: APP/PS1, n = 35, N= 12, wildtype, n = 59, N = 19; 20-24 months: APP/PS1, n = 31, N = 15, wildtype, n = 40, N = 18.

4.5. Carbachol-induced gamma frequency oscillations across the hippocampus

Gamma frequency oscillations were recorded across the hippocampus in order to determine if carbachol-induced gamma frequency oscillations in APP/PS1 mice were altered in a specific region of the hippocampus. Gamma frequency oscillations were induced by the application of carbachol (20 μM) in brain slices taken from three regions – dorsal, medial, and ventral – across the hippocampus (Figure 4.5). The frequency of carbachol-induced gamma frequency oscillations was increased in ventral slices in both APP/PS1 mice and wildtype littermate controls at 9-11 and 20-24 months. The amplitude of carbachol-induced gamma frequency oscillations was reduced in medial slices in APP/PS1 mice at both 9-11 months and 20-24 months.

In wildtype littermate controls at 9-11 and 20-24 months the amplitude of carbachol-induced oscillations was similar across the hippocampus and was not affected by the region recorded. This was demonstrated by the area under the curve which was approximately 600 $\mu V^2 Hz^-$ at 9-11 months and increased with age to approximately 1200 $\mu V^2 Hz^-$ at 20-24 months, across the regions studied. Similarly, the peak amplitude was approximately 50 μV at 9-11 months and increased to approximately 120 μV at 20-24 months across the regions studied. The peak frequency of carbachol-induced gamma frequency oscillations in wildtype littermate controls at 9-11 and 20-24 months was notably increased in slices taken from the ventral region of hippocampus. The peak frequency in these ventral slices was approximately 32 Hz at 9-11 months, compared to 25 Hz in medial and dorsal slices, and was approximately 25 Hz at 20-24 months, compared to 21 Hz in medial and dorsal slices. This preponderance of medial and dorsal slices generating low frequency oscillations may have accounted for the poorly defined peak of carbachol-induced gamma frequency in wildtype littermate controls at 9-11 months. Therefore, in wildtype littermate controls the region recorded from did not have a notable impact on

carbachol-induced gamma frequency oscillation amplitude. However, slices from ventral region of the hippocampus generated higher frequency gamma frequency oscillations in wildtype littermate controls at both 9-11 and 20-24 months.

In APP/PS1 mice at 9-11 and 20-24 months the amplitude of carbachol-induced oscillations was reduced in slices taken from the medial region of the hippocampus relative to the dorsal and ventral regions. This was demonstrated by the area under the curve parameter which was approximately 300 $\mu V^2 Hz^-$ at 9-11 months, and was approximately 800 $\mu V^2 Hz^-$ at 20-24 months, in medial slices. In ventral and dorsal slices the area under the curve was approximately 700 $\mu V^2 Hz^-$ at 9-11 months and was approximately 3,500 $\mu V^2 Hz^-$ at 20-24 months. Similarly, the peak amplitude was approximately 25 μV at 9-11 months, and was approximately 50 μV at 20-24 months, in medial slices. In ventral and dorsal slices the peak amplitude was approximately 125 μV at 9-11 months and was approximately 300 μV at 20-24 months. As in wildtype littermate controls, the peak frequency of carbachol-induced gamma frequency oscillations in APP/PS1 mice at 9-11 and 20-24 months was increased in slices taken from the ventral regions of the hippocampus (approximately: 25 Hz) relative to slices taken from the dorsal and medial regions of the hippocampus (approximately 20 Hz.

There are therefore region-specific changes in carbachol-induced gamma frequency oscillations in both APP/PS1 mice and wildtype littermate controls at 9-11 and 20-24 months. Most notably the peak frequency was significantly increased in ventral slices at 9-11 months ($F_{2, 60} = 4.27$, $p = 0.0184$) and at 20-24 months ($F_{2, 51} = 3.52$, $p = 0.0371$). This effect was not affected by the APP/PS1 genotype (9-11 months: $F_{2, 60} = 0.21$, $p = 0.8124$, 20-24 months: $F_{2, 51} = 0.28$, $p = 0.7580$) nor was there an overall effect of the APP/PS1 genotype on peak frequency (9-11 months: $F_{2, 60} = 1.16$, $p = 0.2854$, 20-24 months: $F_{2, 51} = 0.59$, $p = 0.4476$).

There were also region-specific changes in carbachol-induced gamma frequency oscillation amplitude in APP/PS1 mice. At 9-11 months there was a reduction in gamma frequency oscillation amplitude in slices taken from the medial region of the hippocampus. This reduction caused the area under the curve ($F_{1, 60} = 5.02$, $p = 0.0289$) and peak amplitude ($F_{1, 60} = 4.10$, $p = 0.0473$) to be significantly reduced in APP/PS1 mice at 9-11 months, this effect was not affected by the region recorded (area under the curve: $F_{2, 60} = 0.34$, $p = 0.7117$, peak amplitude: $F_{2, 60} = 0.33$, $p = 0.7179$) nor was there an overall effect of the region recorded (area under the curve: $F_{2, 60} = 0.20$, $p = 0.8183$, peak amplitude: $F_{2, 60} = 0.47$, $p = 0.6293$). At 20-24 months in APP/PS1 mice oscillation amplitude was also reduced in slices taken from the medial region, however this did not lead to a significant reduction in APP/PS1 mice for the area under the curve ($F_{1, 51} = 2.15$, $p = 0.1488$) or in the peak amplitude ($F_{1, 51} = 3.17$, $p = 0.0811$) nor was there a significant effect of the region recorded on either parameter (area under the curve: $F_{2, 51} = 1.39$, $p = 0.2588$, peak amplitude: $F_{2, 51} = 1.71$, $p = 0.1918$). There was also no interaction between the region recorded and the APP/PS1 genotype (area under the curve: $F_{2, 51} = 0.38$, $p = 0.6850$, peak amplitude: $F_{2, 51} = 0.55$, $p = 0.3169$).

Therefore there were significant effects of the region recorded on carbachol-induced gamma frequency oscillation peak frequency and amplitude. For this model of gamma frequency oscillation induction, the region recorded was a significant consideration in the interpretation of gamma frequency oscillations in both APP/PS1 mice and littermate controls.

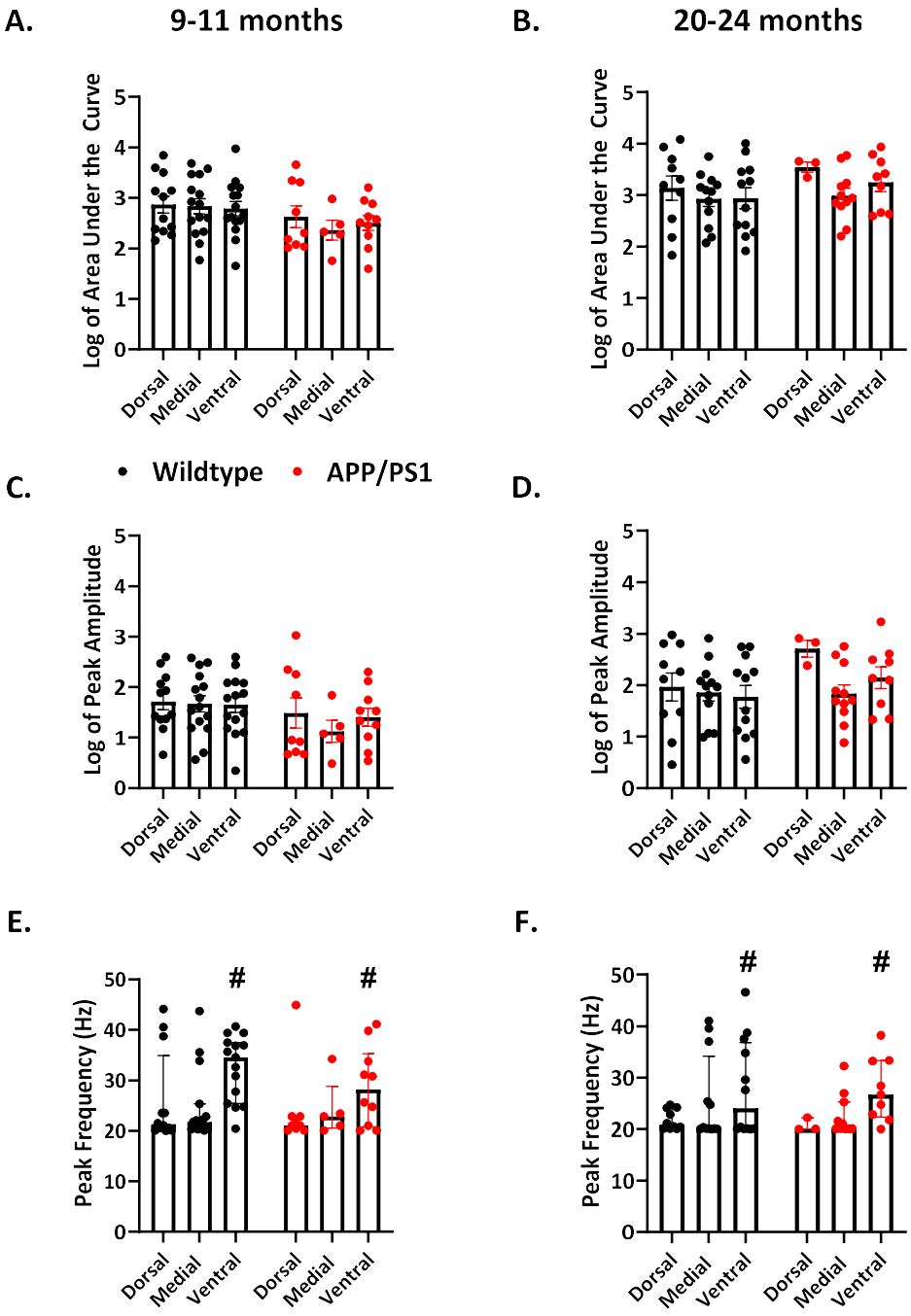

Figure 4.5. Carbachol-induced gamma frequency oscillations across the hippocampus. (A, B) Area under the curve, (C, D) peak amplitude, and (E, F) peak frequency of gamma frequency oscillations induced by carbachol (20 μM) in APP/PS1 (red) and wildtype mice (black) at (A, C, E) 9-11 and (B, D, F) 20-24 months. Data in A-D are log transformed. Median and IQR plotted in E and F. 2-way ANOVA, main effect of region in bold: # = $p < 0.05$. 9-11 months: APP/PS1, n = 35, N = 12, wildtype, n = 59, N= 19; 20-24 months: APP/PS1, n = 31, N = 15, wildtype, n = 40, N = 18.

4.6. Sex differences in carbachol-induced gamma frequency oscillations

As with kainate-induced gamma frequency oscillations, the effect of sex on carbachol-induced gamma frequency oscillations was examined (Figure 4.6). There were no significant sex effects on either APP/PS1 mice or wildtype littermate controls at 9-11 and 20-24 months. The age-associated increase in oscillation amplitude occurred in both sexes in both APP/PS1 mice and wildtype littermate controls.

In wildtype littermate controls at 9-11 months, there were no sex differences in the amplitude and frequency of carbachol-induced gamma frequency oscillations (area under the curve: males: 1553 ± 623.3 $\mu V^2 Hz^-$, females: 1678 ± 892.9 $\mu V^2 Hz^-$, peak amplitude: males: 93.27 ± 29.86 μV, females: 90.85 ± 26.29 μV, peak frequency: males: 26.49 ± 1.09 Hz, females: 26.80 ± 2.12 Hz). In wildtype littermate controls at 20-24 months there were also no sex differences in the amplitude and frequency of carbachol-induced gamma frequency oscillations (area under the curve: males: 2201.26 ± 719.60 $\mu V^2 Hz^-$, females: 3416.05 ± 1119.45 $\mu V^2 Hz^-$, peak amplitude: males: 170.39 ± 56.86 μV, females: 309.82 ± 89.86 μV, peak frequency: males: 24.34 ± 1.89 Hz, females: 28.07 ± 2.99 Hz) Therefore, in wildtype littermate controls, both sexes had an age-associated increase in amplitude and reduction in frequency at 20-24 months relative to 9-11 months.

In APP/PS1 mice at 9-11 months there were no notable sex differences in the peak frequency of carbachol-induced gamma frequency oscillations. However, there was a reduction in oscillation amplitude in female APP/PS1 mice at 9-11 months (area under the curve: males: 1678 ± 892.9 $\mu V^2 Hz^-$, females: 943 ± 444.3 $\mu V^2 Hz^-$, peak amplitude: males: 131.2 ± 46.83 μV, females: 72.47 ± 34.21 μV, peak frequency: males: 26.80 ± 2.12 Hz, females: 26.12 ± 1.62 Hz). In APP/PS1 mice at 20-24 there were no notable sex differences in the amplitude or frequency of carbachol-induced gamma frequency oscillations. The amplitude of carbachol-induced gamma frequency

oscillations were increased in both sexes in APP/PS1 mice at 20-24 months relative mice at 9-11 months (area under the curve: males: 2907.46 ± 950.79 $\mu V^2 Hz^-$, females: 1874.00 ± 527.67 $\mu V^2 Hz^-$, peak amplitude: males: 224.54 ± 93.29 μV, females: 224.54 ± 93.29 μV, peak frequency: males: 25.94 ± 2.60 Hz, females: 23.36 ± 0.91 Hz).

At 9-11 and 20-24 months there was no significant effect of sex on the area under the curve (9-11 months: $F_{1,27} = 0.76$, p = 0.3912, 20-24 months: $F_{1,29} = 0.17$, p = 0.6870), peak amplitude (9-11 months: $F_{1,27} = 1.32$, p = 0.2613, 20-24 months: $F_{1,29} = 0.35$, p = 0.5572), or peak frequency (9-11 months: $F_{1,27} = 0.85$, p = 0.3641, 20-24 months: $F_{1,29} = 0.07$, p = 0.2184). Nor were there any interactions between sex and genotype for the area under the curve (9-11 months: $F_{1,27} = 0.30$, p = 0.5900, 20-24 months: $F_{1,29} = 2.42$, p = 0.1305), peak amplitude (9-11 months: $F_{1,27} = 1.69$, p = 0.2044, 20-24 months: $F_{1,29} = 2.39$, p = 0.1329), or peak frequency (9-11 months: $F_{1,27} = 1.94$, p = 0.1750, 20-24 months: $F_{1,29} = 2.11$, p = 0.1571).

This demonstrated that sex did not have a significant impact on carbachol-induced gamma frequency oscillations in either APP/PS1 mice or wildtype littermate controls at 9-11 and 20-24 months.

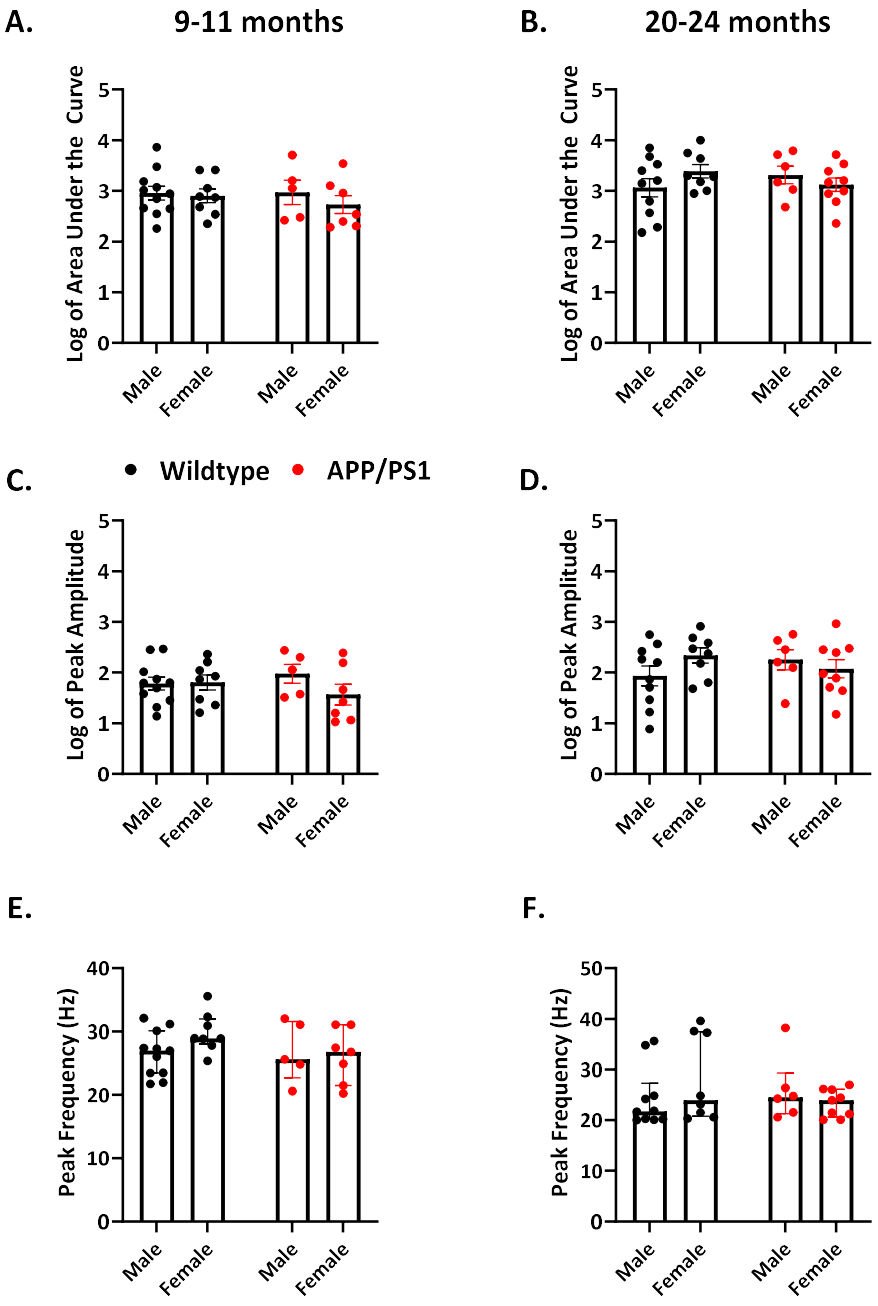

Figure 4.6. Sex effects on carbachol-induced gamma frequency oscillations. (A, B) Area under the curve, (C, D) peak amplitude, and (E, F) peak frequency of gamma frequency oscillations induced by carbachol (20 μM) in APP/PS1 (red) and wildtype mice (black) at (A, C, E) 9-11 and (B, D, F) 20-24 months in both sexes. Data in A-D are log transformed. 2-way ANOVA, main effect of genotype in bold. 9-11 months: male APP/PS1, n = 12, N = 5, female APP/PS1, n = 23, N = 7; male WT, n = 33, N = 11, female WT, n = 26, N = 8; 20-24 months: male APP/PS1, n = 9, N = 6, female APP/PS1, n = 22, N = 9; male WT, n = 22, N = 10, female WT, n = 18, N = 8.

4.7. Epileptiform events embedded in gamma frequency oscillations

Epileptiform activity was commonly observed in certain experiments in which gamma frequency oscillations were induced with kainate (100 nM) or carbachol (20 μM). This activity appeared as sharp, large-amplitude, deflections which were embedded in the ongoing gamma frequency oscillation (Pais et al., 2003). Representative traces of these events are shown in Figures 4.7 and 4.8. This epileptiform activity was automatically detected and quantified by identifying events which were five standard deviations larger than the ongoing gamma frequency oscillation. The incidence of epileptiform activity APP/PS1 mice and wildtype littermate controls at 9-11 and 20-24 months was quantified as well as the frequency (events per minute), amplitude (μV) and length (msec).

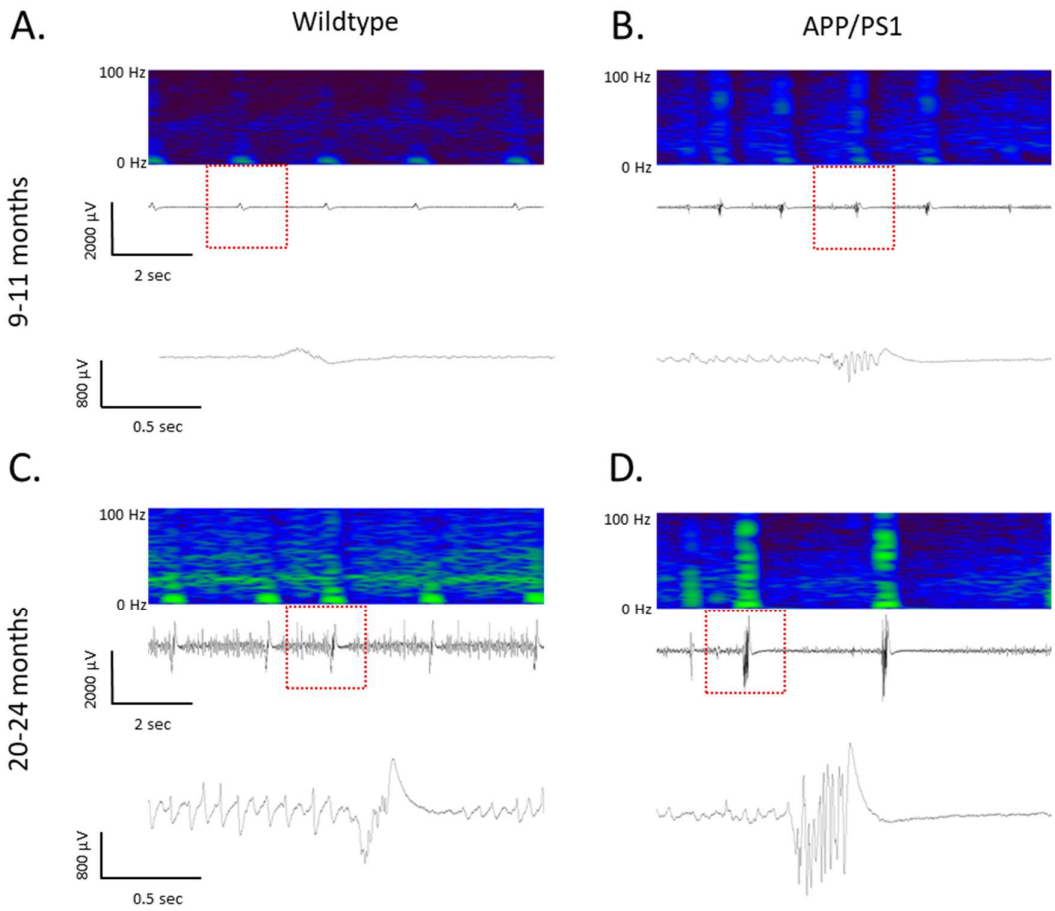

Figure 4.7. Representative epileptiform events in embedded kainate-induced gamma frequency oscillations. Epileptiform events in brain slices with kainate-induced gamma frequency oscillations in wildtype mice (left - A, C) and APP/PS1 mice (right – B, D) at 9-11 (top – A, B) and 20-24 months (bottom – C, D). Shown for each group: a representative 10 second section, a heatmap of the frequency decomposition by Fast Fourier Transform for this 10 second section, and a 1 second section of the recording. The 1 second section is highlighted in red on the 10 second section.

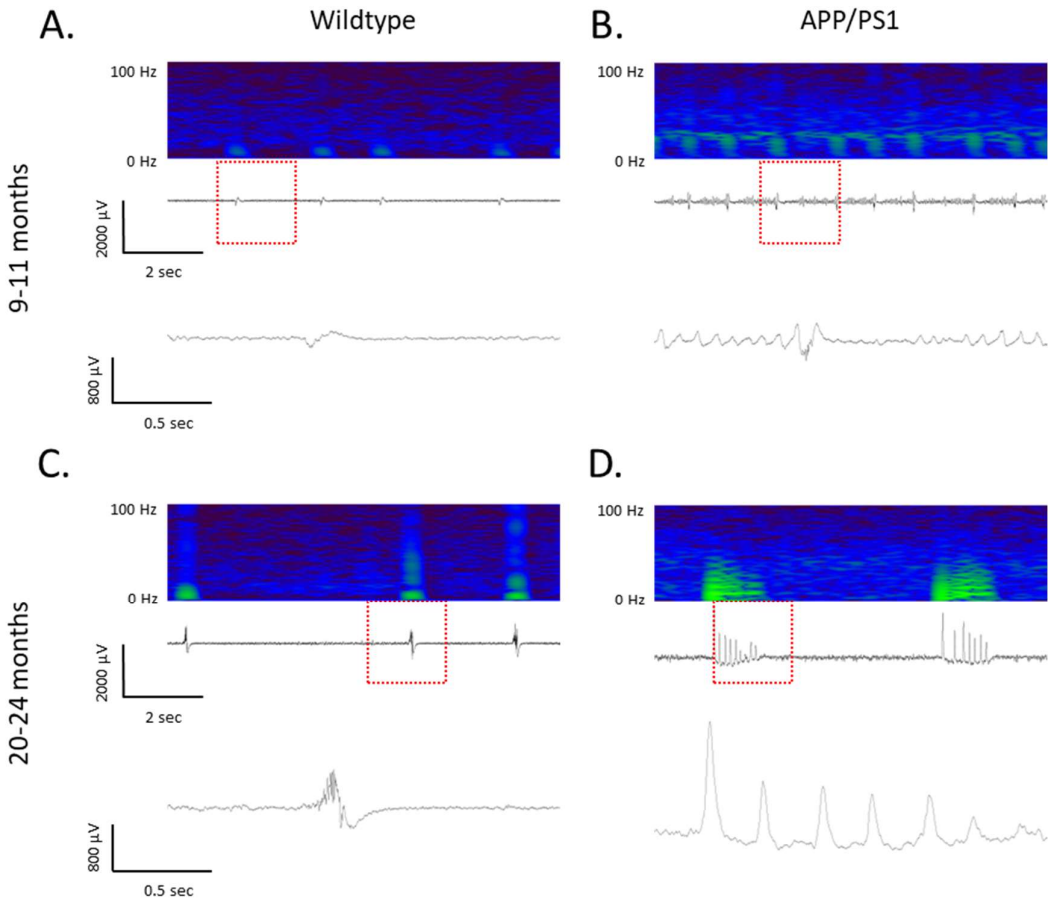

Figure 4.8. Representative epileptiform events embedded in carbachol-induced gamma frequency oscillations. Epileptiform events in brain slices with carbachol-induced gamma frequency oscillations in wildtype mice (left - A, C) and APP/PS1 mice (right – B, D) at 9-11 (top – A, B) and 20-24 months (bottom – C, D). Shown for each group: a representative 10 second section, a heatmap of the frequency decomposition by Fast Fourier Transform for this 10 second section, and a 1 second section of the recording. The 1 second section is highlighted in red on the 10 second section.

4.8. Epileptiform event incidence in APP/PS1 mice

In slices with kainate-induced gamma frequency oscillations the incidence of epileptiform events was quantified (Figure 4.9, A, B). There was a lower incidence of epileptiform events in female relative to male wildtype littermate controls at both 9-11 and 20-24 months (males: 54% of slices, females: 33% of slices). This incidence was similar to that in wildtype littermate controls at 20-24 months in males (54%) and females (22%). There was an increased incidence of epileptiform events in kainate-induced gamma frequency oscillations in APP/PS1 mice at 9-11 months (male: 72%, female: 77%, $p = 0.0048$) and at 20-24 months (male: 88%, female: 62%, $p = 0.0052$). The increase incidence of epileptiform event incidence was especially large in female APP/PS1 mice, relative to the reduced incidence in female wildtype littermate controls.

In slices with carbachol-induced gamma frequency oscillations the incidence of epileptiform events was quantified (Figure 4.9, C, D). There was a similar incidence of epileptiform events in female and male wildtype littermate controls at both 9-11 and 20-24 months. In wildtype littermate controls at 9-11 months 39% of slices from males and 32% of slices from females had epileptiform events. This incidence was increased in wildtype littermate controls at 20-24 months in males (55%) and in females (53%). Relative to wildtype littermate controls, there was an increased incidence of epileptiform events in carbachol-induced gamma frequency oscillations in APP/PS1 mice at 9-11 months, notably in male APP/PS1 mice (male: 91%, female: 52%, $p = 0.0100$) and less notably at 20-24 months (male: 54%, female: 68%, $p = 0.4850$). Epileptiform events incidence was higher in carbachol-induced gamma frequency occurred in aged mice and in APP/PS1 mice relative to wildtype littermate controls at 9-11 months.

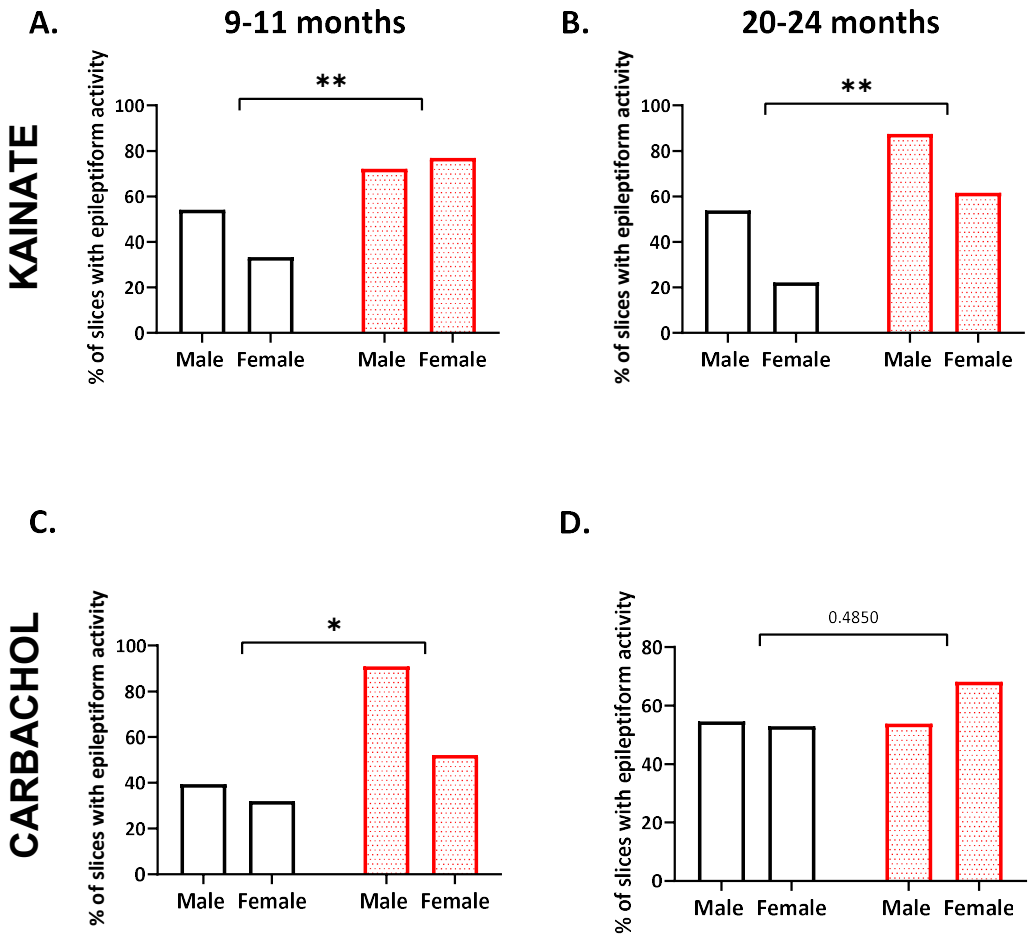

Figure 4.9. Incidence of epileptiform activity in brain slices with kainate- and carbachol-induced gamma frequency oscillations. Brain slices taken from APP/PS1 mice (red) and wildtype mice (black) at (A, C) 9-11 months and (B, D) 20-24 months. Epileptiform event incidence quantified in (A, B) kainate- and (C, D) carbachol-induced gamma frequency oscillations. Kainate: 9-11 months: APP/PS1 male n = 18, N = 5, APP/PS1 female n = 26, N = 7, WT male n = 24, N = 11, WT female n = 21, N = 8. 20-24 months: : APP/PS1 male n = 16, N = 6, APP/PS1 female n = 26, N = 10, WT male n = 22, N = 7, WT female n = 18, N = 7. Carbachol: 9-11 months: APP/PS1 male n = 11, N = 5, APP/PS1 female n = 23, N = 7, WT male n = 33, N = 11, WT female n = 25, N = 8. 20-24 months: : APP/PS1 male n = 13, N = 6, APP/PS1 female n = 22, N = 9, WT male n = 18, N = 7, WT female n = 17, N = 7.

4.9. Epileptiform quantification in kainate-induced gamma frequency oscillations

The frequency (events per minute), amplitude (μV) and length (msec) of the epileptiform events in kainate-induced gamma frequency oscillations were quantified in brain slices from APP/PS1 mice and wildtype littermate controls at 9-11 and 20-24 months (Figure 4.10). As well as having increased incidence, epileptiform events had increased length in APP/PS1 mice – this was suggestive of increased event complexity. In aged mice there is an increase in event amplitude. These findings are described in further detail below.

In wildtype littermate controls at 9-11 months epileptiform events occurred at a frequency of approximately 18 events per minute, with events being more frequent in slices from males than from females (male: 21.78 ± 2.26 events per minute, female: 14.73 ± 2.68 events per minute). Event length was also greater in males than in female wildtype littermate controls at 9-11 months (male: 422.4 ± 106.8 msec, female: 212.3 ± 58.2 msec). Event amplitude was similar in male and female wildtype littermate controls at 9-11 months (male: 573.2 ± 113.4 μV, female: 509.3 ± 170.6 μV). Therefore, as well as event incidence being lower in females relative to males, the events which occurred in females were shorter and had lower frequency than those which occurred in males for wildtype littermate controls at 9-11 months.

At 20-24 months the frequency events occurred at was similar in male and female wildtype littermate controls (16.70 ± 2.29 events per minute, female: 17.75 ± 3.53 events per minute) but amplitude was increased in both male and female wildtype littermate controls at 20-24 months relative to 9-11 months (male: 808.7 ± 208.9 μV, female: 1085 ± 624.7 μV). Event length was also increased in both sexes at 20-24 months relative to 9-11 months. As at 9-11 months, event length was increased in males relative to female wildtype littermate controls at 20-24 months (male: 765.5 ± 522.9 msec, female: 495.3 ± 93.56 msec). Therefore, in wildtype mice at both ages,

these epileptiform events were longer in males than in females which was indicative of increased complexity and pathogenicity. At 20-24 months epileptiform events had increased in amplitude and length relative to wildtype littermate controls at 9-11 months.

In APP/PS1 mice at 9-11 and 20-24 months epileptiform events occurred at a frequency of approximately 15 events per minute with events being more frequent in slices from female mice than in male mice (9-11 months: male: 11.21 ± 1.94 events per minute, female: 16.79 ± 1.40 events per minute, 20-24 months: male: 14.75 ± 2.67 events per minute, female: 15.81 ± 3.52 events per minute). This represented an overall decrease in event frequency in APP/PS1 mice relative to wildtype littermate controls, most notably in male APP/PS1 mice. At 9-11 months epileptiform event amplitude in APP/PS1 mice was similar to event amplitude in wildtype littermate controls (male: 617.3 ± 162.5 μV, female: 592.7 ± 76.3 μV) but was increased at 20-24 months. This increased amplitude was similar to amplitude in wildtype littermate controls at 20-24 months (male: 1512 ± 290.9 μV, female: 983.8 ± 294.9 μV). Epileptiform event length was increased in APP/PS1 mice relative to wildtype littermate controls at 9-11 months (wildtype: male: 765.5 ± 522.9 msec, female: 495.3 ± 93.56 msec; APP/PS1: male: 2590 ± 1727 msec, female: 2176 ± 976.1 msec). Event length was slightly decreased in APP/PS1 mice at 20-24 months relative to 9-11 months but was nonetheless increased relative to wildtype mice at 20-24 months (male: 610.1 ± 236.0 msec, female: 1880 ± 1509 msec). As in wildtype littermate controls, there was an increase in event amplitude in APP/PS1 mice at 20-24 months relative to 9-11 months. Most notably, in APP/PS1 mice there was an increase in epileptiform event length which suggested more complex events occurred in APP/PS1 than in wildtype littermate controls.

There was no significant effect of age ($F_{1, 37} = 0.004$, $p = 0.9479$), genotype ($F_{1, 37} = 2.38$, $p = 0.1311$), or sex ($F_{1, 37} = 0.006$, $p = 0.9371$) on the frequency at which epileptiform events occurred in APP/PS1 mice and wildtype littermate controls at 9-11 and 20-24 months. Nor was there any significant interactions between these factors with regard to event frequency. There was a

significant increase in epileptiform event amplitude in aged mice ($F_{1, 37}$ = 8.34, p = 0.0064). There was no significant effect of genotype ($F_{1, 37}$ = 1.01, p = 0.3214) or sex ($F_{1, 37}$ = 0.22, p = 0.6420) on event amplitude nor was there any significant interactions between these factors. The length of events was significantly increased in APP/PS1 mice relative to wildtype littermate controls ($F_{1, 37}$ = 4.48, p = 0.0411). Event length was not significantly affected by sex ($F_{1, 37}$ = 0.04, p = 0.8512) or by age ($F_{1, 37}$ = 1.40, p = 0.2443). However, there was a significant interaction between age and genotype ($F_{1, 37}$ = 0.78, p = 0.0456) suggesting that the increase in event length in APP/PS1 mice was most notable in APP/PS1 mice at 9-11 months.

Overall, the epileptiform events which occurred in kainate-induced gamma frequency oscillations had higher incidence in APP/PS1 mice relative to wildtype littermate controls. Additionally, epileptiform events had increased length in APP/PS1 mice relative to wildtype littermate controls, most significantly at 9-11 months. Independent of genotype, epileptiform event amplitude was increased in mice at 20-24 months.

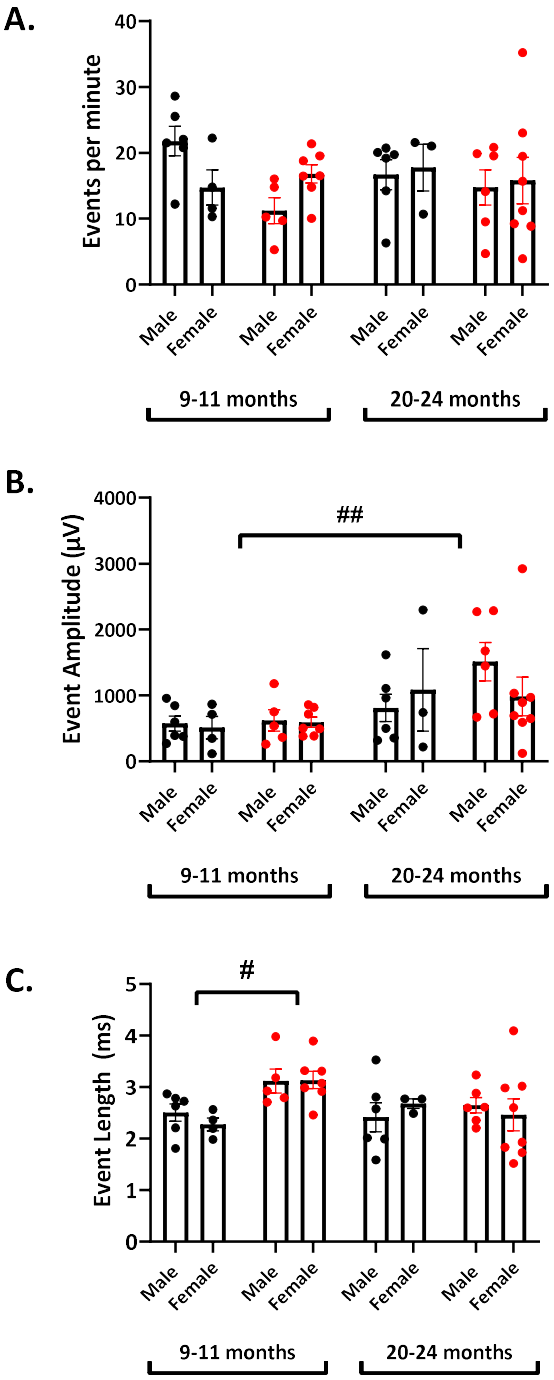

Figure 4.10. Epileptiform event quantification in kainate-induced gamma frequency oscillations. Epileptiform event (A) frequency, (B) amplitude, (C) and length in brain slices with kainate-induced gamma frequency oscillations. Brain slices taken from APP/PS1 (red) and wildtype mice (black) at 9-11 and 20-24 months. Data in C are log transformed. 3-way ANOVA, # = $p < 0.05$, ## = $p < 0.001$ for main effects of ANOVA. 9-11 months: APP/PS1, n = 43, N = 12, WT, n = 49, N = 16; 20-24 months: APP/PS1, n = 40, N = 15, WT, n = 46, N = 17.

4.10. Epileptiform quantification in carbachol-induced gamma frequency oscillations

The frequency (events per minute), amplitude (μV) and length (msec) of the epileptiform events in carbachol-induced gamma frequency oscillations were quantified in brain slices from APP/PS1 mice and wildtype littermate controls at 9-11 and 20-24 months (Figure 4.11). The frequency at which epileptiform events occurred at was slightly increased in APP/PS1 mice at 9-11 months. The amplitude of epileptiform events was increased in mice at 20-24 months.

In wildtype littermate controls at 9-11 months epileptiform events occurred at a frequency of approximately 13 events per minute with no notable sex differences (male: 15.27 ± 3.22 events per minute, female: 11.86 ± 2.12 events per minute). Event amplitude was also similar in both sexes at 9-11 months (male: 526.6 ± 92.44 μV, female: 442.4 ± 153.2 μV). However, event length was increased in males relative to female wildtype littermate controls (male: 1035 ± 422.7 msec, female: 326.7 ± 129.6 msec). Therefore, similar to epileptiform events which occurred during kainate-induced gamma frequency oscillations, the events which occurred in carbachol-induced gamma frequency were shorter in females than those which occurred in male wildtype littermate controls at 9-11 months. At 20-24 months the frequency events occurred at was similar in both sexes of wildtype littermate controls (male: 10.82 ± 2.42 events per minute, female: 17.63 ± 2.57 events per minute). Event amplitude was increased in female wildtype littermate controls at 20-24 months relative to females at 9-11 months but was unchanged in male mice (male: 563.2 ± 185.9 μV, female: 908.1 ± 252.2 μV). Event length was increased at 20-24 months relative to 9-11 months. Similar to event amplitude, event length was increased in females at 20-24 months relative 9-11 months but was unchanged male mice (male: 841.7 ± 645.7 msec, female: 1309 ± 629.8 msec). Therefore, in wildtype littermate controls the epileptiform events which occurred in carbachol-induced gamma frequency oscillations at 9-11 months were less frequent, smaller and

shorter in female mice. However at 20-24 months, there was an increase in epileptiform event frequency, amplitude, and length in female wildtype littermate controls but not in male wildtype littermate controls.

In APP/PS1 mice at 9-11 months epileptiform events occurred at a frequency of approximately 15 events per minute with events being more frequent in slices from female mice than in male mice (male: 21.27 ± 3.84 events per minute, female: 14.05 ± 1.22 events per minute). This represented an overall increase in event frequency in APP/PS1 mice relative to wildtype littermate controls at 9-11 months. In APP/PS1 mice at 9-11 months epileptiform event amplitude was similar to event amplitude in wildtype littermate controls at 9-11 months (male: 416.0 ± 120.3 μV, female: 578.1 ± 143.4 μV). Epileptiform event length was increased in APP/PS1 mice relative to wildtype littermate controls at 9-11 months (male: 1897 ± 1284 msec, female: 1623 ± 403.3 msec). In APP/PS1 mice at 20-24 months epileptiform events occurred at a frequency of approximately 17 events per minute (male: 18.95 ± 2.36 events per minute, female: 17.74 ± 3.29 events per minute), this was similar to the frequency of events in APP/PS1 mice at 9-11 months and the frequency of events in wildtype littermate controls at 20-24 months. Event amplitude was increased in APP/PS1 mice at 20-24 months relative to APP/PS1 mice at 9-11 months, however it was similar to event amplitude in wildtype littermate controls at 20-24 months (male: 1256 ± 429.2 μV, female: 750.1 ± 206.2 μV). Event length was decreased in APP/PS1 mice at 20-24 months relative to event length in APP/PS1 mice at 9-11 months but was increased relative to wildtype littermate controls at 20-24 months (male: 841.7 ± 645.7 msec, female: 1309 ± 629.8 msec). Therefore, in APP/PS1 mice the frequency of events was increased in APP/PS1 mice relative to wildtype littermate controls at 9-11 months, but not at 20-24 months. As in wildtype mice, there was an increase in event amplitude in APP/PS1 mice at 20-24 months relative to APP/PS1 mice at 9-11 months. As with the epileptiform events which occurred in kainate-induced gamma frequency oscillations, in carbachol-induced gamma frequency oscillation

epileptiform events in APP/PS1 mice there was an increase in event length which suggested more complex events occurred in APP/PS1 mice than in wildtype littermate controls.

There was no significant effect of age ($F_{1, 40}$ = 0.094, p = 0.7600), genotype ($F_{1, 40}$ = 3.512, p = 0.0682), or sex ($F_{1, 40}$ = 0.3269, p = 0.5707) on the frequency at which epileptiform events occurred in carbachol-induced gamma frequency oscillations in APP/PS1 mice and wildtype littermate controls at 9-11 months and 20-24 months. Nor was there any significant interaction between these factors with regard to event frequency. There was however a strong trend towards a significant increase in event frequency in APP/PS1 mice relative to wildtype littermate controls. There was a significant increase in epileptiform event amplitude in aged mice ($F_{1, 40}$ = 6.156, p = 0.0174) in both sexes and in both APP/PS1 mice and wildtype littermate controls. There was no significant effect of genotype ($F_{1, 40}$ = 0.8414, p = 0.3645) or sex ($F_{1, 40}$ = 0.018, p = 0.8923) on event amplitude nor was there any significant interactions between these factors. Event length was not significantly affected by genotype ($F_{1, 40}$ = 1.667, p = 0.2040), by sex ($F_{1, 40}$ = 1.002, p = 0.3229) or by age ($F_{1, 40}$ = 0.429, p = 0.5159) nor was there a significant interaction between these factors.

In summary, the epileptiform events which occurred in carbachol-induced gamma frequency oscillations had higher incidence in APP/PS1 mice relative to wildtype littermate controls. There was non-significantly increased frequency and length of epileptiform events in APP/PS1 mice relative to wildtype littermate controls, notably at 9-11 months. Independent of genotype, epileptiform event amplitude was increased in mice at 20-24 months.

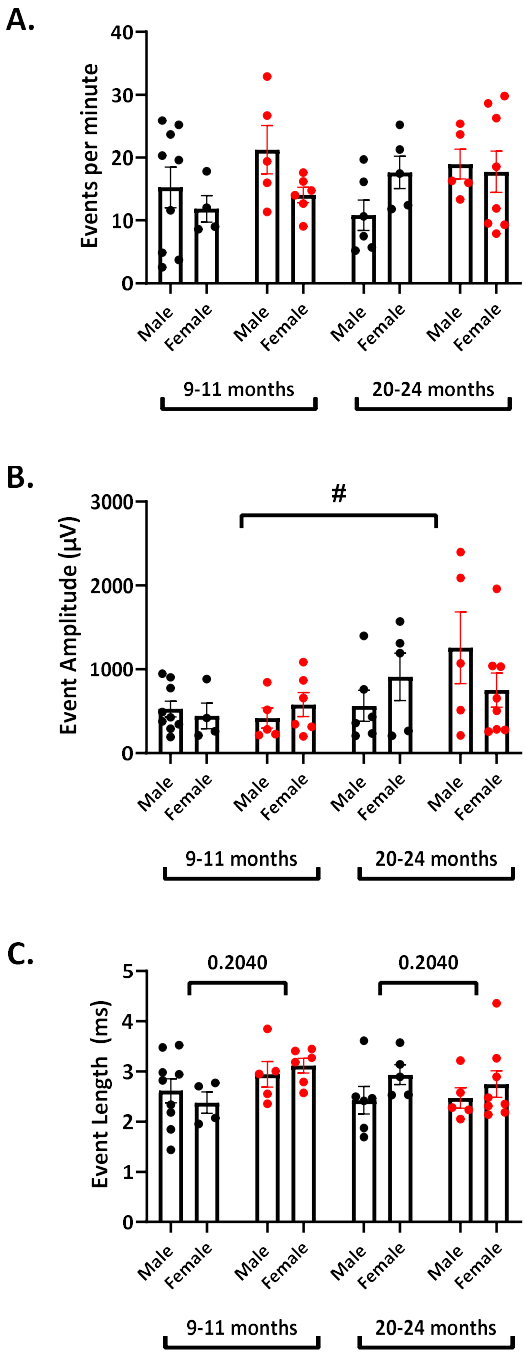

Figure 4.11. Epileptiform event quantification in carbachol-induced gamma frequency oscillations. Epileptiform event (A) frequency, (B) amplitude, (C) and length in brain slices with kainate-induced gamma frequency oscillations. Brain slices taken from APP/PS1 (red) and wildtype mice (black) at 9-11 and 20-24 months. Data in C are log transformed. 3-way ANOVA, # = $p < 0.05$, ## = $p < 0.001$ for main effects of ANOVA. 9-11 months: APP/PS1, n = 35, N = 12, wildtype, n = 59, N = 19; 20-24 months: APP/PS1, n = 31, N= 15 mice, wildtype, n = 40, N = 18.

4.11. Parvalbumin-positive interneuron density in APP/PS1 mice

Parvalbumin-positive interneurons are known to be sufficient and necessary to generate gamma frequency oscillations (Cardin et al., 2009; Sohal et al., 2009). Having established that gamma frequency oscillations were altered in APP/PS1 mice at 9-11 and 20-24 months, parvalbumin-positive interneuron density was investigated using immunohistochemistry in APP/PS1 mice and wildtype littermate controls (Figure 4.12). Briefly, parvalbumin interneuron density was reduced in APP/PS1 mice predominantly in the dentate gyrus and CA3 subregion, and to a greater extent in female APP/PS1 mice. The hippocampus is made up of several subregions: the dentate gyrus and the cornus Ammonis (CA) regions. Parvalbumin-positive interneuron density was examined in three of these hippocampal subregions: the dentate gyrus, the CA3, and the CA1 subregions. Parvalbumin-positive interneurons were observed to be multipolar with extensive dendritic arborisation. In the dentate gyrus, parvalbumin-positive cell bodies were located, almost exclusively, in the stratum granulosum. While, in the CA3 and CA1 subregions, parvalbumin-positive cell bodies were predominantly located in the strata oriens and pyramidale.

Parvalbumin-positive interneurons were significantly reduced in APP/PS1 mice compared to wildtype littermate controls ($F_{1, 22} = 7.24$, $p = 0.0134$). There was a modest but non-significant reduction of parvalbumin-positive interneuron density with age ($F_{1, 22} = 2.07$, $p = 0.1647$), and no interaction between age and genotype ($F_{1, 22} = 0.77$, $p = 0.3904$).

With respect to hippocampal subregions, there was a significant reduction in parvalbumin-positive interneuron density in APP/PS1 mice in the dentate gyrus ($F_{1, 22} = 10.25$, $p = 0.0041$) and the CA3 ($F_{1, 22} = 8.07$, $p = 0.0095$), but not in the CA1 ($F_{1, 22} = 0.26$, $p = 0.6128$). Despite no significant effects of age in the hippocampus as a whole, there was a significant effect of age on parvalbumin-positive interneuron density in the dentate gyrus ($F_{1, 22} = 4.97$, $p = 0.0364$) and a trend towards a significant decrease in the CA3 ($F_{1, 22} = 3.97$, $p = 0.0589$) and CA1 ($F_{1, 22} = 2.24$,

p = 0.1484). There was no significant interaction between age and genotype in any subregion quantified (dentate gyrus: $F_{1, 22} = 2.86$, p = 0.1051, CA3: $F_{1, 22} = 2.41$, p = 0.1346, CA1: $F_{1, 22} = 1.45$, p = 0.2421). Therefore, parvalbumin-positive interneurons were particularly vulnerable in the dentate gyrus and the CA3 in both APP/PS1 and aged mice, while the CA1 was relatively protected.

The hippocampus is also structurally heterogenous along the dorsal-ventral axis. Therefore parvalbumin-positive interneuron density in APP/PS1 mice was compared across dorsal, medial, and ventral sections of the hippocampus (Figure 4.13, A, B). At 9-11 months the APP/PS1-associated reduction in parvalbumin-positive interneuron density was present ($F_{1, 31} = 6.55$, p = 0.0156) and there was no effect of the dorsal-ventral location 48($F_{1, 31} = 0.41$, p = 0.6656). At 20-24 months there was a significant effect of the dorsal-ventral location on parvalbumin-positive interneuron density ($F_{1, 29} = 3.56$, p = 0.0416), with a trend towards parvalbumin loss confined to the dorsal region. Therefore, the APP/PS1-associated reduction in parvalbumin-positive interneuron density was not localised to a specific region of the hippocampus.

Parvalbumin-positive interneuron density was also examined with respect to sex (Figure 4.13, C, D). Parvalbumin-positive interneuron density was significantly reduced in both sexes in APP/PS1 mice ($F_{1, 10} = 6.27$, p = 0.0312). In wildtype mice at 9-11 months there was a trend towards an increase in parvalbumin-positive interneuron density in females relative to males ($F_{1, 10} = 3.55$, p = 0.0890). From this higher baseline, female APP/PS1 mice at 9-11 months have a greater reduction in parvalbumin-positive interneuron density than male APP/PS1 mice and at 20-24 months the APP/PS1-associated parvalbumin reduction was seen exclusively in female APP/PS1 mice (sex: $F_{1, 8} = 30.38$, p = 0.0006, sex X genotype: $F_{1, 8} = 7.21$, p = 0.0277).

In summary, parvalbumin-positive interneuron density was significantly reduced in APP/PS1 mice at 9-11 and 20-24 months, and to a greater extent in female APP/PS1 mice.

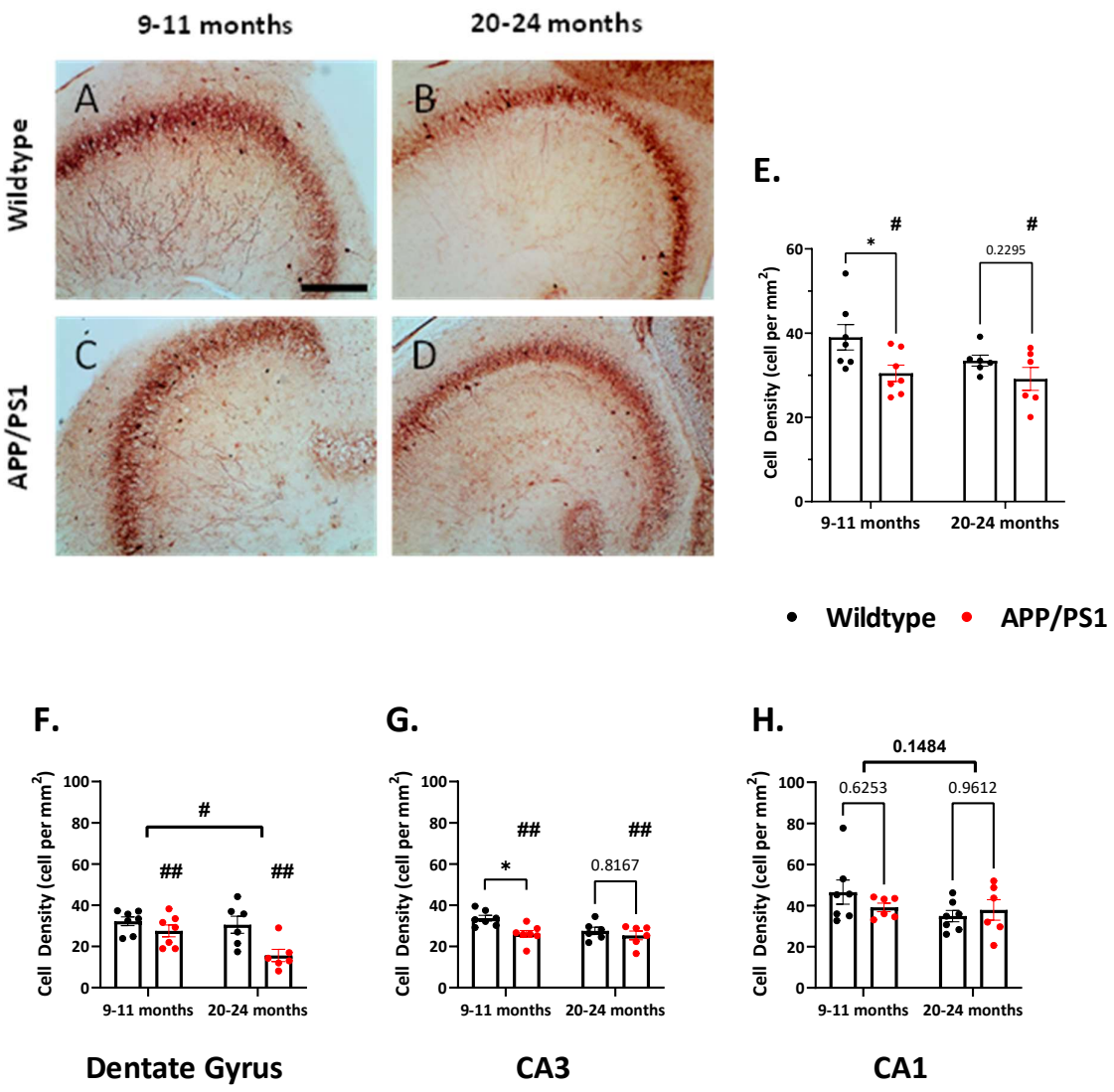

Figure 4.12. Parvalbumin-positive interneuron density in APP/PS1 mice and wildtype mice. (A-D) Representative images of parvalbumin-positive interneuron density in (A, B) wildtype and (C, D) APP/PS1 mice at (A, C) 9-11 months and (B, D) 20-24 months. Parvalbumin-positive interneuron density quantified in hippocampal sections from APP/PS1 (red) and wildtype (black) mice at 9-11 and 20-24 months in (E) the hippocampus, (F) the dentate gyrus, (G) the CA3 subregion, (H) CA1 subregion. 2-way ANOVA, main effects in bold: # = $p < 0.05$, ## = $p < 0.01$, post-hoc comparisons with Tukey corrections in light text: * = $p < 0.05$. Scale bar: 250 μm. 9-11 months: n = 3, N = 7, 20-24 months: n = 3, N = 6.

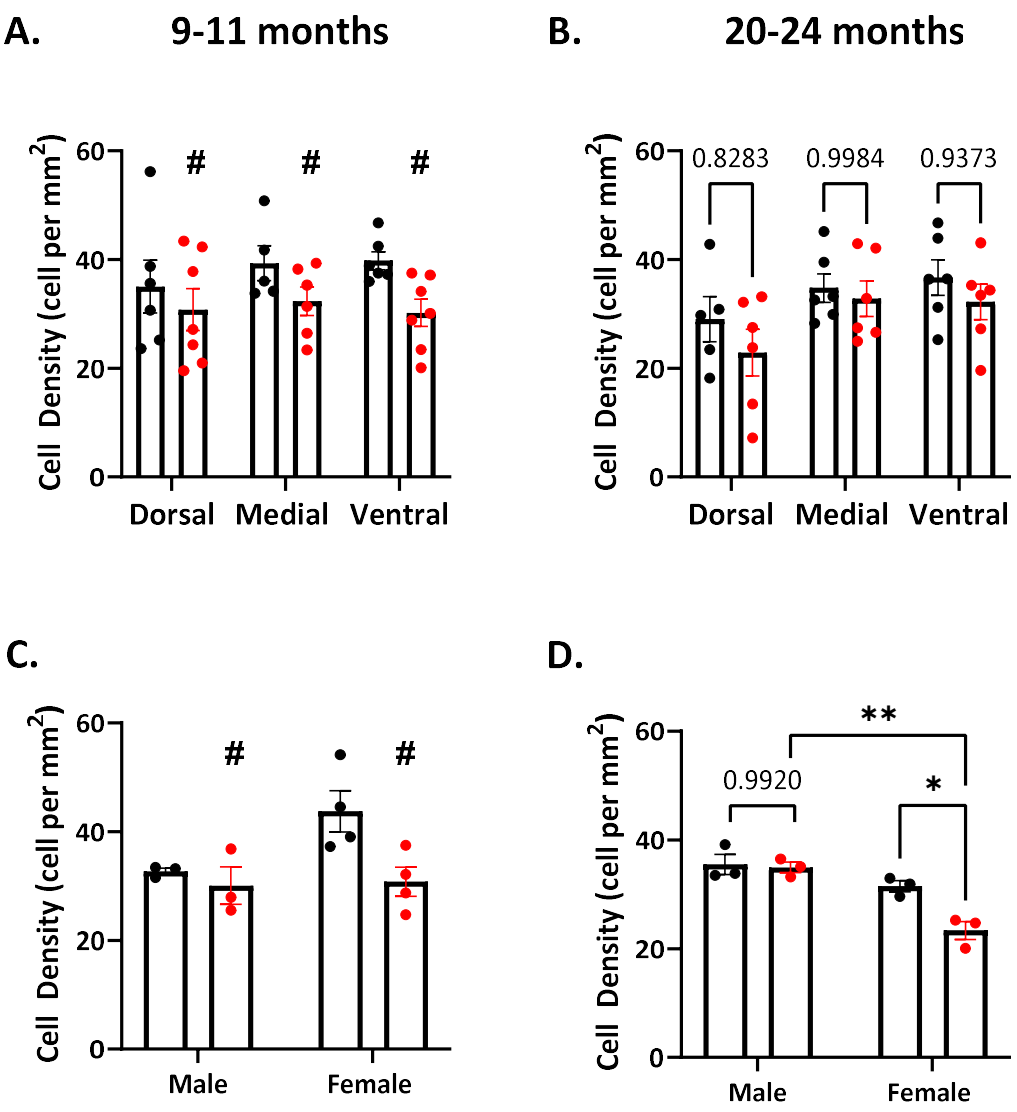

Figure 4.13. Parvalbumin-positive interneuron density across the hippocampus and in both sexes. Parvalbumin-positive interneuron density quantified in hippocampal sections from APP/PS1 (red) and wildtype (black) mice at (A, C) 9-11 and (B, D) 20-24 months (A, B) from three regions – dorsal, medial, ventral – across the hippocampus, and (C, D) in both sexes. 2-way ANOVA, main effects in bold: # = $p < 0.05$, ## = $p < 0.01$, post-hoc comparisons with Tukey corrections in light text, * = $p < 0.05$, ** = $p < 0.01$. 9-11 months: males, N = 3, females, N= 4; 20-24 months: N = 3.

4.12. Somatostatin-positive interneuron density in APP/PS1 mice

Somatostatin-positive interneurons are increasingly considered as important in the generation and maintenance of gamma frequency oscillations (Antonoudiou et al., 2020). Therefore, somatostatin-positive interneuron density was quantified using immunohistochemistry (Figure 4.14). Somatostatin-positive interneuron density was examined in three hippocampal subregions: the dentate gyrus, the CA3, and the CA1 subregion. Briefly, somatostatin interneuron density was reduced in aged mice and non-significantly reduced in APP/PS1 mice at 9-11 months. This reduction predominately occurred in the dentate gyrus and CA3 and in female mice.

Unlike parvalbumin-positive interneurons, only the cell body of somatostatin-positive interneurons were labelled; no processes were visible. In the dentate gyrus, somatostatin-positive cell bodies were located, almost exclusively, in the stratum granulosum. In the CA3 subregion, somatostatin-positive cell bodies were predominantly located in the stratum pyramidale. An intense band of staining was consistently observed in the stratum pyramidale of the CA3 the subregion, which was taken to be synaptic somatostatin. In the CA1 subregion, somatostatin-positive interneurons were predominantly located in the stratum oriens.

There was no main effect of the APP/PS1 genotype on somatostatin-positive interneurons density ($F_{1, 19} = 0.84$, $p = 0.3709$). There was a modest effect of age in that somatostatin-positive interneurons were somewhat, but non-significantly, reduced at 20-24 months relative to 9-11 months ($F_{1, 19} = 3.85$, $p = 0.0647$). There was a reduction in somatostatin-positive interneuron density in APP/PS1 mice relative to wildtype littermate controls at 9-11 months, but the interaction between age and genotype was also not quite significant ($F_{1, 19} = 3.85$, $p = 0.0646$). Moreover, this reduction in somatostatin-positive interneuron density was observed only in the CA3, in this region there was a main effect of age ($F_{1, 19} = 6.74$, $p = 0.0177$). In the dentate gyrus there was a trend towards a modest effect of age ($F_{1, 19} = 3.22$, $p = 0.0888$)

However, at 20-24 months somatostatin-positive interneuron density was comparable in APP/PS1 mice and wildtype littermate controls. There was no overall statistical effect of the APP/PS1 genotype on somatostatin-positive interneuron density. There was a strong trend towards an interaction between age and genotype. This reflected the reduction in somatostatin-positive interneuron density in APP/PS1 mice which occurred at 9-11 months but not at 20-24 months.

The distribution of somatostatin-positive interneuron density across the dorsal-ventral axis of the hippocampus was examined in APP/PS1 and wildtype littermate controls at 9-11 and 20-24 months (Figure 4.15, A, B). There was no significant effect of the location in the hippocampus on somatostatin-positive interneuron density at 9-11 months ($F_{1, 31} = 0.41$, $p = 0.6656$) or at 20-24 months ($F_{2, 20} = 0.68$, $p = 0.5181$). At 9-11 months the reduction in somatostatin-positive interneuron density in APP/PS1 mice was apparent in sections from the dorsal and medial region of the hippocampus, but not in ventral sections.

Somatostatin-positive interneuron density was also examined on the basis of sex (Figure 4.15, C, D). There was no significant effect of sex on somatostatin-positive interneuron density at 9-11 months ($F_{1, 8} = 1.02$, $p = 0.3432$) or at 20-24 months (($F_{1, 7} = 0.24$, $p = 0.6373$). Similar to parvalbumin-positive interneuron density in wildtype female mice at 9-11 months there was a non-significant increase in somatostatin-positive interneuron density relative to males. From this baseline, female APP/PS1 mice had a greater reduction in somatostatin-positive interneuron density than males.

In summary, somatostatin-positive interneuron density was modestly reduced with age and in APP/PS1 mice at 9-11 months. The APP/PS1-associated effect was not apparent at 20-24 months as the age-associated effects on wildtype littermate controls converged with the effect seen in APP/PS1 mice.

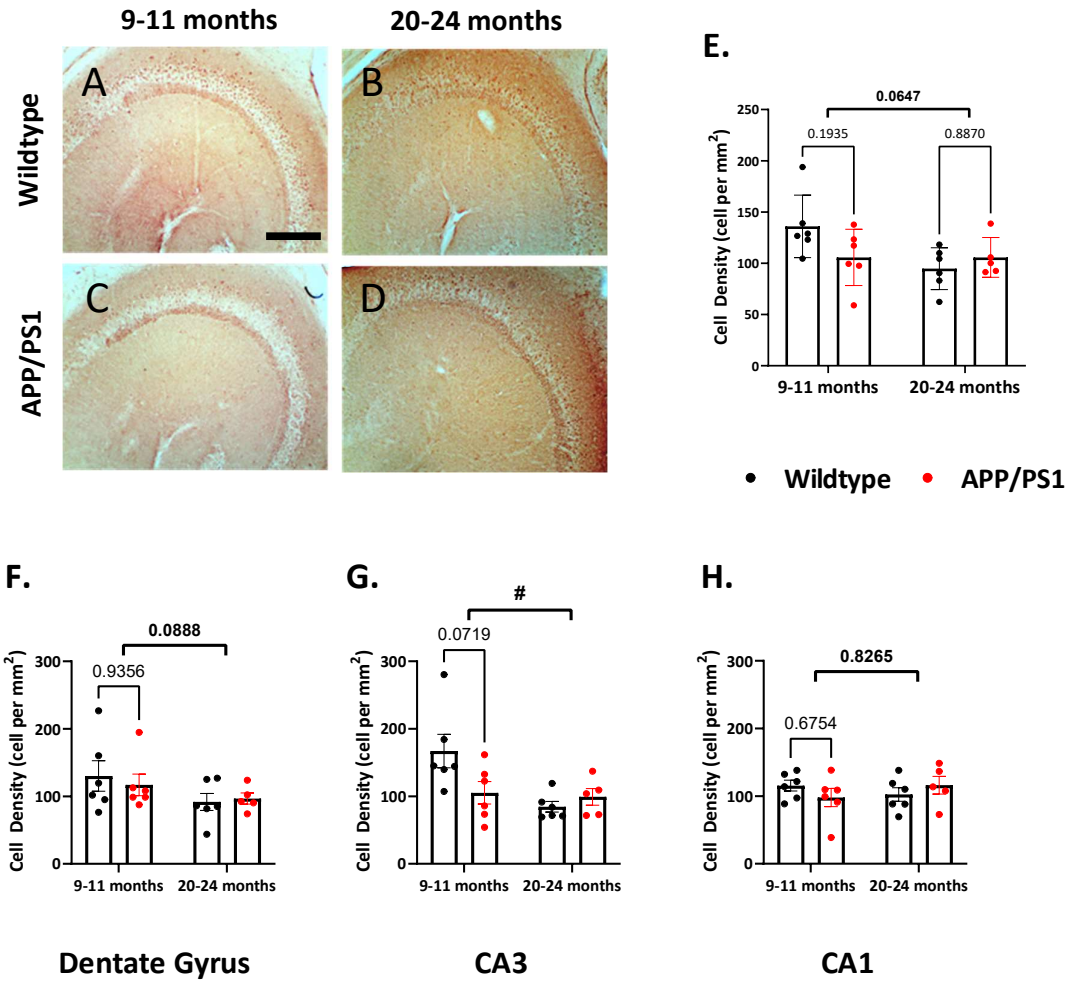

Figure 4.14. Somatostatin-positive interneuron density in APP/PS1 mice and wildtype mice. (A-D) Representative images of somatostatin-positive interneuron density in (A, B) wildtype and (C, D) APP/PS1 mice at (A, C) 9-11 and (B, D) 20-24 months. Somatostatin-positive interneuron density quantified in hippocampal sections from APP/PS1 (red) and wildtype (black) animals at 9-11 and 20-24 months in (E) the hippocampus, (F) the dentate gyrus, (G) the CA3 subregion, (H) CA1 subregion. 2-way ANOVA, main effects in bold: # = $p < 0.05$, ## = $p < 0.01$, post-hoc comparisons with Tukey corrections in light text. Scale bar: 250 μm. 9-11 months: n = 3, N = 6; 20-24 months: APP/PS1, n = 3, N = 5, wildtype, n = 3, N = 6.

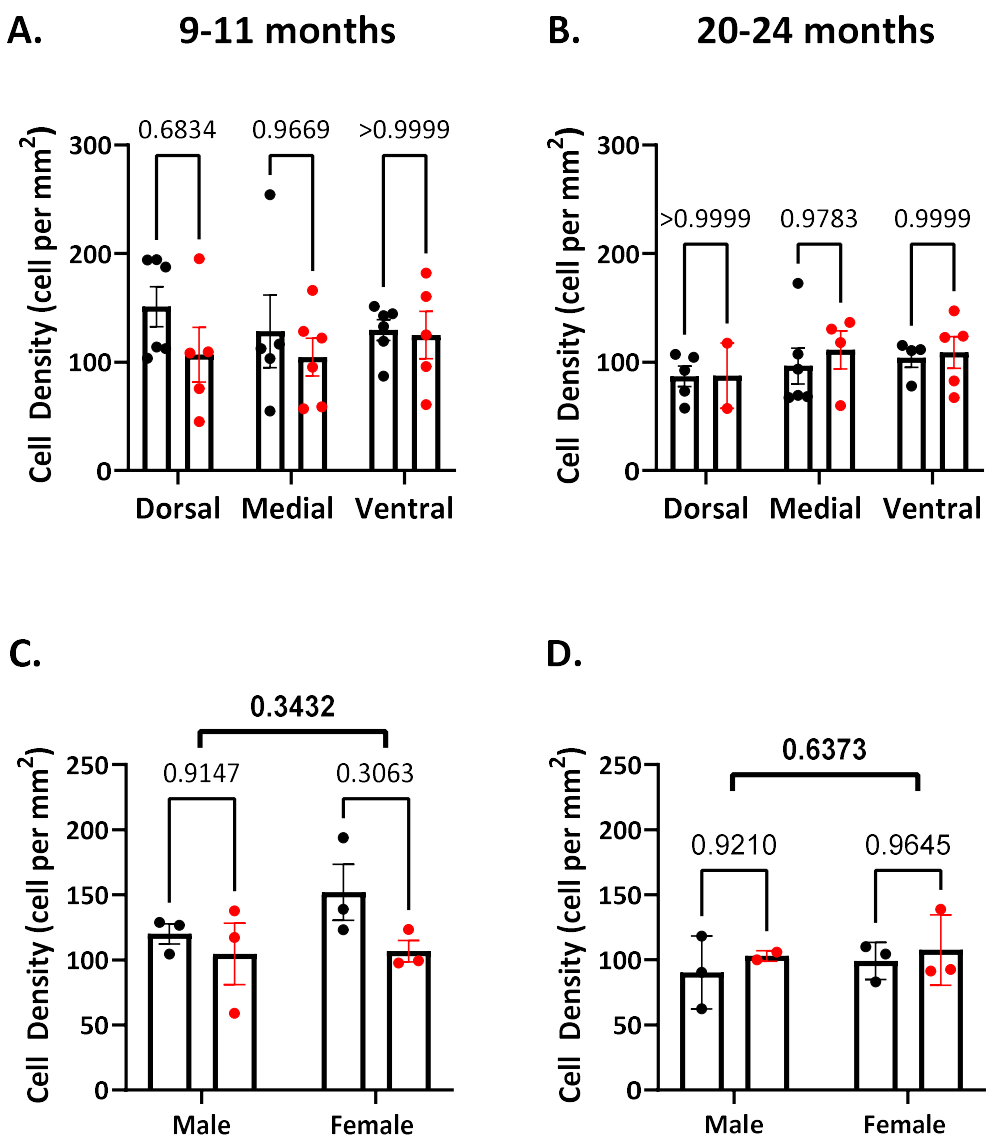

Figure 4.15. Somatostatin-positive interneuron density across the hippocampus and in both sexes. Somatostatin-positive interneuron density quantified in hippocampal sections from APP/PS1 (red) and wildtype (black) animals at (A, C) 9-11 and (B, D) 20-24 months (A, B) from three regions – dorsal, medial, ventral – across the hippocampus, and (C, D) in both sexes. 2-way ANOVA, main effects in bold, post-hoc comparisons with Tukey corrections in light text. 9-11 months: males, N = 3, females, N = 3; 20-24 months: APP/PS1 females and wildtype, N = 3, APP/PS1 males, N = 2.

4.13. Neuronal density in APP/PS1 mice

In order to determine if the observed reductions in parvalbumin- and somatostatin-positive interneuron density were specific reductions in these subpopulations or a feature of a general reduction in neuronal density in APP/PS1 mice, relative to wildtype littermate controls. Neuronal density was quantified using immunohistochemistry (Figure 4.16). The general neuronal marker NeuN was used to label neurons. As this is a predominantly nuclear marker, dendritic and axonal processes were not labelled.

There was no reduction in neuronal density in APP/PS1 mice relative to wildtype littermate controls ($F_{1, 22} = 0.93$, $p = 0.3463$) nor was there a reduction in in aged mice at 20-24 months relative to mice at 9-11 months ($F_{1, 22} = 0.67$, $p = 0.4231$). There was a trend towards a slight reduction in neuronal density in the dentate gyrus (Age: $F_{1, 22} = 0.42$, $p = 0.5261$, Genotype: $F_{1, 22} = 1.64$, $p = 0.2132$) and in the CA3 subregion (Age: $F_{1, 22} = 1.91$, $p = 0.1814$, Genotype: $F_{1, 22} = 0.56$, $p = 0.4623$) of APP/PS1 mice relative to wildtype littermate controls at 20-24 months. Aside from these subregional non-significant reductions, there were no notable differences in neuronal density between APP/PS1 mice and wildtype littermate controls at 9-11 and 20-24 months.

The finding that neuronal density was not reduced in APP/PS1 mice, relative to wildtype littermate controls, at 9-11 or 20-24 months, suggested that the reductions in parvalbumin- and somatostatin-positive interneuron density were specific reductions in these subpopulations.

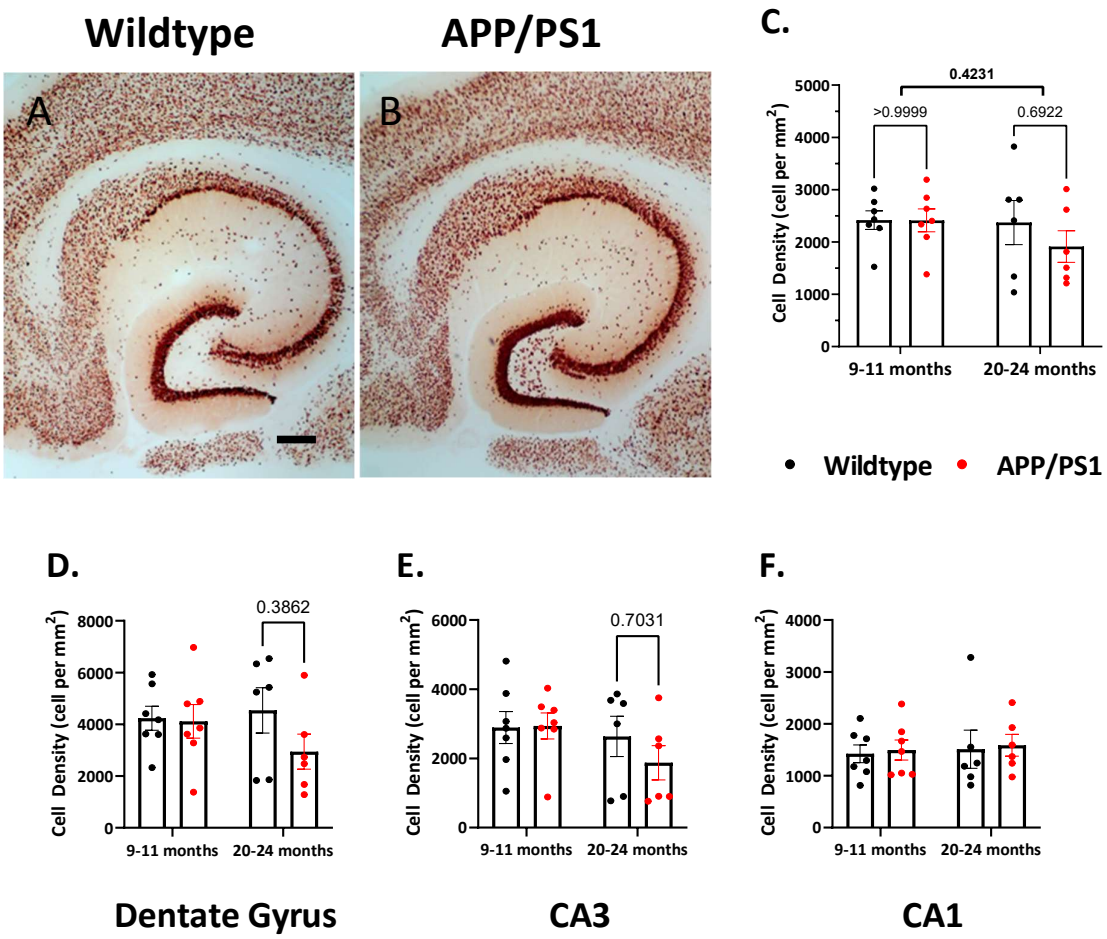

Figure 4.16. Neuronal density in APP/PS1 and wildtype mice. (A-D) Representative images of NeuN-positive interneuron density in (A) wildtype and (B) APP/PS1 mice at 9-11 months. Neuronal density quantified in hippocampal sections from APP/PS1 (red) and wildtype (black) animals at 9-11 and 20-24 months in (E) the hippocampus, (F) the dentate gyrus, (G) the CA3 subregion, (H) CA1 subregion. 2-way ANOVA, main effects in bold, post-hoc comparisons with Tukey corrections in light text. Scale bar: 250 µm. 9-11 months: n = 3, N = 7; 20-24 months: n = 3, N = 6.

4.14. Somatostatin- versus parvalbumin-positive interneuron density

The relationship between parvalbumin-positive interneuron density and somatostatin-positive interneuron density was investigated (Figure 4.17). There was a significant positive correlation between parvalbumin-positive interneuron density and somatostatin-positive interneuron density in APP/PS1 mice and wildtype littermate controls at 9-11 and 20-24 months (Pearson r value: 0.6710, R squared: 0.4502, p = 0.0121). It therefore follows that in mice with low parvalbumin-positive interneuron density, there was likely a low somatostatin-positive interneuron density also.

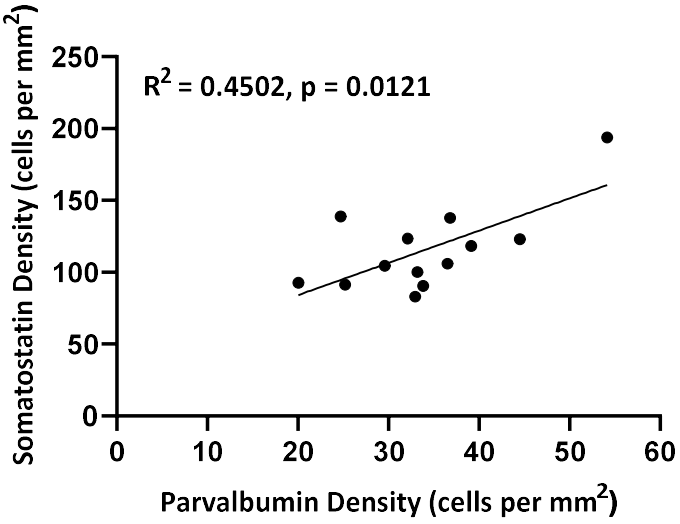

Figure 4.17. The relationship between somatostatin- and parvalbumin-positive interneuron density. Parvalbumin- and somatostatin-positive interneuron density for APP/PS1 and wildtype mice at 9-11 and 20-24 months. Each data point represents a single mouse. Pearson r value: 0.6710, R squared: 0.4502, p = 0.0121. 9-11 months: N = 2; 20-24 months: N = 4-5.

4.15. Inhibitory interneuron density versus gamma frequency oscillations.

As electrophysiological recordings were carried out from the sections in which parvalbumin- and somatostatin-positive interneuron density were quantified, it was possible to correlate the density of the inhibitory interneuron networks to the gamma frequency oscillations generated by the networks (Figure 4.18). These correlations were performed combining all mice for which interneuron density was quantified.

Neither parvalbumin- nor somatostatin-inhibitory interneuron density were significantly correlated to the amplitude of kainate- and carbachol-induced gamma frequency oscillations.

There was a slightly stronger correlation between parvalbumin- and somatostatin-inhibitory interneuron density and the oscillation peak frequency, but this was only statistically significant for somatostatin-positive inhibitory interneuron density versus the peak frequency of kainate-induced gamma frequency oscillations (Pearson r value: 0.6644, R squared: 0.4414, $p = 0.0184$). While parvalbumin-positive inhibitory interneuron density was weakly positively correlated to peak frequency of carbachol-induced gamma frequency oscillations (Pearson r value: 0.3511, R squared: 0.1233, $p = 0.0853$).

Therefore, despite their acknowledged importance, in this relatively small sample there were only weak positive correlation between peak frequency and the density of the inhibitory interneuron network.

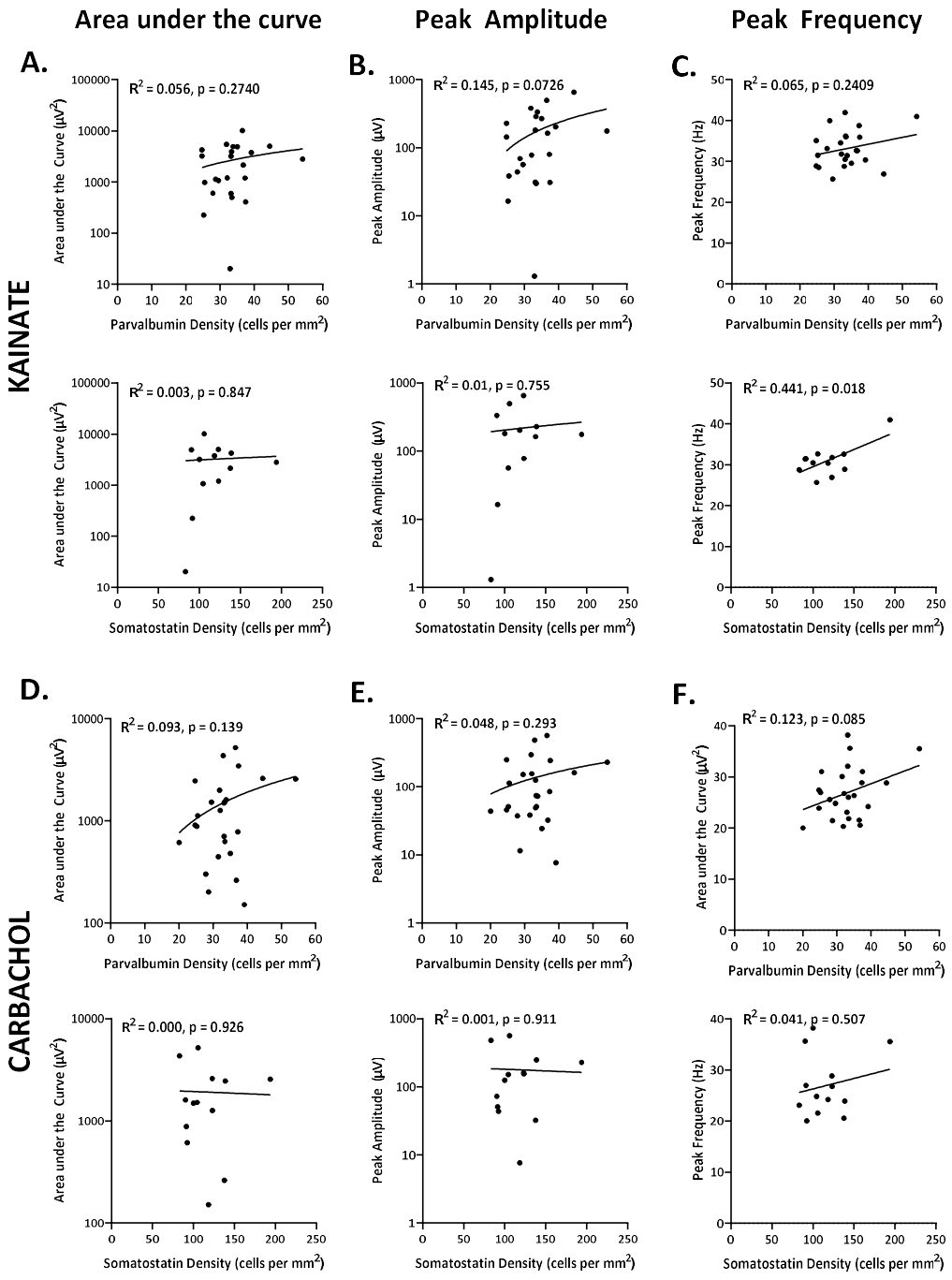

Figure 4.18. The relationship between somatostatin- and parvalbumin-positive interneuron density and kainate- and carbachol-induced gamma frequency oscillations. (A, D) Area under the curve, (B, E) peak amplitude, and (C, F) peak frequency for (A-C) kainate- and (D-F) carbachol-induced gamma frequency oscillations correlated to (top) parvalbumin- and (bottom) somatostatin-positive interneuron density. Parvalbumin Vs Kainate, n = 23, Parvalbumin Vs Carbachol, n = 25, Somatostatin Vs Kainate, n = 12, Somatostatin Vs Carbachol, n = 13. Each data point represents a mouse.

4.16. Blocking GABAergic transmission in APP/PS1 mice

Given the observed changes in gamma frequency oscillations and the epileptiform events in APP/PS1 mice, GABAergic neurotransmission in APP/PS1 mice was investigated. Gamma frequency oscillations are known to be dependent on GABAergic neurotransmission. Additionally, loss of GABAergic neurotransmission is often responsible for increased incidence of epileptiform events. It was therefore hypothesised that APP/PS1 mice would have reduced inhibitory tone relative to wildtype littermate controls. This was investigated by exposing established kainate-induced gamma frequency oscillations in brain slices from APP/PS1 mice and wildtype littermate controls to ascending concentrations of the $GABA_A$ receptor antagonist, gabazine.

In both APP/PS1 mice and wildtype mice the oscillation peak frequency was reduced by exposure to gabazine (wildtype: baseline: 35.16 ± 3.74 Hz, 800 nM gabazine: 21.02 ± 0.58 Hz; APP/PS1: baseline 24.73 ± 2.78 Hz, 800 nM gabazine: 20.29 ± 0.23 Hz). This was demonstrated by the significant effect of gabazine on peak frequency ($F_{1.58, 14.22} = 5.76$, $p = 0.0194$). The peak frequency of the oscillation was reduced in APP/PS1 mice relative to wildtype littermate controls prior to gabazine treatment, therefore the reduction in peak frequency is less notable in APP/PS1 mice. This was demonstrated by the significant interaction between genotype and gabazine treatment ($F_{4, 36} = 3.02$, $p = 0.0304$), however there was no significant main effect of genotype on peak frequency here ($F_{1, 9} = 1.38$, $p = 0.2710$; Figure 4.19, E). As demonstrated at 3-4 months (Figure 3.3) gamma frequency oscillations were abolished by GABAergic blockade in both APP/PS1 mice and wildtype littermate controls, although gamma frequency oscillations were already largely reduced in APP/PS1 mice prior to treatment.

In wildtype mice oscillation amplitude was reduced by gabazine treatment, most notably at 200 nM of gabazine. There was a slight increase in oscillation amplitude at higher concentrations of

gabazine, relative to lower concentrations of gabazine but not relative to the baseline. The pooled Fast Fourier transforms (Figure 4.19, A) demonstrated that this increase occurred at lower frequencies. These changes in oscillation amplitude were demonstrated by the area under the curve (baseline: 3,559.91 ± 1,547.93, gabazine 200 nM: 1,432.96 ± 630.24, gabazine 800 nM: 2,898.18 ± 2,025.78) and the peak amplitude (baseline: 578.82 ± 396.09, gabazine 200 nM: 215.64 ± 108.12, gabazine 800 nM: 396.57 ± 284.67). The overall reduction in oscillation amplitude is further demonstrated by the z-scores calculated for these parameters at 800 nM gabazine (area under the curve: -1.85 ± 1.63, peak amplitude: 2.15 ± 4.25).

In APP/PS1 mice there was a similar response to gabazine, oscillation amplitude was initially reduced by lower concentrations of gabazine and increased at higher concentrations of gabazine. However, the amplitude increase was much larger in APP/PS1 mice at high concentrations of gabazine. The pooled Fast Fourier transforms demonstrated that this increase occurred largely at lower frequencies – this may have represented the emergence of hyperexcitability. These changes in oscillation amplitude are demonstrated by the area under the curve (baseline: 2,048.79 ± 1701.24, gabazine 200 nM: 325.01 ± 150.33, gabazine 800 nM: 2,536.35 ± 1457.87) and the peak amplitude (baseline: 70.17 ± 56.92, gabazine 200 nM: 22.94 ± 10.23, gabazine 800 nM: 268.39 ± 146.59). The large increase in oscillation amplitude at 800 nM of gabazine is further demonstrated by the z-scores calculated for these parameters (area under curve: 3.49 ± 3.29, peak amplitude: 9.38 ± 7.22).

Statistically, there was no significant effect of gabazine treatment on either the area under the curve ($F_{2.02, 18.20} = 2.53$, $p = 0.1066$) or peak amplitude ($F_{4, 36} = 2.53$, $p = 0.5987$). However, there was a clear difference in the response of brain slices from APP/PS1 to high concentrations of gabazine: large amplitude, low frequency emerged to a greater extent than was seen in wildtype littermate controls. This may have represented an increased vulnerability to the emergence of hyperexcitability in APP/PS1 mice.

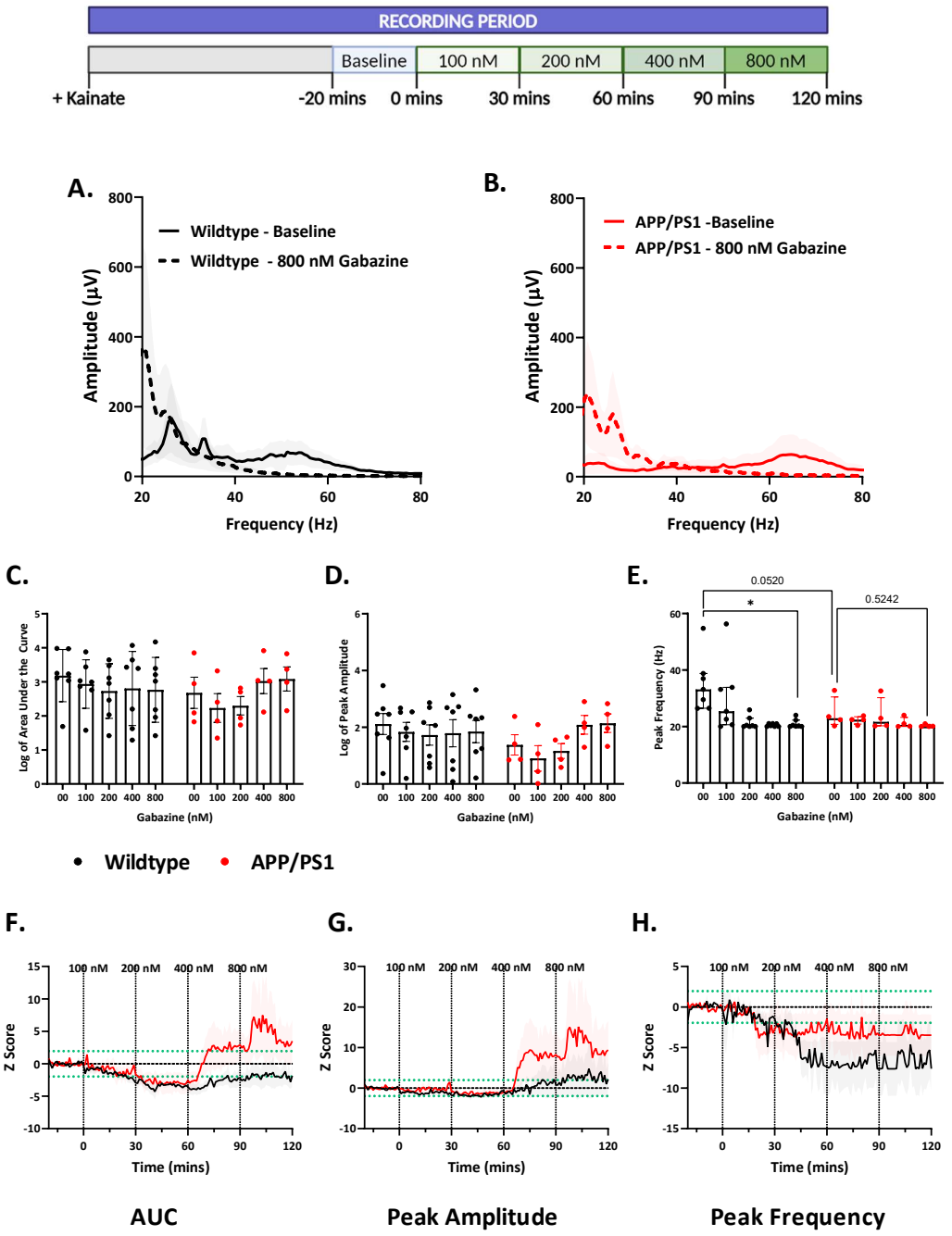

Figure 4.19. Blocking GABAergic transmission with gabazine APP/PS1 and wildtype mice. (A-D) FFTs pooled at baseline (solid lines) and at 800 nM gabazine (dashed lines) for (A) wildtype (black) and (B) APP/PS1 (red) mice. (C) Area under the curve, (D) peak amplitude, (E) peak frequency from FFTs. Data in E and F are log transformed. 2-way ANOVA. (F, G, H) Z-scores of (C, D, E) respectively, dotted green line represents $p < 0.05$. Wildtype, n = 7, N = 7; APP/PS1, n = 4, N = 4.

Discussion

Kainate-induced gamma frequency oscillations were found to be altered in both APP/PS1 and aged mice. In APP/PS1 mice at 9-11 months oscillation amplitude and frequency were reduced and the incidence and complexity of epileptiform events were increased, relative to wildtype littermate controls at the same age. In aged mice oscillation amplitude and the incidence and amplitude of epileptiform events were increased. These changes may be due to the observed reductions in both parvalbumin- and somatostatin-inhibitory interneuron density in both APP/PS1 and aged mice. Additionally, pharmacological intervention by $GABA_A$ receptor blockade further suggested reduced inhibitory tone in APP/PS1 mice.

Kainate-induced gamma frequency oscillations in APP/PS1 mice

Kainate-induced gamma frequency oscillations in APP/PS1 mice were found to be altered relative to wildtype mice at both 9-11 months and 20-24 months. At 9-11 months the amplitude and the frequency of kainate-induced gamma frequency oscillations were reduced in APP/PS1 mice relative to wildtype mice. This deficit was found to be distributed across the hippocampus and was not localised to a specific region of dorsal-ventral axis in the hippocampus. This is indicative of profound impairment in gamma frequency oscillations in APP/PS1 mice at 9-11 months. This finding is consistent with other studies in the field, particularly in amyloidogenic Alzheimer's disease models. In the TAS10 model of Alzheimer's disease at 8 months kainate-induced gamma frequency oscillation amplitude was reduced but frequency was unchanged (Driver et al., 2007). In APP/PS1 mice at 4-5 months kainate-induced gamma frequency oscillations in the lateral entorhinal cortex have reduced frequency and reduced amplitude (Klein et al., 2016). In the 5XFAD model of Alzheimer's disease kainate-induced gamma frequency oscillation amplitude was reduced at 12-19 months but the frequency was unchanged (Mackenzie-Gray Scott et al.,

2022). In the PSAPP model of Alzheimer's disease kainate-induced gamma frequency oscillation amplitude and frequency were reduced at 3 months. Similarly, in freely moving mice expressing excess APP and in 5XFAD mice, gamma frequency oscillation amplitude was reduced, at 8 months in both models (Rubio et al., 2012; Stoiljkovic et al., 2016). At 20-24 months, the frequency of kainate-induced gamma frequency oscillations was reduced in APP/PS1 mice and the amplitude was increased relative to wildtype mice. There have not been many studies on kainate-induced gamma frequency oscillations at 20-24 months therefore it is difficult to situate these findings relative to the work of others. In rats at 22-28 months, brain slices treated with kainate have been shown to have increased epileptiform activity and "less likely to exhibit "physiological" kainate-induced [ ] gamma network oscillations", similar to what was observed here (Kanak et al., 2011). However, kainate-induced gamma frequency oscillation amplitude has also been reported to be reduced in C57BL/6J mice at 22-28 months (C. B. Lu, Hamilton, et al., 2011).

Epileptiform activity was observed to be embedded in kainate-induced gamma frequency oscillations. The incidence of this type of activity, which is a form of hyperexcitability, is increased in APP/PS1 mice relative to wildtype mice. This is consistent with both clinical and preclinical work which suggests that neuronal hyperexcitability and epilepsy are features of Alzheimer's disease (Palop & Mucke, 2016; Rao et al., 2009; Tweedy et al., 2021). The amplitude of these epileptiform events are increased in mice at 20-24 months relative to mice at 9-11 months. The large amplitude of these events may contribute to the increase in amplitude seen in APP/PS1 mice at 20-24 months relative to 9-11 months. Although epileptiform events occurred at a similar frequency per minute in APP/PS1 mice and wildtype mice, the length of the events is significantly increased in APP/PS1 mice. This suggests that the epileptiform events which occurred in APP/PS1 mice were more pathological and were closer to seizure-like events than brief inter-ictal discharges, as occurred in wildtype mice. This is also consistent with the observation that

APP/PS1 mice experience more seizures *in vivo* than their wildtype littermate controls, although this was not investigated here (Reyes-Marin & Nuñez, 2017).

The underlying causes of the impairment in APP/PS1 and aged mice in kainate-induced gamma frequency oscillations and the increase in epileptiform events was investigated by quantifying the density of the inhibitory interneuron networks that generate gamma frequency oscillations. Both parvalbumin and somatostatin interneurons were found to be reduced in APP/PS1 mice and in aged mice. Parvalbumin interneurons have been previously shown to be reduced in the hippocampus and perirhinal cortex of APP/PS1 mice and in post-mortem tissue from individuals with Alzheimer's disease (Sanchez-Mejias et al., 2020; Takahashi et al., 2010). Similar findings of reduced parvalbumin interneuron density have been observed in other Alzheimer's models at different ages, specifically in the TgCRND8 model at 1 month (Hamm et al., 2017; Mahar et al., 2017). Less evidence is available to support the finding that somatostatin interneuron density is reduced in APP/PS1 mice relative to wildtype mice, although the reduction observed here was modest. Somatostatin interneurons have been shown to be reduced in the perirhinal cortex and olfactory bulb of APP/PS1 mice (De la Rosa-Prieto et al., 2016; Sanchez-Mejias et al., 2020). The activity of both of these types of inhibitory interneurons has also been reported as dysregulated in APP/PS1 mice (Algamal et al., 2022). Given the critical role of both parvalbumin and somatostatin inhibitory interneurons in gamma frequency oscillation generation and maintenance, it seems very probable that reductions in these populations could cause impairments in kainate-induced gamma frequency oscillations and lead to the emergence of increased epileptiform events. This interpretation is supported by the finding, made elsewhere and slightly indicated here, that both parvalbumin and somatostatin interneuron density are predictive of gamma frequency oscillation amplitude and frequency (Espinosa et al., 2019). It is also well accepted that loss of inhibitory tone in neuronal networks leads to hyperexcitability and increase the incidence of epileptiform activity (Huberfeld et al., 2015). Therefore, the finding that

inhibitory interneuron density is reduced in APP/PS1 mice is a plausible explanation for the observed deficits in kainate-induced gamma frequency oscillations and increased epileptiform activity in APP/PS1 mice relative to wildtype mice.

It is important to note that the observed reduction in parvalbumin and somatostatin immunoreactivity cannot be interpreted with certainty as being indicative of cell loss. It possible that the observed reductions in parvalbumin and somatostatin are due to reductions in expression of these proteins rather than cell death. For example, during development the neuronal expression of parvalbumin has been shown to be dependent on neuronal activity (Patz et al., 2004). It is possible therefore that the reduced expression of parvalbumin observed here is due to changes in neuronal network activity rather than cell death. Regardless of the exact cause of the loss in parvalbumin and somatostatin immunoreactivity, it is certain that reduced expression of these proteins will have profound consequences on the ability of inhibitory interneurons to carry out their functions. For example, alterations in the levels of parvalbumin directly impact the ability inhibitory neurons to generate inhibitory post-synaptic currents (Vreugdenhil et al., 2003).

No investigation was made here into why parvalbumin and somatostatin interneurons are reduced in APP/PS1 mice. It was shown that these reductions are specific and are not as a result of global loss in neuronal density. Parvalbumin and somatostatin interneurons generate fast-spiking inhibitory activity which is energetically demanding. This leaves these interneuron populations vulnerable to oxidative and metabolic stress – both of which are increased in APP/PS1 mice (Tönnies & Trushina, 2017). Increased oxidative stress has been shown to reduce parvalbumin interneurons in multiple models of schizophrenia and post-traumatic stress disorder (Hardingham & Do, 2016; X. R. Sun et al., 2016). It is also possible that reactive microglia in APP/PS1 mice are selectively removing parvalbumin and somatostatin interneurons. There is also the possibility that the observed reduction in parvalbumin and somatostatin were not due

loss of these neuronal populations but rather due reduced expression of these proteins, this would likely impair their function and calcium buffering capacity.

The hypothesis that excitatory-inhibitory balance is altered in APP/PS1 mice is further supported by the response of brain slices from these mice to treatment with the $GABA_A$ receptor antagonist, gabazine. In response to ascending concentrations of gabazine in brain slices from APP/PS1 mice at 9-11 months the oscillation amplitude increased at low frequencies, this suggested the emergence of hyperexcitable activity following extensive inhibitory blockade. The increased vulnerability to the emergence of this type of activity is consistent with the observation that inhibitory interneuron density was reduced in APP/PS1 mice at this age. Therefore, based on the investigations made here by immunohistochemistry and pharmacological intervention, inhibitory tone appeared to be reduced in APP/PS1 mice at 9-11 months – this likely accounts for the observation that gamma frequency oscillations are reduced and epileptiform activity was increased in these mice.

There are naturally other possible explanations for the observed changes in neuronal network activity in APP/PS1 mice. The previous chapter showed that treating brain slices with pro-inflammatory mediators before inducing gamma frequency oscillations with kainate caused the oscillations which emerged to have reduced frequency and amplitude. Therefore it is possible that the inflammatory environment of the APP/PS1 brain, especially proximal to amyloid-beta plaques, is negatively impacting the ability of neuronal networks to generate and maintain normal gamma frequency oscillations (López-González et al., 2015). It has also been observed that amyloid-beta plaques cause hyperexcitability in neurons which are near to the plaques (Busche et al., 2008, 2012). Additionally, amyloid-beta peptide has been shown to degrade gamma frequency oscillations in a concentration dependent manner (Kurudenkandy et al., 2014). Therefore, there is a possibility that the increasing amyloid burden in APP/PS1 mice is responsible for deficits in kainate-induced gamma frequency oscillations and increase in epileptiform activity.

Sex differences in kainate-induced gamma frequency oscillations

In wildtype mice at 9-11 months kainate-induced gamma frequency oscillations have non-significantly increased amplitude and slightly higher frequency in female mice than in male mice. The incidence of epileptiform events is also non-significantly lower in female wildtype mice than male wildtype mice at 9-11 months, and of the slices that do have epileptiform activity, the frequency per minute of this activity is reduced in female wildtype mice relative to male wildtype mice. This improved quality of kainate-induced gamma frequency oscillations in female wildtype mice is accompanied, and possibly explained, by increased parvalbumin and somatostatin interneuron density in female wildtype mice relative to male wildtype mice at 9-11 months. There have not been many systematic comparisons of sex differences in either kainate-induced gamma frequency oscillations or in inhibitory interneuron density. Gamma frequency oscillations recorded by EEG in humans have been observed to have larger amplitude than in females (Güntekin & Başar, 2007; Vila-Merkle et al., 2023). Inhibitory interneuron density has been found to be unaffected by sex in wildtype mice, however these studies were done on very young mice (Girgenti et al., 2019; Ulrich et al., 2023). A large brain-mapping study found that somatostatin inhibitory interneurons, but not parvalbumin, were increased in female mice (Kim et al., 2017). It is therefore difficult to corroborate the finding that both inhibitory interneuron networks and the activity they generate are increased in female wildtype mice, however the co-occurrence of these findings suggests their validity.

Given these sex differences at baseline in wildtype mice, the deficits in both kainate-induced gamma frequency oscillations and interneuron density in female APP/PS1 mice represent greater reductions than those in male APP/PS1 mice, relative to male wildtype mice. Alzheimer's disease is more common in females and females are at a greater risk of developing the disease (Aggarwal & Mielke, 2023). There are clearly many factors which contribute to this difference, making it

difficult to untangle what are the main causes of this difference. However, this increased vulnerability to Alzheimer's disease in females is also seen in the APP/PS1 model of Alzheimer's disease. Female APP/PS1 mice have greater amyloid burden, increased expression of pro-inflammatory cytokines, increased microgliosis and astrocytosis, and increased synaptic degradation (Jiao et al., 2016). Therefore, Alzheimer's pathology is more aggressive in females both clinically and in disease models. This is represented here in the greater relative deficit in kainate-induced gamma frequency oscillations and inhibitory interneuron density in female APP/PS1 mice (relative to female wildtype mice) than in male APP/PS1 mice (relative to male wildtype mice).

Carbachol-induced gamma frequency oscillations in APP/PS1 mice

Unlike kainate-induced gamma frequency oscillations, it was not possible to induce well defined carbachol-induced gamma frequency oscillations in wildtype mice at 9-11 months or at 20-24 months. Therefore it was difficult to make comparisons between APP/PS1 mice and wildtype mice. Carbachol-induced gamma frequency oscillations have been induced by others in the field in animals at this age, however it appear that carbachol-induced gamma frequency oscillations were not consistently induced as certain slices appear to have been excluded (Mackenzie-Gray Scott et al., 2022). However, the observed significant increase in oscillation amplitude at 20-24 months may be consistent with the observed widespread reduction in inhibitory interneuron density, and by extension reduced inhibitory tone, in aged animals.

Carbachol induces gamma frequency oscillations by activating muscarinic and nicotinic receptors on pyramidal cells. This causes pyramidal cells to activate the inhibitory interneuron network responsible for entraining gamma frequency oscillations. This suggests that in mice at 9-11 months and 20-24 months the excitatory drive from pyramidal cells is insufficient to induce gamma frequency oscillations. This is not observed at 3-4 months. At 3-4 months carbachol-

induced gamma frequency oscillations were successfully generated. It was noted that brain slices from the ventral region of the hippocampus generated higher frequency carbachol-induced gamma frequency oscillations in both wildtype mice and APP/PS1 mice. An increase in acetylcholine muscarinic receptor density has been reported in the ventral hippocampus (Mei et al., 2020). This suggests that carbachol may induce greater excitatory drive in the ventral hippocampus, and so induce higher quality gamma frequency oscillations.

Deficits in cholinergic transmission have been associated with both ageing and Alzheimer's disease. This is the basis of the cholinergic hypothesis which suggests that cholinergic cell loss is an early cause of pathology in Alzheimer's disease (Francis et al., 1999). This hypothesis is also the basis of several Alzheimer's disease therapies which are acetylcholinesterases and act to increase cholinergic transmission (Summers et al., 1986). Cholinergic cells are especially vulnerable to cell death in both ageing and pathology. This is thought to be due to the fact their use of acetyl-CoA for acetylcholine synthesis, as well as for energy production (Schliebs & Arendt, 2011). It is therefore perhaps informative that it was not possible to generate carbachol-induced gamma frequency oscillations in animals beyond 3-4 months. This may be due to a reduction in cholinergic neurons in both wildtype and APP/PS1 mice from 9-11 months. Carbachol-induced gamma frequency oscillations in APP/PS1 mice relative to wildtype mice could be examined more closely by using only brain slices from the ventral region of the hippocampus.

Conclusion

In summary, this chapter has characterised gamma frequency oscillations in both APP/PS1 mice and wildtype mice at 9-11 months and 20-24 months. Both kainate- and carbachol-induced gamma frequency oscillations were characterised. Carbachol-induced gamma frequency oscillations were not well defined in mice at 9-11 months or 20-24 months. A two-fold deficit

was observed in kainate-induced gamma frequency oscillations in APP/PS1 mice at 9-11 months – oscillation amplitude and frequency were reduced and epileptiform events embedded in the oscillation had increased incidence and complexity. In aged mice oscillation and epileptiform event amplitude were observed to be increased. Each of these changes may be explained by the observed reduction in inhibitory interneuron density in APP/PS1 mice at 9-11 months and in aged mice. Therefore, in APP/PS1 mice neuronal networks and the activity they generated were impaired.

Chapter 5

Neuroinflammation and Gamma Frequency Oscillations in APP/PS1 Mice

Introduction

The immune system is now considered a central actor in Alzheimer's disease. The immune system can affect the risk of developing Alzheimer's disease and the manner in which the disease progresses. GWAS have provided evidence that certain mutations in immune-related genes – for example, *Trem2*, and *CD33* – increase the risk of developing Alzheimer's disease (Bertram et al., 2010; Guerreiro et al., 2013; Jonsson et al., 2013). Similarly, routine vaccinations and long-term treatment with anti-inflammatory drugs reduce the risk of Alzheimer's disease (Harris et al., 2023; Hoozemans et al., 2008; Leoutsakos et al., 2012). It is therefore well accepted that alterations in the immune system can contribute to the risk of developing Alzheimer's disease.

Microglia are the primary immune cells of the CNS. Therefore, many of the changes which contribute to the risk of developing Alzheimer's disease occur in microglia, for example reduced phagocytic ability due to certain mutations in TREM2 (Y. Wang et al., 2015). Similarly, much of the immune response caused by Alzheimer's disease occurs in microglia. For example, microglia are chronically activated by the presence of amyloid-beta plaques. Therefore, microglia have central importance when studying the immune system in Alzheimer's disease.

In the previous chapter gamma frequency oscillations were shown to be altered in APP/PS1 mice at 9-11 months relative to wildtype littermate controls. Specifically, this alteration was two-fold in nature: kainate-induced gamma frequency oscillation and frequency were reduced and the incidence of epileptiform activity was increased. Overall, these observations, coupled with the observed reduction in inhibitory interneuron density and function, were suggestive of reduced inhibition in APP/PS1 mice at this age.

Investigating the extent to which these alterations were due to changes in the immune system, specifically in microglia, was a key research question of this thesis. It has been suggested that inducing gamma frequency oscillations in various Alzheimer's disease models improves pathology

by promoting microglial phagocytosis (Iaccarino et al., 2016; Martorell et al., 2019). It has also been shown that reactive microglia can impair gamma frequency oscillations, possibly via NO production (Dikmen et al., 2020; Ta et al., 2019). Additionally, it was shown in chapter 3 that various inflammatory mediators inhibited the emergence and growth of gamma frequency oscillations. Based on these findings, there is evidence that inflammatory mediators and immune cells can modulate gamma frequency oscillations. The effects of both reducing and increasing neuroinflammation on gamma frequency oscillations were therefore investigated.

It was of interest to determine firstly if microglial proliferation contributed to the observed alterations in gamma frequency oscillations in APP/PS1 mice. In order to investigate this, microglial proliferation was inhibited by treating mice with an inhibitor of CSF-1R called GW2580. The drug was administered via the diet at a dose of 1,000 ppm (10 g/kg). It has been shown that at this dose GW2580 inhibits microglia proliferation but does not totally ablate the microglial population (Olmos-Alonso et al., 2016). This treatment was shown to have a protective effect on synaptic degradation and cognitive deficits in APP/PS1 mice, however the effect of this treatment on neuronal network activity was not investigated (Olmos-Alonso et al., 2016). A total ablation of the microglial population is a severe approach which is not likely to be clinically or physiologically relevant. Limiting the proliferation of microglia is a less severe approach which aims to reduce inflammation without entirely removing microglia. Mice began 3 months of GW2580 treatment at 6-7 months. Pathology is established, but not fully developed, in APP/PS1 mice at this age.

Different experimental cohorts underwent different experimental testing, this is described in Figure 5.1. The effects of GW2580 treatment was investigated for: cognitive status (spontaneous alternation in the T-maze and learning in the MWM), neuropathology (immunohistochemistry and histology), gene expression (qPCR on FACS-isolated microglia and astrocytes), and gamma frequency oscillations in *ex vivo* brain slices (both carbachol- and kainate-induced gamma

frequency oscillations). This study aimed to establish the extent to which alterations in gamma frequency oscillations in APP/PS1 mice were caused by increased microglial proliferation and reactivity.

The effects of neuroinflammation on gamma frequency oscillations in APP/PS1 mice were further investigated by exposing brain slices with established kainate-induced gamma frequency oscillations to the pro-inflammatory mediators IL-1β and TNFα. These mediators were among those with the strongest inhibitory effect on established gamma frequency oscillations in C57BL/6J mice at 3-4 months. It was predicted that the growth of established gamma frequency oscillation amplitude would also be inhibited in wildtype mice at 9-11 months. However, given the known alterations in both gamma frequency oscillations and the neuroinflammatory milieu in APP/PS1 mice it was hypothesised that exposure to pro-inflammatory mediators would have a different effect in brain slices from APP/PS1 mice. Lastly, the effects of suppressing endogenous TNFα on gamma frequency oscillations in brain slices from APP/PS1 mice and wildtype littermate controls was investigated using an anti-TNFα antibody. It was hypothesised that reducing neuroinflammation in this manner would have a protective effect on gamma frequency oscillations in APP/PS1 mice.

In summary, this chapter investigated the extent to which the APP/PS1 phenotype observed in chapter 4 is caused by increased neuroinflammation in these mice. Additionally, it investigated the sensitivity of established gamma frequency oscillations in APP/PS1 mice to neuroinflammatory manipulation.

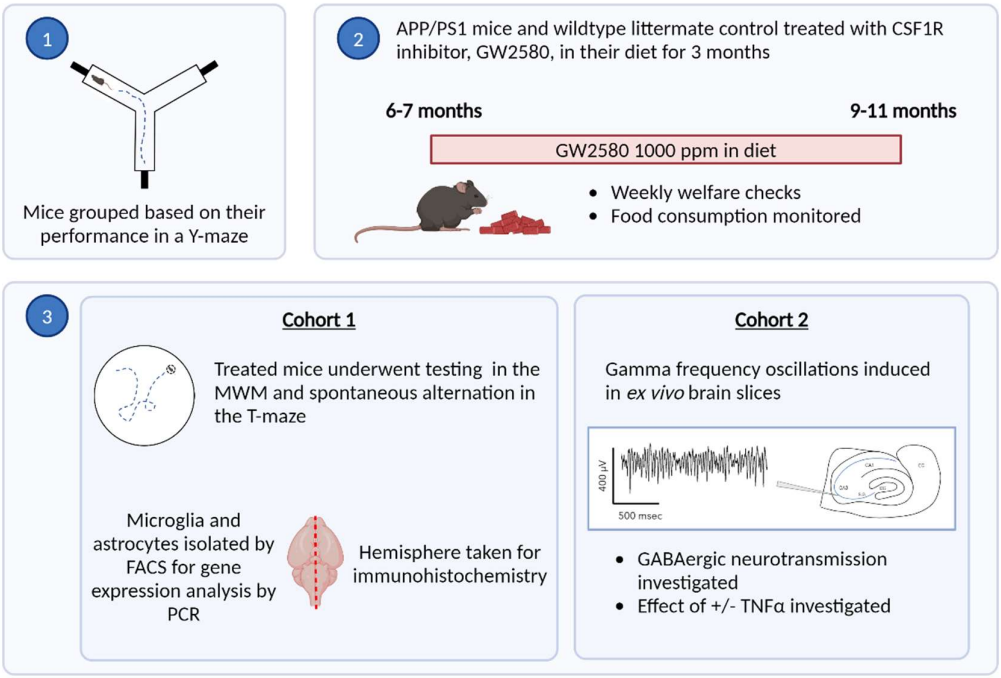

Figure 5.1. Schematic representation of the different investigations made into the effect of GW2580 treatment in APP/PS1 mice. 1. Mice ranked based on their performance in Y-maze, 2. Mice treated for 3 months for GW2580, 3. GW2580-treatd mice underwent various experimental testing, Cohort 1: Behavioural testing, gene expression and neuropathology, Cohort 2: Electrophysiological recordings in *ex vivo* brain slices.

Results

5.1. Baseline cognitive assessment of APP/PS1 mice and wildtype mice

In order to ensure that the treatment groups were balanced with respect to the mice's pre-treatment cognitive status, APP/PS1 mice and wildtype littermate controls were ranked based on their performance in a visuospatial learning task in a Y-maze. Mice were assigned to their treatment groups based on this ranking.

Both APP/PS1 mice and wildtype littermate controls (aged 6-7 months) learned the location of the exit over 48 trials (Figure 5.2, A). There was no significant difference in the rate of learning in APP/PS1 mice and wildtype littermate controls ($F_{3, 168}$ = 37.20, p = 0.2938). APP/PS1 mice and wildtype littermate controls of both sexes learned the location of their exit with similar rates of success (Figure 5.2, C, E). Once mice had learned their exit location, the exit location was changed. The ability of mice to learn this new exit location was assessed over 12 trials. This 'reversal assay' tests the cognitive flexibility of mice. APP/PS1 mice and wildtype littermate controls learned the new exit location at the same rate (Figure 5.2, B). As before, male and female APP/PS1 mice and wildtype littermate controls learned the location of their new exit with similar rates of success (Figure 5.2, D, F).

Based on the combined performance of mice in both training and reversal in the Y-maze mice were ranked and assigned to their treatment groups. The average percentage of correct trails was consistent across treatment groups during visuospatial learning and during the reversal assay.

Therefore, before treatment with GW2580 there were no significant cognitive impairments in APP/PS1 mice. This means the ability of GW2580 to prevent the emergence of cognitive deficits can be studied, without the risk of being confounded by differences which were present before the treatment began.

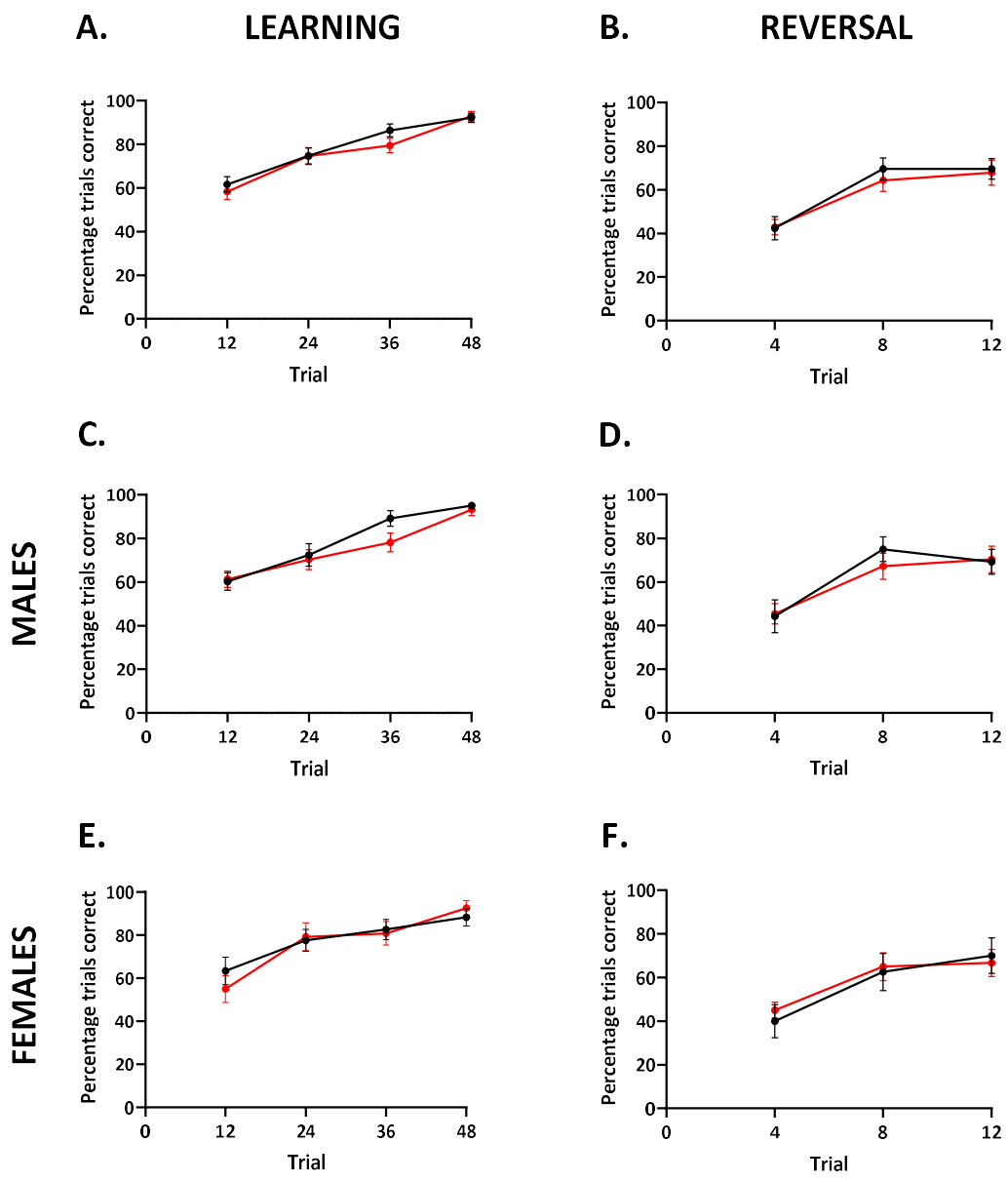

Figure 5.2. Baseline cognitive assessment of APP/PS1 and wildtype mice. Performance of APP/PS1 mice (red) and wildtype mice (black) in (A, C, E) training and (B, D, F) reversal in a Y-maze in (A, B) both sexes, (C, D) males, (E, F) females. Each mouse learned their specific exit over 48 trails. Reversal task was tested over 12 trials. Wildtype males, N = 13, wildtype females, N = 10, APP/PS1 males, N = 11, APP/PS1 females, N = 10.

5.2. Consumption and welfare effects of GW2580-supplemented diet

APP/PS1 mice and wildtype littermate controls were treated with GW2580 via their solid diet from the age of 6-7 months to 9-11 months. Mice in the treatment groups were fed a GW2580-supplemeted diet (1000 ppm/10 g of drug in 10 kg of diet) while control mice received an unmodified diet (normal chow, control diet). The consumption of the GW2580-supplemented diet and control diet was monitored (Figure 5.3, A). Overall, APP/PS1 mice and wildtype littermate controls consumed slightly less when receiving the GW2580-supplemented diet than the control diet. Mice receiving the GW2580-supplemented diet consumed 3.5 g/day on average. This makes the effective dose of GW2580 3.5 mg/day per mouse, on average. This is an approximation as a small of the amount of the diet may have fallen from the food hooper and not actually been consumed by the mice.

Throughout the 3 month treatment of APP/PS1 mice and wildtype littermate controls, GW2580 was well tolerated and did not adversely affect the welfare of the mice. There was an initial weight loss in GW2580-treated mice, compared to control mice (Figure 5.3, B). GW2580-treated mice remained lighter throughout the treatment. However, following this initial weight loss, GW2580-treated mice gained weight at a similar rate as control mice.

Overall, GW2580 treatment via the diet did not appear to significantly affect welfare. Mice receiving GW2580 consumed slightly less of their diet, but there was no indication of any food deprivation related effects.

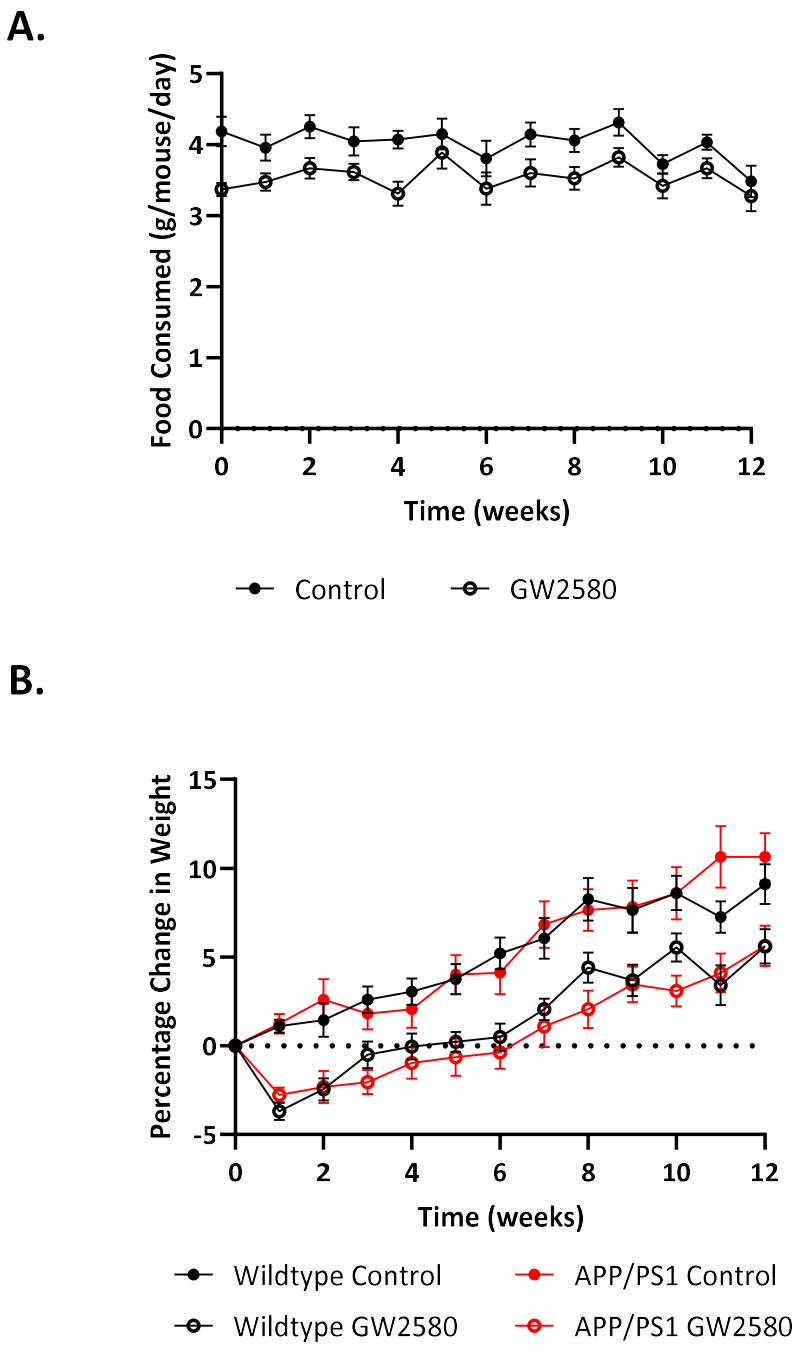

Figure 5.3. Diet consumption and body weight during GW2580 treatment. (A) Diet consumption of APP/PS1 mice and wildtype littermate controls on control diet (solid circle) and GW2580-supplemented diet (clear circle; estimated dose 3.5 mg/day). (B) Percentage change in the weight of wildtype (black) and APP/PS1 (red) mice on control diet (solid circle) and GW2580-supplemented diet (clear circle), Wildtype control, N = 20, wildtype GW2580, N = 22, APP/PS1 control, N = 17, APP/PS1 GW2580, N = 22.

5.3. Effect of GW2580 treatment on spontaneous alternation in the T-maze

The effect of GW2580 treatment on working memory in APP/PS1 mice and wildtype littermate controls was assessed by studying spontaneous alternation rates in a dry T-maze (Figure 5.4, A). Both control and GW2580-treated wildtype mice displayed normal working memory by spontaneously alternating at approximately 80%. There was a significant deficit in working memory in APP/PS1 mice compared to wildtype mice ($F_{1, 80} = 5.63$, $p = 0.02$). There was no significant main effect of GW2580 treatment on working memory ($F_{1, 80} = 0.02$, $p = 0.8832$) and post-hoc analysis (shown on Figure 5.4) did not show a significant protection from GW2580 treatment versus control diet in APP/PS1 mice, in either male or female mice (Figure 5.4, B, C). There may be a trend towards a very modest protective effect in male APP/PS1 mice.

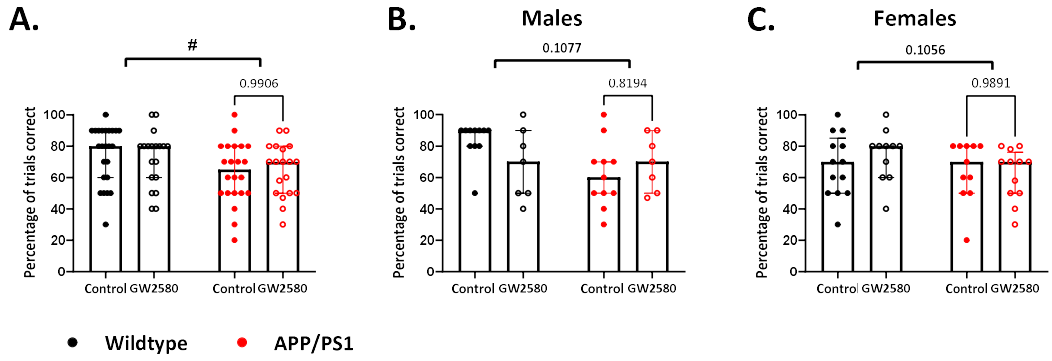

Figure 5.4. The effect of GW2580 treatment on spontaneous alternation in the T-maze. T-maze spontaneous alteration of wildtype (black) and APP/PS1 (red) mice on control diet (solid circles) and GW2580-supplemented diet (empty circles; estimated dose 3.5 mg/day) over 10 trials. 3-way ANOVA, main effect of genotype in bold: # = $p < 0.05$, post-hoc analysis with Tukey corrections for APP/PS1 control versus APP/PS1 GW2580 in light text. Wildtype control, N = 24 (11 males, 13 females), wildtype GW2580, N = 18 (7 males, 11 females), APP/PS1 control, N = 22 (11 males, 11 females), APP/PS1 GW2580, N = 19 (7 males, 12 females).

5.4. Effect of GW2580 treatment on performance in the MWM

The effect of GW2580 treatment on spatial learning was tested using the MWM protocol. Over 5 training days mice learned the location of a hidden platform with reference to extra-maze visual cues (Figure 5.5). The location of the platform was randomly assigned, but fixed, for each mouse, and the start position was altered between trials in a pseudorandom manner.

Both APP/PS1 mice and wildtype littermate controls learned the location of the platform in the MWM over the 5 training days. This was demonstrated by the significant reductions in the latency to platform ($F_{3.66, 292.5} = 104$, $p < 0.0001$) and in the distance travelled to the platform ($F_{3.54, 283.3} = 123.4$, $p < 0.0001$) across the training days (Figure 5.5, A, B). There was a modest but significant deficit in learning in APP/PS1 mice as demonstrated by the increased latency to platform ($F_{1, 80} = 15.92$, $p = 0.0001$) and the increased distance travelled to the platform ($F_{1, 80} = 19.55$, $p < 0.0001$). There was no significant effect of treatment with GW2580 on MWM learning (Latency: $F_{1, 80} = 0.83$, $p = 0.3648$, Distance: $F_{1, 80} = 0.56$, $p = 0.4566$) nor was there an interaction between GW2580 treatment and genotype (Latency: $F_{1, 80} = 0.04$, $p = 0.8457$, Distance: $F_{1, 80} = 0.12$, $p = 0.7254$). Post-hoc analysis showed no significant differences at the end of learning on day 5 between GW2580-treated and control APP/PS1 mice (Latency: $p = 0.9928$, Distance: $p = 0.9936$). Thus, GW2580 treatment did not reverse the modest deficit in spatial learning in the MWM in APP/PS1 mice. This deficit in spatial learning was observed in both male and female APP/PS1 mice and GW2580 treatment did not significantly affect spatial learning in either sex (Figure 5.5, C-F).

During the probe trial, in which the hidden platform was removed, control and GW2580-treated APP/PS1 mice and wildtype littermate controls spent approximately 45% of the time in the quadrant which contained the platform during training (wildtype control: 47.51 ± 3.34%, wildtype GW2580: 45.19 ± 3.24%, APP/PS1 control: 44.27 ± 3.32%, APP/PS1 GW2580: 44.51

± 2.66%; Figure 5.6, A). This demonstrated that mice in each experimental group learned the location of the platform with reference to visuospatial cues and there was no effect of GW2580 treatment in either APP/PS1 mice or wildtype littermate controls. There was no significant effect of sex on performance in the probe trial (Figure 5.6, B, C).

The deficit in spatial learning observed in APP/PS1 mice was not due to differences in swim speeds, which were comparable in APP/PS1 mice and wildtype littermate controls (Figure 5.6, B).

Likewise, deficits were not explained by differences in visual ability, as recorded by the time required to reach a platform with a visible flag (Figure 5.6, C). APP/PS1 mice and wildtype littermate controls had comparable visual ability ($F_{1, 80} = 0.13$, $p = 0.7222$), however, GW2580 treatment appeared to significantly improve visual ability in both wildtype and APP/PS1 mice ($F_{1, 80} = 7.67$, $p = 0.0070$).

In summary, APP/PS1 mice or wildtype littermate controls learned the location of a hidden platform in the MWM. Wildtype mice learned slightly more quickly than APP/PS1 mice. GW2580 treatment did not have an effect on learning in either APP/PS1 mice or wildtype littermate controls.

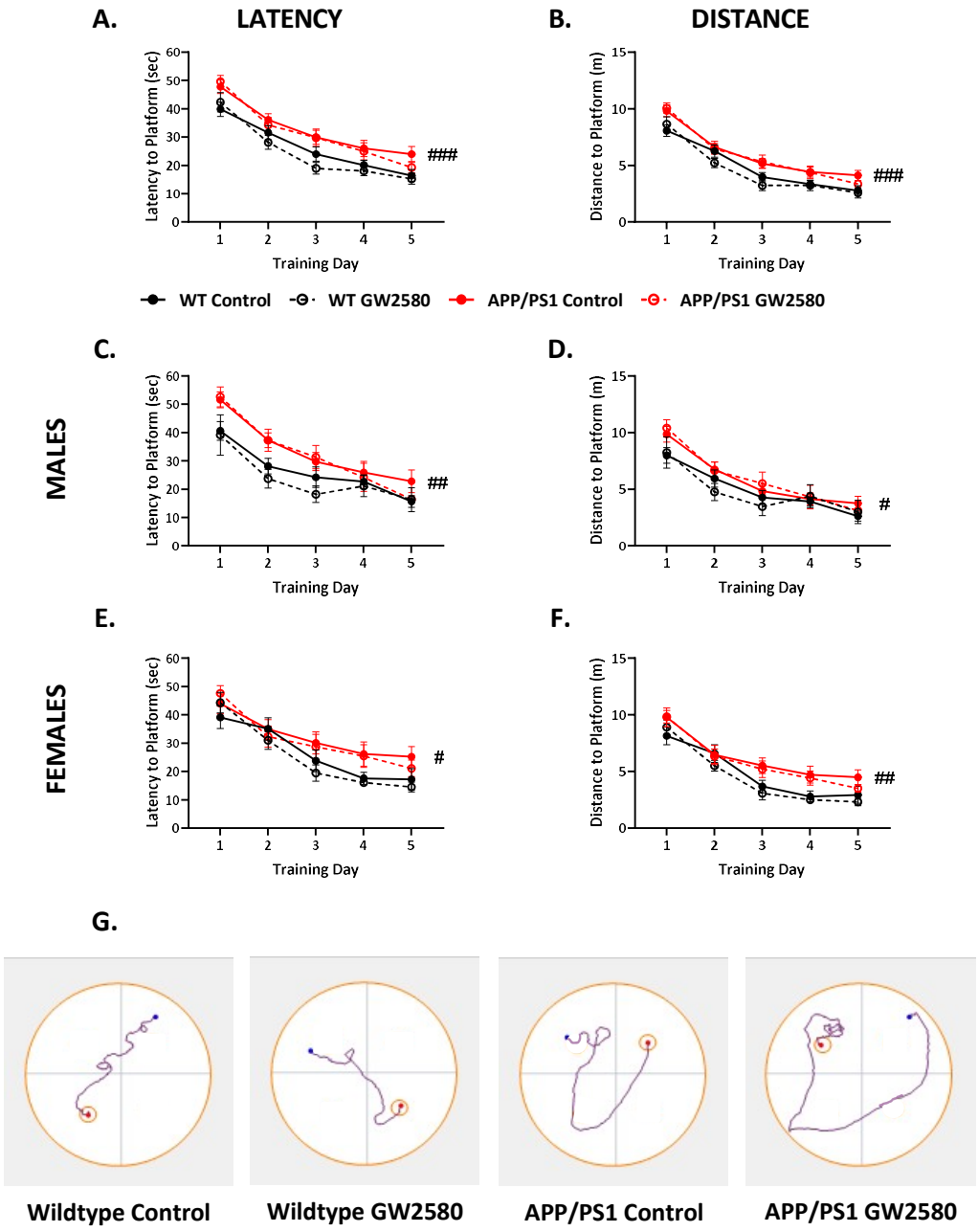

Figure 5.5. The effect of GW2580 treatment on performance in the MWM. (A, C, E) Latency to platform and (B, D, F) distance travelled to platform and (G) representative traces in the Morris water maze for APP/PS1 mice (red) and wildtype mice (black) on a control diet (solid circles) and a GW2580-supplemented diet (empty circles; effective dose 3.5 mg/day) for (A, B) both sexes, (C, D) males, and (E, F) females. 3-way ANOVA, main effect of genotype: # = $p < 0.05$, ## = $p < 0.01$, ### = $p < 0.001$. Wildtype control, N = 24 (12 males, 12 females), wildtype GW2580, N = 18 (7 males, 11 females), APP/PS1 control, N = 22 (11 males, 11 females), APP/PS1 GW2580, N = 20 (8 males, 12 females)

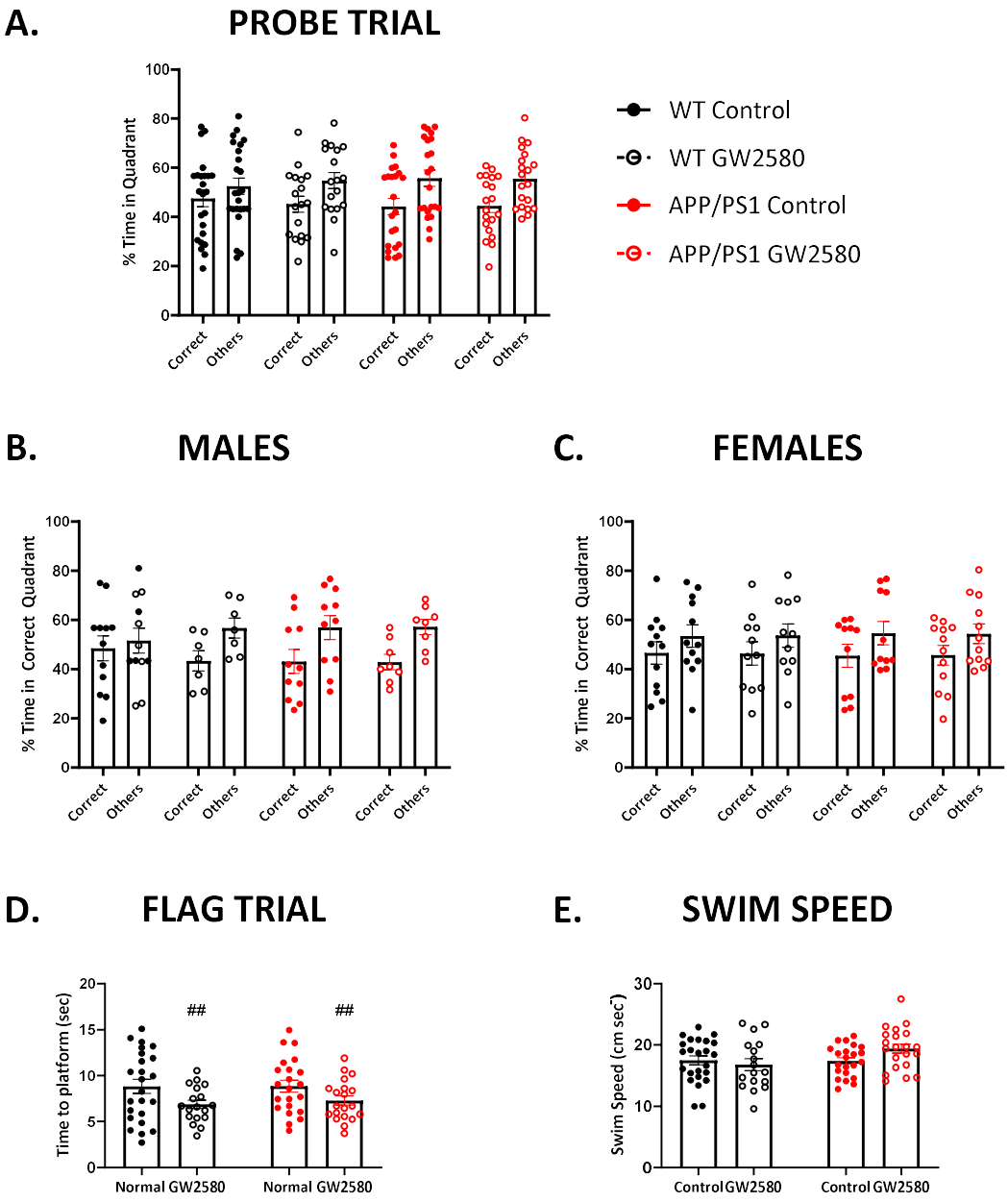

Figure 5.6. The effect of GW2580 treatment on performance in the MWM during the probe trial. (A) Time spent in the correct quadrant and the other three quadrants during the probe trial in (B) males and (C) females. (D) latency to the platform Aduring the flag trial, and (E) average swim speed for wildtype (black) and APP/PS1 (red) mice on control diet (solid circles) and GW2580-supplemented diet (empty circles; estimated dose 3.5 mg/day). 2-way ANOVA, main effect of treatment: ## = $p < 0.01$. Wildtype control, N = 24 (12 males, 12 females), wildtype GW2580, N = 18 (7 males, 11 females), APP/PS1 control, N = 22 (11 males, 11 females), APP/PS1 GW2580, N = 20 (8 males, 12 females)

5.5. The effect of GW2580 treatment on amyloid plaques

The effect of GW2580 treatment on neuropathology was investigated in APP/PS1 mice and wildtype littermate controls. The effect of GW2580 treatment on the number of amyloid-beta plaques was investigated by labelling the plaques. Plaques were labelled using Congo red and quantified across the hippocampus (Figure 5.7). No plaques were detected in wildtype mice. As expected, in APP/PS1 mice there was an increase in amyloid-beta plaques (main effect of genotype: $F_{1, 20} = 44.38$, $p < 0.0001$). There was a slight but non-significant reduction in the number of amyloid-beta plaques stained by Congo red in GW2580-treated APP/PS1 mice relative to control APP/PS1 mice ($p = 0.2660$).

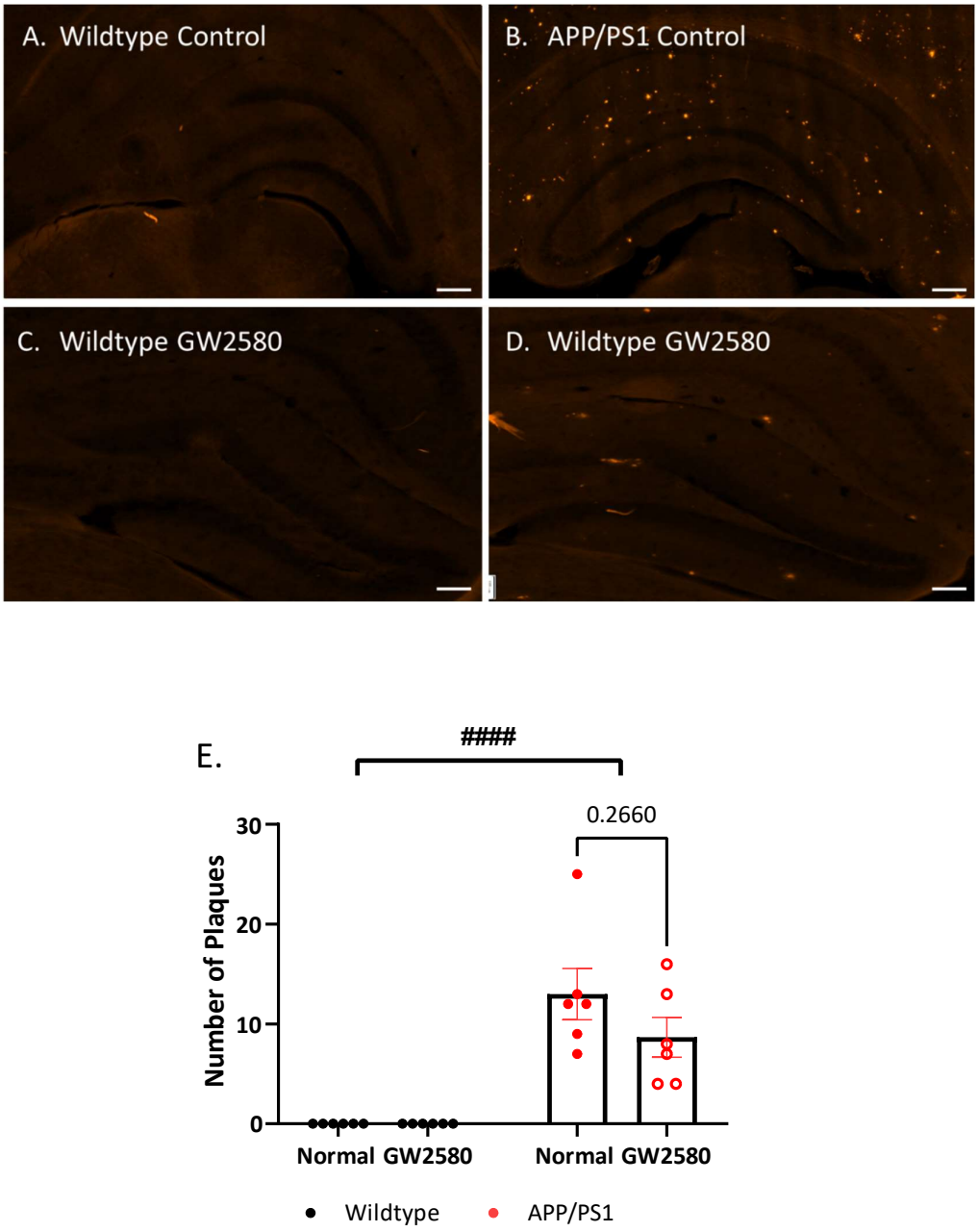

Figure 5.7. The effect of GW2580 treatment on amyloid-beta plaques. Representative images of Congo red staining of amyloid plaques in control (A) wildtype and (B) APP/PS1 mice, and GW2580-treated (C) wildtype and (D) APP/PS1 mice. (E) Quantification of Congo red labelled plaques in the hippocampus of wildtype (black) and APP/PS1 (red) mice on control diet (solid circles) and GW2580-supplemented diet (empty circles)(estimated dose 3.5 mg/day). 2-way ANOVA, main effect of genotype: ### = $p < 0.001$, post-hoc analysis with Tukey's corrections for APP/PS1 control versus APP/PS1 GW2580 in light text. Scale bar: 10 mm. N = 6 for all groups, 3 males, 3 females.

5.6. The effect of GW2580 treatment on microglial numbers and reactivity

Microglia reactivity was quantified by measuring the percentage area labelled by Iba1 in two regions of interest: the dentate gyrus, and the CA1 subregion (Figure 5.8).

In the dentate gyrus the percentage area labelled with Iba1 was significantly increased in APP/PS1 mice relative to wildtype littermate controls ($F_{1, 20} = 41.17$, $p < 0.001$; Figure 5.8, M). The percentage area labelled with Iba1 was significantly reduced by GW2580 treatment in both APP/PS1 mice and wildtype littermate controls ($F_{1, 20} = 6.75$, $p = 0.0172$). In the CA1 region the percentage area labelled with Iba1, or microglial reactivity, was significantly increased in APP/PS1 mice relative to wildtype mice ($F_{1, 20} = 35.27$, $p < 0.001$; Figure 5.8, N). The percentage area labelled with Iba1 was slightly reduced by treatment with GW2580 in APP/PS1 mice and wildtype littermate controls, but this was not statistically significant ($F_{1, 20} = 0.82$, $p = 0.3775$).

Thus, treatment with GW2580 modestly reduced microglial reactivity at gross level in the hippocampus. However, the majority of changes in microglia reactivity and proliferation in APP/PS1 mice occur proximal to amyloid-beta plaques (Olmos-Alonso et al., 2016). Therefore, in order to assess the effect of GW2580 treatment on microglia undergoing the most change, amyloid-beta plaques were stained using Congo red and microglia were labelled with PU.1 in the hippocampus of control and GW2580-treated APP/PS1 mice and wildtype littermate controls. PU.1-labelled microglia were quantified in concentric circles centred on the amyloid-beta plaque. In order to capture microglia density in the absence of plaques, microglia were quantified in concentric circles randomly located in equivalent areas in the hippocampus of control and GW2580-treated wildtype littermate controls (Figure 5.9).

In control and GW2580-treated wildtype littermate controls the number of microglia was relatively uniform across the area quantified. In wildtype mice the number of microglia increased as the distance from the randomly chosen centre increased, reflecting the larger area quantified

as the distance from the centre increased. In APP/PS1 mice there was a significant increase in the number of microglia ($F_{1, 19} = 74.71$, $p < 0.0001$), which peaked at a distance of 30 μm from the centre of the amyloid-beta plaque. In GW2580-treated APP/PS1 mice, proximal to amyloid-beta plaques, there was a significant reduction in the number of microglia relative to untreated APP/PS1 mice. This was reflected in the significant interaction between genotype and GW2580 treatment ($F_{1, 19} = 10.96$, $p = 0.0037$). Therefore, GW2580 treatment reduced microglia proliferation proximal to amyloid-beta plaques.

There was no notable sex difference in this effect with both sexes showing a significant increase in microglia number in APP/PS1 mice (male: $F_{1, 7} = 27.56$, $p = 0.0012$, female: $F_{1, 8} = 31.75$, $p = 0.0005$) and a strong trend towards a significant effect of GW2580 treatment in APP/PS1 mice (male: $F_{1, 7} = 3.68$, $p = 0.0965$, female: $F_{1, 8} = 5.14$, $p = 0.0532$; Figure 5.9, F, G).

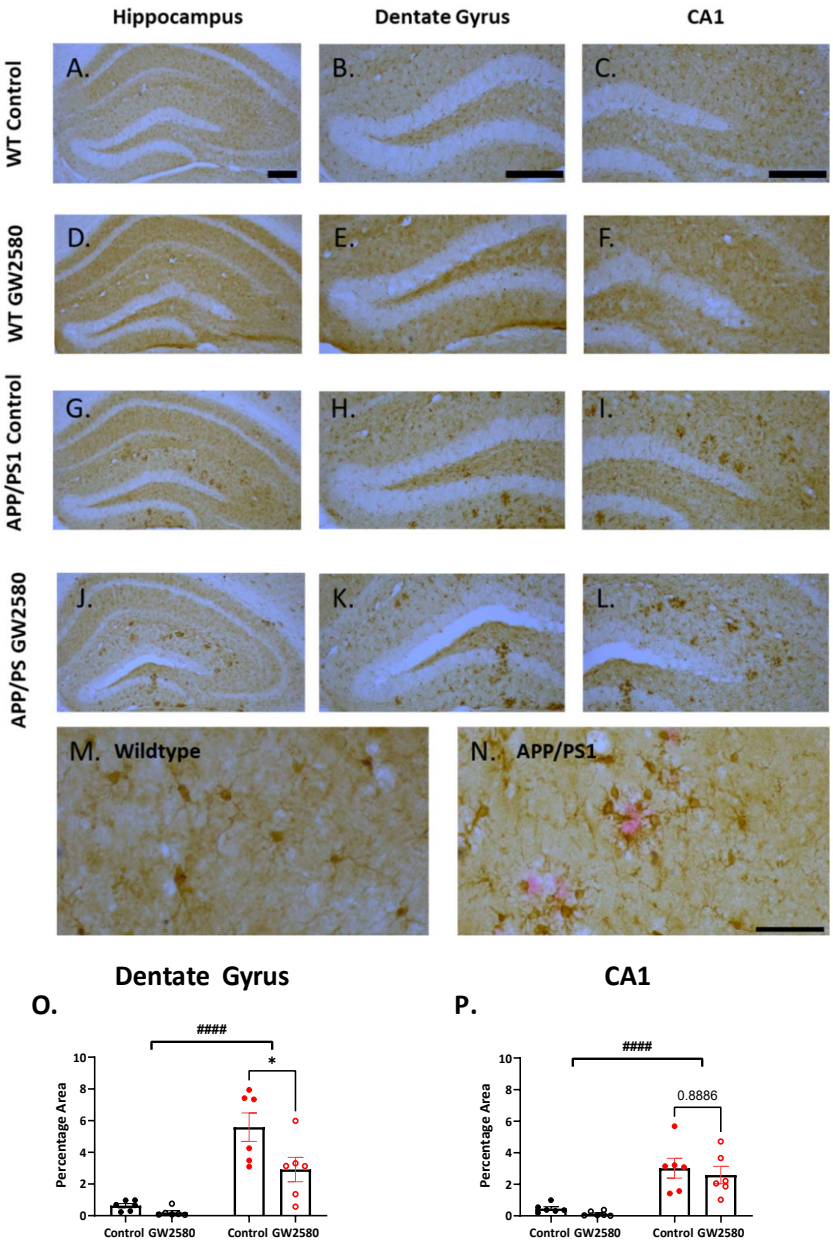

Figure 5.8. The effect of GW2580 treatment on microglia reactivity. Representative images in the (A, D, G, J) hippocampus, (B, E, H, K) dentate gyrus, and (C, F, I, L) CA1 in control (solid circles) and GW2580-treated (empty circles; estimated dose 3.5 mg/day) wildtype (black) and APP/PS1 (red) mice: (A-C) wildtype control, (D-F) wildtype GW2580, (G-I) APP/PS1 control, (J-L) APP/PS1 GW2580. Percentage area labelled quantified in (M) the dentate gyrus, and (N) the CA1 subregion. Microglia labelled with anti-Iba1 antibody and visualised using DAB reaction. 2-way ANOVA, main effect of genotype: #### = $p < 0.0001$, post-hoc analysis with Tukey's post-hoc corrections in light text: * = $p < 0.05$. Hippocampus images at 5X, remainder at 10X. 5X and 10X: Scale bar: 250 µm. 40X: Scale bar: 50 µm. N = 6 for all groups, 3 males and 3 females.

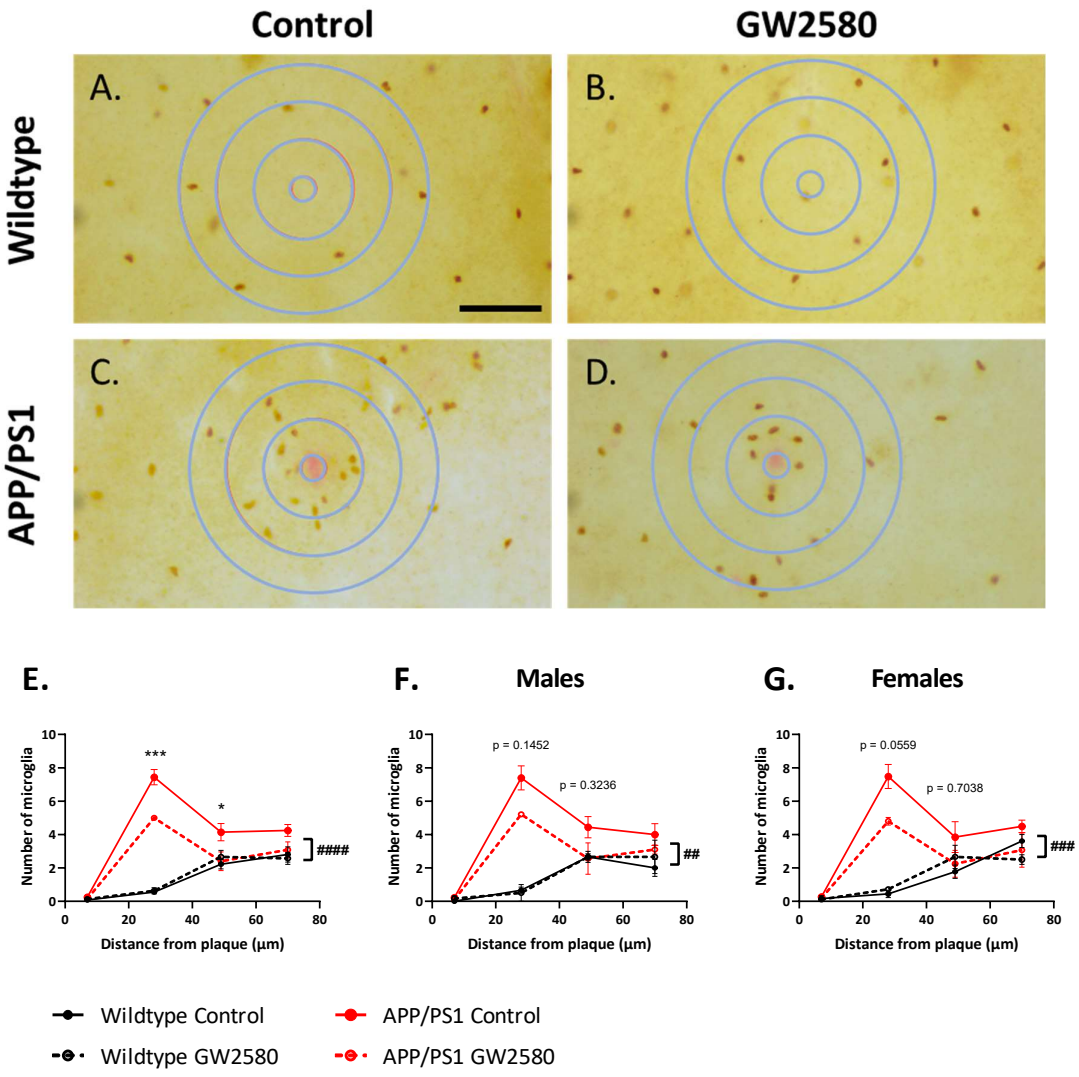

Figure 5.9. The effect of GW2580 treatment on the number of plaque-associated microglia. (A-D) Representative images and (E-F) quantification of microglia labelled with anti-PU.1 antibody in the hippocampus of control (solid lines) and GW2580-treated (dashed lines; estimated dose 3.5 mg/day) wildtype (black) and APP/PS1 (red) mice: (A) wildtype control, (B) Wildtype GW2580, (C) APP/PS1 control, (D) APP/PS1 GW2580. Concentric circles for quantification centred randomly in wildtype mice and on Congo red labelled amyloid plaques in APP/PS1 mice. 3-way ANOVA, main effect of genotype: ## = $p < 0.01$, ### = $p < 0.005$, #### = $p < 0.0001$, post-hoc analysis with Tukey's post-hoc corrections in light text for APP/PS1 control versus APP/PS1 GW2580: * = $p < 0.05$, *** = $p < 0.005$. Images at 40X. Scale bar: 50 µm. N = 6 for all groups, 3 males, 3 females. WT: 3 randomly centred concentric circles analysed, APP/PS1: 11 ± 5 plaque-centred concentric circles analysed.

5.7. The effect of GW2580 treatment on microglial gene expression

The effect of GW2580 treatment on microglial gene expression was investigated in microglia isolated by FACS from control and GW2580-treated APP/PS1 mice and wildtype littermate controls. Gene expression was investigated by quantitative PCR (Figure 5.10). It was confirmed that microglia had been isolated based on the expression of homeostatic microglial genes (*Cd11b*, *Sall1* and *P2ry12*) and the failure to expression astrocyte markers (*Gfap*)(Figure 5.A.1).

The expression of various DAM phenotypic markers was previously quantified in these microglia (Keren-Shaul et al., 2017). In control APP/PS1 mice the expression of *Itgax*, *Clec7a*, and *Apoe* was significantly increased relative to wildtype littermate controls. The expression of *Cst7*, *Cstd*, *Cybb*, and *Lpl* was also non-significantly increased in control APP/PS1 mice relative to wildtype littermate controls. The expression of these DAM phenotype markers was reduced in GW2580-treated APP/PS1 mice relative to control APP/PS1 mice (Islam, 2022). Broadly, therefore, it was understood that the expression of various markers of microglial reactivity was increased in APP/PS1 mice and the expression of these markers was reduced by treatment with GW2580.

The expression of certain pro-inflammatory cytokines and chemokines was quantified here. Overall, the expression of various pro-inflammatory mediators was increased in APP/PS1 mice and trended towards a reduction following treatment with GW2580, both APP/PS1 mice and wildtype littermate controls, although there were some exception to this trend. *Il1b* expression was not significantly affected by genotype ($F_{1, 22} = 0.57$, $p = 0.4601$), probably due to the high expression in control wildtype littermate controls. There was a significant reduction in *Il1b* expression following treatment with GW2580 ($F_{1, 22} = 4.61$, $p = 0.0431$), there was no interaction between genotype and GW2580 treatment ($F_{1, 22} = 0.02$, $p = 0.8811$; Figure 5.10, A). This finding was possibly confounded by the unusually high expression of *Il1b* in control wildtype littermate controls, however there was a notable reduction in *Il1b* expression following treatment with

GW2580 in APP/PS1 mice. There was a significant increase in the pro-inflammatory cytokine *Tnfa* and the chemokines *Ccl3* and *Cxcl10* in APP/PS1 mice (*Tnfa*: $F_{1, 22} = 4.33$, $p = 0.0493$, *Ccl3*: $F_{1, 22} = 9.53$, $p = 0.0054$, *Cxcl10*: $F_{1, 21} = 4.79$, $p = 0.0400$), there was no significant effect of GW2580 treatment (*Tnfa*: $F_{1, 22} = 0.89$, $p = 0.3559$, *Ccl3*: $F_{1, 22} = 0.87$, $p = 0.3625$, *Cxcl10*: $F_{1, 21} = 2.11$, $p = 0.1610$), nor any interaction between GW2580 treatment and genotype (*Tnfa*: $F_{1, 22} = 0.31$, $p = 0.5850$, *Ccl3*: $F_{1, 22} = 0.008$, $p = 0.9294$, *Cxcl10*: $F_{1, 21} = 0.004$, $p = 0.9499$, Figure 5.10, B, C, F). Although post-hoc analysis showed no significant effects, there was a reduction in expression that was consistent across all of these mediators in APP/PS1 mice treated with GW2580 relative to control APP/PS1 mice. Similarly, there was a strong trend towards a significant increase in the expression of *Ccl4* ($F_{1, 22} = 4.15$, $p = 0.0538$), with no significant effect of GW2580 treatment ($F_{1, 22} = 1.99$, $p = 0.1717$) nor any interaction between GW2580 treatment and genotype ($F_{1, 22} = 0.04$, $p = 0.8480$; Figure 5.10, D). Again, there was a non-significant reduction in expression of *Ccl4* in GW2580-treated APP/PS1 mice relative to control APP/PS1 mice.

There was no notable change in the expression of *Ccl2* in APP/PS1 mice relative to wildtype littermate controls ($F_{1, 21} = 2.02$, $p = 0.1697$). There was a reduction in *Ccl2* expression in GW2580-treated wildtype littermate controls, however there was no overall effect of GW2580 treatment ($F_{1, 21} = 1.57$, $p = 0.2247$) nor any interaction between genotype and GW2580 treatment ($F_{1, 21} = 2.44$, $p = 0.1335$; Figure 5.10.E).

Thus, there was a tendency towards increased cytokine expression in APP/PS1 mice and a trend towards reduction with GW2580 treatment.

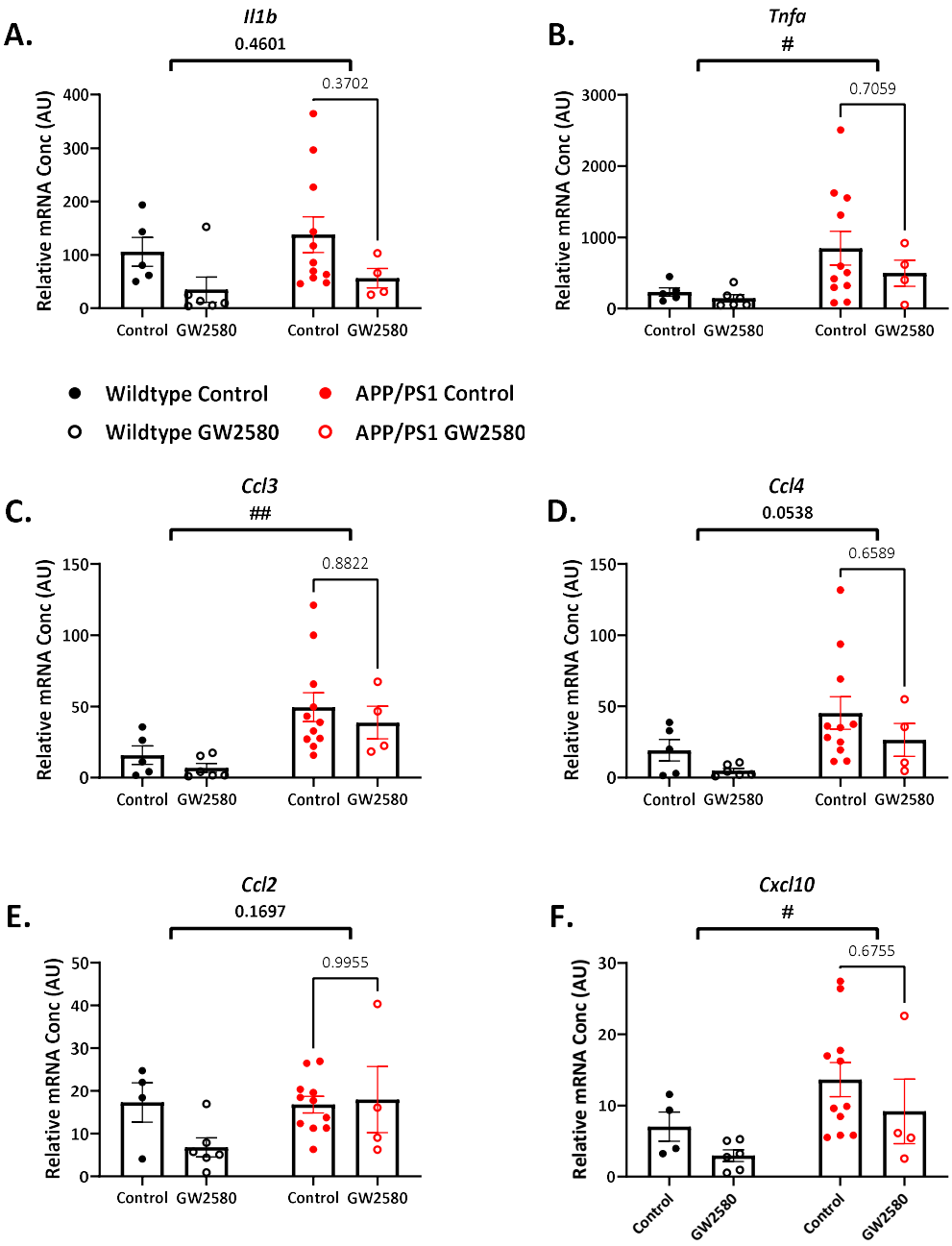

Figure 5.10. The effect of GW2580 treatment on gene expression in isolated microglia from APP/PS1 and wildtype mice. Microglia isolated by FACS from the hippocampus and overlying cortex of APP/PS1 mice (red) and wildtype mice (black) on a control diet (solid circles) and a GW2580-supplemented diet (empty circles). Gene expression quantified by qPCR. All genes normalised to expression of 18s. 2-way ANOVA, main effect of genotype in bold, # = $p < 0.05$, ## = $p < 0.01$, post-hoc analysis with Tukey's corrections in light text for APP/PS1 control versus APP/PS1 GW2580. Wildtype control, N = 5, wildtype GW2580, N = 6, APP/PS1 control, N = 11, APP/PS1 GW2580, N = 4.

5.8. The effect of GW2580 treatment on astrocyte reactivity

Astrocyte reactivity was quantified by measuring the percentage area labelled by GFAP in two regions of interest: the dentate gyrus, and the CA1 subregion (Figure 5.11).

In the dentate gyrus the percentage area labelled with GFAP was significantly increased in APP/PS1 mice relative to wildtype mice ($F_{1, 20} = 27.59$, $p < 0.001$; Figure 5.11, E). The percentage area labelled with GFAP was significantly reduced by GW2580 treatment in wildtype and APP/PS1 mice ($F_{1, 20} = 6.45$, $p = 0.0195$). In the CA1 subregion the percentage area labelled with GFAP was significantly increased in APP/PS1 mice relative to wildtype mice ($F_{1, 20} = 32.51$, $p < 0.001$; Figure 5.11, F). The percentage area labelled with GFAP was significantly reduced by GW2580 treatment in wildtype and APP/PS1 mice ($F_{1, 20} = 7.63$, $p = 0.0120$).

Therefore, astrocyte reactivity was increased in APP/PS1 mice relative to wildtype mice and treatment with GW2580 reduced astrocyte reactivity in the dentate gyrus and CA1 subregion.

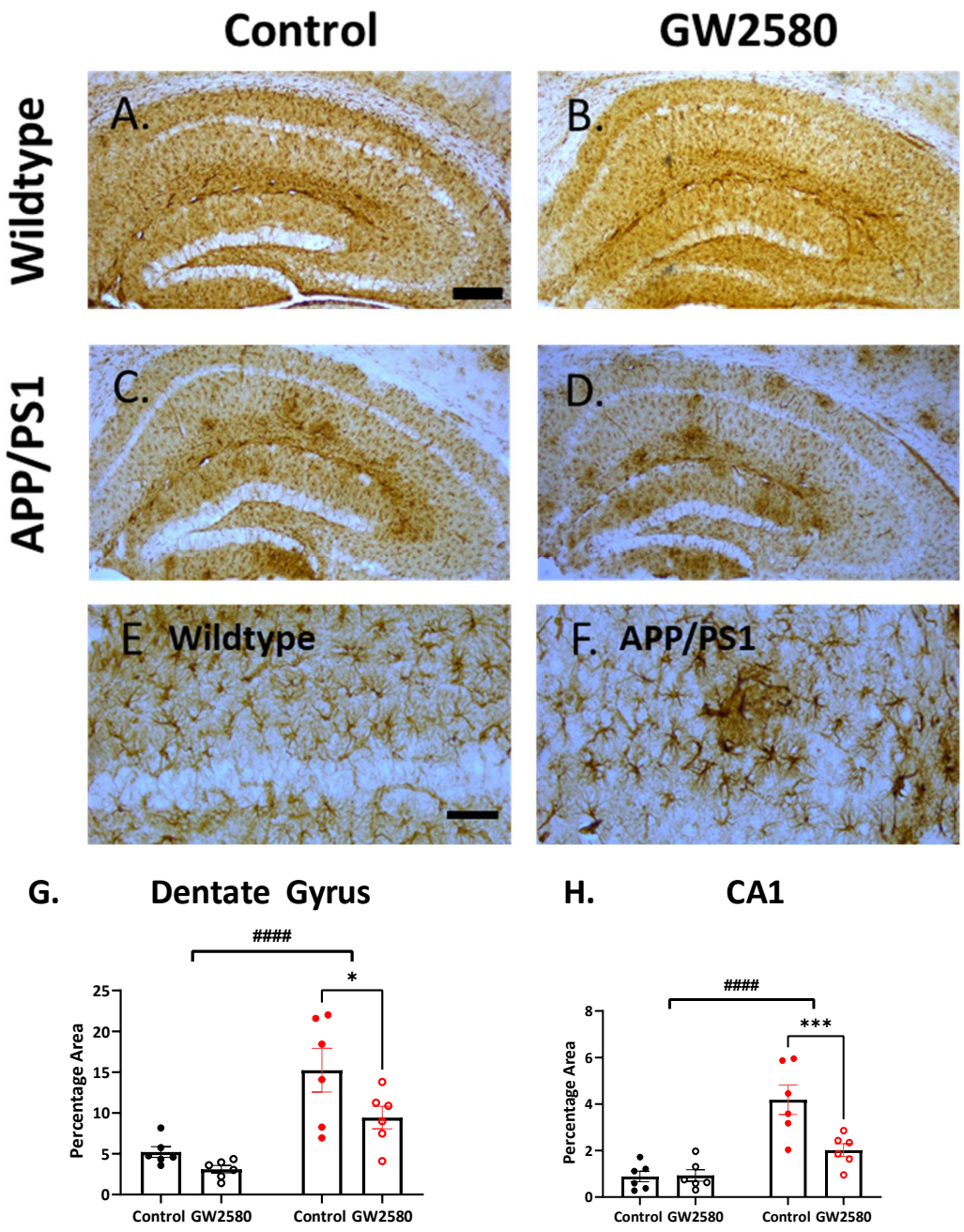

Figure 5.11. The effect of GW2580 treatment on astrocyte reactivity. Representative images in the (A, B, C, D) hippocampus in control (solid circles) and GW2580-treated (empty circles; estimated dose 3.5 mg/day) wildtype (black) and APP/PS1 (red) mice. Percentage area labelled quantified in (M) the dentate gyrus, and (N) the CA1 subregion. Astrocytes labelled with anti-GFAP antibody and visualised using DAB reaction. 2-way ANOVA, main effect of genotype: #### = $p < 0.0001$, post-hoc analysis with Tukey's post-hoc corrections in light text for APP/PS1 control versus APP/PS1 GW2580: * = $p < 0.05$, *** = $p < 0.005$. Images at 5X, Scale bar: 250 µm. N = 6 for all groups, 3 males and 3 females.

5.9. The effect of GW2580 treatment on astrocyte gene expression

The effect of GW2580 treatment on astrocyte gene expression was investigated in astrocytes isolated by FACS from control and GW2580-treated APP/PS1 mice and wildtype littermate controls. Gene expression was investigated by quantitative PCR (Figure 5.12). It was confirmed that astrocytes had been isolated based on the expression of homeostatic astrocyte genes (*Gfap* and *Vimentin*) and the failure to expression microglia markers (*Cd11b*)(Figure 5.A.1).

Astrocyte phenotype was investigated using several markers of astrocyte activity. The most widely used marker of astrocyte reactivity is increased *Gfap* expression. *Gfap* expression was significantly increased in both control and GW2580-treated APP/PS1 mice relative to wildtype littermate controls ($F_{1, 76} = 17.57$, $p < 0.0001$), there was no significant effect of GW2580 treatment ($F_{1, 76} = 0.06$, $p = 0.8095$) nor any interaction between GW2580 treatment and genotype ($F_{1, 76} = 0.77$, $p = 0.3843$; Figure 5.12, A). Increased vimentin (*Vim*) expression has also been used as a marker of astrocyte reactivity (Escartin et al., 2021; Yamada et al., 1992). However, *Vim* expression was not significantly different in APP/PS1 mice relative to wildtype littermate controls ($F_{1, 74} = 0.09$, $p = 0.7665$) nor was it affected by GW2580 treatment ($F_{1, 74} = 3.17$, $p = 0.0793$; Figure 5.12, B). The expression of various proinflammatory cytokines was investigated in FACS-isolated astrocytes. No expression of *Ccl2*, *Tnf*, and *Cxcl10* was detected by PCR (data not shown). *Cxcl1* expression was significantly increased in APP/PS1 mice relative to wildtype littermate controls ($F_{1, 75} = 3.98$, $p = 0.0496$), but there was no effect of GW2580 treatment on *Cxcl1* expression ($F_{1, 77} = 0.02$, $p = 0.9006$) nor any interaction between GW2580 treatment and genotype ($F_{1, 75} = 0.19$, $p = 0.6615$; Figure 5.12, C). Nevertheless, the expression of *Cxcl1* demonstrated that astrocytes in APP/PS1 mice may be producing more pro-inflammatory cytokines relative to wildtype littermate controls and this was not affected by treated with GW2580.

Astrocytes are known to acquire various losses in function in both ageing and Alzheimer's disease (Verkhratsky et al., 2021). Therefore, some gene expression indices of the metabolic profile of FACS-isolated astrocytes were quantified, these included: *Hes5*, which is involved in the functional maturation of astrocytes, specifically relating to glutamate reuptake (Hasel et al., 2017), the glucose transporter gene *Glut1*, and the expression of the glutamine synthetase enzyme gene *Glul*. *Hes5* expression was significantly reduced in APP/PS1 mice relative to wildtype littermate controls ($F_{1, 72}$ = 9.52, p = 0.0029), but there was no effect of GW2580 treatment on *Hes5* expression ($F_{1, 72}$ = 0.45, p = 0.4451) nor any interaction between GW2580 treatment and genotype ($F_{1, 72}$ = 3.09, p = 0.0831; Figure 5.12, D). *Glut1* and *Glul* expression were significantly reduced in APP/PS1 mice relative to wildtype littermate controls (*Glut1*: $F_{1, 70}$ = 11.56, p = 0.0011, *Glul*: $F_{1, 76}$ = 10.50, p = 0.0018), but there was no effect of GW2580 treatment on *Glut1* or *Glul* expression (*Glut1*: $F_{1, 70}$ = 0.43, p = 0.5138, *Glul*: $F_{1, 76}$ = 0.63, p = 0.4284) nor any interaction between GW2580 treatment and genotype (*Glut1*: $F_{1, 70}$ = 0.21, p = 0.6493, *Glul*: $F_{1, 76}$ = 0.17, p = 0.6781; Figure 5.12, E and F).Expression of *Hes5*, *Glut1*, and *Glul* suggested that astrocytes in APP/PS1 mice are metabolically impaired relative to wildtype littermate controls; this metabolic impairment was not affected by GW2580 treatment. The expression of these metabolic genes was correlated to the expression of *Cxcl1* in all mice (shown in appendix, Figure 5.A.2), however, there was no correlation between the expression of *Cxcl1* and the expression of *Hes5*, *Glut1*, and *Glul*. These gene expression changes were to some extent consistent with astrocyte asthenia or senescence (Verkhratsky et al., 2021) but analysis of further genes, descriptive of a state of cellular senescence (*P16*, *P21*, *Pai-1*, *Tgfb1*) did not provide evidence of substantial senescence in this isolated population of astrocytes. In summary, gene expression of markers of reactivity, pro-inflammatory cytokines, and metabolic markers suggested that astrocytes in APP/PS1 mice were altered relative to those in wildtype littermate controls, but there did not appear to be any effect of GW2580 treatment on the indices of astrocytes activation studied here.

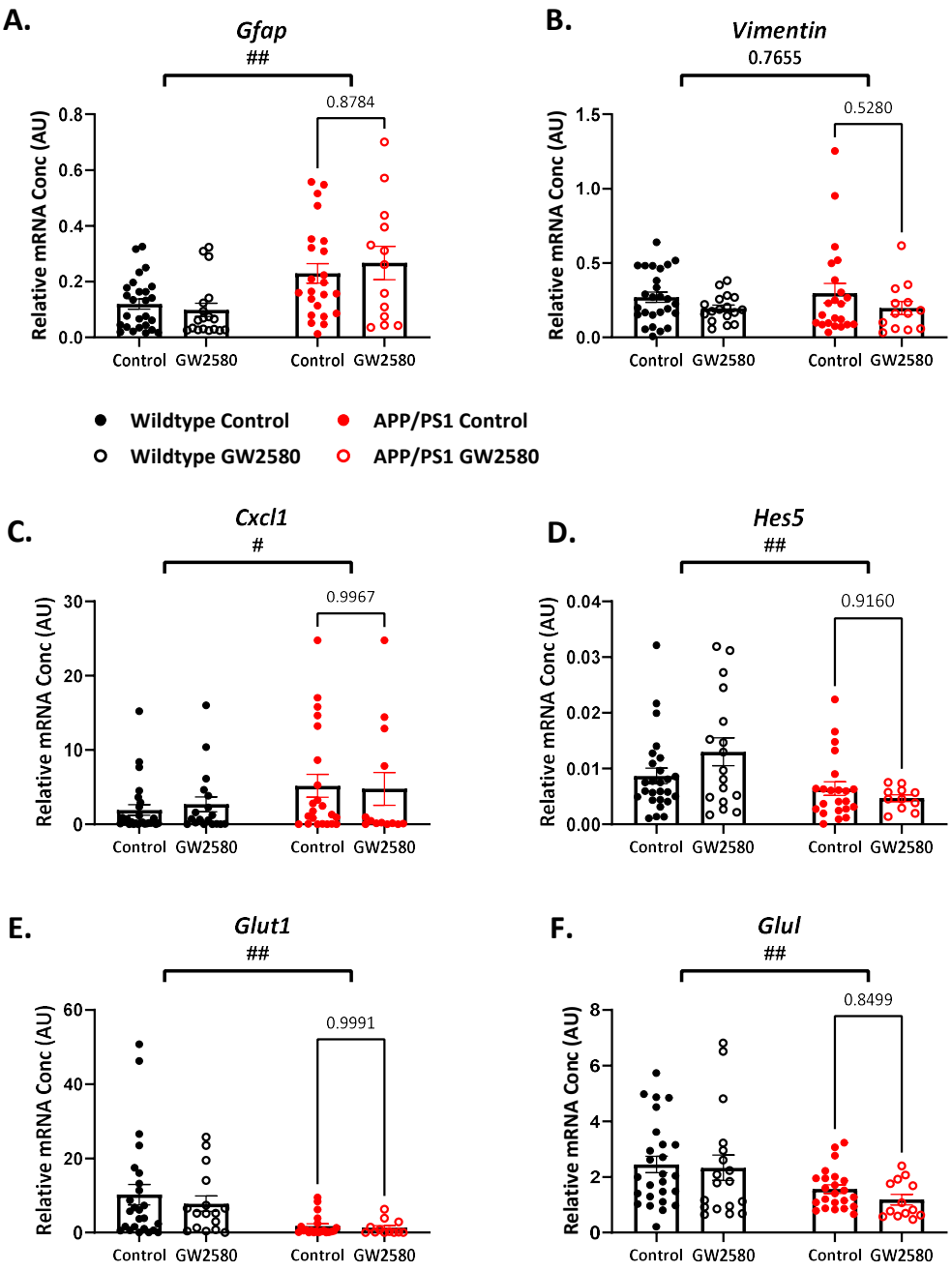

Figure 5.12. The effect of GW2580 treatment on gene expression in isolated astrocytes from APP/PS1 and wildtype mice. Astrocytes isolated by FACS from the hippocampus and overlying cortex of APP/PS1 mice (red) and wildtype mice (black) on a control diet (solid circles) and a GW2580-supplemented diet (empty circles). Gene expression quantified by qPCR. All genes normalised to expression of 18s. 2-way ANOVA, main effect of genotype in bold, # = $p < 0.05$, ## = $p < 0.01$, post-hoc analysis with Tukey's corrections in light text for APP/PS1 control versus APP/PS1 GW2580. Wildtype control, N = 26, wildtype GW2580, N = 18, APP/PS1 control, N = 23, APP/PS1 GW2580, N = 13.

5.10. The effect of GW2580 treatment on gamma frequency oscillations

The effect of GW2580 treatment on gamma frequency oscillations was investigated in brain slices from control and GW2580-treated APP/PS1 mice and wildtype littermate controls. The previously observed reduction in kainate-induced gamma frequency oscillation amplitude and frequency was reproduced in control animals.

In control APP/PS1 mice at 9-11 months the amplitude and frequency of kainate-induced gamma frequency oscillations were reduced relative to wildtype littermate controls. The reduction in amplitude was demonstrated by the area under the curve (wildtype control: 519.44 ± 212.58 μV, APP/PS1 control: 1663.92 ± 270.97 μV^2 Hz^-) and the peak amplitude (wildtype control: 519.44 ± 212.58 μV, APP/PS1 control: 101.25 ± 15.61 μV; Figure 5.13, E, F). The reduction in frequency was demonstrated by the peak frequency (wildtype control: 31.36 ± 1.89 Hz, APP/PS1 control: 26.50 ± 1.25 Hz; Figure 5.13, G). This was a replication of the previous observation that kainate-induced gamma frequency oscillations had reduced amplitude and frequency in APP/PS1 mice relative to wildtype littermate controls at 9-11 months (Figure 4.1).

In wildtype mice there was no significant effect of GW2580 treatment on kainate-induced gamma frequency oscillation amplitude. This was demonstrated by the area under the curve (wildtype control: 5657.87 ± 1884.27 μV^2 Hz^-, wildtype GW2580: 5598.81 ± 1903.74 μV^2 Hz^-) and the peak amplitude (wildtype control: 519.44 ± 212.58 μV, wildtype GW2580: 439.54 ± 108.78 μV; Figure 5.13, E, F). Similarly, in wildtype mice GW2580 treatment did not affect the oscillation peak frequency (wildtype control: 31.36 ± 1.89 Hz, wildtype GW2580: 30.92 ± 1.46 Hz; Figure 5.13, G).

In GW2580-treated APP/PS1 mice there was an increase in oscillation amplitude relative to control APP/PS1 mice. This was demonstrated by the area under the curve (11443.13 ± 3286.33 μV^2 Hz^-) and the peak amplitude (885.97 ± 268.69 μV; Figure 5.13, E, F). There was a significant

main effect of GW2580 treatment on the area under the curve ($F_{1, 32} = 7.14$, $p = 0.0117$) and peak amplitude ($F_{1, 32} = 7.65$, $p = 0.0093$), and a significant interaction between genotype and GW2580 treatment on the area under the curve ($F_{1, 32} = 6.47$, $p = 0.0160$) and the peak amplitude ($F_{1, 32} = 6.33$, $p = 0.0171$). This reflected the increase in kainate-induced gamma frequency oscillation amplitude following treatment with GW2580 in APP/PS1 mice, but not in wildtype littermate controls.

Although this was a reversal of the amplitude reduction observed in APP/PS1 mice, the pooled Fast Fourier transforms show that the activity was not an ordered oscillation, there was a large amount of lower frequency activity present – this was suggestive of hyperexcitability (Figure 5.13, D). Additionally, the peak frequency was reduced in GW2580-treated APP/PS1 mice relative to wildtype littermate controls (APP/PS1 GW2580: 27.64 ± 1.40 Hz, wildtype control: 31.36 ± 1.89 Hz; Figure 5.13, F). The peak frequency was significantly reduced in APP/PS1 mice ($F_{1, 32} = 6.48$, $p = 0.0159$) and was not affected by treatment with GW2580 ($F_{1, 32} = 0.05$, $p = 0.8309$), nor was there any interaction between genotype and treatment ($F_{1, 32} = 0.24$, $p = 0.6245$).

In addition there was an increased incidence of epileptiform events in brain slices from GW2580-treated APP/PS1 mice (Figure 5.13, H). As observed previously, in control APP/PS1 mice there was an increased incidence of epileptiform events relative to wildtype littermate controls (wildtype: 40%, 12 of 30 slices; APP/PS1: 54%, 19 of 35 slices). However, treatment with GW2580 further increased the incidence of epileptiform events in APP/PS1 mice (GW2580 APP/PS1: 71%, 30 of 42 slices). There was a significant effect of experimental group on the incidence of seizing ($p = 0.0031$, Fisher's exact test). This was further evidence that the activity which emerged in APP/PS1 mice following treatment was hyperexcitable and disordered.

In summary, the previously observed reduction in kainate-induced gamma frequency oscillation amplitude and frequency in APP/PS1 mice at 9-11 months was reproduced. Treatment with

GW2580 increased the amplitude of kainate-induced gamma frequency oscillations in APP/PS1 mice relative to control APP/PS1 mice and wildtype littermate controls, but the oscillation frequency remained reduced and the incidence of epileptiform events was increased. Therefore, treatment with GW2580 did reverse the amplitude reduction seen in APP/PS1 mice but the oscillation were different in nature to those in wildtype littermate controls.

As noted previously, carbachol-induced gamma frequency oscillations were not well defined at 9-11 months, nor was there a notable difference in carbachol-induced gamma frequency oscillations in APP/PS1 mice and wildtype littermate controls. Given the poor quality of the carbachol-induced gamma frequency oscillations, these data are not presented in detail but are available in the appendix to this chapter (Figures 5.A.3).

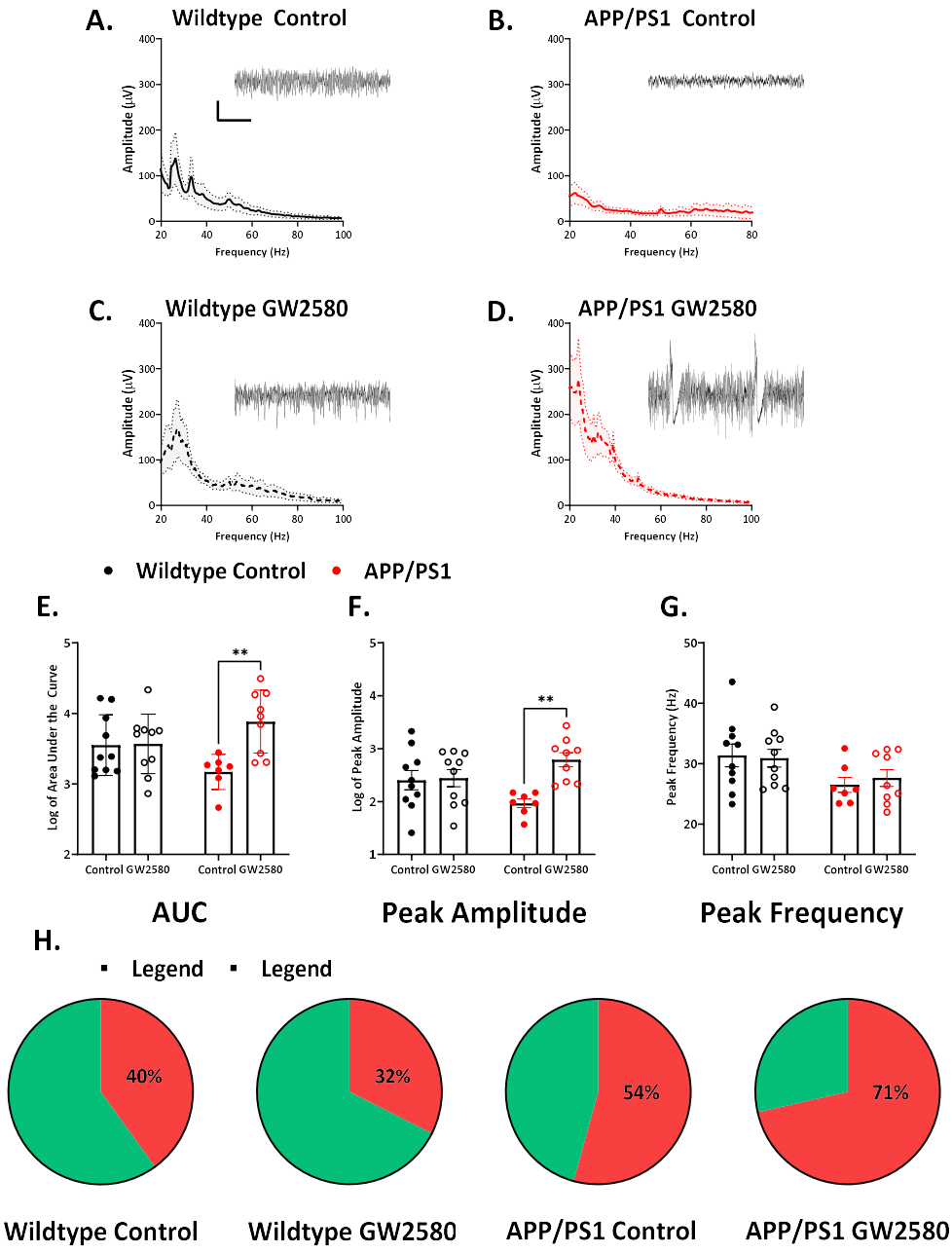

Figure 5.13. The effect of GW2580 treatment on kainate-induced gamma frequency oscillations. (A-D) FFTs pooled and representative traces for (A, C) wildtype (black) and (B, D) APP/PS1 (red) mice on a (A, B) control diet (solid circles/lines) and a (C, D) GW2580-supplemented diet (empty circles/dashed lines; estimated dose 3.5 mg/day). (E) Area under the curve, (F) peak amplitude, (G) peak frequency from FFTs. Data in E and F are log transformed. (H) Incidence of epileptiform events in brain slices. Ed2-way ANOVA, main ANOVA effect of genotype in bold: # = p <0.05, post-hoc analysis with Tukey corrections in light text: ** = p < 0.01. WT control, n = 25, N = 10, WT GW2580, n = 35, N = 10, APP/PS1 control, n = 28, N = 7, APP/PS1 GW2580, n = 38, N = 9. Scale bar: 200 μV, 1 second.

5.11. The effect of time on gamma frequency oscillations in APP/PS1 mice

To facilitate further investigation of the relationship between gamma frequency oscillations and neuroinflammation in APP/PS1 mice, it was necessary to establish how kainate-induced gamma frequency oscillations behaved over time, this served as a reference against which to measure the impact of other intervention on gamma frequency oscillations (Figures 5.14 and 5.15).

In untreated brain slices from wildtype littermate controls, at 9-11 and 20-24 months, and in untreated brain slices from APP/PS1 mice at 9-11 months, kainate-induced gamma frequency oscillations grew in amplitude over time. This was demonstrated by the area under the curve and the peak amplitude (Table 5.1). This was similar to the growth in oscillation amplitude observed in untreated brain slices from C57BL/6J mice at 3-4 months (Figure 3.7) These changes in oscillation amplitude in untreated slices are shown by z-scores calculated at 90 minutes post-baseline for the area under the curve (wildtype 9-11 months: 5.69 ± 3.92, wildtype 20-24 months: 5.02 ± 2.89, APP/PS1 9-11 months: 3.68 ± 3.05) and peak amplitude (wildtype 9-11 months: 3.24 ± 1.75, wildtype 20-24 months: 4.17 ± 2.62, APP/PS1 9-11 months: 6.95 ± 4.83). In untreated brain slices from APP/PS1 mice at 20-24 months oscillation amplitude was relatively stable over time (Table 5.1). This was demonstrated by the z-scores calculated at 90 minutes post-baseline for the area under the curve (0.35 ± 1.93) and peak amplitude (0.63 ± 1.68). Statistically, there was no effect of time on area under the curve at 9-11 months ($F_{2.19, 19.71} = 1.59$, $p = 0.2280$) or at 20-24 months ($F_{1.124, 13.49} = 0.53$, $p = 0.4983$) nor was there any interaction between time and genotype (9-11 months: $F_{3, 27} = 1.13$, $p = 0.3531$, 20-24 months: $F_{2., 24} = 0.21$, $p = 0.8091$). Likewise, there was no significant effect of time on the peak amplitude at 9-11 months ($F_{2.764, 24.88} = 1.61$, $p = 0.2148$) or at 20-24 months ($F_{1.072, 12.87} = 0.52$, $p = 0.4962$) nor was there any interaction between time and genotype (9-11 months: $F_{3, 27} = 0.63$, $p = 0.6052$, 20-24

months: $F_{2., 24} = 0.18$, $p = 0.8388$). Therefore, the changes which were demonstrated by both the raw data and z-scores for the amplitude parameters were not statistically significant.

	Area under the Curve at Baseline ($\mu V^2 Hz^-$)	Area under the Curve at 90 mins post-baseline ($\mu V^2 Hz^-$)	Peak Amplitude at Baseline (μV)	Peak Amplitude at 90 mins post-baseline (μV)
Wildtype 9-11	11,989.56 ± 6,495.06	17,689.19 ± 11,832.88	1,013.88 ± 650.25	1,301.69 ± 1,014.18
Wildtype 20-24	39,255.87 ± 32,121.15	49,675.32 ± 39,718.95	3,679.27 ± 3,018.31	5,081.89 ± 4,208.57
APP/PS1 9-11	1,076.77 ± 540.78	2,844.85 ± 1,274.40	98.69 ± 49.21	277.11 ± 143.33
APP/PS1 20-24	66,304.93 ± 34,020.13	51,675.62 ± 32,8156.06	3,238.30 ± 1,778.29	2,889.48 ± 1,719.23

Table 5.1. Amplitude parameters over time in untreated brain slices from APP/PS1 and wildtype mice.

In untreated brain slices from wildtype mice and from APP/PS1 mice at 20-24 months the oscillation peak frequency is slightly reduced over time (wildtype: 9-11 months: baseline: 33.51 ± 2.56 Hz, 90 minutes post-baseline: 26.51 ± 2.18; wildtype 20-24 months: baseline: 31.44 ± 1.07 Hz, 60 minutes post-baseline: 28.85 ± 1.62, APP/PS1 20-24 months: baseline: 30.63 ± 1.57 Hz, 60 minutes post-baseline: 25.50 ± 1.37). In brain slices from APP/PS1 mice at 9-11 months the oscillation peak frequency is relatively stable over time (baseline: 25.41 ± 1.62 Hz, 90 minutes post-baseline: 29.27 ± 277). There was no significant overall effect of time on peak frequency at 9-11 months ($F_{2.518, 22.67} = 1.36$, $p = 0.2809$), however there was a significant interaction between time and genotype ($F_{3, 27} = 3.72$, $p = 0.0234$). This reflected the decrease in peak frequency in wildtype littermate controls at 9-11 months. There was a significant reduction in peak frequency

with time in mice at 20-24 months ($F_{1.594, 19.13} = 7.87$, $p = 0.0051$) which was not affected by the genotype of the mice ($F_{2, 24} = 1.54$, $p = 0.2349$).

In summary, in untreated slices at 9-11 months, there was a non-significant increase in oscillation amplitude. At 20-24 months, there was also a non-significant increase in oscillation amplitude in wildtype littermate controls but not in APP/PS1 mice. In untreated slice from mice at 9-11 months, the oscillation peak frequency was relatively stable, with a slight decrease in brain slices from wildtype mice. In both APP/PS1 mice and wildtype littermate controls at 20-24 months there was a significant decrease in oscillation frequency with time.

These observations on the behaviour of kainate-induced gamma frequency oscillations in untreated brain slices will be used as a reference against which inflammatory interventions will be compared.

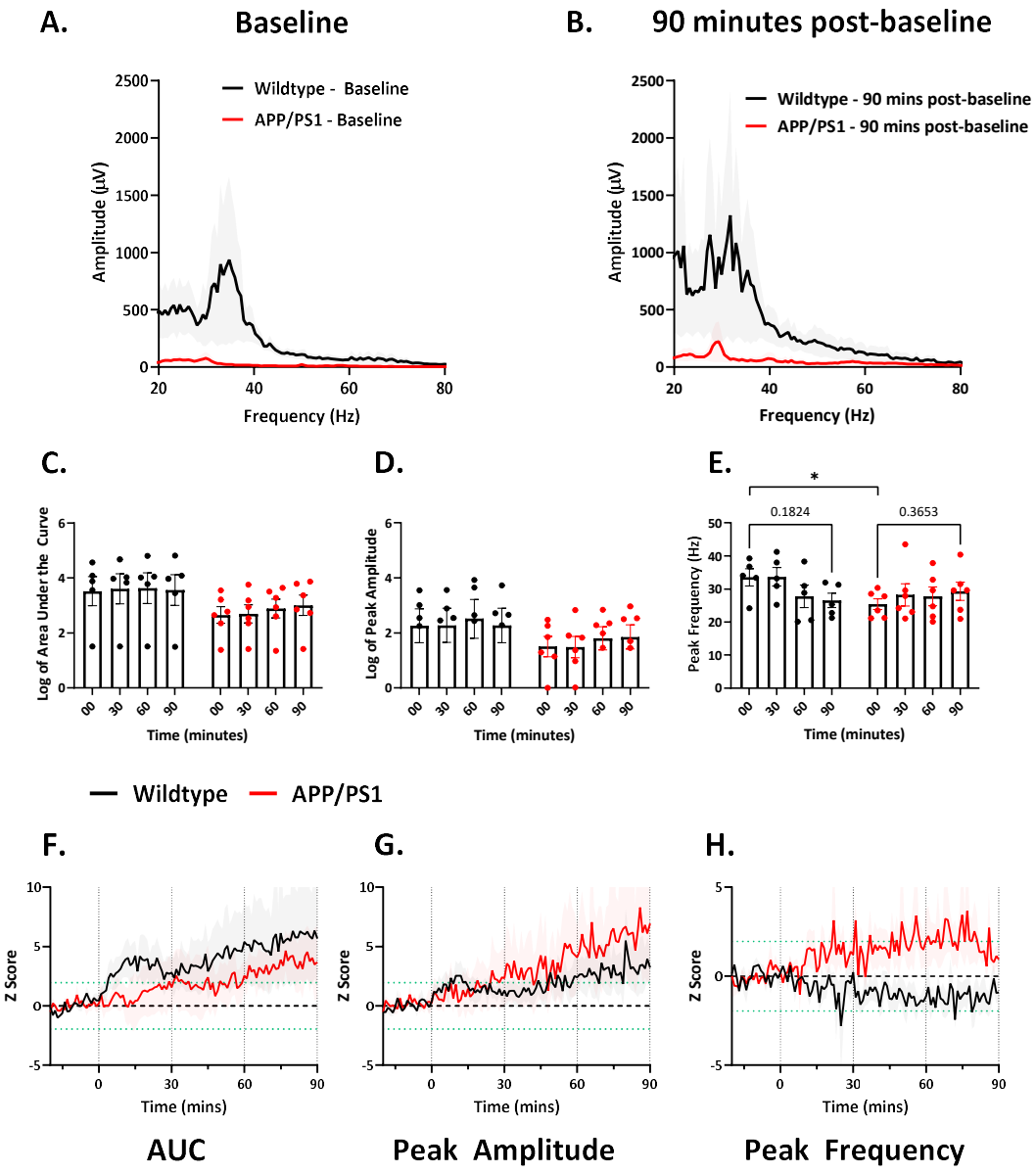

Figure 5.14. The behaviour of established gamma frequency oscillations over time at 9-11 months. (A,B) Pooled FFTs for kainate-induced gamma frequency oscillations at (A) baseline and (B) 60 minutes post-baseline in brain slices from wildtype (black) and APP/PS1 (red) mice. FFT parameters: (C) area under the curve, (D) peak amplitude, (E) peak frequency across 60 minutes. (F, G, H) Z-scores of (C, D, E) respectively, dotted green line represents $p < 0.05$. Data in C and D are log transformed. Wildtype: n = 4, N = 4, APP/PS1: n = 6, N = 6.

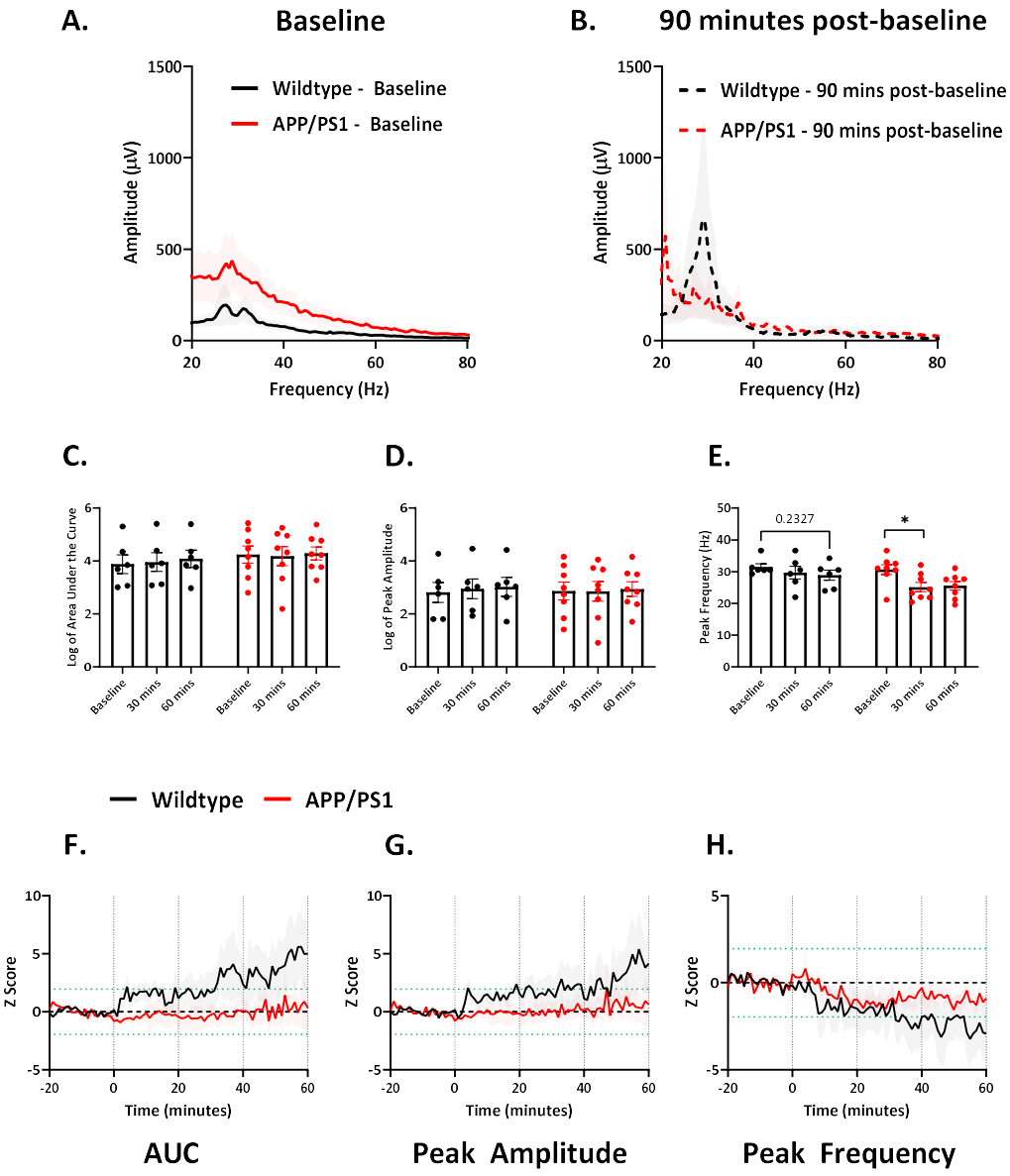

Figure 5.15. The behaviour of established gamma frequency oscillations over time at 20-24 months. (A,B) Pooled FFTs for kainate-induced gamma frequency oscillations at (A) baseline and (B) 60 minutes post-baseline in brain slices from wildtype (black) and APP/PS1 (red) mice. FFT parameters: (C) area under the curve, (D) peak amplitude, (E) peak frequency across 60 minutes. 2-way ANOVA, post-hoc comparisons with Tukey correction in light text, * = $p < 0.05$. (F, G, H) Z-scores of (C, D, E) respectively, dotted green line represents $p < 0.05$. Data in C and D are log transformed. Wildtype: n = 9, N = 6, APP/PS1: n = 13, N = 8.

5.12. The effect of neuroinflammation in brain slices from APP/PS1 mice

Given the observed changes in kainate-induced gamma frequency oscillations in APP/PS1 mice were shown to be sensitive to changes in neuroinflammation via treatment with GW2580, it was of interest to determine how established gamma frequency oscillations in brain slices from APP/PS1 mice and wildtype littermate controls responded to inflammatory manipulations. Brain slices with established gamma frequency oscillations were exposed to IL-1β and TNFα, these pro-inflammatory mediators were shown to inhibit the normal growth in oscillation amplitude in brain slices from C57BL/6J mice at 3-4 months (Figures 3.9, 3.10, and 3.15). It was hypothesised that these pro-inflammatory mediators would have a similar effect in wildtype mice but a different effect in APP/PS1 mice given the altered neuroinflammatory milieu. Additionally, brain slices with established gamma frequency oscillations were exposed to an anti-TNFα antibody. It was hypothesised that this treatment would have a positive effect on gamma frequency oscillation amplitude in APP/PS1 mice, based on the observed effect of GW2580 treatment in APP/PS1.

Brain slices with established gamma frequency oscillations at a stable baseline were exposed to IL-1β (10 ng/mL) or TNFα (10 ng/mL) for 30 minutes. The effect of this exposure was monitored during the exposure and for a further 30 minutes for IL-1β and for a further 60 minutes for TNFα. Alternatively, brain slices with established gamma frequency oscillations at a stable baseline with exposed to anti-TNFα antibody (100 ng/mL) for 90 minutes and the effect of this exposure was monitored throughout (Figure 5.16). The effects of these exposure were compared to the behaviour of gamma frequency oscillations in untreated brain slices (Figure 5.14 and 5.15).

These manipulations of TNFα were also performed on brain slices from GW2580-treated APP/PS1 mice and wildtype littermate controls. These data are available in the appendix to this

chapter (Figures 5.A.6 and 5.A.7). Additionally, data relating to the effect of GW2580-treatment (Figure 5.A.5) and of IL-1β (Figures 5.A.3 and 5.A.4) on carbachol-induced gamma frequency oscillations in brain slices from APP/PS1 mice and wildtype littermate controls are also available in the appendix.

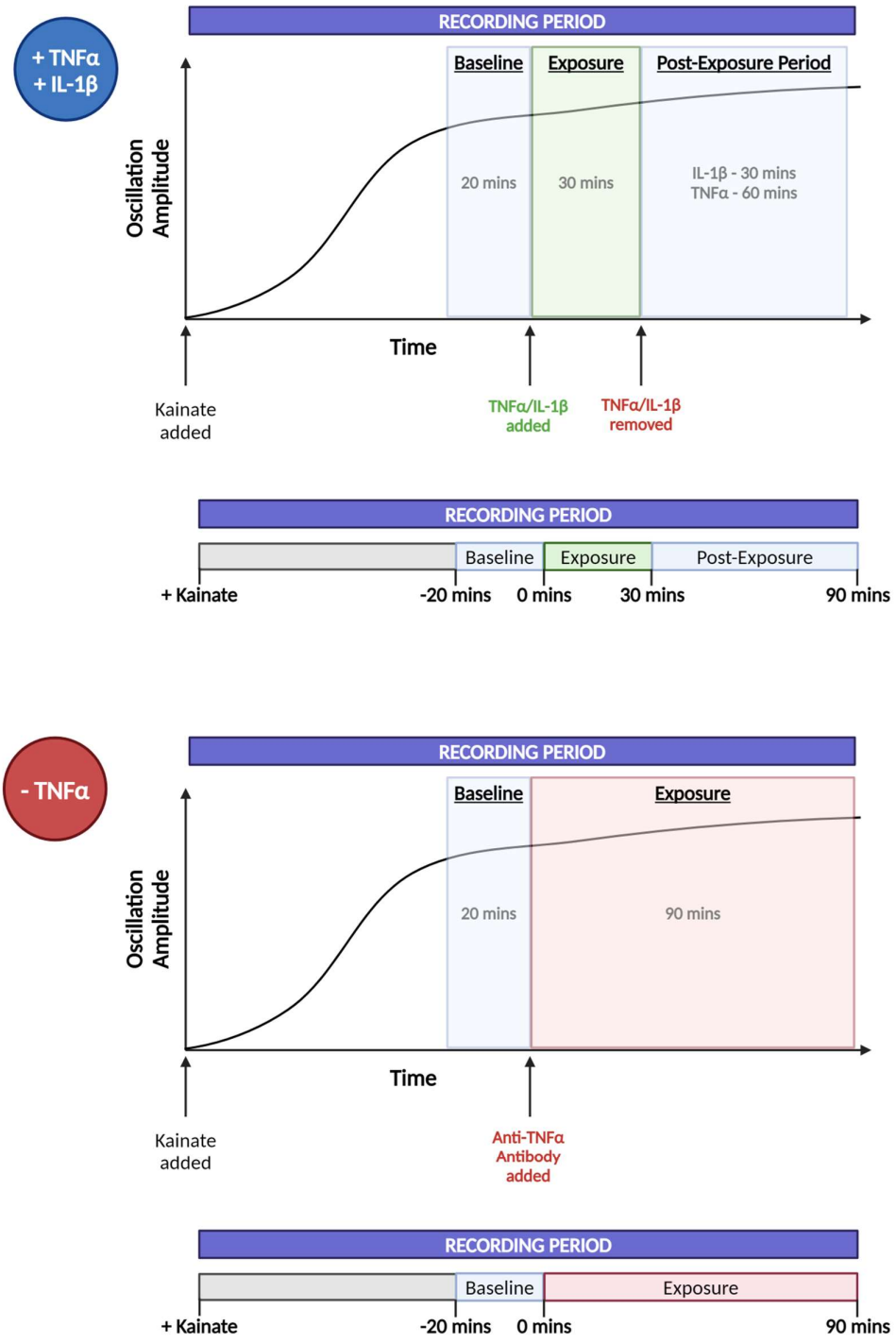

Figure 5.16. Schematic representation of neuroinflammatory manipulations in brain slices with gamma frequency oscillations. Brain slices exposed to (top) TNFα (10 ng/mL) or IL-1β (10 ng/mL) and (bottom) anti-TNFα antibody (100 ng/mL).

5.13. The effect of IL-1β on gamma frequency oscillations in APP/PS1 mice

Gamma frequency oscillations were established with kainate (100 nM). Once gamma frequency oscillations had become established and stabilised in baseline state they were exposed to IL-1β (10 ng/mL) for 30 minutes. The effect of this exposure was monitored both during the exposure and for a further 30 minutes (Figures 5.17 and 5.18).

In untreated brain slices from wildtype mice the gamma frequency oscillation amplitude increased over time and the peak frequency is slightly decreased. In wildtype mice exposure to IL-1β inhibited the normal growth in oscillation amplitude. This was demonstrated by the area under the curve (9-11 months: baseline: 3,000.70 ± 981.92 $\mu V^2 Hz^-$, 60 minutes post-IL-1β: 2,725.22 ± 993.27 $\mu V^2 Hz^-$, 20-24 months: baseline 4,022.626 ± 1,292.908 $\mu V^2 Hz^-$, 60 minutes post-IL-1β: 3,697.654 ± 1261.638 $\mu V^2 Hz^-$) and peak amplitude (9-11 months: baseline: 303.024 ± 128.497 μV, 60 minutes post-IL-1β: 247.47 ± 124.24 μV, 20-24 months: baseline: 327.439 ± 135.854 μV, 60 minutes post-IL-1β: 340.139 ± 148.769 μV) which are reduced 60 minutes after exposure to IL-1β. These changes were further demonstrated by z-scores calculated for these parameters in untreated and IL-1β-treated brain slices (untreated: area under the curve: 9-11 months: 5.69 ± 3.92, 20-24 months: 5.02 ± 2.89, peak amplitude: 9-11 months 3.24 ± 1.75, 20-24 months: 4.17 ± 2.62; IL-1β-treated: area under the curve: 9-11 months: -0.90 ± 1.07, 20-24 months: 0.38 ± 0.81, peak amplitude: 9-11 months: -0.55 ± 0.91, 20-24 months: 0.36 ± 0.54). In wildtype littermate controls, the peak frequency of kainate-induced gamma frequency oscillations was unaffected by exposure to IL-1β at 9-11 months (baseline: 33.39 ± 1.62 Hz, 60 minutes post-IL-1β: 33.91 ± 1.45 Hz), and was reduced at 20-24 months (baseline: 31.62 ± 1.25 Hz, 60 minutes post-IL-1β: 28.55 ± 1.13 Hz). This was similar to the behaviour of oscillation peak frequency in untreated brain slices.

In untreated brain slices from APP/PS1 at 9-11 months gamma frequency oscillation amplitude is increased over time and oscillation peak frequency is stable. In APP/PS1 mice at 9-11 months exposure to IL-1β did not affect the growth in oscillation amplitude which is observed in untreated slices. This was demonstrated by the area under the curve (baseline: 1,169.55 ± 224.81 $\mu V^2 Hz^-$, 60 minutes post-IL-1β: 2031.36 ± 610.54 $\mu V^2 Hz^-$) and peak amplitude (baseline: 74.48 ± 12.06 μV, 60 minutes post-IL-1β: 143.67 ± 45.21 μV) which were increased 60 minutes after exposure to IL-1β. Therefore, in APP/PS1 mice at 9-11 months exposure to IL-1β did not cause kainate-induced gamma frequency oscillations to behave differently than in untreated brain slices. This was further demonstrated by the z-scores for the amplitude parameters (area under the curve: untreated: 3.68 ± 3.05, IL-1β-treated: 5.01 ± 1.07, peak amplitude: untreated: 6.95 ± 4.83, IL-1β-treated: 4.61 ± 0.94). In slices from APP/PS1 mice at 9-11 months the peak frequency was also relatively stable following exposure to IL-1β (baseline: 30.65 ± 1.52 Hz, 60 minutes post-IL-1β: 29.36 ± 1.96 Hz), as it was in untreated brain slices. In untreated brain slices from APP/PS1 mice at 20-24 months, gamma frequency oscillation amplitude is relatively stable over time and oscillation peak frequency is reduced. Following exposure to IL-1β, kainate-induced gamma frequency oscillation amplitude was relatively stable in brain slices from APP/PS1 mice. This was demonstrated by the area under the curve (baseline: 12,409.54 ± 4,144.40 $\mu V^2 Hz^-$, 60 minutes post-IL-1β: 14,113.48 ± 4,856.47 $\mu V^2 Hz^-$) and peak amplitude (baseline: 675.31 ± 210.59 μV, 60 minutes post-IL-1β: 893.08 ± 278.74 μV). This was further demonstrated by the amplitude z-scores (area under the curve: untreated: 0.35 ± 1.93, IL-1β-treated: 2.56 ± 1.24, peak amplitude: untreated: 0.63 ± 1.68, IL-1β-treated: 2.80 ± 1.07). In slices from APP/PS1 mice at 20-24 months exposure to IL-1β reduced the peak frequency of kainate-induced gamma frequency oscillations (baseline: 30.54 ± 1.15 Hz, 60 minutes post-IL-1β: 25.75 ± 1.53 Hz). Therefore, as at 9-11 months, in APP/PS1 mice at 20-24 months exposure to IL-1β did not

cause kainate-induced gamma frequency oscillations to behave differently than they did in untreated brain slices.

At 9-11 months in IL-1β exposed slices the area under the curve was significantly affected by time ($F_{1.96,\ 62.71} = 4.30$, $p = 0.0184$) and this interaction was significantly affected by genotype ($F_{6,\ 64} = 2.25$, $p = 0.0495$). Similarly, the peak amplitude was significantly affected by time in wildtype littermate controls only ($F_{2,\ 46} = 5.28$, $p = 0.0086$). This demonstrated that exposure to IL-1β inhibited the growth of oscillation amplitude in wildtype littermate controls but not in APP/PS1 mice. The peak frequency was not significantly affected by genotype ($F_{1,\ 23} = 2.57$, $p = 0.1229$) or time ($F_{1.746,\ 40.15} = 0.10$, $p = 0.8845$) in IL-1β treated slices at 9-11 months.

At 20-24 months, in IL-1β exposed slices, neither the area under the curve ($F_{1.828,\ 47.53} = 0.57$, $p = 0.5526$) nor the peak amplitude ($F_{1.674,\ 43.53} = 0.76$, $p = 0.4515$) were significantly affected by time. However, the peak frequency was significantly reduced with time in IL-1β-treated slices in both wildtype mice and APP/PS1 mice at 20-24 months ($F_{1.873,\ 48.70} = 8.47$, $p = 0.0009$). This reduction is also seen in untreated brain slices however.

In summary, in wildtype mice, exposure to IL-1β significantly inhibited the growth in oscillation amplitude, as it did in C57BL/6J mice at 3-4 months (Figure 3.15). In APP/PS1 mice exposure to IL-1β did not significantly impact the behaviour of oscillation amplitude, at 9-11 months it increased as normal and at 20-24 months it was stable as normal. Overall, the oscillation frequency was unaffected by treatment with IL-1β.

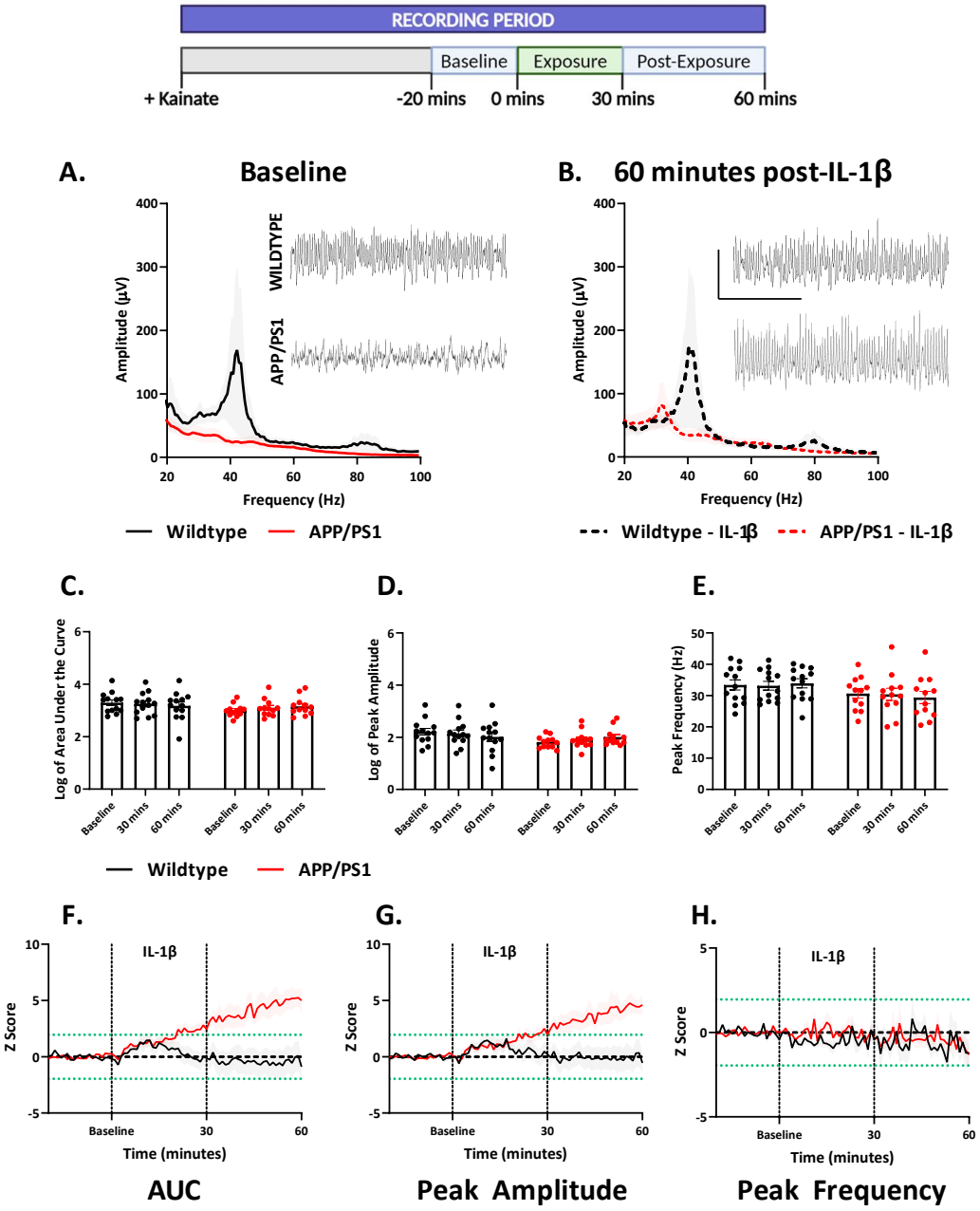

Figure 5.17. The effect of IL-1β on established gamma frequency oscillations in APP/PS1 mice at 9-11 months. (A,B) Pooled FFTs and representative traces for kainate-induced gamma frequency oscillations at (A) baseline and (B) 60 minutes post-baseline in brain slices from wildtype (black) and APP/PS1 (red) mice. FFT parameters: (C) area under the curve, (D) peak amplitude, (E) peak frequency across 60 minutes. 2-way ANOVA. (F, G, H) Z-scores of (C, D, E) respectively, dotted green line represents $p < 0.05$. Scale bar: 200 μV, 1 second. Wildtype: n = 39, N = 13, APP/PS1: n = 44, N = 12.

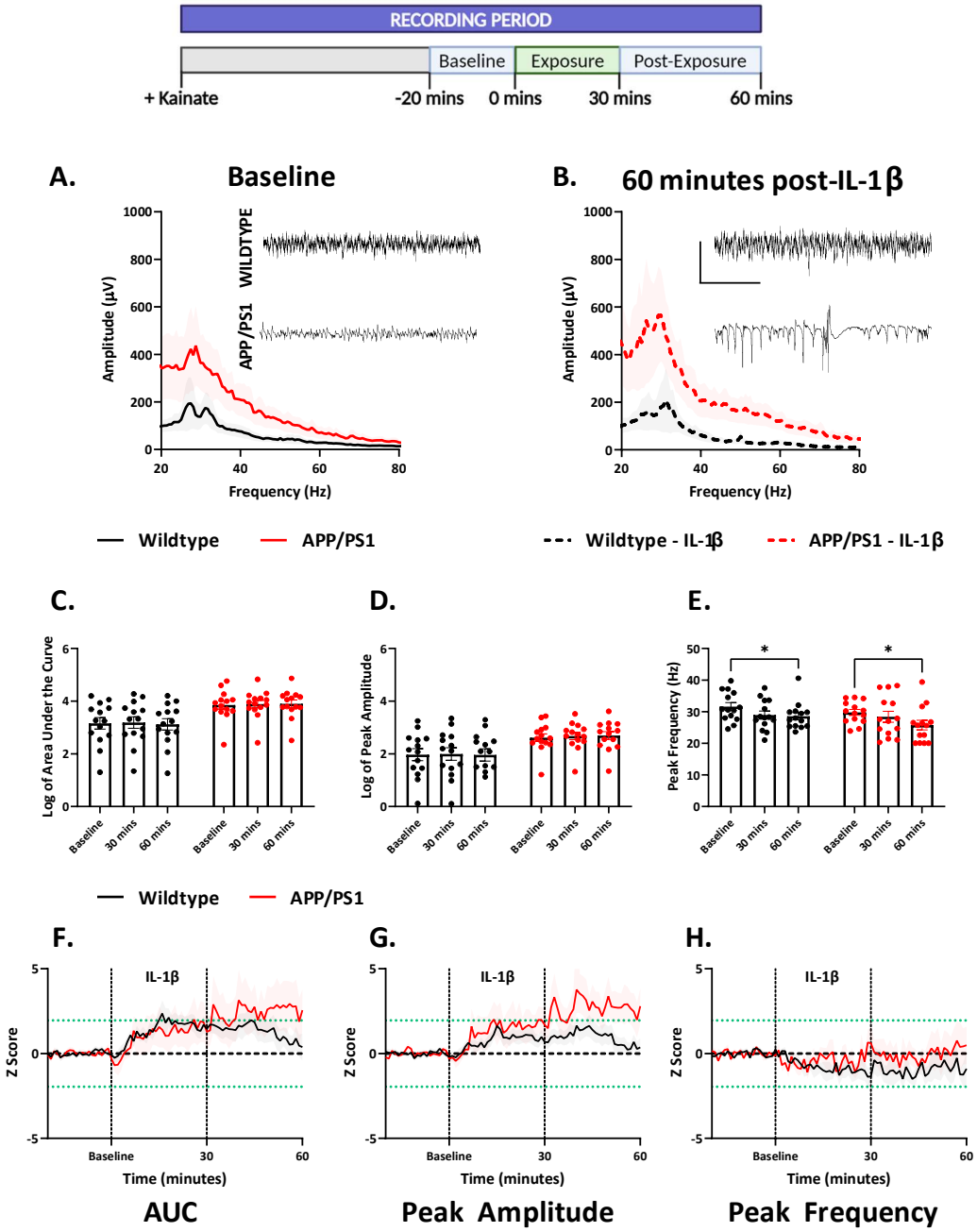

Figure 5.18. The effect of IL-1β on established gamma frequency oscillations in APP/PS1 mice at 20-24 months. (A,B) Pooled FFTs and representative traces for kainate-induced gamma frequency oscillations at (A) baseline and (B) 60 minutes post-baseline in brain slices from wildtype (black) and APP/PS1 (red) mice. FFT parameters: (C) area under the curve, (D) peak amplitude, (E) peak frequency across 60 minutes. 2-way ANOVA, post-hoc comparisons with Tukey correction in light text, * = $p < 0.05$. (F, G, H) Z-scores of (C, D, E) respectively, dotted green line represents $p < 0.05$. Scale bars: 1000 μV, 0.5 seconds. Wildtype: n = 44, N = 15, APP/PS1: n = 35, N = 12.

5.14. The effect of TNFα on gamma frequency oscillations in APP/PS1 mice

Established kainate-induced gamma frequency oscillations in brain slices from APP/PS1 mice and wildtype littermate controls at 9-11 months only were exposed to TNFα (10 ng/mL) for 30 minutes. The effect of this exposure was observed throughout the exposure and for a further 60 minutes.

As demonstrated, in untreated brain slices from APP/PS1 mice and wildtype littermate controls at 9-11 months, oscillation amplitude gradually increased over time (Figure 5.14). Following exposure to TNFα, the growth of oscillation amplitude was inhibited in brain slices from wildtype mice. This was demonstrated by the area under the curve (baseline: 13,072.47 ± 7,680.19 μV^2 Hz^-, 90 minutes post-TNFα: 12,146.37 ± 8,204.82 μV^2 Hz^-) and the peak amplitude (baseline: 1,404.56 ± 1,057.74 μV, 90 minutes post-TNFα: 758.407 ± 478.73 μV; Figure 5.19, E, F). This was similar to the inhibition of growth in oscillation amplitude by exposure to TNFα in C57BL/6J at 3-4 months (Figures 3.9 and 3.10). In brain slices from APP/PS1 mice exposure to TNFα did not affect the normal growth in oscillation amplitude. This was demonstrated by the area under the curve (baseline: 3,179.43 ± 1551.94 μV^2 Hz^-, 90 minutes post-TNFα: 6,448.44 ± 3,112.49 μV^2 Hz^-) and the peak amplitude (baseline: 158.51 ± 68.15 μV, 90 minutes post-TNFα: 321.11 ± 138.64 μV; Figure 5.19, E, F). There was no significant main effect of TNFα treatment on the area under the curve ($F_{1.84, 14.71} = 0.15$, $p = 0.8465$), or peak amplitude ($F_{1, 8} = 0.22$, $p = 0.8093$), however there was a significant interaction between genotype and treatment with TNFα for area under the curve ($F_{3, 24} = 3.27$, $p = 0.0387$), and a trend towards significance for the same interaction in peak amplitude ($F_{3, 24} = 2.18$, $p = 0.1164$). Thus, the previously characterised inhibition of the growth in oscillation amplitude did not occur in APP/PS1 mice.

In untreated brain slices from wildtype littermate controls oscillation peak frequency is slightly reduced over time. While, in untreated brain slices from APP/PS1 mice oscillation peak frequency is relatively stable over time. Exposure to TNFα decreased oscillation peak frequency in brain slices from APP/PS1 mice and wildtype littermate controls (wildtype: baseline: 27.74 ± 1.69 Hz, 90 minutes post-TNFα: 25.76 ± 2.46 Hz, APP/PS1: baseline: 26.67 ± 3.06 Hz, 90 minutes post-TNFα: 21.88 ± 1.38 Hz; Figure 5.19, G). This overall reduction in oscillation frequency following TNFα treatment was demonstrated by the trend towards a significant reduction in peak frequency ($F_{2.02, 16.18} = 2.71$, $p = 0.0965$). There were no interactions between this effect and genotype ($F_{3, 24} = 1.05$, $p = 0.3895$).

Therefore, in summary, exposure to TNFα inhibited the normal growth in oscillation amplitude in brain slices from wildtype mice, but not from APP/PS1 mice. This was similar to the effect observed for IL-1β (Figure 5.17). Exposure to TNFα also reduced the oscillation peak frequency in both APP/PS1 mice and wildtype littermate controls.

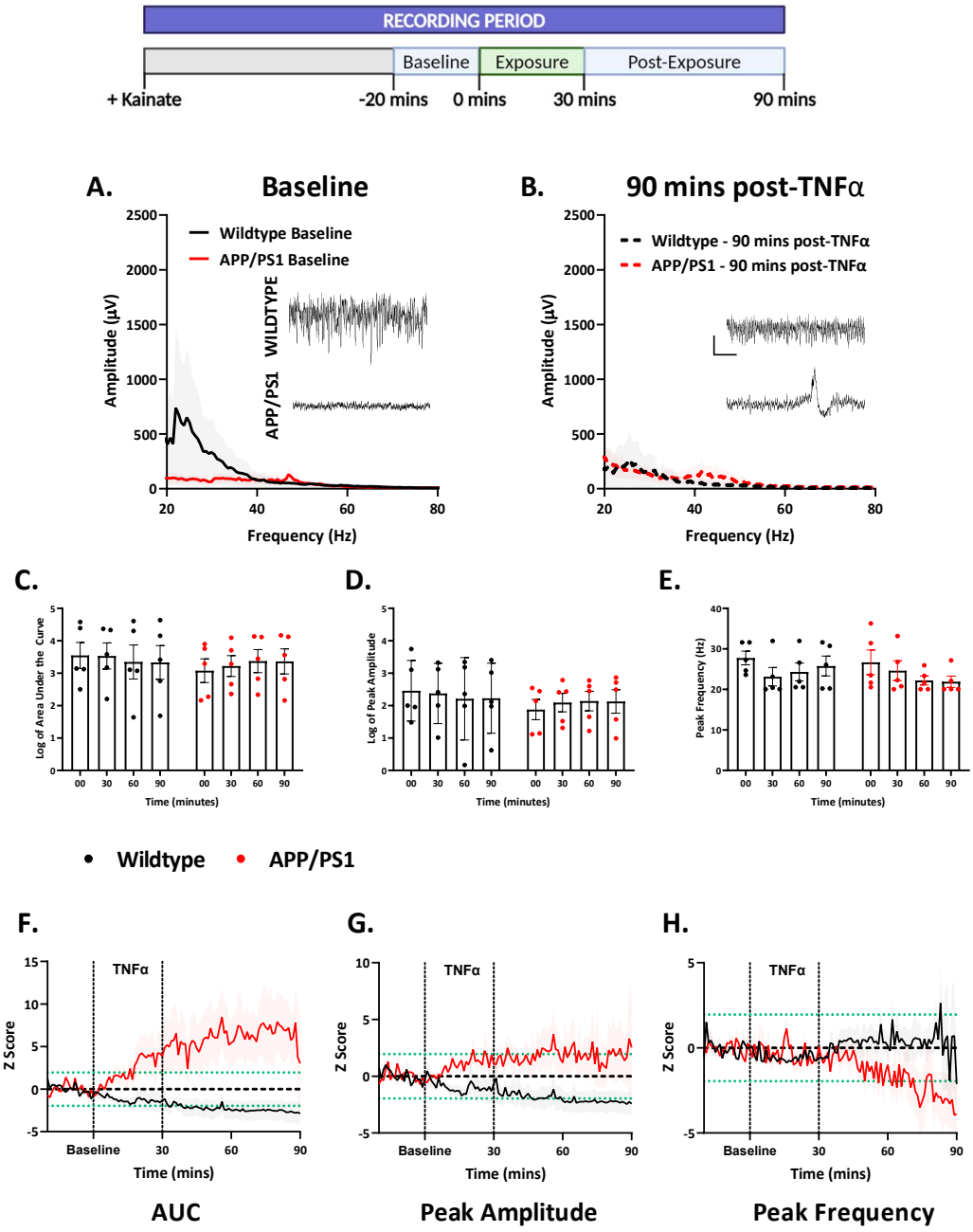

Figure 5.19. The effect of TNFα on established gamma frequency oscillations at in APP/PS1 mice 9-11 months. (A,B) Pooled FFTs and representative traces for kainate-induced gamma frequency oscillations at (A) baseline and (B) 60 minutes post-baseline in brain slices from wildtype (black) and APP/PS1 (red) mice. FFT parameters: (C) area under the curve, (D) peak amplitude, (E) peak frequency across 90 minutes. 2-way ANOVA, post-hoc comparisons with Tukey correction in light text, * = $p < 0.05$. (F, G, H) Z-scores of (C, D, E) respectively, dotted green line represents $p < 0.05$. Scale bar: 1000 μV, 0.5 seconds. Wildtype, n = 5, N = 5; APP/PS1 control, n = 5, N = 5.

5.15. The effect of suppressing TNFα on gamma frequency oscillations in APP/PS1 mice

Established kainate-induced gamma frequency oscillations in brain slices from APP/PS1 mice and wildtype littermate controls at 9-11 months were exposed to an anti-TNFα antibody (100 ng/mL) for 90 minutes. The sample size was relatively small in this experiment therefore conclusions should be moderated, however, it seemed that suppressing TNFα appeared to reduce the growth in oscillation amplitude and possibly reduced oscillation frequency.

In untreated brain slices from both APP/PS1 mice and wildtype littermate controls oscillation amplitude grew over time (Figure 5.14). In brain slices exposed to anti-TNFα antibody oscillation amplitude was reduced over, most notably in brain slices from APP/PS1 mice. This was demonstrated by the area under the curve (wildtype: baseline: 3,634.72 ± 1,724.75 $\mu V^2 Hz^-$, 90 minutes post-anti-TNFα: 2,808.33 ± 1,917.22 $\mu V^2 Hz^-$, APP/PS1: baseline: 187.10 ± 136.48 $\mu V^2 Hz^-$, 90 minutes post-anti-TNFα: 72.07 ± 32.45 $\mu V^2 Hz^-$) and peak amplitude (wildtype: baseline: 104.40 ± 54.54 μV, 90 minutes post-anti-TNFα: 212.99 ± 100.74 μV, APP/PS1: baseline: 11.51 ± 8.65 μV, 90 minutes post-anti-TNFα: 4.54 ± 2.21 μV; Figure 5.20, E, F).

In untreated brain slices oscillation peak frequency was slightly reduced in brain slices from wildtype mice and relatively stable in brain slices from APP/PS1 mice. In brain slices exposed to anti-TNFα antibody the peak frequency was slightly reduced (wildtype: baseline: 32.45 ± 6.94 Hz, 90 minutes post-anti-TNFα: 27.44 ± 3.65 Hz, APP/PS1: baseline: 26.06 ± 2.01 Hz, 90 minutes post-anti-TNFα: 23.41 ± 2.04 Hz; Figure 5.20, G).

Therefore, suppressing TNFα in brain slices from APP/PS1 mice and wildtype littermate controls inhibited the normal growth in oscillation amplitude, most notably in APP/PS1 mice. Exposure to anti-TNFα antibody did not notably affect oscillation peak frequency.

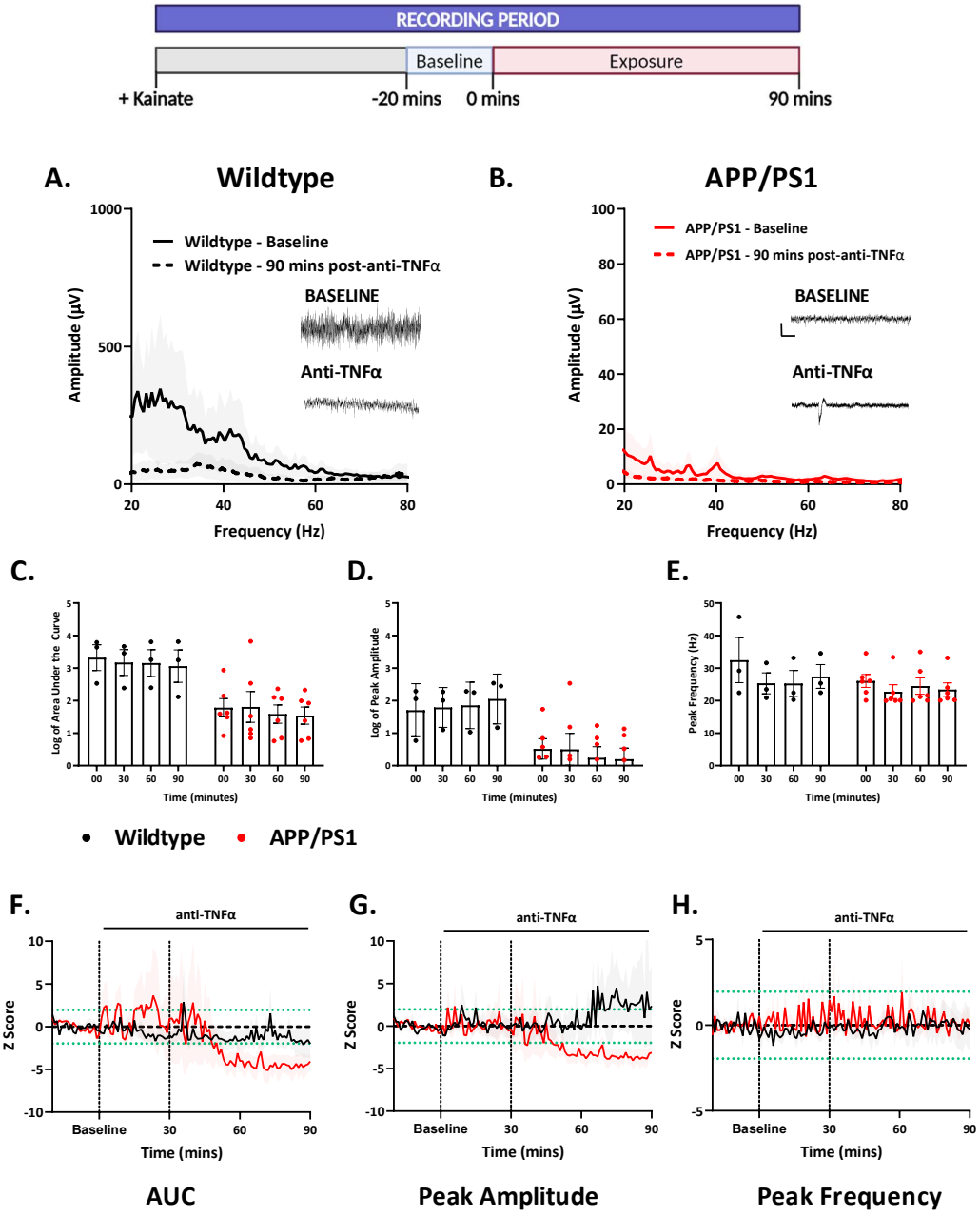

Figure 5.20. The effect of suppressing TNFα on gamma frequency oscillations in APP/PS1 mice at 9-11 months. (A-D) FFTs pooled and representative traces at baseline (solid lines) and at 90 minutes post-anti-TNFα antibody (100 ng/mL) treatment (dashed lines) for (A, B) wildtype (black) and (C, D) APP/PS1 (red) mice on a (A, C) control diet (solid circles/lines) and a (B, D) GW2580-supplemented diet (empty circles/dashed lines; estimated dose 3.5 mg/day). (E) Area under the curve, (F) peak amplitude, (G) peak frequency from FFTs. Data in E and F are log transformed. (H, I, J) Z-scores of (E, F, G) respectively, dotted green line represents $p < 0.05$. Scale bar: 1000 μV, 0.5 seconds. Wildtype control, n = 3, N = 3, wildtype GW2580, n = 6, N = 6, APP/PS1 control, n = 6, N = 6, APP/PS1 GW2580, n = 7, N = 7.

Discussion

In APP/PS1 mice treatment with CSF1R inhibitor GW2580, was shown to: reduce microglial proliferation and reactivity proximal to amyloid-beta plaques, reduce astrocyte reactivity proximal to amyloid-beta plaques, and increase the amplitude and incidence of epileptiform events in kainate-induced gamma frequency oscillations. Treatment with GW2580 did not reverse the behavioural task deficits observed in APP/PS1 mice.

In brain slices from APP/PS1 mice exposure to the pro-inflammatory mediators IL-1β and TNFα did not inhibit the normal growth in oscillation amplitude, as they did in brain slices from wildtype littermate controls and from C57BL/6J mice at 3-4 months (chapter 3). Suppressing TNFα using an anti-TNFα antibody appeared to inhibit the normal growth in oscillation amplitude in both APP/PS1 mice and wildtype littermate controls.

The effects of GW2580 treatment on microglia

In order to investigate the extent to which alterations in gamma frequency oscillations in APP/PS1 mice were due to changes in the immune system, microglial proliferation was inhibited by treatment with GW2580, an inhibitor of CSF1R. This treatment was well-tolerated in wildtype and APP/PS1 mice. This treatment also successfully reduced microglial proliferation in APP/PS1 mice. In areas proximal to amyloid-beta plaques, microglial number was shown to be reduced by treatment with GW2580 in APP/PS1 mice. This was demonstrated by staining microglial nuclei with PU.1. Treatment with GW2580 therefore replicated the reduction in microglia seen previously (Conway et al., 2005).

Further to reducing microglia proliferation, GW2580 treatment reduced microglial reactivity in areas of the hippocampus with high plaque burden (the dentate gyrus and CA1 subregion). The reduction in microglial reactivity was demonstrated by labelling Iba1 using

immunohistochemistry. This reduction in reactive microglia following GW2850 treatment has been seen in a variety of models, including the APP/PS1 Alzheimer's disease model, spinal cord injury models, white matter disease models, and Parkinson's disease models (Askew et al., 2024; Neal et al., 2020; Olmos-Alonso et al., 2016; Perez et al., 2023). This suggests that the microglial proliferation response to the emergence of amyloid-beta plaque pathology was dampened by inhibition of CSF1R. Others have shown that this reduction in reactivity is accompanied by a reduction in phagocytosis (Askew et al., 2024).

The effect of GW2580 treatment on microglia was further demonstrated using qPCR to investigate gene expression in microglia isolated by FACS from these mice. Previously, qPCR was used to investigate the effect of GW2580 treatment on various markers of the DAM phenotype and other markers of microglial reactivity. It was shown that these DAM and reactivity markers (*Itgax*, *Clec7a*, *Apoe*, *Lpl*, *Cstd, Cst7)* had increased expression in APP/PS1 mice and trended towards a reduction following treatment with GW2580 (Islam, 2022). Here, it was shown that the expression of various pro-inflammatory mediators (*Tnfa*, *Ccl3*, *Ccl4*, and *Cxcl10*) was increased in APP/PS1 mice and non-significantly reduced by GW2580 treatment. This was consistent with the observation made by immunohistochemistry that GW2580 treatment reduced microglial reactivity. These analyses of gene expression indicated that beyond simply limiting the proliferation of microglia, the inhibition of CSF1R via GW2580 also appeared to alter microglial phenotype.

It should be noted that interpretation of this gene expression analysis in microglia is limited by the relatively small sample size. This was due to difficulties in the FACS-isolation of microglia; however, these difficulties were not more common in any of the experimental groups therefore it is unlikely they have introduced any bias into the study.

The effects of GW2580 treatment on astrocytes

The reduction in microglial reactivity following GW2580 treatment was accompanied by a reduction in astrocyte reactivity. This was demonstrated by labelling GFAP using immunohistochemistry. A reduction in astrocyte reactivity following a reduction in microglial reactivity is unsurprising as reactive microglia are among the primary inducers of reactive astrocytes (Liddelow et al., 2017). The effects of GW2580 treatment on astrocytes have not been widely studied. In a model of spinal cord injury astrocyte reactivity was reduced following GW2580 treatment (Gerber et al., 2018). However in models of epilepsy and Parkinson's disease treatment with GW2580 had no effect on astrocyte reactivity (Di Nunzio et al., 2021; Neal et al., 2020).

The effect of GW2580 treatment on astrocyte reactivity was not seen at the level of gene expression. Astrocytes isolated from APP/PS1 mice (using FACS) had an increase in reactivity, as demonstrated by the increased expression of reactivity markers (*Gfap*) and the reduced expression of metabolic genes and homeostatic markers (*Glut1*, *Glul*, *Hes5*)(Escartin et al., 2021; Liddelow et al., 2017). These changes in gene expression may be indicative of both an increase in reactivity and a loss of function. Although limited in scope, the reduced expression of metabolism-related genes in APP/PS1 mice is consistent with the idea that astrocytes may be metabolically exhausted and may no longer properly support neurons. This is referred to astrocyte asthenia (Verkhratsky et al., 2021). This could be further investigated by morphological analysis of astrocytes, as asthenic astrocytes are often hypertrophic (Verkhratsky et al., 2023).

Therefore, at the level of gene expression astrocytes reactivity and impairment were increased in APP/PS1 mice. However, the reduction in astrocyte reactivity following GW2580 treatment was not seen at the level of gene expression, as it was when GFAP was labelled using immunohistochemistry. This may be because FACS-isolated astrocytes are from across the entire

hippocampus, whereas GFAP-labelled astrocytes were quantified in areas proximal to amyloid-beta plaques. Amyloid-beta plaques cause the increase in microglial reactivity and subsequent increase in astrocyte reactivity. Therefore, astrocytes proximal to amyloid-beta plaques can be expected to have the greatest increase in reactivity and the greatest effect of GW2580 treatment. Elevated expression of C*xcl10* is a well-recognised marker of astrocyte reactivity (Liddelow et al., 2017; Matusova et al., 2023). Therefore, it is surprising that this chemokine was not detected in APP/PS1 mice and perhaps indicative of suboptimal isolation of astrocytes, whether this was through insufficient selectivity in isolation of reactive astrocytes or possibly even a bias against the selection of reactive astrocytes.

It is possible that the method used to isolate astrocytes introduces a selection bias to the astrocyte population. In the method used, astrocytes were isolated based on the expression of the glutamate aspartate transporter 1 (GLAST1). This may lead to a certain subpopulation of astrocytes being isolated based on differential GLAST1 expression. Indeed it has been reported that GLAST1 expression is reduced in various Alzheimer's disease models (Burnyasheva et al., 2023; Cassano et al., 2012). Therefore it is possible that sorting based on GLAST1 expression is less successful at isolating amyloid-activated astrocytes and therefore selects an unrepresentative subpopulation of astrocytes. This may account for the failure to detect the expression of many pro-inflammatory mediators such as *Ccl2*, *Tnf*, and C*xcl10*.

Overall, the microglia and astrocyte reactivity was increased in APP/PS1 mice – this was demonstrated by both immunohistochemistry and qPCR. Treatment with GW2580 reduced microglial proliferation and reactivity, based on both immunohistochemistry and gene expression analysis by qPCR. GW2580 appeared to reduce astrocyte reactivity, based on GFAP expression, however gene expression analysis by qPCR showed no effect of GW2580 on astrocytes.

The effects of GW2580 treatment on behaviour

A deficit was observed in APP/PS1 mice relative to wildtype littermate controls in both a spontaneous alternation task and in learning in the MWM. Specifically, in the spontaneous alternation task, APP/PS1 mice alternated at a rate of approximately 65%, while wildtype littermate controls alternated at a rate of approximately 80%. This deficit in a spontaneous alternation task is well established by the field (Table 5.2). The rate of alternation seen here in APP/PS1 was not as low as the rate seen by others at 9-10 months; rates as low as 45% and 50% have been observed at this age. However, the alternation rates observed in control mice were also reduced in these studies, relative to the rate observed here in wildtype littermate controls (Gong et al., 2020; Yuan et al., 2021). Therefore, the magnitude of the deficit in spontaneous alternation observed here is consistent with previous observations in the field.

Age	Control Rate	APP/PS1 Rate	Reference
6 months	76.7%	50%	(Filali & Lalonde, 2009)
8 months	76.6 ± 2%	59.7 ± 5%	(Zhang et al., 2020)
9 months	70%	43.3%	(Filali & Lalonde, 2009)
9 months	60%	55%	(Olesen et al., 2017)
9 months	60%	45%	(Yuan et al., 2021)
9 months	65%	50%	(Gong et al., 2020)
12 months	65.3 ± 4%	54.8 ± 2%	(Deacon et al., 2008)
12 months	63.3%	33.3%	(Filali & Lalonde, 2009)
12.5 months	60%	60%	(Othman et al., 2023)
14 months	60%	60%	(L. Liu et al., 2002)

Table 5.2. Spontaneous alternation rates in APP/PS1 mice.

Similarly, the observed deficit in APP/PS1 mice in learning in the MWM is well established by the field (Table 5.3). The learning observed here was notably better than that seen in several other

studies carried out at 9-10 months. In APP/PS1 mice the latency to platform on day 5 of training was approximately 24 seconds, while in wildtype littermate controls it was approximately 16 seconds. This is notably lower relative to some other studies at this age which observed latencies of 37 seconds in controls and 47 seconds in APP/PS1 mice (Lok et al., 2013). Although the extent of learning in both APP/PS1 mice and wildtype littermate controls differed from other studies, the magnitude of the learning deficit observed here was broadly consistent with the findings of others (approximately a 10 second deficit in latency to platform). Given this deficit was relatively small, detecting a statistically significant reduction of that deficit by GW2580 was challenging.

Age	Control Latency	APP/PS1 Latency	Reference
3 months	20 seconds	22 seconds	(Lonnemann et al., 2023)
8 months	30 seconds	40 seconds	(B. Liu et al., 2020)
8 months	21 seconds	45 seconds	(Zhang et al., 2020)
8-9 months	22 seconds	30 seconds	(Gallagher et al., 2012)
9 months	37 seconds	47 seconds	(Lok et al., 2013)
10 months	20 seconds	40 seconds	(Velazquez et al., 2019)
12 months	40 seconds	50 seconds	(Mifflin et al., 2021)
12 months	27 seconds	52 seconds	(Li et al., 2023)
12 months	17 seconds	37 seconds	(Lonnemann et al., 2023)
17 months	15 seconds	30 seconds	(L. Liu et al., 2002)

Table 5.3. Learning in the MWM in APP/PS1 mice.

There were no significant effects of GW2580 treatment on either behavioural task. There was a modest trend towards improvement in the spontaneous alternation task in APP/PS1 mice following treatment with GW2580. The reported effect of GW2580 treatment, and other CSF1R inhibitors, on various behavioural tasks is mixed (Basilico et al., 2022). In APP/PS1 mice

at 9 months, 3 months of GW2580 treatment at 1000 ppm, reversed the deficit in a spontaneous alternation task. However in this study, in which it is difficult to establish the sample size (n = 8-21), the observed deficit in APP/PS1 mice was larger than the deficit observed here (50% alteration versus 65% alternation)(Olmos-Alonso et al., 2016). In the 3xTg Alzheimer's mouse model at 15 months, treatment with the CSF1R inhibitor, PLX5622 (for 3 months at 300 mg/kg), improved performance in a novel place recognition task, but not in novel object recognition, additionally, learning in the MWM was significantly improved by CSF1R inhibition (Dagher et al., 2015). This effect of CSF1R inhibition on learning in the MWM was not replicated here, however the Alzheimer's model used is different, as well as a different CSF1R inhibitor. In a more directly comparable study in which 12 month old APP/PS1 mice were treated with PLX5622 (1200 mg/kg) for 28 days there was no effect of CSF1R inhibition on learning in the MWM (Unger et al., 2018). Similarly, in the Alzheimer's mouse model 5XFAD at 7 months, after 6 months treatment with the CSF1R inhibitor PLX5622, there was no improvement in learning in the MWM (Spangenberg et al., 2019). Therefore, the failure to detect widespread improvement in various cognitive tasks following GW2580 treatment is by no means unique to the current study.

The failure of GW2580 treatment to improve learning in the MWM, and the modest effect of GW2580 on spontaneous alternation, may be due to the small magnitude of the deficit. The magnitude of the deficit is larger in the spontaneous alternation task, this may explain the trend towards in improvement in this task but not in the MWM task. In the MWM mice, despite learning more slowly, APP/PS1 mice did learn the location of the platform. This was demonstrated by the probe trial in which wildtype and APP/PS1 mice spend an equivalent amount of time in the platform which previously contained the platform. Therefore, the deficit in APP/PS1 mice was relatively small. As a result there is not a large window in which to see an effect of GW2580 treatment.

The effects of GW2580 treatment on gamma frequency oscillations

Kainate-induced gamma frequency oscillations were previously observed (in chapter 4) to have reduced amplitude and reduced frequency at 9-11 months in APP/PS1 mice. Following GW2580 treatment this amplitude reduction was largely reversed, however brain slices from these mice also had increased incidence of epileptiform events relative to control APP/PS1 mice. This suggests that inhibiting microglial proliferation had an impact on kainate-induced gamma frequency oscillations, but did not restore oscillations similar to those seen in wildtype mice. This large increase in kainate-induced gamma frequency oscillation amplitude and increased incidence of epileptiform events is suggestive of hyperexcitability. This is especially likely given the low frequency nature of this increased neuronal network activity. A thorough quantification of the frequency, amplitude, and length of this epileptiform activity is required to further establish the effect of GW2580 treatment in on neuronal network activity APP/PS1 mice.

It is possible, when considered alongside the work of others, that the observed changes in oscillation amplitude can be attributed to changes in microglial behaviour following GW2580 treatment. It has been shown that in Alzheimer's disease models microglia selectively target hyperactive synapses via TREM2-mediated recognition of exposed phosphatidylserine positive synapses (Rueda-Carrasco et al., 2023). This was shown in microglial-neuron cocultures and in a cross of the Alzheimer's mouse model (hAPP NL-F KI) and the TREM2 mutant (Trem2 R47H KI) at 6 months. It is plausible that this reduction in excitatory drive mediated via microglial phagocytosis is responsible for the reduced amplitude, and also frequency, of kainate-induced gamma frequency oscillations in control APP/PS1 mice at 9-11 months. Treatment with GW2580 may interfere with the targeting of hyperexcitable synapses by microglia. This is supported by the observation previously made in these mice that the expression of phagocytosis-related genes in microglia was reduced in APP/PS1 mice by GW2580 treatment. These genes

included *Trem2*, *Lpl*, and *Itgax* (Islam, 2022). It has been shown that mice which lacked TREM2, and presumably by extension reduced reactivity and ability to target and engulf hyperactive synapses, were found to have increased synaptic density and enhanced excitatory neurotransmission (Filipello et al., 2018). Similarly, in brain slices with microglia depleted by clodronate liposomes the frequency of excitatory post-synaptic currents was increased. This effect was reversed when microglia were replenished (K. Ji et al., 2013). Furthermore, in a more directly comparable study, in brain slices from mice treated with the CSF1R inhibitor PLX3397 (290 ppm for 3-4 weeks) the frequency of excitatory postsynaptic currents was almost doubled, but their amplitude was unchanged (Y.-J. Liu et al., 2021). It is therefore possible that treatment with GW2580, which reduces microglial proliferation and reactivity, may also reduce the capacity of microglia to target and engulf hyperexcitable synapses. This plausibly could lead to the emergence of neuronal hyperexcitability. This view is supported by the finding that in mice treated with the CSF1R inhibitor PLX3397 (2000 mg/kg for 30 days at 8 months) there was an increase in excitatory dendritic spine density throughout the brain (Rice et al., 2015). It is therefore possible to envision a situation in which an abundance of reactive microglia (in control APP/PS1 mice) overly-degrade excitatory synapses, while insufficient reactive microglia (following GW2580 treatment) leads to an accumulation of hyper-excitable synapses. In both instances, the excitatory-inhibitory balance of the neuronal network would be disturbed and gamma frequency oscillations would be disrupted.

The effect of CSF1R inhibition on neuronal networks has not been widely studied, however it has been described in other models of pathology. Broadly, in the few studies which have used GW2580 to modulate neuronal network activity, treatment with GW2580 does not notably affect neuronal network activity. In an acquired epilepsy model (induced by kainic acid injection) GW2580 treatment reduced the microglial proliferation normally seen in the model, but did not affect the onset or severity of epileptic seizures (Di Nunzio et al., 2021). Similarly, in a model of

traumatic brain injury (TBI), treatment with PLX5622 (another CSF1R agonist) did not reverse the TBI-associated deficits in intrinsic and synaptic excitability (Allen et al., 2020).

In summary, GW2580 treatment had a significant effect on kainate-induced gamma frequency oscillations in APP/PS1 mice at 9-11 months. One part of the two-fold deficit observed in APP/PS1 mice at this age was reversed by GW2580 treatment, namely the amplitude reduction was reversed, however the second part of this deficit was made worse, namely the epileptiform activity increased.

The effect of GW2580 treatment on carbachol-induced gamma frequency oscillations

The effect of treatment with GW2580 on gamma frequency oscillations was investigated also in carbachol-induced gamma frequency oscillations. Previously, it was observed that carbachol-induced gamma frequency oscillations were not successfully induced in APP/PS1 mice or wildtype littermate controls at 9-11 months. In order to investigate if this deficit could be reversed by reducing microglial proliferation, carbachol-induced gamma frequency oscillations were studied in control and GW2580-treated APP/PS1 mice or wildtype littermate controls. As before, carbachol-induced gamma frequency oscillations were not successfully established. This suggests that the deficits responsible for this failure to establish carbachol-induced gamma frequency oscillations were not due to the proliferation or reactivity of microglia. This is not surprising given the deficit was observed in wildtype littermate controls which do not have extensive microglial reactivity or proliferation. It has been suggested that cholinergic loss in Alzheimer's disease is caused by amyloid-beta plaques (Beach et al., 1997; Hampel et al., 2018). Treatment with GW2580 did not have any significant effect on amyloid-beta plaque burden in APP/PS1 mice, therefore it is perhaps not surprising that treatment with GW2580 did not improve carbachol-induced gamma frequency oscillations in APP/PS1 mice.

The relationship between electrophysiology and behaviour

Gamma frequency oscillations are known to be involved in short term memory (Siegel et al., 2009) and selective attention (Tiitinen et al., 1993). Therefore it is very probable that gamma frequency oscillations are required for optimal performance in the spontaneous alternation task and for learning in the MWM. Indeed, it has been shown that in an alteration task in the T-maze, similar to what was performed here, gamma frequency oscillation power, at the CA3-CA1 interface, is increased on the approach to the T-maze junction. This was proposed to coordinate and support memory retrieval (Montgomery & Buzsáki, 2007). Additionally, in a mouse model of schizophrenia, disrupted gamma frequency oscillations were associated with poor performance in a spontaneous alternation task. This deficit was reversed when gamma frequency oscillations were restored (by GSK3 inhibition) (Nakao et al., 2020). Similarly, the reduction of hyperexcitable gamma frequency oscillations in a mouse model of Fragile X syndrome using the $GABA_B$ receptor agonist, baclofen, also improved performance in a spontaneous alternation task (Sinclair et al., 2017). Finally, the inactivation of somatostatin interneurons using optogenetics caused a reduction in gamma frequency oscillation power and reduced performance in a spontaneous alternation task (Espinosa et al., 2019). Given the fact that mice swim in the MWM and the technical difficulties this presents for *in vivo* electrophysiology, gamma frequency oscillations have not been widely studied during this behavioural task. However, in a virtual-reality MWM task carried out in humans, spontaneous gamma power during awake rest correlated with spatial learning – those with the most spatial learning had the most septal hippocampal gamma frequency activity (Cornwell et al., 2014). In adult mice, CA3 gamma frequency oscillation power both *in vivo* and *ex vivo* (in brain slices induced by kainate (100 nM)) was correlated to performance in a Barnes mask task, which is similar to the MWM (C. B. Lu, Jefferys, et al., 2011). This demonstrated that gamma frequency oscillation power can be considered a neurophysiological index of spatial learning, and that *ex vivo* brain slices successfully

capture differences in both *in vivo* gamma frequency oscillations and behavioural performance. Based on these studies, which demonstrate the involvement of gamma frequency oscillations in both spontaneous alternation tasks and spatial reference learning, it seems very probable that the observed reductions in gamma frequency oscillation amplitude and frequency contribute to the deficient performance of APP/PS1 mice at 9-11 months in the spontaneous alteration task and learning in the MWM.

Following treatment with GW2580, gamma frequency oscillation amplitude was increased in APP/PS1 mice, but the oscillations also became more hyperexcitable. This incomplete restoration of gamma frequency oscillations may account for the relatively small effect of GW2580 treatment in the spontaneous alternation task and the absence of an effect on learning in the MWM. Given the reliance of these tasks on gamma frequency oscillations, it follows that partial restoration these oscillations should only partially reverse performance deficits in these tasks. Additionally, the increased emergence of epileptiform activity in GW2580-treated mice can be expected to have had a negative consequence on learning, based on the work of others in this field (Holley & Lugo, 2016; H. Liu et al., 2019).

The effect of IL-1β and TNFα exposure on established gamma frequency oscillations

The extent to which established kainate-induced gamma frequency oscillations in brain slices from APP/PS1 mice were sensitive to the pro-inflammatory mediators IL-1β (10 ng/mL) and TNFα (10 ng/mL) was investigated. It was shown in chapter 3 that these pro-inflammatory cytokines inhibited the normal growth in oscillation amplitude in brain slices from C57BL/6J mice at 3-4 months. It was not clear what was the mechanistic basis of this inhibition. It was further observed here that exposure to IL-1β and TNFα inhibited the growth of oscillation amplitude in brain slices from wildtype mice at 9-11 and 20-24 months (IL-1β only). This effect is likely via IL-1β and TNFα directly modulating the activity of neurons given the short time

scale of action. This is consistent with the long-observed effects of both IL-1β and TNFα on synaptic plasticity in the hippocampus. For example, both IL-1β and TNFα have been shown to inhibit LTP in the hippocampus (A. J. Cunningham et al., 1996; M. A. Lynch, 2015). Additionally, based on the Allen Brain Cell Atlas (Yao et al., 2023), TNFR1 has widespread expression on the immune cells of the brain and also on excitatory neurons. IL1R1 is also widely expressed on immune cells, especially on microglia, and on excitatory neurons; especially on the granule cells of the dentate gyrus. Therefore, based on the expression pattern of the receptors and the extensive literature which suggests a role in neuronal modulation for these cytokines (Nemeth & Quan, 2021; Park & Bowers, 2010), it seems probable that this inhibitory effect is mediated via direct action on neurons.

Exposure to IL-1β or TNFα did not have an effect on the growth of kainate-induced gamma frequency oscillation amplitude in APP/PS1 mice at 9-11 months or at 20-24 months (for IL-1β only). If anything, the pooled Fast Fourier transforms suggest that IL-1β promotes the emergence of a more defined gamma frequency oscillation in APP/PS1 mice. The effect of these exposures on the incidence and severity of epileptiform activity in APP/PS1 mice and wildtype littermate controls is an outstanding question however. It is not clear why treatment with IL-1β or TNFα should have a different effect on kainate-induced gamma frequency oscillations in APP/PS1 mice and in wildtype mice. As suggested in the previous chapter, IL-1β may inhibit the growth in kainate-induced gamma frequency oscillation amplitude by interfering with various synaptic plasticity mechanisms in wildtype mice. In APP/PS1 mice the baseline kainate-induced gamma frequency oscillations are significantly different to those in wildtype mice, therefore it is perhaps reasonable that they should not respond in the same manner to treatment with IL-1β or TNFα. The environment of the brain slice is also significantly different in APP/PS1 mice. It is possible that the widespread changes in microglia and astrocytes, as a result of the Alzheimer's-like pathology in APP/PS1 mice, impedes the effect of treatment with IL-1β or TNFα on gamma

frequency oscillations. Without further investigation it is difficult to comment on this observation. Nevertheless, it is clear that in addition to alterations in kainate-induced gamma frequency oscillations in APP/PS1 mice, kainate-induced gamma frequency oscillations in APP/PS1 mice do not respond in the same manner as those in wildtype mice to treatment with IL-1β or TNFα.

Despite the high possibility that the effects of both IL-1β and TNFα are mediated via there was some evidence that the effect of TNFα on the growth in oscillation amplitude may involve microglia. In control mice (both here and in chapter 3) exposure to TNFα reduced the normal growth in oscillation amplitude, but in brain slices from GW2580-treated wildtype mice TNFα no longer had any effect on the normal growth in oscillation amplitude (data presented in appendix, Figure 5.A.6). Therefore, following GW2580 treatment, TNFα no longer inhibited the growth of oscillation amplitude in wildtype mice. This may be due to differences in microglial activity or phenotype induced by GW2580. There was no suggestion here that microglial number was reduced in wildtype littermate controls treated with GW2580. However, other investigations made in this study have shown a reduction in synaptic density in wildtype littermate controls following GW2580 treatment (Islam, 2022). Therefore, it is plausible that GW2580 treatment impacted on neuronal network connectivity and this resulted in a differential response of network activity to TNFα. The ability of microglia to influence neuronal via TNFα has been suggested previously. In model of chronic pain, LTP was shown to be dependent on TNFα and on the presence of reactive microglia (Y. Liu et al., 2017). Therefore it is quite plausible that the inhibitory effect of exposure to TNFα on kainate-induced gamma frequency oscillation amplitude growth should involve microglia also.

In summary, exposure to the pro-inflammatory cytokines IL-1β and TNFα reduced the normal growth in oscillation in amplitude in brain slices from wildtype mice but not from APP/PS1 mice. Therefore, gamma frequency oscillations were not only impaired in brain slices from APP/PS1

mice, they also did not respond to IL-1β and TNFα in the same manner as brain slices from control mice.

The effect of suppressing TNFα on established gamma frequency oscillations

Given observed effects of GW2580 treatment on gamma frequency oscillations in APP/PS1 mice, the effect of suppressing TNFα were investigated using an anti-TNFα antibody (100 ng/mL). It was hypothesised that suppressing TNFα would reverse some part of the APP/PS1-associated deficit in gamma frequency oscillations, in a manner similar to GW2580 treatment.

The concentration of anti-TNFα antibody was chosen based on the neutralisation dose of the antibody (0.15-0.75 μg/mL in the presence of 0.25 ng/mL recombinant Mouse TNF-α, this is a 600-30,000-fold excess of antibody to cytokine) and the expected concentration of TNFα present in the APP/PS1 brain. It is difficult to establish how much TNFα there is in the APP/PS1 brain, however based on reported findings it seems likely there is less than 100 pg/mL present (Y. Hu et al., 2022; Sahu et al., 2021; J. Sun et al., 2020). Therefore, at a concentration of 100 ng/mL, the anti- TNFα antibody is in a 1000-fold excess to expected levels of TNFα. This is well within the reported neutralisation dose of the antibody.

Exposure to anti-TNFα antibody appeared to reduce the normal growth in kainate-induced gamma frequency oscillation amplitude both APP/PS1 mice and wildtype littermate controls. Therefore, reducing neuroinflammation did not have a positive effect on gamma frequency oscillations in APP/PS1, although the effect of this treatment on epileptiform activity needs to be investigated. The inhibition of normal oscillation amplitude growth suggested that this phenomenon is actually reliant on TNFα; even though exogenously added TNFα inhibited that growth at concentrations of 1 ng/mL, 10 ng/mL, and 50 ng/mL. This may because the reduction in TNFα levels by the anti-TNFα antibody leads to a loss in the synaptic strengthening mechanisms (discussed in chapter 3) which underly the normal increase in oscillation amplitude

over time. This is supported by the finding that TNFα is required for the process of synaptic scaling (Heir et al., 2024; Stellwagen & Malenka, 2006). It is possible that TNFα is required for synaptic strengthening at low concentrations and that TNFα inhibits synaptic strengthening at high concentrations. This U-shaped response of neurons to cytokines and chemokines (in which they are required at low concentrations and inhibitory at high concentrations) has been previously described (Salvador et al., 2021).

It is also possible that the exposure of the brain slices in all experimental groups to the anti-TNFα antibody induces an immune response which leads to widespread disruption of the neuronal network activity. The anti-TNFα antibody binds to multiple molecules of TNFα which likely results in the formation of large multi-protein complexes (Horiuchi et al., 2010). It is not possible to determine therefore if the effects observed following exposure to the anti-TNFα antibody are due to a reduction in the activity of TNFα or the presence of large amounts of the anti-TNFα antibody. This could be investigated by exposing slices to an anti-TNFα antibody with impaired ability to bind TNFα.

In summary, suppressing TNFα did not appear to have a restorative effect on gamma frequency oscillations in APP/PS1 mice, as was predicted. The observation that normal oscillation growth was inhibited in brain slices with suppressed TNFα suggests a central role for TNFα in mediating the synaptic mechanisms which underly the growth of kainate-induced gamma frequency oscillations over time.

Conclusion

Gamma frequency oscillations were found to be sensitive to neuroinflammatory manipulation in APP/PS1 mice at 9-11 months. This was shown by reducing neuroinflammation (GW2580

treatment, anti-TNFα antibody treatment) and by increasing neuroinflammation (treatment with IL-1β and TNFα).

Treatment of APP/PS1 mice with GW2580 reduced the extent of microglial proliferation, reactivity, and, tentatively, cytokine production in APP/PS1 mice. Therefore, treatment with GW2580 had the intended effect of reducing microgliosis in the APP/PS1 brain. GW2580 treatment did not have significant effects on the performance of APP/PS1 mice in behavioural tasks. There were modest but non-significant improvements in performance in the spontaneous alternation task for GW2580-treated APP/PS1 mice and no improvement in learning in the MWM for APP/PS1 mice treated with GW2580.

This minimal effect of GW2580 treatment on the cognitive status of APP/PS1 mice may be accounted for the observed effects in kainate-induced gamma frequency oscillations. Gamma frequency oscillation amplitude, which was reduced in APP/PS1 mice at 9-11 months, was increased by GW2580 treatment. This amplitude increase, which occurred largely at low frequencies, as well as the increased incidence of epileptiform events, may represent a further increase in hyperexcitability in APP/PS1 treated with GW2580. This may be due to an disruption of the role microglia play in maintaining excitatory-inhibitory balance in the brain. Therefore, inhibiting microglial proliferation lead to the incomplete restoration of kainate-induced gamma frequency oscillations in APP/PS1 mice. The ability of neuronal networks to generate gamma frequency oscillations was clearly altered by the inhibition of microglia, however the activity generated was not directly comparable to the activity in wildtype littermate controls. There is possibly a sweet spot for the modulation of microglial behaviour which would lead to the complete restoration of gamma frequency oscillations. This would lie somewhere between the large increase in reactive microglia which prune excitatory synapses (as seen in APP/PS1 mice) and the reduction in reactive microglia which don't prune excitatory synapses and causes network hyperexcitability (as seen in GW2580-treated APP/PS1 mice).

Additionally, the inhibitory effect of IL-1β and TNFα on gamma frequency oscillation growth was lost in APP/PS1 mice. This suggests that gamma frequency oscillations in APP/PS1 mice are not sensitive to increased neuroinflammation as in control mice. This suggests a further dysfunction in this neuronal network activity in APP/PS1 mice.

Overall, these findings highlight the complexity of the interactions between the immune system and neuronal networks and the difficulty of modulating these interactions in a manner that leads to improved network activity.

Appendix

5.A.1 Microglia and astrocyte homeostatic genes and purity marker genes

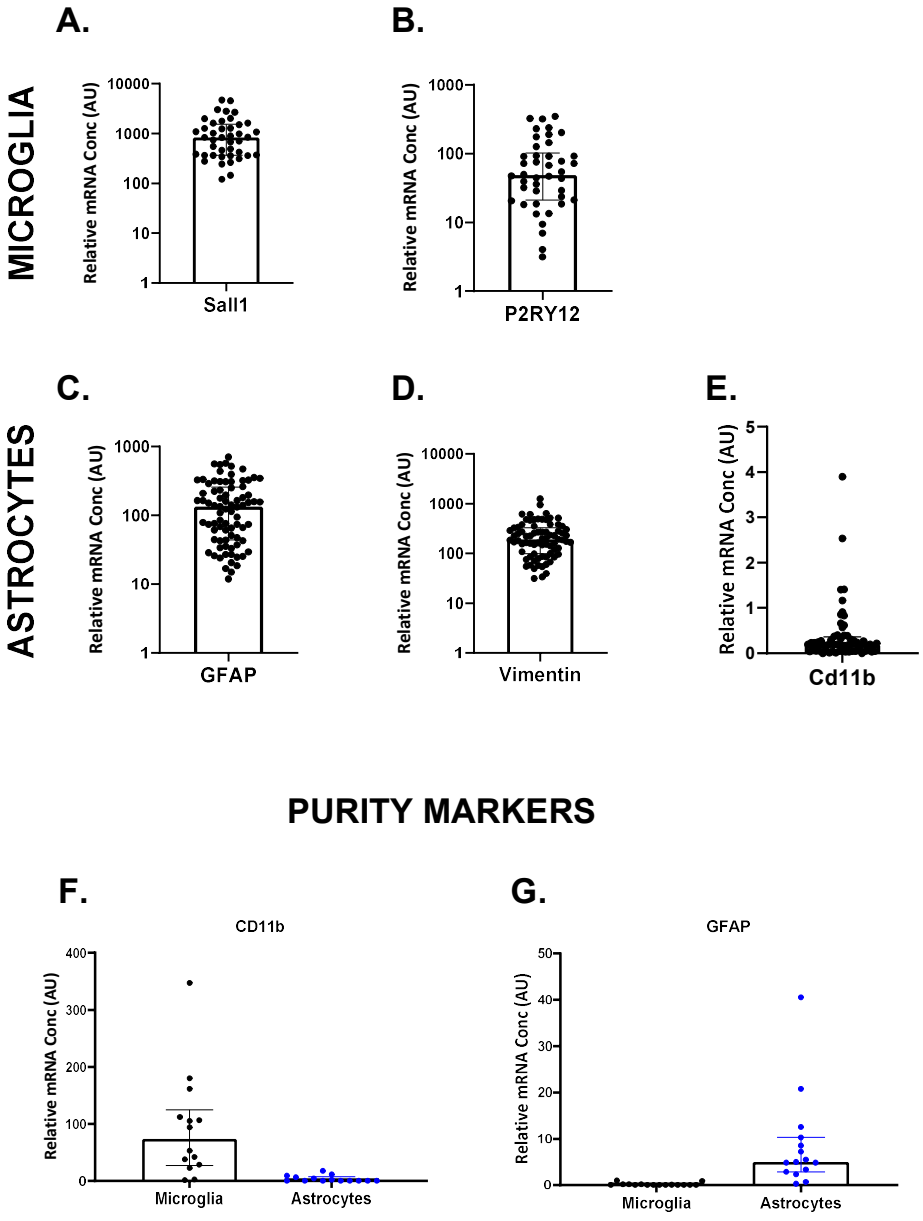

Figure 5.A.1 Homeostatic genes and purity markers in FACS-isolated microglia and astrocytes. Expression of microglia (*Sall1*, *P2ry12, Cd11b*) and astrocytes (*Gfap*, *Vimentin*) homeostatic markers in FACS-isolated microglia and astrocytes. (A-E) Microglia, N = 42, Astrocytes, N = 80; (F, G) Microglia, N = 14, Astrocytes, N = 14.

5.A.2 Astrocyte metabolic genes correlated to *Cxcl1* expression

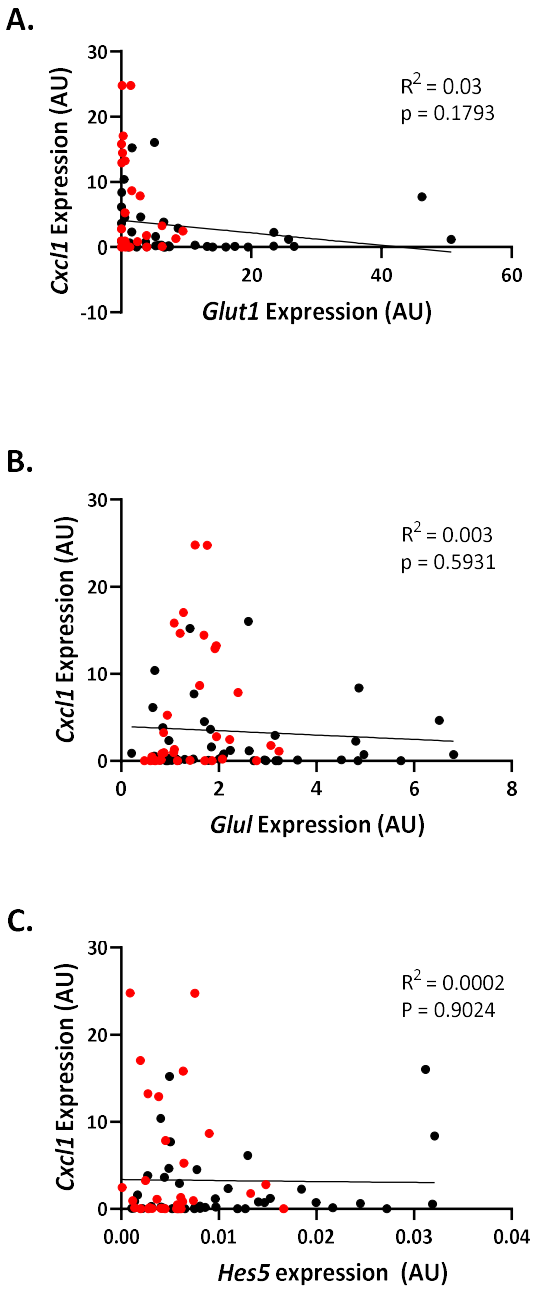

Figure 5.A.2. Correlation between *Cxcl1* expression and metabolic gene expression – (A, B) *Glut1*, (C, D) *Glul*, (E, F) *Hes5* – in FACS-isolated astrocytes from APP/PS1 mice (red circles) and wildtype littermate controls (black circles). Simple linear regression. APP/PS1: N = 36, Wildtype: N = 44.

5.A.3. The effect of IL-1β on carbachol-induced gamma frequency oscillations

Established carbachol-induced gamma frequency oscillations in brain slices from APP/PS1 mice and wildtype littermate controls at 9-11 and 20-24 months were exposed to IL-1β (10 ng/mL) for 30 minutes. The effect of this exposure was monitored during the exposure and for a further 30 minutes. Fast Fourier transforms were performed to quantify the oscillation amplitude (area under the curve and peak amplitude) and oscillation frequency (peak frequency). In order to account for the slice-to-slice variability z-scores were calculated for the three parameters extracted from the Fast Fourier transform (Figures 5.A.3 and 5.A.4).

No significant effects of IL-1β were observed for carbachol-induced gamma frequency oscillations in APP/PS1 mice or wildtype littermate controls.

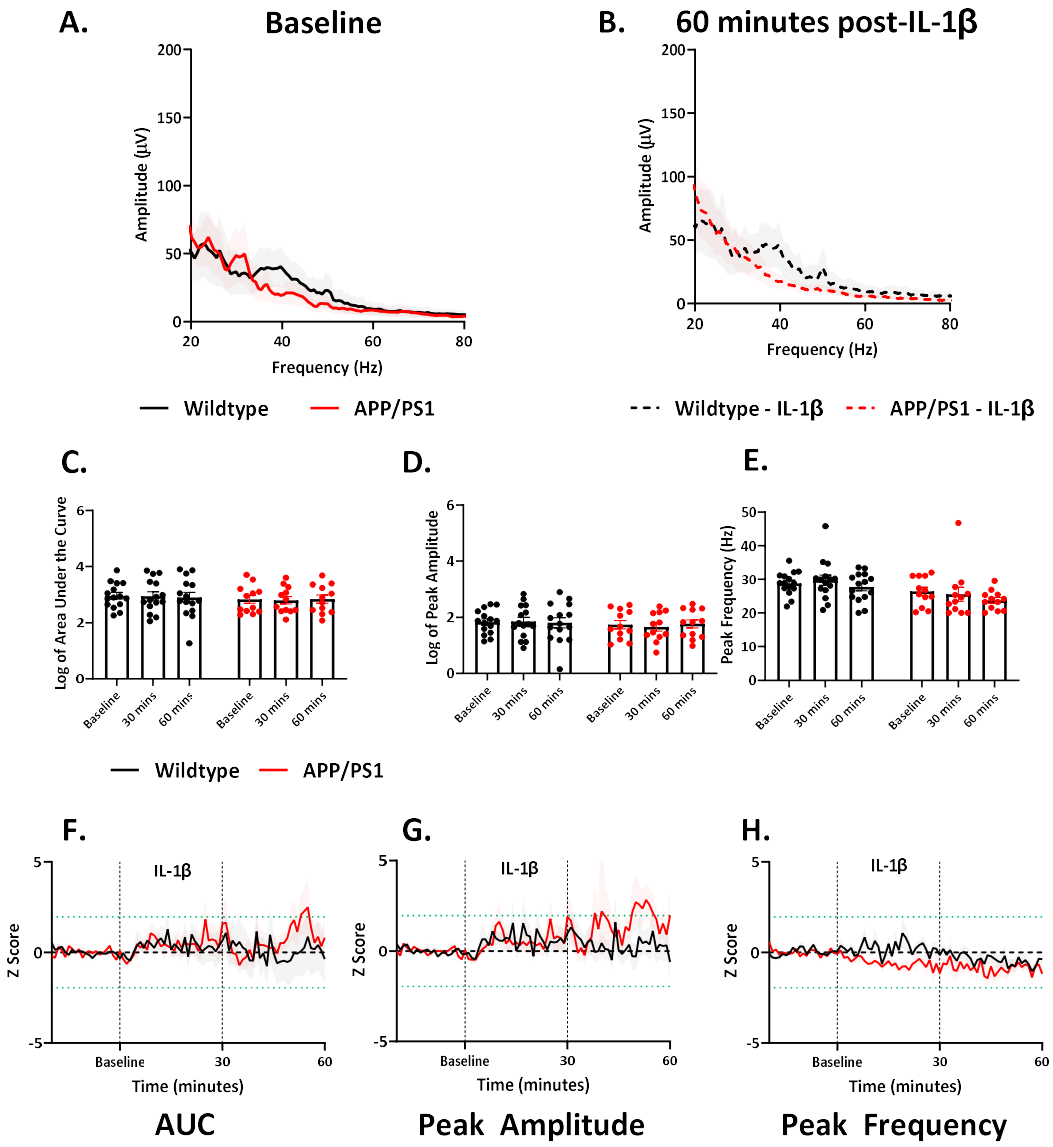

Figure 5.A.3. The effect of IL-1β on carbachol-induced gamma frequency oscillations in APP/PS1 mice at 9-11 months. (A,B) Pooled FFTs for kainate-induced gamma frequency oscillations at (A) baseline and (B) 60 minutes post-baseline in brain slices from wildtype (black) and APP/PS1 (red) mice. FFT parameters: (C) area under the curve, (D) peak amplitude, (E) peak frequency across 60 minutes. 2-way ANOVA. (F, G, H) Z-scores of (C, D, E) respectively, dotted green line represents $p < 0.05$. Wildtype: n = 44, N = 15, APP/PS1: n = 35, N = 12.

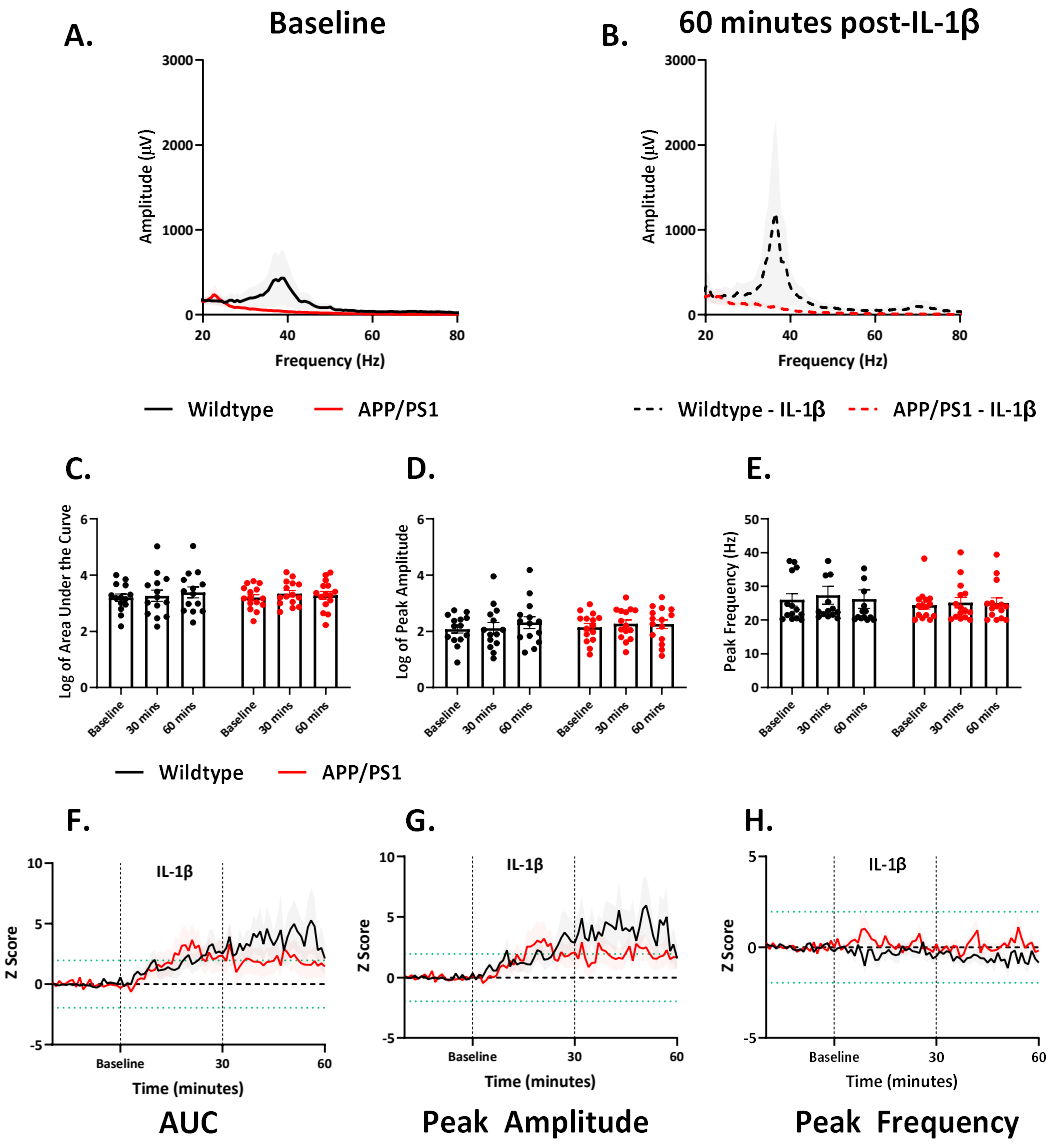

Figure 5.A.4. The effect of IL-1β on carbachol-induced gamma frequency oscillations at in APP/PS1 mice 20-24 months. (A,B) Pooled FFTs for kainate-induced gamma frequency oscillations at (A) baseline and (B) 60 minutes post-baseline in brain slices from wildtype (black) and APP/PS1 (red) mice. FFT parameters: (C) area under the curve, (D) peak amplitude, (E) peak frequency across 60 minutes. 2-way ANOVA. (F, G, H) Z-scores of (C, D, E) respectively, dotted green line represents $p < 0.05$. Wildtype: n = 33, N = 14, APP/PS1: n = 26, N = 15.

5.A.4. Carbachol-induced gamma frequency oscillations in GW2580-treated APP/PS1 mice

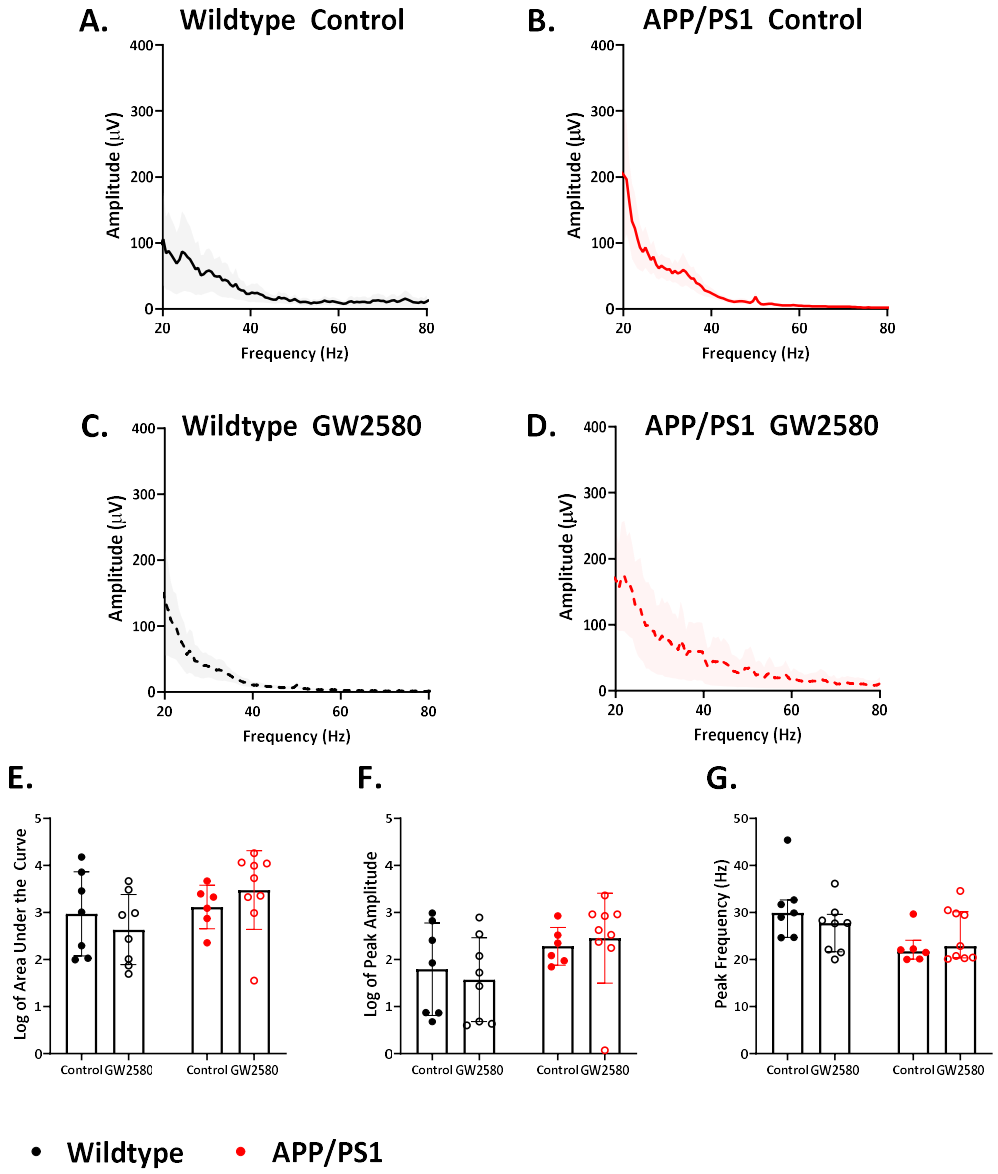

Figure 5.A.5. The effect of GW2580 treatment on carbachol-induced gamma frequency oscillations. (A-D) FFTs pooled and representative traces for (A, C) wildtype (black) and (B, D) APP/PS1 (red) mice on a (A, B) control diet (solid circles/lines) and a (C, D) GW2580-supplemented diet (empty circles/dashed lines; estimated dose 3.5 mg/day). (E) Area under the curve, (F) peak amplitude, (G) peak frequency from FFTs. Data in E and F are log transformed. WT control, n = 10, N = 7, WT GW2580, n = 13, N = 8, APP/PS1 control, n = 10, N = 6, APP/PS1 GW2580, n = 15, N = 9.

5.A.5. The effect of TNFα on gamma frequency oscillations in GW2580-treated APP/PS1 mice

Established kainate-induced gamma frequency oscillations in brain slices from control and GW2580-treated APP/PS1 mice and wildtype littermate controls were exposed to:

1. TNFα (10 ng/mL) for 30 minutes. The effect of this exposure was monitored throughout and for a further 60 minutes, as per the schematic below.

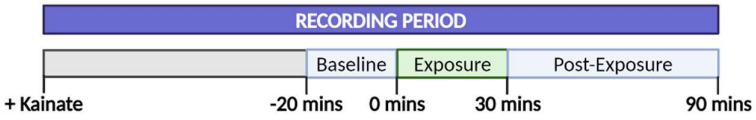

No significant differences were observed in the response of GW2580-treated brain slices to TNFα exposure, however in brain slices from GW2580-treated wildtype mice, TNFα did not inhibit the growth of oscillation amplitude, as it did in brain slices from control wildtype mice.

2. Anti-TNFα antibody (100 ng/mL) for 90 minutes. The effect of this exposure was monitored throughout, as per the schematic below.

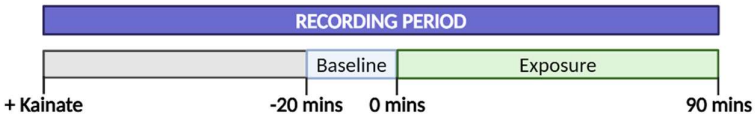

No notable or significant differences were observed in the response of GW2580-treated brain slices to anti-TNFα antibody exposure.

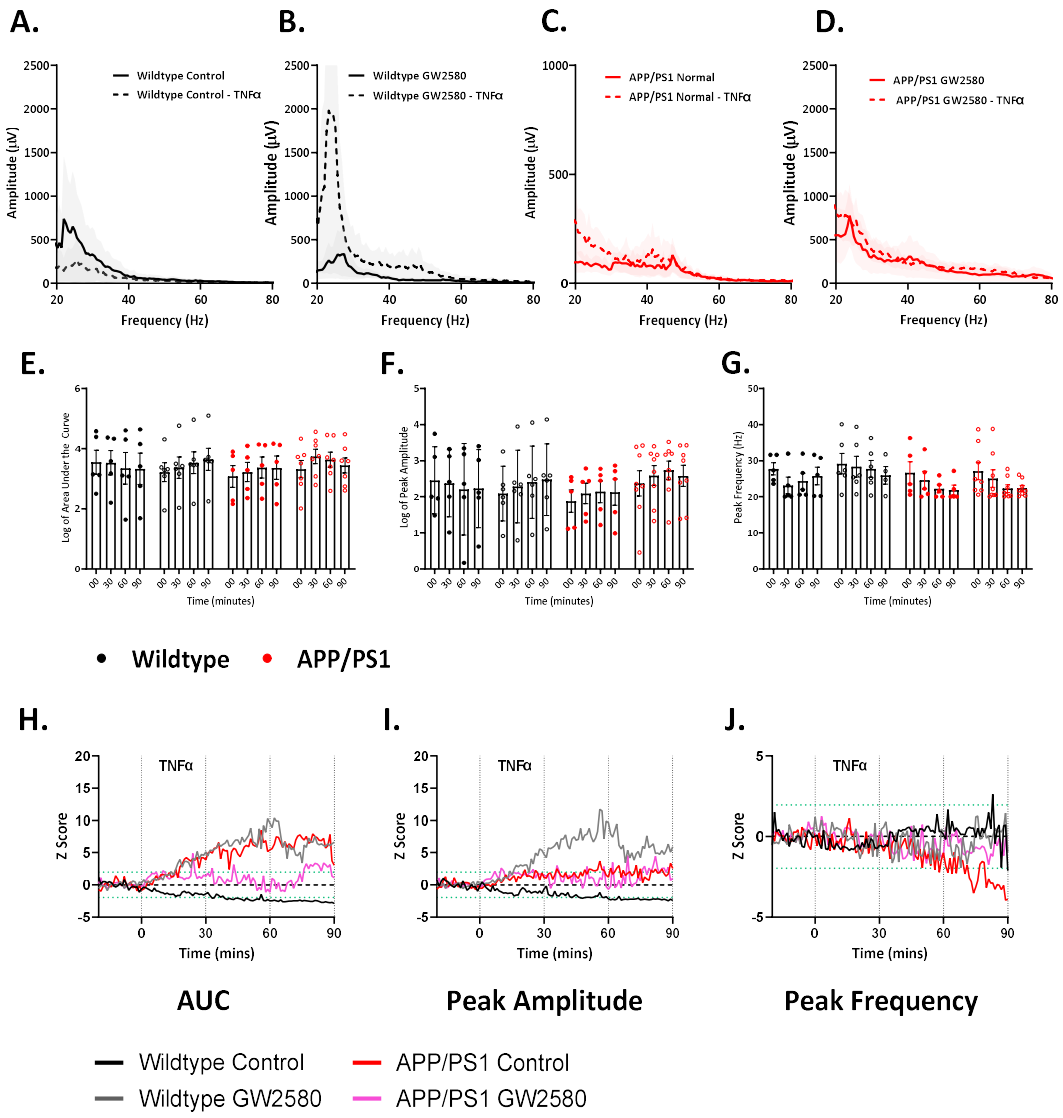

Figure 5.A.6. The effect of TNFα on gamma frequency oscillations in in control and GW2580-treated wildtype and APP/PS1 mice. (A-D) FFTs pooled at baseline (solid lines) and at 90 minutes post-TNFα (10 ng/mL) treatment (dashed lines) for (A, B) wildtype (black) and (C, D) APP/PS1 (red) mice on a (A, C) control diet (solid circles/lines) and a (B, D) GW2580-supplemented diet (empty circles/dashed lines; estimated dose 3.5 mg/day). (E) Area under the curve, (F) peak amplitude, (G) peak frequency from FFTs. Data in E and F are log transformed. 3-way ANOVA. (H, I, J) Z-scores of (E, F, G) respectively, dotted green line represents $p < 0.05$. Wildtype control, n = 5, N = 5, wildtype GW2580, n = 6, N = 6, APP/PS1 control, n = 5, N = 5, APP/PS1 GW2580, n = 8, N = 8.

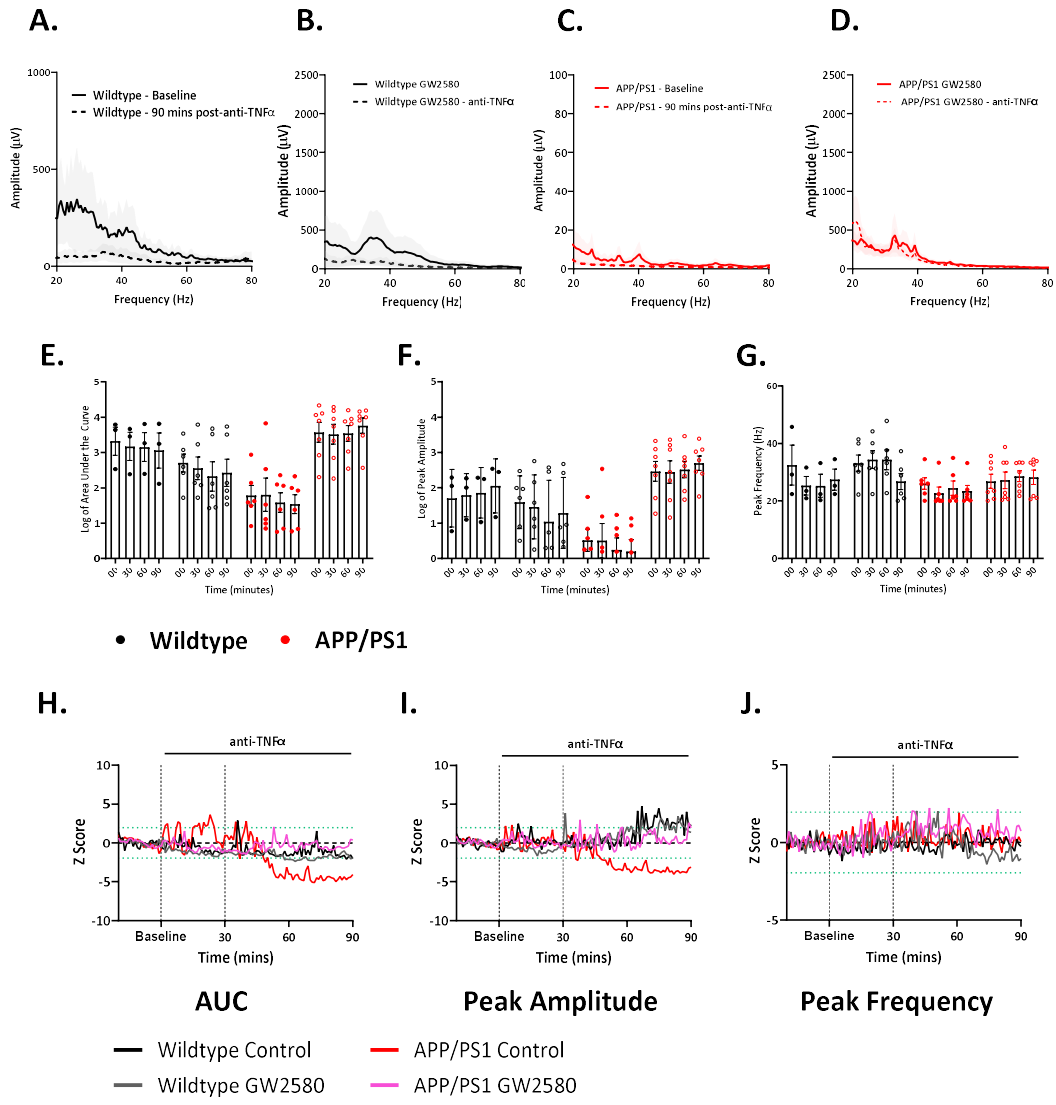

Figure 5.A.7. The effect of suppressing TNFα on gamma frequency oscillations in control and GW2580-treated wildtype and APP/PS1 mice. (A-D) FFTs pooled at baseline (solid lines) and at 90 minutes post-anti-TNFα antibody (100 ng/mL) treatment (dashed lines) for (A, B) wildtype (black) and (C, D) APP/PS1 (red) mice on a (A, C) control diet (solid circles/lines) and a (B, D) GW2580-supplemented diet (empty circles/dashed lines; estimated dose 3.5 mg/day). (E) Area under the curve, (F) peak amplitude, (G) peak frequency from FFTs. Data in E and F are log transformed. 3-way ANOVA. (H, I, J) Z-scores of (E, F, G) respectively, dotted green line represents $p < 0.05$. Wildtype control, n = 3, N = 3, wildtype GW2580, n = 6, N = 6, APP/PS1 control, n = 6, N = 6, APP/PS1 GW2580, n = 7, N = 7.

Chapter 6

Discussion

Overall Discussion

The primary findings of these thesis are:

1. Gamma frequency oscillations in brain slices from healthy control mice were inhibited by various pro-inflammatory mediators. Specifically, the emergence of gamma frequency oscillations was inhibited in brain slices treated with TNFα, CCL2, PGE2, and CXL10. Additionally, the growth in established oscillation amplitude was inhibited by exposure to TNFα, IL-1β, and CCL2, and to a lesser extent by exposure to PGE2 and CXL10.

2. Gamma frequency oscillations were disrupted in brain slices from APP/PS1 mice. Specifically, oscillation amplitude and frequency were reduced in APP/PS1 mice at 9-11 months, and oscillation amplitude was increased and frequency was reduced at 20-24 months. These changes were accompanied by reductions in inhibitory interneuron network density and function in APP/PS1 mice.

3. Gamma frequency oscillations in brain slices from APP/PS1 mice were sensitive to neuroinflammatory manipulations.
    a. Treatment with the CSF1R inhibitor GW2580 had complex effects on gamma frequency oscillations in brain slices from APP/PS1 mice. At 9-11 months, the APP/PS1-associated reduction in oscillation amplitude was reversed by GW2580 treatment, however the oscillation appeared to become hyperexcitable and had increased epileptiform activity.
    b. Unlike their effects in brain slices from young, healthy mice, IL-1β and TNFα did not inhibit the growth of gamma frequency oscillation amplitude in brain slices from APP/PS1 mice.

Taken together, these findings demonstrate that immune cells and inflammatory mediators modulate gamma frequency oscillations in both APP/PS1 and control mice. These findings are summarised in Figure 6.1 and their interrelations are discussed below.

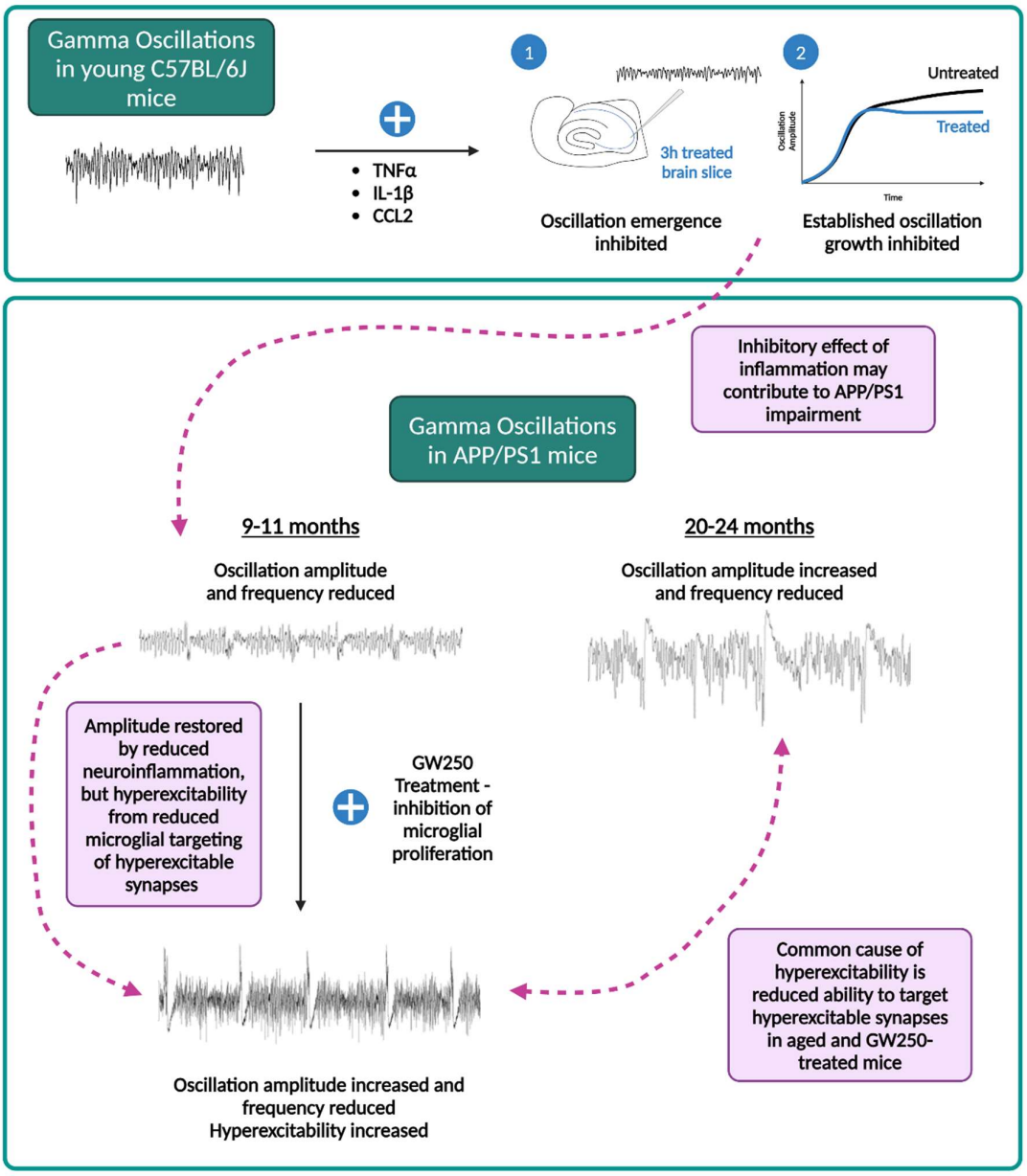

Figure 6.1. Scheme of the main findings relating to immune effects on gamma frequency oscillations in young C57BL/6J mice and APP/PS1 mice. Possible explanation of and interactions between findings are described in pink boxes. Figure created using BioRender.

Gamma frequency oscillations in APP/PS1 mice

One of the main findings of this thesis is that gamma frequency oscillations are disrupted in APP/PS1 mice. Specifically, at 9-11 months oscillation amplitude and frequency are reduced, and at 20-24 months oscillation amplitude is increased and oscillation frequency is reduced. In addition, the incidence and severity of epileptiform activity was increased. These observations were likely to due to observed deficit in inhibitory interneuron density in APP/PS1 mice – this was shown by both immunohistochemistry and pharmacological manipulation of the neuronal network. Therefore, in APP/PS1 at 9-11 months there was an impairment in inhibitory neuronal networks which led to two forms of impairment – reduced gamma frequency oscillation and increased epileptiform activity. The increase in oscillation amplitude at 20-24 months may be due to the further loss of inhibitory interneuron density and increase in epileptiform activity in these mice. These observations provide useful further detail to a body of work which suggests that gamma frequency oscillations, along with other neuronal network activities, are altered in Alzheimer's disease.

Incidentally, there is a view that these changes in neuronal network activity could be used as a diagnostic tool in Alzheimer's disease via cortical EEG recordings (Babiloni et al., 2021). This has been posited as potential means to diagnosis individuals with Alzheimer's disease at the prodromal stage. The alterations observed here in hippocampal gamma frequency oscillations in APP/PS1 mice at 9-11 months were concurrent with only moderate, but significant, behavioural impairment. This suggests that there were profound changes in neuronal network activity which preceded severe behavioural impairment. This makes these changes in hippocampal gamma frequency oscillation potentially diagnostically informative, although alterations to cortical gamma frequency oscillations would be more readily observable by EEG in the clinic. The thorough characterisation made here of gamma frequency oscillations induced in APP/PS1 mice

and wildtype littermate controls using two models, at different ages, in both sexes, using slices from across the dorsal-ventral axis, represents a useful contribution to understanding these changes in neuronal network activity in Alzheimer's disease. Based on a thorough literature review, gamma frequency oscillations do not appear to have been previously characterised in an Alzheimer's disease model on the basis of sex or across the dorsal-ventral axis (indeed this has not been widely reported on in healthy mice). Furthermore, the investigations made here into the density and function of inhibitory interneuron networks represent a novel study into the cellular basis of gamma frequency oscillation impairment in Alzheimer's disease.

The observed reductions in inhibitory interneuron density made here are consistent with observations made in post-mortem Alzheimer's disease tissue (Brady & Mufson, 1997; Sanchez-Mejias et al., 2020; Solodkin et al., 1996). Indeed, the selective targeting of these neuronal populations has been proposed as a therapeutic strategy for Alzheimer's disease (Xu et al., 2020). Given, the known dependence of gamma frequency oscillations on both parvalbumin- and somatostatin-positive interneurons, it seems likely that the observed disruptions in gamma frequency oscillations in APP/PS1 mice are due to the reduction in the density of these interneurons, as well as the reduction in GABAergic neurotransmission (revealed by $GABA_AR$ blockade) observed in these mice. It is possible that the observed reductions in the inhibitory interneuron networks which generate gamma frequency oscillations may be due to neuroinflammatory changes in APP/PS1 mice. Increased neuroinflammation is known to be associated with both metabolic and oxidative stress (Teleanu et al., 2022). Although not investigated here, it can be expected that metabolic and oxidative stress are increased in brain slices from APP/PS1 mice. Both parvalbumin- and somatostatin-positive inhibitory interneurons are known to be sensitive to both metabolic and oxidative stress (Kann et al., 2016). Indeed, it is likely the heightened sensitivity of these networks to such stressors which resulted in the specific loss of these populations in APP/PS1 mice (which were found not to have global neuronal loss

by NeuN immunohistochemistry). Therefore, it is possible that neuroinflammatory-driven changes in inhibitory interneuron networks may account for the observed deficits in gamma frequency oscillations in APP/PS1 mice. This possibility is further supported by the observation that brain slices from C57BL/6J mice which were treated with various pro-inflammatory mediators for 3 hours, had gamma frequency oscillations with reduced amplitude and frequency. It was not investigated if these changes were due to reductions in inhibitory interneuron networks in these brain slices, but is it very possible that they were. This could be further investigated by using immunohistochemistry to label parvalbumin- and somatostatin-inhibitory interneurons in these brain slices treated with pro-inflammatory mediators. In conclusion, further experiments are necessary to establish if the observed reduction in inhibitory interneuron networks was driven by neuroinflammatory changes, however immune-drive increases in metabolic and oxidative stress seem the probable cause for loss of these populations. These observations, taken with the observed inhibition of gamma frequency oscillations in brain slice with pro-inflammatory mediators, suggest that neuroinflammation is capable of driving impairments in neuronal network activity in APP/PS1 mice. This contributes to the view that the immune system is not a passive bystander in Alzheimer's disease, but is instead an active contributor to pathology development and progression.

The effects of GW2580 treatment on gamma frequency oscillations in APP/PS1 mice

Based on the finding that gamma frequency oscillations were impaired in APP/PS1 mice at 9-11 months, and these impairments may have arisen from loss of inhibitory interneuron density as a result of increased neuroinflammation, it was of interest to determine if dampening the immune response in APP/PS1 would impact gamma frequency oscillations. This was done by inhibiting

microglial proliferation via the CSF1R inhibitor GW2580. This drug was shown to effectively reduce microglial proliferation and reactivity proximal to amyloid-beta plaques. The hypothesis for this experiment was that reducing microglial proliferation and reactivity would reduce the pro-inflammatory environment of the brain and restore gamma frequency oscillations to their homeostatic state. The impact of CSF1R was complex and not easily characterised as beneficial or detrimental. The amplitude of gamma frequency oscillation was restored to similar levels as healthy controls following GW2580 treatment APP/PS1 mice, however the oscillatory activity had increased low frequency amplitude and increased incidence of epileptiform events. This suggested that as well as restoring the neuronal network's ability to generate gamma frequency oscillations, treatment with GW2580 caused the neuronal network to become hyperexcitable. In other words, one half of the two-fold impairment in APP/PS1 neuronal networks activity at 9-11 months was restored, but the other half was exacerbated. This suggested that GW2580 treatment increased the already present hyperexcitability in APP/PS1 mice.

The restoration of GW2580 treatment of oscillation amplitude in APP/PS1 mice may be due to preservation of inhibitory interneuron density in these mice as a result of reduced neuroinflammation. This possibility is a pertinent outstanding question which should be addressed by immunohistochemistry in GW2580-treated APP/PS1 mice. Although it seems probable that reduced neuroinflammation would be beneficial for inhibitory interneuron density, the observed increase in epileptiform activity suggests that the excitatory-inhibitory remained altered in GW2580-treated APP/PS1 mice and inhibition was not fully rescued.

The observation that hyperexcitability was further increased by microglial inhibition was consistent with a number of other findings in the field which show that following microglial depletion neuronal networks become hyperexcitable (K. Ji et al., 2013; Y.-J. Liu et al., 2021). It has been shown that in Alzheimer's disease models, microglia target and engulf hyperexcitable synapses (Rueda-Carrasco et al., 2023). Although this process may be overly active in Alzheimer's

disease, it presumably has a beneficial purpose which may be lost following treatment with GW2580, this possibility is supported by the observation previously made that key phagocytic markers (*Trem2*, *Lpl*, and *Itgax*) were reduced in microglia isolated from GW2580-treated APP/PS1 mice (Islam, 2022). This reduction in the phagocytosis of hyperexcitable synapses may account for the emergence of network hyperexcitability in these mice. This may be consistent with the finding made here that in aged APP/PS1 mice gamma frequency oscillations became hyperexcitable, with an increased emergence of epileptiform events. It is possible, although not investigated here or elsewhere, that in aged mice senescent microglia, which are known to accumulate, lose their ability to target and engulf hyperexcitable synapses (Ng et al., 2023).

Overall, this result demonstrated that although the pro-inflammatory environment of the brain was reduced by GW2580 treatment, and this may account for the partial improvement in gamma frequency oscillations, the behaviour of microglia was also altered by GW2580 treatment and this had consequences on the excitatory-inhibitory balance of the neuronal networks. This study is consistent with the known complexity of neuroimmune interactions and may predict difficulties in modulating these interactions. These findings are perhaps cautionary for treatment strategies which aim to reduce neuroinflammation in the treatment of Alzheimer's disease, although this may have some beneficial effects it may also lead to the loss of critical elements of the immune response and the worsening of certain elements of pathology, as occurred here.

The effects of inflammatory mediators on gamma frequency oscillations

It was shown here that gamma frequency oscillations were inhibited by various pro-inflammatory mediators in healthy control animals. Specifically, the growth of oscillation amplitude was inhibited by exposure to various pro-inflammatory mediators. The consistency of the effect of treatment with different pro-inflammatory mediators was surprising. All of the mediators tested,

except for CCL11, had an inhibitory effect on gamma frequency oscillations, however the magnitude of this effect varied. It is difficult to establish if this is because exposure to various pro-inflammatory mediators causes some common change which inhibits gamma frequency oscillations, or if via a variety of mechanisms exposure to various pro-inflammatory mediators leads to the same outcome of inhibiting gamma frequency oscillations, for example, do each of these pro-inflammatory mediators cause the increased expression of NO, which has been consistently shown to inhibit gamma frequency oscillations (Papageorgiou et al., 2016; Schilling et al., 2021; Ta et al., 2019). This possible shared mechanism could be investigated by simultaneously treating brain slices with an inflammatory mediator and an iNOS inhibitor.

However, it is difficult here to establish the exact mechanism of this impairment, this is primarily due to a lack of understanding regarding the normal growth in oscillation amplitude over time. This normal growth in amplitude was proposed here to be due to a number of possible synaptic strengthening mechanisms (discussion of chapter 3). It is possible that TNFα is somehow required for this strengthening, as treatment with anti-TNFα antibody appeared to inhibit the growth in oscillation amplitude over time in all mice. This is consistent with the work of Malenka and Stellwagen which showed that TNFα is required for the process of synaptic scaling (Beattie et al., 2002; Stellwagen & Malenka, 2006). However, it likely that this process extends beyond a reliance on a singular molecular such as TNFα. Understanding the exact nature of this growth in oscillation amplitude over time is a significant outstanding question of this thesis. This lack of understanding makes it difficult to interpret the findings that various pro-inflammatory mediators inhibit the normal growth in oscillation amplitude and that this inhibition does not occur in APP/PS1 mice.

Although it seems very likely, based on the short time scale on which this effect occurs, that this inhibitory effect in control mice occurs via direct action of these mediators on neurons, there is a possibility that microglia are required in this process. This is suggested by the location of the

receptors for the three mediators with the strongest effects, CCL2, IL-1β, and TNFα. Based on the Allen Brain Cell Atlas (Yao et al., 2023), TNFR1 has widespread expression on both immune cells of the brain and neurons. IL1R1 is also expressed on immune cells, especially on microglia, and on excitatory neurons. However, the receptors of CCL2 (CCR2 and CCR4) are not widely expressed on neurons, they are more widely expressed on microglia. Of course each of the mediators may cause the same inhibitory effect via different mechanisms, however if there is a shared mechanism it is likely via mediated via microglia as the receptors for CCL2 are not widely expressed on neurons. The involvement of microglia in the inhibitory effect of pro-inflammatory mediators is further suggested by the observation that in brain slices from GW2580-treated wildtype mice, treatment with TNFα did not inhibit the growth of oscillation amplitude over time. Therefore, modulation of the microglial phenotype by GW2580 resulted in TNFα no longer having an inhibitory effect on oscillation amplitude growth. This finding requires further investigation to determine what changes may be responsible for this effect (for example have microglia in GW2580-treated wildtype mice fewer TNFα receptors) and the extent to which it generalises to other inflammatory mediators. Nevertheless, this observation, along with the known locations of the receptors for these mediators, suggest a role for microglia in the mediation of the inhibitory effect on gamma frequency oscillations of the chemokines and cytokines tested here.

The final element which is difficult to interpret is the finding that in APP/PS1 mice the normal growth in oscillation amplitude is not affected by exposure to IL-1β and TNFα. This may be due a desensitisation effect in APP/PS1, as the background levels of IL-1β and TNFα are significantly higher in APP/PS1 mice. This may also be due to alterations in microglia if, as suggested, the mechanisms by which IL-1β and TNFα act to inhibit the growth in oscillation amplitude is mediated via microglia. This failure to respond to IL-1β and TNFα in brain slices

from APP/PS1 mice represents a further impairment in gamma frequency oscillations in APP/PS1 mice.

Regardless of the mechanism by which the inflammatory mediators studied here inhibit gamma frequency oscillations, there is clear evidence that inflammatory mediators are capable of negatively interacting with gamma frequency oscillations in healthy tissue.

Limitations

The work presented in this thesis naturally has limitations. Experimental models do not capture the full complexity of disease, indeed this reduction of complexity is what makes them extremely useful experimental tools. However, consideration must be given to certain features of the models which may impact the observed findings or may not generalise beyond the experimental model.

The model of Alzheimer's disease used here has certain features which are relevant to the interpretation of the observations made here. Firstly, the APP/PS1 mouse model does not express tau tangles, as is observed in Alzheimer's disease. Tau has been shown to impair neuronal network activity (Busche et al., 2019). Therefore, similar to amyloid-beta, the accumulation of tau in Alzheimer's disease has an impact on neuronal network activity. This feature of pathology is not captured in the APP/PS1 mouse model. This may result in certain findings relating to neuronal network activity in APP/PS1 mice failing to transfer to the clinical presentation of Alzheimer's disease. Overall, however, the APP/PS1 model is an appropriate model in which to study how amyloidosis, and its associated immune response, impacts neuronal network activity.

The main experimental model used here was *ex vivo* brain slice electrophysiology. This model has significant strengths, however it also has several pertinent limitations. Firstly, the preparation of brain slices is a stressful event for the tissue, this can be expected to cause an immune response. Given the focus here on the interactions between neuronal network activity and the cells of the

immune system, background inflammation in the brain slice as a result of brain slice preparation is a significant consideration. Furthermore, there is a possibility that brain slices prepared from APP/PS1 mice experience a greater immune response following brain slice preparation. A thorough characterisation of the extent of the immune response to brain slice preparation is required to establish if this limitation may have affected the experimental observations made here. A second limitation of the brain slice model is the nature of the gamma frequency oscillations induced. In the brain gamma frequency oscillations emerge as brief epochs which do not persist (Bragin et al., 1995). However, kainate- and carbachol-induced gamma frequency oscillations persist for hours. This makes the behaviour of gamma frequency oscillations in brain slices significantly different from *in vivo* oscillations, however findings in brain slices have been shown to correlate with *in vivo* EEG and animal behaviour (C. B. Lu, Jefferys, et al., 2011). Therefore, despite this difference in duration, *ex vivo* brain slices are a useful tool to study neuronal oscillations. A final relevant limitation of *ex vivo* brain slices is the removal of the peripheral immune system. It has not been discussed or examined here, but the cells of the peripheral immune system can infiltrate the brain in Alzheimer's disease – these cells include peripheral macrophages and T cells (Ní Chasaide & Lynch, 2020). For example, in APP/PS1 the increased expression of CXCL10 and CCL3 was shown to recruit peripheral T cells to brain (McManus et al., 2014). This phenomenon is not captured in the experiments which exposed brain slices to various pro-inflammatory mediators. Broadly, despite several limitations, *ex vivo* brain slice electrophysiology was a suitable experimental approach to investigate the impact of immune cells and their mediators on gamma frequency oscillations

Conclusion

In APP/PS1 mice gamma frequency oscillations were found to be altered in a manner that reflected the observed reduction in inhibitory interneuron density and function – specifically

oscillation amplitude was reduced and epileptiform activity was increased. These deficits in inhibitory interneurons are likely driven by increased neuroinflammation in APP/PS1 mice. In brain slices from healthy mice, treatment with various pro-inflammatory mediators inhibited the emergence of gamma frequency oscillations. Further supporting the view that increased neuroinflammation in APP/PS1 mice drove gamma frequency oscillation deficits. However, the inhibition of microglial proliferation and reactivity via GW2580 treatment, demonstrated that these changes were not simply reversed by reducing neuroinflammation. The restoration of gamma frequency oscillation amplitude following GW2580 treatment may be attributable to the reduction in neuroinflammation, however the increase in epileptiform activity suggested the network became even more hyperexcitable, this may be due to loss of function in microglia following GW2580 treatment.

In addition to the described deficits in APP/PS1 mice, established gamma frequency oscillations in brain slices from APP/PS1 mice were found to not be sensitive to inhibition by IL-1β and TNFα in the same manner as gamma frequency oscillations in brain slices from healthy animals. Further work is required to establish the nature of this impairment in healthy mice and why it was lost in APP/PS1 mice. Nevertheless, this finding represents a further impairment in gamma frequency oscillations in APP/PS1 mice.

Overall, the work carried out here demonstrated that neuronal networks and the activity they generate are sensitive to immune cells and their mediators in both health and Alzheimer's disease. The increased neuroinflammation observed in Alzheimer's disease is capable of driving profound impairments in neuronal network activity. Therefore, neuroinflammation should be considered a causative factor in Alzheimer's disease progression. However, various manipulations with immune cells and their mediators demonstrated that neuroimmune interactions are complex and require careful characterisation prior to therapeutic targeting.

References

A Armstrong, R. (2019). Risk factors for Alzheimer's disease. *Folia Neuropathologica*, *57*(2), 87–105. https://doi.org/10.5114/fn.2019.85929

Abdul Kadir, L., Stacey, M., & Barrett-Jolley, R. (2018). Emerging Roles of the Membrane Potential: Action Beyond the Action Potential. *Frontiers in Physiology*, *9*, 1661. https://doi.org/10.3389/fphys.2018.01661

Adaikkan, C., & Tsai, L. H. (2020). Gamma Entrainment: Impact on Neurocircuits, Glia, and Therapeutic Opportunities. *Trends in Neurosciences*, *43*(1), 24–41. https://doi.org/10.1016/j.tins.2019.11.001

Aggarwal, N. T., & Mielke, M. M. (2023). Sex Differences in Alzheimer's Disease. *Neurologic Clinics*, *41*(2), 343–358. https://doi.org/10.1016/j.ncl.2023.01.001

Agostini, J. V., & Inouye, S. K. (2003). Delirium. In W. R. Hazzard, J. P. Blass, J. B. Halter, J. G. Ouslander, & M. E. Tinetti (Eds.), *Principles of Geriatric Medicine and Gerontology* (pp. 1503–1515). McGraw-Hill Companies.

Ahnaou, A., Walsh, C., Manyakov, N. V., Youssef, S. A., & Drinkenburg, W. H. (2019). Early Electrophysiological Disintegration of Hippocampal Neural Networks in a Novel Locus Coeruleus Tau-Seeding Mouse Model of Alzheimer's Disease. *Neural Plasticity*, *2019*. https://doi.org/10.1155/2019/6981268

Algamal, M., Russ, A. N., Miller, M. R., Hou, S. S., Maci, M., Munting, L. P., Zhao, Q., Gerashchenko, D., Bacskai, B. J., & Kastanenka, K. V. (2022). Reduced excitatory neuron activity and interneuron-type-specific deficits in a mouse model of Alzheimer's disease. *Communications Biology*, *5*, 1323. https://doi.org/10.1038/s42003-022-04268-x

Allen, B. D., Syage, A. R., Maroso, M., Baddour, A. A. D., Luong, V., Minasyan, H., Giedzinski, E., West, B. L., Soltesz, I., Limoli, C. L., Baulch, J. E., & Acharya, M. M. (2020). Mitigation of helium irradiation-induced brain injury by microglia depletion. *Journal of Neuroinflammation*, *17*, 159. https://doi.org/10.1186/s12974-020-01790-9

Alzheimer, V. A. (1911). *Uber eigenartige Krankheitsfalle des spateren Alters*. 356–385.

Alzheimer's Association Report. (2023). *2023 Alzheimer's disease facts and figures*.

Alzheimer's Association Report. (2024). *Alzheimer's Disease Facts and Figures*.

Alzheimer's Disease International. (2019). *World Alzheimer Report 2019: Attitudes to dementia* (p. 13). Alzheimer's Disease International.

Amatniek, J. C., Hauser, W. A., DelCastillo-Castaneda, C., Jacobs, D. M., Marder, K., Bell, K., Albert, M., Brandt, J., & Stern, Y. (2006). Incidence and Predictors of Seizures in Patients with Alzheimer's Disease. *Epilepsia*, *47*(5), 867–872. https://doi.org/10.1111/j.1528-1167.2006.00554.x

Antonoudiou, P., Tan, Y. L., Kontou, G., Upton, A. L., & Mann, E. O. (2020). Parvalbumin and Somatostatin Interneurons Contribute to the Generation of Hippocampal Gamma Oscillations. *The Journal of Neuroscience: The Official Journal of the Society for Neuroscience*, *40*(40), 7668–7687. https://doi.org/10.1523/JNEUROSCI.0261-20.2020

Araque, A., Parpura, V., Sanzgiri, R. P., Haydon, P. G., Araque, A., Parpura, V., Sanzgiri, R. P., & Haydon, P. G. (1999). Tripartite synapses: Glia, the unacknowledged partner. *Trends in Neurosciences*, *22*(5), 208–215. https://doi.org/10.1016/S0166-2236(98)01349-6

Askew, K. E., Beverley, J., Sigfridsson, E., Szymkowiak, S., Emelianova, K., Dando, O., Hardingham, G. E., Duncombe, J., Hennessy, E., Koudelka, J., Samarasekera, N., Salman, R. A.-S., Smith, C., Tavares, A. A. S., Gomez-Nicola, D., Kalaria, R. N., McColl, B. W., & Horsburgh, K. (2024). Inhibiting CSF1R alleviates cerebrovascular white matter disease and cognitive impairment. *Glia*, *72*(2), 375–395. https://doi.org/10.1002/glia.24481

Astrup, J., Sørensen, P. M., & Sørensen, H. R. (1981). Oxygen and glucose consumption related to Na+-K+ transport in canine brain. *Stroke*, *12*(6), 726–730. https://doi.org/10.1161/01.STR.12.6.726

Babiloni, C., Arakaki, X., Azami, H., Bennys, K., Blinowska, K., Bonanni, L., Bujan, A., Carrillo, M. C., Cichocki, A., de Frutos-Lucas, J., Del Percio, C., Dubois, B., Edelmayer, R., Egan, G., Epelbaum, S., Escudero, J., Evans, A., Farina, F., Fargo, K., … Guntekin, B. (2021). Measures of resting state EEG rhythms for clinical trials in Alzheimer's disease: Recommendations of an expert panel. *Alzheimer's & Dementia*, *17*(9), 1528–1553. https://doi.org/10.1002/alz.12311

Babiloni, C., Blinowska, K., Bonanni, L., Cichocki, A., De Haan, W., Del Percio, C., Dubois, B., Escudero, J., Fernández, A., Frisoni, G., Guntekin, B., Hajos, M., Hampel, H., Ifeachor, E., Kilborn, K., Kumar, S., Johnsen, K., Johannsson, M., Jeong, J., … Randall, F. (2020). What electrophysiology tells us about Alzheimer's disease: A window into the synchronization and connectivity of brain neurons. *Neurobiology of Aging*, *85*, 58–73. https://doi.org/10.1016/j.neurobiolaging.2019.09.008

Baik, S. H., Kang, S., Lee, W., Choi, H., Chung, S., Kim, J.-I., & Mook-Jung, I. (2019). A Breakdown in Metabolic Reprogramming Causes Microglia Dysfunction in Alzheimer's Disease. *Cell Metabolism*, *30*(3), 493-507.e6. https://doi.org/10.1016/j.cmet.2019.06.005

Bakker, A., Krauss, G. L., Albert, M. S., Speck, C. L., Jones, L. R., Stark, C. E., Yassa, M. A., Bassett, S. S., Shelton, A. L., & Gallagher, M. (2012). Reduction of Hippocampal Hyperactivity Improves Cognition in Amnestic Mild Cognitive Impairment. *Neuron*, *74*(3), 467–474. https://doi.org/10.1016/j.neuron.2012.03.023

Barker, W. W., Luis, C. A., Kashuba, A., Luis, M., Harwood, D. G., Loewenstein, D., Waters, C., Jimison, P., Shepherd, E., Sevush, S., Graff-Radford, N., Newland, D., Todd, M., Miller, B., Gold, M., Heilman, K., Doty, L., Goodman, I., Robinson, B., … Duara, R. (2002). Relative Frequencies of Alzheimer Disease, Lewy Body, Vascular and Frontotemporal Dementia, and Hippocampal Sclerosis in the State of Florida Brain Bank. *Alzheimer Disease & Associated Disorders*, *16*(4), 203–212. https://doi.org/10.1097/00002093-200210000-00001

Barros, L. F., Courjaret, R., Jakoby, P., Loaiza, A., Lohr, C., & Deitmer, J. W. (2009). Preferential transport and metabolism of glucose in Bergmann glia over Purkinje cells: A multiphoton study of cerebellar slices. *Glia*, *57*(9), 962–970. https://doi.org/10.1002/glia.20820

Barth, A. M. I., Ferando, I., & Mody, I. (2014). Ovarian cycle-linked plasticity of δ-GABAA receptor subunits in hippocampal interneurons affects γ oscillations in vivo. *Frontiers in Cellular Neuroscience*, *8*(AUG). https://doi.org/10.3389/fncel.2014.00222

Başar, E., Emek-Savaş, D. D., Güntekin, B., & Yener, G. G. (2016). Delay of cognitive gamma responses in Alzheimer's disease. *NeuroImage: Clinical*, *11*, 106–115. https://doi.org/10.1016/j.nicl.2016.01.015

Basilico, B., Ferrucci, L., Khan, A., Di Angelantonio, S., Ragozzino, D., & Reverte, I. (2022). What microglia depletion approaches tell us about the role of microglia on synaptic function and behavior. *Frontiers in Cellular Neuroscience*, *16*. https://doi.org/10.3389/fncel.2022.1022431

Bayer, J., Schultz, H., Gamer, M., & Sommer, T. (2014). Menstrual-cycle dependent fluctuations in ovarian hormones affect emotional memory. *Neurobiology of Learning and Memory*, *110*, 55–63. https://doi.org/10.1016/j.nlm.2014.01.017

Beach, T. G., Honer, W. G., & Hughes, L. H. (1997). Cholinergic fibre loss associated with diffuse plaques in the non-demented elderly: The preclinical stage of Alzheimer's disease? *Acta Neuropathologica*, *93*(2), 146–153. https://doi.org/10.1007/s004010050595

Beattie, E. C., Stellwagen, D., Morishita, W., Bresnahan, J. C., Byeong, K. H., Von Zastrow, M., Beattie, M. S., & Malenka, R. C. (2002). Control of synaptic strength by glial TNFα. *Science*, *295*(5563), 2282–2285. https://doi.org/10.1126/science.1067859

Bellot-Saez, A., Cohen, G., van Schaik, A., Ooi, L., W Morley, J., & Buskila, Y. (2018). Astrocytic modulation of cortical oscillations. *Scientific Reports*, *8*(1), 11565. https://doi.org/10.1038/s41598-018-30003-w

Bertram, L., Lange, C., Mullin, K., Parkinson, M., Hsiao, M., Hogan, M. F., Schjeide, B. M. M., Hooli, B., DiVito, J., Ionita, I., Jiang, H., Laird, N., Moscarillo, T., Ohlsen, K. L., Elliott, K., Wang, X., Hu-Lince, D., Ryder, M., Murphy, A., … Tanzi, R. E. (2008). Genome-wide Association Analysis Reveals Putative Alzheimer's Disease Susceptibility

Loci in Addition to APOE. *American Journal of Human Genetics*, *83*(5), 623. https://doi.org/10.1016/J.AJHG.2008.10.008

Bertram, L., Lill, C. M., & Tanzi, R. E. (2010). The Genetics of Alzheimer Disease: Back to the Future. *Neuron*, *68*(2), 270–281. https://doi.org/10.1016/J.NEURON.2010.10.013

Bezaire, M. J., & Soltesz, I. (2013). Quantitative assessment of CA1 local circuits: Knowledge base for interneuron-pyramidal cell connectivity. *Hippocampus*, *23*(9), 751–785. https://doi.org/10.1002/hipo.22141

Blank, T., & Prinz, M. (2017). Type I interferon pathway in CNS homeostasis and neurological disorders. *Glia*, *65*(9), 1397–1406. https://doi.org/10.1002/glia.23154

Booker, S. A., & Vida, I. (2018). Morphological diversity and connectivity of hippocampal interneurons. *Cell and Tissue Research*, *373*(3), 619–641. https://doi.org/10.1007/s00441-018-2882-2

Brady, D. R., & Mufson, E. J. (1997). Parvalbumin-immunoreactive neurons in the hippocampal formation of Alzheimer's diseased brain. *Neuroscience*, *80*(4), 1113–1125. https://doi.org/10.1016/S0306-4522(97)00068-7

Bragin, A., Jando, G., Nadasdy, Z., Hetke, J., Wise, K., & Buzsaki, G. (1995). Gamma (40-100 Hz) oscillation in the hippocampus of the behaving rat. *Journal of Neuroscience*, *15*(1 I), 47–60. https://doi.org/10.1523/jneurosci.15-01-00047.1995

Bray, N., Burrows, F. E., Jones, M., Berwick, J., Allan, S. M., & Schiessl, I. (2016). Decreased haemodynamic response and decoupling of cortical gamma-band activity and tissue oxygen perfusion after striatal interleukin-1 injection. *Journal of Neuroinflammation*, *13*(1), 195. https://doi.org/10.1186/s12974-016-0664-x

Bressler, S. L., & Freeman, W. J. (1980). Frequency analysis of olfactory system EEG in cat, rabbit, and rat. *Electroencephalography and Clinical Neurophysiology*, *50*(1–2), 19–24. https://doi.org/10.1016/0013-4694(80)90319-3

Brockett, A. T., Kane, G. A., Monari, P. K., Briones, B. A., Vigneron, P. A., Barber, G. A., Bermudez, A., Dieffenbach, U., Kloth, A. D., Buschman, T. J., & Gould, E. (2018). Evidence supporting a role for astrocytes in the regulation of cognitive flexibility and neuronal oscillations through the Ca2+ binding protein S100β. *PLoS ONE*, *13*(4), e0195726. https://doi.org/10.1371/journal.pone.0195726

Buhl, E. H., Halasy, K., & Somogyi, P. (1994). Diverse sources of hippocampal unitary inhibitory postsynaptic potentials and the number of synaptic release sites. *Nature*, *368*(6474), 823–828. https://doi.org/10.1038/368823a0

Bullock, T. H. (1997). Signals and signs in the nervous system: The dynamic anatomy of electrical activity is probably information-rich. *Proceedings of the National Academy of Sciences*, *94*(1), 1–6. https://doi.org/10.1073/PNAS.94.1.1

Burnyasheva, A. O., Stefanova, N. A., Kolosova, N. G., & Telegina, D. V. (2023). Changes in the Glutamate/GABA System in the Hippocampus of Rats with Age and during Alzheimer's Disease Signs Development. *Biochemistry (Moscow)*, *88*(12), 1972–1986. https://doi.org/10.1134/S0006297923120027

Busche, M. A., Chen, X., Henning, H. A., Reichwald, J., Staufenbiel, M., Sakmann, B., & Konnerth, A. (2012). Critical role of soluble amyloid-β for early hippocampal hyperactivity in a mouse model of Alzheimer's disease. *Proceedings of the National Academy of Sciences of the United States of America*, *109*(22), 8740–8745. https://doi.org/10.1073/pnas.1206171109

Busche, M. A., Eichhoff, G., Adelsberger, H., Abramowski, D., Wiederhold, K.-H., Haass, C., Staufenbiel, M., Konnerth, A., & Garaschuk, O. (2008). Clusters of hyperactive neurons near amyloid plaques in a mouse model of Alzheimer's disease. *Science (New York, N.Y.)*, *321*(5896), 1686–1689. https://doi.org/10.1126/science.1162844

Busche, M. A., Wegmann, S., Dujardin, S., Commins, C., Schiantarelli, J., Klickstein, N., Kamath, T. V., Carlson, G. A., Nelken, I., & Hyman, B. T. (2019). Tau impairs neural circuits, dominating amyloid-β effects, in Alzheimer models in vivo. *Nature Neuroscience*, *22*(1), 57–64. https://doi.org/10.1038/s41593-018-0289-8

Bushong, E. A., Martone, M. E., Jones, Y. Z., & Ellisman, M. H. (2002). Protoplasmic astrocytes in CA1 stratum radiatum occupy separate anatomical domains. *The Journal of Neuroscience: The Official Journal of the Society for Neuroscience*, *22*(1), 183–192. https://doi.org/10.1523/JNEUROSCI.22-01-00183.2002

Buzsáki, G., & Draguhn, A. (2004). Neuronal oscillations in cortical networks. *Science (New York, N.Y.)*, *304*(5679), 1926–1929. https://doi.org/10.1126/science.1099745

Buzsáki, G., & Wang, X.-J. (2012). Mechanisms of Gamma Oscillations. *Annual Review of Neuroscience*, *35*(1), 203–225. https://doi.org/10.1146/annurev-neuro-062111-150444

Cabrejo, L., Guyant-Marechal, L., Laquerriere, A., Vercelletto, M., De La Fourniere, F., Thomas-Anterion, C., Verny, C., Letournel, F., Pasquier, F., Vital, A., Checler, F., Frebourg, T., Campion, D., & Hannequin, D. (2006). Phenotype associated with APP duplication in five families. *Brain*, *129*(11), 2966–2976. https://doi.org/10.1093/brain/awl237

Cabungcal, J. H., Steullet, P., Morishita, H., Kraftsik, R., Cuenod, M., Hensch, T. K., & Do, K. Q. (2013). Perineuronal nets protect fast-spiking interneurons against oxidative stress. *Proceedings of the National Academy of Sciences of the United States of America*, *110*(22), 9130–9135. https://doi.org/10.1073/pnas.1300454110

Cahoy, J. D., Emery, B., Kaushal, A., Foo, L. C., Zamanian, J. L., Christopherson, K. S., Xing, Y., Lubischer, J. L., Krieg, P. A., Krupenko, S. A., Thompson, W. J., & Barres, B. A. (2008). A Transcriptome Database for Astrocytes, Neurons, and Oligodendrocytes: A

New Resource for Understanding Brain Development and Function. *Journal of Neuroscience*, *28*(1), 264–278. https://doi.org/10.1523/JNEUROSCI.4178-07.2008

Caioli, S., Pieri, M., Antonini, A., Guglielmotti, A., Severini, C., & Zona, C. (2013). Monocyte Chemoattractant Protein-1 upregulates GABA-induced current: Evidence of modified GABAA subunit composition in cortical neurons from the G93A mouse model of Amyotrophic Lateral Sclerosis. *Neuropharmacology*, *73*, 247–260. https://doi.org/10.1016/J.NEUROPHARM.2013.05.045

Capogna, M., Castillo, P. E., & Maffei, A. (2021). The ins and outs of inhibitory synaptic plasticity: Neuron types, molecular mechanisms and functional roles. *The European Journal of Neuroscience*, *54*(8), 6882–6901. https://doi.org/10.1111/ejn.14907

Cardin, J. A., Carlén, M., Meletis, K., Knoblich, U., Zhang, F., Deisseroth, K., Tsai, L.-H., & Moore, C. I. (2009). Driving fast-spiking cells induces gamma rhythm and controls sensory responses. *Nature*, *459*(7247), 663–667. https://doi.org/10.1038/nature08002

Cassano, T., Serviddio, G., Gaetani, S., Romano, A., Dipasquale, P., Cianci, S., Bellanti, F., Laconca, L., Romano, A. D., Padalino, I., LaFerla, F. M., Nicoletti, F., Cuomo, V., & Vendemiale, G. (2012). Glutamatergic alterations and mitochondrial impairment in a murine model of Alzheimer disease. *Neurobiology of Aging*, *33*(6), 1121.e1-12. https://doi.org/10.1016/j.neurobiolaging.2011.09.021

Castelhano, J., Duarte, I., Bernardino, I., Pelle, F., Francione, S., Sales, F., & Castelo-Branco, M. (2022). Intracranial recordings in humans reveal specific hippocampal spectral and dorsal vs. Ventral connectivity signatures during visual, attention and memory tasks. *Scientific Reports*, *12*(1), 3488. https://doi.org/10.1038/s41598-022-07225-0

Cataldo, A. M., & Broadwell, R. D. (1986). Cytochemical identification of cerebral glycogen and glucose-6-phosphatase activity under normal and experimental conditions. II. Choroid plexus and ependymal epithelia, endothelia and pericytes. *Journal of Neurocytology*, *15*(4), 511–524. https://doi.org/10.1007/BF01611733

Celio, M. R. (1986). Parvalbumin in most γ-aminobutyric acid-containing neurons of the rat cerebral cortex. *Science*, *231*(4741), 995–997. https://doi.org/10.1126/science.3945815

Chan, D., Suk, H.-J., Jackson, B. L., Milman, N. P., Stark, D., Klerman, E. B., Kitchener, E., Fernandez Avalos, V. S., de Weck, G., Banerjee, A., Beach, S. D., Blanchard, J., Stearns, C., Boes, A. D., Uitermarkt, B., Gander, P., Howard, M., Sternberg, E. J., Nieto-Castanon, A., … Tsai, L.-H. (2022). Gamma frequency sensory stimulation in mild probable Alzheimer's dementia patients: Results of feasibility and pilot studies. *PloS One*, *17*(12), e0278412. https://doi.org/10.1371/journal.pone.0278412

Chen, Z., Jalabi, W., Hu, W., Park, H. J., Gale, J. T., Kidd, G. J., Bernatowicz, R., Gossman, Z. C., Chen, J. T., Dutta, R., & Trapp, B. D. (2014). Microglial displacement of

inhibitory synapses provides neuroprotection in the adult brain. *Nature Communications*, *5*(1), 4486. https://doi.org/10.1038/ncomms5486

Cho, J., Nelson, T. E., Bajova, H., & Gruol, D. L. (2009). Chronic CXCL10 alters neuronal properties in rat hippocampal culture. *Journal of Neuroimmunology*, *207*(1), 92–100. https://doi.org/10.1016/j.jneuroim.2008.12.007

Cole, A. E., & Nicoll, R. A. (1984). The pharmacology of cholinergic excitatory responses in hippocampal pyramidal cells. *Brain Research*, *305*(2), 283–290. https://doi.org/10.1016/0006-8993(84)90434-7

Consoli, D. C., Spitznagel, B. D., Owen, B. M., Kang, H., Roberson, S. W., Pandharipande, P., Ely, E. W., Nobis, W. P., Bastarache, J. A., & Harrison, F. E. (2023). Altered EEG, Disrupted Hippocampal Long-Term Potentiation and Neurobehavioral Deficits Implicate a Delirium-like state in a Mouse Model of Sepsis. *Brain, Behavior, and Immunity*, *107*, 165–178. https://doi.org/10.1016/j.bbi.2022.10.003

Conway, J. G., McDonald, B., Parham, J., Keith, B., Rusnak, D. W., Shaw, E., Jansen, M., Lin, P., Payne, A., Crosby, R. M., Johnson, J. H., Frick, L., Lin, M.-H. J., Depee, S., Tadepalli, S., Votta, B., James, I., Fuller, K., Chambers, T. J., … Hutchins, J. T. (2005). Inhibition of colony-stimulating-factor-1 signaling in vivo with the orally bioavailable cFMS kinase inhibitor GW2580. *Proceedings of the National Academy of Sciences of the United States of America*, *102*(44), 16078–16083. https://doi.org/10.1073/pnas.0502000102

Cook, M., Baker, N., Lanes, S., Bullock, R., Wentworth, C., & Arrighi, H. M. (2015). Incidence of stroke and seizure in Alzheimer's disease dementia. *Age and Ageing*, *44*(4), 695–699. https://doi.org/10.1093/ageing/afv061

Corder, E., Saunders, A., Strittmatter, W., Schmechel, D., Gaskell, P., Small, G., Roses, A., Haines, J., & Pericak-Vance, M. (1993). Gene dose of apolipoprotein E type 4 allele and the risk of Alzheimer's disease in late onset families. *Science*, *261*(5123), 921–923. https://doi.org/10.1126/science.8346443

Cornwell, B. R., Overstreet, C., & Grillon, C. (2014). Spontaneous fast gamma activity in the septal hippocampal region correlates with spatial learning in humans. *Behavioural Brain Research*, *261*, 258–264. https://doi.org/10.1016/j.bbr.2013.12.031

Cossart, R., Esclapez, M., Hirsch, J. C., Bernard, C., & Ben-Ari, Y. (1998). GluR5 kainate receptor activation in interneurons increases tonic inhibition of pyramidal cells. *Nature Neuroscience*, *1*(6), Article 6. https://doi.org/10.1038/2185

Cramer, P. E., Cirrito, J. R., Wesson, D. W., Lee, C. Y. D., Karlo, J. C., Zinn, A. E., Casali, B. T., Restivo, J. L., Goebel, W. D., James, M. J., Brunden, K. R., Wilson, D. A., & Landreth, G. E. (2012). ApoE-directed therapeutics rapidly clear β-amyloid and reverse

deficits in AD mouse models. *Science*, *335*(6075), 1503–1506. https://doi.org/10.1126/science.1217697

Cretin, B., Sellal, F., Philippi, N., Bousiges, O., Di Bitonto, L., Martin-Hunyadi, C., & Blanc, F. (2016). Epileptic Prodromal Alzheimer's Disease, a Retrospective Study of 13 New Cases: Expanding the Spectrum of Alzheimer's Disease to an Epileptic Variant? *Journal of Alzheimer's Disease*, *52*(3), 1125–1133. https://doi.org/10.3233/JAD-150096

Crocker, P. R., McMillan, S. J., & Richards, H. E. (2012). CD33-related siglecs as potential modulators of inflammatory responses. *Annals of the New York Academy of Sciences*, *1253*, 102–111. https://doi.org/10.1111/j.1749-6632.2011.06449.x

Cunningham, A. J., Murray, C. A., O'Neill, L. A. J., Lynch, M. A., & O'Connor, J. J. (1996). Interleukin-1β (IL-1β) and tumour necrosis factor (TNF) inhibit long-term potentiation in the rat dentate gyrus in vitro. *Neuroscience Letters*, *203*(1), 17–20. https://doi.org/10.1016/0304-3940(95)12252-4

Cunningham, C., Campion, S., Lunnon, K., Murray, C. L., Woods, J. F. C., Deacon, R. M. J., Rawlins, J. N. P., & Perry, V. H. (2009). Systemic inflammation induces acute behavioral and cognitive changes and accelerates neurodegenerative disease. *Biological Psychiatry*, *65*(4), 304–312. https://doi.org/10.1016/j.biopsych.2008.07.024

Cunningham, C., Campion, S., Teeling, J., Felton, L., & Perry, V. H. (2007). The sickness behaviour and CNS inflammatory mediator profile induced by systemic challenge of mice with synthetic double-stranded RNA (poly I:C). *Brain, Behavior, and Immunity*, *21*(4), 490–502. https://doi.org/10.1016/j.bbi.2006.12.007

Cunningham, C., Wilcockson, D. C., Campion, S., Lunnon, K., & Perry, V. H. (2005). Central and systemic endotoxin challenges exacerbate the local inflammatory response and increase neuronal death during chronic neurodegeneration. *Journal of Neuroscience*, *25*(40), 9275–9284. https://doi.org/10.1523/JNEUROSCI.2614-05.2005

Cunningham, M. O. (Unpublished). *Brain slice preparation comparison*.

Cunningham, M. O., Davies, C. H., Buhl, E. H., Kopell, N., & Whittington, M. A. (2003). Gamma oscillations induced by kainate receptor activation in the entorhinal cortex in vitro. *The Journal of Neuroscience: The Official Journal of the Society for Neuroscience*, *23*(30), 9761–9769. https://doi.org/10.1523/JNEUROSCI.23-30-09761.2003

Dagher, N. N., Najafi, A. R., Kayala, K. M. N., Elmore, M. R. P., White, T. E., Medeiros, R., West, B. L., & Green, K. N. (2015). Colony-stimulating factor 1 receptor inhibition prevents microglial plaque association and improves cognition in 3xTg-AD mice. *Journal of Neuroinflammation*, *12*(1), 139. https://doi.org/10.1186/s12974-015-0366-9

Danbolt, N. C. (2001). Glutamate uptake. *Progress in Neurobiology*, *65*(1), 1–105. https://doi.org/10.1016/S0301-0082(00)00067-8

Davalos, D., Grutzendler, J., Yang, G., Kim, J. V., Zuo, Y., Jung, S., Littman, D. R., Dustin, M. L., & Gan, W.-B. (2005). ATP mediates rapid microglial response to local brain injury in vivo. *Nature Neuroscience*, *8*(6), Article 6. https://doi.org/10.1038/nn1472

Davis, D. H. J., Muniz Terrera, G., Keage, H., Rahkonen, T., Oinas, M., Matthews, F. E., Cunningham, C., Polvikoski, T., Sulkava, R., MacLullich, A. M. J., & Brayne, C. (2012). Delirium is a strong risk factor for dementia in the oldest-old: A population-based cohort study. *Brain: A Journal of Neurology*, *135*(Pt 9), 2809–2816. https://doi.org/10.1093/brain/aws190

De la Rosa-Prieto, C., Saiz-Sanchez, D., Ubeda-Banon, I., Flores-Cuadrado, A., & Martinez-Marcos, A. (2016). Neurogenesis, Neurodegeneration, Interneuron Vulnerability, and Amyloid-β in the Olfactory Bulb of APP/PS1 Mouse Model of Alzheimer's Disease. *Frontiers in Neuroscience*, *10*, 227. https://doi.org/10.3389/fnins.2016.00227

Deacon, R. M. J., Cholerton, L. L., Talbot, K., Nair-Roberts, R. G., Sanderson, D. J., Romberg, C., Koros, E., Bornemann, K. D., & Rawlins, J. N. P. (2008). Age-dependent and -independent behavioral deficits in Tg2576 mice. *Behavioural Brain Research*, *189*(1), 126–138. https://doi.org/10.1016/j.bbr.2007.12.024

Deacon, R. M. J., & Rawlins, J. N. P. (2006). T-maze alternation in the rodent. *Nature Protocols*, *1*(1), 7–12. https://doi.org/10.1038/nprot.2006.2

DeKosky, S. T., Scheff, S. W., & Styren, S. D. (1996). Structural correlates of cognition in dementia: Quantification and assessment of synapse change. *Neurodegeneration*, *5*(4), 417–421. https://doi.org/10.1006/neur.1996.0056

Devlin, B. A., Smith, C. J., & Bilbo, S. D. (2021). Sickness and the Social Brain: How the Immune System Regulates Behavior across Species. *Brain Behavior and Evolution*, *97*(3–4), 197–210. https://doi.org/10.1159/000521476

Di Nunzio, M., Di Sapia, R., Sorrentino, D., Kebede, V., Cerovic, M., Gullotta, G. S., Bacigaluppi, M., Audinat, E., Marchi, N., Ravizza, T., & Vezzani, A. (2021). Microglia proliferation plays distinct roles in acquired epilepsy depending on disease stages. *Epilepsia*, *62*(8), 1931–1945. https://doi.org/10.1111/epi.16956

Dickerson, B. C., Salat, D. H., Greve, D. N., Chua, E. F., Rand-Giovannetti, E., Rentz, D. M., Bertram, L., Mullin, K., Tanzi, R. E., Blacker, D., Albert, M. S., & Sperling, R. A. (2005). Increased hippocampal activation in mild cognitive impairment compared to normal aging and AD. *Neurology*, *65*(3), 404–411. https://doi.org/10.1212/01.wnl.0000171450.97464.49

Dikmen, H. O., Hemmerich, M., Lewen, A., Hollnagel, J.-O., Chausse, B., & Kann, O. (2020). GM-CSF induces noninflammatory proliferation of microglia and disturbs electrical neuronal network rhythms in situ. *Journal of Neuroinflammation*, *17*, 235. https://doi.org/10.1186/s12974-020-01903-4

Djurisic, M. (2020). Minimizing Hypoxia in Hippocampal Slices from Adult and Aging Mice. *JoVE (Journal of Visualized Experiments)*, *2020*(161), e61377. https://doi.org/10.3791/61377

Dos Santos, S. E., Medeiros, M., Porfirio, J., Tavares, W., Pessôa, L., Grinberg, L., Leite, R. E. P., Ferretti-Rebustini, R. E. L., Suemoto, C. K., Filho, W. J., Noctor, S. C., Sherwood, C. C., Kaas, J. H., Manger, P. R., & Herculano-Houzel, S. (2020). Similar Microglial Cell Densities across Brain Structures and Mammalian Species: Implications for Brain Tissue Function. *The Journal of Neuroscience*, *40*(24), 4622–4643. https://doi.org/10.1523/JNEUROSCI.2339-19.2020

Driver, J. E., Racca, C., Cunningham, M. O., Towers, S. K., Davies, C. H., Whittington, M. A., & LeBeau, F. E. N. (2007). Impairment of hippocampal gamma (γ)-frequency oscillations in vitro in mice overexpressing human amyloid precursor protein (APP). *European Journal of Neuroscience*, *26*(5), 1280–1288. https://doi.org/10.1111/j.1460-9568.2007.05705.x

Dunot, J., Ribera, A., Pousinha, P. A., & Marie, H. (2023). Spatiotemporal insights of APP function. *Current Opinion in Neurobiology*, *82*, 102754. https://doi.org/10.1016/j.conb.2023.102754

Easley-Neal, C., Foreman, O., Sharma, N., Zarrin, A. A., & Weimer, R. M. (2019). CSF1R Ligands IL-34 and CSF1 Are Differentially Required for Microglia Development and Maintenance in White and Gray Matter Brain Regions. *Frontiers in Immunology*, *10*. https://doi.org/10.3389/fimmu.2019.02199

Eckhorn, R., Bauer, R., Jordan, W., Brosch, M., Kruse, W., Munk, M., & Reitboeck, H. J. (1988). Coherent oscillations: A mechanism of feature linking in the visual cortex? *Biological Cybernetics*, *60*(2), 121–130. https://doi.org/10.1007/BF00202899

Eisenberger, N. I., Inagaki, T. K., Mashal, N. M., & Irwin, M. R. (2010). Inflammation and social experience: An inflammatory challenge induces feelings of social disconnection in addition to depressed mood. *Brain, Behavior, and Immunity*, *24*(4), 558–563. https://doi.org/10.1016/j.bbi.2009.12.009

Elmore, M. R. P., Najafi, A. R., Koike, M. A., Dagher, N. N., Spangenberg, E. E., Rice, R. A., Kitazawa, M., Matusow, B., Nguyen, H., West, B. L., & Green, K. N. (2014). Colony-stimulating factor 1 receptor signaling is necessary for microglia viability, unmasking a microglia progenitor cell in the adult brain. *Neuron*, *82*(2), 380–397. https://doi.org/10.1016/j.neuron.2014.02.040

Elzoheiry, S., Lewen, A., Schneider, J., Both, M., Hefter, D., Boffi, J. C., Hollnagel, J.-O., & Kann, O. (2020). Mild metabolic stress is sufficient to disturb the formation of pyramidal cell ensembles during gamma oscillations. *Journal of Cerebral Blood Flow & Metabolism*, *40*(12), 2401–2415. https://doi.org/10.1177/0271678X19892657

Engel, A. K., König, P., Kreiter, A. K., Schillen, T. B., & Singer, W. (1992). Temporal coding in the visual cortex: New vistas on integration in the nervous system. *Trends in Neurosciences*, *15*(6), 218–226. https://doi.org/10.1016/0166-2236(92)90039-B

Erickson, M. A., & Banks, W. A. (2011). Cytokine and chemokine responses in serum and brain after single and repeated injections of lipopolysaccharide: Multiplex quantification with path analysis. *Brain, Behavior, and Immunity*, *25*(8), 1637–1648. https://doi.org/10.1016/j.bbi.2011.06.006

Escartin, C., Galea, E., Lakatos, A., O'Callaghan, J. P., Petzold, G. C., Serrano-Pozo, A., Steinhäuser, C., Volterra, A., Carmignoto, G., Agarwal, A., Allen, N. J., Araque, A., Barbeito, L., Barzilai, A., Bergles, D. E., Bonvento, G., Butt, A. M., Chen, W.-T., Cohen-Salmon, M., … Verkhratsky, A. (2021). Reactive astrocyte nomenclature, definitions, and future directions. *Nature Neuroscience*, *24*(3), 312–325. https://doi.org/10.1038/s41593-020-00783-4

Espinosa, N., Alonso, A., Lara-Vasquez, A., & Fuentealba, P. (2019). Basal forebrain somatostatin cells differentially regulate local gamma oscillations and functionally segregate motor and cognitive circuits. *Scientific Reports*, *9*(1), 2570. https://doi.org/10.1038/s41598-019-39203-4

Ethridge, L. E., White, S. P., Mosconi, M. W., Wang, J., Byerly, M. J., & Sweeney, J. A. (2016). Reduced habituation of auditory evoked potentials indicate cortical hyper-excitability in Fragile X Syndrome. *Translational Psychiatry*, *6*(4), Article 4. https://doi.org/10.1038/tp.2016.48

Evenhuis, H. M. (1990). The Natural History of Dementia in Down's Syndrome. *Archives of Neurology*, *47*(3), 263–267. https://doi.org/10.1001/archneur.1990.00530030029011

Fan, Z., Brooks, D. J., Okello, A., & Edison, P. (2017). An early and late peak in microglial activation in Alzheimer's disease trajectory. *Brain*, *140*(3), 792–803. https://doi.org/10.1093/brain/aww349

Femminella, G. D., Dani, M., Wood, M., Fan, Z., Calsolaro, V., Atkinson, R., Edginton, T., Hinz, R., Brooks, D. J., & Edison, P. (2019). Microglial activation in early Alzheimer trajectory is associated with higher gray matter volume. *Neurology*, *92*(12), e1331–e1343. https://doi.org/10.1212/WNL.0000000000007133

Fernández-Castañeda, A., Lu, P., Geraghty, A. C., Song, E., Lee, M.-H., Wood, J., Yalçın, B., Taylor, K. R., Dutton, S., Acosta-Alvarez, L., Ni, L., Contreras-Esquivel, D., Gehlhausen, J. R., Klein, J., Lucas, C., Mao, T., Silva, J., Peña-Hernández, M. A., Tabachnikova, A., … Monje, M. (2022). Mild respiratory SARS-CoV-2 infection can cause multi-lineage cellular dysregulation and myelin loss in the brain. *bioRxiv: The Preprint Server for Biology*, 2022.01.07.475453. https://doi.org/10.1101/2022.01.07.475453

Field, R., Campion, S., Warren, C., Murray, C., & Cunningham, C. (2010). Systemic challenge with the TLR3 agonist poly I:C induces amplified IFNα/β and IL-1β responses in the diseased brain and exacerbates chronic neurodegeneration. *Brain, Behavior, and Immunity*, *24*(6), 996–1007. https://doi.org/10.1016/j.bbi.2010.04.004

Filali, M., & Lalonde, R. (2009). Age-related cognitive decline and nesting behavior in an APPswe/PS1 bigenic model of Alzheimer's disease. *Brain Research*, *1292*, 93–99. https://doi.org/10.1016/j.brainres.2009.07.066

Filiano, A. J., Xu, Y., Tustison, N. J., Marsh, R. L., Baker, W., Smirnov, I., Overall, C. C., Gadani, S. P., Turner, S. D., Weng, Z., Peerzade, S. N., Chen, H., Lee, K. S., Scott, M. M., Beenhakker, M. P., Litvak, V., & Kipnis, J. (2016). Unexpected role of interferon-γ 3 in regulating neuronal connectivity and social behaviour. *Nature*, *535*(7612), 425–429. https://doi.org/10.1038/nature18626

Filipello, F., Morini, R., Corradini, I., Zerbi, V., Canzi, A., Michalski, B., Erreni, M., Markicevic, M., Starvaggi-Cucuzza, C., Otero, K., Piccio, L., Cignarella, F., Perrucci, F., Tamborini, M., Genua, M., Rajendran, L., Menna, E., Vetrano, S., Fahnestock, M., … Matteoli, M. (2018). The Microglial Innate Immune Receptor TREM2 Is Required for Synapse Elimination and Normal Brain Connectivity. *Immunity*, *48*(5), 979-991.e8. https://doi.org/10.1016/j.immuni.2018.04.016

Fisahn, A., Contractor, A., Traub, R. D., Buhl, E. H., Heinemann, S. F., & McBain, C. J. (2004). Distinct Roles for the Kainate Receptor Subunits GluR5 and GluR6 in Kainate-Induced Hippocampal Gamma Oscillations. *The Journal of Neuroscience*, *24*(43), 9658–9668. https://doi.org/10.1523/JNEUROSCI.2973-04.2004

Fisahn, A., Neddens, J., Yan, L., & Buonanno, A. (2009). Neuregulin-1 modulates hippocampal gamma oscillations: Implications for schizophrenia. *Cerebral Cortex*, *19*(3), 612–618. https://doi.org/10.1093/cercor/bhn107

Fisahn, A., Pike, F. G., Buhl, E. H., & Paulsen, O. (1998). Cholinergic induction of network oscillations at 40 Hz in the hippocampus in vitro. *Nature 1998 394:6689*, *394*(6689), 186–189. https://doi.org/10.1038/28179

Fitzgerald, P. J., & Watson, B. O. (2018). Gamma oscillations as a biomarker for major depression: An emerging topic. *Translational Psychiatry*, *8*(1), Article 1. https://doi.org/10.1038/s41398-018-0239-y

Fong, T. G., Jones, R. N., Shi, P., Marcantonio, E. R., Yap, L., Rudolph, J. L., Yang, F. M., Kiely, D. K., & Inouye, S. K. (2009). Delirium accelerates cognitive decline in alzheimer disease. *Neurology*, *72*(18), 1570–1575. https://doi.org/10.1212/WNL.0b013e3181a4129a

Francis, P. T., Palmer, A. M., Snape, M., & Wilcock, G. K. (1999). The cholinergic hypothesis of Alzheimer's disease: A review of progress. In *J Neurol Neurosurg Psychiatry* (Vol. 66, pp. 137–147).

Franklin, B. S., Bossaller, L., De Nardo, D., Ratter, J. M., Stutz, A., Engels, G., Brenker, C., Nordhoff, M., Mirandola, S. R., Al-Amoudi, A., Mangan, M. S., Zimmer, S., Monks, B. G., Fricke, M., Schmidt, R. E., Espevik, T., Jones, B., Jarnicki, A. G., Hansbro, P. M., … Latz, E. (2014). The adaptor ASC has extracellular and "prionoid" activities that propagate inflammation. *Nature Immunology*, *15*(8), 727–737. https://doi.org/10.1038/ni.2913

Fries, P. (2009). Neuronal gamma-band synchronization as a fundamental process in cortical computation. *Annual Review of Neuroscience*, *32*, 209–224. https://doi.org/10.1146/annurev.neuro.051508.135603

Fuchs, E. C., Zivkovic, A. R., Cunningham, M. O., Middleton, S., LeBeau, F. E. N., Bannerman, D. M., Rozov, A., Whittington, M. A., Traub, R. D., Rawlins, J. N. P., & Monyer, H. (2007). Recruitment of Parvalbumin-Positive Interneurons Determines Hippocampal Function and Associated Behavior. *Neuron*, *53*(4), 591–604. https://doi.org/10.1016/j.neuron.2007.01.031

Fukuda, T., Kosaka, T., Singer, W., & Galuske, R. A. W. (2006). Gap junctions among dendrites of cortical GABAergic neurons establish a dense and widespread intercolumnar network. *Journal of Neuroscience*, *26*(13), 3434–3443. https://doi.org/10.1523/JNEUROSCI.4076-05.2006

Gallagher, J. J., Minogue, A. M., & Lynch, M. A. (2012). Impaired Performance of Female APP/PS1 Mice in the Morris Water Maze Is Coupled with Increased Aβ Accumulation and Microglial Activation. *Neurodegenerative Diseases*, *11*(1), 33–41. https://doi.org/10.1159/000337458

Galow, L. V., Schneider, J., Lewen, A., Ta, T.-T., Papageorgiou, I. E., & Kann, O. (2014). Energy substrates that fuel fast neuronal network oscillations. *Frontiers in Neuroscience*, *8*, 398. https://doi.org/10.3389/fnins.2014.00398

Gangoiti, P., Granado, M. H., Wang, S. W., Kong, J. Y., Steinbrecher, U. P., & Gómez-Muñoz, A. (2008). Ceramide 1-phosphate stimulates macrophage proliferation through activation of the PI3-kinase/PKB, JNK and ERK1/2 pathways. *Cellular Signalling*, *20*(4), 726–736. https://doi.org/10.1016/j.cellsig.2007.12.008

Gao, R., Ji, M. huo, Gao, D. peng, Yang, R. hua, Zhang, S. gang, Yang, J. jun, & Shen, J. chun. (2017). Neuroinflammation-Induced Downregulation of Hippocampacal Neuregulin 1-ErbB4 Signaling in the Parvalbumin Interneurons Might Contribute to Cognitive Impairment in a Mouse Model of Sepsis-Associated Encephalopathy. *Inflammation*, *40*(2), 387–400. https://doi.org/10.1007/s10753-016-0484-2

Garza, K. M., Zhang, L., Borron, B., Wood, L. B., & Singer, A. C. (2020). Gamma visual stimulation induces a neuroimmune signaling profile distinct from acute neuroinflammation. *Journal of Neuroscience*, *40*(6), 1211–1225. https://doi.org/10.1523/JNEUROSCI.1511-19.2019

Gatz, M., Reynolds, C. A., Fratiglioni, L., Johansson, B., Mortimer, J. A., Berg, S., Fiske, A., & Pedersen, N. L. (2006). Role of Genes and Environments for Explaining Alzheimer Disease. *Archives of General Psychiatry*, *63*(2), 168. https://doi.org/10.1001/archpsyc.63.2.168

Gaubert, S., Raimondo, F., Houot, M., Corsi, M.-C., Naccache, L., Diego Sitt, J., Hermann, B., Oudiette, D., Gagliardi, G., Habert, M.-O., Dubois, B., De Vico Fallani, F., Bakardjian, H., Epelbaum, S., & Alzheimer's Disease Neuroimaging Initiative. (2019). EEG evidence of compensatory mechanisms in preclinical Alzheimer's disease. *Brain*, *142*(7), 2096–2112. https://doi.org/10.1093/brain/awz150

Ge, W.-P., Miyawaki, A., Gage, F. H., Jan, Y. N., & Jan, L. Y. (2012). Local generation of glia is a major astrocyte source in postnatal cortex. *Nature*, *484*(7394), 376–380. https://doi.org/10.1038/nature10959

Gerber, Y. N., Saint-Martin, G. P., Bringuier, C. M., Bartolami, S., Goze-Bac, C., Noristani, H. N., & Perrin, F. E. (2018). CSF1R Inhibition Reduces Microglia Proliferation, Promotes Tissue Preservation and Improves Motor Recovery After Spinal Cord Injury. *Frontiers in Cellular Neuroscience*, *12*, 368. https://doi.org/10.3389/fncel.2018.00368

Ginhoux, F., Greter, M., Leboeuf, M., Nandi, S., See, P., Gokhan, S., Mehler, M. F., Conway, S. J., Ng, L. G., Stanley, E. R., Samokhvalov, I. M., & Merad, M. (2010). Fate Mapping Analysis Reveals That Adult Microglia Derive from Primitive Macrophages. *Science*, *330*(6005), 841–845. https://doi.org/10.1126/science.1194637

Girgenti, M. J., Wohleb, E. S., Mehta, S., Ghosal, S., Fogaca, M. V., & Duman, R. S. (2019). Prefrontal cortex interneurons display dynamic sex-specific stress-induced transcriptomes. *Translational Psychiatry*, *9*, 292. https://doi.org/10.1038/s41398-019-0642-z

Giulian, D., Baker, T. J., Shih, L. C., & Lachman, L. B. (1986). Interleukin 1 of the central nervous system is produced by ameboid microglia. *The Journal of Experimental Medicine*, *164*(2), 594–604. https://doi.org/10.1084/jem.164.2.594

Glenner, G. G., & Murphy, M. A. (1989). Amyloidosis of the nervous system. *Journal of the Neurological Sciences*, *94*(1–3), 1–28. https://doi.org/10.1016/0022-510x(89)90214-1

Goate, A., Chartier-Harlin, M.-C., Mullan, M., Brown, J., Crawford, F., Fidani, L., Giuffra, L., Haynes, A., Irving, N., James, L., Mant, R., Newton, P., Rooke, K., Roques, P., Talbot, C., Pericak-Vance, M., Roses, A., Williamson, R., Rossor, M., … Hardy, J. (1991). Segregation of a missense mutation in the amyloid precursor protein gene with

familial Alzheimer's disease. *Nature*, *349*(6311), 704–706. https://doi.org/10.1038/349704a0

Godbout, J. P., Chen, J., Abraham, J., Richwine, A. F., Berg, B. M., Kelley, K. W., & Johnson, R. W. (2005). Exaggerated neuroinflammation and sickness behavior in aged mice following activation of the peripheral innate immune system. *FASEB Journal: Official Publication of the Federation of American Societies for Experimental Biology*, *19*(10), 1329–1331. https://doi.org/10.1096/fj.05-3776fje

Goedert, M., Wischik, C. M., Crowther, R. A., Walker, J. E., & Klug, A. (1988). Cloning and sequencing of the cDNA encoding a core protein of the paired helical filament of Alzheimer disease: Identification as the microtubule-associated protein tau. *Proceedings of the National Academy of Sciences*, *85*(11), 4051–4055. https://doi.org/10.1073/pnas.85.11.4051

Gong, Y., Chen, J., Jin, Y., Wang, C., Zheng, M., & He, L. (2020). GW9508 ameliorates cognitive impairment via the cAMP-CREB and JNK pathways in APPswe/PS1dE9 mouse model of Alzheimer's disease. *Neuropharmacology*, *164*, 107899. https://doi.org/10.1016/j.neuropharm.2019.107899

Goutagny, R., Gu, N., Cavanagh, C., Jackson, J., Chabot, J. G., Quirion, R., Krantic, S., & Williams, S. (2013). Alterations in hippocampal network oscillations and theta-gamma coupling arise before Aβ overproduction in a mouse model of Alzheimer's disease. *European Journal of Neuroscience*, *37*(12), 1896–1902. https://doi.org/10.1111/ejn.12233

Gray, C. M. (1994). Synchronous oscillations in neuronal systems: Mechanisms and functions. *Journal of Computational Neuroscience*, *1*(1–2), 11–38. https://doi.org/10.1007/BF00962716

Gray, C. M., König, P., Engel, A. K., & Singer, W. (1989). Oscillatory responses in cat visual cortex exhibit inter-columnar synchronization which reflects global stimulus properties. *Nature*, *338*(6213), 334–337. https://doi.org/10.1038/338334a0

Griciuc, A., Federico, A. N., Natasan, J., Forte, A. M., McGinty, D., Nguyen, H., Volak, A., LeRoy, S., Gandhi, S., Lerner, E. P., Hudry, E., Tanzi, R. E., & Maguire, C. A. (2020). Gene therapy for Alzheimer's disease targeting CD33 reduces amyloid beta accumulation and neuroinflammation. *Human Molecular Genetics*, *29*(17), 2920–2935. https://doi.org/10.1093/hmg/ddaa179

Griciuc, A., Serrano-Pozo, A., Parrado, A. R., Lesinski, A. N., Asselin, C. N., Mullin, K., Hooli, B., Choi, S. H., Hyman, B. T., & Tanzi, R. E. (2013). Alzheimer's disease risk gene CD33 inhibits microglial uptake of amyloid beta. *Neuron*, *78*(4), 631–643. https://doi.org/10.1016/j.neuron.2013.04.014

Grubman, A., Chew, G., Ouyang, J. F., Sun, G., Choo, X. Y., McLean, C., Simmons, R. K., Buckberry, S., Vargas-Landin, D. B., Poppe, D., Pflueger, J., Lister, R., Rackham, O. J.

L., Petretto, E., & Polo, J. M. (2019). A single-cell atlas of entorhinal cortex from individuals with Alzheimer's disease reveals cell-type-specific gene expression regulation. *Nature Neuroscience*, *22*(12), 2087–2097. https://doi.org/10.1038/s41593-019-0539-4

Gu, X., Wu, H., Xie, Y., Xu, L., Liu, X., & Wang, W. (2021). Caspase-1/IL-1β represses membrane transport of GluA1 by inhibiting the interaction between Stargazin and GluA1 in Alzheimer's disease. *Molecular Medicine*, *27*(1), 8. https://doi.org/10.1186/s10020-021-00273-8

Guerra, A., Colella, D., Giangrosso, M., Cannavacciuolo, A., Paparella, G., Fabbrini, G., Suppa, A., Berardelli, A., & Bologna, M. (2022). Driving motor cortex oscillations modulates bradykinesia in Parkinson's disease. *Brain: A Journal of Neurology*, *145*(1), 224–236. https://doi.org/10.1093/brain/awab257

Guerreiro, R., Wojtas, A., Bras, J., Carrasquillo, M., Rogaeva, E., Majounie, E., Cruchaga, C., Sassi, C., Kauwe, J. S. K., Younkin, S., Hazrati, L., Collinge, J., Pocock, J., Lashley, T., Williams, J., Lambert, J.-C., Amouyel, P., Goate, A., Rademakers, R., … Hardy, J. (2013). TREM2 Variants in Alzheimer's Disease. *New England Journal of Medicine*, *368*(2), 117–127. https://doi.org/10.1056/nejmoa1211851

Gulen, M. F., Samson, N., Keller, A., Schwabenland, M., Liu, C., Glück, S., Thacker, V. V., Favre, L., Mangeat, B., Kroese, L. J., Krimpenfort, P., Prinz, M., & Ablasser, A. (2023). cGAS-STING drives ageing-related inflammation and neurodegeneration. *Nature*, *620*(7973), 374–380. https://doi.org/10.1038/s41586-023-06373-1

Gulyás, A. I., Buzsáki, G., Freund, T. F., & Hirase, H. (2006). Populations of hippocampal inhibitory neurons express different levels of cytochrome c. *European Journal of Neuroscience*, *23*(10), 2581–2594. https://doi.org/10.1111/j.1460-9568.2006.04814.x

Gulyás, A. I., Megías, M., Emri, Z., & Freund, T. F. (1999). Total number and ratio of excitatory and inhibitory synapses converging onto single interneurons of different types in the CA1 area of the rat hippocampus. *Journal of Neuroscience*, *19*(22), 10082–10097. https://doi.org/10.1523/jneurosci.19-22-10082.1999

Güntekin, B., & Başar, E. (2007). Brain oscillations are highly influenced by gender differences. *International Journal of Psychophysiology*, *65*(3), 294–299. https://doi.org/10.1016/j.ijpsycho.2007.03.009

Güntekin, B., Erdal, F., Bölükbaş, B., Hanoğlu, L., Yener, G., & Duygun, R. (2023). Alterations of resting-state Gamma frequency characteristics in aging and Alzheimer's disease. *Cognitive Neurodynamics*, *17*(4), 829–844. https://doi.org/10.1007/s11571-022-09873-4

Gurevicius, K., Lipponen, A., & Tanila, H. (2012). Increased Cortical and Thalamic Excitability in Freely Moving APPswe/PS1dE9 Mice Modeling Epileptic Activity Associated with Alzheimer's Disease. *Cerebral Cortex*, *23*(5), 1148–1158.

Hamm, V., Héraud, C., Bott, J. B., Herbeaux, K., Strittmatter, C., Mathis, C., & Goutagny, R. (2017). Differential contribution of APP metabolites to early cognitive deficits in a TgCRND8 mouse model of Alzheimer's disease. *Science Advances*, *3*(2), e1601068. https://doi.org/10.1126/sciadv.1601068

Hampel, H., Mesulam, M. M., Cuello, A. C., Farlow, M. R., Giacobini, E., Grossberg, G. T., Khachaturian, A. S., Vergallo, A., Cavedo, E., Snyder, P. J., & Khachaturian, Z. S. (2018). The cholinergic system in the pathophysiology and treatment of Alzheimer's disease. *Brain*, *141*(7), 1917–1933. https://doi.org/10.1093/brain/awy132

Hardingham, G. E., & Do, K. Q. (2016). Linking early-life NMDAR hypofunction and oxidative stress in schizophrenia pathogenesis. *Nature Reviews. Neuroscience*, *17*(2), 125–134. https://doi.org/10.1038/nrn.2015.19

Harris, K., Ling, Y., Bukhbinder, A. S., Chen, L., Phelps, K. N., Cruz, G., Thomas, J., Kim, Y., Jiang, X., & Schulz, P. E. (2023). The Impact of Routine Vaccinations on Alzheimer's Disease Risk in Persons 65 Years and Older: A Claims-Based Cohort Study using Propensity Score Matching. *Journal of Alzheimer's Disease*, *95*(2), 703–718. https://doi.org/10.3233/JAD-221231

Hart, B. L. (1988). Biological basis of the behavior of sick animals. *Neuroscience and Biobehavioral Reviews*, *12*(2), 123–137. https://doi.org/10.1016/s0149-7634(88)80004-6

Hasam-Henderson, L. A., Gotti, G. C., Mishto, M., Klisch, C., Gerevich, Z., Geiger, J. R. P., & Kovács, R. (2018). NMDA-receptor inhibition and oxidative stress during hippocampal maturation differentially alter parvalbumin expression and gamma-band activity. *Scientific Reports*, *8*, 9545. https://doi.org/10.1038/s41598-018-27830-2

Hasel, P., Aisenberg, W. H., Bennett, F. C., & Liddelow, S. A. (2023). Molecular and metabolic heterogeneity of astrocytes and microglia. *Cell Metabolism*, *35*(4), 555–570. https://doi.org/10.1016/j.cmet.2023.03.006

Hasel, P., Dando, O., Jiwaji, Z., Baxter, P., Todd, A. C., Heron, S., Márkus, N. M., McQueen, J., Hampton, D. W., Torvell, M., Tiwari, S. S., McKay, S., Eraso-Pichot, A., Zorzano, A., Masgrau, R., Galea, E., Chandran, S., Wyllie, D. J. A., Simpson, T. I., & Hardingham, G. E. (2017). Neurons and neuronal activity control gene expression in astrocytes to regulate their development and metabolism. *Nature Communications*, *8*(1), 15132. https://doi.org/10.1038/ncomms15132

Hasel, P., Rose, I. V. L., Sadick, J. S., Kim, R. D., & Liddelow, S. A. (2021). Neuroinflammatory astrocyte subtypes in the mouse brain. *Nature Neuroscience*, *24*(10), 1475–1487. https://doi.org/10.1038/s41593-021-00905-6

Hauser, W. A., Morris, M. L., Heston, L. L., & Anderson, V. E. (1986). Seizures and myoclonus in patients with Alzheimer's disease. *Neurology*, *36*(9), 1226–1230. https://doi.org/10.1212/wnl.36.9.1226

Hayashi, F., Smith, K. D., Ozinsky, A., Hawn, T. R., Yi, E. C., Goodlett, D. R., Eng, J. K., Akira, S., Underhill, D. M., & Aderem, A. (2001). The innate immune response to bacterial flagellin is mediated by Toll-like receptor 5. *Nature*, *410*(6832), 1099–1103. https://doi.org/10.1038/35074106

Haynes, S. E., Hollopeter, G., Yang, G., Kurpius, D., Dailey, M. E., Gan, W.-B., & Julius, D. (2006). The P2Y12 receptor regulates microglial activation by extracellular nucleotides. *Nature Neuroscience*, *9*(12), 1512–1519. https://doi.org/10.1038/nn1805

He, X., Li, J., Zhou, G., Yang, J., McKenzie, S., Li, Y., Li, W., Yu, J., Wang, Y., Qu, J., Wu, Z., Hu, H., Duan, S., & Ma, H. (2021). Gating of hippocampal rhythms and memory by synaptic plasticity in inhibitory interneurons. *Neuron*, *109*(6), 1013-1028.e9. https://doi.org/10.1016/j.neuron.2021.01.014

Hebert, L. E., Weuve, J., Scherr, P. A., & Evans, D. A. (2013). Alzheimer disease in the United States (2010–2050) estimated using the 2010 census. *Neurology*, *80*(19), 1778. https://doi.org/10.1212/WNL.0B013E31828726F5

Heir, R., Abbasi, Z., Komal, P., Altimimi, H. F., Franquin, M., Moschou, D., Chambon, J., & Stellwagen, D. (2024). Astrocytes Are the Source of TNF Mediating Homeostatic Synaptic Plasticity. *Journal of Neuroscience*, *44*(14). https://doi.org/10.1523/JNEUROSCI.2278-22.2024

Heneka, M. T., Kummer, M. P., Stutz, A., Delekate, A., Schwartz, S., Vieira-Saecker, A., Griep, A., Axt, D., Remus, A., Tzeng, T.-C., Gelpi, E., Halle, A., Korte, M., Latz, E., & Golenbock, D. T. (2013). NLRP3 is activated in Alzheimer's disease and contributes to pathology in APP/PS1 mice. *Nature*, *493*(7434), 674–678. https://doi.org/10.1038/nature11729

Hennessy, E., Griffin, E. W., & Cunningham, C. (2015). Astrocytes are primed by chronic neurodegeneration to produce exaggerated chemokine and cell infiltration responses to acute stimulation with the cytokines IL-1β and TNF-α. *Journal of Neuroscience*, *35*(22), 8411–8422. https://doi.org/10.1523/JNEUROSCI.2745-14.2015

Herculano-Houzel, S. (2009). The Human Brain in Numbers: A Linearly Scaled-up Primate Brain. *Frontiers in Human Neuroscience*, *3*, 31. https://doi.org/10.3389/neuro.09.031.2009

Herreras, O. (2016). Local Field Potentials: Myths and Misunderstandings. *Frontiers in Neural Circuits*, *10*. https://www.frontiersin.org/articles/10.3389/fncir.2016.00101

Herrmann, C. S., & Demiralp, T. (2005). *Human EEG gamma oscillations in neuropsychiatric disorders*. https://doi.org/10.1016/j.clinph.2005.07.007

Hertz, L., Dringen, R., Schousboe, A., & Robinson, S. R. (1999). Astrocytes: Glutamate producers for neurons. *Journal of Neuroscience Research*, *57*(4), 417–428.

Hesdorffer, D. C., Hauser, W. A., Annegers, J. F., Kokmen, E., & Rocca, W. A. (1996). Dementia and adult-onset unprovoked seizures. *Neurology*, *46*(3), 727–730. https://doi.org/10.1212/wnl.46.3.727

Hide, I., Tanaka, M., Inoue, A., Nakajima, K., Kohsaka, S., Inoue, K., & Nakata, Y. (2000). Extracellular ATP triggers tumor necrosis factor-alpha release from rat microglia. *Journal of Neurochemistry*, *75*(3), 965–972. https://doi.org/10.1046/j.1471-4159.2000.0750965.x

Hijazi, S., Heistek, T. S., Scheltens, P., Neumann, U., Shimshek, D. R., Mansvelder, H. D., Smit, A. B., & Kesteren, R. E. van. (2020). Early restoration of parvalbumin interneuron activity prevents memory loss and network hyperexcitability in a mouse model of Alzheimer's disease. *Molecular Psychiatry*, *25*(12), 3380. https://doi.org/10.1038/S41380-019-0483-4

Hijazi, S., Smit, A. B., & Van Kesteren, R. E. (2023). Fast-spiking parvalbumin-positive interneurons in brain physiology and Alzheimer's disease. *Molecular Psychiatry*. https://doi.org/10.1038/s41380-023-02168-y

Hirtz, D., Thurman, D. J., Gwinn-Hardy, K., Mohamed, M., Chaudhuri, A. R., & Zalutsky, R. (2007). How common are the "common" neurologic disorders? *Neurology*, *68*(5), 326–337. https://doi.org/10.1212/01.wnl.0000252807.38124.a3

Hoek, R. M., Ruuls, S. R., Murphy, C. A., Wright, G. J., Goddard, R., Zurawski, S. M., Blom, B., Homola, M. E., Streit, W. J., Brown, M. H., Barclay, A. N., & Sedgwick, J. D. (2000). Down-Regulation of the Macrophage Lineage Through Interaction with OX2 (CD200). *Science*, *290*(5497), 1768–1771. https://doi.org/10.1126/science.290.5497.1768

Holley, A. J., & Lugo, J. N. (2016). Effects of an Acute Seizure on Associative Learning and Memory. *Epilepsy & Behavior : E&B*, *54*, 51–57. https://doi.org/10.1016/j.yebeh.2015.11.001

Hollnagel, J. O., Elzoheiry, S., Gorgas, K., Kins, S., Beretta, C. A., Kirsch, J., Kuhse, J., Kann, O., & Kiss, E. (2019). Early alterations in hippocampal perisomatic GABAergic synapses and network oscillations in a mouse model of Alzheimer's disease amyloidosis. *PLoS ONE*, *14*(1), e0209228. https://doi.org/10.1371/journal.pone.0209228

Holm, T. H., Draeby, D., & Owens, T. (2012). Microglia are required for astroglial Toll-like receptor 4 response and for optimal TLR2 and TLR3 response. *Glia*, *60*(4), 630–638. https://doi.org/10.1002/glia.22296

Holmes, C., Cunningham, C., Zotova, E., Woolford, J., Dean, C., Kerr, S., Culliford, D., & Perry, V. H. (2009). Systemic inflammation and disease progression in Alzheimer disease. *Neurology*, *73*(10), 768. https://doi.org/10.1212/WNL.0B013E3181B6BB95

Holtman, I. R., Raj, D. D., Miller, J. A., Schaafsma, W., Yin, Z., Brouwer, N., Wes, P. D., Möller, T., Orre, M., Kamphuis, W., Hol, E. M., Boddeke, E. W. G. M., & Eggen, B.

J. L. (2015). Induction of a common microglia gene expression signature by aging and neurodegenerative conditions: A co-expression meta-analysis. *Acta Neuropathologica Communications*, *3*(1), 31. https://doi.org/10.1186/s40478-015-0203-5

Holtzman, D. M., Fagan, A. M., Mackey, B., Tenkova, T., Sartorius, L., Paul, S. M., Bales, K., Ashe, K. H., Irizarry, M. C., & Hyman, B. T. (2000). Apolipoprotein E facilitates neuritic and cerebrovascular plaque formation in an Alzheimer's disease model. *Annals of Neurology*, *47*(6), 739–747.

Hong, S., Beja-Glasser, V. F., Nfonoyim, B. M., Frouin, A., Li, S., Ramakrishnan, S., Merry, K. M., Shi, Q., Rosenthal, A., Barres, B. A., Lemere, C. A., Selkoe, D. J., & Stevens, B. (2016). Complement and Microglia Mediate Early Synapse Loss in Alzheimer Mouse Models. *Science (New York, N.Y.)*, *352*(6286), 712–716. https://doi.org/10.1126/science.aad8373

Hoozemans, J. J. M., Rozemuller, J. M., van Haastert, E. S., Veerhuis, R., & Eikelenboom, P. (2008). Cyclooxygenase-1 and -2 in the different stages of Alzheimer's disease pathology. *Current Pharmaceutical Design*, *14*(14), 1419–1427. https://doi.org/10.2174/138161208784480171

Horiuchi, T., Mitoma, H., Harashima, S., Tsukamoto, H., & Shimoda, T. (2010). Transmembrane TNF-α: Structure, function and interaction with anti-TNF agents. *Rheumatology*, *49*(7), 1215–1228. https://doi.org/10.1093/rheumatology/keq031

Hormuzdi, S. G., Pais, I., LeBeau, F. E. N., Towers, S. K., Rozov, A., Buhl, E. H., Whittington, M. A., & Monyer, H. (2001). Impaired Electrical Signaling Disrupts Gamma Frequency Oscillations in Connexin 36-Deficient Mice. *Neuron*, *31*(3), 487–495. https://doi.org/10.1016/S0896-6273(01)00387-7

Hu, H., & Jonas, P. (2014). A supercritical density of Na+ channels ensures fast signaling in GABAergic interneuron axons. *Nature Neuroscience*, *17*(5), 686–693. https://doi.org/10.1038/nn.3678

Hu, H., Martina, M., & Jonas, P. (2010). Dendritic mechanisms underlying rapid synaptic activation of fast-spiking hippocampal interneurons. *Science*, *327*(5961), 52–58. https://doi.org/10.1126/science.1177876

Hu, Y., Huang, Y., Xing, S., Chen, C., Shen, D., & Chen, J. (2022). Aβ promotes CD38 expression in senescent microglia in Alzheimer's disease. *Biological Research*, *55*(1), 10. https://doi.org/10.1186/s40659-022-00379-1

Huang, C., Wahlund, L. O., Dierks, T., Julin, P., Winblad, B., & Jelic, V. (2000). Discrimination of Alzheimer's disease and mild cognitive impairment by equivalent EEG sources: A cross-sectional and longitudinal study. *Clinical Neurophysiology*, *111*(11), 1961–1967. https://doi.org/10.1016/S1388-2457(00)00454-5

Huberfeld, G., Blauwblomme, T., & Miles, R. (2015). Hippocampus and epilepsy: Findings from human tissues. *Revue Neurologique*, *171*(3), 236–251. https://doi.org/10.1016/j.neurol.2015.01.563

Hughes, M. M., Field, R. H., Perry, V. H., Murray, C. L., & Cunningham, C. (2010). Microglia in the degenerating brain are capable of phagocytosis of beads and of apoptotic cells, but do not efficiently remove PrPSc, even upon LPS stimulation. *Glia*, *58*(16), 2017–2030. https://doi.org/10.1002/glia.21070

Iaccarino, H. F., Singer, A. C., Martorell, A. J., Rudenko, A., Gao, F., Gillingham, T. Z., Mathys, H., Seo, J., Kritskiy, O., Abdurrob, F., Adaikkan, C., Canter, R. G., Rueda, R., Brown, E. N., Boyden, E. S., & Tsai, L. H. (2016). Gamma frequency entrainment attenuates amyloid load and modifies microglia. *Nature*, *540*(7632), 230–235. https://doi.org/10.1038/nature20587

Ince, P. G. (2001). Pathological correlates of late-onset dementia in a multicentre, community-based population in England and Wales. *The Lancet*, *357*(9251), 169–175. https://doi.org/10.1016/S0140-6736(00)03589-3

Inouye, S. K. (2006). Delirium in older persons. *New England Journal of Medicine*, *354*(11), 1157–1165. https://doi.org/10.1056/NEJMra052321

Irizarry, M. C., Jin, S., He, F., Emond, J. A., Raman, R., Thomas, R. G., Sano, M., Quinn, J. F., Tariot, P. N., Galasko, D. R., Ishihara, L. S., Weil, J. G., & Aisen, P. S. (2012). Incidence of New-Onset Seizures in Mild to Moderate Alzheimer Disease. *Archives of Neurology*, *69*(3), 368. https://doi.org/10.1001/archneurol.2011.830

Islam, S. (2022). *The role of Colony Stimulating Factor 1 Receptor in microglial phenotype and function in vitro and in vivo*. University of Dublin, Trinity College.

Ittner, A. A., Gladbach, A., Bertz, J., Suh, L. S., & Ittner, L. M. (2014). p38 MAP kinase-mediated NMDA receptor-dependent suppression of hippocampal hypersynchronicity in a mouse model of Alzheimer's disease. Acta Neuropathologica Communications, 2(1) | 10.1186/s40478-014-0149-z. *Acta Neuropathologica Communications*, *2*(149). https://sci-hub.si/https://link.springer.com/article/10.1186/s40478-014-0149-z

Jarrett, J. T., Berger, E. P., & Lansbury, P. T. (1993). The Carboxy Terminus of the β Amyloid Protein Is Critical for the Seeding of Amyloid Formation: Implications for the Pathogenesis of Alzheimer's Disease. *Biochemistry*, *32*(18), 4693–4697. https://doi.org/10.1021/bi00069a001

Jasper, H. H., & Andrews, H. L. (1938). BRAIN POTENTIALS AND VOLUNTARY MUSCLE ACTIVITY IN MAN. *Journal of Neurophysiology*, *1*(2), 87–100. https://doi.org/10.1152/jn.1938.1.2.87

Jefferies, C., Bowie, A., Brady, G., Cooke, E.-L., Li, X., & O'Neill, L. A. J. (2001). Transactivation by the p65 Subunit of NF-κB in Response to Interleukin-1 (IL-1)

Involves MyD88, IL-1 Receptor-Associated Kinase 1, TRAF-6, and Rac1. *Molecular and Cellular Biology*, *21*(14), 4544–4552. https://doi.org/10.1128/MCB.21.14.4544-4552.2001

Jekabsone, A., Mander, P. K., Tickler, A., Sharpe, M., & Brown, G. C. (2006). Fibrillar beta-amyloid peptide Aβ1–40 activates microglial proliferation via stimulating TNF-α release and H2O2 derived from NADPH oxidase: A cell culture study. *Journal of Neuroinflammation*, *3*, 24. https://doi.org/10.1186/1742-2094-3-24

Jelic, V., Shigeta, M., Julin, P., Almkvist, O., Winblad, B., & Wahlund, L. O. (1996). Quantitative electroencephalography power and coherence in alzheimer's disease and mild cognitive impairment. *Dementia and Geriatric Cognitive Disorders*, *7*(6), 314–323. https://doi.org/10.1159/000106897

Jendresen, C., Årskog, V., Daws, M. R., & Nilsson, L. N. G. (2017). The Alzheimer's disease risk factors apolipoprotein E and TREM2 are linked in a receptor signaling pathway. *Journal of Neuroinflammation*, *14*(1), 59. https://doi.org/10.1186/s12974-017-0835-4

Jensen, O., & Colgin, L. L. (2007). Cross-frequency coupling between neuronal oscillations. *Trends in Cognitive Sciences*, *11*(7), 267–269. https://doi.org/10.1016/j.tics.2007.05.003

Ji, K., Akgul, G., Wollmuth, L. P., & Tsirka, S. E. (2013). Microglia actively regulate the number of functional synapses. *PloS One*, *8*(2), e56293. https://doi.org/10.1371/journal.pone.0056293

Ji, M., Li, S., Zhang, L., Gao, Y., Zeng, Q., Mao, M., & Yang, J. (2020). Sepsis induced cognitive impairments by disrupting hippocampal parvalbumin interneuron-mediated inhibitory network via a D4-receptor mechanism. *Aging*, *12*(3), 2471–2484. https://doi.org/10.18632/aging.102755

Jiang, Q., Lee, C. Y. D., Mandrekar, S., Wilkinson, B., Cramer, P., Zelcer, N., Mann, K., Lamb, B., Willson, T. M., Collins, J. L., Richardson, J. C., Smith, J. D., Comery, T. A., Riddell, D., Holtzman, D. M., Tontonoz, P., & Landreth, G. E. (2008). ApoE Promotes the Proteolytic Degradation of Aβ. *Neuron*, *58*(5), 681–693. https://doi.org/10.1016/j.neuron.2008.04.010

Jiao, S.-S., Bu, X.-L., Liu, Y.-H., Zhu, C., Wang, Q.-H., Shen, L.-L., Liu, C.-H., Wang, Y.-R., Yao, X.-Q., & Wang, Y.-J. (2016). Sex Dimorphism Profile of Alzheimer's Disease-Type Pathologies in an APP/PS1 Mouse Model. *Neurotoxicity Research*, *29*(2), 256–266. https://doi.org/10.1007/s12640-015-9589-x

Jin, N., Lipponen, A., Koivisto, H., Gurevicius, K., & Tanila, H. (2018). Increased cortical beta power and spike-wave discharges in middle-aged APP/PS1 mice. *Neurobiology of Aging*, *71*, 127–141. https://doi.org/10.1016/j.neurobiolaging.2018.07.009

Jones, D. T., Graff-Radford, J., Lowe, V. J., Wiste, H. J., Gunter, J. L., Senjem, M. L., Botha, H., Kantarci, K., Boeve, B. F., Knopman, D. S., Petersen, R. C., & Jack, C. R. (2017).

Tau, amyloid, and cascading network failure across the Alzheimer's disease spectrum. *Cortex*, *97*, 143–159. https://doi.org/10.1016/j.cortex.2017.09.018

Jonsson, T., Stefansson, H., Steinberg, S., Jonsdottir, I., Jonsson, P. V., Snaedal, J., Bjornsson, S., Huttenlocher, J., Levey, A. I., Lah, J. J., Rujescu, D., Hampel, H., Giegling, I., Andreassen, O. A., Engedal, K., Ulstein, I., Djurovic, S., Ibrahim-Verbaas, C., Hofman, A., … Stefansson, K. (2013). Variant of TREM2 Associated with the Risk of Alzheimer's Disease. *New England Journal of Medicine*, *368*(2), 107–116. https://doi.org/10.1056/nejmoa1211103

Kaczmarek, L. K., & Zhang, Y. (2017). Kv3 channels: Enablers of rapid firing, neurotransmitter release, and neuronal endurance. *Physiological Reviews*, *97*(4), 1431–1468. https://doi.org/10.1152/physrev.00002.2017

Kanak, D. J., Jones, R. T., Tokhi, A., Willingham, A. L., Zaveri, H. P., Rose, G. M., & Patrylo, P. R. (2011). Electrical and Pharmacological Stimuli Reveal a Greater Susceptibility for CA3 Network Excitability in Hippocampal Slices from Aged vs. Adult Fischer 344 Rats. *Aging and Disease*, *2*(4), 318–331.

Kandel, E. R., Schwartz, J. H., & Jessell, T. M. (2000). *Principles of Neural Science* (4th ed.). McGraw-Hill Companies.

Kann, O., Hollnagel, J.-O., Elzoheiry, S., & Schneider, J. (2016). Energy and Potassium Ion Homeostasis during Gamma Oscillations. *Frontiers in Molecular Neuroscience*, *9*, 47. https://doi.org/10.3389/fnmol.2016.00047

Kapasi, A., DeCarli, C., & Schneider, J. A. (2017). Impact of multiple pathologies on the threshold for clinically overt dementia. *Acta Neuropathologica*, *134*(2), 171–186. https://doi.org/10.1007/s00401-017-1717-7

Katsuki, H., Nakai, S., Hirai, Y., Akaji, K., Kiso, Y., & Satoh, M. (1990). Interleukin-1 beta inhibits long-term potentiation in the CA3 region of mouse hippocampal slices. *European Journal of Pharmacology*, *181*(3), 323–326. https://doi.org/10.1016/0014-2999(90)90099-r

Katz, L. C., & Shatz, C. J. (1996). Synaptic Activity and the Construction of Cortical Circuits. *Science*, *274*(5290), 1133–1138. https://doi.org/10.1126/science.274.5290.1133

Kawaguchi, Y., Katsumaru, H., Kosaka, T., Heizmann, C. W., & Hama, K. (1987). Fast spiking cells in rat hippocampus (CA1 region) contain the calcium-binding protein parvalbumin. *Brain Research*, *416*(2), 369–374. https://doi.org/10.1016/0006-8993(87)90921-8

Kawanokuchi, J., Mizuno, T., Takeuchi, H., Kato, H., Wang, J., Mitsuma, N., & Suzumura, A. (2006). Production of interferon-gamma by microglia. *Multiple Sclerosis (Houndmills, Basingstoke, England)*, *12*(5), 558–564. https://doi.org/10.1177/1352458506070763

Kelley, T. W., Graham, M. M., Doseff, A. I., Pomerantz, R. W., Lau, S. M., Ostrowski, M. C., Franke, T. F., & Marsh, C. B. (1999). Macrophage colony-stimulating factor promotes

cell survival through Akt/protein kinase B. *The Journal of Biological Chemistry*, *274*(37), 26393–26398. https://doi.org/10.1074/jbc.274.37.26393

Keren-Shaul, H., Spinrad, A., Weiner, A., Matcovitch-Natan, O., Dvir-Szternfeld, R., Ulland, T. K., David, E., Baruch, K., Lara-Astaiso, D., Toth, B., Itzkovitz, S., Colonna, M., Schwartz, M., & Amit, I. (2017). A Unique Microglia Type Associated with Restricting Development of Alzheimer's Disease. *Cell*, *169*(7), 1276-1290.e17. https://doi.org/10.1016/j.cell.2017.05.018

Kersanté, F., Rowley, S. C. S., Pavlov, I., Gutièrrez-Mecinas, M., Semyanov, A., Reul, J. M. H. M., Walker, M. C., & Linthorst, A. C. E. (2013). A functional role for both -aminobutyric acid (GABA) transporter-1 and GABA transporter-3 in the modulation of extracellular GABA and GABAergic tonic conductances in the rat hippocampus. *The Journal of Physiology*, *591*(10), 2429–2441. https://doi.org/10.1113/jphysiol.2012.246298

Kesika, P., Suganthy, N., Sivamaruthi, B. S., & Chaiyasut, C. (2021). Role of gut-brain axis, gut microbial composition, and probiotic intervention in Alzheimer's disease. *Life Sciences*, *264*, 118627. https://doi.org/10.1016/j.lfs.2020.118627

Kettenmann, H. (2007). The brain's garbage men. *Nature*, *446*(7139), Article 7139. https://doi.org/10.1038/nature05713

Khazipov, R., & Holmes, G. L. (2003). Synchronization of Kainate-Induced Epileptic Activity via GABAergic Inhibition in the Superfused Rat Hippocampus In Vivo. *The Journal of Neuroscience*, *23*(12), 5337–5341. https://doi.org/10.1523/JNEUROSCI.23-12-05337.2003

Kidd, M. (1963). Paired Helical Filaments in Electron Microscopy of Alzheimer's Disease. *Nature*, *197*(4863), 192–193. https://doi.org/10.1038/197192b0

Killin, L. O. J., Starr, J. M., Shiue, I. J., & Russ, T. C. (2016). Environmental risk factors for dementia: A systematic review. *BMC Geriatrics*, *16*, 175. https://doi.org/10.1186/s12877-016-0342-y

Kim, Y., Yang, G. R., Pradhan, K., Venkataraju, K. U., Bota, M., Molino, L. C. G. del, Fitzgerald, G., Ram, K., He, M., Levine, J. M., Mitra, P., Huang, Z. J., Wang, X.-J., & Osten, P. (2017). Brain-wide Maps Reveal Stereotyped Cell-Type-Based Cortical Architecture and Subcortical Sexual Dimorphism. *Cell*, *171*(2), 456-469.e22. https://doi.org/10.1016/j.cell.2017.09.020

Klein, A. S., Donoso, J. R., Kempter, R., Schmitz, D., & Beed, P. (2016). Early cortical changes in gamma oscillations in alzheimer's disease. *Frontiers in Systems Neuroscience*, *10*(OCT). https://doi.org/10.3389/fnsys.2016.00083

Koenig, T., Prichep, L., Dierks, T., Hubl, D., Wahlund, L. O., John, E. R., & Jelic, V. (2005). Decreased EEG synchronization in Alzheimer's disease and mild cognitive impairment.

Neurobiology of Aging, *26*(2), 165–171. https://doi.org/10.1016/j.neurobiolaging.2004.03.008

Koizumi, S., Shigemoto-Mogami, Y., Nasu-Tada, K., Shinozaki, Y., Ohsawa, K., Tsuda, M., Joshi, B. V., Jacobson, K. A., Kohsaka, S., & Inoue, K. (2007). UDP acting at P2Y6 receptors is a mediator of microglial phagocytosis. *Nature*, *446*(7139), Article 7139. https://doi.org/10.1038/nature05704

Korin, B., Ben-Shaanan, T. L., Schiller, M., Dubovik, T., Azulay-Debby, H., Boshnak, N. T., Koren, T., & Rolls, A. (2017). High-dimensional, single-cell characterization of the brain's immune compartment. *Nature Neuroscience*, *20*(9), 1300–1309. https://doi.org/10.1038/nn.4610

Kosaka, T., Katsumaru, H., Hama, K., Wu, J. Y., & Heizmann, C. W. (1987). GABAergic neurons containing the Ca2+-binding protein parvalbumin in the rat hippocampus and dentate gyrus. *Brain Research*, *419*(1–2), 119–130. https://doi.org/10.1016/0006-8993(87)90575-0

Krasemann, S., Madore, C., Cialic, R., Baufeld, C., Calcagno, N., El Fatimy, R., Beckers, L., O'Loughlin, E., Xu, Y., Fanek, Z., Greco, D. J., Smith, S. T., Tweet, G., Humulock, Z., Zrzavy, T., Conde-Sanroman, P., Gacias, M., Weng, Z., Chen, H., … Butovsky, O. (2017). The TREM2-APOE pathway drives the transcriptional phenotype of dysfunctional microglia in neurodegenerative diseases. *Immunity*, *47*(3), 566-581.e9. https://doi.org/10.1016/j.immuni.2017.08.008

Kriegstein, A., & Alvarez-Buylla, A. (2009). The Glial Nature of Embryonic and Adult Neural Stem Cells. *Annual Review of Neuroscience*, *32*, 149–184. https://doi.org/10.1146/annurev.neuro.051508.135600

Kuhn, S. A., van Landeghem, F. K. H., Zacharias, R., Färber, K., Rappert, A., Pavlovic, S., Hoffmann, A., Nolte, C., & Kettenmann, H. (2004). Microglia express GABAB receptors to modulate interleukin release. *Molecular and Cellular Neuroscience*, *25*(2), 312–322. https://doi.org/10.1016/j.mcn.2003.10.023

Kunkle, B. W., Grenier-Boley, B., Sims, R., Bis, J. C., Damotte, V., Naj, A. C., Boland, A., Vronskaya, M., Lee, S. J. van der, Amlie-Wolf, A., Bellenguez, C., Frizatti, A., Chouraki, V., Martin, E. R., Sleegers, K., Badarinarayan, N., Jakobsdottir, J., Hamilton-Nelson, K. L., Moreno-Grau, S., … Pericak-Vance, M. A. (2019). Genetic meta-analysis of diagnosed Alzheimer's disease identifies new risk loci and implicates Aβ, tau, immunity and lipid processing. *Nature Genetics*, *51*(3), 414. https://doi.org/10.1038/S41588-019-0358-2

Kuramoto, E., Tanaka, Y. R., Hioki, H., Goto, T., & Kaneko, T. (2022). Local Connections of Pyramidal Neurons to Parvalbumin-Producing Interneurons in Motor-Associated Cortical Areas of Mice. *eNeuro*, *9*(1). https://doi.org/10.1523/ENEURO.0567-20.2021

Kurudenkandy, F. R., Zilberter, M., Biverstål, H., Presto, J., Honcharenko, D., Strömberg, R., Johansson, J., Winblad, B., & Fisahn, A. (2014). Amyloid-β-induced action potential desynchronization and degradation of hippocampal gamma oscillations is prevented by interference with peptide conformation change and aggregation. *Journal of Neuroscience*, *34*(34), 11416–11425. https://doi.org/10.1523/JNEUROSCI.1195-14.2014

Lai, F., & Williams, R. S. (1989). A Prospective Study of Alzheimer Disease in Down Syndrome. *Archives of Neurology*, *46*(8), 849–853. https://doi.org/10.1001/archneur.1989.00520440031017

Lara, D. R., Gama, C. S., Belmonte-De-Abreu, P., Portela, L. V. C., Gonçalves, C. A., Fonseca, M., Hauck, S., & Souza, D. O. (2001). Increased serum S100B protein in schizophrenia: A study in medication-free patients. *Journal of Psychiatric Research*, *35*(1), 11–14. https://doi.org/10.1016/S0022-3956(01)00003-6

Larner, A. J., & Doran, M. (2006). Clinical phenotypic heterogeneity of Alzheimer's disease associated with mutations of the presenilin–1 gene. *Journal of Neurology*, *253*(2), 139–158. https://doi.org/10.1007/s00415-005-0019-5

Lee, H. S., Ghetti, A., Pinto-Duarte, A., Wang, X., Dziewczapolski, G., Galimi, F., Huitron-Resendiz, S., Piña-Crespo, J. C., Roberts, A. J., Verma, I. M., Sejnowski, T. J., & Heinemann, S. F. (2014). Astrocytes contribute to gamma oscillations and recognition memory. *Proceedings of the National Academy of Sciences*, *111*(32), E3343–E3352. https://doi.org/10.1073/pnas.1410893111

Lenz, K. M., Wright, C. L., Martin, R. C., & McCarthy, M. M. (2011). Prostaglandin E2 Regulates AMPA Receptor Phosphorylation and Promotes Membrane Insertion in Preoptic Area Neurons and Glia during Sexual Differentiation. *PLOS ONE*, *6*(4), e18500. https://doi.org/10.1371/journal.pone.0018500

Leoutsakos, J.-M. S., Muthen, B. O., Breitner, J. C. S., Lyketsos, C. G., & ADAPT Research Team. (2012). Effects of non-steroidal anti-inflammatory drug treatments on cognitive decline vary by phase of pre-clinical Alzheimer disease: Findings from the randomized controlled Alzheimer's Disease Anti-inflammatory Prevention Trial. *International Journal of Geriatric Psychiatry*, *27*(4), 364–374. https://doi.org/10.1002/gps.2723

Levy-Lahad, E., Wasco, W., Poorkaj, P., Romano, D., Oshima, J., Pettingell, W., Yu, C., Jondro, P., Schmidt, S., Wang, K., & al., e. (1995). Candidate gene for the chromosome 1 familial Alzheimer's disease locus. *Science*, *269*(5226), 973–977. https://doi.org/10.1126/science.7638622

Lewen, A., Ta, T., Cesetti, T., Hollnagel, J., Papageorgiou, I. E., Chausse, B., & Kann, O. (2020). Neuronal gamma oscillations and activity-dependent potassium transients remain regular after depletion of microglia in postnatal cortex tissue. *Journal of Neuroscience Research*, *98*(10), 1953–1967. https://doi.org/10.1002/jnr.24689

Li, S., Wang, Y., Zhang, X., Xiong, X., Zhou, F., Li, X., Fan, J., Liang, X., Li, G., Peng, Y., & Li, Y. (2023). Mitochondrial damage-induced abnormal glucose metabolism with ageing in the hippocampus of APP/PS1 mice. *Metabolomics*, *19*(6), 56. https://doi.org/10.1007/s11306-023-02023-9

Liang, K.-G., Mu, R.-Z., Liu, Y., Jiang, D., Jia, T.-T., & Huang, Y.-J. (2019). Increased Serum S100B Levels in Patients With Epilepsy: A Systematic Review and Meta-Analysis Study. *Frontiers in Neuroscience*, *13*(MAY), 456. https://doi.org/10.3389/fnins.2019.00456

Liddelow, S. A., Guttenplan, K. A., Clarke, L. E., Bennett, F. C., Bohlen, C. J., Schirmer, L., Bennett, M. L., Münch, A. E., Chung, W.-S., Peterson, T. C., Wilton, D. K., Frouin, A., Napier, B. A., Panicker, N., Kumar, M., Buckwalter, M. S., Rowitch, D. H., Dawson, V. L., Dawson, T. M., … Barres, B. A. (2017). Neurotoxic reactive astrocytes are induced by activated microglia. *Nature*, *541*(7638), Article 7638. https://doi.org/10.1038/nature21029

Lin, H., Lee, E., Hestir, K., Leo, C., Huang, M., Bosch, E., Halenbeck, R., Wu, G., Zhou, A., Behrens, D., Hollenbaugh, D., Linnemann, T., Qin, M., Wong, J., Chu, K., Doberstein, S. K., & Williams, L. T. (2008). Discovery of a cytokine and its receptor by functional screening of the extracellular proteome. *Science (New York, N.Y.)*, *320*(5877), 807–811. https://doi.org/10.1126/science.1154370

Lin, Y.-T., Seo, J., Gao, F., Feldman, H. M., Wen, H.-L., Penney, J., Cam, H. P., Gjoneska, E., Raja, W. K., Cheng, J., Rueda, R., Kritskiy, O., Abdurrob, F., Peng, Z., Milo, B., Yu, C. J., Elmsaouri, S., Dey, D., Ko, T., … Tsai, L.-H. (2018). APOE4 Causes Widespread Molecular and Cellular Alterations Associated with Alzheimer's Disease Phenotypes in Human iPSC-Derived Brain Cell Types. *Neuron*, *98*(6), 1141-1154.e7. https://doi.org/10.1016/j.neuron.2018.05.008

Liu, B., Kou, J., Li, F., Huo, D., Xu, J., Zhou, X., Meng, D., Ghulam, M., Artyom, B., Gao, X., Ma, N., & Han, D. (2020). Lemon essential oil ameliorates age-associated cognitive dysfunction via modulating hippocampal synaptic density and inhibiting acetylcholinesterase. *Aging (Albany NY)*, *12*(9), 8622–8639. https://doi.org/10.18632/aging.103179

Liu, C. C., Zhao, N., Fu, Y., Wang, N., Linares, C., Tsai, C. W., & Bu, G. (2017). ApoE4 Accelerates Early Seeding of Amyloid Pathology. *Neuron*, *96*(5), 1024-1032.e3. https://doi.org/10.1016/j.neuron.2017.11.013

Liu, H., Stover, K. R., Sivanenthiran, N., Chow, J., Cheng, C., Liu, Y., Lim, S., Wu, C., Weaver, D. F., Eubanks, J. H., Song, H., & Zhang, L. (2019). Impaired Spatial Learning and Memory in Middle-Aged Mice with Kindling-Induced Spontaneous Recurrent Seizures. *Frontiers in Pharmacology*, *10*, 1077. https://doi.org/10.3389/fphar.2019.01077

Liu, L., Ikonen, S., Heikkinen, T., Heikkilä, M., Puoliväli, J., van Groen, T., & Tanila, H. (2002). Effects of fimbria-fornix lesion and amyloid pathology on spatial learning and memory in transgenic APP+PS1 mice. *Behavioural Brain Research*, *134*(1–2), 433–445. https://doi.org/10.1016/s0166-4328(02)00058-x

Liu, Y., Walter, S., Stagi, M., Cherny, D., Letiembre, M., Schulz-Schaeffer, W., Heine, H., Penke, B., Neumann, H., & Fassbender, K. (2005). LPS receptor (CD14): A receptor for phagocytosis of Alzheimer's amyloid peptide. *Brain: A Journal of Neurology*, *128*(Pt 8), 1778–1789. https://doi.org/10.1093/brain/awh531

Liu, Y., Zhou, L.-J., Wang, J., Li, D., Ren, W.-J., Peng, J., Wei, X., Xu, T., Xin, W.-J., Pang, R.-P., Li, Y.-Y., Qin, Z.-H., Murugan, M., Mattson, M. P., Wu, L.-J., & Liu, X.-G. (2017). TNF-α Differentially Regulates Synaptic Plasticity in the Hippocampus and Spinal Cord by Microglia-Dependent Mechanisms after Peripheral Nerve Injury. *The Journal of Neuroscience: The Official Journal of the Society for Neuroscience*, *37*(4), 871–881. https://doi.org/10.1523/JNEUROSCI.2235-16.2016

Liu, Y.-J., Spangenberg, E. E., Tang, B., Holmes, T. C., Green, K. N., & Xu, X. (2021). Microglia Elimination Increases Neural Circuit Connectivity and Activity in Adult Mouse Cortex. *Journal of Neuroscience*, *41*(6), 1274–1287. https://doi.org/10.1523/JNEUROSCI.2140-20.2020

Livingston, G., Huntley, J., Liu, K. Y., Costafreda, S. G., Selbæk, G., Alladi, S., Ames, D., Banerjee, S., Burns, A., Brayne, C., Fox, N. C., Ferri, C. P., Gitlin, L. N., Howard, R., Kales, H. C., Kivimäki, M., Larson, E. B., Nakasujja, N., Rockwood, K., … Mukadam, N. (2024). Dementia prevention, intervention, and care: 2024 report of the Lancet standing Commission. *The Lancet*, *404*(10452), 572–628. https://doi.org/10.1016/S0140-6736(24)01296-0

Llinas, R., & Ribary, U. (1993). Coherent 40-Hz oscillation characterizes dream state in humans. *Proceedings of the National Academy of Sciences*, *90*(5), 2078–2081. https://doi.org/10.1073/pnas.90.5.2078

Lofredi, R., Neumann, W.-J., Bock, A., Horn, A., Huebl, J., Siegert, S., Schneider, G.-H., Krauss, J. K., & Kühn, A. A. (2018). Dopamine-dependent scaling of subthalamic gamma bursts with movement velocity in patients with Parkinson's disease. *eLife*, *7*, e31895. https://doi.org/10.7554/eLife.31895

Lok, K., Zhao, H., Shen, H., Wang, Z., Gao, X., Zhao, W., & Yin, M. (2013). Characterization of the APP/PS1 mouse model of Alzheimer's disease in senescence accelerated background. *Neuroscience Letters*, *557*, 84–89. https://doi.org/10.1016/j.neulet.2013.10.051

Lonart, G., Wang, J., & Johnson, K. M. (1992). Nitric oxide induces neurotransmitter release from hippocampal slices. *European Journal of Pharmacology*, *220*(2), 271–272. https://doi.org/10.1016/0014-2999(92)90759-W

Lonnemann, N., Korte, M., & Hosseini, S. (2023). Repeated performance of spatial memory tasks ameliorates cognitive decline in APP/PS1 mice. *Behavioural Brain Research*, *438*, 114218. https://doi.org/10.1016/j.bbr.2022.114218

López-González, I., Schlüter, A., Aso, E., Garcia-Esparcia, P., Ansoleaga, B., LLorens, F., Carmona, M., Moreno, J., Fuso, A., Portero-Otin, M., Pamplona, R., Pujol, A., & Ferrer, I. (2015). Neuroinflammatory signals in Alzheimer disease and APP/PS1 transgenic mice: Correlations with plaques, tangles, and oligomeric species. *Journal of Neuropathology and Experimental Neurology*, *74*(4), 319–344. https://doi.org/10.1097/NEN.0000000000000176

López-Otín, C., Blasco, M. A., Partridge, L., Serrano, M., & Kroemer, G. (2013). The hallmarks of aging. *Cell*, *153*(6), 1194. https://doi.org/10.1016/j.cell.2013.05.039

Lopez-Rodriguez, A. B., Hennessy, E., Murray, C. L., Nazmi, A., Delaney, H. J., Healy, D., Fagan, S. G., Rooney, M., Stewart, E., Lewis, A., Barra, N. de, Scarry, P., Riggs-Miller, L., Boche, D., Cunningham, M. O., & Cunningham, C. (2021). Acute systemic inflammation exacerbates neuroinflammation in Alzheimer's disease: IL-1β drives amplified responses in primed astrocytes and neuronal network dysfunction. *Alzheimer's & Dementia*. https://doi.org/10.1002/ALZ.12341

Lourenço, J., Pacioni, S., Rebola, N., van Woerden, G. M., Marinelli, S., DiGregorio, D., & Bacci, A. (2014). Non-associative Potentiation of Perisomatic Inhibition Alters the Temporal Coding of Neocortical Layer 5 Pyramidal Neurons. *PLoS Biology*, *12*(7), e1001903. https://doi.org/10.1371/journal.pbio.1001903

Lu, C. B., Hamilton, J. B., Powell, A. D., Toescu, E. C., & Vreugdenhil, M. (2011). Effect of ageing on CA3 interneuron sAHP and gamma oscillations is activity-dependent. *Neurobiology of Aging*, *32*(5), 956–965. https://doi.org/10.1016/j.neurobiolaging.2009.05.006

Lu, C. B., Jefferys, J. G. R., Toescu, E. C., & Vreugdenhil, M. (2011). In vitro hippocampal gamma oscillation power as an index of in vivo CA3 gamma oscillation strength and spatial reference memory. *Neurobiology of Learning and Memory*, *95*(3), 221–230. https://doi.org/10.1016/j.nlm.2010.11.008

Lu, C., Wang, Z., Zhou, Y., & Vreugdenhil, M. (2012). Temperature- and concentration-dependence of kainate-induced γ oscillation in rat hippocampal slices under submerged condition. *Acta Pharmacologica Sinica*, *33*(2), 214–220. https://doi.org/10.1038/aps.2011.159

Lynch, B. A., Lambeng, N., Nocka, K., Kensel-Hammes, P., Bajjalieh, S. M., Matagne, A., & Fuks, B. (2004). The synaptic vesicle protein SV2A is the binding site for the antiepileptic drug levetiracetam. *Proceedings of the National Academy of Sciences*, *101*(26), 9861–9866. https://doi.org/10.1073/PNAS.0308208101

Lynch, M. A. (2015). Neuroinflammatory changes negatively impact on LTP: A focus on IL-1β. *Brain Research*, *1621*, 197–204. https://doi.org/10.1016/j.brainres.2014.08.040

Lytton, W. W., & Sejnowski, T. J. (1991). Simulations of cortical pyramidal neurons synchronized by inhibitory interneurons. *Journal of Neurophysiology*, *66*(3), 1059–1079. https://doi.org/10.1152/jn.1991.66.3.1059

Ma, L., & Patel, M. (2022). Mechanism of carbachol-induced 40 Hz gamma oscillations and the effects of NMDA activation on oscillatory dynamics in a model of the CA3 subfield of the hippocampus. *Journal of Theoretical Biology*, *548*, 111200. https://doi.org/10.1016/j.jtbi.2022.111200

Maciejewski-Lenoir, D., Chen, S., Feng, L., Maki, R., & Bacon, K. B. (1999). Characterization of fractalkine in rat brain cells: Migratory and activation signals for CX3CR-1-expressing microglia. *Journal of Immunology (Baltimore, Md.: 1950)*, *163*(3), 1628–1635.

Mackenzie-Gray Scott, C. A., Pelkey, K. A., Caccavano, A. P., Abebe, D., Lai, M., Black, K. N., Brown, N. D., Trevelyan, A. J., & McBain, C. J. (2022). Resilient Hippocampal Gamma Rhythmogenesis and Parvalbumin-Expressing Interneuron Function Before and After Plaque Burden in 5xFAD Alzheimer's Disease Model. *Frontiers in Synaptic Neuroscience*, *14*, 857608. https://doi.org/10.3389/fnsyn.2022.857608

MacVicar, B. A., & Newman, E. A. (2015). Astrocyte Regulation of Blood Flow in the Brain. *Cold Spring Harbor Perspectives in Biology*, *7*(5), a020388. https://doi.org/10.1101/cshperspect.a020388

Mahar, I., Albuquerque, M. S., Mondragon-Rodriguez, S., Cavanagh, C., Davoli, M. A., Chabot, J. G., Williams, S., Mechawar, N., Quirion, R., & Krantic, S. (2017). Phenotypic alterations in hippocampal NPY- and PV-expressing interneurons in a presymptomatic transgenic mouse model of Alzheimer's disease. *Frontiers in Aging Neuroscience*, *8*(JAN). https://doi.org/10.3389/fnagi.2016.00327

Makar, T. K., Nedergaard, M., Preuss, A., Gelbard, A. S., Perumal, A. S., & Cooper, A. J. (1994). Vitamin E, ascorbate, glutathione, glutathione disulfide, and enzymes of glutathione metabolism in cultures of chick astrocytes and neurons: Evidence that astrocytes play an important role in antioxidative processes in the brain. *Journal of Neurochemistry*, *62*(1), 45–53. https://doi.org/10.1046/j.1471-4159.1994.62010045.x

Mamad, O., Islam, N., Cunningham, C., & Tsanov, M. (2018). Differential response of hippocampal and prefrontal oscillations to systemic LPS application. *Brain Research*, *1681*, 64–74. https://doi.org/10.1016/j.brainres.2017.12.036

Mander, P. K., Jekabsone, A., & Brown, G. C. (2006). Microglia proliferation is regulated by hydrogen peroxide from NADPH oxidase. *Journal of Immunology (Baltimore, Md.: 1950)*, *176*(2), 1046–1052. https://doi.org/10.4049/jimmunol.176.2.1046

Mann, D. M. A., Pickering-Brown, S. M., Takeuchi, A., & Iwatsubo, T. (2001). Amyloid Angiopathy and Variability in Amyloid β Deposition Is Determined by Mutation Position in Presenilin-1-Linked Alzheimer's Disease. *The American Journal of Pathology*, *158*(6), 2165–2175. https://doi.org/10.1016/S0002-9440(10)64688-3

Mapunda, J. A., Tibar, H., Regragui, W., & Engelhardt, B. (2022). How Does the Immune System Enter the Brain? *Frontiers in Immunology*, *13*. https://www.frontiersin.org/articles/10.3389/fimmu.2022.805657

Marinelli, S., Basilico, B., Marrone, M. C., & Ragozzino, D. (2019). Microglia-neuron crosstalk: Signaling mechanism and control of synaptic transmission. *Seminars in Cell & Developmental Biology*, *94*, 138–151. https://doi.org/10.1016/j.semcdb.2019.05.017

Martinon, F., Burns, K., & Tschopp, J. (2002). The Inflammasome: A Molecular Platform Triggering Activation of Inflammatory Caspases and Processing of proIL-β. *Molecular Cell*, *10*(2), 417–426. https://doi.org/10.1016/S1097-2765(02)00599-3

Martorell, A. J., Paulson, A. L., Suk, H. J., Abdurrob, F., Drummond, G. T., Guan, W., Young, J. Z., Kim, D. N. W., Kritskiy, O., Barker, S. J., Mangena, V., Prince, S. M., Brown, E. N., Chung, K., Boyden, E. S., Singer, A. C., & Tsai, L. H. (2019). Multi-sensory Gamma Stimulation Ameliorates Alzheimer's-Associated Pathology and Improves Cognition. *Cell*, *177*(2), 256-271.e22. https://doi.org/10.1016/j.cell.2019.02.014

Masters, C. L., & Beyreuther, K. (1987). Neuronal Origin of Cerebral Amyloidogenic Proteins: Their Role in Alzheimer's Disease and Unconventional Virus Diseases of the Nervous System. In *Ciba Foundation symposium* (Vol. 126, pp. 49–64). https://doi.org/10.1002/9780470513422.ch4

Mathiisen, T. M., Lehre, K. P., Danbolt, N. C., & Ottersen, O. P. (2010). The perivascular astroglial sheath provides a complete covering of the brain microvessels: An electron microscopic 3D reconstruction. *Glia*, *58*(9), 1094–1103. https://doi.org/10.1002/glia.20990

Matusova, Z., Hol, E. M., Pekny, M., Kubista, M., & Valihrach, L. (2023). Reactive astrogliosis in the era of single-cell transcriptomics. *Frontiers in Cellular Neuroscience*, *17*, 1173200. https://doi.org/10.3389/fncel.2023.1173200

McDonald, D. R., Brunden, K. R., & Landreth, G. E. (1997). Amyloid fibrils activate tyrosine kinase-dependent signaling and superoxide production in microglia. *The Journal of Neuroscience: The Official Journal of the Society for Neuroscience*, *17*(7), 2284–2294. https://doi.org/10.1523/JNEUROSCI.17-07-02284.1997

McKhann, G. M., Knopman, D. S., Chertkow, H., Hyman, B. T., Jack, C. R., Kawas, C. H., Klunk, W. E., Koroshetz, W. J., Manly, J. J., Mayeux, R., Mohs, R. C., Morris, J. C., Rossor, M. N., Scheltens, P., Carrillo, M. C., Thies, B., Weintraub, S., & Phelps, C. H. (2011). The diagnosis of dementia due to Alzheimer's disease: Recommendations from the National Institute on Aging-Alzheimer's Association workgroups on diagnostic guidelines for Alzheimer's disease. *Alzheimer's & Dementia*, *7*(3), 263–269. https://doi.org/10.1016/j.jalz.2011.03.005

McManus, R. M., Higgins, S. C., Mills, K. H. G., & Lynch, M. A. (2014). Respiratory infection promotes T cell infiltration and amyloid-β deposition in APP/PS1 mice. *Neurobiology of Aging*, *35*(1), 109–121. https://doi.org/10.1016/j.neurobiolaging.2013.07.025

Meda, L., Cassatella, M. A., Szendrei, G. I., Otvos, L., Baron, P., Villalba, M., Ferrari, D., & Rossi, F. (1995). Activation of microglial cells by beta-amyloid protein and interferon-gamma. *Nature*, *374*(6523), 647–650. https://doi.org/10.1038/374647a0

Medawar, P. B. (1948). Immunity to homologous grafted skin; the fate of skin homografts transplanted to the brain, to subcutaneous tissue, and to the anterior chamber of the eye. *British Journal of Experimental Pathology*, *29*(1), 58–69.

Mei, L., Zhou, Y., Sun, Y., Liu, H., Zhang, D., Liu, P., & Shu, H. (2020). Acetylcholine Muscarinic Receptors in Ventral Hippocampus Modulate Stress-Induced Anxiety-Like Behaviors in Mice. *Frontiers in Molecular Neuroscience*, *13*, 598811. https://doi.org/10.3389/fnmol.2020.598811

Metea, M. R., & Newman, E. A. (2006). Glial Cells Dilate and Constrict Blood Vessels: A Mechanism of Neurovascular Coupling. *The Journal of Neuroscience*, *26*(11), 2862–2870. https://doi.org/10.1523/JNEUROSCI.4048-05.2006

Micheau, O., & Tschopp, J. (2003). Induction of TNF Receptor I-Mediated Apoptosis via Two Sequential Signaling Complexes. *Cell*, *114*(2), 181–190. https://doi.org/10.1016/S0092-8674(03)00521-X

Mifflin, M. A., Winslow, W., Surendra, L., Tallino, S., Vural, A. S., & Velazquez, R. (2021). Sex differences in the IntelliCage and the Morris water maze in the APP/PS1 mouse model of amyloidosis. *Neurobiology of Aging*, *101*, 130–140. https://doi.org/10.1016/j.neurobiolaging.2021.01.018

Miltner, W. H. R., Braun, C., Arnold, M., Witte, H., & Taub, E. (1999). Coherence of gamma-band EEG activity as a basis for associative learning. *Nature*, *397*(6718), 434–436. https://doi.org/10.1038/17126

Moehlmann, T., Winkler, E., Xia, X., Edbauer, D., Murrell, J., Capell, A., Kaether, C., Zheng, H., Ghetti, B., Haass, C., & Steiner, H. (2002). Presenilin-1 mutations of leucine 166 equally affect the generation of the Notch and APP intracellular domains independent of their effect on Abeta 42 production. *Proceedings of the National Academy of Sciences of*

the United States of America, *99*(12), 8025–8030. https://doi.org/10.1073/pnas.112686799

Momtazmanesh, S., Perry, G., & Rezaei, N. (2020). Toll-like receptors in Alzheimer's disease. *Journal of Neuroimmunology*, *348*. https://doi.org/10.1016/j.jneuroim.2020.577362

Montgomery, S. M., & Buzsáki, G. (2007). Gamma oscillations dynamically couple hippocampal CA3 and CA1 regions during memory task performance. *Proceedings of the National Academy of Sciences*, *104*(36), 14495–14500. https://doi.org/10.1073/pnas.0701826104

Morawski, M., Reinert, T., Meyer-Klaucke, W., Wagner, F. E., Tröger, W., Reinert, A., Jäger, C., Brückner, G., & Arendt, T. (2015). Ion exchanger in the brain: Quantitative analysis of perineuronally fixed anionic binding sites suggests diffusion barriers with ion sorting properties. *Scientific Reports*, *5*(1), 16471. https://doi.org/10.1038/srep16471

Morquette, P., Verdier, D., Kadala, A., Féthière, J., Philippe, A. G., Robitaille, R., & Kolta, A. (2015). An astrocyte-dependent mechanism for neuronal rhythmogenesis. *Nature Neuroscience*, *18*(6), 844–854. https://doi.org/10.1038/nn.4013

Müller, C., & Remy, S. (2014). Dendritic inhibition mediated by O-LM and bistratified interneurons in the hippocampus. *Frontiers in Synaptic Neuroscience*, *6*, 23. https://doi.org/10.3389/fnsyn.2014.00023

Murdock, M. H., Yang, C.-Y., Sun, N., Pao, P.-C., Blanco-Duque, C., Kahn, M. C., Kim, T., Lavoie, N. S., Victor, M. B., Islam, M. R., Galiana, F., Leary, N., Wang, S., Bubnys, A., Ma, E., Akay, L. A., Sneve, M., Qian, Y., Lai, C., … Tsai, L.-H. (2024). Multisensory gamma stimulation promotes glymphatic clearance of amyloid. *Nature*. https://doi.org/10.1038/s41586-024-07132-6

Murphy, P. G., Borthwick, L. A., Altares, M., Gauldie, J., Kaplan, D., & Richardson, P. M. (2000). Reciprocal actions of interleukin-6 and brain-derived neurotrophic factor on rat and mouse primary sensory neurons. *The European Journal of Neuroscience*, *12*(6), 1891–1899. https://doi.org/10.1046/j.1460-9568.2000.00074.x

Murray, C., Sanderson, D. J., Barkus, C., Deacon, R. M. J., Rawlins, J. N. P., Bannerman, D. M., & Cunningham, C. (2012). Systemic inflammation induces acute working memory deficits in the primed brain: Relevance for delirium. *Neurobiology of Aging*, *33*(3), 603-616.e3. https://doi.org/10.1016/j.neurobiolaging.2010.04.002

Nakao, K., Singh, M., Sapkota, K., Hagler, B. C., Hunter, R. N., Raman, C., Hablitz, J. J., & Nakazawa, K. (2020). GSK3β inhibition restores cortical gamma oscillation and cognitive behavior in a mouse model of NMDA receptor hypofunction relevant to schizophrenia. *Neuropsychopharmacology*, *45*(13), 2207–2218. https://doi.org/10.1038/s41386-020-00819-0

Nakazono, T., Lam, T. N., Patel, A. Y., Kitazawa, M., Saito, T., Saido, T. C., & Igarashi, K. M. (2017). Impaired In Vivo Gamma Oscillations in the Medial Entorhinal Cortex of

Knock-in Alzheimer Model. *Frontiers in Systems Neuroscience*, *11*, 48. https://doi.org/10.3389/fnsys.2017.00048

Neal, M. L., Fleming, S. M., Budge, K. M., Boyle, A. M., Kim, C., Alam, G., Beier, E. E., Wu, L.-J., & Richardson, J. R. (2020). Pharmacological inhibition of CSF1R by GW2580 reduces microglial proliferation and is protective against neuroinflammation and dopaminergic neurodegeneration. *FASEB Journal: Official Publication of the Federation of American Societies for Experimental Biology*, *34*(1), 1679–1694. https://doi.org/10.1096/fj.201900567RR

Neher, J. J., & Cunningham, C. (2019). Priming Microglia for Innate Immune Memory in the Brain. *Trends in Immunology*, *40*(4), 358–374. https://doi.org/10.1016/j.it.2019.02.001

Nelson, T. E., & Gruol, D. L. (2004). The chemokine CXCL10 modulates excitatory activity and intracellular calcium signaling in cultured hippocampal neurons. *Journal of Neuroimmunology*, *156*(1–2), 74–87. https://doi.org/10.1016/j.jneuroim.2004.07.009

Nemeth, D. P., & Quan, N. (2021). Modulation of Neural Networks by Interleukin-1. *Brain Plasticity*, *7*(1), 17–32. https://doi.org/10.3233/BPL-200109

Ng, P. Y., McNeely, T. L., & Baker, D. J. (2023). Untangling senescent and damage-associated microglia in the aging and diseased brain. *The FEBS Journal*, *290*(5), 1326–1339. https://doi.org/10.1111/febs.16315

Ní Chasaide, C., & Lynch, M. A. (2020). The role of the immune system in driving neuroinflammation. *Brain and Neuroscience Advances*, *4*, 2398212819901082. https://doi.org/10.1177/2398212819901082

Nidai Ozes, O., Mayo, L. D., Gustin, J. A., Pfeffer, S. R., Pfeffer, L. M., & Donner, D. B. (1999). NF-κB activation by tumour necrosis factor requires the Akt serine–threonine kinase. *Nature*, *401*(6748), Article 6748. https://doi.org/10.1038/43466

Nimmerjahn, A., Kirchhoff, F., & Helmchen, F. (2005). Resting Microglial Cells Are Highly Dynamic Surveillants of Brain Parenchyma in Vivo. *Science*, *308*(5726), 1314–1318. https://doi.org/10.1126/SCIENCE.1110647

Nimmervoll, B., White, R., Yang, J.-W., An, S., Henn, C., Sun, J.-J., & Luhmann, H. J. (2013). LPS-Induced Microglial Secretion of TNFα Increases Activity-Dependent Neuronal Apoptosis in the Neonatal Cerebral Cortex. *Cerebral Cortex*, *23*(7), 1742–1755. https://doi.org/10.1093/CERCOR

Nishiyori, A., Minami, M., Ohtani, Y., Takami, S., Yamamoto, J., Kawaguchi, N., Kume, T., Akaike, A., & Satoh, M. (1998). Localization of fractalkine and CX3CR1 mRNAs in rat brain: Does fractalkine play a role in signaling from neuron to microglia? *FEBS Letters*, *429*(2), 167–172. https://doi.org/10.1016/s0014-5793(98)00583-3

Nishizawa, Y., Yamanashi, T., Saito, T., Marra, P., Crutchley, K. J., Wahba, N. E., Malicoat, J., Shibata, K., Nishiguchi, T., Lee, S., Cho, H. R., Kanazawa, T., & Shinozaki, G. (2023).

Bispectral EEG (BSEEG) Algorithm Captures High Mortality Risk Among 1,077 Patients: Its Relationship to Delirium Motor Subtype. *The American Journal of Geriatric Psychiatry: Official Journal of the American Association for Geriatric Psychiatry*, *31*(9), 704–715. https://doi.org/10.1016/j.jagp.2023.03.002

Nisticò, R., Mango, D., Mandolesi, G., Piccinin, S., & Berretta, N. (2013). Inflammation Subverts Hippocampal Synaptic Plasticity in Experimental Multiple Sclerosis. *PLoS ONE*, *8*(1), 54666. https://doi.org/10.1371/journal.pone.0054666

Noda, M., Nakanishi, H., Nabekura, J., & Akaike, N. (2000). AMPA–Kainate Subtypes of Glutamate Receptor in Rat Cerebral Microglia. *Journal of Neuroscience*, *20*(1), 251–258. https://doi.org/10.1523/JNEUROSCI.20-01-00251.2000

Numan, T., Slooter, A. J. C., van der Kooi, A. W., Hoekman, A. M. L., Suyker, W. J. L., Stam, C. J., & van Dellen, E. (2017). Functional connectivity and network analysis during hypoactive delirium and recovery from anesthesia. *Clinical Neurophysiology: Official Journal of the International Federation of Clinical Neurophysiology*, *128*(6), 914–924. https://doi.org/10.1016/j.clinph.2017.02.022

Ogiwara, I., Miyamoto, H., Morita, N., Atapour, N., Mazaki, E., Inoue, I., Takeuchi, T., Itohara, S., Yanagawa, Y., Obata, K., Furuichi, T., Hensch, T. K., & Yamakawa, K. (2007). Nav1.1 localizes to axons of parvalbumin-positive inhibitory interneurons: A circuit basis for epileptic seizures in mice carrying an Scn1a gene mutation. *Journal of Neuroscience*, *27*(22), 5903–5914. https://doi.org/10.1523/JNEUROSCI.5270-06.2007

Oikawa, N., & Walter, J. (2019). Presenilins and γ-Secretase in Membrane Proteostasis. *Cells*, *8*(3), 209. https://doi.org/10.3390/cells8030209

O'Keefe, J., & Recce, M. L. (1993). Phase relationship between hippocampal place units and the EEG theta rhythm. *Hippocampus*, *3*(3), 317–330. https://doi.org/10.1002/hipo.450030307

Olesen, L. Ø., Sivasaravanaparan, M., Severino, M., Babcock, A. A., Bouzinova, E. V., West, M. J., Wiborg, O., & Finsen, B. (2017). Neuron and neuroblast numbers and cytogenesis in the dentate gyrus of aged APPswe/PS1dE9 transgenic mice: Effect of long-term treatment with paroxetine. *Neurobiology of Disease*, *104*, 50–60. https://doi.org/10.1016/j.nbd.2017.04.021

Olmos-Alonso, A., Schetters, S. T. T., Sri, S., Askew, K., Mancuso, R., Vargas-Caballero, M., Holscher, C., Perry, V. H., & Gomez-Nicola, D. (2016). Pharmacological targeting of CSF1R inhibits microglial proliferation and prevents the progression of Alzheimer's-like pathology. *Brain*, *139*(3), 891–907. https://doi.org/10.1093/brain/awv379

Osipova, D., Pekkonen, E., & Ahveninen, J. (2006). Enhanced magnetic auditory steady-state response in early Alzheimer's disease. *Clinical Neurophysiology*, *117*(9), 1990–1995. https://doi.org/10.1016/j.clinph.2006.05.034

Othman, O., Marshall, H., Masterson, M., Winlow, P., Gibson, G., Ding, Y., & Pardon, M.-C. (2023). Thymosin beta 4 prevents systemic lipopolysaccharide-induced plaque load in middle-age APP/PS1 mice. *International Immunopharmacology*, *117*, 109951. https://doi.org/10.1016/j.intimp.2023.109951

Pais, I., Hormuzdi, S. G., Monyer, H., Traub, R. D., Wood, I. C., Buhl, E. H., Whittington, M. A., & LeBeau, F. E. N. (2003). Sharp wave-like activity in the hippocampus in vitro in mice lacking the gap junction protein connexin 36. *Journal of Neurophysiology*, *89*(4), 2046–2054. https://doi.org/10.1152/jn.00549.2002

Palop, J. J., Chin, J., Roberson, E. D., Wang, J., Thwin, M. T., Bien-Ly, N., Yoo, J., Ho, K. O., Yu, G. Q., Kreitzer, A., Finkbeiner, S., Noebels, J. L., & Mucke, L. (2007). Aberrant Excitatory Neuronal Activity and Compensatory Remodeling of Inhibitory Hippocampal Circuits in Mouse Models of Alzheimer's Disease. *Neuron*, *55*(5), 697–711. https://doi.org/10.1016/j.neuron.2007.07.025

Palop, J. J., & Mucke, L. (2016). Network abnormalities and interneuron dysfunction in Alzheimer disease. *Nature Reviews Neuroscience*, *17*(12), 777–792. https://doi.org/10.1038/nrn.2016.141

Pantev, C., Makeig, S., Hoke, M., Galambos, R., Hampson, S., & Gallen, C. (1991). Human auditory evoked gamma-band magnetic fields. *Proceedings of the National Academy of Sciences of the United States of America*, *88*(20), 8996–9000. https://doi.org/10.1073/pnas.88.20.8996

Paolicelli, R. C., Sierra, A., Stevens, B., Tremblay, M.-E., Aguzzi, A., Ajami, B., Amit, I., Audinat, E., Bechmann, I., Bennett, M., Bennett, F., Bessis, A., Biber, K., Bilbo, S., Blurton-Jones, M., Boddeke, E., Brites, D., Brône, B., Brown, G. C., … Wyss-Coray, T. (2022). Microglia states and nomenclature: A field at its crossroads. *Neuron*, *110*(21), 3458–3483. https://doi.org/10.1016/j.neuron.2022.10.020

Papageorgiou, I. E., Lewen, A., Galow, L. V., Cesetti, T., Scheffel, J., Regen, T., Hanisch, U. K., & Kann, O. (2016). TLR4-activated microglia require IFN-γ to induce severe neuronal dysfunction and death in situ. *Proceedings of the National Academy of Sciences of the United States of America*, *113*(1), 212–217. https://doi.org/10.1073/pnas.1513853113

Papazoglou, A., Soos, J., Lundt, A., Wormuth, C., Ginde, V. R., Müller, R., Henseler, C., Broich, K., Xie, K., Ehninger, D., Haenisch, B., & Weiergräber, M. (2016). *Gender-Specific Hippocampal Dysrhythmia and Aberrant Hippocampal and Cortical Excitability in the APPswePS1dE9 Model of Alzheimer's Disease*. https://doi.org/10.1155/2016/7167358

Park, K. M., & Bowers, W. J. (2010). Tumor Necrosis Factor-alpha Mediated Signaling in Neuronal Homeostasis and Dysfunction. *Cellular Signalling*, *22*(7), 977–983. https://doi.org/10.1016/j.cellsig.2010.01.010

Patz, S., J, G., T, G., Mj, W., & P, W. (2004). Parvalbumin expression in visual cortical interneurons depends on neuronal activity and TrkB ligands during an Early period of postnatal development. *Cerebral Cortex (New York, N.Y.: 1991)*, *14*(3). https://doi.org/10.1093/cercor/bhg132

Paulson, O. B., & Newman, E. A. (1987). Does the Release of Potassium from Astrocyte Endfeet Regulate Cerebral Blood Flow? *Science (New York, N.Y.)*, *237*(4817), 896–898.

Pellerin, L., & Magistretti, P. J. (1994). Glutamate uptake into astrocytes stimulates aerobic glycolysis: A mechanism coupling neuronal activity to glucose utilization. *Proceedings of the National Academy of Sciences of the United States of America*, *91*(22), 10625–10629. https://doi.org/10.1073/pnas.91.22.10625

Pelvig, D. P., Pakkenberg, H., Stark, A. K., & Pakkenberg, B. (2008). Neocortical glial cell numbers in human brains. *Neurobiology of Aging*, *29*(11), 1754–1762. https://doi.org/10.1016/j.neurobiolaging.2007.04.013

Perez, J.-C., Poulen, G., Cardoso, M., Boukhaddaoui, H., Gazard, C. M., Courtand, G., Bertrand, S. S., Gerber, Y. N., & Perrin, F. E. (2023). CSF1R inhibition at chronic stage after spinal cord injury modulates microglia proliferation. *Glia*, *71*(12), 2782–2798. https://doi.org/10.1002/glia.24451

Peskind, E. R., Griffin, W. S. T., Akama, K. T., Raskind, M. A., & Van Eldik, L. J. (2001). Cerebrospinal fluid S100B is elevated in the earlier stages of Alzheimer's disease. *Neurochemistry International*, *39*(5–6), 409–413. https://doi.org/10.1016/S0197-0186(01)00048-1

Pisani, M. A., McNicoll, L., & Inouye, S. K. (2003). Cognitive impairment in the intensive care unit. *Clinics in Chest Medicine*, *24*(4), 727–737. https://doi.org/10.1016/S0272-5231(03)00092-3

Poltorak, A., He, X., Smirnova, I., Liu, M. Y., Van Huffel, C., Du, X., Birdwell, D., Alejos, E., Silva, M., Galanos, C., Freudenberg, M., Ricciardi-Castagnoli, P., Layton, B., & Beutler, B. (1998). Defective LPS signaling in C3H/HeJ and C57BL/10ScCr mice: Mutations in Tlr4 gene. *Science (New York, N.Y.)*, *282*(5396), 2085–2088. https://doi.org/10.1126/science.282.5396.2085

Pósfai, B., Cserép, C., Orsolits, B., & Dénes, Á. (2019). New Insights into Microglia–Neuron Interactions: A Neuron's Perspective. *Neuroscience*, *405*, 103–117. https://doi.org/10.1016/j.neuroscience.2018.04.046

Pott Godoy, M. C., Tarelli, R., Ferrari, C. C., Sarchi, M. I., & Pitossi, F. J. (2008). Central and systemic IL-1 exacerbates neurodegeneration and motor symptoms in a model of Parkinson's disease. *Brain: A Journal of Neurology*, *131*(Pt 7), 1880–1894. https://doi.org/10.1093/brain/awn101

Pulvermüller, F., Lutzenberger, W., Preissl, H., & Birbaumer, N. (1995). Spectral responses in the gamma-band: Physiological signs of higher cognitive processes? *Neuroreport*, *6*(15), 2059–2064. https://doi.org/10.1097/00001756-199510010-00025

Radde, R., Bolmont, T., Kaeser, S. A., Coomaraswamy, J., Lindau, D., Stoltze, L., Calhoun, M. E., Jäggi, F., Wolburg, H., Gengler, S., Haass, C., Ghetti, B., Czech, C., Hölscher, C., Mathews, P. M., & Jucker, M. (2006). Abeta42-driven cerebral amyloidosis in transgenic mice reveals early and robust pathology. *EMBO Reports*, *7*(9), 940–946. https://doi.org/10.1038/sj.embor.7400784

Rao, S. C., Dove, G., Cascino, G. D., & Petersen, R. C. (2009). Recurrent seizures in patients with dementia: Frequency, seizure types, and treatment outcome. *Epilepsy & Behavior*, *14*(1), 118–120. https://doi.org/10.1016/j.yebeh.2008.08.012

Reed-Geaghan, E. G., Savage, J. C., Hise, A. G., & Landreth, G. E. (2009). CD14 and toll-like receptors 2 and 4 are required for fibrillar A{beta}-stimulated microglial activation. *The Journal of Neuroscience: The Official Journal of the Society for Neuroscience*, *29*(38), 11982–11992. https://doi.org/10.1523/JNEUROSCI.3158-09.2009

Reiman, E. M., Arboleda-Velasquez, J. F., Quiroz, Y. T., Huentelman, M. J., Beach, T. G., Caselli, R. J., Chen, Y., Su, Y., Myers, A. J., Hardy, J., Paul Vonsattel, J., Younkin, S. G., Bennett, D. A., De Jager, P. L., Larson, E. B., Crane, P. K., Keene, C. D., Kamboh, M. I., Kofler, J. K., … Jun, G. R. (2020). Exceptionally low likelihood of Alzheimer's dementia in APOE2 homozygotes from a 5,000-person neuropathological study. *Nature Communications*, *11*, 667. https://doi.org/10.1038/s41467-019-14279-8

Ren, S., Breuillaud, L., Yao, W., Yin, T., Norris, K. A., Zehntner, S. P., & D'Adamio, L. (2021). TNF-α–mediated reduction in inhibitory neurotransmission precedes sporadic Alzheimer's disease pathology in young Trem2R47H rats. *Journal of Biological Chemistry*, *296*. https://doi.org/10.1074/jbc.RA120.016395

Reyes-Marin, K. E., & Nuñez, A. (2017). Seizure susceptibility in the APP/PS1 mouse model of Alzheimer's disease and relationship with amyloid β plaques. *Brain Research*, *1677*, 93–100. https://doi.org/10.1016/j.brainres.2017.09.026

Ribary, U., Ioannides, A. A., Singh, K. D., Hasson, R., Bolton, J. P. R., Lado, F., Mogilner, A., & Llinás, R. (1991). Magnetic field tomography of coherent thalamocortical 40-Hz oscillations in humans. *Proceedings of the National Academy of Sciences of the United States of America*, *88*(24), 11037–11041. https://doi.org/10.1073/pnas.88.24.11037

Rice, R. A., Spangenberg, E. E., Yamate-Morgan, H., Lee, R. J., Arora, R. P. S., Hernandez, M. X., Tenner, A. J., West, B. L., & Green, K. N. (2015). Elimination of Microglia Improves Functional Outcomes Following Extensive Neuronal Loss in the Hippocampus. *Journal of Neuroscience*, *35*(27), 9977–9989. https://doi.org/10.1523/JNEUROSCI.0336-15.2015

Risse, S. C., Lampe, T. H., Bird, T. D., Nochlin, D., Sumi, S. M., Keenan, T., Cubberley, L., Peskind, E., & Raskind, M. A. (1990). Myoclonus, Seizures, and Paratonia in Alzheimer Disease. *Alzheimer Disease & Associated Disorders*, *4*(4), 217–225. https://doi.org/10.1097/00002093-199040400-00003

Robinson, J. H., & Deadwyler, S. A. (1981). Kainic acid produces depolarization of CA3 pyramidal cells in the in vitro hippocampal slice. *Brain Research*, *221*(1), 117–127. https://doi.org/10.1016/0006-8993(81)91067-2

Rocca, W. A., Hofman, A., Brayne, C., Breteler, M. M. B., Clarke, M., Copeland, J. R. M., Dartigues, J.-F., Engedal, K., Hagnell, O., Heeren, T. J., Jonker, C., Lindesay, J., Lobo, A., Mann, A. H., Mölsä, P. K., Morgan, K., O'Connor, D. W., Droux, A. da S., Sulkava, R., … Amaducci, L. (1991). Frequency and distribution of Alzheimer's disease in Europe: A collaborative study of 1980-1990 prevalence findings. *Annals of Neurology*, *30*(3), 381–390. https://doi.org/10.1002/ana.410300310

Romanelli, M. F., Morris, J. C., Ashkin, K., & Coben, L. A. (1990). Advanced Alzheimer's Disease Is a Risk Factor for Late-Onset Seizures. *Archives of Neurology*, *47*(8), 847–850. https://doi.org/10.1001/archneur.1990.00530080029006

Roskies, A. L. (1999). The Binding Problem. *Neuron*, *24*, 7–9.

Rostène, W., Kitabgi, P., & Parsadaniantz, S. M. (2007). Chemokines: A new class of neuromodulator? *Nature Reviews Neuroscience*, *8*(11), 895–903. https://doi.org/10.1038/nrn2255

Rubio, S. E., Vega-Flores, G., Martínez, A., Bosch, C., Pérez-Mediavilla, A., Del Río, J., Gruart, A., Delgado-García, J. M., Soriano, E., & Pascual, M. (2012). Accelerated aging of the GABAergic septohippocampal pathway and decreased hippocampal rhythms in a mouse model of Alzheimer's disease. *FASEB Journal*, *26*(11), 4458–4467. https://doi.org/10.1096/fj.12-208413

Rudzinski, L. A., Fletcher, R. M., Dickson, D. W., Crook, R., Hutton, M. L., Adamson, J., & Graff-Radford, N. R. (2008). Early onset familial Alzheimer Disease with spastic paraparesis, dysarthria, and seizures and N135S mutation in PSEN1. *Alzheimer Disease and Associated Disorders*, *22*(3), 299–307. https://doi.org/10.1097/WAD.0b013e3181732399

Rueda-Carrasco, J., Sokolova, D., Lee, S., Childs, T., Jurčáková, N., Crowley, G., De Schepper, S., Ge, J. Z., Lachica, J. I., Toomey, C. E., Freeman, O. J., Hardy, J., Barnes, S. J., Lashley, T., Stevens, B., Chang, S., & Hong, S. (2023). Microglia-synapse engulfment via PtdSer-TREM2 ameliorates neuronal hyperactivity in Alzheimer's disease models. *The EMBO Journal*, *42*(19), e113246. https://doi.org/10.15252/embj.2022113246

Rupp, N. J., Wegenast-Braun, B. M., Radde, R., Calhoun, M. E., & Jucker, M. (2011). Early onset amyloid lesions lead to severe neuritic abnormalities and local, but not global

neuron loss in APPPS1 transgenic mice. *Neurobiology of Aging*, *32*(12), 2324.e1-6. https://doi.org/10.1016/j.neurobiolaging.2010.08.014

Sahu, B., Mackos, A. R., Floden, A. M., Wold, L. E., & Combs, C. K. (2021). Particulate Matter Exposure Exacerbates Amyloid-β Plaque Deposition and Gliosis in APP/PS1 Mice. *Journal of Alzheimer's Disease*, *80*(2), 761–774. https://doi.org/10.3233/JAD-200919

Sakatani, S., Seto-Ohshima, A., Shinohara, Y., Yamamoto, Y., Yamamoto, H., Itohara, S., & Hirase, H. (2008). Neural-activity-dependent release of S100B from astrocytes enhances kainate-induced gmma oscillations in vivo. *Journal of Neuroscience*, *28*(43), 10928–10936. https://doi.org/10.1523/JNEUROSCI.3693-08.2008

Salvador, A. F., Lima, K. A. de, & Kipnis, J. (2021). Neuromodulation by the immune system: A focus on cytokines. *Nature Reviews Immunology 2021*, 1–16. https://doi.org/10.1038/s41577-021-00508-z

Sanchez, P. E., Zhu, L., Verret, L., Vossel, K. A., Orr, A. G., Cirrito, J. R., Devidze, N., Ho, K., Yu, G. Q., Palop, J. J., & Mucke, L. (2012). Levetiracetam suppresses neuronal network dysfunction and reverses synaptic and cognitive deficits in an Alzheimer's disease model. *Proceedings of the National Academy of Sciences of the United States of America*, *109*(42), E2895–E2903. https://doi.org/10.1073/pnas.1121081109

Sanchez-Mejias, E., Nuñez-Diaz, C., Sanchez-Varo, R., Gomez-Arboledas, A., Garcia-Leon, J. A., Fernandez-Valenzuela, J. J., Mejias-Ortega, M., Trujillo-Estrada, L., Baglietto-Vargas, D., Moreno-Gonzalez, I., Davila, J. C., Vitorica, J., & Gutierrez, A. (2020). Distinct disease-sensitive GABAergic neurons in the perirhinal cortex of Alzheimer's mice and patients. *Brain Pathology*, *30*(2), 345–363. https://doi.org/10.1111/bpa.12785

Sang, N., Zhang, J., Marcheselli, V., Bazan, N. G., & Chen, C. (2005). Postsynaptically synthesized prostaglandin E2 (PGE2) modulates hippocampal synaptic transmission via a presynaptic PGE2 EP2 receptor. *The Journal of Neuroscience: The Official Journal of the Society for Neuroscience*, *25*(43), 9858–9870. https://doi.org/10.1523/JNEUROSCI.2392-05.2005

Saper, C. B., Romanovsky, A. A., & Scammell, T. E. (2012). Neural circuitry engaged by prostaglandins during the sickness syndrome. *Nature Neuroscience*, *15*(8), 1088–1095. https://doi.org/10.1038/nn.3159

Scarmeas, N., Honig, L. S., Choi, H., Cantero, J., Brandt, J., Blacker, D., Albert, M., Amatniek, J. C., Marder, K., Bell, K., Hauser, W. A., & Stern, Y. (2009). Seizures in Alzheimer Disease. *Archives of Neurology*, *66*(8), 992–997. https://doi.org/10.1001/archneurol.2009.130

Schafer, D. P., Lehrman, E. K., Kautzman, A. G., Koyama, R., Mardinly, A. R., Yamasaki, R., Ransohoff, R. M., Greenberg, M. E., Barres, B. A., & Stevens, B. (2012). Microglia

Sculpt Postnatal Neural Circuits in an Activity and Complement-Dependent Manner. *Neuron*, *74*(4), 691–705. https://doi.org/10.1016/j.neuron.2012.03.026

Scheuner, D., Eckman, C., Jensen, M., Song, X., Citron, M., Suzuki, N., Bird, T., Hardy, J., Hutton, M., Kukull, W., Larson, E., Levy-Lahad, E., Viitanen, M., Peskind, E., Poorkaj, P., Schellenberg, G., Tanzi, R., Wasco, W., Lannfelt, L., … Younkin, S. (1996). Secreted amyloid beta-protein similar to that in the senile plaques of Alzheimer's disease is increased in vivo by the presenilin 1 and 2 and APP mutations linked to familial Alzheimer's disease. *Nature Medicine*, *2*(8), 864–870. https://doi.org/10.1038/NM0896-864

Schilling, S., Chausse, B., Dikmen, H. O., Almouhanna, F., Hollnagel, J.-O., Lewen, A., & Kann, O. (2021). TLR2- and TLR3-activated microglia induce different levels of neuronal network dysfunction in a context-dependent manner. *Brain, Behavior, and Immunity*, *96*, 80–91. https://doi.org/10.1016/j.bbi.2021.05.013

Schindelin, J., Rueden, C. T., Hiner, M. C., & Eliceiri, K. W. (2015). The ImageJ ecosystem: An open platform for biomedical image analysis. *Molecular Reproduction and Development*, *82*(7–8), 518–529. https://doi.org/10.1002/mrd.22489

Schlepckow, K., Morenas-Rodríguez, E., Hong, S., & Haass, C. (2023). Stimulation of TREM2 with agonistic antibodies-an emerging therapeutic option for Alzheimer's disease. *The Lancet. Neurology*, *22*(11), 1048–1060. https://doi.org/10.1016/S1474-4422(23)00247-8

Schliebs, R., & Arendt, T. (2011). The cholinergic system in aging and neuronal degeneration. *Behavioural Brain Research*, *221*(2), 555–563. https://doi.org/10.1016/J.BBR.2010.11.058

Schmidt-Hieber, C., Jonas, P., & Bischofberger, J. (2008). Action potential initiation and propagation in hippocampal mossy fibre axons. *Journal of Physiology*, *586*(7), 1849–1857. https://doi.org/10.1113/jphysiol.2007.150151

Schmöle, A.-C., Lundt, R., Ternes, S., Albayram, Ö., Ulas, T., Schultze, J. L., Bano, D., Nicotera, P., Alferink, J., & Zimmer, A. (2015). Cannabinoid receptor 2 deficiency results in reduced neuroinflammation in an Alzheimer's disease mouse model. *Neurobiology of Aging*, *36*(2), 710–719. https://doi.org/10.1016/j.neurobiolaging.2014.09.019

Schwartzkroin, P. A., & Mathers, L. H. (1978). Physiological and morphological identification of a nonpyramidal hippocampal cell type. *Brain Research*, *157*(1), 1–10. https://doi.org/10.1016/0006-8993(78)90991-5

Serrano-Pozo, A., Das, S., & Hyman, B. T. (2021). APOE and Alzheimer's Disease: Advances in Genetics, Pathophysiology, and Therapeutic Approaches. *The Lancet. Neurology*, *20*(1), 68–80. https://doi.org/10.1016/S1474-4422(20)30412-9

Sessa, G., Podini, P., Mariani, M., Meroni, A., Spreafico, R., Sinigaglia, F., Colonna, M., Panina, P., & Meldolesi, J. (2004). Distribution and signaling of TREM2/DAP12, the receptor system mutated in human polycystic lipomembraneous osteodysplasia with sclerosing leukoencephalopathy dementia. *European Journal of Neuroscience*, *20*(10), 2617–2628. https://doi.org/10.1111/j.1460-9568.2004.03729.x

Sherrington, R., Rogaev, E. I., Liang, Y., Rogaeva, E. A., Levesque, G., Ikeda, M., Chi, H., Lin, C., Li, G., Holman, K., Tsuda, T., Mar, L., Foncin, J.-F., Bruni, A. C., Montesi, M. P., Sorbi, S., Rainero, I., Pinessi, L., Nee, L., … St George-Hyslop, P. H. (1995). Cloning of a gene bearing missense mutations in early-onset familial Alzheimer's disease. *Nature*, *375*(6534), 754–760. https://doi.org/10.1038/375754a0

Shinozaki, G., Chan, A. C., Sparr, N. A., Zarei, K., Gaul, L. N., Heinzman, J. T., Robles, J., Yuki, K., Chronis, T. J., Ando, T., Wong, T., Sabbagh, S., Weckmann, M. T., Lee, S., Yamada, T., Karam, M. D., Noiseux, N. O., Shinozaki, E., & Cromwell, J. W. (2018). Delirium detection by a novel bispectral electroencephalography device in general hospital. *Psychiatry and Clinical Neurosciences*, *72*(12), 856–863. https://doi.org/10.1111/pcn.12783

Shrimpton, A. E., Schelper, R. L., Linke, R. P., Hardy, J., Crook, R., Dickson, D. W., Ishizawa, T., & Davis, R. L. (2007). A presenilin 1 mutation (L420R) in a family with early onset Alzheimer disease, seizures and cotton wool plaques, but not spastic paraparesis. *Neuropathology*, *27*(3), 228–232. https://doi.org/10.1111/j.1440-1789.2007.00766.x

Siegel, M., Warden, M. R., & Miller, E. K. (2009). Phase-dependent neuronal coding of objects in short-term memory. *Proceedings of the National Academy of Sciences of the United States of America*, *106*(50), 21341–21346. https://doi.org/10.1073/pnas.0908193106

Sik, A., Penttonen, M., Ylinen, A., & Buzsáki, G. (1995). Hippocampal CA1 interneurons: An in vivo intracellular labeling study. *Journal of Neuroscience*, *15*(10), 6651–6665. https://doi.org/10.1523/jneurosci.15-10-06651.1995

Sinclair, D., Featherstone, R., Naschek, M., Nam, J., Du, A., Wright, S., Pance, K., Melnychenko, O., Weger, R., Akuzawa, S., Matsumoto, M., & Siegel, S. J. (2017). GABA-B Agonist Baclofen Normalizes Auditory-Evoked Neural Oscillations and Behavioral Deficits in the Fmr1 Knockout Mouse Model of Fragile X Syndrome. *eNeuro*, *4*(1). https://doi.org/10.1523/ENEURO.0380-16.2017

Singer, W., & Gray, C. M. (1995). Visual Feature Integration and the Temporal Correlation Hypothesis. *Annual Review of Neuroscience*, *18*(1), 555–586. https://doi.org/10.1146/annurev.ne.18.030195.003011

Singh, A., Jones, O. D., Mockett, B. G., Ohline, S. M., & Abraham, W. C. (2019). Tumor Necrosis Factor-α-Mediated Metaplastic Inhibition of LTP Is Constitutively Engaged

in an Alzheimer's Disease Model. *Journal of Neuroscience*, *39*(46), 9083–9097. https://doi.org/10.1523/JNEUROSCI.1492-19.2019

Sirota, A., Csicsvari, J., Buhl, D., & Buzsáki, G. (2003). Communication between neocortex and hippocampus during sleep in rodents. *Proceedings of the National Academy of Sciences of the United States of America*, *100*(4), 2065–2069. https://doi.org/10.1073/pnas.0437938100

Sleegers, K., Brouwers, N., Gijselinck, I., Theuns, J., Goossens, D., Wauters, J., Del-Favero, J., Cruts, M., Duijn, C. M. v., & Broeckhoven, C. V. (2006). APP duplication is sufficient to cause early onset Alzheimer's dementia with cerebral amyloid angiopathy. *Brain*, *129*(11), 2977–2983. https://doi.org/10.1093/brain/awl203

Sofroniew, M. V. (2009). Molecular dissection of reactive astrogliosis and glial scar formation. *Trends in Neurosciences*, *32*(12), 638–647. https://doi.org/10.1016/j.tins.2009.08.002

Sofroniew, M. V., & Vinters, H. V. (2010). Astrocytes: Biology and pathology. *Acta Neuropathologica*, *119*(1), 7–35. https://doi.org/10.1007/s00401-009-0619-8

Sohal, V. S. (2022). Transforming Discoveries About Cortical Microcircuits and Gamma Oscillations Into New Treatments for Cognitive Deficits in Schizophrenia. *The American Journal of Psychiatry*, *179*(4), 267–276. https://doi.org/10.1176/appi.ajp.20220147

Sohal, V. S., Zhang, F., Yizhar, O., & Deisseroth, K. (2009). Parvalbumin neurons and gamma rhythms enhance cortical circuit performance. *Nature*, *459*(7247), 698–702. https://doi.org/10.1038/nature07991

Solodkin, A., Veldhuizen, S. D., & Van Hoesen, G. W. (1996). Contingent vulnerability of entorhinal parvalbumin-containing neurons in Alzheimer's disease. *The Journal of Neuroscience: The Official Journal of the Society for Neuroscience*, *16*(10), 3311–3321. https://doi.org/10.1523/JNEUROSCI.16-10-03311.1996

Sommer, W. (1880). Erkrankung des Ammonshorns als aetiologisches Moment der Epilepsie. *Archiv Für Psychiatrie Und Nervenkrankheiten*, *10*(3), 631–675. https://doi.org/10.1007/BF02224538

Soula, M., Martín-Ávila, A., Zhang, Y., Dhingra, A., Nitzan, N., Sadowski, M. J., Gan, W.-B., & Buzsáki, G. (2023). Forty-hertz light stimulation does not entrain native gamma oscillations in Alzheimer's disease model mice. *Nature Neuroscience*, *26*(4), 570–578. https://doi.org/10.1038/s41593-023-01270-2

Spangenberg, E., Severson, P. L., Hohsfield, L. A., Crapser, J., Zhang, J., Burton, E. A., Zhang, Y., Spevak, W., Lin, J., Phan, N. Y., Habets, G., Rymar, A., Tsang, G., Walters, J., Nespi, M., Singh, P., Broome, S., Ibrahim, P., Zhang, C., … Green, K. N. (2019). Sustained microglial depletion with CSF1R inhibitor impairs parenchymal plaque development in an Alzheimer's disease model. *Nature Communications*, *10*(1), 3758. https://doi.org/10.1038/s41467-019-11674-z

Stadler, K., Bierwirth, C., Stoenica, L., Battefeld, A., Reetz, O., Mix, E., Schuchmann, S., Velmans, T., Rosenberger, K., Bräuer, A. U., Lehnardt, S., Nitsch, R., Budt, M., Wolff, T., Kole, M. H. P., & Strauss, U. (2014). Elevation in Type I Interferons Inhibits HCN1 and Slows Cortical Neuronal Oscillations. *Cerebral Cortex*, *24*(1), 199–210. https://doi.org/10.1093/cercor/bhs305

Stam, C. J., Van Cappellen van Walsum, A. M., Pijnenburg, Y. A. L., Berendse, H. W., De Munck, J. C., Scheltens, P., & Van Dijk, B. W. (2002). Generalized synchronization of MEG recordings in Alzheimer's disease: Evidence for involvement of the gamma band. *Journal of Clinical Neurophysiology*, *19*(6), 562–574. https://doi.org/10.1097/00004691-200212000-00010

Stanley, E. R., & Chitu, V. (2014). CSF-1 Receptor Signaling in Myeloid Cells. *Cold Spring Harbor Perspectives in Biology*, *6*(6), a021857–a021857. https://doi.org/10.1101/cshperspect.a021857

Stellwagen, D., Beattie, E. C., Seo, J. Y., & Malenka, R. C. (2005). Differential regulation of AMPA receptor and GABA receptor trafficking by tumor necrosis factor-α. *Journal of Neuroscience*, *25*(12), 3219–3228. https://doi.org/10.1523/JNEUROSCI.4486-04.2005

Stellwagen, D., & Malenka, R. C. (2006). Synaptic scaling mediated by glial TNF-α. *Nature*, *440*(7087), 1054–1059. https://doi.org/10.1038/nature04671

Stence, N., Waite, M., & Dailey, M. E. (2001). Dynamics of microglial activation: A confocal time-lapse analysis in hippocampal slices. *Glia*, *33*(3), 256–266. https://doi.org/10.1002/1098-1136(200103)33:3<256::AID-GLIA1024>3.0.CO;2-J

Stevens, B., Allen, N. J., Vazquez, L. E., Howell, G. R., Christopherson, K. S., Nouri, N., Micheva, K. D., Mehalow, A. K., Huberman, A. D., Stafford, B., Sher, A., Litke, A. M., Lambris, J. D., Smith, S. J., John, S. W. M., & Barres, B. A. (2007). The Classical Complement Cascade Mediates CNS Synapse Elimination. *Cell*, *131*(6), 1164–1178. https://doi.org/10.1016/j.cell.2007.10.036

Stewart, C. R., Stuart, L. M., Wilkinson, K., van Gils, J. M., Deng, J., Halle, A., Rayner, K. J., Boyer, L., Zhong, R., Frazier, W. A., Lacy-Hulbert, A., El Khoury, J., Golenbock, D. T., & Moore, K. J. (2010). CD36 ligands promote sterile inflammation through assembly of a Toll-like receptor 4 and 6 heterodimer. *Nature Immunology*, *11*(2), 155–161. https://doi.org/10.1038/ni.1836

Stoiljkovic, M., Kelley, C., Hajós, G. P., Nagy, D., Koenig, G., Leventhal, L., & Hajós, M. (2016). Hippocampal network dynamics in response to α7 nACh receptors activation in amyloid-β overproducing transgenic mice. *Neurobiology of Aging*, *45*, 161–168. https://doi.org/10.1016/j.neurobiolaging.2016.05.021

Streit, W. J., Hurley, S. D., McGraw, T. S., & Semple-Rowland, S. L. (2000). Comparative evaluation of cytokine profiles and reactive gliosis supports a critical role for interleukin-

6 in neuron-glia signaling during regeneration. *Journal of Neuroscience Research*, *61*(1), 10–20. https://doi.org/10.1002/1097-4547(20000701)61:1<10::AID-JNR2>3.0.CO;2-E

Strittmatter, W. J., Saunders, A. M., Schmechel, D., Pericak-Vance, M., Enghild, J., Salvesen, G. S., & Roses, A. D. (1993). Apolipoprotein E: high-avidity binding to beta-amyloid and increased frequency of type 4 allele in late-onset familial Alzheimer disease. *Proceedings of the National Academy of Sciences*, *90*(5), 1977–1981. https://doi.org/10.1073/pnas.90.5.1977

Summers, W. K., Majovski, L. V., Marsh, G. M., Tachiki, K., & Kling, A. (1986). Oral tetrahydroaminoacridine in long-term treatment of senile dementia, Alzheimer type. *The New England Journal of Medicine*, *315*(20), 1241–1245. https://doi.org/10.1056/NEJM198611133152001

Sun, J., Xu, J., Yang, B., Chen, K., Kong, Y., Fang, N., Gong, T., Wang, F., Ling, Z., & Liu, J. (2020). Effect of Clostridium butyricum against Microglia-Mediated Neuroinflammation in Alzheimer's Disease via Regulating Gut Microbiota and Metabolites Butyrate. *Molecular Nutrition & Food Research*, *64*(2), 1900636. https://doi.org/10.1002/mnfr.201900636

Sun, X. R., Zhang, H., Zhao, H. T., Ji, M. H., Li, H. H., Wu, J., Li, K. Y., & Yang, J. J. (2016). Amelioration of oxidative stress-induced phenotype loss of parvalbumin interneurons might contribute to the beneficial effects of environmental enrichment in a rat model of post-traumatic stress disorder. *Behavioural Brain Research*, *312*, 84–92. https://doi.org/10.1016/j.bbr.2016.06.016

Suzumura, A., Mezitis, S. G., Gonatas, N. K., & Silberberg, D. H. (1987). MHC antigen expression on bulk isolated macrophage-microglia from newborn mouse brain: Induction of Ia antigen expression by gamma-interferon. *Journal of Neuroimmunology*, *15*(3), 263–278. https://doi.org/10.1016/0165-5728(87)90121-4

Suzumura, A., Sawada, M., & Marunouchi, T. (1996). Selective induction of interleukin-6 in mouse microglia by granulocyte-macrophage colony-stimulating factor. *Brain Research*, *713*(1–2), 192–198. https://doi.org/10.1016/0006-8993(95)01535-3

Ta, T. T., Dikmen, H. O., Schilling, S., Chausse, B., Lewen, A., Hollnagel, J. O., & Kann, O. (2019). Priming of microglia with IFN-γ slows neuronal gamma oscillations in situ. *Proceedings of the National Academy of Sciences of the United States of America*, *116*(10), 4637–4642. https://doi.org/10.1073/pnas.1813562116

Takahashi, H., Brasnjevic, I., Rutten, B. P. F., Van Der Kolk, N., Perl, D. P., Bouras, C., Steinbusch, H. W. M., Schmitz, C., Hof, P. R., & Dickstein, D. L. (2010). Hippocampal interneuron loss in an APP/PS1 double mutant mouse and in Alzheimer's disease. *Brain Structure and Function*, *214*(2–3), 145–160. https://doi.org/10.1007/s00429-010-0242-4

Tamás, G., Buhl, E. H., Lörincz, A., & Somogyi, P. (2000). Proximally targeted GABAergic synapses and gap junctions synchronize cortical interneurons. *Nature Neuroscience*, *3*(4), 366–371. https://doi.org/10.1038/73936

Tang, Y., Nyengaard, J. R., De Groot, D. M., & Gundersen, H. J. (2001). Total regional and global number of synapses in the human brain neocortex. *Synapse (New York, N.Y.)*, *41*(3), 258–273. https://doi.org/10.1002/syn.1083

Tao, H. Y., & Tian, X. (2005). Coherence Characteristics of Gamma-band EEG during rest and cognitive task in MCI and AD. *Annual International Conference of the IEEE Engineering in Medicine and Biology - Proceedings*, *7 VOLS*, 2747–2750. https://doi.org/10.1109/iembs.2005.1617040

Targa Dias Anastacio, H., Matosin, N., & Ooi, L. (2022). Neuronal hyperexcitability in Alzheimer's disease: What are the drivers behind this aberrant phenotype? *Translational Psychiatry*, *12*(1), 1–14. https://doi.org/10.1038/s41398-022-02024-7

Teleanu, D. M., Niculescu, A.-G., Lungu, I. I., Radu, C. I., Vladâcenco, O., Roza, E., Costăchescu, B., Grumezescu, A. M., & Teleanu, R. I. (2022). An Overview of Oxidative Stress, Neuroinflammation, and Neurodegenerative Diseases. *International Journal of Molecular Sciences*, *23*(11), 5938. https://doi.org/10.3390/ijms23115938

Terry, R. D., Gonatas, N. K., & Weiss, M. (1964). ULTRASTRUCTURAL STUDIES IN ALZHEIMER'S PRESENILE DEMENTIA. *The American Journal of Pathology*, *44*(2), 269–297.

Terry, R. D., Masliah, E., Salmon, D. P., Butters, N., DeTeresa, R., Hill, R., Hansen, L. A., & Katzman, R. (1991). Physical basis of cognitive alterations in alzheimer's disease: Synapse loss is the major correlate of cognitive impairment. *Annals of Neurology*, *30*(4), 572–580. https://doi.org/10.1002/ana.410300410

Testa, D., Prochiantz, A., & Di Nardo, A. A. (2019). Perineuronal nets in brain physiology and disease. *Seminars in Cell and Developmental Biology*, *89*, 125–135. https://doi.org/10.1016/j.semcdb.2018.09.011

Thornton, P., Pinteaux, E., Gibson, R. M., Allan, S. M., & Rothwell, N. J. (2006). Interleukin-1-induced neurotoxicity is mediated by glia and requires caspase activation and free radical release. *Journal of Neurochemistry*, *98*(1), 258–266. https://doi.org/10.1111/j.1471-4159.2006.03872.x

Tiesinga, P., & Sejnowski, T. J. (2009). Cortical Enlightenment: Are Attentional Gamma Oscillations Driven by ING or PING? *Neuron*, *63*(6), 727–732. https://doi.org/10.1016/j.neuron.2009.09.009

Tiitinen, H. T., Sinkkonen, J., Reinikainen, K., Alho, K., Lavikainen, J., & Näätänen, R. (1993). Selective attention enhances the auditory 40-Hz transient response in humans. *Nature*, *364*(6432), 59–60. https://doi.org/10.1038/364059a0

Tönnies, E., & Trushina, E. (2017). Oxidative Stress, Synaptic Dysfunction, and Alzheimer's Disease. *Journal of Alzheimer's Disease: JAD*, *57*(4), 1105–1121. https://doi.org/10.3233/JAD-161088

Tortora, F., Rendina, A., Angiolillo, A., Di Costanzo, A., Aniello, F., Donizetti, A., Febbraio, F., & Vitale, E. (2022). CD33 rs2455069 SNP: Correlation with Alzheimer's Disease and Hypothesis of Functional Role. *International Journal of Molecular Sciences*, *23*(7), 3629. https://doi.org/10.3390/ijms23073629

Torvell, M., Hampton, D. W., Connick, P., MacLullich, A. M. J., Cunningham, C., & Chandran, S. (2019). A single systemic inflammatory insult causes acute motor deficits and accelerates disease progression in a mouse model of human tauopathy. *Alzheimer's & Dementia (New York, N. Y.)*, *5*, 579–591. https://doi.org/10.1016/j.trci.2019.09.001

Town, T., Jeng, D., Alexopoulou, L., Tan, J., & Flavell, R. A. (2006). Microglia recognize double-stranded RNA via TLR3. *Journal of Immunology (Baltimore, Md.: 1950)*, *176*(6), 3804–3812. https://doi.org/10.4049/jimmunol.176.6.3804

Traub, R. D., Bibbig, A., Fisahn, A., LeBeau, F. E. N., Whittington, M. A., & Buhl, E. H. (2000). A model of gamma-frequency network oscillations induced in the rat CA3 region by carbachol in vitro. *European Journal of Neuroscience*, *12*(11), 4093–4106. https://doi.org/10.1046/j.1460-9568.2000.00300.x

Traub, R. D., Bibbig, A., LeBeau, F. E. N., Buhl, E. H., & Whittington, M. A. (2004). CELLULAR MECHANISMS OF NEURONAL POPULATION OSCILLATIONS IN THE HIPPOCAMPUS IN VITRO. *Annual Review of Neuroscience*, *27*(1), 247–278. https://doi.org/10.1146/annurev.neuro.27.070203.144303

Traub, R. D., Whittington, M. A., Colling, S. B., Buzsáki, G., & Jefferys, J. G. (1996). Analysis of gamma rhythms in the rat hippocampus in vitro and in vivo. *The Journal of Physiology*, *493*(Pt 2), 471–484.

Traub, R. D., Whittington, M. A., Stanford, I. M., & Jefferys, J. G. R. (1996). A mechanism for generation of long-range synchronous fast oscillations in the cortex. *Nature*, *383*(6601), Article 6601. https://doi.org/10.1038/383621a0

Tukker, J. J., Lasztóczi, B., Katona, L., Roberts, J. D. B., Pissadaki, E. K., Dalezios, Y., Márton, L., Zhang, L., Klausberger, T., & Somogyi, P. (2013). Distinct dendritic arborization and in vivo firing patterns of parvalbumin-expressing basket cells in the hippocampal area CA3. *Journal of Neuroscience*, *33*(16), 6809–6825. https://doi.org/10.1523/JNEUROSCI.5052-12.2013

Tweedy, C., Kindred, N., Curry, J., Williams, C., Taylor, J.-P., Atkinson, P., Randall, F., Erskine, D., Morris, C. M., Reeve, A. K., Clowry, G. J., & LeBeau, F. E. N. (2021). Hippocampal network hyperexcitability in young transgenic mice expressing human

mutant alpha-synuclein. *Neurobiology of Disease*, *149*, 105226. https://doi.org/10.1016/j.nbd.2020.105226

Uchihara, T., Duyckaerts, C., He, Y., Kobayashi, K., Seilhean, D., Amouyel, P., & Hauw, J. J. (1995). ApoE immunoreactivity and microglial cells in Alzheimer's disease brain. *Neuroscience Letters*, *195*(1), 5–8. https://doi.org/10.1016/0304-3940(95)11763-m

Ulland, T. K., & Colonna, M. (2018). TREM2—A key player in microglial biology and Alzheimer disease. *Nature Reviews Neurology*, *14*(11), 667–675. https://doi.org/10.1038/s41582-018-0072-1

Ulland, T. K., Song, W. M., Huang, S. C.-C., Ulrich, J. D., Sergushichev, A., Beatty, W. L., Loboda, A. A., Zhou, Y., Cairns, N. J., Kambal, A., Loginicheva, E., Gilfillan, S., Cella, M., Virgin, H. W., Unanue, E. R., Wang, Y., Artyomov, M. N., Holtzman, D. M., & Colonna, M. (2017). TREM2 Maintains Microglial Metabolic Fitness in Alzheimer's Disease. *Cell*, *170*(4), 649-663.e13. https://doi.org/10.1016/j.cell.2017.07.023

Ulrich, M., Pollali, E., Çalışkan, G., Stork, O., & Albrecht, A. (2023). Sex differences in anxiety and threat avoidance in GAD65 knock-out mice. *Neurobiology of Disease*, *183*, 106165. https://doi.org/10.1016/j.nbd.2023.106165

Unger, M. S., Schernthaner, P., Marschallinger, J., Mrowetz, H., & Aigner, L. (2018). Microglia prevent peripheral immune cell invasion and promote an anti-inflammatory environment in the brain of APP-PS1 transgenic mice. *Journal of Neuroinflammation*, *15*(1), 274. https://doi.org/10.1186/s12974-018-1304-4

United Nations. (2019). *World Population Prospects—Population Division—United Nations*. https://population.un.org/wpp/DataSources/231

van Dellen, E., van der Kooi, A. W., Numan, T., Koek, H. L., Klijn, F. A. M., Buijsrogge, M. P., Stam, C. J., & Slooter, A. J. C. (2014). Decreased functional connectivity and disturbed directionality of information flow in the electroencephalography of intensive care unit patients with delirium after cardiac surgery. *Anesthesiology*, *121*(2), 328–335. https://doi.org/10.1097/ALN.0000000000000329

van Deursen, J. A., Vuurman, E. F. P. M., van Kranen-Mastenbroek, V. H. J. M., Verhey, F. R. J., & Riedel, W. J. (2011). 40-Hz steady state response in Alzheimer's disease and mild cognitive impairment. *Neurobiology of Aging*, *32*(1), 24–30. https://doi.org/10.1016/j.neurobiolaging.2009.01.002

Van Deursen, J. A., Vuurman, E. F. P. M., Verhey, F. R. J., Van Kranen-Mastenbroek, V. H. J. M., & Riedel, W. J. (2008). Increased EEG gamma band activity in Alzheimer's disease and mild cognitive impairment. *Journal of Neural Transmission*, *115*(9), 1301–1311. https://doi.org/10.1007/s00702-008-0083-y

Veit, J., Hakim, R., Jadi, M. P., Sejnowski, T. J., & Adesnik, H. (2017). Cortical gamma band synchronization through somatostatin interneurons. *Nature Neuroscience*, *20*(7), 951–959. https://doi.org/10.1038/nn.4562

Velazquez, R., Ferreira, E., Knowles, S., Fux, C., Rodin, A., Winslow, W., & Oddo, S. (2019). Lifelong choline supplementation ameliorates Alzheimer's disease pathology and associated cognitive deficits by attenuating microglia activation. *Aging Cell*, *18*(6), e13037. https://doi.org/10.1111/acel.13037

Venegas, C., Kumar, S., Franklin, B. S., Dierkes, T., Brinkschulte, R., Tejera, D., Vieira-Saecker, A., Schwartz, S., Santarelli, F., Kummer, M. P., Griep, A., Gelpi, E., Beilharz, M., Riedel, D., Golenbock, D. T., Geyer, M., Walter, J., Latz, E., & Heneka, M. T. (2017). Microglia-derived ASC specks cross-seed amyloid-β in Alzheimer's disease. *Nature*, *552*(7685), 355–361. https://doi.org/10.1038/nature25158

Verkhratsky, A., Augusto-Oliveira, M., Pivoriūnas, A., Popov, A., Brazhe, A., & Semyanov, A. (2021). Astroglial asthenia and loss of function, rather than reactivity, contribute to the ageing of the brain. *Pflügers Archiv - European Journal of Physiology*, *473*(5), 753–774. https://doi.org/10.1007/s00424-020-02465-3

Verkhratsky, A., Butt, A., Li, B., Illes, P., Zorec, R., Semyanov, A., Tang, Y., & Sofroniew, M. V. (2023). Astrocytes in human central nervous system diseases: A frontier for new therapies. *Signal Transduction and Targeted Therapy*, *8*(1), 1–37. https://doi.org/10.1038/s41392-023-01628-9

Verkhratsky, A., & Nedergaard, M. (2018). Physiology of astroglia. *Physiological Reviews*, *98*(1), 239–389. https://doi.org/10.1152/physrev.00042.2016

Verret, L., Mann, E. O., Hang, G. B., Barth, A. M. I., Cobos, I., Ho, K., Devidze, N., Masliah, E., Kreitzer, A. C., Mody, I., Mucke, L., & Palop, J. J. (2012). Inhibitory interneuron deficit links altered network activity and cognitive dysfunction in alzheimer model. *Cell*, *149*(3), 708–721. https://doi.org/10.1016/j.cell.2012.02.046

Vezzani, A., & Viviani, B. (2015). Neuromodulatory properties of inflammatory cytokines and their impact on neuronal excitability. *Neuropharmacology*, *96*(Pt A), 70–82. https://doi.org/10.1016/j.neuropharm.2014.10.027

Vila-Merkle, H., González-Martínez, A., Campos-Jiménez, R., Martínez-Ricós, J., Teruel-Martí, V., Lloret, A., Blasco-Serra, A., & Cervera-Ferri, A. (2023). Sex differences in amygdalohippocampal oscillations and neuronal activation in a rodent anxiety model and in response to infralimbic deep brain stimulation. *Frontiers in Behavioral Neuroscience*, *17*. https://www.frontiersin.org/articles/10.3389/fnbeh.2023.1122163

Villeda, S. A., Luo, J., Mosher, K. I., Zou, B., Britschgi, M., Bieri, G., Stan, T. M., Fainberg, N., Ding, Z., Eggel, A., Lucin, K. M., Czirr, E., Park, J.-S., Couillard-Després, S., Aigner, L., Li, G., Peskind, E. R., Kaye, J. A., Quinn, J. F., … Wyss-Coray, T. (2011).

The ageing systemic milieu negatively regulates neurogenesis and cognitive function. *Nature*, *477*(7362), 90–94. https://doi.org/10.1038/nature10357

Viriyopase, A., Memmesheimer, R.-M., & Gielen, S. (2016). Cooperation and competition of gamma oscillation mechanisms. *Journal of Neurophysiology*, *116*(2), 232–251. https://doi.org/10.1152/jn.00493.2015

Viviani, B., Bartesaghi, S., Gardoni, F., Vezzani, A., Behrens, M. M., Bartfai, T., Binaglia, M., Corsini, E., Di Luca, M., Galli, C. L., & Marinovich, M. (2003). Interleukin-1beta enhances NMDA receptor-mediated intracellular calcium increase through activation of the Src family of kinases. *The Journal of Neuroscience: The Official Journal of the Society for Neuroscience*, *23*(25), 8692–8700. https://doi.org/10.1523/JNEUROSCI.23-25-08692.2003

Volicer, L., Smith, S., & Volicer, B. J. (1995). Effect of Seizures on Progression of Dementia of the Alzheimer Type. *Dementia and Geriatric Cognitive Disorders*, *6*(5), 258–263. https://doi.org/10.1159/000106956

Vossel, K. A., Beagle, A. J., Rabinovici, G. D., Shu, H., Lee, S. E., Naasan, G., Hegde, M., Cornes, S. B., Henry, M. L., Nelson, A. B., Seeley, W. W., Geschwind, M. D., Gorno-Tempini, M. L., Shih, T., Kirsch, H. E., Garcia, P. A., Miller, B. L., & Mucke, L. (2013). Seizures and Epileptiform Activity in the Early Stages of Alzheimer Disease. *JAMA Neurology*, *70*(9), 1158. https://doi.org/10.1001/jamaneurol.2013.136

Vossel, K. A., Ranasinghe, K. G., Beagle, A. J., Mizuiri, D., Honma, S. M., Dowling, A. F., Darwish, S. M., Van Berlo, V., Barnes, D. E., Mantle, M., Karydas, A. M., Coppola, G., Roberson, E. D., Miller, B. L., Garcia, P. A., Kirsch, H. E., Mucke, L., & Nagarajan, S. S. (2016). Incidence and impact of subclinical epileptiform activity in Alzheimer's disease. *Annals of Neurology*, *80*(6), 858–870. https://doi.org/10.1002/ana.24794

Vreugdenhil, M., Jefferys, J. G. R., Celio, M. R., & Schwaller, B. (2003). Parvalbumin-Deficiency Facilitates Repetitive IPSCs and Gamma Oscillations in the Hippocampus. *Journal of Neurophysiology*, *89*(3), 1414–1422. https://doi.org/10.1152/jn.00576.2002

Waddington, C. H. (1957). *The Strategy of the Genes*. Routledge.

Wake, H., Moorhouse, A. J., Jinno, S., Kohsaka, S., & Nabekura, J. (2009). Resting microglia directly monitor the functional state of synapses in vivo and determine the fate of ischemic terminals. *The Journal of Neuroscience: The Official Journal of the Society for Neuroscience*, *29*(13), 3974–3980. https://doi.org/10.1523/JNEUROSCI.4363-08.2009

Wallon, D., Rousseau, S., Rovelet-Lecrux, A., Quillard-Muraine, M., Guyant-Maréchal, L., Martinaud, O., Pariente, J., Puel, M., Rollin-Sillaire, A., Pasquier, F., Le Ber, I., Sarazin, M., Croisile, B., Boutoleau-Bretonnière, C., Thomas-Antérion, C., Paquet, C., Moreaud, O., Gabelle, A., Sellal, F., … collaborators of GMAJ project. (2012). The French Series of Autosomal Dominant Early Onset Alzheimer's Disease Cases:

Mutation Spectrum and Cerebrospinal Fluid Biomarkers. *Journal of Alzheimer's Disease*, *30*(4), 847–856. https://doi.org/10.3233/JAD-2012-120172

Walz, W. (2000). Role of astrocytes in the clearance of excess extracellular potassium. *Neurochemistry International*, *36*(4–5), 291–300. https://doi.org/10.1016/s0197-0186(99)00137-0

Wang, J., Fang, Y., Wang, X., Yang, H., Yu, X., & Wang, H. (2017). Enhanced Gamma Activity and Cross-Frequency Interaction of Resting-State Electroencephalographic Oscillations in Patients with Alzheimer's Disease. *Frontiers in Aging Neuroscience*, *9*(JUL), 243. https://doi.org/10.3389/fnagi.2017.00243

Wang, J., Ikonen, S., Gurevicius, K., Van Groen, T., & Tanila, H. (2002). Alteration of cortical EEG in mice carrying mutated human APP transgene. *Brain Research*, *943*(2), 181–190. https://doi.org/10.1016/S0006-8993(02)02617-3

Wang, X.-J., & Buzsáki, G. (1996). Gamma Oscillation by Synaptic Inhibition in a Hippocampal Interneuronal Network Model. *The Journal of Neuroscience*, *16*(20), 6402–6413. https://doi.org/10.1523/JNEUROSCI.16-20-06402.1996

Wang, Y., Cella, M., Mallinson, K., Ulrich, J. D., Young, K. L., Robinette, M. L., Gilfillan, S., Krishnan, G. M., Sudhakar, S., Zinselmeyer, B. H., Holtzman, D. M., Cirrito, J. R., & Colonna, M. (2015). TREM2 lipid sensing sustains the microglial response in an Alzheimer's disease model. *Cell*, *160*(6), 1061–1071. https://doi.org/10.1016/j.cell.2015.01.049

White, J. A., Chow, C. C., Rit, J., Soto-Treviño, C., & Kopell, N. (1998). Synchronization and Oscillatory Dynamics in Heterogeneous, Mutually Inhibited Neurons. *Journal of Computational Neuroscience*, *5*(1), 5–16. https://doi.org/10.1023/A:1008841325921

Whittington, M. A., Traub, R. D., Faulkner, H. J., Stanford, I. M., & Jefferys, J. G. R. (1997). Recurrent excitatory postsynaptic potentials induced by synchronized fast cortical oscillations. *Proceedings of the National Academy of Sciences*, *94*(22), 12198–12203. https://doi.org/10.1073/pnas.94.22.12198

Whittington, M. A., Traub, R. D., & Jefferys, J. G. R. (1995). Synchronized oscillations in interneuron networks driven by metabotropic glutamate receptor activation. *Nature*, *373*(6515), 612–615. https://doi.org/10.1038/373612a0

Whittington, M. A., Traub, R. D., Kopell, N., Ermentrout, B., & Buhl, E. H. (2000). Inhibition-based rhythms: Experimental and mathematical observations on network dynamics. *International Journal of Psychophysiology*, *38*(3), 315–336. https://doi.org/10.1016/S0167-8760(00)00173-2

WHO. (2001). World Health Organization: Epilepsy: Epidemiology, aetiology and prognosis. *WHO Factsheet*.

Wiesman, A. I., Murman, D. L., May, P. E., Schantell, M., Wolfson, S. L., Johnson, C. M., & Wilson, T. W. (2021). Visuospatial alpha and gamma oscillations scale with the severity of cognitive dysfunction in patients on the Alzheimer's disease spectrum. *Alzheimer's Research & Therapy*, *13*(1), 139. https://doi.org/10.1186/s13195-021-00881-w

Wilhelmsson, U., Bushong, E. A., Price, D. L., Smarr, B. L., Phung, V., Terada, M., Ellisman, M. H., & Pekny, M. (2006). Redefining the concept of reactive astrocytes as cells that remain within their unique domains upon reaction to injury. *Proceedings of the National Academy of Sciences of the United States of America*, *103*(46), 17513–17518. https://doi.org/10.1073/pnas.0602841103

Wißfeld, J., Nozaki, I., Mathews, M., Raschka, T., Ebeling, C., Hornung, V., Brüstle, O., & Neumann, H. (2021). Deletion of Alzheimer's disease-associated CD33 results in an inflammatory human microglia phenotype. *Glia*, *69*(6), 1393–1412. https://doi.org/10.1002/glia.23968

Witlox, J., Eurelings, L. S. M., De Jonghe, J. F. M., Kalisvaart, K. J., Eikelenboom, P., & Van Gool, W. A. (2010). Delirium in elderly patients and the risk of postdischarge mortality, institutionalization, and dementia: A meta-analysis. *JAMA - Journal of the American Medical Association*, *304*(4), 443–451. https://doi.org/10.1001/jama.2010.1013

Wójtowicz, A. M., Van Boom, L. D., Chakrabarty, A., Maggio, N., Haq, R. U., Behrens, C. J., & Heinemann, U. (2009). Monoamines block kainate- And carbachol-induced. γ-oscillations but augment stimulus-induced γ-oscillations in rat hippocampus in vitro. *Hippocampus*, *19*(3), 273–288. https://doi.org/10.1002/HIPO.20508

Xu, Y., Zhao, M., Han, Y., & Zhang, H. (2020). GABAergic Inhibitory Interneuron Deficits in Alzheimer's Disease: Implications for Treatment. *Frontiers in Neuroscience*, *14*. https://doi.org/10.3389/fnins.2020.00660

Yamada, T., Kawamata, T., Walker, D. G., & McGeer, P. L. (1992). Vimentin immunoreactivity in normal and pathological human brain tissue. *Acta Neuropathologica*, *84*(2), 157–162. https://doi.org/10.1007/BF00311389

Yao, Z., van Velthoven, C. T. J., Kunst, M., Zhang, M., McMillen, D., Lee, C., Jung, W., Goldy, J., Abdelhak, A., Aitken, M., Baker, K., Baker, P., Barkan, E., Bertagnolli, D., Bhandiwad, A., Bielstein, C., Bishwakarma, P., Campos, J., Carey, D., … Zeng, H. (2023). A high-resolution transcriptomic and spatial atlas of cell types in the whole mouse brain. *Nature*, *624*(7991), 317–332. https://doi.org/10.1038/s41586-023-06812-z

Ye, J., Coulouris, G., Zaretskaya, I., Cutcutache, I., Rozen, S., & Madden, T. L. (2012). Primer-BLAST: A tool to design target-specific primers for polymerase chain reaction. *BMC Bioinformatics*, *13*, 134. https://doi.org/10.1186/1471-2105-13-134

Yuan, L., Zhang, J., Guo, J.-H., Holscher, C., Yang, J.-T., Wu, M.-N., Wang, Z.-J., Cai, H.-Y., Han, L.-N., Shi, H., Han, Y.-F., & Qi, J.-S. (2021). DAla2-GIP-GLU-PAL Protects Against Cognitive Deficits and Pathology in APP/PS1 Mice by Inhibiting Neuroinflammation and Upregulating cAMP/PKA/CREB Signaling Pathways. *Journal of Alzheimer's Disease*, *80*(2), 695–713. https://doi.org/10.3233/JAD-201262

Zamanian, J. L., Xu, L., Foo, L. C., Nouri, N., Zhou, L., Giffard, R. G., & Barres, B. A. (2012). Genomic Analysis of Reactive Astrogliosis. *The Journal of Neuroscience*, *32*(18), 6391–6410. https://doi.org/10.1523/JNEUROSCI.6221-11.2012

Zhang, X., Zhao, F., Wang, C., Zhang, J., Bai, Y., Zhou, F., Wang, Z., Wu, M., Yang, W., Guo, J., & Qi, J. (2020). AVP(4-8) Improves Cognitive Behaviors and Hippocampal Synaptic Plasticity in the APP/PS1 Mouse Model of Alzheimer's Disease. *Neuroscience Bulletin*, *36*(3), 254–262. https://doi.org/10.1007/s12264-019-00434-0

Zhao, L. (2018). CD33 in Alzheimer's Disease – Biology, Pathogenesis, and Therapeutics: A Mini-Review. *Gerontology*, *65*(4), 323–331. https://doi.org/10.1159/000492596

Zhao, N., Ren, Y., Yamazaki, Y., Qiao, W., Li, F., Felton, L. M., Mahmoudiandehkordi, S., Kueider-Paisley, A., Sonoustoun, B., Arnold, M., Shue, F., Zheng, J., Attrebi, O. N., Martens, Y. A., Li, Z., Bastea, L., Meneses, A. D., Chen, K., Thompson, J. W., … Bu, G. (2020). Alzheimer's risk factors age, APOE genotype, and sex drive distinct molecular pathways. *Neuron*, *106*(5), 727-742.e6. https://doi.org/10.1016/j.neuron.2020.02.034

Zhao, Y., Wu, X., Li, X., Jiang, L.-L., Gui, X., Liu, Y., Sun, Y., Zhu, B., Piña-Crespo, J. C., Zhang, M., Zhang, N., Chen, X., Bu, G., An, Z., Huang, T. Y., & Xu, H. (2018). TREM2 Is a Receptor for β-Amyloid that Mediates Microglial Function. *Neuron*, *97*(5), 1023-1031.e7. https://doi.org/10.1016/j.neuron.2018.01.031

Zhou, Y., Song, W. M., Andhey, P. S., Swain, A., Levy, T., Miller, K. R., Poliani, P. L., Cominelli, M., Grover, S., Gilfillan, S., Cella, M., Ulland, T. K., Zaitsev, K., Miyashita, A., Ikeuchi, T., Sainouchi, M., Kakita, A., Bennett, D. A., Schneider, J. A., … Colonna, M. (2020). Human and mouse single-nucleus transcriptomics reveal TREM2-dependent and TREM2-independent cellular responses in Alzheimer's disease. *Nature Medicine*, *26*(1), 131–142. https://doi.org/10.1038/s41591-019-0695-9

Zhou, Y., Tang, H., Liu, J., Dong, J., & Xiong, H. (2011). Chemokine CCL2 modulation of neuronal excitability and synaptic transmission in rat hippocampal slices. *Journal of Neurochemistry*, *116*(3), 406. https://doi.org/10.1111/J.1471-4159.2010.07121.X

Zhu, X.-C., Tan, L., Wang, H.-F., Jiang, T., Cao, L., Wang, C., Wang, J., Tan, C.-C., Meng, X.-F., & Yu, J.-T. (2015). Rate of early onset Alzheimer's disease: A systematic review and meta-analysis. *Annals of Translational Medicine*, *3*(3), 38. https://doi.org/10.3978/j.issn.2305-5839.2015.01.19

Zipp, F., Bittner, S., & Schafer, D. P. (2023). Cytokines as emerging regulators of central nervous system synapses. *Immunity*, *56*(5), 914–925. https://doi.org/10.1016/j.immuni.2023.04.011

Zonta, M., Angulo, M. C., Gobbo, S., Rosengarten, B., Hossmann, K.-A., Pozzan, T., & Carmignoto, G. (2003). Neuron-to-astrocyte signaling is central to the dynamic control of brain microcirculation. *Nature Neuroscience*, *6*(1), 43–50. https://doi.org/10.1038/nn980